Summary
of Activities
2013

CANADA-NUNAVUT
GEOSCIENCE OFFICE

ᑲᓇᑕᐅᑉ−ᓄᓇᕗᒡᒍ
ᐅᔭᖅᑲᓃᑦ ᖃᐅᔨᓴᕐᕕᖓᑦᑕ

BUREAU GÉOSCIENTIFIQUE
CANADA-NUNAVUT

KANATAMI-NUNAVUMI
GEOSCIENCE TITIGAKVIIT

CANADA-NUNAVUT
GEOSCIENCE OFFICE

ᑲᓇᑕᐅᑉᐴᓄᓇ ᢒᓗ
ᐅᔅᖃᖃᓂᖅ ᖃᐅᐱᔅᖃᑎᖕᑎᑦ

BUREAU GÉOSCIENTIFIQUE
CANADA-NUNAVUT

KANATAMI-NUNAVUMI
GEOSCIENCE TITIGAKVIIT

SUMMARY OF ACTIVITIES 2013

Front cover photo: Candice Sudlovenick (left) and Patricia Peyton (right) record observations while mapping on northern Hall Peninsula. Photo by Holly Steenkamp, Canada-Nunavut Geoscience Office.

Back cover photo: East-vergent fold of metapelite (brown), metabasite (black) and granitic orthogneiss (grey), northeastern Hall Peninsula. Photo by Diane Skipton, University of Ottawa.

Foreword

The Canada-Nunavut Geoscience Office (CNGO) was established in 1999 to help foster the development of Nunavut's mineral and energy resources and infrastructure. It is a partnership between the Government of Nunavut (GN), Natural Resources Canada (NRCan), and Aboriginal Affairs and Northern Development Canada (AANDC). Nunavut Tunngavik Incorporated (NTI) is an ex-officio member of the office. Fully staffed, the office consists of six employees with expertise in Precambrian, Paleozoic and Quaternary geology; GIS; and online data dissemination. In February 2013, the CNGO moved its office into the new Inuksugait Phase IV building in downtown Iqaluit.

The mandate of the CNGO is to provide accessible geoscience information and expertise in Nunavut that supports 1) responsible resource exploration and development, 2) responsible infrastructure development, 3) geoscience-capacity building, 4) education and training, and 5) geoscience awareness and outreach. The CNGO geoscience program concentrates on new geoscience mapping and research, supporting geoscience-capacity building, disseminating geoscience information and developing collaborative partnerships of strategic importance to Nunavut.

The CNGO is pleased to once again be presenting results from its numerous collaborative geoscience projects in its 2013 Canada-Nunavut Geoscience Office Summary of Activities volume. This is the second publication in this series, which continues to be an exciting undertaking for the office and a vehicle for disseminating results from field research in a timely manner. This year, the CNGO proudly introduces a new publication series named the 'Geoscience Data Series'. The intent of this series is to disseminate digital datasets (e.g., analytical datasets, polygon files, point data) so stakeholders can incorporate this information into decision-making processes. This series will provide the digital data to support papers in the Summary of Activities, as well as disseminate additional data collected by the CNGO. Where appropriate, this series will be referenced in Summary of Activities papers, with links provided to the online repository. This is truly an exciting time for data dissemination at the CNGO.

This year's volume is divided into six sections and consists of 22 papers. The sections are 'Mineral deposit studies', 'Regional geoscience', 'Geoscience for infrastructure', 'Carving stone', 'Aggregate and industrial minerals', and 'Outreach and capacity building'. The latter two sections are new this year and demonstrate more fully the breadth of research conducted by the CNGO. All papers will be available for download at www.cngo.ca.

The 'Mineral deposit studies' section focuses on studies in the Mesoproterozoic Borden Basin and on Hall Peninsula. Work in the Borden Basin focuses on the Ikpiarjuk Formation mounds, with an emphasis on determining the composition of the vent fluid that formed them and hence the potential for SEDEX deposits in the area. This work is part of a Ph.D. project led by Laurentian University. Two additional papers discuss the natural resource potential on Hall Peninsula. The first discusses the economic significance of the numerous ultramafic rocks occurring in the region. Emphasis is placed on the discovery of new layered mafic-ultramafic intrusions that could show potential for Ni-Cu-platinum group element mineralization and the potential for carving stone in hydrated ultramafic rocks. The second paper provides an update on the diamond sources beneath Hall Peninsula, including the diamond residence history, and carbon and nitrogen isotopic characteristics.

The papers in the 'Regional geoscience' section focus on observations and results from the Hall Peninsula Integrated Geoscience Program (HPIGP). The HPIGP is being led by the Canada-Nunavut Geoscience Office in collaboration with Dalhousie University, University of Alberta, Université Laval, University of Manitoba, University of Ottawa, University of Saskatchewan, Arctic College and the Geological Survey of Canada. Papers from Oxford University and the University of Texas at Austin also make a contribution to this year's work on Hall Peninsula. The focus is once again on bedrock and surficial mapping, and a range of thematic studies. New results from the southern portion of Hall Peninsula, including geochronology, till geochemistry, geochemistry of mafic and ultramafic rocks, and Paleoproterozoic deformation and metamorphism, are presented along with a regional overview of the geology on the northern part of the peninsula.

This year's 'Geoscience for infrastructure' section highlights a broad range of collaborative research conducted by the Earth Sciences Sector (ESS) of Natural Resources Canada and Canadian universities, with the support of the CNGO. The first paper provides preliminary results from new geohazards research led by the ESS Public Safety Geoscience Program in Baffin Bay. The aim of this work is to assess seafloor stability, sediment transport, earthquake history, seabed mass movements and natural hydrocarbon seeps in the area. Results from permafrost research at the Iqaluit International Airport and an update on coastal climate-change work being conducted by the ESS Climate Change Geoscience Program are also provided. The runway, taxiways and apron at the airport experience instability and subsidence that are likely related to permafrost degradation and drainage conditions. New geophysical data are being collected to better characterize permafrost conditions and processes in the area. An update of coastal climate-change issues across Nunavut is also presented, with an emphasis on coastal

mapping work in southern Coronation Gulf and sea-level change in Hudson Bay. Finally, a series of four papers summarizing observations from reconnaissance landscape-hazard assessments in Kugluktuk, Cambridge Bay, Whale Cove and Arviat is presented. These assessments were part of the Nunavut Climate Change Partnership and will contribute to planning processes for climate-change adaptation in each of these communities.

The 'Carving stone' section consists of a paper focused on the geology and the remaining resource potential at the Kangiqsukutaaq quarry (Korok Inlet). This quarry has been producing high-quality carving stone for Inuit carvers in south Baffin and across Nunavut for more than 50 years. A collaboration between the CNGO, Qikiqtani Inuit Association, the Government of Nunavut and DeBeers Canada aims to identify the extent of remaining at-surface or surface-accessible resources at the quarry, as well as inform a site management plan at the quarry.

Papers are being published in the 'Aggregate and industrial minerals' and the 'Outreach and capacity building' sections for the first time. In 2013, new fieldwork focused on the industrial limestone potential of the Lower Silurian Ekwan River and Attawapiskat formations on western Southampton Island. Preliminary data suggest that high-calcium limestone occurs in the Ekwan River Formation. This is a new discovery that could stimulate the development of Nunavut's first industrial limestone quarry. Finally, an overview of a new pilot geoscience-training program for Nunavut students reports on a collaborative effort between the CNGO and Dalhousie University that provided training opportunities for two students from Nunavut Arctic College and serves as a model that could be expanded upon in future years.

Finally, this volume is dedicated to Dr. Eric Prosh and Mannasie Qillaq, who both passed away suddenly this fall. Both Eric and Mannasie were close friends and colleagues with staff at the CNGO and made significant contributions to the evolution of the office and delivery of its geoscience programs. They will be missed.

Acknowledgments

David Mate
Chief Geologist
Canada-Nunavut Geoscience Office
www.cngo.ca/

In Memoriam
Eric Charles Prosh, Ph.D., P.Geo. (1957–2013)

Eric died suddenly on September 3rd while travelling through Ottawa en route to Iqaluit. He had been with the Government of Nunavut (GN) for more than 6 years, most recently as the Director of Minerals & Petroleum Resources. He had ties to northern geoscience that spanned nearly 30 years, in the form of scholarly work in the Paleozoic rocks of the islands in the High Arctic. Eric's experience in mineral exploration and geology was diverse, and strongly rooted in the north. He had many years of mineral industry experience and broad knowledge of mineral policy and practice, both domestically and internationally. He also consulted in both the exploration and mine reclamation sectors.

Eric worked with a wide range of Nunavut agencies regarding mineral and oil-and-gas exploration and development, including the Canada-Nunavut Geoscience Office (CNGO), where he sat as the territorial representative on the Management Board. He was always a strong and unwavering champion for the growth, evolution and programming of the office. This support has continued to push the development of the office into a stand-alone geological survey for the territory. Some of the highlights are noted in the paragraphs below.

Eric significantly increased GN leadership in, and administrative support for, field operations at the CNGO. The main beneficiary of this support was the CNGO's flagship Hall Peninsula Integrated Geoscience Program. This program was a massive undertaking that could not have been delivered without administrative know-how from Nunavut. This support included critical contracting for both camp building and camp cooks while also negotiating an agreement with industry to rent an exploration camp for 2013 fieldwork. Nunavut is arguably the most complex jurisdiction in Canada in which to operate, and Eric's dedication to improving operational capacity for the CNGO made a significant impact. It has also helped demonstrate that the Government of Nunavut is capable of playing a greater leadership role in geosciences in advance of devolution.

Eric was also a visionary for the geoscience research needs of the territory. In 2009, he implemented a first-of-its-kind evaluation program for carving stone deposits that was co-delivered by the GN and the CNGO. Carving stone is a mineral commodity unique to the Canadian Arctic and key for Inuit art—a cultural icon for the country and an economic mainstay for many Inuit. This four-year program aimed to verify, locate and examine more than 200 carving stone occurrences near Nunavut communities and document their suitability as artisanal resources. This carving stone work has had the added benefit of demonstrating the value of geoscience mapping to Nunavut communities.

Eric was also active in field research with the CNGO. In this capacity, he contributed to a first-of-its-kind program for Nunavut focused on industrial limestone. Fieldwork has been focused on Southampton Island and, in 2013, the resource potential of the Lower Silurian Ekwan River and Attawapiskat formations was investigated. Three major areas underlain by these formations were explored on the western part of the island, and preliminary data suggest that high-purity limestone exists. This discovery could lead to the development of Nunavut's first industrial limestone quarry. Such a discovery would have made Eric proud.

Eric was also committed to geoscience training and capacity building. Recently, he worked with the Greenland School of Minerals and Petroleum to provide diamond-drill training for two young men from Coral Harbour, Nunavut. The training took place in Sisimiut, Greenland and consisted of surface drilling, underground horizontal drilling and classwork. Eric's hope was that this training would lead to more advanced careers for these two men, as well as provide a larger pool of qualified workers for industry in Nunavut. Additionally, as part of his work with CNGO, he ensured that its private-sector camp cook contracts required the hiring and training of assistant cooks from the Nunavut Arctic College Camp Cook program. This provided an advanced training opportunity for Nunavumiut and set them on an industry career path in their field. He also frequently gave lectures on Nunavut's mineral and petroleum potential to students in the Nunavut Arctic College's Environmental Technology Program.

Born in Montreal, Eric was schooled at Queen's University and the University of Western Ontario, and completed his postdoctoral fellowship at McGill. He is survived by his sister Linda, who lives with her family near North Bay.

In Memoriam
Mannasie Qillaq (1966–2013)

Mannasie died suddenly on November 5th at his daughter's home in Ottawa. Born in Clyde River. Mannasie was unwavering in his support of elders and always helpful to anyone he met. His obsession was the land and he enjoyed camping, hunting and eating country food. He was a natural born teacher who was a teaching assistant at the Clyde River Secondary School and taught soapstone carving to First Nations and Inuit youth at the Wabano Centre in Ottawa.

Most recently (summer 2012 to summer 2013), Manna provided expert and committed service to the Canada-Nunavut Geoscience Office (CNGO), where he touched many people and made an impact. He was a consummate professional in everything he did and he could always be depended upon. With the CNGO, he managed the operations at large (more than 20 person) geoscience field camps as part of the Hall Peninsula Integrated Geoscience Program. This included winter fuel caching, erecting Weatherhaven tents, being a carpenter and electrician, monitoring wildlife, keeping the camp clean, providing camp tours to visitors, cutting rock samples and teaching staff about Inuit use of the land. His wide range of skills provided a calming influence on daily camp operations because you knew there would never be a problem or a challenge that could not be overcome.
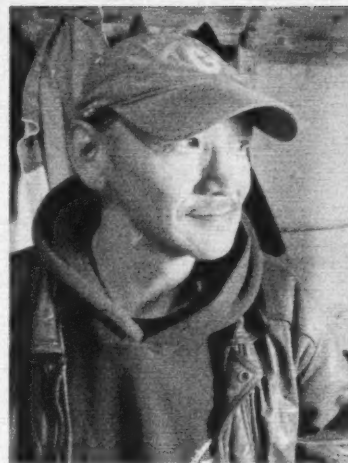
Mannasie also used his experience from working with geologists on Hall Peninsula and his teaching ability to help communicate results of geoscience research to the Nunavut communities of Iqaluit and Pangnirtung. This included giving community presentations, speaking over community radio, discussing with elders and elder committees, and presenting to hunter and trapper associations. His Inuit perspectives, combined with his geoscience experience, enabled the CNGO to plan and deliver its programming effectively and respectfully.

Finally, Mannasie assisted the CNGO with the move into its new office space. In this role, he unpacked and sorted a daunting number of books and organized large volumes of files. His attention to detail and patience ensured that these tasks were completed to perfection and ensured a smooth transition.

Mannasie was a loving and committed family man. When in Nunavut, he would always take the time to visit relatives and, while in Ottawa, he was dedicated in his support of his daughter Karen and grandson Doyle Atagootsiak. Not a day would go by without Mannasie talking about Doyle, whom he adored and would walk to school regularly.

Mannasie is survived by a large number of children and siblings. His children include daughter Karen Atagootsiak in Ottawa and son Randy Atagootsiak and daughter Georgina Pewatoalook in Pond Inlet. His siblings include brothers James Qillaq, Moses Qillaq and Joamie Apak, while his sisters include Angugasa Poisey, Nunujie Palituq, Annie Pewatoalook, Elisapee Qillaq, Reena Qillaq and Leah Sheatie. His parents were the late Ipeelie and Arnaujumajuq Qillaq, and his brothers Tupinga and Kippomee Qillaq are also deceased.

Préface

Le Bureau géoscientifique Canada-Nunavut a été créé en 1999 en vue de promouvoir le développement des ressources ainsi que de l'infrastructure minière et énergétique du Nunavut. Il s'agit d'un partenariat entre le gouvernement du Nunavut, Ressources naturelles Canada (RNCan) et le ministère des Affaires autochtones et Développement du Nord Canada. La société Nunavut Tunngavik Incorporated (NTI) est membre d'office du Bureau. Lorsque tous les postes y sont occupés, celui-ci regroupe six employés spécialisés dans la géologie du Précambrien, du Paléozoïque et du Quaternaire, le système d'information géographique et la diffusion de données en ligne. En février 2013, le Bureau a aménagé dans le nouvel immeuble Inuksugait, Phase IV, au centre-ville d'Iqaluit.

Le mandat du Bureau géoscientifique Canada-Nunavut est de fournir des données et un savoir-faire géoscientifiques à la portée de tous en appui 1) à l'exploration et à l'exploitation responsables des ressources, 2) à l'aménagement responsable de l'infrastructure, 3) au renforcement des capacités géoscientifiques, 4) à l'enseignement et à la formation, et 5) à la sensibilisation et à l'information du public sur les enjeux géoscientifiques. Le Bureau concentre ses efforts sur la cartographie des enjeux géoscientifiques émergents et les recherches connexes, sur le soutien du renforcement des capacités géoscientifiques, sur la diffusion de données géoscientifiques et sur la mise en place de partenariats efficaces d'importance stratégique pour le Nunavut.

Le Bureau se félicite de pouvoir partager de nouveau les résultats de ses nombreux projets de collaboration géoscientifique grâce à cette édition 2013 de son *Sommaire des activités*. Cette série s'avère un projet stimulant pour le Bureau, et sert aussi à diffuser de façon opportune les résultats de recherches entreprises sur le terrain. Cette année, le Bureau est fier de lancer une nouvelle publication en série intitulée « Série des données géoscientifiques ». Cette série a pour objet de diffuser des ensembles de données numériques (par ex., des ensembles de données analytiques, polygonales et ponctuelles) que les intervenants pourront par la suite intégrer à leurs processus de prise de décision. En outre, cette série fournira les données numériques à l'appui des rapports publiés dans le *Sommaire des activités* et servira aussi à diffuser des données supplémentaires recueillies par le Bureau géoscientifique Canada-Nunavut. Le cas échéant, la série sera citée en référence dans les rapports paraissant dans le *Sommaire des activités* et un lien permettra l'accès au dépôt de données électronique. Grâce à l'introduction de cette nouvelle forme de diffusion des données, le Bureau vit vraiment des moments emballants.

La présente édition du volume comprend six sections et un total de 22 articles. Les sections sont les suivantes : Études sur les gisements minéraux, Études géoscientifiques régionales, Études géoscientifiques liées à l'infrastructure, Pierre à sculpter, Agrégats et minéraux industriels, et Sensibilisation du public et renforcement des capacités. Les deux dernières sections font leurs débuts cette année et mettent en valeur encore plus l'ampleur des travaux menés par le Bureau géoscientifique Canada-Nunavut. Tous les articles seront publiés (en anglais seulement, accompagnés de résumés en français) sur Internet et pourront être téléchargés depuis le www.cngo.ca.

La section Études sur les gisements minéraux présente des études du bassin de Borden d'âge mésoprotérozoïque dans la péninsule Hall. Les travaux dans le bassin de Borden portent sur les monticules carbonatés de la formation d'Ikpiarjuk, en mettant l'accent sur l'identification de la composition des fluides émis par les griffons qui sont à leur origine et qui peuvent donc indiquer la présence possible dans la région de gisements sédimentaires exhalatifs. Ces travaux s'inscrivent dans le cadre d'un projet de thèse de doctorat dirigé par l'Université Laurentienne. Deux autres rapports portent sur le potentiel en ressources naturelles de la péninsule Hall. Le premier se penche sur l'importance économique des nombreuses roches ultramafiques qui se trouvent disséminées dans la région. L'accent est mis sur la découverte de nouvelles intrusions mafiques-ultramafiques rubanées susceptibles de renfermer une minéralisation en Ni-Cu-éléments du groupe du platine et sur la possibilité de trouver de la pierre à sculpter dans les roches ultramafiques hydratées. Le deuxième rapport est une mise à jour de l'état des ressources diamantifères gisant sous la péninsule Hall, traitant notamment des antécédents de la période de résidence des diamants à cet endroit et décrivant les caractéristiques des isotopes du carbone et de l'azote.

Les rapports réunis dans la section Études géoscientifiques régionales portent sur la recherche et les résultats liées au Projet géoscientifique intégré de la péninsule Hall. Ce programme est dirigé par le Bureau géoscientifique Canada-Nunavut en collaboration avec l'Université Dalhousie, l'Université de l'Alberta, l'Université Laval, l'Université du Manitoba, l'Université d'Ottawa, l'Université de la Saskatchewan, le Collège de l'Arctique et la Commission géologique du Canada. Cette année, le Projet géoscientifique intégré de la péninsule Hall compte aussi des contributions étrangères sous la forme de rapports provenant de l'Université d'Oxford et de l'Université du Texas à Austin. Le projet met une fois encore l'accent sur la cartographie du substratum rocheux et de la géologie de surface, et comprend une gamme d'études thématiques. Des recherches menées dans la partie méridionale de la péninsule ont fournis de nouveaux résultats portant sur la géochronol-

ogie, la géochimie du till, la géochimie des roches mafiques et ultramafiques, et la déformation et le métamorphisme paléoprotérozoïques. En plus de ces résultats, le présent volume comporte un aperçu régional de la géologie de la partie septentrionale de la péninsule.

La section Études géoscientifiques liées à l'infrastructure traite des recherches de nature collaborative menées par le Secteur des sciences de la Terre de Ressources naturelles Canada et l'Université Laval, avec l'appui du Bureau géoscientifique Canada-Nunavut. Le premier rapport fait état des résultats préliminaires provenant de travaux de recherche sur les géorisques dirigés par le Secteur des sciences de la Terre dans le cadre de son programme Géoscience pour la sécurité publique réalisé dans la baie de Baffin. Ces travaux ont pour objet de fournir une évaluation régionale du degré de stabilité des fonds océaniques, des modes de transport des sédiments, de la périodicité des tremblements de terre, des mouvements de masses se produisant sur les fonds marins et des suintements d'hydrocarbures naturels. Le rapport présenté aussi les résultats provenant des recherches menées sur le pergélisol dans la région de l'aéroport international d'Iqaluit et une mise à jour des travaux portant sur l'incidence des changements climatiques sur les zones côtières entrepris par le Secteur des sciences de la Terre dans le cadre de son programme Géosciences des changements climatiques. La piste de l'aéroport, ses voies de circulation et son aire de trafic sont sujet à des phénomènes d'instabilité et d'affaissement du sol probablement liés à la dégradation du pergélisol et aux conditions de drainage. Les nouvelles données géophysiques recueillies permettront de mieux décrire les conditions et les processus liés au pergélisol dans cette région. Une mise à jour des questions relatives à l'incidence des changements climatiques sur les zones côtières à l'échelle du Nunavut fait également l'objet d'un rapport, qui met l'accent sur les travaux de cartographie des zones côtières entrepris dans le golfe Coronation et sur le changement du niveau marin dans la baie d'Hudson. Enfin, une série de quatre rapports résume les observations faites à partir d'évaluations de reconnaissance des risques géomorphologiques relevés dans les collectivités de Kugluktuk, Cambridge Bay, Whale Cove et Arviat. Ces évaluations découlent du Partenariat sur les changements climatiques du Nunavut et devraient jouer un rôle au niveau des processus de planification suivis en vue de l'adoption par chacune de ces collectivités de mesures d'adaptation aux changements climatiques.

La contribution de la section Pierre à sculpter comporte un rapport axé sur la géologie et le potentiel en ressources que recèle encore la carrière Kangiqsuktaaq (à la baie Korok). Cette carrière fournit depuis plus de 50 ans de la pierre de haute qualité aux sculpteurs inuits de la région méridionale de l'île de Baffin ainsi qu'à l'ensemble du Nunavut. Des travaux entrepris par le Bureau géoscientifique Canada-Nunavut en collaboration avec l'Association des Inuites Qitiqtani, le gouvernement du Nunavut et la société DeBeers Canada Exploration Inc. ont pour objet d'identifier l'étendue des ressources en pierre encore disponibles à la carrière, qu'il s'agisse de ressources en surface ou accessibles à partir de la surface, et de fournir les renseignements nécessaires à la mise en place d'un plan de gestion pour la carrière.

La section des Agrégats et des minéraux industriels et la section de la Sensibilisation du public et renforcement des capacités présentent pour la première fois des rapports. En 2013, de nouveaux travaux sur le terrain ont porté sur les ressources possibles en calcaire industriel que pourraient renfermer les formations d'Ekwan River et d'Attawapiskat du Silurien inférieur dans le la partie occidentale de l'île Southampton. Les données préliminaires semblent indiquer que la formation d'Ekwan River contient du calcaire à forte teneur en calcium. Il s'agit-là d'une découverte importante susceptible de mener à la mise en valeur de la première carrière de calcaire industriel au Nunavut. Un autre rapport présente un aperçu d'un nouveau programme-pilote de formation en géoscience mis sur pied à l'intention des étudiants du Nunavut; il y est question de la collaboration entre le Bureau et l'Université Dalhousie qui a permis à ces organismes d'offrir des occasions de formation à deux étudiants provenant du Collège de l'Arctique, au Nunavut, soit un projet susceptible de servir de modèle à des efforts semblables, et même plus ambitieux, dans les années à venir.

Enfin, le présent volume est dédié à Eric Prosh (Ph.D.) et Mannasie Qillaq, qui tous deux sont décédés soudainement cet automne. Eric et Mannasie étaient de bons amis et collègues des membres du personnel du Bureau géoscientifique Canada-Nunavut, et ont contribué de manière importante au développement de ce bureau et à l'exécution de ses programmes géoscientifiques. Ils nous manqueront tous les deux.

Remerciements

Michel Allard, Université Laval
Carl Bilodeau, Ministère des ressources naturelles du Québec
Alfredo Camacho, Université du Manitoba
Ingrid Chinn, DeBeers Canada Exploration Inc.
Lisel Currie, Commission géologique du Canada
Keith Dewing, Commission géologique du Canada
Mike Ellerbeck, Commission géologique du Canada
Don Forbes, Commission géologique du Canada
Phil Hill, Commission géologique du Canada
Michel Houle, Commission géologique du Canada
Donald James, Gouvernement de la Nouvelle-Écosse
Don Kellett, Commission géologique du Canada
Anne-Marie LeBlanc, Commission géologique du Canada

Dave Lentz, Université du Nouveau-Brunswick
Roger Paulen, Commission géologique du Canada
Rob Rainbird, Commission géologique du Canada
Nicole Rayner, Commission géologique du Canada
Wendy Sladen, Commission géologique du Canada
David Schneider, Université d'Ottawa
David Scott, Commission canadienne des affaires polaires
Marc St-Onge, Commission géologique du Canada
Holly Steenkamp, Bureau géoscientifique Canada-Nunavut
Tommy Tremblay, Bureau géoscientifique Canada-Nunavut
Dave Waters, Université d'Oxford

David Mate
Géologue en chef
Bureau géoscientifique Canada-Nunavut
www.cngo.ca/

In Memoriam
Eric Charles Prosh, Ph.D., P.Geo. (1957–2013)

Eric est décédé soudainement le 3 septembre de passage à Ottawa, en route vers Iqaluit. Il travaillait pour le gouvernement du Nunavut depuis plus de 6 ans, son poste le plus récent ayant été celui de Directeur des ressources minérales et pétrolières. Ses antécédents dans le domaine géoscientifique remontaient à plus de 30 ans, alors qu'il avait réalisé un travail de recherche académique portant sur les roches paléozoïques des îles de l'Extrême-Arctique. Son expérience diverse dans les domaines de l'exploration minérale et de la géologie était fortement ancrée dans le nord. Il a œuvré de nombreuses années au sein de l'industrie minérale, y acquérant une vaste connaissance des politiques et pratiques qui régissent le domaine minéral, aussi bien au Canada qu'ailleurs dans le monde. Il a aussi agi à titre de consultant en matière d'exploration et de restauration minière.

Eric a travaillé pour le compte d'un grand nombre d'agences du Nunavut œuvrant dans le domaine de l'exploration minérale et celui du pétrole et du gaz, notamment le Bureau géoscientifique Canada-Nunavut, où il a d'ailleurs siégé sur le conseil de gestion à titre de représentant territorial. Il s'est toujours montré un champion indéfectible et fidèle du développement, de la progression et des programmes du Bureau. Grâce à ce soutien acharné, le Bureau a pris de l'essor et est devenu une commission géologique autonome au service du territoire. Quelques uns des points saillants de cette évolution sont décrits ci-dessous.

Les efforts d'Eric ont contribué de façon significative à accroître au niveau du gouvernement du Nunavut la maîtrise des opérations sur le terrain menées par le Bureau, ainsi que la prestation des services administratifs qui leur étaient liés. Le principal bénéficiaire de ce soutien fut le Projet géoscientifique intégré de la péninsule Hall dirigé par le Bureau géoscientifique Canada-Nunavut. Il s'agissait d'une énorme entreprise qui n'aurait jamais pu réussir sans le savoir-faire administratif offert par le Nunavut. Ce soutien comprenait l'octroi de contrats pour la construction des camps et l'embauchage des cuisiniers de camp, tout en négociant une entente avec le secteur industriel en vue de la location d'un camp d'exploration minière à l'intention des équipes responsables des travaux sur le terrain en 2013. Il ne fait aucun doute que le Nunavut s'avère la compétence la plus complexe au Canada où entreprendre des activités et le dévouement dont Eric a fait preuve en vue d'améliorer les capacités opérationnelles du Bureau a porté fruit. Ce geste a en outre contribué à mettre en valeur la capacité du gouvernement du Nunavut à assumer un plus grand rôle de chef de file dans le domaine des géosciences en prévision du transfert de responsabilités.

Eric était un visionnaire lorsqu'il s'agissait de cerner les besoins du territoire en matière de travaux de recherche géoscientifique. En 2009, il a mis sur pied un programme d'évaluation des gisements de pierre à sculpter unique en son genre réalisé par le gouvernement du Nunavut et le Bureau. La pierre à sculpter est un produit minéral de l'Arctique canadien à caractère unique et un élément essentiel de l'expression artistique inuite–un symbole culturel du pays et un pilier économique pour plusieurs Inuits. Le programme de quatre ans avait comme tâche de vérifier, de localiser et d'examiner plus de 200 venues de pierre à sculpter gisant à proximité de collectivités du Nunavut, et de déterminer si elles étaient aptes à servir de ressources artisanales. Les travaux entrepris dans le cadre de ce programme ont eu l'avantage supplémentaire de mettre en valeur l'importance de la cartographie géoscientifique auprès des collectivités du Nunavut.

Eric a également activement participé à des recherches sur le terrain menées par le Bureau. À ce titre, il a contribué à la mise sur pied d'un programme unique en son genre axé sur le calcaire industriel du Nunavut. Les travaux sur le terrain se sont déroulés dans l'île Southampton, menant en 2013 à l'étude du potentiel en ressources calcaires des formations d'Ekwan River et d'Attawapiskat du Silurien inférieur. Trois zones principales recouvrant ces formations ont fait l'objet d'explorations dans la partie occidentale de l'île et les données préliminaires semblent indiquer la présence de calcaire de grande pureté. Cette découverte pourrait mener à la mise en valeur de la première carrière de calcaire industriel du Nunavut. Une telle découverte aurait rendu Eric très fier.

Eric se consacrait également à la formation dans le domaine géoscientifique et au renforcement des capacités. Tout récemment, il a travaillé avec l'École des mines et du pétrole du Groenland en vue d'offrir à deux jeunes hommes de Coral Harbour, au Nunavut, une formation dans les techniques de forage au diamant. Cette formation a eu lieu à Sisimiut, au Groenland, et

était divisé en trois composantes: les techniques de forage effectués en surface, les techniques de forages souterrains effectués horizontalement et le travail en classe. Eric espérait que cette formation ferait progresser les carrières de ces jeunes hommes, tout en créant un plus vaste bassin de travailleurs qualifiés dont pourrait bénéficier le secteur industriel au Nunavut. En outre, dans le cadre de son travail pour le compte du Bureau, il s'est assuré que les contrats dotant le camp de cuisiniers issus du secteur privé incluait une clause prévoyant la formation et l'embauche d'aides-cuisiniers inscrits au programme de cuisiniers de camp du Collège de l'Arctique. Il mettait ainsi à la disposition des résidants du Nunavut une occasion unique de formation avancée, leur ouvrant les portes à des carrières dans un domaine de leur choix. Il donnait aussi fréquemment des conférences au sujet des ressources potentielles en minéraux et en pétrole du Nunavut aux étudiants faisant partie du programme de techniques environnementales du Collège de l'Arctique.

Né à Montréal, Eric a fait ses études à l'Université Queen's et à l'Université de Western Ontario, terminant son programme de bourses postdoctorales à McGill. Il laisse dans le deuil sa sœur Linda, qui demeure avec sa famille près de North Bay.

In Memoriam
Mannasie Qillaq (1966-2013)

Mannasie Qillaq est décédé soudainement le 5 novembre à la maison de sa fille, à Ottawa. Né à Clyde River, Mannasie a toujours offert son appui indéfectible aux aînés et était toujours prêt à venir en aide à quiconque. Sa passion était la terre et ses moments les plus heureux étaient passés à s'adonner au camping, à la chasse et à la dégustation de nourriture traditionnelle. Il avait des dons innés d'enseignant et partageait son temps entre un emploi d'aide-professeur à l'école secondaire de Clyde River et le Centre Wabano, à Ottawa, où il enseignait l'art de sculpter la pierre de savon aux jeunes, aussi bien inuits que des Premières nations.

Plus récemment (de l'été 2012 à l'été 2013), Manna a mis ses connaissances au service du Bureau géoscientifique Canada-Nunavut où il a touché de façon positive la vie de bien des gens. Tout ce qu'il entreprenait était empreint d'une grande rigueur professionnelle et on pouvait toujours se fier à lui. Sa prestation auprès du Bureau l'a amené à diriger les opérations liées à la gestion des grands camps sur le terrain (plus de 20 personnes) mis sur pied dans le cadre du Projet géoscientifique intégré de la péninsule Hall. Ses tâches incluaient le contrôle du stockage de carburant pour l'hiver, le montage des tentes Weatherhaven, de menus travaux de charpenterie et d'électricité, la surveillance de la faune, l'entretien du campement, l'encadrement des visiteurs au campement, la taille des échantillons de roche et le partage de ses connaissances avec le personnel du Bureau au sujet de la perception inuite de l'utilisation des terres. Sa vaste gamme de compétences permettait à une atmosphère de calme de régner sur le camp, car il semblait à tous impossible qu'un problème puisse se présenter qu'il n'était pas en mesure de régler.
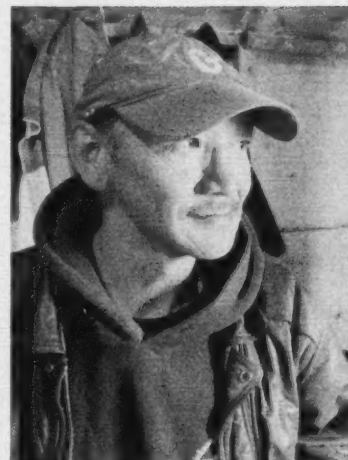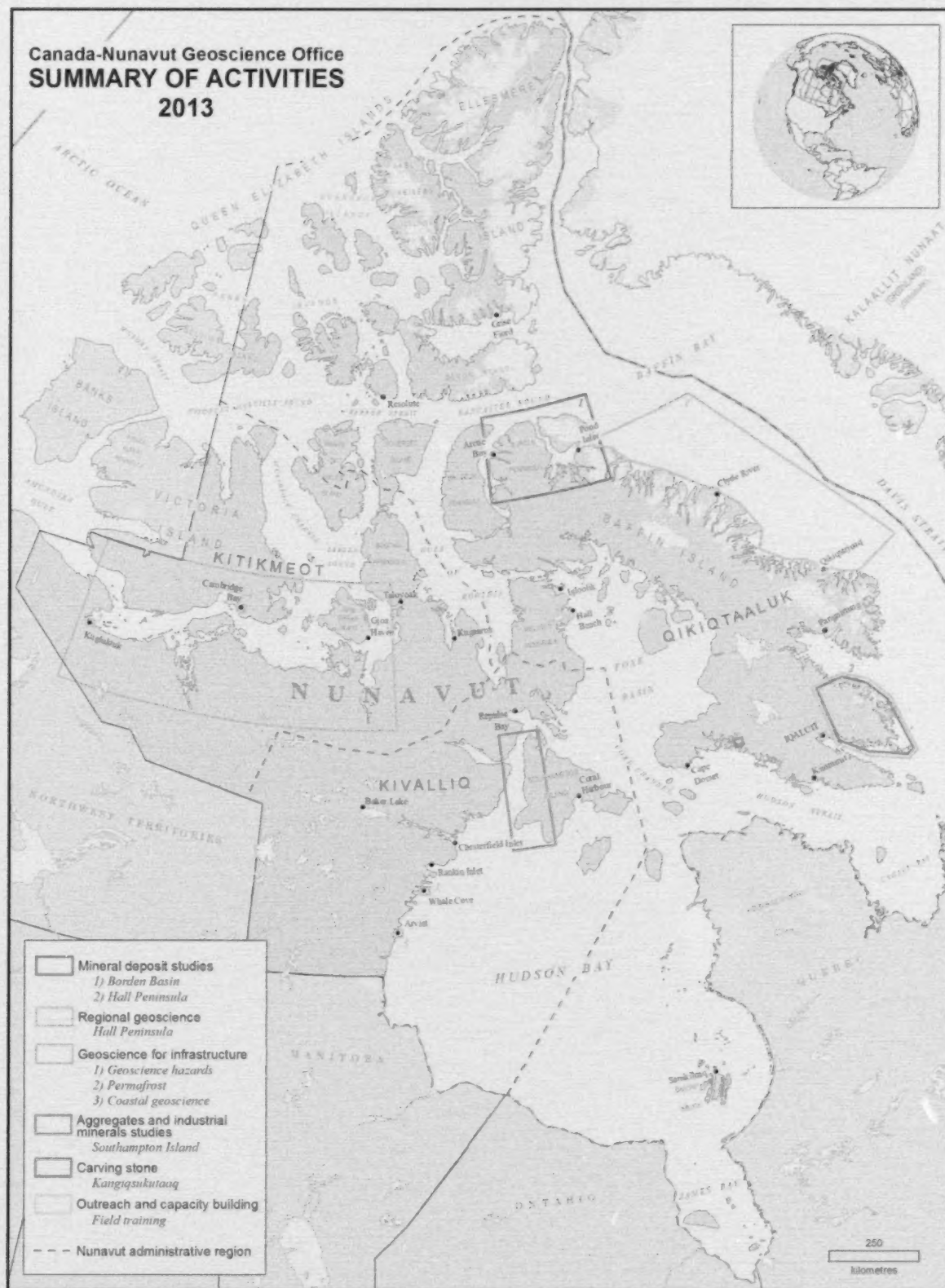
L'expérience que Mannasie a acquise en travaillant avec les géologues dans la péninsule Hall et ses talents d'enseignant lui ont valu d'être la personne toute indiquée pour partager avec les membres des collectivités d'Iqaluit et de Pangnirtung, au Nunavut, les résultats de ces travaux géoscientifiques. Pour ce faire, il a présenté des exposés dans les collectivités, animé des programmes de radio communautaire, pris part à des discussions avec des aînés et des comités d'aînés, et fait des présentations aux associations de chasseurs et de trappeurs. Son point de vue spécifiquement inuit, allié à son expérience dans le domaine géoscientifique, ont fait qu'il a été possible pour le Bureau de planifier et de mener à bien son programme de façon efficace et respectueuse.

Enfin, Mannasie est venu en aide au Bureau lors de son aménagement dans ses nouveaux locaux. Il lui incombait de déballer et de mettre en ordre un nombre déconcertant de livres, et d'organiser un aussi grand nombre de dossiers. Sa minutie et sa patience ont fait en sorte que ces tâches ont été accomplies à la perfection, assurant ainsi une transition sans heurt dans les nouveaux locaux.

Mannasie était un homme affectueux, attaché aux valeurs familiales. Lorsque de passage au Nunavut, il ne manquait jamais de rendre visite à des parents et, pendant ses séjours à Ottawa, il faisait preuve du plus grand dévouement envers sa fille Karen et son petit-fils Doyle Atagootsiak. Pas un seul jour ne s'écoulait sans que Mannasie ne mentionne Doyle, qu'il adorait et qu'il accompagnait régulièrement à l'école.

Mannasie laisse dans le deuil un grand nombre d'enfants et de frères et sœurs. Il s'agit de sa fille Karen Atagootsiak, à Ottawa, et de son fils Randy Atagootsiak et sa fille Georgina Pewatoalook, tous deux de Pond Inlet. Il laisse aussi ses frères James Qillaq, Moses Qillaq et Joamie Apak, ainsi que ses sœurs Angugasa Poisey, Nunujie Palituk, Annie Pewatoalook, Elisapee Qillaq, Reena Qillaq et Leah Sheatie. Ses parents, feux Ipeelie et Arnaujumajuk Qillaq, et ses frères Tupinga et Kippomee Qillaq l'ont précédé dans la mort.

Canada-Nunavut Geoscience Office
SUMMARY OF ACTIVITIES
2013

Mineral deposit studies
  1) Borden Basin
  2) Hall Peninsula

Regional geoscience
  Hall Peninsula

Geoscience for infrastructure
  1) Geoscience hazards
  2) Permafrost
  3) Coastal geoscience

Aggregates and industrial
minerals studies
  Southampton Island

Carving stone
  Kangiqsukutaaq

Outreach and capacity building
  Field training

– – – Nunavut administrative region

Contents

High-precision trace-element analysis of deep-water, vent-related dolostone in the Borden Basin, northwestern Baffin Island, Nunavut

K.E. Hahn[1] and E.C. Turner[2]

[1]*Department of Earth Sciences, Laurentian University, Sudbury, Ontario, kx_hahn@laurentian.ca*
[2]*Department of Earth Sciences, Laurentian University, Sudbury, Ontario*

Abstract

The Mesoproterozoic Borden Basin in northeastern Nunavut, which contains the carbonate-hosted Nanisivik Zn-Pb deposit, is one of the tectonostratigraphically complex Bylot basins. The Ikpiarjuk Formation, preserved in the Milne Inlet graben of the Borden Basin, consists of unusually large, deep-water dolostone mounds. The linear mounds, which consist of featureless dolomudstone that precipitated in the water column (pelagic) and clotted dolostone that formed on the seafloor (benthic), are centred on and parallel to synsedimentary faults, and formed during an interval of extensional faulting and accumulation of black shale.

The Ikpiarjuk Formation mounds are interpreted to be fossilized cold-seep deposits that accumulated during fluid expulsion along active faults on the seafloor. The composition of the vent fluid is unknown, but rare-earth element (REE)+Y analyses show that the seawater with which the vent fluid mixed was in a redox-stratified water column. Such characteristics, occurring in a basin undergoing syndepositional extensional faulting, are considered to be fundamental prerequisites for the formation of sedimentary-exhalative (SEDEX) deposits. There is currently no evidence for SEDEX-type venting of metalliferous fluids in the basin, but the pronounced local venting of subsurface fluid to produce benthic and pelagic dolostone of the Ikpiarjuk Formation mounds indicates that low-temperature fluids were voluminously and locally expelled at line or point sources on the basin floor during deposition of black shale.

Résumé

Le bassin mésoprotérozoïque de Borden (au Nunavut), qui renferme le gisement de Zn-Pb sur roches carbonatées de Nanisivik, fait partie des bassins de Bylot qui se distinguent par leur nature tectonostratigraphique complexe. La formation d'Ikpiarjuk, mise en place dans le graben de Milne Inlet du bassin de Borden, se compose de buttes de dolomie remarquables en raison de leur grande taille et dont la mise en place a eu lieu en eau profonde. Ces buttes, qui adoptent une forme linéaire et qui sont constitués de mudstone dolomitique sans traits caractéristiques issu de la précipitation dans la colonne d'eau (pélagique) et de dolomie grumeleuse mise en place sur le fond océanique (benthique), se situent autour de failles synsédimentaires ou s'allongent parallèles à ces dernières. Leur formation est associée à un intervalle au cours duquel ont eu lieu des épisodes de formation de failles d'extension et de sédimentation de schiste ampéliteux.

On estime que les buttes de la formation d'Ikpiarjuk sont des dépôts fossilisés dont la formation est liée à des suintements froids et dont l'accumulation aurait eu lieu au cours d'épisodes d'expulsion de fluides le long de failles actives sur le fond océanique. La composition des fluides provenant de ces évents est inconnue, mais les analyses des éléments du groupe des terres rares, incluant l'yttrium, ont établi que l'eau de mer à laquelle ces fluides provenant d'évents viennent se mélanger se trouvait dans une colonne d'eau stratifiée à gradients redox. Un tel phénomène, qui se produit au sein d'un bassin subissant un épisode de formation de failles d'extension de nature synsédimentaire, constitue l'une des conditions préalables les plus fondamentales requises pour la formation de gisements sédimentaires exhalatifs (SEDEX). Aucune preuve d'exhalaison de fluides métallifères de type SEDEX n'a été trouvée dans le bassin, mais la forte exhalaison de fluides de subsurface à l'échelle régionale, responsable de la formation de la dolomie benthique et pélagique des buttes de la formation d'Ikpiarjuk, témoigne du fait qu'une expulsion volumineuse de fluides de basse température se produisant localement à partir de sources ponctuelles ou linéaire sur le fond du bassin aurait eu lieu au cours de l'épisode de sédimentation du schiste ampéliteux.

Introduction

The Borden Basin Project is a multiyear academic study that was developed to evaluate the geological history and economic potential of the Mesoproterozoic basins of eastern Nunavut (Figure 1; Turner et al., 2012). Although part of the basin is a known Zn district, which hosted the Nanisivik mine (in operation from 1976 to 2002), the basin is relatively underexplored for both Zn and other metals. The main objective of the Borden Basin Project is to understand the geological evolution of eastern Nunavut's Mesoproterozoic sedimentary basins, and identify the potential for further economic mineral deposits. This paper reports on one of the currently active components of the project.

Mapping of carbonate rock units in the Milne Inlet graben identified very large and unusual dolostone mounds (Turner, 2004a, 2009). These mounds are the focus of a Ph.D.

project at Laurentian University that examines their origin and implications. Fieldwork for this project was completed during two 6-week field seasons in 2011 and 2012, the results of which are summarized in Hahn and Turner (2013). The project has now entered the analytical phase and this paper summarizes results from work completed in 2013.

This phase of the project involved analyzing rare-earth elements (REEs) and several other trace elements in the different phases (benthic precipitates and pelagic carbonate mud) of the mound dolostone. The objective of this work is to evaluate the composition of seawater in the basin, characterize the composition of the fluids venting into the basin, and establish if there was potential for a vent-related economic mineral deposit to have formed during the voluminous fluid venting. The study is based largely on the inter-
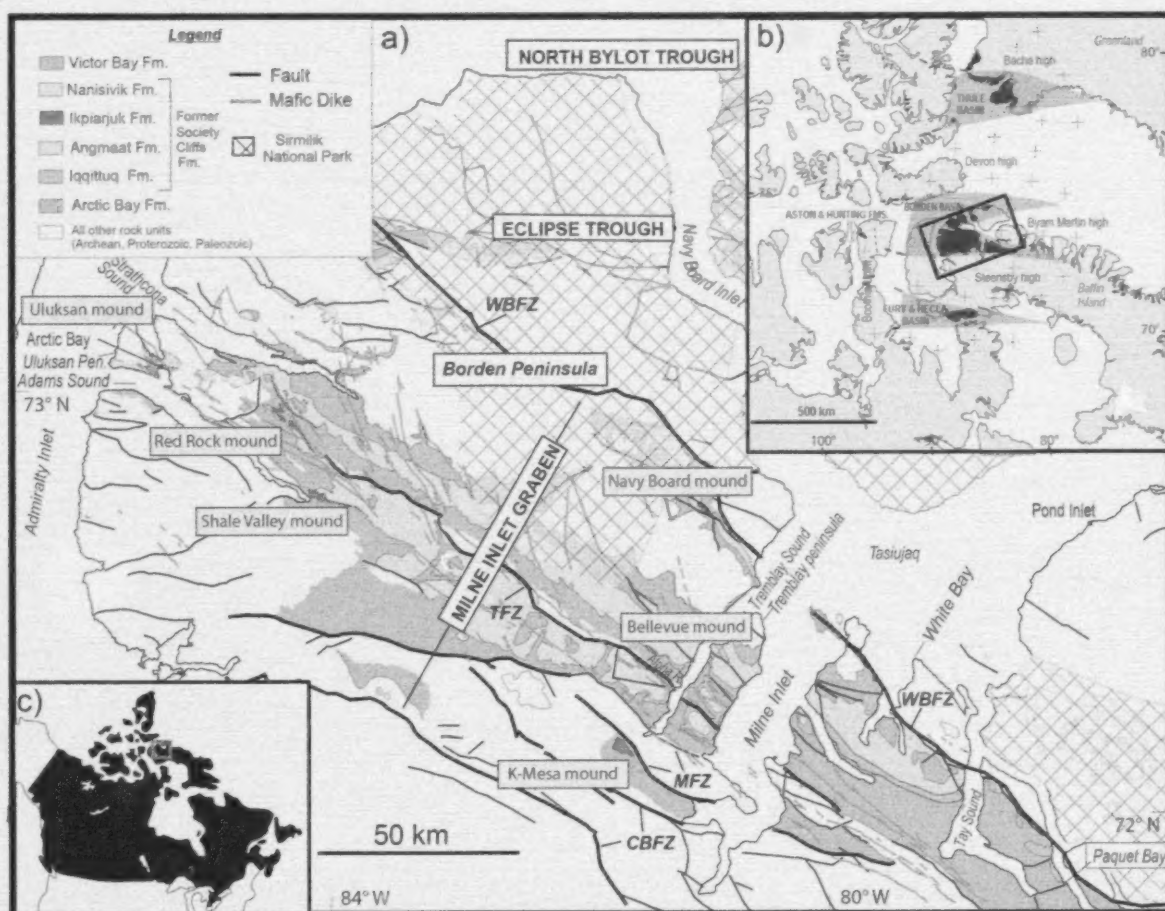
Figure 1: a) Geology of the Milne Inlet graben (MIG), northern Baffin Island, northwestern Nunavut; only the Mesoproterozoic units are shown. Seven areas of mound lithofacies are known from outcrop (modified from Scott and de Kemp, 1998; Turner, 2009). Prominent fault zones are labelled (CBFZ, Central Baffin fault zone; MFZ, Magda fault zone; TFZ, Tikirarjuaq fault zone; WBFZ, White Bay fault zone). Place name with the generic in lower case is unofficial. **b)** Bylot basins of the Canadian Arctic islands, with the Borden Basin highlighted. Dark blue zones represent the extent of the present-day exposure, and pale blue zones are the inferred former basin margins (after Jackson and Iannelli, 1981). **c)** Location of the Bylot basins.

pretation of shale-normalized REE+Y patterns. which are useful tracers of oceanic redox conditions.

Geological setting

The Borden Basin is one of the Bylot basins. a group of four basins exposed in northeastern Nunavut and northwestern Greenland. The basins were interpreted to have formed during rifting related to the Mackenzie igneous event (ca. 1270 Ma; LeCheminant and Heaman, 1989). Correlations were based on geochemical similarities between basalt of the Mackenzie igneous event and basalt preserved at the base of the basin-filling succession in the Bylot basins (Nauyat Formation; Jackson and Iannelli, 1981; Dostal et al., 1989). The depositional age of black shale near the base of the basin is now known to be ca. 1.1 Ga, and rifting during deposition of the black shale has been linked to tectonic stress associated with the amalgamation of Rodinia (Long and Turner, 2012; Turner and Kamber, 2012). The entire basin is cut by dikes of the Franklin large igneous province (ca. 720 Ma; Heaman et al., 1992; Pehrsson and Buchan, 1999; Denyszyn et al., 2009).

The Borden Basin contains three fault-bounded troughs. the largest of which is the Milne Inlet graben (MIG), which contains both the Nanisivik Zn-Pb deposit and the unusual dolostone mounds of the Ikpiarjuk Formation. The MIG is bounded by northwest-trending synsedimentary faults and

is filled with ~6 km of sedimentary rocks referred to as the 'Bylot Supergroup' (Jackson and Iannelli, 1981).

The tectonic history of the basin is complex and has been recently revised (e.g., Turner, 2011; Long and Turner, 2012; Turner and Kamber, 2012; Figure 2). The current model proposes that the Borden Basin initially formed during mild extension accompanying the Mackenzie igneous event. Tholeiitic basalt erupted subaqueously during this phase and was then overlain by marine sand represented by the Adams Sound Formation, deposited during a phase of thermal relaxation (Long and Turner, 2012).

Significant extension began during deposition of the Arctic Bay Formation (Turner and Kamber, 2012) with the first appearance of graben-like geomorphic features. During this stage, the basin deepened to the west and deepened upward. This stage of basin development was characterized by synsedimentary slope failures adjacent to deep-water fault zones. which resulted in pronounced lateral thickness and lithofacies changes (Turner and Kamber, 2012). Wedges of detrital material (Fabricius Fiord Formation; Jackson and Iannelli, 1981; Scott and deKemp, 1998) were deposited at the margins of the MIG, marking the initiation of localized sedimentation into newly formed grabens, and also in the vicinity of subaqueous fault scarps (Turner, 2004b). During a phase of extension that coincided with deposition of black shale of the upper Arctic Bay Formation, fluid venting through active faults resulted in the volumi-

Formation		Tectonic history	Sedimentary environment	Reference
	Sinasiuvik Fm.	Unknown	Locally derived material and externally supplied terrigenous clastic sediment. Complex paleotopography	Knight and Jackson (1994)
	Aqigilik Fm.			
	Strathcona Sound Fm. & Athole Point Fm.	Uplift	Uplift and karsting in west end; Drowning and deepening in east (Athole Point Fm.)	Sherman et al. (2002)
	Victor Bay Fm.	Quiescence	Resubmersion, northwest-deepening ramp	Sherman et al. (2001) Turner (2009) Turner (2011) Turner and Kamber (2012)
	Nanisivik Fm. / Angmaat Fm.	Uplift/tilting	Dramatic uplift and tilting to the northeast; erosion	
	Ikpiarjuk Fm. (mounds) / Iqqituq Fm. / Fabricus Fiord Fm	Extension	Northwest deepening Alluvial fans (Fabricus Fiord Fm.) at graben margins Active faults, local debris flows, soft sediment deformation. Prograding carbonate ramp to platform in southeast Fault-related carbonate mounds throughout Milne Inlet graben	
	Arctic Bay Fm.			
	Adams Sound Fm.	Sag basin	Shallow marine sandstone	Long and Turner (2012)
	Nauyat Fm.	Thermal doming	Basalt	

(left margin spanning: Bylot Supergroup)

Rae Province basement

Figure 2: Stratigraphy of the Bylot Supergroup, with associated tectonic and depositional environments (after Turner, 2009, 2011; Long and Turner, 2012; Turner and Kamber, 2012).

nous accumulation of deep-water dolostone, the highly distinctive carbonate mounds of the Ikpiarjuk Formation (Turner, 2004a; 2009).

The dolostone mounds (Ikpiarjuk Formation) are underlain and surrounded by black shale of the Arctic Bay Formation, and are interpreted to have formed beneath wave base and below the photic zone (Turner 2004a, 2009; Hahn and Turner, 2013; Figure 3a, b). The mounds are linear in plan view and are parallel to mapped or inferred faults that were known to be active during their formation. The mounds are characterized by two dominant lithofacies: clotted carbonate that formed as a benthic precipitate and characterizes large zones in the mound centres (Figure 3c), and featureless carbonate, which formed as a mud-grade water-column precipitate and represents the bulk of the mounds, including voids among benthic clots (Figure 3d). Field relationships show that the mounds formed during subaqueous fluid venting along fault zones during accumulation of black shale. Several of the mounds are associated with smaller 'moundlets' (tens of metres in scale) that are stratigraphically lower than the main mound and are dominated by the clotted (benthic) lithofacies (Figure 3e, f).

Fluid expulsion ended at the same time as an abrupt shift from deposition of black shale to accumulation of deep-water, laminated carbonate strata in the northwestern part of the MIG (Nanisivik Formation; Turner 2009, 2011).

Following deposition of the Nanisivik and laterally equivalent (southeast) Angmaat formations, the basin was uplifted and tilted to the northeast, and underwent significant subaerial erosion (Turner, 2011). The basin was then resubmerged, as revealed by overlying shale and limestone of the Victor Bay Formation that were deposited throughout the basin as a northwest-deepening ramp during an interval of tectonic quiescence (Sherman et al., 2000, 2001, 2002; Turner, 2011). The Victor Bay Formation was then tilted to the northeast such that northwestern strata were subaerially weathered, but southeastern strata were drowned (Athole Point Formation; Sherman et al., 2002; Figure 2). The tectonic history of the upper part of the succession (Nunatsiaq Group) records a major influx of terrigenous clastic material in a shallowing-upward succession (Knight and Jackson, 1994).

Methods

Stratigraphic sections were measured through cliff exposures up to 250 m thick, and were sampled approximately every 5 m (Hahn and Turner, 2013). Detailed petrographic work was completed in order to identify the least-altered samples, and then laser-ablation inductively coupled mass-mass spectrometry (LA-ICP-MS; at Laurentian University) was undertaken on the least-altered samples. Of the samples that were analyzed using LA-ICP-MS, 33 were chosen for further high-precision solution ICP-MS in order

to measure the abundance of REEs and other trace elements in different dolomitic phases. The samples that were analyzed using solution ICP-MS were very small (<0.1 mg) and required a custom analysis, undertaken at Trinity College, Dublin, Ireland.

Results and interpretation

The REE+Y patterns from the samples were normalized both to an upper continental crust composite (MUQ; Kamber et al., 2005) and to a black shale from the Arctic Bay Formation, calculated as an average of black-shale samples measured by Turner and Kamber (2012) from the Milne Inlet graben. Normalized to the crustal composite, most REE+Y patterns are flat to very slightly negatively sloped, which is not what is expected of REE+Y patterns from sediment deposited under normal seawater (e.g., Webb and Kamber, 2000; Kamber et al., 2004; Planavsky et al., 2010). When the samples are normalized to the Arctic Bay Formation shale, the REE+Y patterns are steeper and expected anomalies (e.g., positive La, Gd and Y anomalies) are present. This indicates that basin water was restricted from the open ocean, that the input of local sediment greatly affected the distribution of the REEs, and that MUQ is not an appropriate composite for normalizing raw data. All results presented in this paper are normalized instead to the Arctic Bay Formation shale.

The amount of contamination due to siliciclastic detrital material was monitored by tracking the abundance of Al (a measure of the abundance of clay minerals), and Zr, Th and Nb (a measure of the abundance of heavy minerals). Only samples deemed uncontaminated are discussed below.

Red Rock mound (Milne block)

The REE+Y patterns at Red Rock mound exhibit slightly positive to distinctly positive slopes, positive Y and Ce anomalies and, in most cases, a negative Eu anomaly (Figure 4a). The positive slope of the patterns, as well as the calculated positive Y and La anomalies, are characteristics of normal Proterozoic seawater (e.g., Webb and Kamber, 2000; Kamber et al., 2004; Planavsky et al., 2010). The positive Ce anomaly indicates that the material formed beneath a chemocline: a particle shuttle carried oxidized Ce from shallow water into deeper water, where it was reduced and dissolved away from the shuttle particles to accumulate in the sediment. The origin of the negative Eu anomaly is unknown; it may be related to the composition of the vent fluid from which the mounds are derived, or it may be a primary feature of seawater in the Milne Inlet graben.

The redox-sensitive metals V, Mo and U were normalized to Al and plotted stratigraphically (Figure 5). Vanadium and Mo show similar patterns, whereas U has much more scatter. Enrichment in these metals was most prominent at the base of the section, with one notable sample that had a
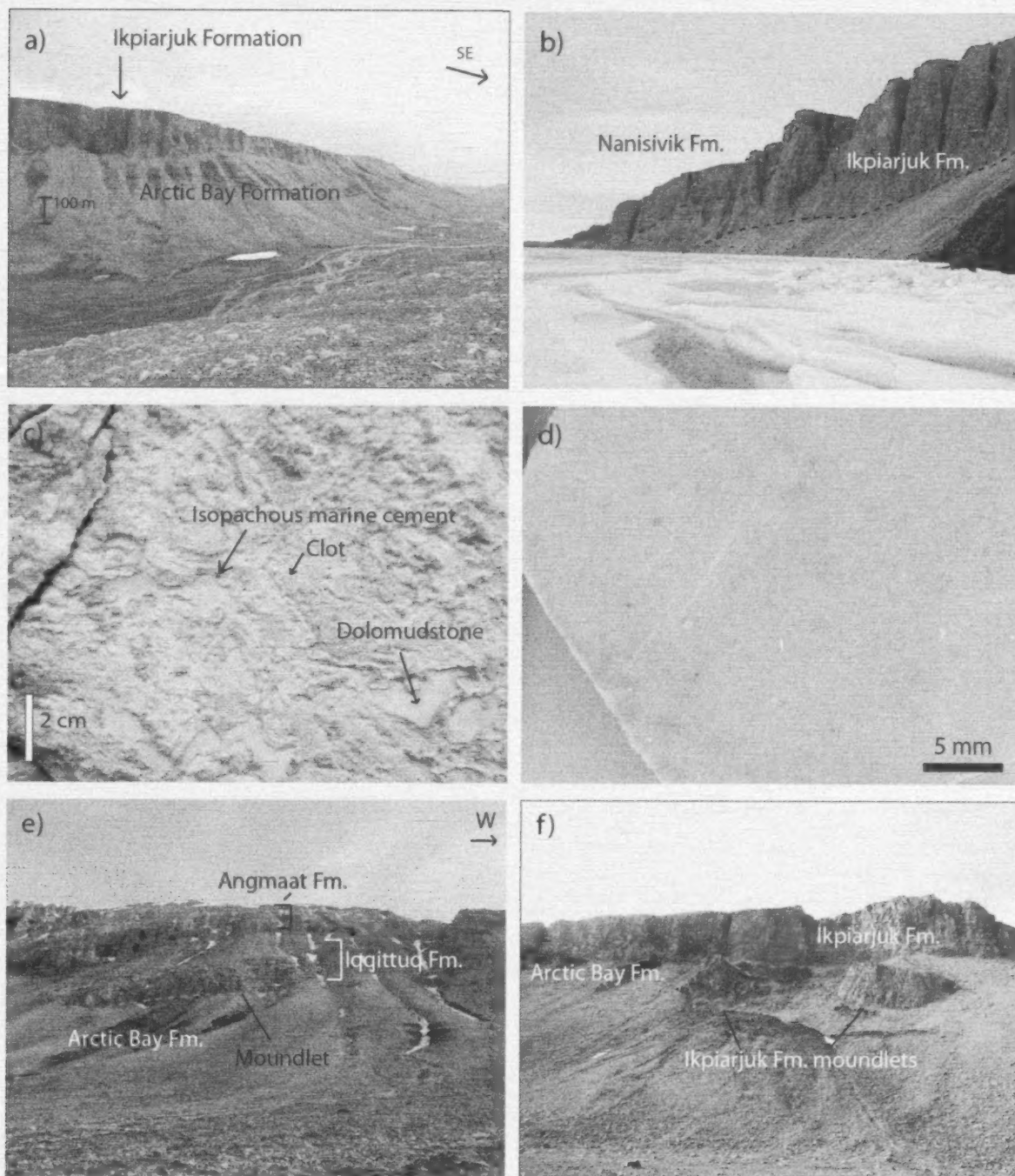
Figure 3: Field exposures of the Ikpiarjuk Formation, northern Baffin Island, northwestern Nunavut: **a)** Red Rock mound (arrow), which pinches out at its base and gradually climbs upsection toward the southeast, relative to Arctic Bay Formation black shale; **b)** main exposure of Uluksan mound; the core is largely inaccessible, but it can be distinguished from the overlying Nanisivik Formation by a subtle colour change and the presence of faint layering in the upper parts of the cliffs; **c)** example of the clotted lithofacies that is present in most mounds, Red Rock mound; note the resistant rims of isopachous marine cement surrounding clots, and carbonate mudstone in voids among the clots; **d)** example of the massive dolostone facies from Red Rock mound, interpreted as a water-column precipitate identical to the inter-clot mud in the clotted lithofacies; **e)** small 'moundlet' of Ikpiarjuk Formation enclosed by outer-ramp strata of the Iqqittuq Formation near Belle-vue mound; **f)** 'moundlets' of the Ikpiarjuk Formation enclosed by black shale of the Arctic Bay Formation, directly beneath the main cliff-forming exposure of K-Mesa mound.
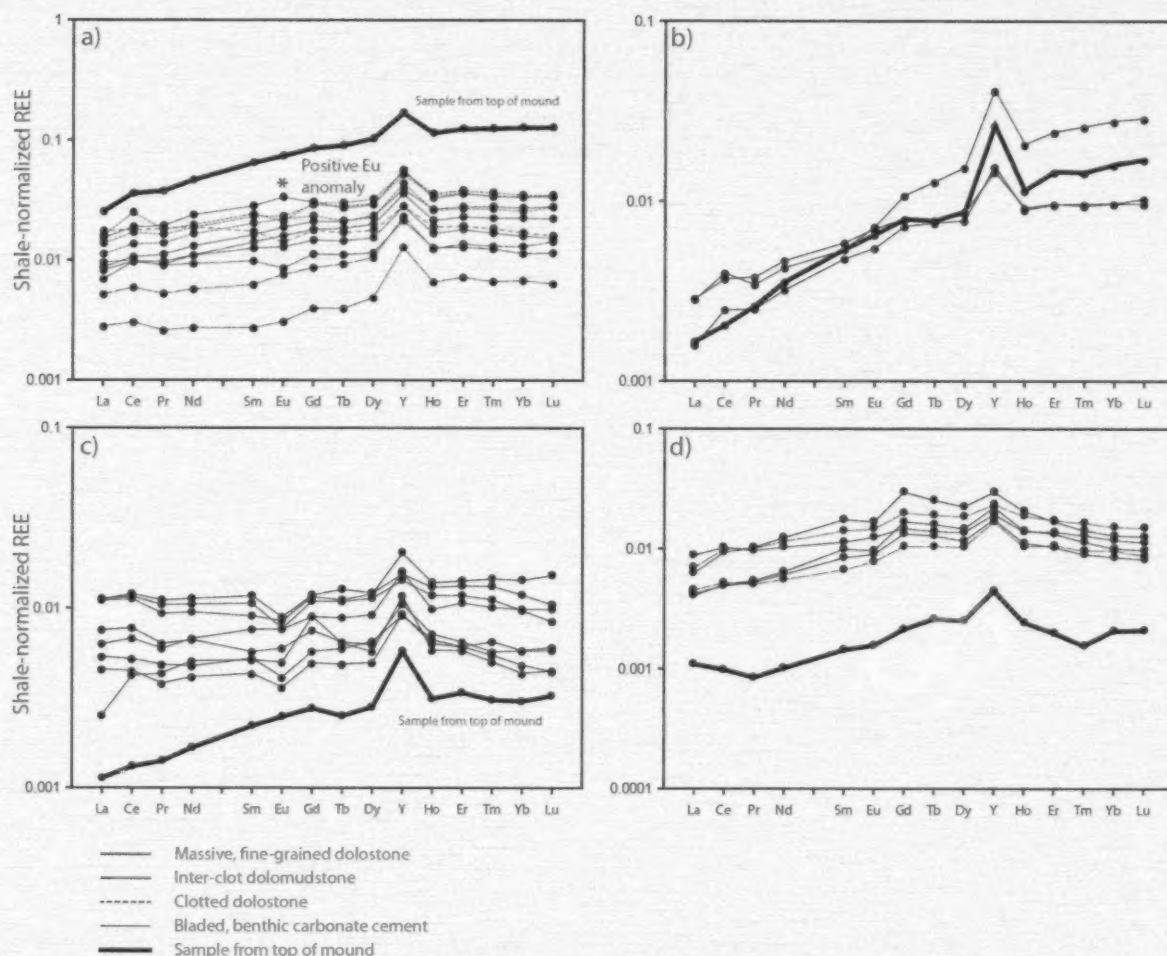
Figure 4: Shale-normalized (Arctic Bay Formation) REE+Y plots for selected samples from each of four mounds studied, northern Baffin Island, northwestern Nunavut: **a)** Red Rock mound (northwestern Milne Inlet graben, Milne block) exhibits a negative Eu anomaly in most samples; **b)** Uluksan mound (northwestern Milne Inlet graben, Milne block) exhibits steep patterns, as compared to those from other sample locations; **c)** Bellevue mound (southeastern Milne Inlet graben, Tremblay block) exhibits a significant negative Eu anomaly in all but one sample, indicating that the mound-derived carbonate was restricted from the open ocean; **d)** K-Mesa mound (southeastern Milne Inlet graben, Magda block) patterns are irregular as compared to expected seawater patterns but still preserve the main aspects of seawater, such as positive Y, Gd and La anomalies, and overall enrichment of heavy rare-earth elements.

significant enrichment in V and Mo. This enriched sample was of 'particulate' carbonate mud (i.e., precipitated in the water column, not benthically) and corresponds to a positive Eu anomaly.

Uluksan mound (Milne block)

All samples analyzed display a steep, positive REE+Y slope and strong positive Ce and Y anomalies (Figure 4b). The patterns are characteristic of normal Proterozoic seawater that was deposited beneath a chemocline (e.g., Webb and Kamber, 2000; Kamber et al., 2004; Planavsky et al., 2010).

Concentrations of the trace metals Mo, V and U are low in all samples from Uluksan mound. In general, the trace metals all behave similarly and correlate well with one another.

Bellevue mound (Tremblay block)

The REE+Y patterns at Bellevue mound have a flat to slightly positive slope, significant negative Eu anomalies and positive La, Ce and Y anomalies (Figure 4c). They are interpreted to have been derived from seawater due to the presence of the positive slope and normal seawater anomalies. As in the other mounds, the negative Eu anomaly is interpreted as a function either of the local seawater or the vent fluid.

The abundance of the trace metals Mo, V and U is low through most of the mound (Figure 5b). When the elements are normalized to Al and plotted against stratigraphic position, an enrichment is observed in one sample from the uppermost part of the mound (Figure 5b). This sample has no
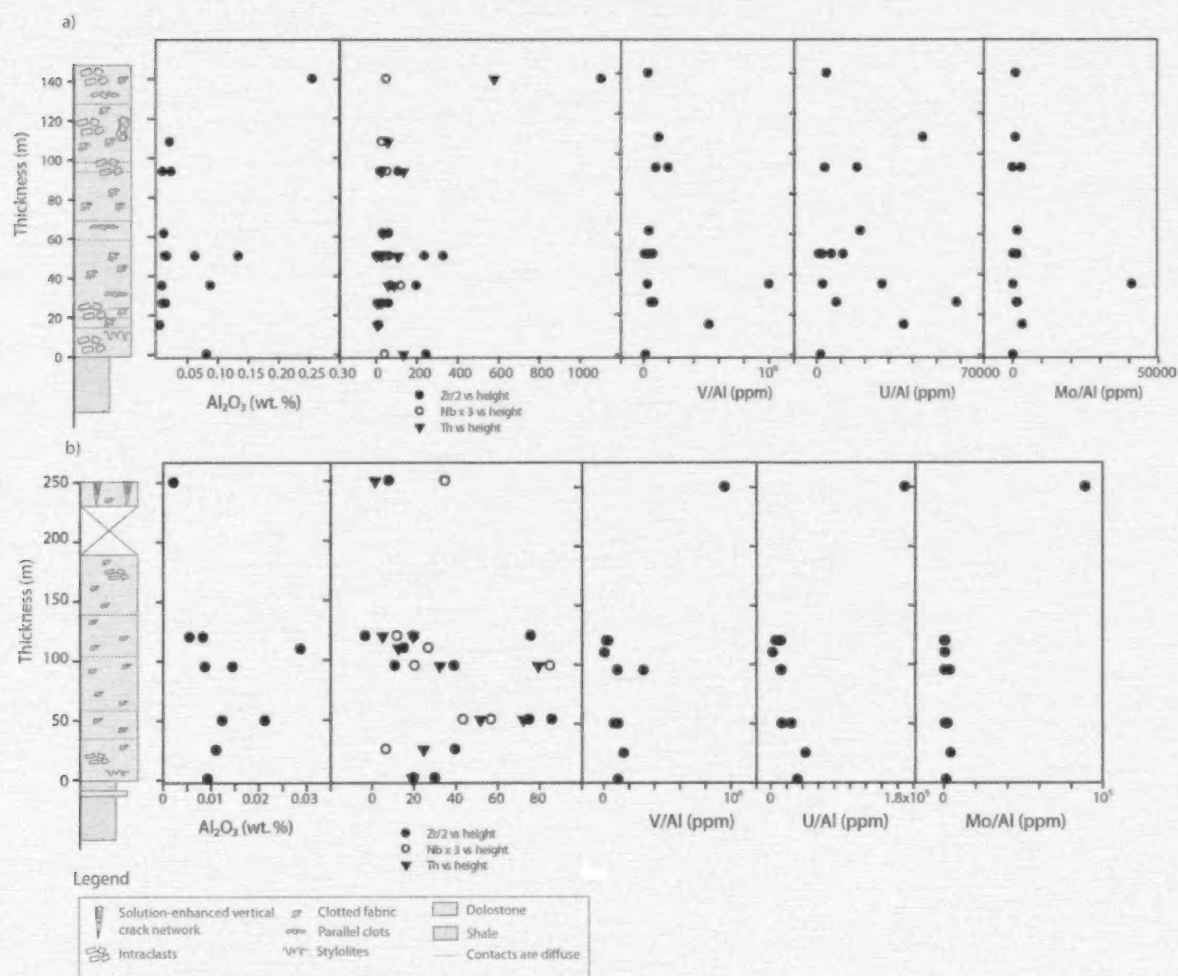
Figure 5: Stratigraphic plots of Red Rock mound **(a)** and Bellevue mound **(b)**, northern Baffin Island, northwestern Nunavut, illustrating the elements used to detect detrital contamination, and several redox-sensitive trace elements. Detrital contamination at Bellevue mound is low. The contamination from heavy minerals (Th, Zr, Nb) is very low, and their peaks do not correspond to any unusual REE+Y patterns. The clay content (Al_2O_3) is also low and has not influenced the REE+Y patterns. The detrital component in Red Rock mound is much higher than that of Bellevue mound, and may have affected the REE+Y patterns very slightly, but the REE+Y patterns are interpreted as a faithful representation of paleoseawater solutes.

Eu anomaly and exhibits the steepest, most seawater-like REE+Y pattern. The redox-sensitive elements all display a positive correlation with the magnitude of the Eu anomaly. These results imply that the carbonate at the top of the mound was derived from more open and well mixed seawater.

K-Mesa mound (Magda block)

The REE+Y patterns at K-Mesa mound are highly unusual, showing very low abundance of REE+Y. There is a significant bulge in the middle REEs, although an overprint of normal seawater patterns is observed (Figure 4d). The unusual REE+Y patterns at K-Mesa are unrelated to diagenesis because diagenetic cements exhibit a much different REE+Y pattern, including extreme La depletion. Only samples that were considered very well preserved were analyzed. The entire mound is crosscut by enigmatic solution breccia, and the solutions that generated the breccia may have modified the REE patterns in mound rock away from an original seawater signature. It is possible that K-Mesa mound was in a completely isolated sub-basin with a completely different vent-fluid composition, and that the composition of the vent fluid had a larger control on the composition of the REEs in this location. The abundance of the trace metals V, Mo and U is low.

Discussion

The strong positive Ce anomaly in the REE patterns of the Ikpiarjuk Formation, together with results from previous

work on related strata (Turner and Kamber, 2012), give strong evidence that the basin water was chemically stratified with respect to oxygen (redoxcline) during deposition of the mounds. The subtle differences in the REE+Y patterns among the mounds are probably due to the fact that each mound formed in a separate, fault-bounded sub-basin in the MIG. One sample of ooid grainstone from a mound top displays a positive Ce anomaly (i.e., it accumulated below the redoxcline), which indicates that the redoxcline was above fair-weather wave base (where ooids form). This unusual presence of anoxia in shallow water is not completely unknown: the modern Black Sea has a redoxcline that reaches the base of the photic zone (Algeo and Tribovillard, 2009). Although the depth of wave base and extent of fetch in the MIG are unknown, other lines of evidence point to an unusually shallow storm-wave base and limited fetch for other parts of the Bylot Supergroup in the MIG (Turner, 2009). These factors may have contributed to the lack of mixing among subaqueous, fault-bounded sub-basins. The type of basement rock beneath the Bylot Supergoup is unknown in many parts of the basin, and it is possible that spatial variability in its composition was a local influence on the vent fluid in each sub-basin.

Economic considerations

Although the solute composition of the vent fluids that drove deep-water carbonate precipitation in the Ikpiarjuk Formation remains largely unresolved, mound accumulation in the MIG records characteristics that are known attributes of SEDEX, base-metal–hosting basins (e.g., Leach et al., 2005; Goodfellow and Lydon, 2007; Leach et al., 2010). These include a stratified basin with anoxic to euxinic bottom water, black shale, fault-bounded sub-basins and voluminous fluid venting. It remains unknown whether the vent fluids in the Borden Basin were hydrothermal, and if they carried metals at some stage or location. The centres of all exposed mounds were removed by Pleistocene glacial erosion, which formed valleys that follow the weaknesses representing fault structures. Consequently, the true spatial distribution of lithofacies in mound centres, and the potential for them to contain sulphidic exhalites, remains unknown. Recent study on black shale in the MIG suggested that bottom water was euxinic at times and that, if voluminous venting had occurred, then there was good potential for SEDEX mineralization to develop (Turner and Kamber, 2012).

The Lost City vent field in the mid–Atlantic Ocean is an off-axis vent field where carbonate chimneys are produced on the seafloor from vent fluids produced during serpentinization reactions between ultramafic rocks and seawater (Kelley et al., 2001). The Lost City vents are at approximately 30 km from sulphide-producing black-smoker–type vents. It is also known that hydrothermal fluids produced during serpentinization reactions are highly reducing (McCollom

and Seewald, 2013), a phenomenon that may help explain the negative Eu anomaly documented in the Ikpiarjuk Formation mounds. If the Ikpiarjuk Formation mounds formed as a result of a mechanism similar to that in effect at the Lost City vent field, or had locations or phases of development that were characterized by venting of more metalliferous fluids, then there is potential for as-yet undiscovered proximal hydrothermal precipitates in the MIG.

Acknowledgments

References

Algeo, T.J. and Tribovillard, N. 2009: Environmental analysis of paleoceanographic systems based on molybdenum-uranium covariation; Chemical Geology, v. 268, no. 3–4, p. 211–215.

Denyszyn, S.W., Halls, H.C., Davis, D.W. and Evans, A.D. 2009: Paleomagnetism and U-Pb geochronology of Franklin Dykes in High Arctic Canada and Greenland: a revised age and paleomagnetic pole constraining block rotations in the Nares Strait region; Canadian Journal of Earth Sciences, v. 46, no. 9, p. 689–705.

Dostal, J., Jackson, G.D. and Galley, A. 1989: Geochemistry of Neohelikian Nauyat plateau basalts, Borden rift basin, northwestern Baffin Island, Canada; Canadian Journal of Earth Sciences, v. 26, no. 11, p. 2214–2223.

Goodfellow, W.D. and Lydon, J.W. 2007: Sedimentary exhalative (SEDEX) deposits; in Mineral Deposits of Canada: A Synthesis of Major Deposit Types, District Metallogeny, the Evolution of Geological Provinces, and Exploration Methods; Geological Association of Canada, Special Publication 5, p. 163–183.

Hahn, K.E. and Turner, E.C. 2013: Deep-water carbonate mound lithofacies, Borden Basin, Nunavut; Geological Survey of Canada, Current Research 2013-11, 14 p., URL <ftp://ftp2.cits.rncan.gc.ca/pub/geott/ess_pubs/292/292439/cr_2013_11_gsc.pdf> [September 2013], doi:10.4095/292439

Heaman, L.M., LeCheminant, A.N. and Rainbird, R.H. 1992: Nature and timing of Franklin igneous events, Canada: implications for a late Proterozoic mantle plume and the break-up of Laurentia; Earth and Planetary Science Letters, v. 109, no 1–2, p. 117–131.

Jackson, G.D. and Iannelli, T.R. 1981: Rift-related cyclic sedimentation in the Neohelikian Borden Basin, northern Baffin Island; in Proterozoic Basins of Canada; Geological Survey of Canada, Paper 81-10, p. 269–302.

Kamber, B.S., Bolhar, R. and Webb, G.E. 2004: Geochemistry of late Archaean stromatolites from Zimbabwe: evidence for microbial life in restricted epicontinental seas; Precambrian Research, v. 132, no. 4, p. 379–399.

Kamber, B.S., Greig, A. and Collerson, K.D. 2005: A new estimate for the composition of weathered young upper continental crust from alluvial sediments, Queensland, Australia; Geochimica et Cosmochimica Acta, v. 69, no. 4, p. 1041–1058.

Kelley, D.S., Karson, J.A., Blackman, D.K., Frueh-Green, G.L., Butterfield, D.A., Lilley, M.D., Olson, E.J., Schrenk, M.O., Roe, K.K., Lebon, G.T. and Rivizzignot, P. 2001: An off-axis hydrothermal vent field near the mid-Atlantic ridge at 30°N; Nature, v. 412, p. 145–149.

Knight, R.D. and Jackson, G.D. 1994: Sedimentology and stratigraphy of the Mesoproterozoic Elwin Subgroup (Aqigilik and Sinasiuvik formations), uppermost Bylot Supergroup, Borden rift basin, northern Baffin Island; Geological Survey of Canada, Bulletin 455, p. 48.

Leach, D.L., Bradley, D.C., Huston, D., Pisarevsky, S.A., Taylor, R.D. and Gardoll, S.J. 2010: Sediment-hosted lead-zinc deposits in Earth history; Economic Geology, v. 105, p. 593–625.

Leach, D.L., Sangster, D.F., Kelley, K.D., Large, R.R., Garven, G., Allen, C.R., Gutzmer, J. and Walters, S. 2005: Sediment-hosted lead-zinc deposits: a global perspective; Economic Geology, 100th Anniversary Volume, p. 561–607.

LeCheminant, A.N. and Heaman L.M. 1989: Mackenzie igneous events, Canada: Middle Proterozoic hotspot magmatism associated with ocean opening; Earth and Planetary Science Letters, v. 96, no. 1–2, p. 38–48.

Long, D.G.F. and Turner, E.C. 2012: Tectonic, sedimentary and metallogenic re-evaluation of basal strata in the Mesoproterozoic Bylot basins, Nunavut, Canada: are unconformity-type uranium concentrations a realistic expectation?; Precambrian Research, v. 214–215, p. 192–209.

McCollom, T.M. and Seewald, J.S. 2013: Serpentinites, hydrogen, and life; Elements, v. 9, p. 129–134.

Pehrsson, S.J. and Buchan, K.L. 1999: Borden dykes of Baffin Island, Northwest Territories: a Franklin U-Pb baddeleyite age and a paleomagnetic reinterpretation; Canadian Journal of Earth Sciences, v. 36, no. 1, p. 65–73.

Planavsky, N., Bekker, A., Rouxel, O.J., Kamber, B.S., Hofmann, A., Knudsen, A. and Lyons, T.W. 2010: Rare earth element and yttrium compositions of Archean and Paleoproterozoic Fe formations revisited: new perspectives on the significance and mechanisms of deposition; Geochimica et Cosmochimica Acta, v. 74, no. 22, p. 6387–6405.

Scott, D.J. and de Kemp, E.A. 1998: Bedrock geology compilation, northern Baffin Island and northern Melville Peninsula, Northwest Territories; Geological Survey of Canada, Open File 3633.

Sherman, A.G., James, N.P. and Narbonne, G.M. 2000: Sedimentology of a late Mesoproterozoic muddy carbonate ramp, northern Baffin Island, Arctic Canada; in Carbonate Sedimentation and Diagenesis in the Evolving Precambrian World, J.P. Grotzinger and N.P. James (ed.), Society for Sedimentary Geology (SEPM), Special Publication 67, p. 275–294.

Sherman, A.G., James, N.P. and Narbonne, G.M. 2001: Anatomy of a cyclically packaged Mesoproterozoic ramp in northern Canada; Sedimentary Geology, v. 139, p. 171–203.

Sherman, A.G., James, N.P. and Narbonne, G.M. 2002: Evidence for reversal of basin polarity during carbonate ramp development in the Mesoproterozoic Borden Basin, Baffin Island; Canadian Journal of Earth Sciences, v. 39, p. 519–538.

Turner, E.C. 2004a: Kilometre-scale carbonate mounds in basinal strata: implications for base-metal mineralization in the Mesoproterozoic Arctic Bay and Society Cliffs formations, Borden Basin, Nunavut; Geological Survey of Canada, Current Research 2004-B4, 12 p., <ftp://ftp2.cits.rncan.gc.ca/pub/geott/ess_pubs/215/215337/cr_2004_b04.pdf> [September 2013].

Turner, E.C. 2004b: Origin of basinal carbonate laminites of the Mesoproterozoic Society Cliffs Formation (Borden Basin, Nunavut), and implications for base-metal mineralization; Geological Survey of Canada, Current Research 2004-B2, 1 CD-ROM, <ftp://ftp2.cits.rncan.gc.ca/pub/geott/ess_pubs/215/215334/cr_2004_b02.pdf> [September 2013].

Turner, E.C. 2009: Mesoproterozoic carbonate systems in the Borden Basin, Nunavut; Canadian Journal of Earth Sciences, v. 46, no. 12, p. 915–938.

Turner, E.C. 2011: Structural and stratigraphic controls on carbonate-hosted base metal mineralization in the Mesoproterozoic Borden Basin (Nanisivik District), Nunavut; Economic Geology, v. 106, no. 7, p. 1197–1223.

Turner, E.C. and Kamber, B.S. 2012: Arctic Bay Formation, Borden Basin, Nunavut (Canada): basin evolution, black shale, and dissolved metal systematics in the Mesoproterozoic ocean; Precambrian Research, v. 208–211, p. 1–18.

Turner, E.C., Kamber, B.S., Kontak, D.J., Long, D.G.F., Hnatyshin, D., Creaser, R., Morden, R. and Hahn, K. 2012: Economic potential of the Mesoproterozoic Borden Basin zinc district, northern Baffin Island, Nunavut: update 2011–2012; in Summary of Activities 2012, Canada-Nunavut Geoscience Office, p. 1–12.

Webb, G.E. and Kamber, B.S. 2000: Rare earth elements in Holocene reefal microbialites: a new shallow seawater proxy; Geochimica et Cosmochimica Acta, v. 64, no. 9, p. 1557–1565.

Altered ultramafic and layered mafic-ultramafic intrusions: new economic and carving stone potential on northern Hall Peninsula, Baffin Island, Nunavut

H.M. Steenkamp[1], E.R. Bros[2] and M.R. St-Onge[3]

[1]Canada-Nunavut Geoscience Office, Iqaluit, Nunavut, holly.steenkamp@nrcan.gc.ca

[2]Department of Earth Sciences, Dalhousie University, Halifax, Nova Scotia

[3]Geological Survey of Canada, Natural Resources Canada, Ottawa, Ontario

Abstract

Regional bedrock mapping stemming from the 2012–2014 Hall Peninsula Integrated Geoscience Project has led to the discovery and documentation of a number of localities of potential economic interest. Two large layered mafic-ultramafic intrusions, identified in the northern and southwestern portions of the peninsula, show potential for Ni-Cu-platinum element group mineralization. The compositional layering and geological setting of the mafic-ultramafic intrusions appear comparable to those reported for the Raglan-type deposits in the Cape Smith Belt of northern Quebec. Several ultramafic intrusions dominantly exposed on the eastern side of northern Hall Peninsula exhibit postemplacement hydrothermally altered mineral assemblages. Altered ultramafic rock is the most common type of carving stone used in Nunavut, a valuable commodity that is currently in high demand as the traditional art form expands to reach new global markets. Understanding the precise geological context and tectonic evolution of potentially economic sites on Hall Peninsula is critical when exploring for similar resources elsewhere in the territory.

Résumé

La cartographie régionale du substratum rocheux réalisée en 2012–2014 dans le cadre du Projet géoscientifique intégré de la péninsule Hall a permis de découvrir et de documenter un certain nombre de sites présentant un intérêt économique. Deux grandes intrusions mafiques-ultramafiques rubanées découvertes dans le nord et le sud-ouest de la péninsule présentent des signes de minéralisation possible en Ni-Cu-éléments du groupe du platine. La différentiation pétrographique et le cadre géologique de ces intrusions mafiques-ultramafiques s'apparentent à ceux qui caractérisent les gisements de type Raglan de la ceinture de Cape Smith dans le nord du Québec. Quelques intrusions ultramafiques affleurant dans la partie orientale du nord de la péninsule Hall présentent des assemblages minéraux qui ont été altérés par des fluides hydrothermaux après la mise en place des intrusions. Les roches ultramafiques altérées constituent le type de pierre à sculpter utilisé le plus couramment au Nunavut; il s'agit d'un produit précieux pour lequel la demande est actuellement très élevée en raison de l'entrée sur de nouveaux marchés mondiaux de cette forme d'expression artistique traditionnelle. Une bonne compréhension du contexte géologique précis et de l'histoire tectonique des sites d'intérêt économique possibles dans la péninsule Hall s'impose lorsqu'il s'agit de découvrir des ressources semblables ailleurs dans le territoire.

Introduction

Regional bedrock mapping was conducted in the summer of 2013 on northern Hall Peninsula as part of the 2012–2014 Hall Peninsula Integrated Geoscience Project (Machado et al., 2013; Steenkamp and St-Onge, 2014). Hall Peninsula is an area of high economic potential, as demonstrated by the presence of the Chidliak diamond district currently held by Peregrine Diamonds Ltd. The Chidliak property, discovered in 2008, boasts 64 kimberlite occurrences, of which seven are considered potentially economic (O'Connor and Coopersmith, 2013). Late Jurassic to Early Cretaceous kimberlites are emplaced in Archean orthogneiss, approximately 120 km northeast of Iqaluit (Heaman et al., 2012; Nichols et al., 2013; Pell et al., 2013; Rayner, 2014). In addition to kimberlitic diamonds, bedrock mapping on southern Hall Peninsula in 2012 led to the discovery of several ultramafic intrusions with carving stone and Ni-Cu-platinum group element potential (Beauregard et al., 2013; Machado et al., 2013; Senkow, 2013).

Observations, early geological interpretations and economic considerations related to two layered mafic-ultramafic intrusions and several altered ultramafic intrusions examined during the 2013 mapping campaign on northern Hall Peninsula (Figure 1) are reported in this paper. The mafic-ultramafic bodies are high priorities for further geochemical investigation and may be of interest to the exploration industry. The altered ultramafic intrusions may be useful as carving stone sources, a highly sought commodity for local artisans.

Regional setting

Southern Baffin Island is situated within the upper-plate collage (Churchill Plate) of the Paleoproterozoic Trans-Hudson Orogen (THO; Hoffman, 1988; Lewry and Collerson, 1990). Hall Peninsula (Figure 1) preserves a midcrustal cross-section of a progressive transition from orogenic foreland in the east to hinterland in the west, and comprises Archean basement orthogneiss (Scott, 1999; From et al., 2014) and Paleoproterozoic supracrustal rocks (Braden, 2013; MacKay et al., 2013; Rayner, 2014; Skipton and St-Onge, 2014). A gradual east-to-west increase in metamorphic grade and three distinct deformation phases attributed to the terminal collision of the THO have been documented across the peninsula (St-Onge et al., 2009; Dyck and St-Onge, 2014; From et al., 2014; Skipton and St-Onge, 2014; Steenkamp and St-Onge, 2014).

The polymetamorphic Archean orthogneiss dominates the eastern half of Hall Peninsula and contains several felsic phases, ranging in composition from tonalite to granite, with variably distributed intrusive syenogranitic to monzogranitic dikes (Scott, 1999; From et al., 2013; Machado et al., 2013; From et al., 2014; Rayner, 2014). Paleoproterozoic metasedimentary supracrustal strata disconformably overlie the basement orthogneiss and dominantly comprise quartzite, psammite, semipelite, pelite, amphibolite, calcsilicate and ironstone (Machado et al., 2013; Skipton et al., 2013; Rayner, 2014; Skipton and St-Onge, 2014; Steenkamp and St-Onge, 2014). Discrete sections of supracrustal strata are present within thick-skinned, east-verging thrust imbricates that have been documented across the eastern field area (Steenkamp and St-Onge, 2014). Supracrustal strata dominate the peninsula west of Chidliak Bay and are intruded by panels of Paleoproterozoic tonalite to quartz diorite, which locally contain orthopyroxene, clinopyroxene and/or magnetite (Rayner, 2014; Steenkamp and St-Onge 2014).

Layered mafic-ultramafic intrusions

Two separate layered mafic-ultramafic intrusive sills hosted in Paleoproterozoic metasedimentary rocks were discovered in southwestern and northern Hall Peninsula (Figure 1). Both supracrustal and intrusive units have been imbricated, folded and thrust to the east due to east-west crustal shortening during the terminal collision of the THO (St-Onge et al., 2009; Dyck and St-Onge, 2014; Skipton and St-Onge, 2014; Steenkamp and St-Onge, 2014).

The northern sill (lat. 64°33.683'N, long. 66°55.006'W; Figure 2) is located approximately 28 km west of the southern end of Ptarmigan Fiord, within the Chidliak property held by Peregrine Diamonds Ltd. This intrusion is well-exposed in three segments, separated by low-relief till cover that extends parallel to the regional moderately-dipping north-south foliation. The southwestern sill (63°21.937'N, 66°52.961'W) is located approximately 90 km southeast of Iqaluit, between two ultramafic rock localities noted during mapping of the southern Hall Peninsula in 2012 (Machado et al., 2013). The main body is approximately 100 m wide, 300 m long and foliated parallel to the regional subvertical north-south fabric (Figure 3a). The body thins to only tens of metres at the southern end, but outcrops intermittently along strike for about another 3 km to the south.

Field relationships

The field relationships described here specifically pertain to the three outcrop segments of the northern sill. The northern segment (Figure 2) is approximately 250 m wide by 1400 m long and contains a complete ultramafic-to-mafic layered compositional sequence (Figure 2b, 3b). It outcrops on the overturned west-dipping limb of an antiform in the footwall of an east-verging imbricate thrust. This interpretation is supported by the observed inversion of the ultramafic-to-mafic compositional sequence and the discovery of several in situ rip-up clasts of the country rock embedded in well-exposed basal clinopyroxenite on the western side of the outcrop (Figure 3c). A matching mafic-ultramafic body in the hangingwall of the east-verging thrust was not observed to the west. This may be due to
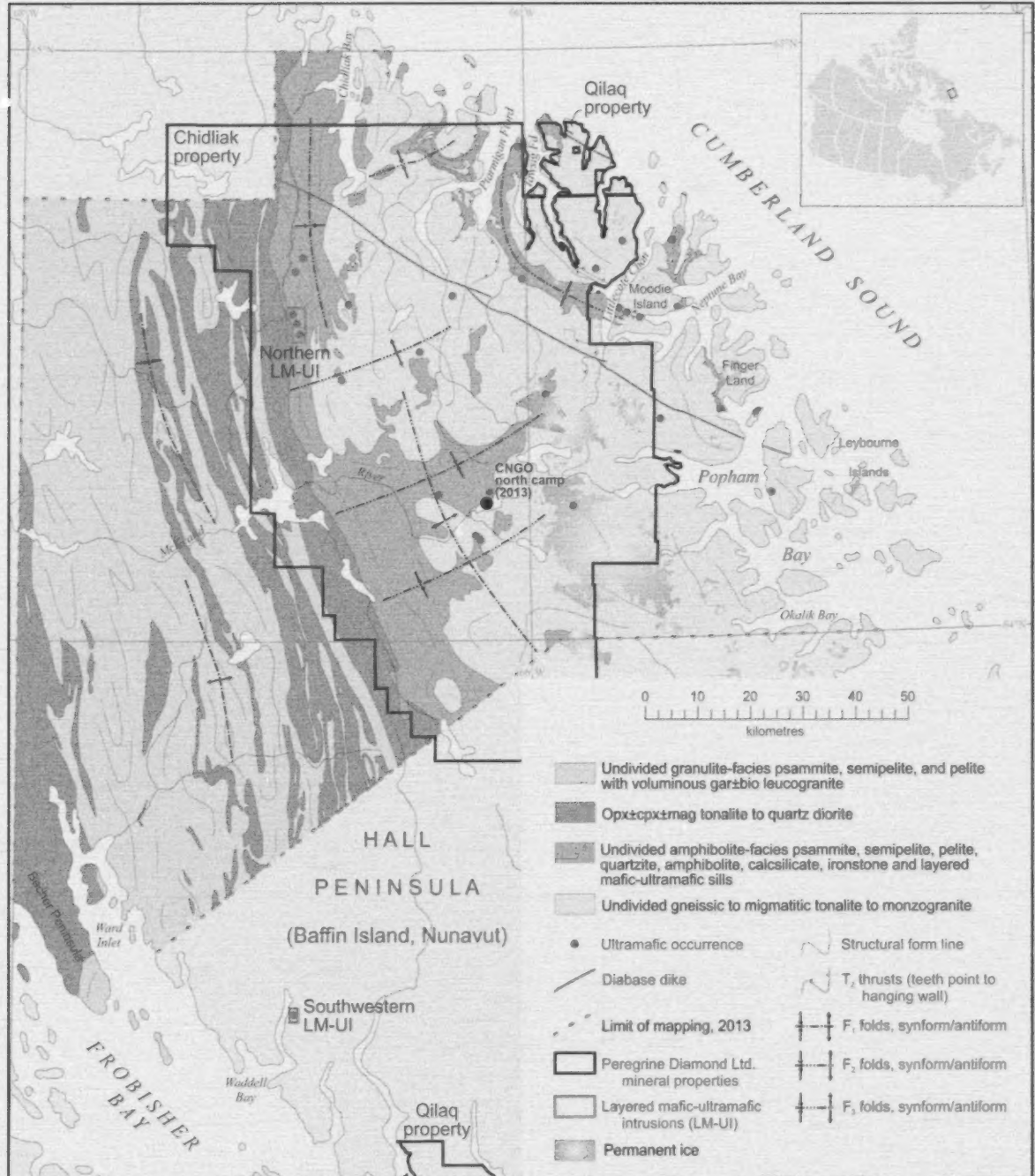
Figure 1: Simplified geology of Hall Peninsula (after Steenkamp and St-Onge, 2014), Nunavut, indicating the locations of the southwestern and northern (detailed in Figure 2) layered mafic-ultramafic intrusions (LM-UI) and altered ultramafic occurrences. The Chidliak and Qilaq mineral claims held by Peregrine Diamonds Ltd. are overlain for reference (boundaries current as of November 2013). Abbreviations: bio, biotite; cpx, clinopyroxene; gar, garnet; mag, magnetite; opx, orthopyroxene.

structural displacement on the east-verging thrust and/or subsequent erosion of the hangingwall.

The central segment is preserved in an overturned south-plunging antiform (Figure 2a). The eastern limb outcrop is 1600 m long by 50 m thick and the western limb, which is 20 m thick, discontinuously outcrops for 1400 m.

The southern segment is interpreted as an outcrop constituting the two limbs of a south-plunging synform (Figure 3d). The western limb outcrop measures about 2600 m in length and up to 85 m in width, whereas the eastern limb outcrop is 300 m long by 75 m wide. In total, the northern sill outcrops along a 6.7 km distance oriented north-south.

The relative timing of emplacement of the northern mafic-ultramafic intrusion is constrained by observed field relationships and the timing of deformation events. The sill intrudes Paleoproterozoic metasedimentary cover rocks, requiring emplacement after sedimentary deposition. Both the intrusion and the host metasedimentary units are folded and later cut by leucogranitic dikes associated with peak-metamorphic conditions related to the THO on Hall Peninsula (Dyck and St-Onge, 2014; Steenkamp and St-Onge, 2014).

Internal magmatic stratigraphy

Detailed textural and compositional observations of the northern segment, described in this section, were recorded from the footwall psammitic metasedimentary strata to the stratigraphic top of the layered intrusive body. Representative samples of each compositional layer were taken for whole-rock geochemical and assay analyses to be completed in early 2014.

The exposed base of the intrusion is parallel to compositional layering in the underlying, grey-weathering to locally gossanous garnet-biotite psammite. The basal composition of the intrusion is a clinopyroxenite layer 0.5–1 m thick containing thinly-spaced (3–10 cm) clinopyroxene+orthopyroxene laminae. In general, this layer has a cumulate texture comprising coarse clinopyroxene (5–8 mm long grains) and minor, fine-grained interstitial orthopyroxene and magnetite. Metamorphosed rip-up clasts of psammite 10–20 cm long were identified in situ in the basal clinopyroxenite (Figure 3c), and appear to be completely recrystallized (indurated) with minor magnetite and phlogopite at their rims.

Stratigraphically above (and structurally below) the basal clinopyroxenite is a compositionally layered peridotite up

Figure 2: Northern layered mafic-ultramafic intrusion (LM-UI) on Hall Peninsula, Nunavut: a) simplified geology illustrating field relationships and the locations of major structures; b) close-up showing approximate (dashed) internal compositional stratigraphy, strike and dip of compositional layering, and geochemistry and geochronology sample locations in the northern segment outcrop. Abbreviations: bio, biotite; gar, garnet.
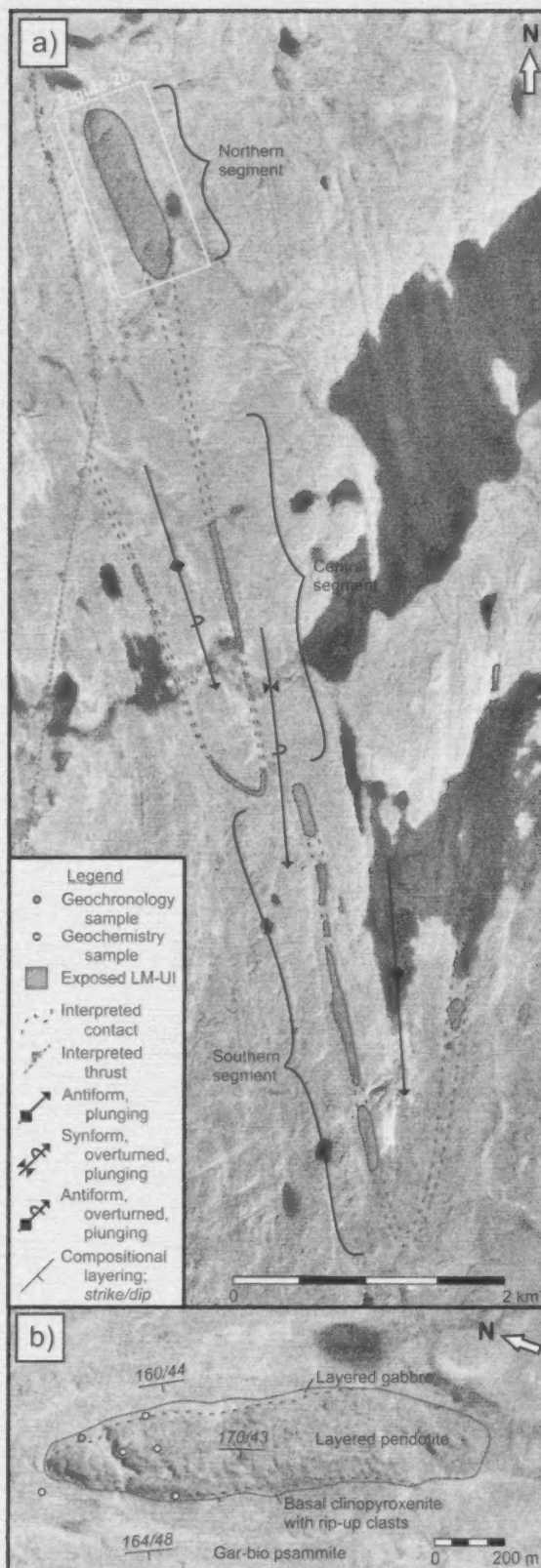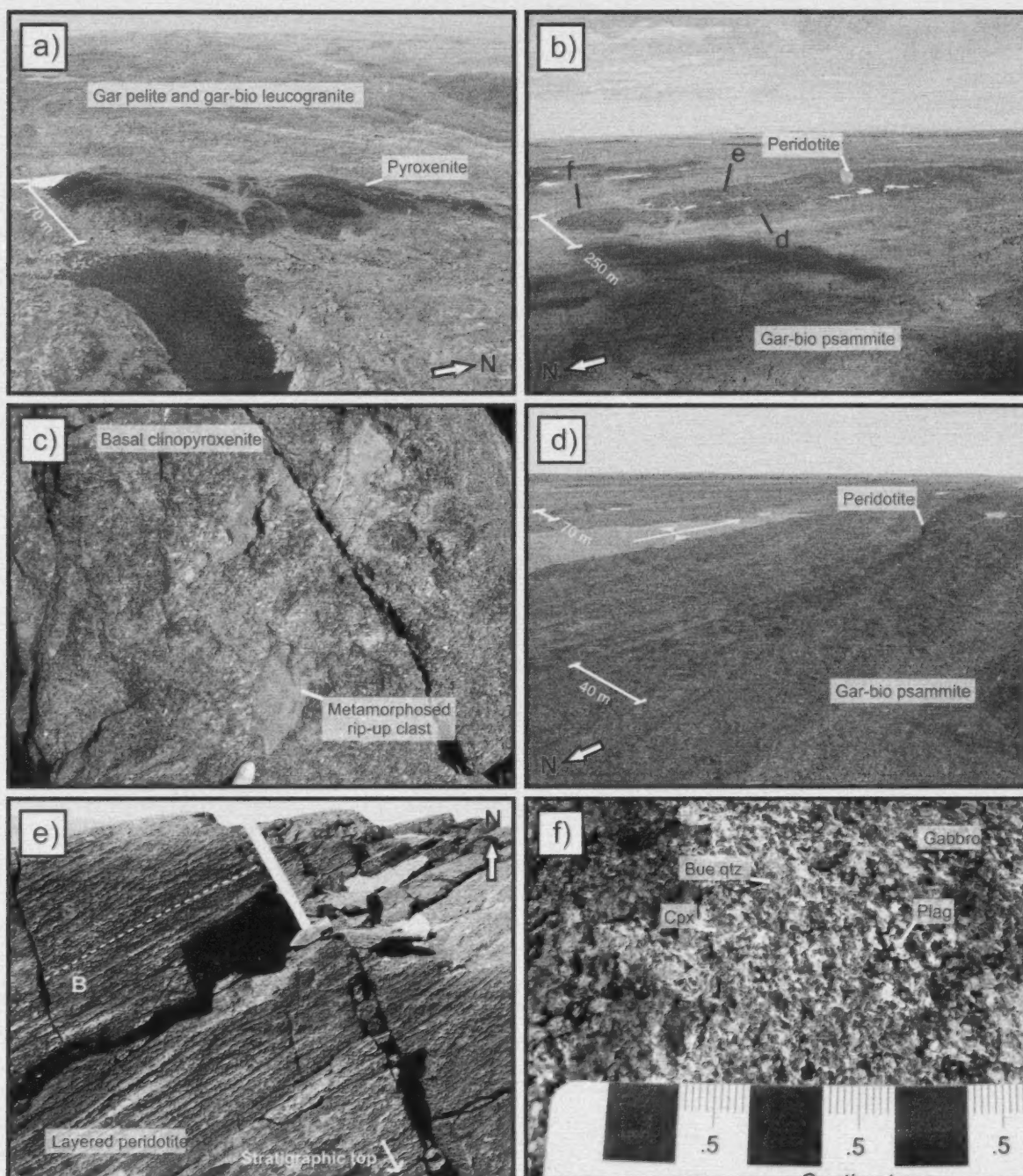
Figure 3: Layered mafic-ultramafic sills on Hall Peninsula, Nunavut: **a)** view looking west at the southwestern sill; **b)** view of the northern segment of the northern sill looking east-southeast (d, e, f refer to the respective images in this figure); **c)** in situ metamorphosed rip-up clasts embedded in basal clinopyroxenite on the western side of the northern segment outcrop; **d)** view looking southeast at the southern segment of the northern sill; the intrusion outcrops as the western (foreground) and eastern limbs (background) of a south-plunging synform (approximate hinge indicated in yellow); **e)** looking north at a cross-section of compositionally-layered peridotite (B; yellow dashed line) with superimposed mineral fabric (S; red dashed line) defined by flattened orthopyroxene phenocrysts in the northern segment outcrop; **f)** gabbro containing blue quartz, plagioclase and clinopyroxene on the eastern side of the northern segment outcrop. Hammer for scale in photograph is 40 cm long. Abbreviations: bio, biotite; cpx, clinopyroxene; gar, garnet; plag, plagioclase; qtz, quartz.

to 150 m in stratigraphic thickness, containing minor laterally continuous clinopyroxenite layers 5–10 cm wide. Compositional layering is defined by changing proportions of olivine relative to orthopyroxene and clinopyroxene (Figure 3e). The peridotite contains flattened orthopyroxene phenocrysts that define a mineral fabric that is parallel to the regional north-south foliation and slightly steeper than the internal compositional layering.

At the stratigraphic top of the peridotite, the composition of the layered sill gradually changes from ultramafic to mafic. The mafic phase is a medium- to very coarse-grained gabbro, with clinopyroxene crystals up to 1 cm long. The gabbro ranges in stratigraphic thickness from 15 m to 25 m along the eastern side of the northern segment outcrop. Blue quartz was locally observed in the gabbro (Figure 3f) and a sample was collected for U-Pb zircon geochronology to determine the age of emplacement of the mafic-ultramafic intrusion.

In one location on the eastern side of the northern segment outcrop, the gabbro was observed to compositionally grade into an anorthositic layer up to 6 cm thick. The plagioclase is flattened into a ribbon-like texture, which may be related to either crystallization concurrent with internal flow, or deformation due to the emplacement of a second, overlying, compositionally layered mafic-ultramafic sequence 2 m thick. The upper stratigraphic contact of the northern segment of the mafic-ultramafic intrusion with the host garnet-biotite psammite cover unit was not observed.

Altered ultramafic intrusions

In addition to the previously described layered mafic-ultramafic intrusions, 25 variably altered ultramafic intrusions with primary compositions likely ranging from pyroxenite to peridotite were documented on northern Hall Peninsula (Figure 1). Most of these intrusions were identified in the eastern portion of the field area, and were typically recognized by their distinctive dull brown- to orange-weathering colour that contrasts well with both the grey-weathering Archean orthogneiss complex and the grey- to white-weathering psammite and pelite that dominate the supracrustal stratigraphy (Steenkamp and St-Onge, 2014).

Field relationships

The ultramafic intrusions on northern Hall Peninsula can be grouped, based on field relationships, into basement hosted or supracrustal hosted. Some ultramafic intrusions hosted in Archean basement orthogneiss are well-exposed, small-scale isolated plugs up to 60 m wide (Figure 4a). Locally, the basement orthogneiss is more strongly foliated in proximity to the ultramafic contact, with the basement fabric wrapping around the plug. Other ultramafic rocks hosted in crystalline basement generally occur as discontinuous, variably boudinaged dikes intermittently exposed over

100–500 m. One exception is a discontinuous ultramafic dike exposed in the 4.5 km long valley between the southern end of Tawsig Fiord and Littlecote Channel (Figure 4b). Most of the basement-hosted ultramafic intrusions are characterized by a weakly-developed west-dipping foliation, defined by platy minerals or elongated phenocrysts, consistent with the regional S_{1a} fabric attributed to east-west crustal shortening on Hall Peninsula during the THO (Skipton and St-Onge, 2014; Steenkamp and St-Onge, 2014).

Ultramafic intrusions hosted in Paleoproterozoic supracrustal strata typically occur as laterally continuous sills up to 30 m thick. These sills were commonly documented within psammite and pelite near the base of the supracrustal strata. At some localities, metagabbro and amphibolite, locally containing garnet, were found at the upper and lower contacts of the supracrustal-hosted sills. On an island southeast of the Finger Land area, where supracrustal units containing ultramafic pods are exposed in the footwall of a D_2 thick-skinned thrust (Steenkamp and St-Onge, 2014), a schuppen zone comprising outcrop-scale fold and thrust imbricates and a chaotic reorientation of the supracrustal units and metamorphic fabrics around partially boudinaged ultramafic sills was documented (Figure 4c). The schuppen zone is interpreted as having developed in response to the strong rheological contrast between the relatively rigid ultramafic sill and the more pliable supracrustal rocks. In general, most ultramafic sills preserve a pervasive S_{1a} foliation defined by platy minerals; this fabric has locally been reoriented by D_2 east-verging imbricate folding and thrusting, and later D_3 north-south crustal shortening (Figure 4d; Dyck and St-Onge, 2014; Steenkamp and St-Onge, 2014). A single ultramafic plug-type intrusion 5 m wide was documented in the lower supracrustal strata between the southern ends of Ptarmigan Fiord and Tawsig Fiord.

Mineralogy

On northern Hall Peninsula, all of the observed ultramafic intrusions are variably altered. The original pyroxenite to peridotite compositions have dominantly been replaced by hydrated mineral assemblages. The most commonly observed mineral assemblages include tremolite+actinolite+phlogopite+magnetite±serpentine±talc, with minor amounts of primary orthopyroxene+clinopyroxene±olivine remaining.

In general, the interiors of basement-hosted plug-type and sill intrusions are dominated by massive, fine- to medium-grained tremolite, actinolite and phlogopite that partially to completely replace primary orthopyroxene, clinopyroxene and olivine. Minor disseminated magnetite was noted at most localities. At the contact with the surrounding host orthogneiss, outcrop-scale alteration zones penetrate up to 5 m into the ultramafic intrusion and contain medium- to coarse-grained prismatic tremolite and/or actinolite, with minor talc and/or serpentine (Figure 4b). Fibrous tremolite
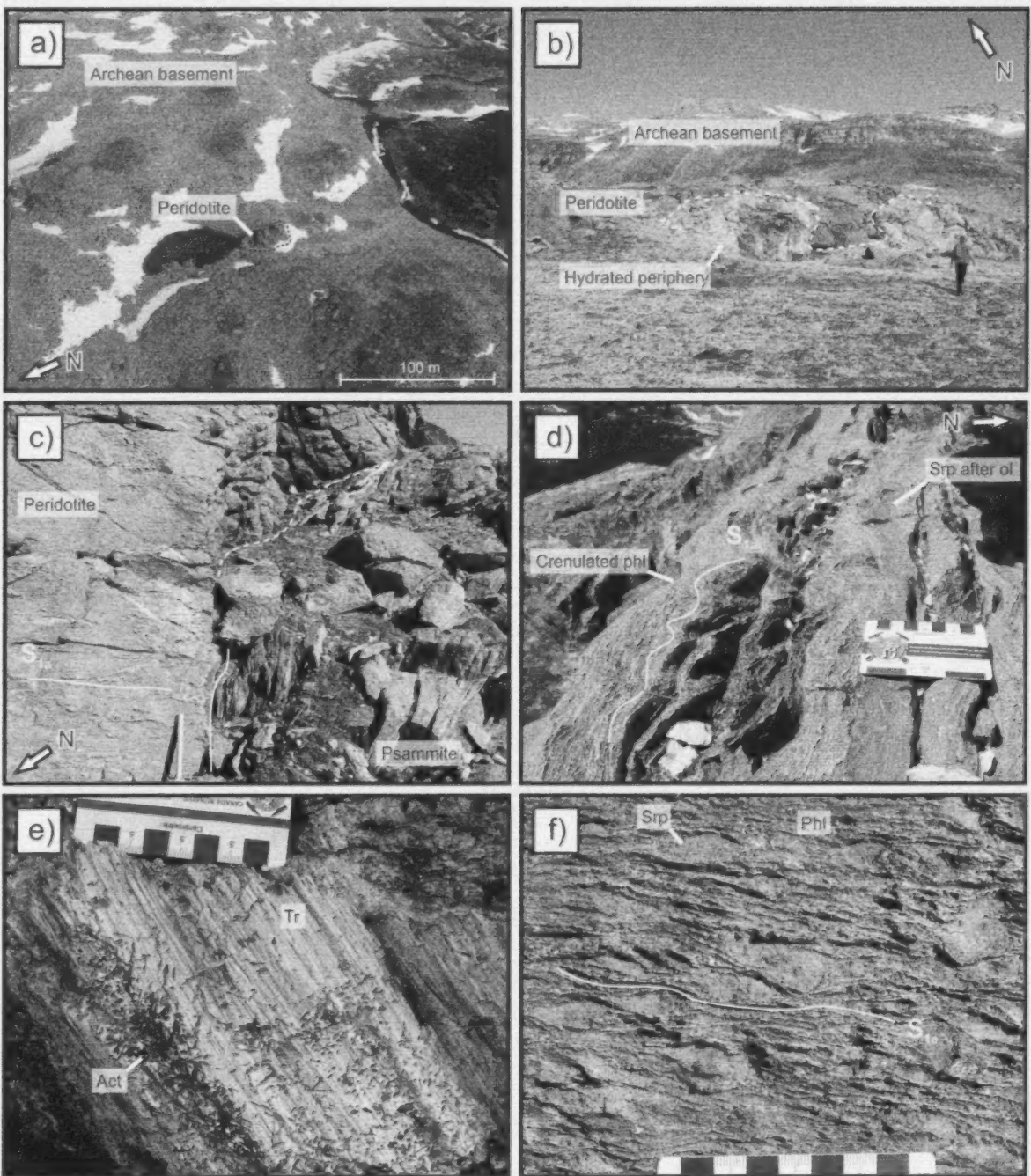
Figure 4: Hydrothermally altered ultramafic intrusions on Hall Peninsula, Nunavut: **a)** aerial view of a plug-type ultramafic intrusion (within black dashed outline) hosted in Archean basement orthogneiss; **b)** laterally discontinuous ultramafic dike in Archean basement orthogneiss at Tawsig Fiord; the white- to green- weathering periphery of the intrusion contains a hydrated mineral assemblage, whereas the brown-weathering interior (labelled peridotite) preserves some primary mineralogy (photo courtesy of Z. Braden); **c)** foliation in Paleoproterozoic psammite (S_2) is deflected around a peridotite sill with preserved S_{1a} mineral fabric in the footwall of a D_2 thrust; the contact between psammite and peridotite is delineated by the white line (solid, confirmed; dashed, approximate); **d)** preserved S_{1a} mineral fabric defined by aligned phlogopite and F_{1b} folds in a Paleoproterozoic supracrustal-hosted hydrated ultramafic sill reoriented by later D_2 east-west, and D_3 north-south crustal-shortening events (view to the west); **e)** massive fibrolitic tremolite with medium-grained, euhedral actinolite inclusions at the periphery of the Tawsig Fiord basement-hosted ultramafic dike; **f)** fine-grained serpentine clots wrapped by phlogopite define the pervasive S_{1a} mineral fabric in the supracrustal-hosted ultramafic sills (photo courtesy of R. From). Hammer for scale in photographs is 40 cm long. Abbreviations: act, actinolite; ol, olivine; phl, phlogopite; srp, serpentine; tr, tremolite.

and actinolite were documented at two basement-hosted localities, including Tawsig Fiord (Figure 4e). The single plug-type deposit hosted in the supracrustal strata contains radiating acicular actinolite that creates florets 1 cm wide. The documented alteration mineral assemblages, and the intensity and location of altered areas, suggest penetrative hydrothermal activity throughout most basement-hosted intrusions, with the most thorough alteration taking place at the boundary between the ultramafic intrusions and the host orthogneiss.

The primary ultramafic mineral assemblages in supracrustal-hosted intrusions are completely replaced by hydrated mineral assemblages. Aligned phlogopite was observed in many of the supracrustal-hosted sills to define the S_{1a} mineral fabric (Figure 4d; Steenkamp and St-Onge, 2014). Locally the fabric deflects around knots comprising varying proportions of tremolite, actinolite and/or serpentine, creating an augen texture (Figure 4f). Magnetite was observed disseminated throughout the intrusions, concentrated in thin ribbons and/or in rare clots up to 2 cm wide.

In general, the abundance of tremolite and actinolite (in the presence of serpentine) in compositionally altered ultramafic rocks implies silica-saturated hydrothermal breakdown of calcic clinopyroxene, namely diopside, at amphibolite-facies conditions (for a list of possible reactions, see Frost and Beard, 2007). Olivine and orthopyroxene breakdown to serpentine+talc can occur over a range of temperatures and pressures, provided amenable silica and fluid activities exist (Frost and Beard, 2007). The source of the hydrothermal fluids is not clear from field observations on northern Hall Peninsula, although one potential mechanism is progressive dehydration of pelitic strata during prograde metamorphism related to the THO. The interpreted S_{1a} mineral fabric is locally defined by the hydrated mineral assemblage, which supports the hypothesis of alteration of the ultramafic intrusions during prograde metamorphism.

Economic considerations

A broad group of potentially economic deposits containing nickel, copper and platinum group elements are associated with a variety of mafic and ultramafic magmatic rocks (Eckstrand et al., 2004; Naldrett, 2004; Eckstrand and Hulbert, 2007). On Hall Peninsula, the discovery of two layered mafic-ultramafic sills hosted in supracrustal strata warrants further field and analytical investigations. The observed internal magmatic layering and field relationships of the mafic-ultramafic sills on Hall Peninsula are comparable with those of the higher-level Raglan deposit of the Cape Smith Belt in northern Quebec (St-Onge and Lucas, 1993; Lesher, 2007). The Ni-Cu-platinum group element sulphide mineralization in the Raglan horizon is attributed to ultramafic sills (or flows) emplaced in pelitic metased-

imentary rocks, from which sulphur was assimilated (St-Onge and Lucas, 1993; Lesher, 2007).

Hydrothermally altered ultramafic rocks, such as serpentinite and soapstone, are the most sought after carving stone materials in Nunavut (Beauregard et al., 2013; Senkow, 2013). As traditional Inuit carvings become increasingly desirable in an expanding worldwide market, the demand for locally sourced, high-quality carving materials is increasing. The discovery and documentation of altered ultramafic bodies in the territory helps to meet this need and can also lead to a better understanding of the metasomatic processes and geological settings required to generate carving stone materials. Such information can help to identify areas with increased potential for hosting ultramafic rocks, allowing for more targeted and efficient exploration of new sources of carving stone. Samples from the most prospective ultramafic intrusions on Hall Peninsula have been sent to a local artisan, who will produce test carvings and evaluate the quality of the stone. Representative samples of the hydrated mineral assemblages were also collected for further petrological analyses.

Acknowledgments

References

Beauregard, M. A., Ell, J., Pikor, R.K. and Ham, L.J. 2013; Nunavut Carving Stone Deposit Evaluation Program (2010–2013): third year results; *in* Summary of Activities 2012, Canada-Nunavut Geoscience Office, p. 151–162.

Braden, Z.M. 2013: Paleoproterozoic pressure-temperature-deformation path in the Newton Fiord region, eastern Baffin Island, Nunavut; B.Sc. thesis, Dalhousie University, Halifax, 95 p.

Dyck, B.J. and St-Onge, M.R. 2014: Dehydration-melting reactions, leucogranite emplacement and the Paleoproterozoic structural evolution of Hall Peninsula, Baffin Island, Nunavut; *in* Canada-Nunavut Geoscience Office, Summary of Activities 2013, p. 73–84.

Eckstrand, O.R., Good, D.J., Yakubchuk, A. and Gall, Q. 2004: World distribution of Ni, Cu, PGE and Cr deposits and camps; Geological Survey of Canada, unpublished update of Open File 3791a.

Eckstrand, O.R. and Hulbert, L.J. 2007: Magmatic nickel-copper-platinum group element deposits; *in* Mineral Deposits of Canada: a Synthesis of Major Deposit Types, District

Metallogeny, the Evolution of Geological Provinces, and Exploration Methods; W.D. Goodfellow, (ed), Geological Association of Canada, Special Publication, v. 5, p. 205–222.

From, R.E., Camacho, A.L. and St-Onge, M.R. 2013: Preliminary observations on the nature and origin of the eastern orthogneiss complex of southern Hall Peninsula, Baffin Island, Nunavut; *in* Summary of Activities 2012, Canada-Nunavut Geoscience Office, p. 43–54.

From, R.E., St-Onge, M.R. and Camacho, A.L. 2014: Preliminary characterization of the Archean orthogneiss complex of Hall Peninsula, Baffin Island, Nunavut; *in* Summary of Activities 2013, Canada-Nunavut Geoscience Office, p. 53–62.

Frost, B.R. and Beard, J.S. 2007: On silica activity and serpentinization; Journal of Petrology, v. 48, no. 7, p. 1351–1368, doi: 10.1093/petrology/egml021.

Heaman, L.M., Grütter, H.S., Pell, J. Holmes, P. and Grenon, H. 2012: U-Pb geochronology, Sr- and Nd-isotope compositions of groundmass perovskite from the Chidliak and Qilaq kimberlites, Baffin Island, Nunavut; *in* Proceedings of 10th International Kimberlite Conference, D.G. Pearson (ed.), Geological Society of India, Special Issue, conference CD, abstract 193.

Hoffman, P.F. 1988: United Plates of America, the birth of a craton: Early Proterozoic assembly and growth of Laurentia; Annual Review of Earth and Planetary Sciences, v. 16, p. 543–603.

Lesher, C.M., 2007. Ni-Cu-(PGE) deposits in the Raglan area, Cape Smith Belt, New Quebec; *in* Mineral Deposits of Canada: a Synthesis of Major Deposit Types, District Metallogeny, the Evolution of Geological Provinces, and Exploration Methods, W.D. Goodfellow (ed), Geological Association of Canada, Special Publication, v. 5, p. 351–386.

Lewry, J. F. and Collerson, K. D. 1990: The Trans-Hudson Orogen: extent, subdivision, and problems; *in* The Early Proterozoic Trans-Hudson Orogen of North America, J.F. Lewry and M.R. Stauffer (ed.), Geological Association of Canada, Special Paper, v. 37, 1–14.

Machado, G., Bilodeau, C., Takpanie, R., St-Onge, M.R., Rayner, N.M., Skipton, D.R., From, R.E., MacKay, C.B., Creason, C.G. and Braden, Z.M. 2013: Hall Peninsula regional bedrock mapping, Baffin Island, Nunavut: summary of fieldwork; *in* Summary of Activities 2012, Canada-Nunavut Geoscience Office, p. 13–22.

MacKay, C.B., Ansdell, K.M., St-Onge, M.R., Machado, G. and Bilodeau, C. 2013: Geological relationships in the Qaqqanittuaq area, southern Hall Peninsula, Baffin Island, Nunavut; *in* Summary of Activities 2012, Canada-Nunavut Geoscience Office, p. 55–64.

Naldrett, A.J. 2004: Magmatic Sulfide Deposits: Geology, Geochemistry and Exploration; Heidelberg, Springer Verlag, 727 p.

Nichols, K.M. A., Stachel, T., Pell, J. A. and Mate, D.J. 2013: Diamond sources beneath the Hall Peninsula, Baffin Island, Nunavut: preliminary assessment based on microdiamonds; *in* Summary of Activities 2012, Canada-Nunavut Geoscience Office, p. 113–120.

O'Connor, A. and Coopersmith, H. 2013: Peregrine provides Chidliak update and announces discovery of three new kimberlites; Peregrine Diamonds Ltd, press release, September 9, 2013, URL <http://www.pdiam.com/s/Press Releases.Asp?DateRange=2013/01/01..2013/12/31> [October 2013].

Pell, J., Grütter, H., Neilson, S., Lockhart, G., Dempsey, S. and Grenon, H. 2013: Exploration and discovery of the Chidliak kimberlite province, Baffin Island, Nunavut: Canada's newest diamond district; *in* Proceedings of 10th International Kimberlite Conference, D.G. Pearson (ed.), Geological Society of India, Special Issue, v. 2, p. 209–227, doi: 10.1007/978-81-322-1173-0-14.

Rayner, N.M. 2014: New U-Pb geochronological results from Hall Peninsula, Baffin Island, Nunavut; *in* Summary of Activities 2013, Canada-Nunavut Geoscience Office, p. 39–52.

Scott, D.J. 1999: U-Pb geochronology of the eastern Hall Peninsula, southern Baffin Island, Canada: a northern link between the Archean of West Greenland and the Paleoproterozoic Torngat Orogen of northern Labrador; Precambrian Research, v. 93, p. 5–26.

Senkow, M.D. 2013: Characterization of ultramafic occurrences on southern Hall Peninsula, Baffin Island, Nunavut, and evaluation of their potential as a source of carving stone; *in* Summary of Activities 2012, Canada-Nunavut Geoscience Office, p. 163–168.

Skipton, D.R. and St-Onge, M.R., 2014: Paleoproterozoic deformation and metamorphism in metasedimentary rocks west of Okalik Bay: a field template for the evolution of eastern Hall Peninsula, Baffin Island, Nunavut; *in* Summary of Activities 2013, Canada-Nunavut Geoscience Office, p. 63–72.

St-Onge, M.R. and Lucas, S.B. 1993: Controls on the regional distribution of iron-nickel-copper-platinum-group element sulfide mineralization in the eastern Cape Smith Belt, Quebec; Canadian Journal of Earth Sciences, v. 31, p. 206–218.

St-Onge, M.R., Van Gool, J. A.M., Garde, A. A. and Scott, D.J. 2009: Correlation of Archaean and Palaeoproterozoic units between northeastern Canada and western Greenland: constraining the pre-collisional upper plate accretionary history of the Trans-Hudson orogen; *in* Earth Accretionary Systems in Space and Time, P. A. Cawood and A. Kröner (ed), The Geological Society, London, Special Publications, v. 318, p. 193–235.

Steenkamp, H.M. and St-Onge, M.R. 2014: Overview of the 2013 regional bedrock mapping program on northern Hall Peninsula, Baffin Island, Nunavut: *in* Summary of Activities 2013, Canada-Nunavut Geoscience Office, p. 27–38.

Diamond sources beneath the Hall Peninsula, Baffin Island, Nunavut: an update of the preliminary assessment

K.M.A. Nichols[1], T. Stachel[2,3], R.A. Stern[3], J.A. Pell[4] and D.J. Mate[5]

[1]*Department of Earth and Atmospheric Sciences, University of Alberta, Edmonton, Alberta, hogberg@ualberta.ca*

[2]*Department of Earth and Atmospheric Sciences, University of Alberta, Edmonton, Alberta*

[3]*Canadian Centre for Isotopic Microanalysis, University of Alberta, Edmonton, Alberta*

[4]*Peregrine Diamonds, Vancouver, British Columbia*

[5]*Canada-Nunavut Geoscience Office, Iqaluit, Nunavut*

Nichols, K.M.A., Stachel, T., Stern, R.A., Pell, J.A. and Mate D.J. 2014: Diamond sources beneath the Hall Peninsula, Baffin Island, Nunavut: an update of the preliminary assessment; *in* Summary of Activities 2013, Canada-Nunavut Geoscience Office, p. 21–26.

Abstract

The physical description, scanning electron microscope imaging and initial results on nitrogen content and aggregation state (determined by Fourier-transform infrared spectroscopy) of the Chidliak diamonds were presented in CNGO's 2012 *Summary of Activities*. Here we provide an update on the diamond residence history based on nitrogen concentration-aggregation relationships, and carbon and nitrogen isotopic characteristics.

Résumé

Le *Sommaire des activités* paru en 2013 faisait état de la description physique, des images obtenues au microscope électronique à balayage et des résultats préliminaires du contenu en azote, et de son état d'agrégation (ces derniers établis au moyen de la spectroscopie infrarouge à transformée de Fourier), des diamants de Chidliak. Le but de la présente étude est de faire le point sur les antécédents de la période de résidence des diamants en fonction des rapports observés entre les taux de concentration et d'agrégation de l'azote, ainsi que des caractéristiques isotopiques du carbone et de l'azote.

Introduction

The Chidliak kimberlites are located, 120 km northeast of Iqaluit on the Hall Peninsula, southern Baffin Island, Nunavut. Many of the discovered kimberlites have proven to be diamondiferous; currently, there are 67 kimberlites identified in the Chidliak kimberlite field, 64 in the area covered by the Chidliak project and 3 at the neighbouring Qilaq project. Diamonds were recovered during kimberlite sampling that was part of an intensive period of diamond exploration in this region that began in 2005; approximately 740 have been provided by Peregrine Diamonds Ltd., of which 210 (size range from 212 to 600 μm) have been utilized for geochemical analyses. In this study, the stones were subdivided into two groups, from ≥425 to 600 μm and from ≥212 to <425 μm; diamonds <212 μm were not included.

The purpose of this paper is to update Nichols et al., (2013), which was published in CNGO's inaugural *Summary of Activities* volume. The paper includes an update on the carbon isotopic compositions and nitrogen characteristics of Chidliak diamonds, which will be used to constrain diamond sources in the cratonic root and determine the diamond mantle residence history, as well as conditions of diamond formation and preservation beneath the Hall Peninsula.

Methods and results

A Zeiss EVO 15 scanning electron microscope, equipped for cathodoluminescence (CL) imaging, was used to characterize polished diamonds and to identify internal growth structures prior to ion-probe analysis. The diamonds imaged by CL were not oriented crystallographically, due to mounting procedures. Mounting of the diamonds includes sorting them according to weight and size, then placing them on double-sided thermal tape, followed by casting of epoxy pucks and finally polishing. Polishing is done in order to expose the diamond; the imaged surfaces are randomly oriented and, as a consequence, do not necessarily show systematic growth layers. Octahedral, cuboid and aggregate growth patterns were identified, in addition to extremely complex internal growth structures (Figure 1).

Carbon stable isotope compositions and nitrogen contents were measured in situ (multicollector–secondary-ion mass spectrometry, MC-SIMS) for 94 diamonds at high spatial resolution (~15 μm spot size). The $\delta^{13}C$ value, defined as:

$$\delta^{13}C_{(sample)} = ([\{^{13}C/^{12}C\}_{sample}/\{^{13}C/^{12}C\}_{std}] - 1) \times 1000,$$

ranges from –1.3 to –28.6‰, with a primary mode about –6‰; the accepted mantle value of carbon is –5‰ ±1‰ (e.g., Deines et al., 1980; Cartigny, 2005). Chidliak diamonds show a second minor mode about –15‰ (Figure 2). The $\delta^{13}C$ distribution of eclogitic diamonds from worldwide sources is well documented as having a main mode about –5‰ with a skewness toward lower $\delta^{13}C$ values (e.g., McCandless and Gurney, 1997; Cartigny et al., 2001; Stachel et al., 2009). Diamonds of peridotitic paragenesis have carbon isotopic compositions showing a much narrower range (from ~0 to –10‰) than eclogitic diamonds (from +5 to –40‰; e.g., Kirkley et al., 1991; Stachel et al., 2009). The $\delta^{13}C$ distribution of Chidliak diamonds is very similar to that of the well-known eclogitic diamond distribution, and compares well with eclogitic diamonds from Canada and from worldwide sources (Figure 2).

Nitrogen was subsequently measured on the same spot locations as the carbon isotopes. Chidliak diamonds have nitrogen contents ranging from 0.2 to 3830 atomic ppm (at. ppm), with a median of 1130 at. ppm (Figure 3).
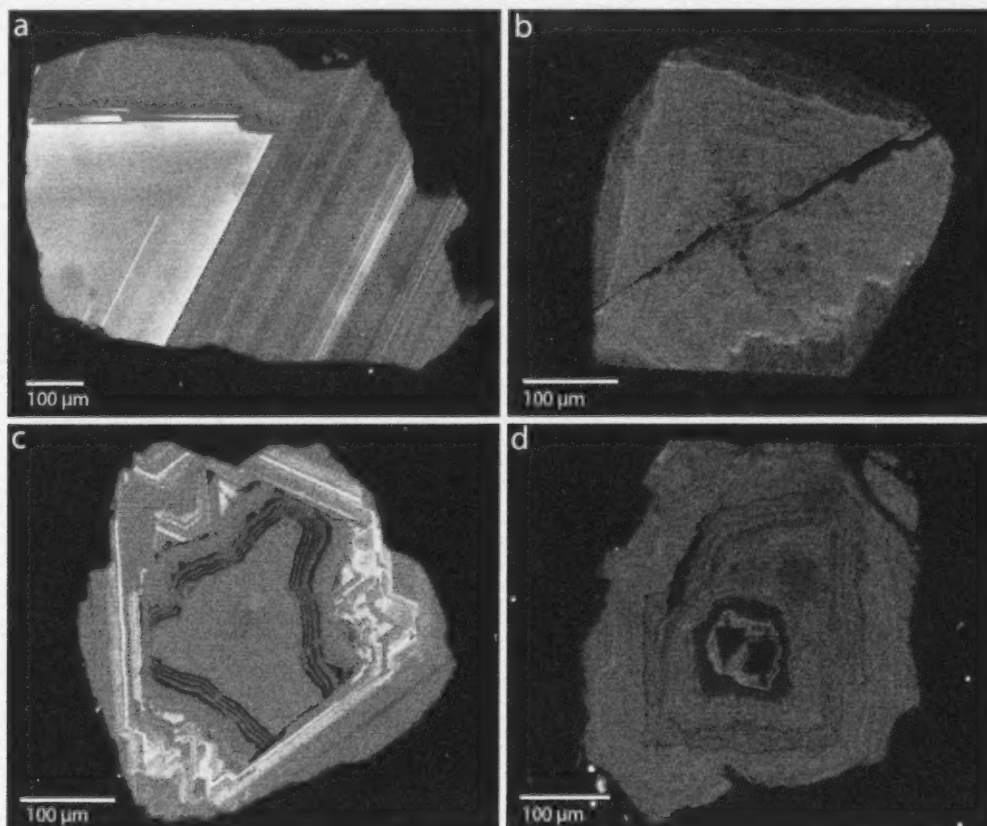
Figure 1: Cathodoluminescence images of diamonds from Hall Peninsula, Nunavut: **a)** octahedral growth layers, **b)** cuboid growth layers, **c)** centre-cross pattern caused by competition between octahedral and cuboid growth, **d)** diamond aggregate.
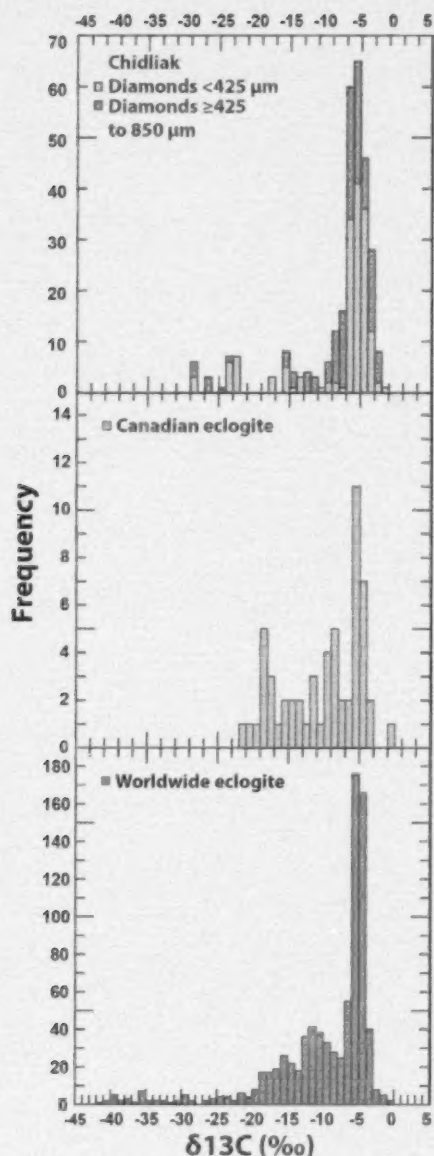
Figure 2: Carbon isotopic composition of Chidliak diamonds (Hall Peninsula, Nunavut) compared to Canadian and worldwide eclogitic diamond distributions from the database of Stachel and Harris (2008). Chidliak diamonds have a range in $\delta^{13}C$ from −1.3 to −28.6‰, with a primary mode about −6‰ and a secondary mode about −15‰. The larger diamond size fraction (≥425 to 600 μm) is separated from the finer size fraction (<425 μm) and shows similar trends.

Figure 3: Averaged nitrogen content of Chidliak diamonds (Hall Peninsula, Nunavut) compared to the worldwide eclogitic and peridotitic database of Stachel and Harris (2008). The Chidliak diamonds are nitrogen rich, with a median value of 1130 at. ppm and include 28 diamonds containing >1500 at. ppm. The larger diamond size fraction (≥425 to 600 μm) is separated from the finer size fraction (<425 μm) and shows similar trends.

Determination of nitrogen concentrations and aggregation states were carried out using a Thermo Scientific Nicolet FT-IR spectrometer. Spectra were collected for 200s; after subtraction of a 1 cm pure Type II diamond spectrum, the spectra were converted into absorption coefficients. The spectra were then deconvoluted into A, B and D compo-

nents using software provided by D. Fisher (The Diamond Trading Company). Diamonds yielding high quality spectra show similar nitrogen contents to SIMS measurements, ranging from below the limit of detection (~10 at. ppm) to 3360 at. ppm, with a median nitrogen concentration of 1100 at. ppm.

Assuming a mantle residence time of 1 b.y., it is possible to use the measured nitrogen abundance and aggregation to calculate time-averaged mantle residence temperatures (Taylor et al., 1990; Leahy and Taylor, 1997). Only high quality
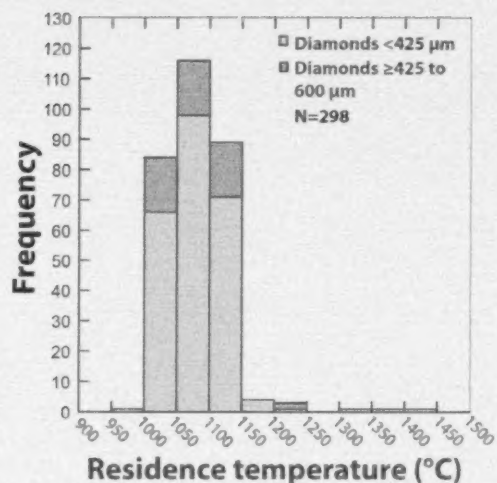
Figure 4: Time-averaged mantle residence temperatures calculated using high quality spectra and an assumed residence time of 1 b.y. (diamonds from kimberlite samples P5500 and P6807). Two points per diamond were recorded when possible. Temperature range observed was from ~980 to 1410°C, but the main population was between 1000 and 1150°C.

Figure 5: Chidliak diamond mantle residence temperatures (main population represented by yellow bands), are plotted along the paleogeotherm of Pell et al., 2012 (black circles are Nimis and Taylor [2000] thermobarometry results from Chidliak clinopyroxene) corresponding to depths of ~150–190 km.

infrared spectra are used in determining temperature. For diamonds that are pure Type IaA (0% nitrogen in the B centre), an assumed value of 0.5% B was used for the temperature calculations (i.e., calculated temperatures for these diamonds represent a maximum value). The temperatures derived by this method are usually comparable to those obtained by inclusion geothermobarometry (Leahy and Taylor, 1997). The Chidliak diamonds show a range in temperature from ~980 to 1410°C for an assumed mantle residence time of 1 b.y. (Figure 4); ranges in temperature for different diamond types are as follows: Type IaA: 978–1130°C, Type IaAB: 1038–1209°C, Type IaB: 1246–1408°C. When projected onto the local paleogeotherm of Pell et al. (2012), this corresponds to a depth range of formation at ~150–190 km (Figure 5).

Economic considerations

Since the diamonds in the ≥425 µm and <425 µm size ranges have similar characteristics they can be considered together in this study. Chidliak diamonds formed at mantle residence temperatures of approximately 980–1410°C and corresponding depths of approximately 150–190 km. The $\delta^{13}C$ distribution of Chidliak diamonds, showing a distinct skewness toward ^{13}C depleted compositions, and overall high nitrogen contents, suggest that there is a strong eclogitic component in the Chidliak diamond suite. This would lead to a suggested approach for future exploration work that targets eclogitic kimberlite indicator minerals when exploring for kimberlite pipes in the region.

References

Cartigny, P., Harris, J.W. and Javoy, M. 2001: Diamond genesis, mantle fractionations and mantle nitrogen content: a study of $\delta^{13}C$–N concentrations in diamonds; Earth and Planetary Science Letters v. 185, no. 1–2, p. 85–98.

Cartigny, P. 2005: Stable isotopes and the origin of diamond; Elements, v. 1, no. 2, p. 79–84.

Deines, P. 1980: The carbon isotopic composition of diamonds: relationship to diamond shape, color, occurrence and vapor composition; Geochimica et Cosmochimica Acta, v. 44 no 7, p. 943-961.

Kirkley, M.B., Gurney, J.J., Otter, M.L., Hill, S.J. and Daniels, L.R. 1991: The application of C isotope measurements to the identification of the sources of C in diamonds: a review; Applied Geochemistry v. 6, no. 5, p. 477–494.

Leahy, K. and Taylor, W.R. 1997: The influence of the Glennie domain deep structure on diamonds in Saskatchewan kimberlites; Russian Geology and Geophysics, v. 38, no. 2, p. 481–491.

McCandless, T.E. and Gurney, J.J. 1997: Diamond eclogites: comparison with carbonaceous chondrites, carbonaceous shales, and microbial carbon-enriched MORB; Russian Geology and Geophysics, v. 38, no. 2, p. 371–381.

Nichols, K.M.A., Stachel, T., Pell, J.A. and Mate D.J. 2013: Diamond sources beneath the Hall Peninsula, Baffin Island, Nunavut: preliminary assessment based on microdiamonds; *in* Summary of Activities 2012, Canada-Nunavut Geoscience Office, p. 113–120.

Nimis, P. and Taylor, W.R. 2000: Single clinopyroxene thermobarometry for garnet peridotites, Part 1: calibration and testing of a Cr-in-Cpx barometer and an enstatite-in-Cpx thermometer; Contributions to Mineralogy and Petrology, v. 139, p. 541–554.

Pell, J., Grütter, H., Dempsey, S. and Neilson, S. 2012: Exploration and discovery of the Chidliak kimberlite province, Baffin Island, Nunavut: Canada's newest diamond district; 10th International Kimberlite Conference, Bangalore, India, conference CD, abstract 40.

Taylor, W.R., Jacques, A.L. and Ridd, M. 1990: Nitrogen-defect aggregation characteristics of some Australian diamonds: time-temperature constraints on the source regions of pipe and alluvial diamonds; American Mineralogist, p. 1290–1320.

Stachel, T. and Harris, J.W. 2008: The origin of cratonic diamonds—constraints from mineral inclusions; Ore Geology Reviews, v. 34, no. 1–2, p. 5–32.

Stachel, T., Harris, J.W. and Muehlenbachs, K. 2009: Sources of carbon in inclusion bearing diamonds; Lithos, p. 625–637.

Overview of the 2013 regional bedrock mapping program on northern Hall Peninsula, Baffin Island, Nunavut

H.M. Steenkamp[1] and M.R. St-Onge[2]

[1]*Canada-Nunavut Geoscience Office, Iqaluit, Nunavut, holly.steenkamp@nrcan.gc.ca*
[2]*Geological Survey of Canada, Natural Resources Canada, Ottawa, Ontario*

Abstract

This paper reports field observations, initial interpretations and implications from six weeks of geological investigation on northern Hall Peninsula of southern Baffin Island, Nunavut. As part of the Canada-Nunavut Geoscience Office's 2012–2014 Hall Peninsula Integrated Geoscience Program, the 2013 fieldwork was focused on furthering geoscience knowledge and documenting the economic potential of the area. Interpretations of field observations suggest that the geology underlying Hall Peninsula represents a transition from an orogenic foreland to hinterland, progressing east to west, related to the terminal collision of the Paleoproterozoic Trans-Hudson Orogen. Three associated phases of deformation were documented, as well as an east-to-west increase in metamorphic grade. Regional-scale east-verging folds and thrust imbricates have structurally thickened Archean basement and Paleoproterozoic supracrustal units on Hall Peninsula. The supracrustal stratigraphy is interpreted as representing a gradational change from a proximal shallow-marine to a more distal slope to slope-rise depositional setting, with close proximity to a local rifting environment. Economically interesting discoveries on northern Hall Peninsula include layered mafic-ultramafic intrusions with potential for Ni-Cu-platinum group element mineralization, silicified pyrite- and pyrrhotite-bearing gossanous metasediments, granitic pegmatites with rare-earth element potential, many prospective carving stone sites and a semi-precious gem showing. The 2013 field campaign involved several Canadian university collaborators, the Geological Survey of Canada, and Aboriginal Affairs and Northern Development Canada, all of whom continue to gather geoscience data on Hall Peninsula through ongoing analytical research.

Résumé

Le présent rapport fait état des observations sur le terrain, des interprétations préliminaires et des conséquences qui découlent de six semaines d'enquête géologique dans le nord de la péninsule Hall, située au sud de l'île de Baffin, au Nunavut. Dans le cadre du Programme géoscientifique intégré de la péninsule Hall, dirigé par le Bureau géoscientifique Canada-Nunavut entre 2012 et 2014, les travaux sur le terrain réalisés en 2013 ont surtout cherché à ajouter à la base de connaissances géoscientifiques relatives à cette région et à documenter son potentiel économique. Les observations recueillies semblent indiquer que les formations géologiques gisant sous la péninsule Hall attestent d'une transition qui aurait eu lieu d'une zone orogénique d'avant-pays à une zone d'arrière-pays, s'étendant d'est en ouest, à l'époque où s'est produit l'épisode final de collision de l'orogène trans-hudsonien du Paléoprotérozoïque. Trois phases de déformation connexes ont été relevées et on a également noté une augmentation, d'est en ouest, du degré de métamorphisme. Des plis et des chevauchements imbriqués à vergence est d'échelle régionale ont contribué à un épaississement structural du socle archéen et des roches supracrustales paléoprotérozoïques de la péninsule Hall. On estime que la stratigraphie supracrustale correspond à un changement graduel d'un milieu de sédimentation proximal marin en eau peu profonde à un milieu plus distal de

pente ou de glacis, le tout situé à proximité d'un milieu de rifting d'échelle régionale. On compte parmi les découvertes intéressantes, d'un point de vue économique, faites dans le nord de la péninsule Hall des intrusions stratifiées mafiques-ultramafiques susceptibles de renfermer une minéralisation en Ni-Cu-éléments du groupe du platine, des métasédiments rouillés silicifiés contenant de la pyrite et de la pyrrhotite, des pegmatites granitiques pouvant contenir des éléments des terres rares, de nombreux sites possibles propices à l'exploitation de la pierre à sculpter et une venue de pierre semi-précieuse. La campagne 2013 de travaux sur le terrain a réunis les efforts de nombreux collaborateurs du milieu universi-taire canadien, de la Commission géologique du Canada et du ministère des Affaires autochtones et Développement du Nord Canada. Leur tâche ne s'arrête pas là car tous continuent de recueillir des données géoscientifiques ayant trait à la péninsule Hall par le biais de leurs recherches analytiques.

Introduction

The primary objective of the 2012–2014 Hall Peninsula In-tegrated Geoscience Program (HPIGP) is to gather geos-cience information to aid in accurately interpreting the tectonostratigraphic and structural/metamorphic evolution of Hall Peninsula, and evaluating the potential for eco-nomic resources within this key area of eastern Nunavut. The results of the 2013 bedrock mapping campaign sum-marized in this paper stem from the second field season of the HPIGP—the northern continuation to the complemen-tary 2012 southern Hall Peninsula bedrock map presented in Machado et al. (2013a, b). Fieldwork was supported by a 20–24 person team, including a 12-person bedrock-map-ping crew. The project ran from June 29th to July 9th based in Iqaluit, and from July 10th to August 15th based in an indus-try camp (rented from Peregrine Diamonds Ltd.) located approximately 130 km northeast of Iqaluit. Fieldwork was supported by helicopter and conducted mostly on foot, ex-cept for coastal areas of high topographic relief, islands and areas where outcrop is sparse, which were mapped by mak-ing targeted helicopter stops. Topographically, the western and central portions of northern Hall Peninsula are low in relief and are dominated by unconsolidated glacial till, felsenmeers, lakes and marshes. The rare bedrock outcrops in this area are found mostly in river cuts and are strongly weathered. The eastern and northern coastlines are charac-terized by dramatic topographic relief dominated by deeply carved glacial fiords. Excellent vertical cross-sections are exposed in the fiord walls and the bedrock is generally less vegetated there than inland. An ice cap near the eastern coast marks the highest elevation point on the peninsula.

Bedrock mapping at a scale of 1:250 000 (Figure 1) and sur-ficial-sediment mapping at a scale of 1:100 000 were the continued focus of the 2013 fieldwork, as well as several ongoing and new thematic studies carried out with univer-sity and government collaborators. These include contin-ued research on the tectonic history and affinity of Archean basement rocks (From et al., 2013; From et al., 2014), the tectonostratigraphy of Paleoproterozoic strata (MacKay et al., 2013, MacKay and Ansdell, 2014), metamorphism and deformation related to the Paleoproterozoic Trans-Hudson Orogen (St-Onge et al., 2002, 2006, 2007; Braden, 2013;

Skipton et al., 2013; Dyck and St-Onge, 2014; Skipton and St-Onge, 2014), regional geochronology (Rayner et al., 2013; Rayner, 2014), and Quaternary glaciation and per-mafrost on Hall Peninsula (Leblanc-Dumas et al., 2013; Tremblay et al., 2013; Tremblay et al., 2014). New thematic studies include the economic potential of layered mafic-ultramafic sills and hydrated ultramafic bodies for metals and carving stone deposits (Steenkamp et al., 2014).

Hall Peninsula has benefited from previous reconnais-sance-scale bedrock mapping conducted by the Geological Survey of Canada during Operation Amadjuak (Blackadar, 1967), and limited detailed mapping and U-Pb geochronol-ogy by Scott (1996, 1999). Regional airborne aeromagnetic surveys were flown in 1996–1997 at an altitude of 150 m and with 800 m flight-line spacing (Pilkington and Oneschuk, 2007), and in 2009 at an altitude of 150 m and with 400 m line spacing(Dumont and Dostaler, 2010a–g). Recent diamond exploration at the Chidliak kimberlite field has led to small-scale, detailed bedrock mapping (Ansdell et al., 2012), kimberlite emplacement studies (Nichols et al., 2013; Pell et al., 2013) and ongoing research on the Paleozoic rock record on southern Baffin Island, evi-dence of which only exists as xenoliths in the kimberlite in-trusions (Zhang and Pell, 2013; Zhang and Pell, work in progress).

Mapping by Machado et al. (2013b) on southern Hall Pen-insula in 2012 revealed that the eastern half of the field area is underlain by Archean polymetamorphic tonalitic to gra-nitic orthogneiss basement (Scott, 1999; Rayner, 2014) with secondary infolded and overlying supracrustal meta-sedimentary cover, including semipelite, psammite, amphi-bolite, quartzite, and rare marble and calcsilicate compo-nents. The western half of the southern field area was mapped as alternating panels of high-grade pelitic to psam-mitic metasedimentary rocks and typically orthopyroxene-bearing diorite to monzogranite intrusive rocks (Machado et al., 2013b). Rayner (2014) constrains Paleoproterozoic sedimentary deposition across the southern field area using maximum depositional ages that range from 2126 ±16 Ma to 1906 ±9 Ma and minimum depositional ages, provided by the crystallization of crosscutting orthopyroxene-bear-ing monzogranite intrusions, at ca. 1.89 Ga. These rock
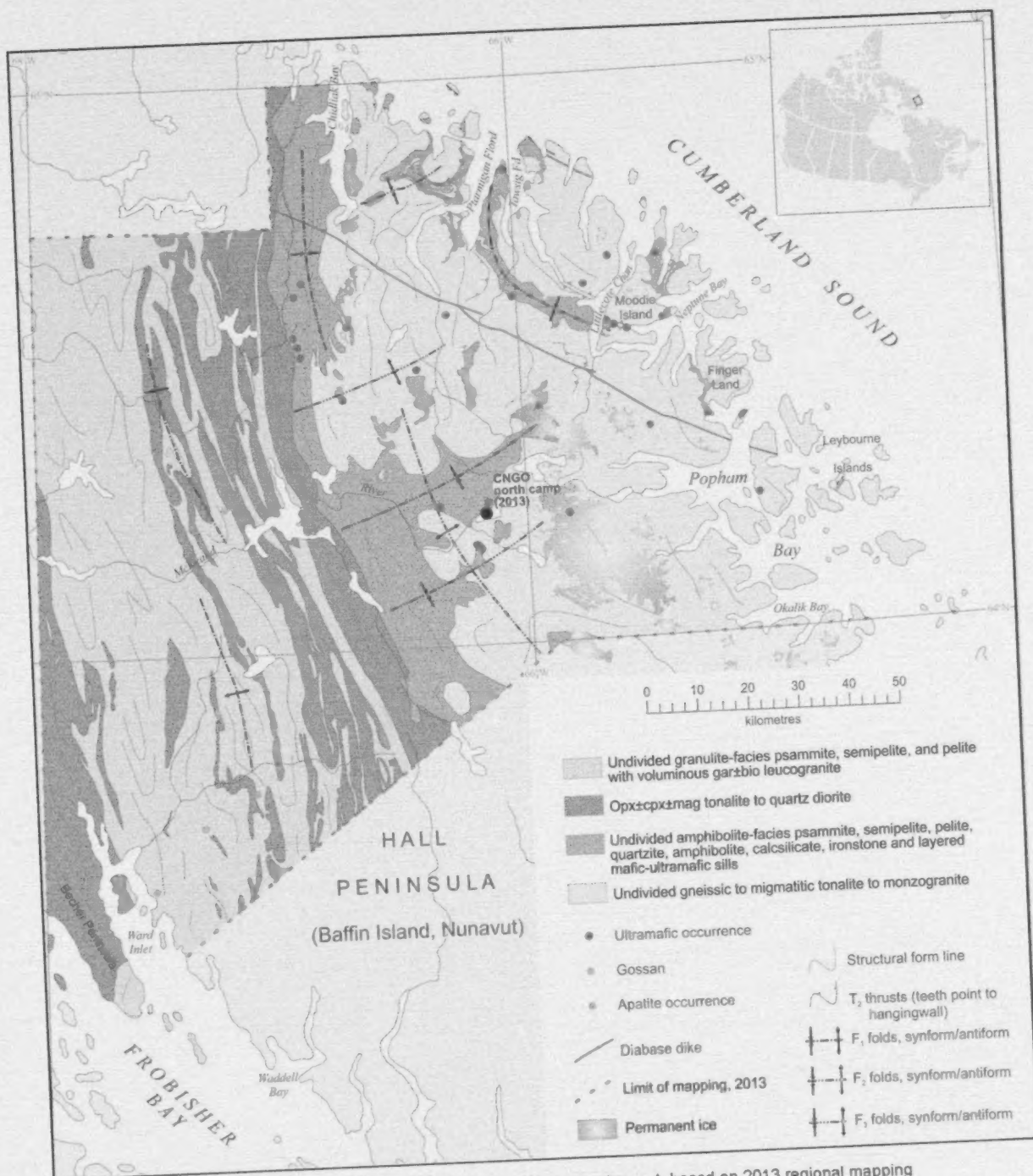
Figure 1: Simplified geology of northern Hall Peninsula, Nunavut, based on 2013 regional mapping

units are intruded by 1867 ±8 Ma (Rayner, 2014) garnet-leucogranite, interpreted as derived from partial melting of local metasedimentary units (Braden, 2013; Machado et al., 2013a; Dyck and St-Onge, 2014).

Regional observations

Similar to the southern portion of the peninsula, northern Hall Peninsula is underlain by Archean orthogneiss basement and supracrustal metasedimentary cover in the east, and by pelitic to psammitic metasedimentary strata inter-leaved with orthopyroxene-bearing diorite to monzogranite in the west (Figure 1). Due to the paucity of outcrop in the peninsula's interior, the nature of the boundary between the eastern and western lithological assemblages had remained enigmatic, with Machado et al. (2013a) inferring a major lithological boundary on southern Hall Peninsula obscured by intrusive plutonic rocks, based on an interpretation of regional aeromagnetic patterns (Figure 2) and traverse observations from the 2012 field season. Observations from the northernmost portion of the 2013 field area have instead revealed a gradational transition from
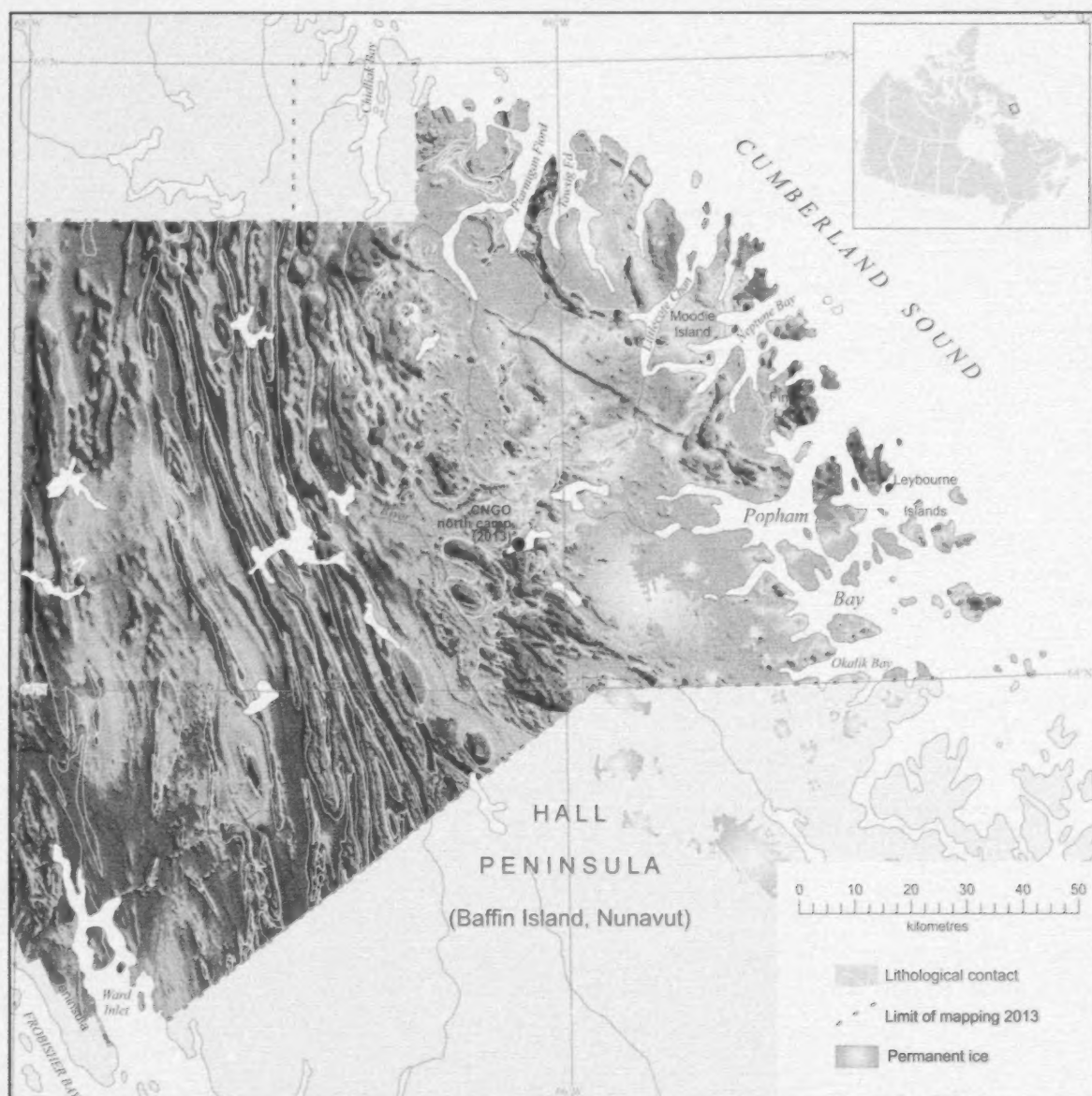
Figure 2: Lithological contacts overlain on the total-field magnetic susceptibility from the 1996–1997 and 2009 surveys (Pilkington and Oneschuk, 2007; Dumont and Dostaler, 2010a-g) on northern Hall Peninsula, Nunavut

crystalline basement- to metasedimentary strata-dominated map units, with the basement and cover rock units imbricated by a set of east-verging folds and thick-skinned thrusts. Additionally, a gradual increase in metamorphic grade preserved in supracrustal units, and a progression from lower to higher structural levels, were documented from east to west across northern Hall Peninsula. The sum of these observations, described more fully below, is regionally interpreted as characteristics of a normal transition from an orogenic foreland in the east to hinterland in the west.

Trans-Hudson Orogen

The Trans-Hudson Orogen (THO) is a Paleoproterozoic collisional orogenic belt that extends in a broad arcuate shape from northeastern to south-central North America (Hoffman 1988; Lewry and Collerson, 1990) and separates the lower-plate Superior craton from an upper-plate collage of Archean crustal blocks (Churchill Plate). On Baffin Island, the continental collisional zone records the southward migration of the Churchill Plate and its terminal collision with the Superior craton at 1.82–1.80 Ga (St-Onge et al., 2009). On Hall Peninsula, lithological associations and field observations in 2012 and 2013 allow for the field characterization of major map units as either predating, postdating or being synchronous with the THO continental collision.

Pre-THO rock units

Archean orthogneiss complex

The Archean basement orthogneiss complex is dominantly exposed on the eastern side of Hall Peninsula (NTS 026A; Figure 1). It comprises mostly gneissic to migmatitic tonalite to monzogranite, with local enclaves and pods of amphibolite, and crosscutting granite to syenogranite dikes (Machado et al., 2013a; From et al., 2014). A pervasive fabric is defined by compositional banding, and the alignment of biotite and hornblende, where present (Figure 3a). Crystallization ages of two basement samples, a tonalite gneiss and deformed megacrystic granite, collected on southern Hall Peninsula, indicate emplacement of these components at ca. 2.84 and 2.70 Ga, respectively (Rayner, 2014). Several hydrated ultramafic intrusions crosscut the basement orthogneiss and are locally wrapped by the pervasive gneissic foliation (Steenkamp et al., 2014). It is postulated that these ultramafic bodies may be associated with the emplacement of the mafic-ultramafic dikes and layered sills observed in the overlying cover stratigraphy.

The Archean orthogneiss has recorded several deformational, metamorphic and plutonic events. Detailed mapping of the basement orthogneiss by From et al. (2014) outlines a minimum of eight components, ranging in composition from tonalite to biotite-hornblende-monzogranite and syenogranite; each component is temporally defined using rela-

tive crosscutting relationships. The affinity of this crustal block, the characterization of the plutonic components, their respective emplacement ages and subsequent deformational features are currently under investigation (From et al., 2014).

Paleoproterozoic metasedimentary units

The Archean orthogneiss complex is disconformably overlain locally by a variably metamorphosed supracrustal sequence. The supracrustal units exposed in the eastern map area vary greatly in composition compared to the units in the western map area. The basal unit is a blue-grey quartzite with relic heavy-mineral bands defining the primary bedding. The quartzite ranges from about 1 m to 25 m in thickness (Figure 3b) and was clearly observed in contact with the Archean basement orthogneiss at several locations on northern Hall Peninsula. Overlying the quartzite is a unit of alternating psammite, semipelite and pelite (Figure 3c). This unit is ~600 m thick in places and weathers grey to rusty brown.

Above this lies a compositionally variable unit 100–400 m thick comprising semipelite, calcsilicate, meta-ironstone and compositionally variable amphibolite layers interpreted as metamorphosed volcaniclastic sedimentary rocks and rare subaerial mafic flows (Figure 3d; Mackay et al., 2013; MacKay and Ansdell, 2014). Additionally, beige quartzite and silicified gossanous layers are locally present in this unit.

From just west of Ptarmigan Fiord through to the western map boundary, the supracrustal stratigraphy becomes compositionally more homogeneous and is dominated by pelite and psammite. The observed compositional transition from margin-proximal supracrustal units with mafic components in the east to dominantly distal, deeper-water pelitic strata in the west suggests a progressive change in paleodepositional environment from east to west across northern Hall Peninsula. The whole supracrustal sequence is interpreted as representing a proximal shallow-marine to more distal continental-shelf and slope-rise setting with input of mafic material, possibly from a local rifting environment. In the east, slivers and panels of lower, margin-proximal supracrustal strata are contained within thick-skinned (basement and cover) imbricate folds and thrusts. Toward the west, a transition to imbricate fold and thrust structures involving stratigraphically higher and more distal supracrustal units was documented.

Mafic-ultramafic units

Ultramafic intrusions were documented in both the basement gneisses and within supracrustal strata. In the crystalline basement, peridotite bodies occur as isolated dikes or plugs that locally have been wrapped by the pervasive gneissic foliation. Ultramafic and mafic bodies ranging in composition from amphibolite and gabbro to peridotite
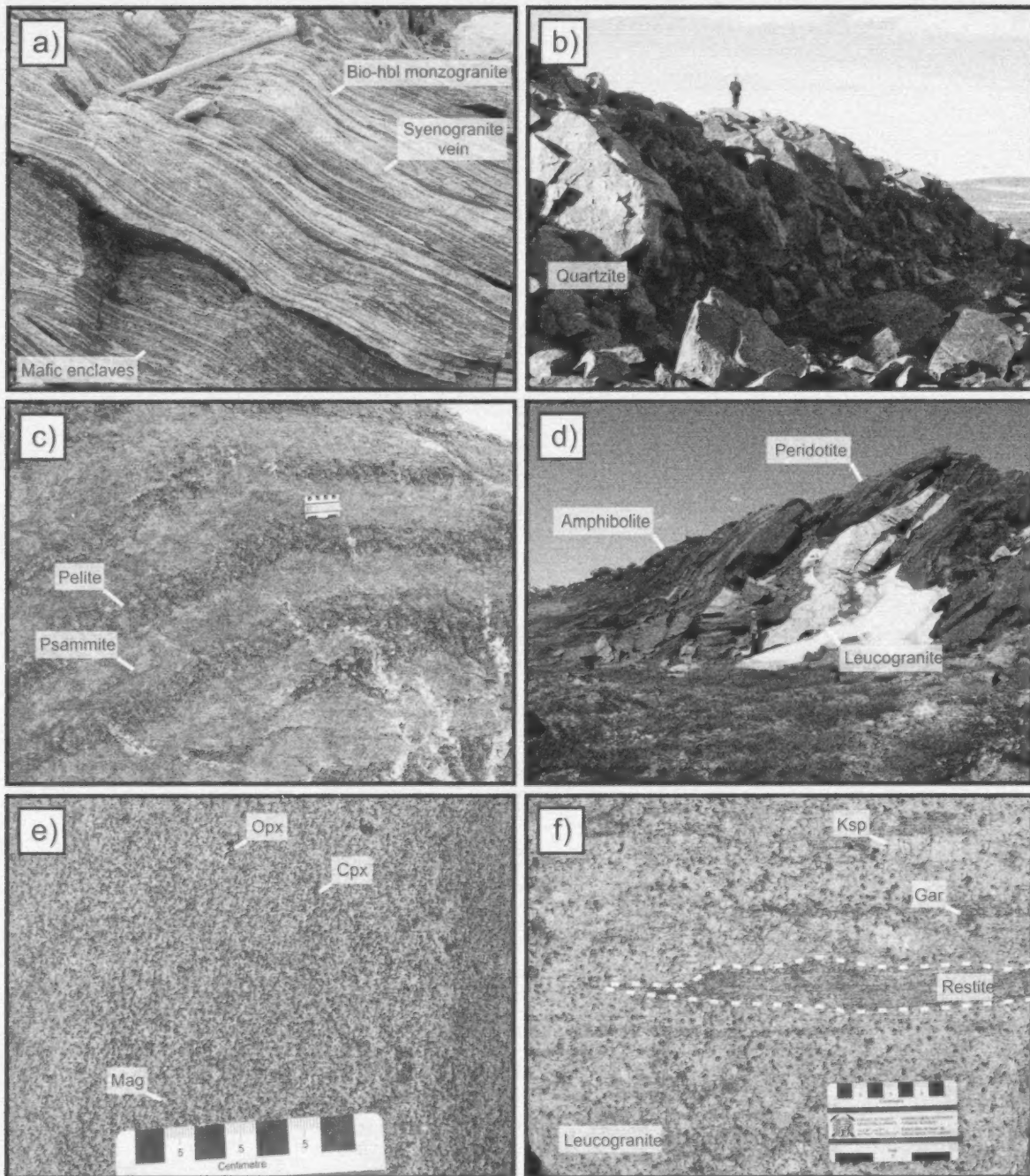
Figure 3: Lithological associations on northern Hall Peninsula, Nunavut, showing **a)** Archean basement of biotite-hornblende monzogranite with abundant mafic enclaves cut by a syenogranite vein; **b)** basal blue-grey supracrustal quartzite outcrop 24 m thick in contact with the underlying Archean basement behind the geologist (for scale); **c)** relict bedding locally remains clearly visible in eastern outcrops of the supracrustal pelitic to psammitic unit (photo courtesy of B. Dyck); **d)** supracrustal amphibolite intruded by peridotite and later by a muscovite-sillimanite-garnet leucogranite sill, with all rock units subsequently deformed; **e)** foliated mafic tonalite commonly observed in the western portion of the map area containing the granulite-facies mineral assemblage consisting of orthopyroxene+clinopyroxene+magnetite (photo courtesy of B. Dyck); **f)** restitic pelite surrounded by garnet-leucogranite with porphyroblastic K-feldspar likely derived from biotite dehydration-melting commonly found in the western portion of the map area. Hammer for scale in photograph is 90 cm long. Abbreviations: bio, biotite; cpx, clinopyroxene; gar, garnet; hbl, hornblende; ksp, K-feldspar; mag, magnetite; opx, orthopyroxene.

were commonly observed emplaced in the supracrustal rocks (Figure 3d) in the eastern map area. These become less common toward the west, where nevertheless a large layered mafic-ultramafic sill is well exposed (Steenkamp et al., 2014). Most ultramafic bodies have a metamorphic mineral assemblage consisting of tremolite, actinolite, phlogopite and serpentine, indicating postemplacement hydrothermal alteration. A regionally consistent mineral foliation, defined dominantly by aligned phlogopite and/or recrystallized elongate orthopyroxene and olivine, was observed at most peridotite localities (Steenkamp et al., 2014). Based on field relationships and evidence of deformation in both the ultramafic-mafic intrusions and their host, the relative timing of their emplacement followed sedimentary deposition of the Paleoproterozoic supracrustal sequence and preceded regional deformation associated with the THO.

Syn-THO rock units

West of Chidliak Fiord, several laterally continuous felsic intrusions cut into the psammitic to pelitic supracrustal strata. The panels range in width from 100 m to several kilometres and are elongated with a north-south orientation. The intrusive units typically contain megacrystic K-feldspar and, locally, minor proportions of orthopyroxene, clinopyroxene, garnet, biotite, hornblende and magnetite (Figure 3e). Rayner (2014) interprets the crystallization of a compositionally equivalent sample taken from a laterally contiguous panel in the southern field area at ca. 1.89 Ga.

Leucogranite was identified across northern Hall Peninsula, present as sills and dikes within the supracrustal sequence. The mineral assemblage muscovite+sillimanite+K-feldspar±garnet was observed in leucogranite sills up to 4 m thick in the east (Figure 3d). Toward the west, a gradational transition to the metamorphic mineral assemblage garnet+K-feldspar±biotite, and an increase in the abundance of leucogranite was documented (Figure 3f). Dyck and St-Onge (2014) suggest dehydration melting of muscovite and biotite in the psammitic to pelitic supracrustal units as the source of leucogranitic melt generation. The observed change in metamorphic mineral assemblages, coupled with a notable increase in the volume of leucogranite, suggests that metamorphic temperature conditions increased from east to west across the peninsula.

Deformation and metamorphism related to the THO

Evidence of deformation and metamorphism related to the THO is ubiquitous on Hall Peninsula. Three major deformation events are interpreted from the field observations collected during the 2013 mapping campaign. Evidence of these events, organized in order of their relative chronology, is described below and summarized in Figure 4.

D_1 east-west shortening (pre- to synthermal peak of metamorphism)

The earliest regional deformation features associated with the THO observed on Hall Peninsula indicate east-west crustal shortening (D_1). East-verging isoclinal folds (F_{1a}) of primary bedding (S_0; Figure 3c) in the supracrustal stratigraphy are generally moderately west-dipping. A metamorphic mineral foliation (S_{1a}) axial planar to F_{1a} is typically defined by the alignment of platy minerals in amphibolite-facies assemblages, such as biotite, muscovite and/or flattened faserkiesel sillimanite in pelitic metasedimentary rocks (Skipton and St-Onge, 2014). The S_{1a} fabric is pervasive throughout the basement orthogneiss.

Toward the western portion of the field area, the amphibolite-facies S_{1a} fabric is progressively refolded by a second set of pervasive granulite-facies, regional-scale east-verging isoclinal folds (F_{1b}), resulting in laterally continuous panels of alternating pelitic and psammitic supracrustal units (Figure 5a), leucogranite, and foliated tonalite to monzogranite (Dyck and St-Onge, 2014). Granulite-facies mineral assemblages progressively develop westward from Ptarmigan Fiord and overprint the amphibolite-facies assemblages and mineral textures. Garnet porphyroblasts, melt seams and elongated orthopyroxene crystals define a new metamorphic foliation (S_{1b}; Figure 5b) axial planar to F_{1b}. The earlier amphibolite-facies S_{1a} fabric is only preserved as inclusion trails in granulite-facies minerals, such as garnet, in the westernmost field area (Braden, 2013).

D_2 east-west shortening (post-thermal peak metamorphism)

Further east-west shortening (D_2) is exemplified by several east-verging, thick-skinned imbricate thrusts (T_2), which were observed along the northern and eastern coastline of Hall Peninsula in well-exposed cliff sections (Figure 5c). It

Paleoproterozoic structural development

- S_0: Bedding

D_1: east-west shortening (*pre- to syn-thermal peak*)
  - F_{1a} isoclinal folds of S_0 bedding
  - S_{1a} metamorphic foliation axial planar to F_{1a}
  - F_{1b} isoclinal folds of S_{1a}
  - S_{1b} metamorphic foliation axial planar to F_{1b}

D_2: east-west shortening (*post-thermal peak*)
  - T_2 thick-skinned thrusts
  - L_2 mineral stretching and elongate growth
  - F_2 thick-skinned folds

D_3: north-south shortening
  - F_3 thick-skinned folds
  - S_3 Crenulation cleavage axial planar to F_3

Figure 4: Relative sequence of observed textures and fabrics associated with the three interpreted regional deformation events of the Trans-Hudson Orogen on northern Hall Peninsula, Nunavut.
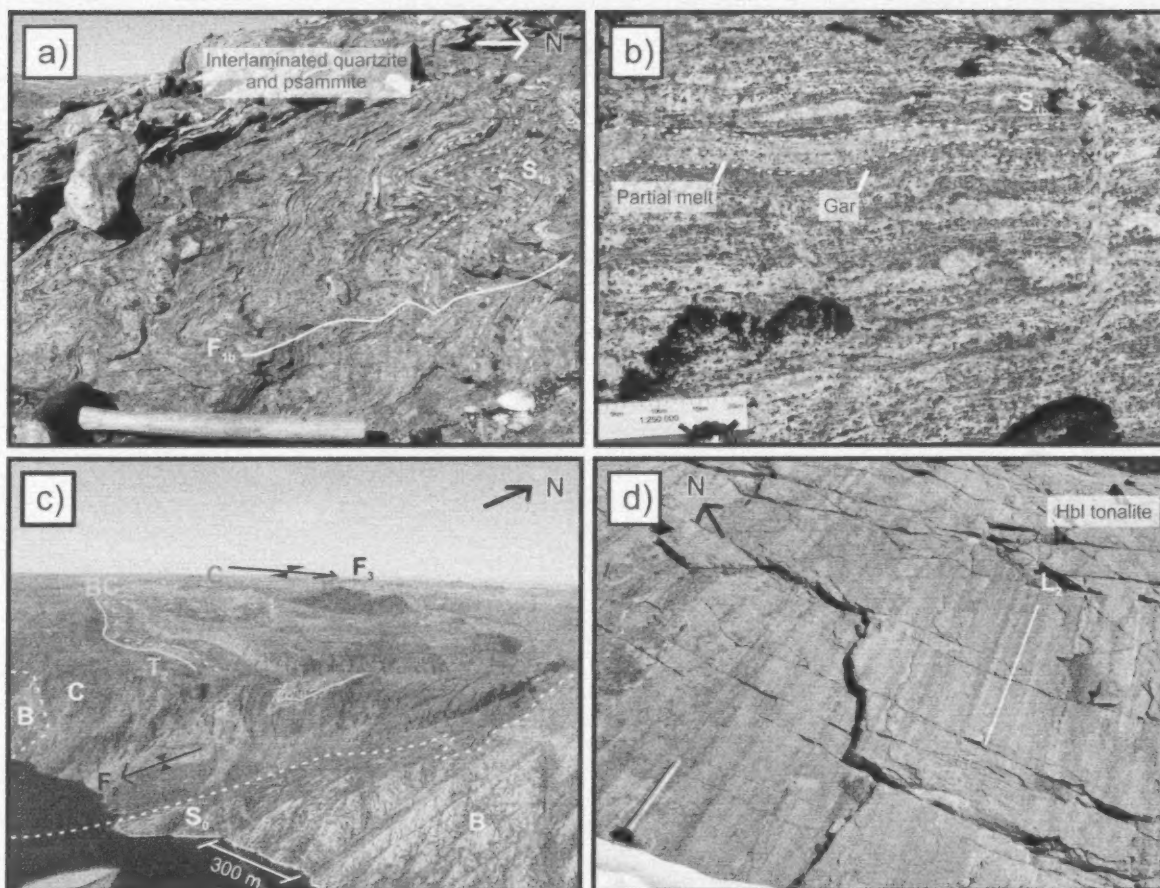
Figure 5: Structural features observed on northern Hall Peninsula, Nunavut: **a)** S_{1a} fabric in supracrustal interlaminated quartzite and psammite is disharmonically folded axial planar to F_{1b}; **b)** partial melt lenses and layers, and garnet porphyroblasts define the granulite-facies S_{1b} fabric in supracrustal pelitic strata; **c)** three T_2 thrust imbricates (lower in yellow, middle in orange and upper in red) exposed in multiple cliff cross-sections at Ptarmigan Fiord; dashed lines represent depositional basement-cover contacts and solid lines represent thrust contacts; the lowest imbricate folded axial planar to F_2 and all three imbricates later folded axial planar to F_3; **d)** L_2 lineations defined by recrystallized quartz and feldspar mineral aggregates in basement hornblende-tonalite at a T_2 thrust contact over supracrustal units. Hammer for scale in photographs is 40 cm long. Abbreviations: B, basement; C, cover; Gar, garnet; Hbl, hornblende.

is thought that these large-scale structures exist across the peninsula and south into the 2012 field area, although the extent and quality of outcrop exposure does not unequivocally demonstrate this. The observed thrusts incorporate slices of Archean basement and associated overlying supracrustal cover, and are characterized by strongly-deformed to mylonitic shear zones at the thrust contacts. Lineations (L_2) associated with T_2 are defined by elongate growth of amphibolite-facies mineral assemblages and recrystallized stretched mineral aggregates (quartz and feldspar rodding), oriented east to northeast (Figure 5d). Mafic enclaves in basement orthogneiss are documented as having clinopyroxene-bearing cores rimmed by hornblende oriented parallel to L_2. Where supracrustal units contain ultramafic sills in the footwalls of thrusts, chaotic folding and fabric reorientation was noted. The rigid ultramafic sills are commonly boudinaged, whereas the more

pliable pelite and psammite host wraps around and between the ultramafic pods.

Following T_2, east-west shortening continued with thick-skinned regional-scale folding (F_2) that resulted in variable reorientation of the thick-skinned thrust imbricates. Sub-vertical to overturned imbricates were observed in the Finger Land and Moodie Island areas (Figure 1).

D_3 north-south shortening

Regional-scale east- and west-plunging folds (F_3) have been identified across Hall Peninsula (Machado et al., 2013a). The F_3 folds are south verging and representative of north-south crustal shortening (D_3). Intersection of F_3 and F_{1b} or F_2 is responsible for the common ovoid map patterns. An S_3 crenulation cleavage, defined by muscovite, biotite and faserkiesel sillimanite reoriented axial planar to

F_3, is well developed in pelitic supracrustal units in the south-eastern portion of the field area (Skipton and St-Onge, 2014).

Late- to post-THO rock units

On northern Hall Peninsula, pegmatite dikes were recognized during the 2013 mapping efforts. They are mostly concentrated on the eastern side of the field area, crosscut all regional deformational fabrics and have not been subsequently deformed. The pegmatite dikes commonly comprise varying proportions of K-feldspar, plagioclase and quartz, with lesser amounts of muscovite, biotite, magnetite and black tourmaline. Graphic intergrowth of feldspar and quartz was documented at several localities.

Two laterally continuous, brown-weathering diabase dikes were observed in the northernmost field area. These are up to 12 m wide, strike east-southeast and crosscut all regional fabrics and felsic pegmatite dikes. They are likely related to the ca. 721–712 Ma Franklin magmatic event that emplaced mafic dikes and sills over a 2500 km lateral distance between Arctic Canada and Greenland (Heaman et al., 1992; Denyszyn et al., 2009). Additionally, a kimberlite dike 1 m wide was discovered within Peregrine Diamond Ltd.'s Chidliak property during the 2013 mapping program.

Economic considerations

A variety of geological features and occurrences with potential economic implications were recognized during the 2013 bedrock-mapping campaign on northern Hall Peninsula. Mafic-ultramafic dikes and layered sills with a similar geological context to that documented on Hall Peninsula have elsewhere been linked with Ni-Cu-platinum group element mineralization (e.g., the Raglan deposit in the Cape Smith Belt of northern Quebec; St-Onge and Lucas, 1993; Lesher, 2007; Steenkamp et al., 2014). Additionally, ultramafic bodies that have hydrated mineral assemblages may be suitable as carving stone. Several sites with carving stone potential were sampled on the peninsula and test carvings are currently being made. Possible mineralization in supracrustal meta-ironstone and pyrite- and pyrrhotite-bearing silicified gossanous layers is also being assessed. Investigations into the age, textures and geochemistry of the above rock units are to be carried out within the next year.

Abundant pegmatites on Hall Peninsula, containing muscovite, biotite and locally tourmaline, have been flagged for further investigation into their rare-earth element mineralization potential.

Supracrustal calcsilicate layers containing 3–5 mm long, pale-blue euhedral fluorapatite crystals were discovered in the west-central field area. High-quality fluorapatite crystals are a semiprecious gem that can be used in jewellery. Furthermore, these calcsilicate layers also locally contain lenses of impure marble, which could be harvested for carving purposes.

Ongoing development of the Archean basement-hosted Chidliak diamond property, currently held by Peregrine Diamonds Ltd., continues to uncover new kimberlite occurrences. Outside of this property, the potential to make new kimberlite discoveries remains.

Acknowledgments

References

Ansdell, K., Hunchak, A. and Pell, J. 2012: Precambrian basement rocks in the vicinity of the Chidliak kimberlites: initial mapping on the Hall Peninsula, Baffin Island; Geological Association of Canada-Mineralogical Association of Canada, Joint Annual Meeting, St. John's, Newfoundland, program with Abstracts, v. 35, p. 5–6.

Blackadar, R.G. 1967: Geological reconnaissance, southern Baffin Island, District of Franklin; Geological Survey of Canada, Paper 66-47.

Braden, Z.M. 2013: Paleoproterozoic pressure-temperature-deformation path in the Newton Fiord region, eastern Baffin Island, Nunavut; B.Sc. thesis, Dalhousie University, 95 p.

Denyszyn, S.W., Halls, H.C., Davis, D.W. and Evans, D. A.D. 2009: Paleomagnetism and U-Pb geochronology of Franklin dykes in High Arctic Canada and Greenland: a revised age and paleomagnetic pole constraining block rotations in the Nares Strait region; Canadian Journal of Earth Science, v. 46, p. 689–705.

Dumont, R. and Dostaler, F. 2010a: Geophysical Series, NTS 25-O/NE, Aeromagnetic Survey Hall Peninsula, Nunavut; Geological Survey of Canada, Open File 6419, scale 1:100 000.

Dumont, R. and Dostaler, F. 2010b: Geophysical Series, NTS 25-O/NW, Aeromagnetic Survey Hall Peninsula, Nunavut;

Geological Survey of Canada, Open File 6420, scale 1:100 000.

Dumont, R. and Dostaler, F. 2010c: Geophysical Series, NTS 26 A/SE, Aeromagnetic Survey Hall Peninsula, Nunavut; Geological Survey of Canada, Open File 6425, scale 1:100 000.

Dumont, R. and Dostaler, F. 2010d: Geophysical Series, NTS 6 A/SW, Aeromagnetic Survey Hall Peninsula, Nunavut; Geological Survey of Canada, Open File 6426, scale 1:100 000.

Dumont, R. and Dostaler, F. 2010e: Geophysical Series, NTS 26 A/NW and part of 26 A/NE, Aeromagnetic Survey Hall Peninsula, Nunavut; Geological Survey of Canada, Open File 6427, scale 1:100 000.

Dumont, R. and Dostaler, F. 2010f: Geophysical Series, NTS 26 B/SE, Aeromagnetic Survey Hall Peninsula, Nunavut; Geological Survey of Canada, Open File 6428, scale 1:100 000.

Dumont, R. and Dostaler, F. 2010g: Geophysical Series, NTS 26 B/NE, Aeromagnetic Survey Hall Peninsula, Nunavut; Geological Survey of Canada, Open File 6429, scale 1:100 000.

Dyck, B.J. and St-Onge, M.R. 2014: Dehydration melting reactions, leucogranite emplacement and the Paleoproterozoic structural evolution of Hall Peninsula, Baffin Island, Nunavut; *in* Summary of Activities 2013, Canada-Nunavut Geoscience Office, p. 73–84.

From, R.E., Camacho, A.L. and St-Onge, M.R. 2013: Preliminary observations on the nature and origin of the eastern orthogneiss complex of southern Hall Peninsula, Baffin Island, Nunavut; *in* Summary of Activities 2012, Canada-Nunavut Geoscience Office, p. 43–54.

From, R.E., St-Onge, M.R. and Camacho, A.L. 2014: Preliminary characterization of the Archean orthogneiss complex of Hall Peninsula, Baffin Island, Nunavut: insights from the 'snow bowl' study area; *in* Summary of Activities 2013, Canada-Nunavut Geoscience Office, p. 53–62.

Heaman, L.M., LeCheminant, A.N. and Rainbird, R.H. 1992: Nature and timing of Franklin igneous events, Canada: implications for a Late Proterozoic mantle plume and the breakup of Laurentia; Earth and Planetary Science Letters, v. 109, no. 1–2, p. 117–131.

Hoffman, P.F. 1988: United Plates of America, the birth of a craton: Early Proterozoic assembly and growth of Laurentia; Annual Review of Earth and Planetary Sciences, v. 16, p. 543–603.

Leblanc-Dumas, J., Allard, M. and Tremblay, T. 2013: Quaternary geology and permafrost characteristics in central Hall Peninsula, Baffin Island, Nunavut; *in* Summary of Activities 2012, Canada-Nunavut Geoscience Office, p. 101–108.

Lesher, C.M. 2007: Ni-Cu-(PGE) deposits in the Raglan area, Cape Smith Belt, New Quebec; *in* Mineral Deposits of Canada: a Synthesis of Major Deposit Types, District Metallogeny, the Evolution of Geological Provinces, and Exploration Methods, W.D. Goodfellow (ed.), Geological Association of Canada, Special Publication, v. 5, p. 351–386.

Lewry, J. F. and Collerson, K. D. 1990: The Trans-Hudson Orogen: extent, subdivision, and problems; *in* The Early Proterozoic Trans-Hudson Orogen of North America, J.F. Lewry and M.R. Stauffer (ed.), Geological Association of Canada, Special Paper, v. 37, p. 1–14.

Machado, G., Bilodeau, C., Takpanie, R., St-Onge, M.R., Rayner, N.M., Skipton, D.R., From, R.E., MacKay, C.B., Creason, C.G. and Braden, Z.M. 2013a: Hall Peninsula regional bedrock mapping, Baffin Island, Nunavut: summary of fieldwork; *in* Summary of Activities 2012, Canada-Nunavut Geoscience Office, p. 13–22.

Machado, G., Bilodeau, C. and St-Onge, M.R. 2013b: Geology, southern part of Hall Peninsula, south Baffin Island, Nunavut; Geological Survey of Canada, Canadian Geoscience Map 135 (preliminary); Canada-Nunavut Geoscience Office, Open File Map 2013-1, scale 1:250 000. doi:10.4095/292443.

MacKay, C.B., Ansdell, K.M., St-Onge, M.R., Machado, G. and Bilodeau, C. 2013: Geological relationships in the Qaqqanittuaq area, southern Hall Peninsula, Baffin Island, Nunavut; *in* Summary of Activities 2012, Canada-Nunavut Geoscience Office, p. 55–64.

MacKay, C.B. and Ansdell, K.M. 2014: Geochemical study of mafic and ultramafic rocks from southern Hall Peninsula, Baffin Island, Nunavut; *in* Summary of Activities 2013, Canada-Nunavut Geoscience Office, p. 85–92.

Nichols, K.M.A., Stachel, T., Pell, J. A. and Mate, D.J. 2013: Diamond sources beneath the Hall Peninsula, Baffin Island, Nunavut: preliminary assessment based on microdiamonds; *in* Summary of Activities 2012, Canada-Nunavut Geoscience Office, p. 113–120.

Pell, J., Grütter, H., Neilson, S., Lockhart, G., Dempsey, S. and Grenon, H. 2013: Exploration and discovery of the Chidliak kimberlite province, Baffin Island, Nunavut: Canada's newest diamond district; *in* Proceedings of 10th International Kimberlite Conference, D.G. Pearson (ed.), Geological Society of India, Special Issue, v. 2, p. 209–227, doi: 10.1007/978-81-322-1173-0-14.

Pilkington, M. and Oneschuk, D. 2007: Aeromagnetic and gravity; *in* Digital Geoscience Atlas of Baffin Island (south of 70°N and east of 80°W), Nunavut, Geological Survey of Canada, Open File 5116.

Rayner, N.M., Machado, G., Bilodeau, C. and St-Onge, M.R. 2013: Uranium-lead geochronological studies of Hall Peninsula, Baffin Island, Nunavut: contributions to mapping and tectonics; *in* Summary of Activities 2012, Canada-Nunavut Geoscience Office, p. 23–28.

Rayner, N.M. 2014: New U-Pb geochronological results from Hall Peninsula, Baffin Island, Nunavut; *in* Summary of Activities 2013, Canada-Nunavut Geoscience Office, p. 39–53.

Scott, D.J. 1996: Geology of the Hall Peninsula east of Iqaluit, southern Baffin Island; *in* Current Research 1996-C, Geological Survey of Canada, p. 83–91.

Scott, D.J. 1999: U-Pb geochronology of the eastern Hall Peninsula, southern Baffin Island, Canada: a northern link between the Archean of West Greenland and the Paleoproterozoic Torngat Orogen of northern Labrador; Precambrian Research, v. 93, p. 5–26.

Skipton, D.R., Schneider, D. A. and St-Onge, M.R. 2013: Preliminary observations on Archean and Paleoproterozoic metamorphism and deformation of the southern Hall Peninsula, Baffin Island, Nunavut; *in* Summary of Activities 2012, Canada-Nunavut Geoscience Office, p. 29–42.

Skipton, D.R. and St-Onge, M.R., 2014: Paleoproterozoic deformation and metamorphism in metasedimentary rocks west of Okalik Bay: a field template for the evolution of eastern Hall Peninsula, Baffin Island, Nunavut; *in* Summary of Activities 2013, Canada-Nunavut Geoscience Office, p. 63–72.

St-Onge, M.R. and Lucas, S.B. 1993: Controls on the regional distribution of iron-nickel-copper-platinum-group element sul-

fide mineralization in the eastern Cape Smith Belt, Quebec; Canadian Journal of Earth Sciences, v. 31, p. 206–218.

St-Onge, M.R., Scott, D.J. and Wodicka, N. 2002: Review of crustal architecture and evolution in the Ungava Peninsula–Baffin Island area: connection to the Lithoprobe ECSOOT transect; Canadian Journal of Earth Sciences, v. 39, p. 589–610.

St-Onge, M.R., Searle, M.P. and Wodicka, N. 2006: Trans-Hudson Orogen of North America and Himalaya-Karakoram-Tibetan Orogen of Asia: structural and thermal characteristics of the lower and upper plates; Tectonics, v. 25, p. 1–22, doi: 10.1029/2005TC001907.

St-Onge, M.R., Wodicka, N. and Ijewliw, O., 2007: Polymetamorphic evolution of the Trans-Hudson Orogen, Baffin Island, Canada: integration of petrological, structural and geochronological data; Journal of Petrology, v. 48, p. 271–302, doi: 10.1093/petrology/eg1060.

St-Onge, M.R., Van Goole, J.A.M., Garde, A.A. and Scott, D.J. 2009: Correlation of Archaean and Palaeoproterozoic units between northeastern Canada and western Greenland: constraining the pre-collisional upper plate accretionary history of the Trans-Hudson Orogen; in Earth Accretionary Systems in Space and Time, P.A. Cawood and A. Kröner (ed.); The Geological Society, London, Special Publications, v. 318, p. 193–235.

Steenkamp, H.M., Bros, E.R. and St-Onge, M.R. 2014: Altered ultramafic and layered mafic-ultramafic intrusions: new economic and carving stone potential on northern Hall Peninsula, Baffin Island, Nunavut; in Summary of Activities 2013, Canada-Nunavut Geoscience Office, p. 11–20.

Tremblay, T., Leblanc-Dumas, J., Allard, M., Gosse, J.C., Creason, C.G., Peyton, P., Budkewitsch, P. and LeBlanc, A.M. 2013: in Summary of Activities 2012, Canada-Nunavut Geoscience Office, p. 93–100.

Tremblay, T., Leblanc-Dumas, J., Allard, M., Ross, M. and Johnson, C. 2014: Surficial geology of central Hall Peninsula, Baffin Island, Nunavut: summary of the 2013 field season; in Summary of Activities 2013, Canada-Nunavut Geoscience Office, p. 109–120.

Zhang, S. and Pell, J. 2013: Study of sedimentary rock xenoliths from kimberlites on Hall Peninsula, Baffin Island, Nunavut; in Summary of Activities 2012, Canada-Nunavut Geoscience Office, p. 107–112.

New U-Pb geochronological results from Hall Peninsula, Baffin Island, Nunavut

N.M. Rayner[1]

[1]Geological Survey of Canada, Natural Resources Canada, Ottawa, Ontario, nrayner@nrcan.gc.ca

Abstract

Ages for ten bedrock samples from across southern Hall Peninsula, Baffin Island, Nunavut were determined by zircon U-Pb geochronology. Ages for the basement complex in the eastern portion of the peninsula include tonalite gneiss dated at 2841± 3 Ma and deformed megacrystic granite with a crystallization age of 2701 ±2 Ma. Four metasedimentary samples from locations across the peninsula are demonstrably Paleoproterozoic, with a significant 2.1–1.9 Ga zircon population and maximum ages of deposition that range from 2126 ±16 to 1906 ±9 Ma. A quartzite sampled from within the gneissic basement–dominated eastern half of the peninsula contains only Archean detritus and is interpreted to represent a locally sourced, basal clastic package. Metasedimentary rocks in the west are cut by extensive granulite-grade diorite to monzogranite dated at 1892 ±7 Ma. White-weathering monzogranite cutting psammite and amphibolite yields an age of 1873 ±6 Ma. Because this monzogranite was subsequently affected by a regionally pervasive, east-west shortening, deformation episode (D_1), this age is also a maximum age constraint on the timing of D_1 deformation. A sample of weakly to undeformed leucogranite with distinct lilac-coloured garnet is dated at 1867 ±8 Ma, bracketing the end of D_1.

Résumé

Les âges radiométriques de dix échantillons provenant de localités dans le sud de la péninsule Hall, dans l'île de Baffin, au Nunavut, ont été obtenus au moyen de la datation U-Pb sur zircon. Les âges associés au socle de la partie orientale de la péninsule proviennent d'un gneiss tonalitique dont l'âge a été établi à 2841 ±3 Ma et d'un granite mégacristallin dont l'âge de cristallisation a été fixé à 2701 ±2 Ma. Quatre échantillons métasédimentaires provenant de localités situées dans l'ensemble de la péninsule datent du Paléoprotérozoïque, ainsi que le démontre une population de zircons notable dont l'âge a été établi à 2,1–1,9 Ga et une période de sédimentation qui aurait eu lieu, au maximum, entre il y a 2126 ±16 Ma et 1906 ±9 Ma. Un échantillon de quartzite provenant du socle gneissique, qui caractérise la partie orientale de la péninsule, ne renferme que des débris archéens et on estime qu'il s'agit d'un ensemble clastique basal d'origine locale. Les roches métasédimentaires à l'ouest sont recoupées par de grandes unités dioritiques à monzogranitiques métamorphisées au faciès des granulites dont l'âge a été établi à 1892 ±7 Ma. Un monzogranite, auquel l'altération confère une teinte blanchâtre, recoupe la psammite et l'amphibole et a donné un âge U-Pb de 1873±6 Ma. La phase de déformation intense d'échelle régionale caractérisée par un raccourcissement est-ouest (D_1) qu'a subi subséquemment le monzogranite fait que l'âge établi représente également la limite maximum d'âge pouvant correspondre à la phase de déformation D_1. Un échantillon de leucogranite à grenats de couleur lilas distinctive et dont le degré de déformation varie de faible à inexistant permet de fixer la fin de l'épisode D_1 à 1867 ±8 Ma.

Introduction

The Hall Peninsula Integrated Geoscience Project (HPIGP) is being led by the Canada-Nunavut Geoscience Office in collaboration with Geological Survey of Canada (GSC) and a number of university and community partners. The focus is on bedrock and surficial mapping and a range of thematic studies that includes Archean and Paleoproterozoic tectonics and geochronology. This paper presents the first results from a comprehensive U-Pb geochronology research program carried out by the geochronology laboratories of the GSC in support of new 1:250 000 geological maps of Hall Peninsula, Baffin Island, Nunavut (Figure 1; Machado et al., 2013a). A detailed summary of the geology of Hall Peninsula can be found in Machado et al. (2013b), but is briefly summarized here. The eastern half of the peninsula is dominated by an orthogneiss complex ranging in composition from tonalite to syenogranite. Clastic metasedimentary rocks ranging from quartzite to psammite to semipelite, from the central and eastern part of the peninsula, are commonly interbedded with thin mafic horizons tentatively interpreted as gabbroic sills, minor marble or calcsilicate and minor iron formation (Machado et al., 2013a, b). Psammite and minor quartzite in the west are more rarely observed in association with mafic or calcareous rocks, and instead are intruded by voluminous granulite-grade monzogranite to diorite as well as white-weathering, garnet-biotite leucogranite, interpreted as the product of partial melting of the metasedimentary rocks.

In this paper, zircon U-Pb results from 10 samples from across Hall Peninsula are presented. The samples were analyzed using the sensitive high-resolution ion microprobe (SHRIMP) at the GSC. A separate section for each sample contains lithological and zircon descriptions, as well as a discussion of the geochronological results and interpretation. The objective of the geochronology research component of the Hall Peninsula Integrated Geoscience Project is to provide temporal pins for the geological observations. The suite of dated samples achieves this objective by characterizing the age range of the exposed tectonostratigraphic basement, constraining the maximum age of deposition of extensive metasedimentary assemblages and characterizing their provenance signature, and bracketing the timing of deformation through age determinations of Paleoproterozoic plutonic suites.

Analytical procedures

Seven of the ten samples were disaggregated using standard crushing and pulverizing techniques followed by density separation using a Wilfley table; the remaining three samples were comminuted using a CNT Spark-2 electric pulse disaggregator (EPD; Rudashevsky et al., 1995). All samples were subsequently separated by density using heavy liquids. A magnetic separator was used to isolate a zircon separate. Details regarding the procedure, or any deviations from it, are noted in the sections relating to specific samples.

The SHRIMP analytical procedures followed those described by Stern (1997), with standards and U-Pb calibration methods following Stern and Amelin (2003). Briefly, zircons were cast in 2.5 cm diameter epoxy mounts (GSC epoxy mounts #670, 677, 679, 690) along with fragments of the GSC laboratory standard zircon (z6266, with ^{206}Pb/^{238}U age = 559 Ma). The midsections of the zircons were exposed using 9, 6 and 1 μm diamond compounds, and the internal features of the zircons (such as zoning, structures and alteration) were characterized in backscattered electron (BSE) mode using a Zeiss Evo® 50 scanning electron microscope. The count rates of 11 masses including background were sequentially measured with a single electron multiplier. Offline data processing was accomplished using SQUID2 (version 2.22.08.04.30, revised April 30, 2008). The 1σ external errors of ^{206}Pb/^{238}U ratios reported in the data table incorporate the error in calibrating the standard. Common Pb correction used the Pb composition of the surface blank (Stern, 1997). Details of the analytical session, including spot size, number of scans, calibration error and the applications of any intra-element fractionation corrections are given in the footnotes of the data table (Rayner, 2014[2]). Isoplot v. 3.00 (Ludwig, 2003) was used to generate concordia plots and calculate weighted means. The error ellipses on the concordia diagrams and the weighted mean errors in the text and on the figures are reported at the 2σ uncertainty level. Probability density diagrams were generated using AgeDisplay (Sircombe, 2004).

Results

Basement rocks

Tonalite, Beekman Peninsula (12MBC-F105A)

Sample description

A sample of tonalite gneiss was collected on Beekman Peninsula, to contribute to the age characterization of the eastern, tonalite-dominated portion of Hall Peninsula (Figure 1). The tonalite sample is exposed in contact with, and structurally above, a metasedimentary panel comprising psammite, semipelite, calcsilicate and garnet amphibolite. The contact between the tonalite and the metasedimentary package is parallel with the penetrative fabric found in both units, although the intensity of the fabric increases with proximity to the contact. The tonalite is characterized by banding corresponding to the injection of thin monzogranite stringers (Figure 2a) that are not present in the adja-
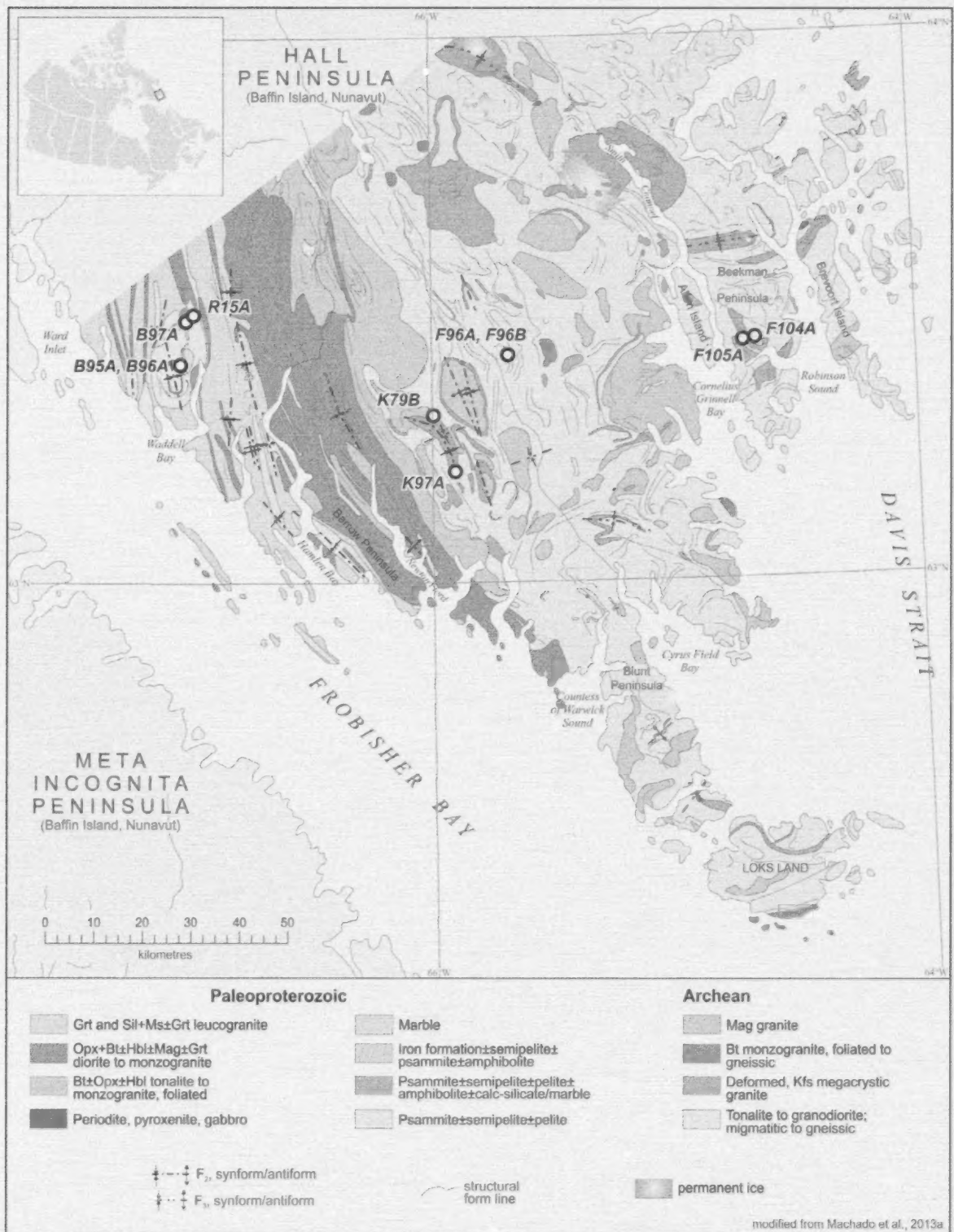
Figure 1: Simplified geology of Hall Peninsula, Nunavut (modified from Machado et al., 2013a), showing the locations of zircon geochronology samples described in this paper. Abbreviated sample names are given for clarity. The prefix 12MBC- is used for all samples in the text. Mineral abbreviations: Bi, biotite; Grt, garnet; Hbl, hornblende; Kfs, potassium feldspar; Mag, magnetite; Ms, muscovite; Opx, orthopyroxene; Sil, sillimanite.

cent supracrustal units. These stringers were avoided during sampling for geochronology.

Zircon description

This sample was disaggregated using standard crushing and grinding procedures. A magnetic separator was used to isolate a zircon separate and the grains were hand-picked from the nonmagnetic @ 3° side-slope fraction. Abundant, large zircon grains were recovered. The zircon population consistently exhibits oscillatory zoning (Figure 3a, b). Rare grains have thin, unzoned, high-U (bright in BSE images) rims (Figure 3b, grain 60).

Results and interpretation

A total of 38 analyses were conducted on 28 separate zircon grains, yielding $^{207}Pb/^{206}Pb$ ages between 2869 Ma and 1779 Ma (Rayner, 2014). The majority of the analyses form a cluster with a mean age of 2841 ±3 Ma (n = 20, mean square of weighted deviates [MSWD] = 1.7), which is interpreted as the crystallization age of the tonalite (Figure 3c). Two zircons yield slightly older ages of ca. 2.87 Ga, interpreted as an inherited component. Younger ages not included in the calculation of the weighted mean include analyses from zircon rims, as well as replicate analyses within zircon cores. These younger ages are largely nonreproducible. Analysis of two high-U, low U-Th unzoned rims suggest a ca. 1.8 Ga metamorphic overprint. This overprint may be responsible for minor Pb loss from the Archean zircon, accounting for some of the scatter to younger ages. A third high-U, low U-Th rim yields a discordant $^{207}Pb/^{206}Pb$ age of ca. 2.1 Ga, interpreted as a mixed age due to overlap of the analytical spot onto an Archean core.

Strongly deformed megacrystic granite, central Hall Peninsula (12MBC-F96A)

Sample description

A basement sample of strongly deformed, K-feldspar megacrystic granite was collected from within east-central Hall Peninsula, approximately 40 km west of Allen Island (Figures 1, 2b, c). This unit was formerly described as rapakivi granite (Machado et al., 2013a, b). The granite is in contact with, and is structurally above, a west-dipping metasedimentary assemblage including psammite-semipelite, as well as minor marble, quartzite and diorite. It is inferred that the plutonic phase is part of the eastern basement gneiss complex. The contact between the metasedimentary assemblage and the deformed megacrystic granite is tectonized, and clear intrusive relationships are not preserved.

Zircon description

This sample was disaggregated using standard crushing and grinding procedures. A magnetic separator was used to isolate a zircon separate and the grains were hand-picked from the nonmagnetic @ 3° side-slope fraction. Abundant, large, prismatic zircon grains were recovered (Figure 3d).
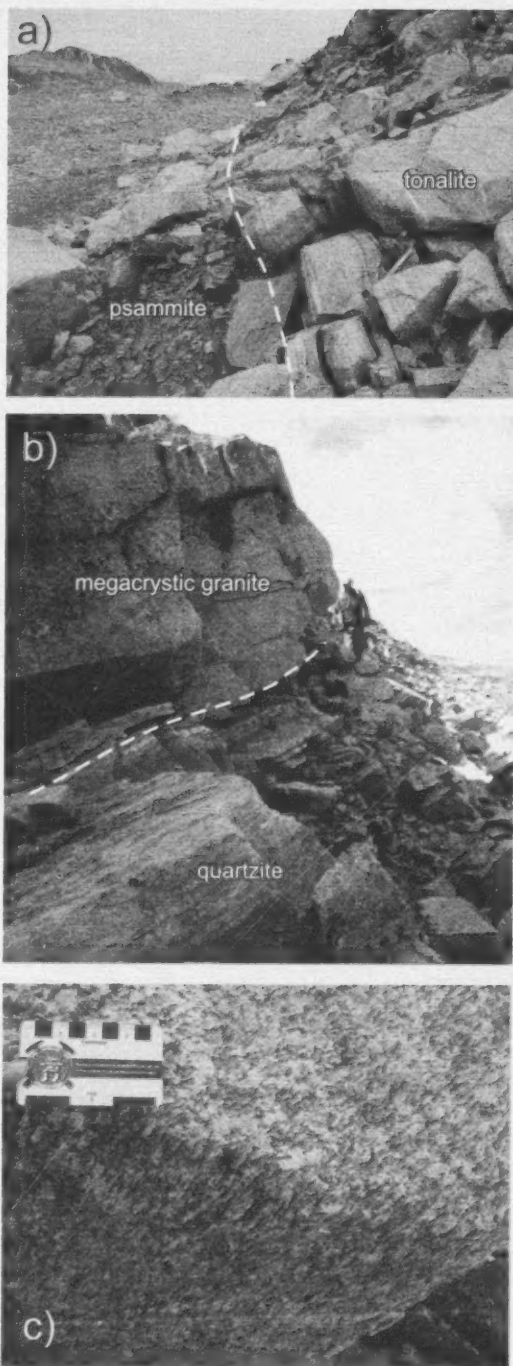
Figure 2: Field photographs of the basement samples and relationships discussed in this paper: a) contact between structurally overlying foliated grey tonalite gneiss (sample 12MBC-F105A) and flaggy, rusty psammite equivalent to sample 12MBC-F104A; view to the southeast, hammer is 40 cm long; b) strongly deformed megacrystic pink granite (sample 12MBC-F96A) structurally overlying white quartzite (sample 12MBC-F96B)+marble+psammite assemblage; view to the north, geologist is 170 cm tall; c) detail of strongly flattened and lineated K-feldspar phenocrysts (augen) in sample 12MBC-F96A.
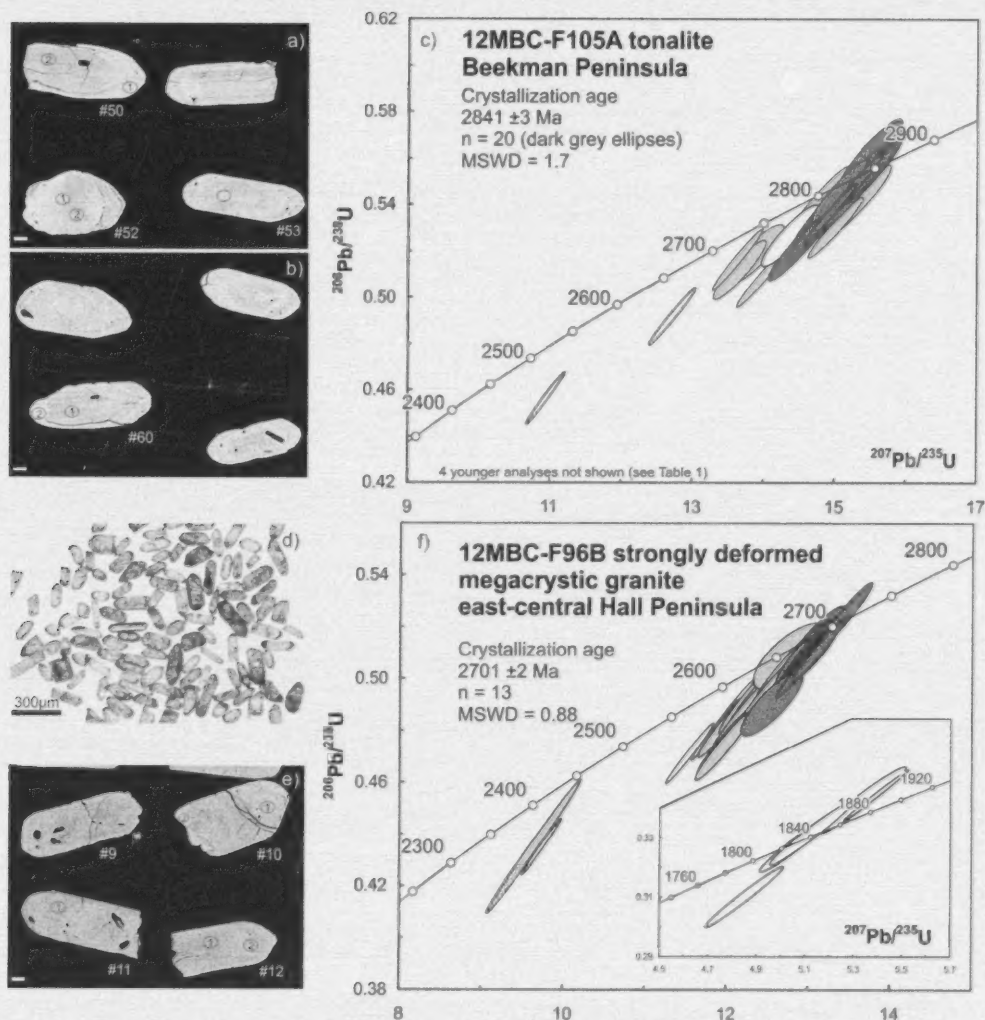
Figure 3: Zircon images and concordia diagrams for Hall Peninsula, Nunavut, basement samples. Ellipses plotted and mean ages reported at the 2σ confidence level: **a, b)** backscattered electron (BSE) images of zircons from sample 12MBC-F105A; white scale bar is 20 μm; white grain numbers and black ellipses with spot numbers correspond to analyses in Rayner (2014); **c)** concordia diagram of U-Pb results from sample 12MBC-F105A; dark grey ellipses correspond to analyses included in the calculation of the weighted mean, light grey ellipses are excluded from the calculation, unfilled ellipses denote analyses from zircon rims (see text for discussion); **d)** transmitted light image of zircon grains recovered from sample 12MBC-F96A; **e)** BSE images of zircons from sample 12MBC-F96A; white scale bar is 20 μm,; white grain numbers and black ellipses with spot numbers correspond to analyses in Rayner (2014); **f)** concordia diagram of U-Pb results from sample 12MBC-F96A; dark grey ellipses correspond to analyses included in the calculation of the weighted mean, light grey ellipses are excluded from the calculation, unfilled ellipses (including inset) denote analyses from zircon rims (see text for discussion).

In BSE images, the zircons are commonly oscillatory zoned (Figure 3e). Rare grains have thin, unzoned, high-U (bright in BSE images) rims (Figure 3e, grain 10).

Results and interpretation

A total of 38 analyses were conducted on 27 separate zircon grains, yielding $^{207}Pb/^{206}Pb$ ages between 2708 and 1832 Ma (Rayner, 2014). A cluster of the 13 oldest zircons yield a weighted mean $^{207}Pb/^{206}Pb$ age of 2701 ±2 Ma (MSWD = 0.9), which is interpreted as the crystallization age of the tonalite (Figure 3f). Twenty analyses yield dates between 2689 and 2463 Ma and are not included in the calculation of the weighted mean. These younger ages are generally not reproduced by replicate analyses on the same grain and are interpreted to represent nonzero age Pb loss. Analysis of five high-U, low U-Th unzoned rims yield ages between 1856 and 1832 Ma. These ages are interpreted to record a metamorphic overprint related to the Trans-Hud-

son Orogen; however, due to the limited number of analyses and their nonreproducibility, no metamorphic age is reported here.

Supracrustal rocks

Psammite, Beekman Peninsula (12MBC-F104A)

Sample description

Sample 12MBC-F104A is a biotite-garnet psammite from an extensive metasedimentary panel exposed on Beekman Peninsula (Figure 1). The metasedimentary assemblage includes minor semipelite, calcsilicate and garnet amphibolite. An early, pervasive metamorphic foliation defined by aligned biotite and sillimanite knots (S_{1a}) dips to the southwest and is subsequently folded. The sampled psammite was collected from approximately 100 m structurally below the tonalite gneiss described earlier (sample 12MBC-F105A). The psammite is progressively more flaggy approaching the contact with the strongly foliated tonalite. The sampled horizon is steeply west-dipping and characterized by a well-developed parting parallel to foliation (Figure 4a). This sample was collected for U-Pb detrital zircon geochronology to characterize the metasedimentary packages from eastern Hall Peninsula and to test whether these include Archean and/or Paleoproterozoic strata.

Zircon description

This sample was disaggregated using standard crushing and grinding procedures. A magnetic separator was used to isolate a zircon separate and the grains were hand-picked from the nonmagnetic @ 10° side-slope fraction. Abundant, large, zircon grains were recovered, ranging in colour from colourless to dark brown (Figure 5a). Most grains do not preserve well-defined facets and appear subrounded, either due to sedimentary transport or metamorphic resorption. Oscillatory zonation is commonly observed in BSE images, as are thin, high-U rims.

Results and interpretation

A total of 68 analyses were conducted from the internal zones/cores of 63 separate grains (Rayner, 2014). An additional seven analyses were carried out on zircon rims. The maximum age of deposition of this psammite is 1959 ±12 Ma, defined by three replicates on the youngest detrital zircon (grain 90). This grain is part of a significant population of Paleoproterozoic detritus with important modes at 1.96 and 2.0 Ga (Figure 5a). Older Paleoproterozoic detritus is sparsely represented, with a significant, secondary detrital population yielding Archean ages between 2.95 and 2.65 Ga. These ages are consistent with those reported from the basement tonalite (sample 12MBC-F105A; Scott, 1999). These results unequivocally demonstrate the presence of Paleoproterozoic sedimentary sequences that, in this case, occur structurally below Archean tonalite in eastern Hall Peninsula. The contact between the tonalite and the supracrustal rocks is tentatively interpreted as a tonalite

overthrust on the basis of strain recorded along the contact and the lack of evidence for symmetry or repetition of supracrustal rock types. Zircon overgrowths record nonreproducible dates between 1.87 and 1.79 Ga and low U-Th ratios. These are interpreted to record a prolonged metamorphic overprint; however, given the scatter in the results, no specific age determination is made.

Quartzite, central Hall Peninsula (12MBC-F96B)

Sample description

A west-dipping metasedimentary assemblage dominated by psammite-semipelite within the east-central portion of the peninsula (40 km west of Allen Island; see also sample 12MBC-F96A, Figure 1) is of limited strike length but unique in the preservation of a relatively pure marble horizon. A 30 cm thick quartzite horizon interbedded with psammite was collected for geochronology (Figures 2b, 4b). The psammite-quartzite is structurally overlain by deformed megacrystic granite (12MBC-F96A). No evidence for an intrusive contact is preserved (Figure 2b).

Zircon description

This sample was disaggregated using standard crushing and grinding procedures. A magnetic separator was used to isolate a zircon separate and the grains were hand-picked from the nonmagnetic @ 10° side-slope fraction. The zircons are highly variable in colour and morphology with some grains preserving facets and terminations, whereas others are well rounded. Small tips and overgrowths are observed in plane light (Figure 5b).

Results and interpretation

A total of 67 analyses were conducted from the internal zones/cores of 65 separate grains. Only Archean detrital ages are preserved in the quartzite (Figure 5b; Rayner, 2014). The youngest, concordant grain yields a single spot $^{207}Pb/^{206}Pb$ age of 2678 ±8 Ma, interpreted as the maximum age of deposition of the sediment. Replicate analyses on younger grains were not reproducible and therefore not considered as a reliable measure of the youngest detrital zircon. Significant detrital modes are present at 2.68, 2.72, 2.78 and 2.8–2.85 Ga (Figure 5b), which correspond to recently determined ages of basement on Hall Peninsula, including the overlying deformed megacrystic granite (this paper; Scott, 1999). An additional six analyses were carried out on zircon rims, yielding ages between 1878 and 1769 Ma (Rayner, 2014). A small cluster of four analyses yielded an imprecisely constrained mean $^{207}Pb/^{206}Pb$ age of 1861 ±25 Ma, interpreted to represent a metamorphic overprint and the minimum age of deposition. Based on the similarity of its lithological associations and deformation state with other metasedimentary sequences described herein, this quartzite is interpreted to be part of the Paleoproterozoic assemblage. As both the quartzite-psammite and overlying deformed megacrystic granite are strongly

lineated, the interface does not represent simply an unmodified depositional contact. Based on the presence of exclusively Archean sources, however, the author tentatively proposes that the quartzite represents a basal sequence containing locally sourced detritus.

Quartzite, central Hall Peninsula (12MBC-K97A)

Sample description

The quartzite sample was collected from a doubly plunging synformal basin in the central part of the peninsula (Figure 1). The quartzite panel is a minor constituent of an amphibolite–metasedimentary assemblage, which is cut by ultramafic and monzogranitic plutonic bodies, subsequently deformed then bisected by undeformed pegmatite dikes. This quartzite sample is part of the Qaqqanittuaq area described in greater detail in MacKay et al. (2013a, b) and was collected for U-Pb detrital zircon geochronology to further characterize the metasedimentary packages on Hall Peninsula.
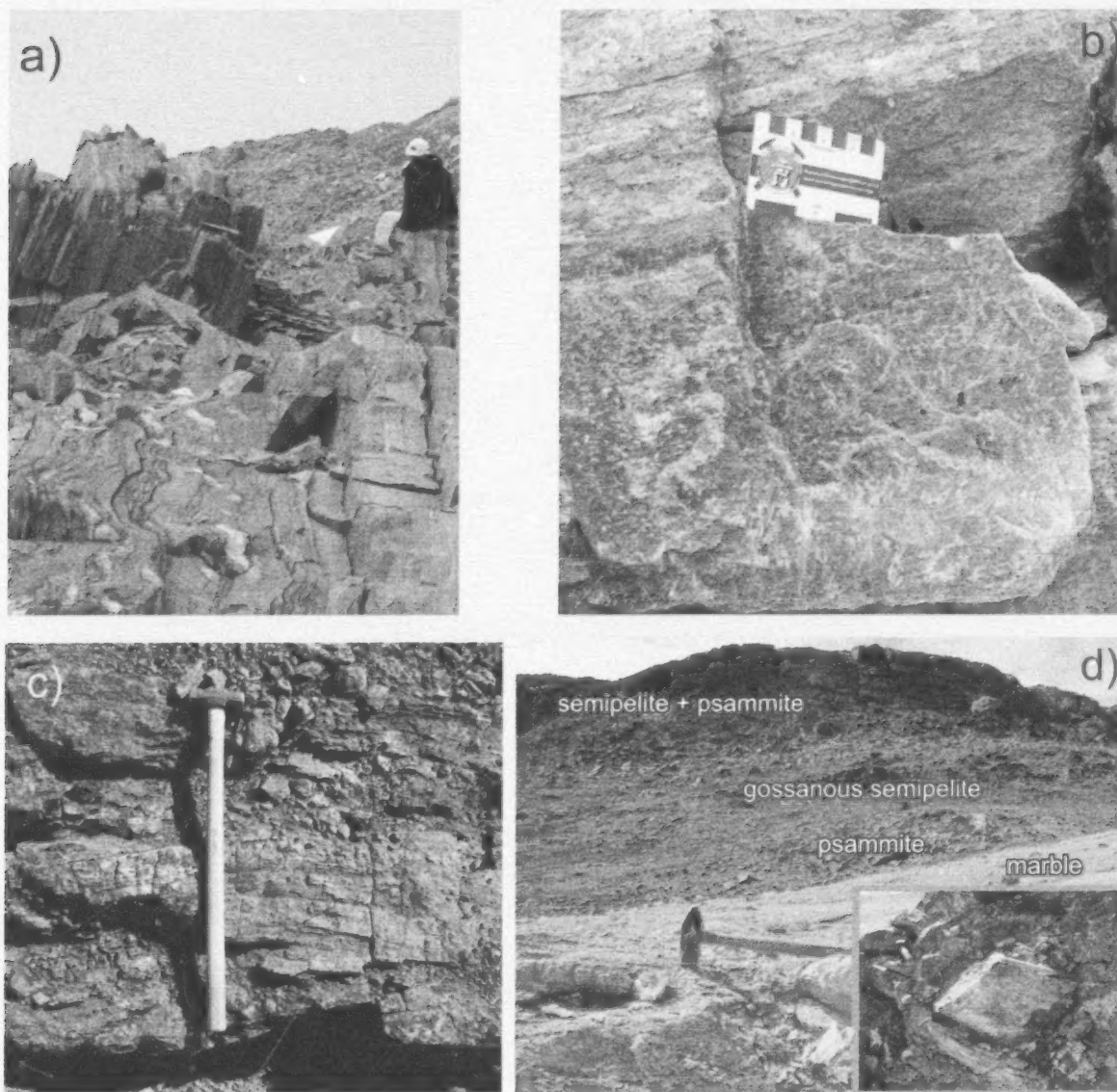
Figure 4: Sedimentary samples and field relationships, Hall Peninsula: **a)** geochronology sample location (block beneath hammer) of flaggy psammite (12MBC-F104A); view to northwest, geologist is 170 cm tall; **b)** detail of quartzite sample 12MBC-F96B; **c)** horizontal exposure of quartz-rich psammite (sample 12MBC-R15A) collected for geochronology, hammer is 90 cm long; **d)** overview of locality for sample 12MBC-B95A; marble in foreground overlain by psammite (white-cream weathering), which is in turn overlain by gossanous semipelite and finally by semipelite with minor psammite, forming the cliff; view to west, hammer is 40 cm long; inset: detail of sample collected from the upper horizon of semipelite in the cliff; pen magnet is 12 cm long.

Zircon description

The sample was disaggregated using standard crushing and grinding procedures. A magnetic separator was used to isolate a zircon separate and the grains were hand-picked from the nonmagnetic@ 10° side-slope fraction. Detrital zircons recovered from the quartzite are commonly colourless to medium brown (Figure 5c). Many are well rounded, presumably due to sedimentary transport.

Results and interpretation

A total of 68 analyses were conducted on 63 separate zircon grains to define the detrital zircon provenance profile for quartzite sample 12MBC-K97A (Figure 5c; Rayner, 2014). Nine analyses form a cluster at ca. 2.13 Ga, and the maximum age of deposition is constrained by four replicates on grain 42 with a mean $^{207}Pb/^{206}Pb$ age of 2126 ±16 Ma. The majority of the detrital zircons yield Archean ages with prominent modes between 2880 and 2700 Ma, similar to the prominent modes recorded in sample 12MBC-F96B and consistent with the age of basement documented on Hall Peninsula. Twenty analyses yield Mesoarchean to Eoarchean ages (3.78–2.96 Ga), ages hitherto undocumented on Hall Peninsula.

Quartzite, western Hall Peninsula (12MBC-R15A)

Sample description

A sample was collected from a thin (15 cm) panel of quartzite (Figure 4c) sitting within a more extensive exposure of psammite and structurally below a large outcrop of marble. Although there is little evidence in this location for the extensive in situ partial melting observed elsewhere in the western portion of Hall Peninsula, the psammite is intruded by white-weathering, lilac garnet–bearing leucogranite and minor orange-weathering, biotite-orthopyroxene monzogranite. Every effort was made to avoid the plutonic phases during sampling. This sample was chosen for detrital zircon analysis to more fully characterize the provenance profile of sedimentary rocks across Hall Peninsula and for comparison with the demonstrably Paleoproterozoic se-

Figure 5: Probability density diagrams and histograms for detrital zircon samples from Hall Peninsula. Dark grey curves include only data that fall within the ±5% concordance threshold; light grey curves incorporate all data. Replicates and metamorphic overgrowths are not plotted, regardless of concordance. The bin width is 10 Ma. Maximum ages of deposition (MDA) are reported at the 2σ confidence level (see text for discussion and Rayner [2014] for results). Results are presented with the sample in the lowest structural setting at the bottom of the page (a) and the sample with the highest structural setting at the top of the page (e): **a)** results from sample 12MBC-F104A; inset: transmitted light image of recovered zircons; scale bar is 300 µm; **b)** results from sample 12MBC-F96B; inset: transmitted light image of recovered zircons, scale bar is 300 µm; arrows indicate metamorphic overgrowths; **c)** results from sample 12MBC-K97A; inset: transmitted light image of recovered zircons, scale bar is 300 µm; **d)** results from sample 12MBC-R15A; inset: transmitted light image of recovered zircons, scale bar is 300 µm; **e)** results from sample 12MBC-B95A; inset: transmitted light image of recovered zircons, scale bar is 300 µm.

e) **12MBC-B95, psammite, western Hall Penin.**
n = 27/31,
MDA = 1907 ±9 Ma
grain 1, n = 3
MSWD = 0.38

d) **12MBC-R15 quartzite, western Hall Penin.**
n = 48/57
MDA = 1906 ±9 Ma
grain 11, n = 3
MSWD = 0.60

c) **12MBC-K97A quartzite, central Hall Penin.**
n = 59/63
MDA = 2126 ±16 Ma
grain 42, n = 4
MSWD = 0.80

b) **12MBC-F96B, quartzite, east-central Hall Pen.**
n = 58/65
MDA = 2678 ±8 Ma
no replicates

a) **12MBC-F104A psammite, Beekman Penin.**
n = 60/63
MDA = 1959 ±12 Ma
n = 3, grain 90
MSWD = 2.5
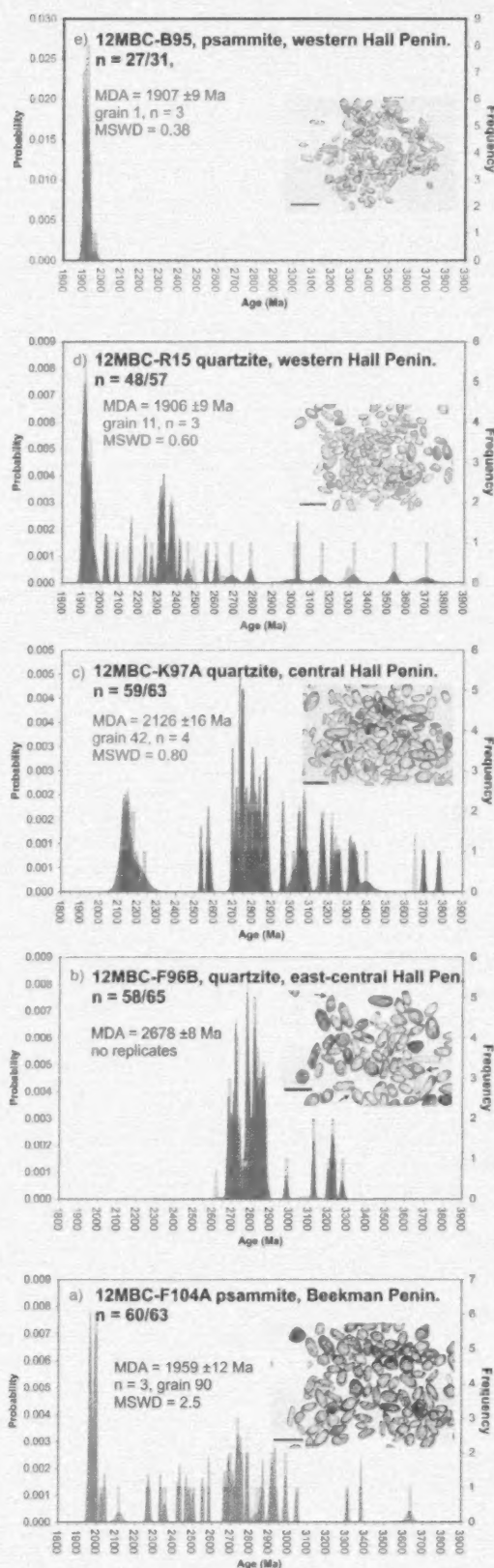
quences identified to the east (samples 12MBC-F104A, -F96B, -K97A).

Zircon description

This sample was disaggregated using standard crushing and grinding procedures. A magnetic separator was used to isolate a zircon separate and the grains were hand-picked from the nonmagnetic @ 10° side-slope fraction. Zircons recovered from the quartzite are commonly subrounded, with aspect ratios of 2:1–4:1, pale brown to medium brown, with oscillatory zoning visible in plane light (Figure 5d). A distinct population of equant, clear, colourless, inclusion- and fracture-free grains is also present. In BSE images, many grains exhibit unzoned overgrowths and the equant and colourless grains are also typically unzoned.

Results and interpretation

A total of 86 analyses were carried out on 71 individual zircon grains yielding dates ranging from 3701 to 1827 Ma (Figure 5d; Rayner, 2014). There is a small cluster of ages between 2.4 and 2.3 Ga that is not apparent in the other samples of this study. Older ages are represented by single data points, whereas the majority of the analyses are younger than 2.0 Ga. Given the prevalence of monzogranite injection at the sampling site, as well as the high metamorphic grade inferred from the extensive partial melting of semipelitic phases elsewhere in the western portion of the peninsula, some of these young results likely represent a metamorphic overprint or thin magmatic injection and not the youngest detrital component. Examination of the morphological and zoning characteristics of the analyzed zircon, as well as replicate analyses to evaluate reproducibility, were necessary to identify the youngest demonstrably detrital grain and constrain the maximum age of deposition. Unzoned tips, rims and equant zircon grains generally yield the youngest dates (1886–1832 Ma) and are inferred to represent a metamorphic overprint. Replicate analyses on both unzoned and zoned zircon are commonly nonreproducible. The youngest zoned zircon with reproducible analyses (grain 11; Rayner, 2014) yielded a weighted mean ^{207}Pb/^{206}Pb age of 1906 ±9 Ma, which is considered to be the maximum age of deposition of the quartzite-psammite assemblage.

Quartzite, western Hall Peninsula (12MBC-B95A)

Sample description

Sample 12MBC-B95A was collected approximately 10 km south-southwest of sample 12MBC-R15A described above. It comprises psammite and gossanous semipelite with extensive partial melting, and has been intruded by lilac garnet–bearing leucogranite. It lies structurally above a small exposure of marble, which is the along-strike equivalent of the large marble outcrop described above as adjacent to sample 12MBC-R15A. Given the consistent westerly dips across the western portion of the peninsula, this sam-

ple is the structurally highest unit targeted for geochronology. The sample was taken from a thin (50 cm) horizon of relatively pure quartzite within the psammite (Figure 4d).

Zircon description

This sample was disaggregated using standard crushing and grinding procedures. A magnetic separator was used to isolate a zircon separate and the grains were hand-picked from the nonmagnetic @ 10° side-slope fraction. Zircons recovered from the quartzite are equant to elongate, colourless to medium yellow-brown to medium brown (Figure 5e). Most are well rounded. The majority of zircon crystals have distinct high-U (bright in BSE) rims. In some cases, these clearly truncate internal zoning, indicating a later phase of zircon growth (Figure 5e). In other cases, the high-U zircon is concordant with zoning in the inner part of the grain and may simply represent a change in zircon composition during growth.

Results and interpretation

A total of 56 analyses were carried out on 49 zircon grains, yielding a virtually unimodal age range from 1967 to 1837 Ma (Figure 5e; Rayner, 2014). As in sample 12MBC-R15A, some of these young results likely represent a metamorphic overprint and not the youngest detrital component. Twelve of the fourteen youngest analyses are from zircon with elevated U content (greater than 1500 ppm, most greater than 2000 ppm). Many are unzoned or faintly zoned and some are from distinct secondary phases (rims, patchy overgrowths). Although these do not form a statistically significant age cluster, the author interprets these to represent new zircon growth and/or a disturbance of the U-Pb isotopic system and therefore does not consider their ages to be detrital or a good measure of the age of the youngest detrital zircon. The youngest low-U, clearly zoned zircon with reproducible results yields a weighted mean ^{207}Pb/^{206}Pb age of 1907 ±9 Ma, which is considered as the maximum age of deposition of the psammite. The age constraint is statistically equivalent to the maximum age constraint presented for sample 12MBC-R15A above.

Paleoproterozoic plutonic rocks

Biotite-orthopyroxene monzogranite, western Hall Peninsula (12MBC-B97A)

Sample description

Orange-brown–weathering, biotite–hornblende±orthopyroxene±magnetite–bearing granodiorite to granite is a major unit in western Hall Peninsula. It was observed to cut the metasedimentary package and is itself cut by a white-weathering, lilac garnet–bearing leucogranite. Fine-grained varieties are commonly very friable in outcrop. The unit sampled for geochronology is medium grained (5–10 mm) and forms cliffs at the intrusive contact with marble (Figure 6a).
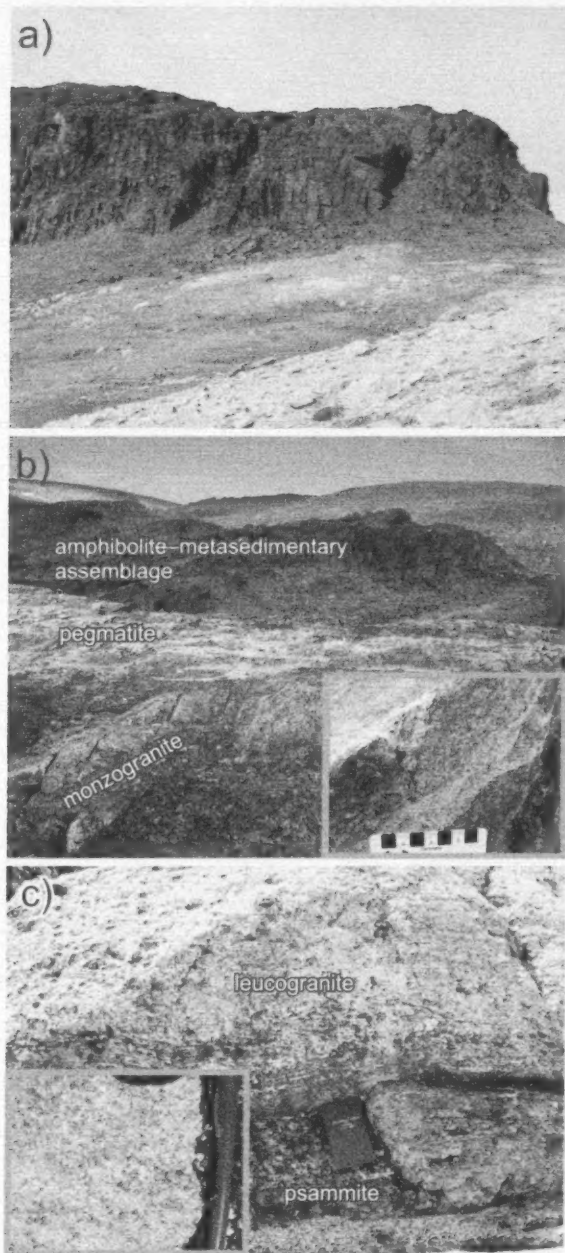
Figure 6: Paleoproterozoic plutonic samples and field relationships, Hall Peninsula: **a)** cliff exposure (height approximately 100 m) of biotite–orthopyroxene±garnet monzogranite cutting marble at station 12MBC-B97A; **b)** amphibolite–metasedimentary assemblage (background) cut by monzogranite (grey resistant unit in foreground, station 12MBC-K79B), both deformed; cut by undeformed pegmatite (white, rubbly unit in midground); inset: detail of geochronology sample illustrating foliation; **c)** weakly to undeformed lilac garnet–bearing monzogranite (sample 12MBC-B96A) cutting well-foliated psammite, notebook is 16 cm long; inset of geochronology sample illustrating weak to absent fabric development. Field of view is approximately 10 cm high.

Zircon description

Electric pulse disaggregation was used to comminute this sample. A magnetic separator was used to isolate a zircon separate and the grains were hand-picked from the non-magnetic @ 5° side-slope fraction. Abundant pale to medium brown zircons with resorbed or rounded facets were recovered from a sample of orthopyroxene-bearing monzogranite. Clear, colourless prismatic zircon is rare. In some cases this morphology is present as cores with pale to medium brown rims (Figure 7a).

Results and interpretation

A total of 40 analyses were carried out on 30 separate zircon grains, yielding ages between 2516 and 1802 Ma (Rayner, 2014). Ages older than 1.92 Ga are not clustered and mainly occur as unique results. These are most often recorded in zoned zircon cores. Two clusters of results occur at ca. 1.89 Ga and 1.83 Ga. The older cluster comprises analyses of zoned and unzoned zircon, whereas the younger cluster comprises only unzoned zircon (Figure 7b). Both groups have similar ranges of U and U-Th values. Replicate analyses of young (ca. 1.83 Ga) unzoned zircon are commonly nonreproducible and also record older, ca. 1.89 Ga, ages (see Rayner, 2014; grains 42, 56, 80, 105). On the basis of zoning and the preservation of older ages in some portions of unzoned zircon grains, the older cluster of results are interpreted to represent the crystallization age of the monzogranite at 1892 ±7 Ma (weighted mean $^{207}Pb/^{206}Pb$ age; MSWD = 1.6; Figure 5c). The younger cluster at 1828 ±3 Ma (MSWD = 0.75), including reproducible repli-

▶

Figure 7: Zircon images and concordia diagrams for the western Hall Peninsula plutonic rocks. Ellipses plotted and mean ages are reported at the 2σ confidence level; black scale bars on transmitted light images are 300 μm, white scale bars on backscattered electron (BSE) images are 20 μm: **a)** transmitted light image of zircon grains recovered from sample 12MBC-B97A; **b)** BSE images of zircons from sample 12MBC-B97A; white grain numbers and black ellipses correspond to analyses in Rayner (2014); **c)** concordia diagram of U-Pb results from sample 12MBC-B97A; dark grey ellipses correspond to analyses included in the calculation of the crystallization age, light grey ellipses are included in the calculation of the age of the metamorphic overprint, white ellipses are excluded from any age calculations (see text for discussion), abbreviation: opx, orthopyroxene; **d)** transmitted light image of zircon grains recovered from sample 12MBC-K79B; **e)** BSE images of zircons from sample 12MBC-K79B; white grain numbers and black ellipses with spot numbers correspond to analyses in Rayner (2014); **f)** concordia diagram of U-Pb results from sample 12MBC-K79B; dark grey ellipses correspond to analyses included in the calculation of the weighted mean, light grey ellipses are excluded from the calculation (shown in detail in inset); unfilled ellipses are interpreted as inherited (see text for discussion); **g)** transmitted light image of zircon grains recovered from sample 12MBC-B96A; **h)** BSE images of zircons from sample 12MBC-B96A; white grain numbers and black ellipses with spot numbers correspond to analyses in Rayner (2014); **i)** concordia diagram of U-Pb results from sample 12MBC-B96A; all data shown in the concordia plot were used to calculate the crystallization age; data with UO/U higher than 7.5 were not plotted or included in calculations (see text for discussion).

c) **12MBC-B97A opx-monzogranite western Hall Peninsula**

Crystallization age
1892 ±7 Ma
n = 10
MSWD = 1.6

Metamorphic overprint
1828 ±3 Ma
n = 7
MSWD = 0.75

f) **12MBC-K79B monzogranite central Hall Peninsula**

Crystallization age
1873 ±6 Ma
n = 8 (dark grey ellipses)
MSWD = 1.7

i) **12MBC-B96A lilac garnet monzogranite western Hall Peninsula**

Crystallization age
1867 ±8 Ma
n = 9 (dark grey ellipses, UO/U < 7.5)
MSWD = 2.6
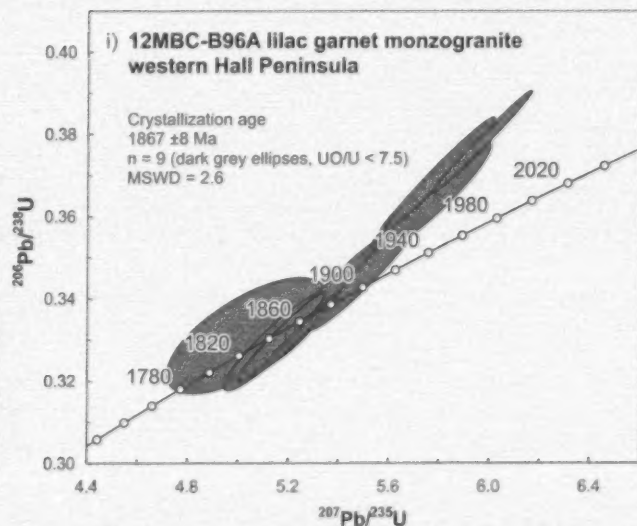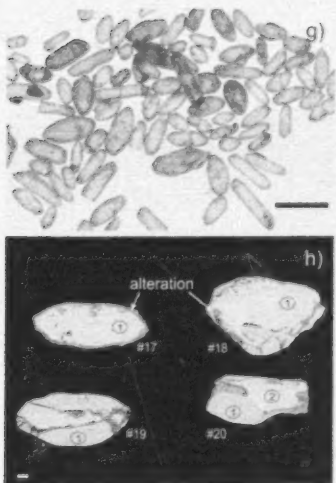
cates, is interpreted to represent a metamorphic overprint resulting in the partial to complete recrystallization of igneous zircon.

Monzogranite, central Hall Peninsula (12MBC-K79B)

Sample description

Within the doubly plunging synformal basin in the Qaqqanittuaq area (see MacKay 2013a, b) is a monzogranitic dike that cuts the amphibolite/metasedimentary assemblage (see station 12MBC-K97A, this paper) and has been subsequently deformed (Figure 6b). The age of the monzogranite will constrain the minimum age of the deposition of the sedimentary assemblage into which it intrudes as well as the maximum age of the pervasive east-vergent deformation ($D_1 + D_2$; see Steenkamp et al., 2014).

Zircon description

Electric pulse disaggregation was used to comminute this sample. A magnetic separator was used to isolate a zircon separate and the grains were hand-picked from the nonmagnetic @ 3° side-slope 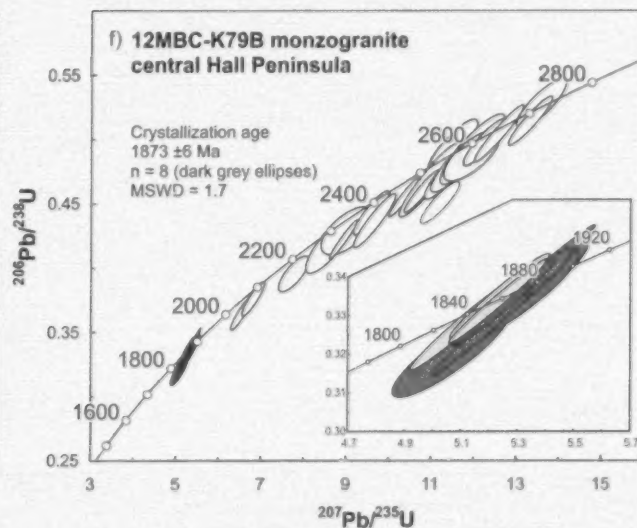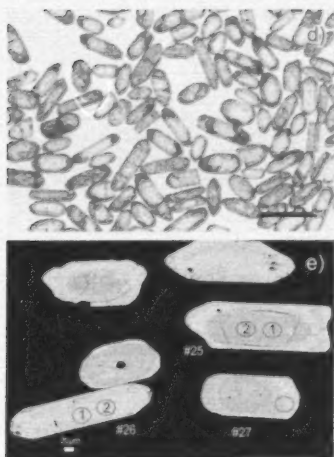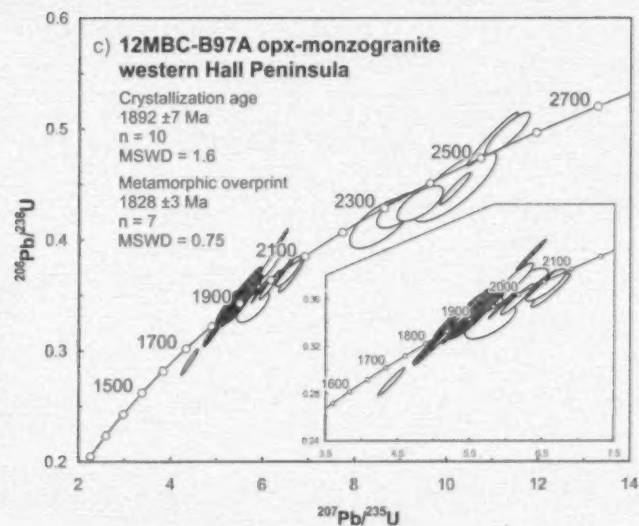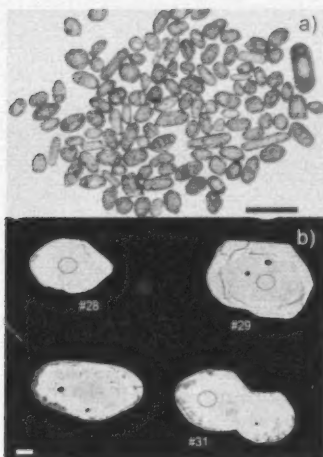fraction. From the abundant recovery, two main morphological zircon types are recognized. Clear, colourless, prismatic and well-faceted zircon is present as discrete grains as well as cores (Figure 7d). Pale brown, elongate, prismatic, highly fractured zircon comprises overgrowths around colourless zircon cores as well as entire grains.

Results and interpretation

A total of 35 analyses were carried out on 25 separate zircon grains, yielding ages from 2722 to 1849 Ma (Rayner, 2014). The crystallization age of the monzogranite is recorded in high-U zircon and zircon rims with a weighted mean $^{207}Pb/^{206}Pb$ age of 1873 ±6 Ma (n = 8, MSWD = 1.7). Three slightly younger analyses are excluded from the calculation of the weighted mean and are considered to have been affected by a small amount of Pb loss. Ages older than 2.1 Ga are recorded in low-U zircon grains and zircon cores and are interpreted to represent inherited material. Replicate analyses from the low-U zircon grains form a linear array on the concordia diagram (Figure 7f) but are nonreproducible (see Rayner [2014], grains 13, 25, 34, 49; Figure 7e). The spread along an apparent discordia curve as well as the nonreproducibility of results suggests that some or all of the spread in ages is due to a disturbance in the U-Pb isotopic system, either through diffusive Pb loss or zircon recrystallization. The ca. 2.7 Ga upper intercept of this 'discordia' cannot represent the crystallization age of the monzogranite because field relationships indicate it cuts sedimentary rocks with a maximum age of deposition of 2126 ±16 Ma (sample 12MBC-K97A).

Lilac garnet leucogranite, western Hall Peninsula (12MBC-B96A)

Sample description

A weakly to undeformed, white-weathering, lilac garnet-bearing leucogranite cuts the strongly foliated psammite-semipelite assemblage of sample 12MBC-B95A described above (Figure 6c). Correlative units are interpreted to intrude into the orange-brown–weathering, orthopyroxene-bearing plutonic suite (e.g., sample 12MBC-B97A), thus yielding the characteristic alternating bands of rusty-white and brown rocks across western Hall Peninsula. The age of the monzogranite provides an additional constraint on the minimum age of deposition of the metasedimentary units. The low degree of strain recorded in the leucogranite suggests that pervasive east-west shortening ($D_1 + D_2$) was largely over by the time of emplacement.

Zircon description

Electric pulse disaggregation was used to comminute this sample. A magnetic separator was used to isolate a zircon separate and the grains were hand-picked from the non-magnetic @ 10° side-slope fraction. The zircon grains are prismatic but strongly resorbed, with few facets preserved (Figure 7g). The BSE images reveal unzoned zircon inner regions separated from unzoned zircon outer regions by a zone of vermicular zircon alteration (Figure 7h). The alteration appears relatively dark in BSE images, likely due to the increased presence of OH⁻, Ca and Ba, which reduces the mineral density (and BSE response) relative to unaltered zircon. The unzoned outer parts of the grains are typically very thin (>5 µm) but in some cases are wide enough to permit analysis (see Rayner, 2014; grain 36).

Results and interpretation

A total of 25 analyses were carried out on 20 separate zircon grains. Zircon outboard of the zone of alteration has lower U concentrations (400–900 ppm) than zircon inside the alteration zone (typically 6000 ppm, up to 12 000 ppm). There is no correlation between age and analysis location either inside or outside the alteration zone. Due to the anomalously high U concentrations of some of these zircon grains and their effect on the zircon crystal lattice, the ionization and sputtering behaviour of these grains differs from the zircon standard used to calibrate U-Pb fractionation. This anomalous behaviour is best recognized in the measured $^{238}U^{16}O/^{238}U$ ratio of the sample in comparison to the zircon standard. The U-Pb age determined by ion probe depends on a fractionation correction that involves UO/U (Stern, 1997). The measured UO/U ratio of the standard during this analytical session is 6.7–7.3. The measured UO/U ratio for the sample over the same session is 6.3–8.3; therefore, the U-Pb age of any analysis with a UO/U value outside of the calibration range (>7.5) is not considered reliable. For this reason, such results are not plotted on the concordia diagram (Figure 7i). The weighted mean $^{207}Pb/$

^{206}Pb ages of the nine remaining zircons is 1867 ±8 Ma (MSWD = 2.6), which is interpreted as the crystallization age of the lilac garnet–bearing leucogranite. Although the ^{207}Pb/^{206}Pb ages should be unaffected by the calibration effect, their high-U content makes them prone to isotopic disturbance and therefore analyses with high UO/U were also excluded from the calculation of the weighted mean.

Economic considerations

Precise, absolute age constraints are an essential component of modern mapping because they provide temporal calibration of geological observations, strengthen regional correlations and place time brackets on tectonometamorphic events. The geochronology results presented in this paper set the stage for further understanding of the basement substrate, host to diamondiferous kimberlites at Chidliak (Pell et al., 2012; From et al., 2014). The clear recognition of a Paleoproterozoic age for sedimentary rocks across Hall Peninsula permits continued study of the origin and evolution of these base-metal prospective rocks. Further comparisons of the provenance profiles of sedimentary rocks across Hall Peninsula with similar datasets from Lake Harbour Group rocks on southern Baffin Island (host to coloured gemstones), Tasiuyak gneiss in Labrador (Scott and Gauthier, 1996; Scott, 1999) or possible equivalents in Greenland (Thrane and Connelly, 2006) will contribute to the assessment of regional tectonostratigraphic correlations.

Conclusions

The crystallization age of 2844 ±3 Ma for a tonalite gneiss from Beekman Peninsula (12MBC-F105A) replicates the basement ages reported by Scott (1999) from nearby Allen Island (2835 ±11 Ma) and Brevoort Island (2844 ±6 Ma), as well as at Okalik Bay (2848 ±3 Ma), roughly 60 km to the north. A crystallization age of 2701 ±2 Ma for a distinct, strongly deformed megacrystic granite containing K-feldspar porphyroclasts rimmed by plagioclase (sample 12MBC-F96A) is inferred to correspond to a similar rock type extensively exposed at the head of Smith Channel (unit Ergr from Machado, 2013a). Four of the five metasedimentary samples described in this paper are demonstrably Paleoproterozoic, with significant 2.1–1.9 Ga detritus and maximum ages of deposition that range from 2126 ±16 to 1906 ±9 Ma. These Paleoproterozoic sedimentary units are distributed across the entire map area. Those from the east contain dominant to subdominant Archean detritus, whereas this detrital component is less pronounced to absent in the west. One quartzite sample (sample 12MBC-F96B), associated with marble and mafic sills within the gneissic basement–dominated eastern half of the peninsula, contains only Archean detritus and may represent a locally derived, basal sedimentary package. The 1892 ±7 Ma orthopyroxene-bearing monzogranite (sample

12MBC-B97A) is consistent with that of a comparable lithology dated by Scott (1999, sample D350, 1890 ±3 Ma) and located roughly along strike, approximately 30 km to the north. Likewise, white-weathering monzogranite and leucogranite samples 12MBC-K79B and -B96A yield overlapping ages of 1873 ±6 Ma and 1867 ±8 Ma, respectively, which also correspond to the results for similar rock types described by Scott (1999, samples D320, D108).

References

Ludwig, K.R. 2003: User's manual for Isoplot/Ex rev. 3.00: a geochronological toolkit for Microsoft Excel; Berkeley Geochronology Center, Special Publication 4, 70 p.

Machado, G., Bilodeau, C. and St-Onge, M.R. 2013a: Geology, southern part of Hall Peninsula, south Baffin Island, Nunavut; Geological Survey of Canada, Canadian Geoscience Map 135 (preliminary), Open File Map 2013-1, scale 1:250 000, doi:10.4095/292443

Machado, G., Bilodeau, C., Takpanie, R., St-Onge, M.R., Rayner, N.M., Skipton, D.R., From, R.E., MacKay, C.B., Creason, C.G. and Braden, Z.M. 2013b: Hall Peninsula regional bedrock mapping, Baffin Island, Nunavut: summary of fieldwork; in Summary of Activities 2012, Canada-Nunavut Geoscience Office, p. 13–22.

MacKay, C.B., Ansdell, K.M., St-Onge, M.R., Machado, G. and Bilodeau, C. 2013a: Geological relationships in the Qaqqanittuaq area, southern Hall Peninsula, Baffin Island, Nunavut; in Summary of Activities 2012, Canada-Nunavut Geoscience Office, p. 55–64.

MacKay, C.B., Ansdell, K.M., St-Onge, M.R., Rayner, N.M. and Mate, D. 2013b: Geological, age and geochemical constraints on the evolution of the northeastern Paleoproterozoic Trans-Hudson Orogen from southern Hall Peninsula, Baffin Island, Canada; Geological Society of America An-

nual Meeting 2013, Program with Abstracts, v. 45, no. 7, p. 309.

Pell, J., Grütter, H., Neilson, S., Lockhard, G., Dempsey, S. and Grenon, H. 2012: Exploration and discovery of the Chidliak kimberlite province, Baffin Island, Nunavut: Canada's newest diamond district; *in* Proceedings of 10th International Kimberlite Conference, D.G. Pearson et al. (eds.), v. 2, Special Issue of the Journal of the Geological Society of India, p. 209–227.

Rayner, N.M. 2014: Data table accompanying "New U-Pb geochronological results from Hall Peninsula, Baffin Island, Nunavut"; Canada-Nunavut Geoscience Office, Geoscience Data Series GDS2014-001, Microsoft® Excel® file, URL <http://cngo.ca/summary-of-activities/2013/> [November 2013].

Rudashevsky, N.S., Burakov, B.E., Lupal, S.D., Thalhammer, O.A.R. and Saini-Eidukat, B. 1995: Liberation of accessory minerals from various rock types by electric-pulse disintegration—method and application; Transactions of the Institute of Mining and Metallurgy, v. 104, p. C25–C29.

Scott, D.J. 1999: U-Pb geochronology of the eastern Hall Peninsula, southern Baffin Island, Canada: a northern link between the Archean of West Greenland and the Paleoproterozoic Torngat Orogen of northern Labrador; Precambrian Research, v. 93, p. 5–26.

Scott, D.J. and Gauthier, G. 1996: Comparison of TIMS (U-Pb) and laser ablation microprobe ICP-MS (Pb) techniques for age determination of detrital zircons from Paleoproterozoic metasedimentary rocks from northeastern Laurentia, Canada, with tectonic implications; Chemical Geology, v. 131, p. 127–142.

Sircombe, K.N. 2004: AgeDisplay: an Excel workbook to evaluate and display univariate geochronological data using binned frequency histograms and probability density distributions; Computers and Geosciences, v. 30, p. 21–31.

Stern, R.A. 1997: The GSC sensitive high resolution ion microprobe (SHRIMP): analytical techniques of zircon U-Th-Pb age determinations and performance evaluation; *in* Radiogenic Age and Isotopic Studies Report 10, Geological Survey of Canada, Current Research 1997-F, p. 1–31.

Stern, R.A. and Amelin, Y. 2003: Assessment of errors in SIMS zircon U-Pb geochronology using a natural zircon standard and NIST SRM 610 glass; Chemical Geology, v. 197, p. 111–146.

Thrane, K. and Connelly, J.N. 2006: Zircon geochronology from the Kangaatsiaq–Qasigiannguit region, the northern part of the 1.9–1.8 Ga Nagssugtoqidian orogen, West Greenland; Geological Survey of Denmark and Greenland Bulletin, v. 11, p. 87–99.

Preliminary characterization of the Archean orthogneiss complex of Hall Peninsula, Baffin Island, Nunavut

R.E. From[1], M.R. St-Onge[2] and A.L. Camacho[3]

[1]Department of Geological Sciences, University of Manitoba, Winnipeg, Manitoba, jnrfrom@gmail.com
[2]Geological Survey of Canada, Natural Resources Canada, Ottawa, Ontario
[3]Department of Geological Sciences, University of Manitoba, Winnipeg, Manitoba

Abstract

Archean gneissic rocks of the study area on Hall Peninsula, Baffin Island, were mapped at a scale of 1:6000 along a transect 600 m in length. The study area was selected for its spectacular exposures of continuous, lichen-free outcrops within the Archean orthogneiss complex of Hall Peninsula. Mapping delineated eight distinct lithological units within the orthogneiss complex. Unequivocal crosscutting relationships observed in the field played a vital role in establishing age relationships. A unit of porphyroclastic monzogranite dominates the study area, entraining older units of magnetite-bearing monzogranite, 'ribbon' granite, mafic monzogranite, 'leopard' gneiss, grey tonalite gneiss and pyroxene diorite. Characterizing eight units within the Hall Peninsula orthogneiss complex is in marked contrast to the general character of this complex, which was previously mapped as tonalite and monzogranite gneiss. Petrography, petrology, geochemistry, geochronology and Lu-Hf isotopic work will constitute the first step in identifying a fingerprint for the Archean orthogneiss complex of Hall Peninsula, which can then be used for comparison with adjacent Archean terrains, and in providing insight into paleoplate reconstructions for the Baffin Island and subarctic region.

Résumé

Les roches gneissiques archéennes de la zone d'étude dans la péninsule Hall, dans l'île de Baffin, ont été cartographiées à l'échelle de 1/6000 le long d'un transect de 600 m. Cette zone d'étude a été choisie en raison du fait que cette section du complexe d'orthogneiss archéen de la péninsule Hall présente de spectaculaires affleurements continus exempts de lichens. À l'aide de la cartographie, on a pu délimiter huit unités lithologiques distinctes au sein du socle d'orthogneiss archéen. Les liens sans équivoque qui existent au niveau des structures transversales remarquées sur le terrain ont joué un rôle de première importance dans la détermination des rapports qui existent entre les âges. Une unité de monzogranite porphyroclastique, prépondérante dans la zone d'étude, a entraîné des unités plus anciennes de monzogranite renfermant de la magnétite, du granite « rubané », du monzogranite mafique, du gneiss « léopard », du gneiss à tonalite gris et de la diorite à pyroxène. Le fait que huit unités ont pu être caractérisées au sein du compelxe d'orthogneiss de la péninsule Hall va à l'encontre du caractère général de ce complexe que des cartes géologiques antérieures décrivent comme étant composé de tonalite et de gneiss monzogranitique. Des travaux pétrographiques, pétrologiques, géochimiques, géochronologiques et isotopiques (méthode Lu-Hf) serviront de première étape à l'identification de l'empreinte géologique du complexe d'orthogneiss archéen de la péninsule Hall. À l'aide de cette empreinte, il sera alors possible d'établir des corrélations avec les terrains archéens voisins et faire le point sur les reconstructions des paléoplatesformes de la région subarctique et de l'île de Baffin.

Introduction

This study is part of the Canada-Nunavut Geoscience Office's Hall Peninsula Integrated Geoscience Program (HPIGP), a multiyear bedrock and surficial geology mapping program with associated thematic studies (e.g., Creason et al., 2013; Leblanc-Dumas et al., 2013; MacKay et al., 2013; Skipton et al., 2013). In the summer of 2013, the northern portion of Hall Peninsula (NTS 026A, B) was mapped at the scale of 1:250 000, completing the second and last year of HPIGP fieldwork (Figure 1).

A transition in dominant rock types, from the eastern to the western portion of Hall Peninsula, was documented during the 2012 and 2013 field seasons. Steenkamp and St-Onge (2014) provide an overview of the geology of Hall Peninsula and a brief outline is presented herein. The eastern portion of Hall Peninsula is dominated by an Archean tonalite-trondhjemite-granodiorite plutonic suite with tectonically interleaved panels of Paleoproterozoic metasedimentary rocks (Scott, 1999; Rayner, 2014). The western portion of Hall Peninsula is dominated by a plutonic suite of granodiorite to orthopyroxene-bearing monzogranite with intervening metasedimentary panels; the plutonic suite and the metasedimentary rocks are both inferred to be Paleoproterozoic (Scott, 1999; Rayner, 2014).

This paper focuses on the multitude of metamorphosed, plutonic units that dominate the geographic eastern portion of Hall Peninsula, referred to herein as the Archean orthogneiss complex of Hall Peninsula. The Archean orthogneiss complex is very similar in age and appearance to Archean tonalitic to granitic gneiss found elsewhere throughout Baffin Island and the subarctic region as a whole (St-Onge et al., 2009). Characterizing the Archean rocks of Hall Peninsula will allow comparison to and correlation with similar age rocks in the surrounding cratonic blocks (e.g., Rae craton, Meta Incognita microcontinent, Aasiaat domain, North Atlantic craton) and help better define the regional tectonic assembly of northeastern Laurentia. Future work in the study area, which will include petrography, petrology, geochronology, whole-rock and isotope geochemistry, will constitute the first step in characterizing this Archean terrain.

Geological background and previous work

The Archean orthogneiss complex of Hall Peninsula was previously described by Blackadar (1967), Scott (1996, 1999) and From et al. (2013). The orthogneisses are broadly similar in age, lithological characteristics and texture to Archean tonalitic to granitic gneiss found elsewhere throughout Baffin Island and the surrounding subarctic region (St-Onge et al., 2009). Previous work in adjacent terranes has elucidated the nature of different crustal blocks, although there are multiple working hypotheses as to the location of postulated intervening sutures (Figure 2), due in part to the absence of detailed geological work on Hall Peninsula (Cor-

rigan et al., 2009; St-Onge et al., 2009; Whalen et al., 2010). Based on lithological similarities, geochronology, geochemistry and aeromagnetic characteristics, the Archean rocks of central and northern Baffin Island have been correlated with the Rae craton of the north-central Canadian Shield and northern West Greenland (Hoffman, 1988). Archean rocks of the Meta Incognita microcontinent found in southern Baffin Island may correlate with the Aasiaat domain of west-central Greenland (Hollis et al., 2006; Thrane and Connelly, 2006; St-Onge et al., 2009). Other correlations between the Nain craton of northern Labrador and the North Atlantic craton of southern Greenland have also been proposed (van Gool et al., 2004). In addition, Paleoproterozoic Lake Harbour Group metasedimentary rocks have been correlated with the Meta Incognita microcontinent to the south and into the core zone of northern Labrador and northeastern Quebec (Knight and Morgan, 1981; Scott and Gauthier, 1996, Scott, 1999). Hall Peninsula Archean rocks have yet to be unequivocally correlated with any of the surrounding crustal blocks and remain enigmatic in terms of how they fit into the regional tectonic assembly of Baffin Island. Correlating the Archean orthogneiss complex of Hall Peninsula with the adjacent crustal blocks, such as the Meta Incognita microcontinent to the west (St-Onge et al., 2009), the Rae craton to the north, the Aasiaat domain of central West Greenland to the east (Hollis et al., 2006; Thrane and Connelly, 2006) and the Nain craton to the south (Scott and Campbell, 1993; Scott, 1999; Connelly, 2001; Wardle et al., 2002), or presenting it as a unique and distinct microcontinent, will directly impact its role in the continually developing story of tectonic assembly for the subarctic region.

Analytical work on the Hall Peninsula orthogneiss complex has been carried out by Scott (1999) and Rayner (2014). Uranium-lead zircon geochronology by Scott (1999) produced ages ranging from 2920 to 2797 +8/-15 Ma for the plutonic rocks, which were interpreted as magmatic. In addition, Scott (1999) suggested the zircons provided evidence of tectonothermal overprints at ca. 2770 Ma, and between 1844 and 1736 Ma.

Uranium-lead geochronology was carried out by Rayner (2014) using the sensitive high resolution ion microprobe (SHRIMP) on zircon grain separates from a tonalite gneiss and K-feldspar porphyritic granite located on the Beekman Peninsula (Figure 1). Zircons from the tonalite gneiss sample yielded an age of 2841 ±3 Ma, which is interpreted as the crystallization age of the rock (Rayner, 2014). In contrast, a sample of strongly deformed K-feldspar porphyritic granite, collected about 40 km west of Allen Island (Figure 1), has a crystallization age of 2701 ±2 Ma (Rayner, 2014). These preliminary results support an Archean age for the orthogneiss complex.

In addition, Scott (1999) and Rayner (2014) have produced U-Pb zircon data suggesting the Archean rocks record tec-
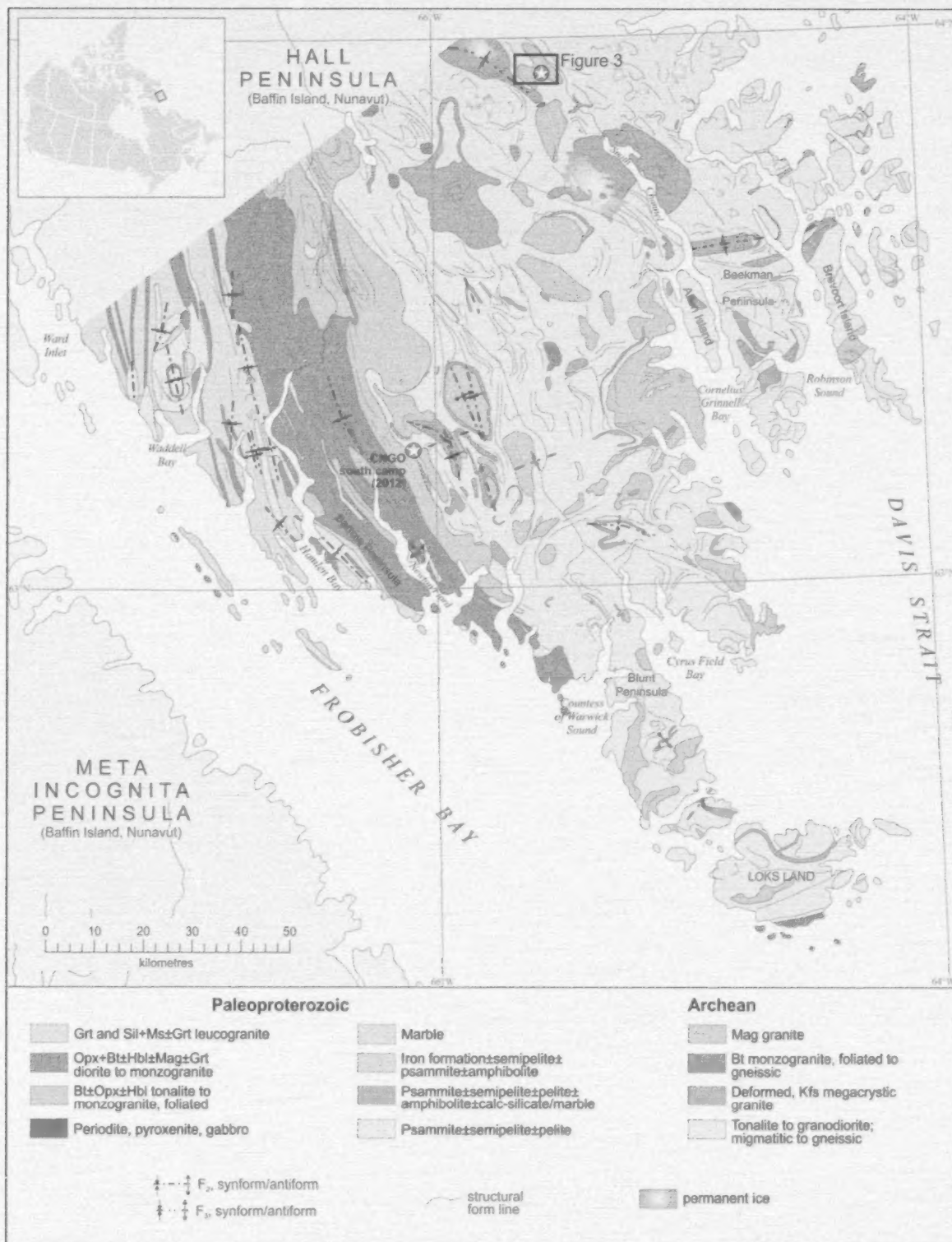
Figure 1: Compilation map of Hall Peninsula, Nunavut, from data collected during the 2012 and 2013 field seasons, showing the distribution of the principal tectonostratigraphic units (modified from Machado et al., 2013). Locations of the southern CNGO camp and the study area are shown with red stars. Abbreviations: bio, biotite; gar, garnet; hbl, hornblende; kfs, K-feldspar; mag, magnetite; mus, muscovite; opx, orthopyroxene; sil, sillimanite.

tonic events at ca. 2700 Ma and between 1856 and 1736 Ma.

Geology of the study area

The study area, is located in the central region of Hall Peninsula, about 80 km northeast of the southern CNGO camp (Figure 1) and 43 km southeast of the northern CNGO camp (Steenkamp and St-Onge, 2014, Figure 1). The study area forms part of what is informally referred to as the orthogneiss complex of Hall Peninsula, as described by From et al. (2013). The majority of rocks are metamorphosed, pervasively deformed and gneissic in character, and the prefix 'meta' is omitted from rock units for brevity. This study area was chosen due to the absence of lichen over most of the bedrock. A northeast-trending transect was mapped at the scale of 1:6000, documenting eight plutonic units within the orthogneiss complex (seven of which are represented on Figure 3). These lithological units are described from oldest to youngest below.

Description of lithological units

Pyroxene diorite (unit 1)

Unit 1 consists of clinopyroxene±orthopyroxene–bearing diorite that varies locally to quartz diorite. The rocks are grey to reddish brown on the weathered surface and have a dark grey to black fresh surface. Typically, the rocks are fine grained with local concentrations of clinopyroxene± orthopyroxene. This unit occurs within some of the younger units in the shape of enclaves and panels varying in size from centimetres to metres, respectively (Figure 4a).

Grey tonalite gneiss (unit 2)

Unit 2 consists of a grey, biotite- and hornblende-bearing tonalite gneiss. The rocks are distinctly grey weathering and have a salt-and-pepper fresh surface. The rocks are fine to medium grained with thin, millimetre-scale trondhjemitic segregations (Figure 4b) and boudinaged relicts of pyroxene diorite from unit 1. Felsic monzogranite to syenogranite intrude the tonalite gneiss of unit 2 parallel to the gneissosity in the host rocks of unit 2 (Figure 4c).

'Leopard' gneiss (unit 3)

Unit 3 consists of a hornblende+biotite+epidote megacrystic granodiorite that is informally named 'leopard' gneiss based on its archetypal 'leopard'-like, spotted appearance. The rocks are black and white on the weathered and fresh surfaces. They are medium to coarse grained and commonly have an L-tectonite fabric defined by elongated, relict plagioclase phenocrysts (Figure 4d). The plagioclase phenocrysts are commonly surrounded by hornblende and locally by K-feldspar phenocrysts. This unit is further character-
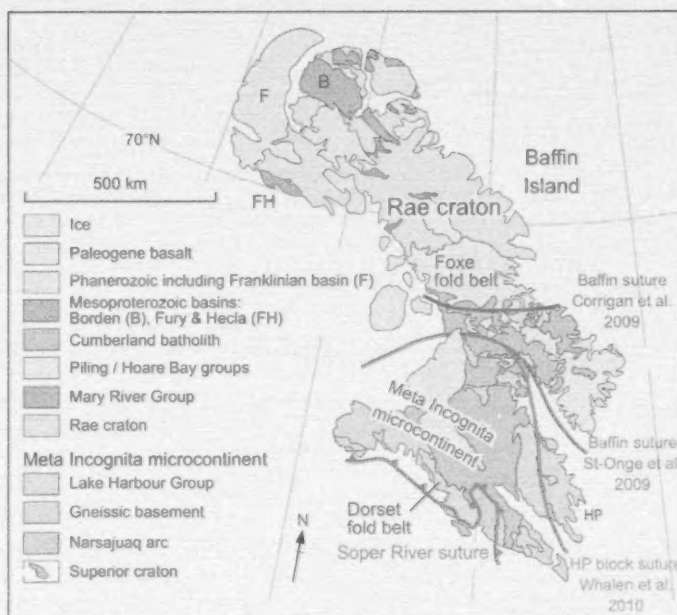
Figure 2: Compilation map of Baffin Island, Nunavut, which predates the initiation of the Canada-Nunavut Geoscience Office's Hall Peninsula Integrated Geoscience Program, showing the alternative hypotheses for suture locations on Baffin Island with specific convergence on Hall Peninsula (modified from St-Onge et al., 2009). Abbreviation: HP, Hall Peninsula.

ized by entrained, fine-grained enclaves of hornblende+biotite+epidote quartz diorite very similar in composition to unit 1 (Figure 4e).

Mafic monzogranite gneiss (unit 4)

Unit 4 consists of biotite- and hornblende-bearing monzogranite containing abundant mafic enclaves. These fine- to medium-grained rocks are typically whitish grey to black on the weathered and fresh surfaces. Unit 4 is distinguished by an abundance of mafic material occurring as angular enclaves and discrete layers, creating a black-and-white striped gneissosity. The mafic material is biotite±clinopyroxene± orthopyroxene quartz diorite, which is provisionally correlated with unit 1. The gneissosity in rocks from unit 4 is irregularly and complexly folded (Figure 4f).

'Ribbon' granite gneiss (unit 5)

The 'ribbon' granite gneiss unit consists of a hornblende- and biotite-bearing monzogranite. These fine- to medium-grained rocks are reddish grey to black on the weathered and fresh surfaces, and contain schlieren composed of hornblende, quartz and diorite similar in composition to unit 1, as well as crosscutting felsic monzogranite and syenogranite veins several centimetres in width. As its name suggests, the unit is characterized by a 'ribbon' layering texture defined by alternating pinkish, grey and black bands in K-feldspar–, plagioclase- and hornblende-rich layers (Figure 5a). Thin red layers a few millimetres thick contain minor amounts of pyrite, which has produced a deep red stain
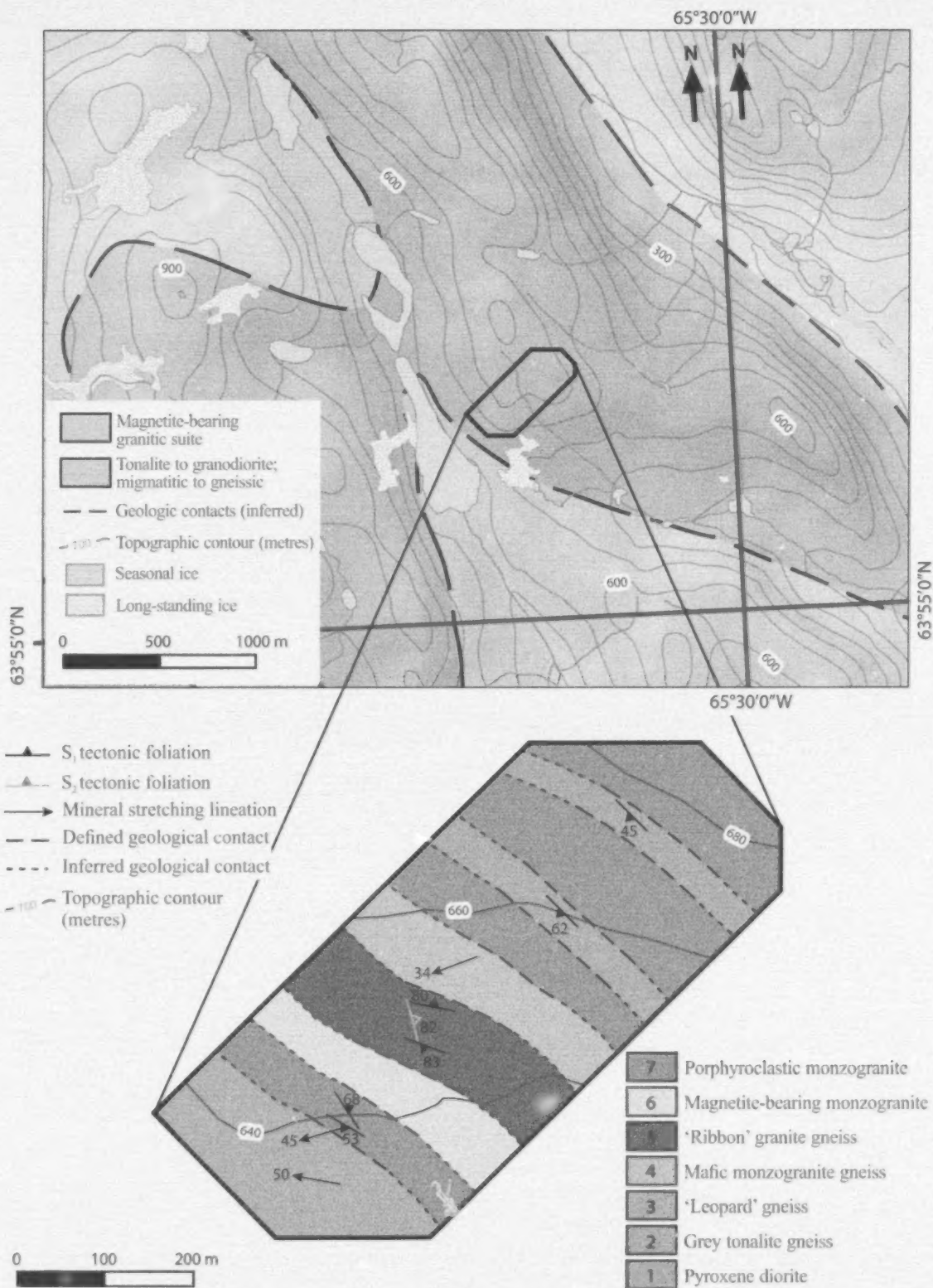
Figure 3: Detailed map of the study area region on Hall Peninsula, Nunavut, with inset showing the preliminary geology of the study area. The geological unit legend of the study area lists units from oldest (1) to youngest (7), as described in the text.
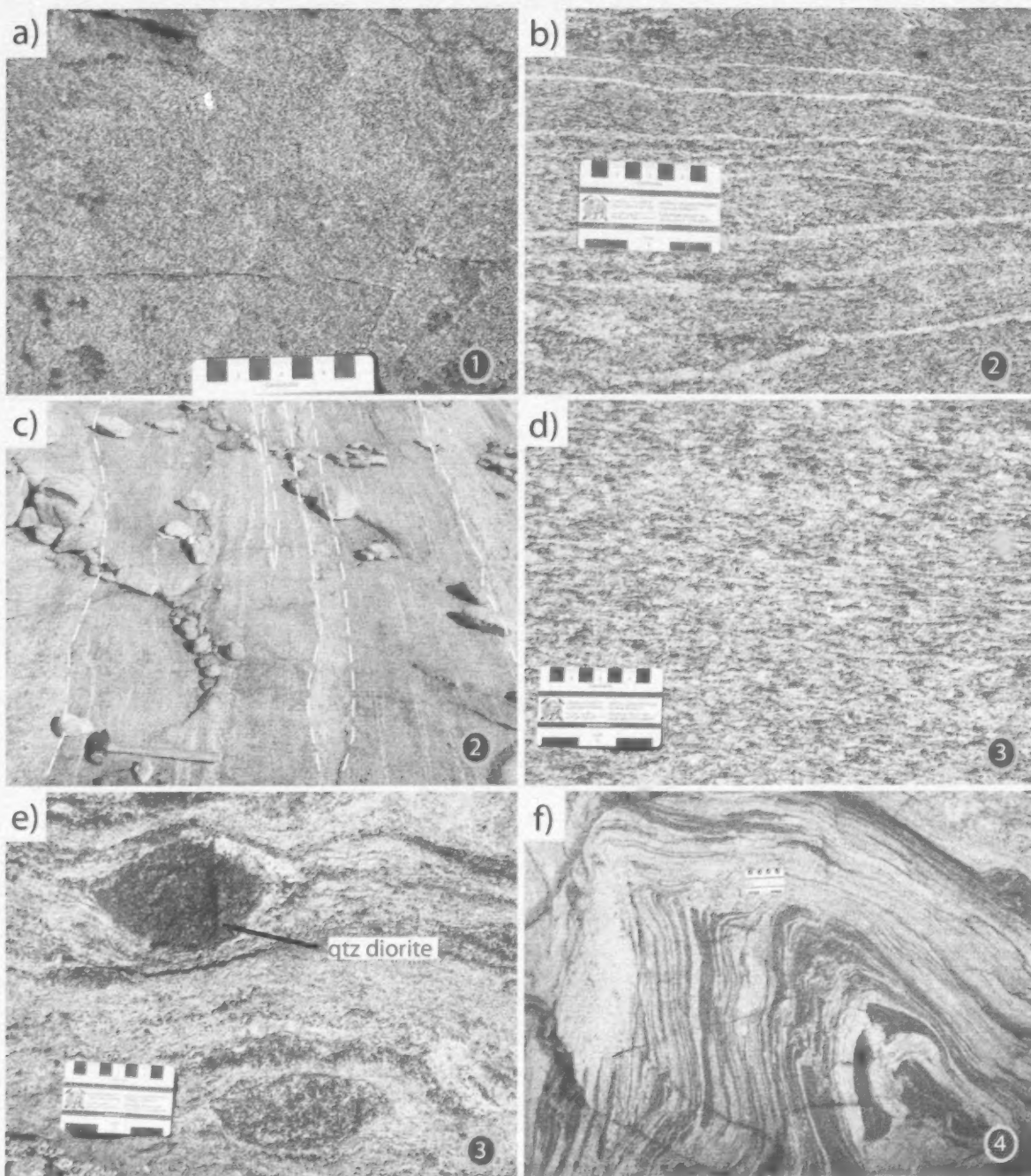
Figure 4: Field photographs from the study area, Hall Peninsula, Nunavut. Unit numbers and colour codes correspond to those of Figure 3 and are shown in the bottom right corner of each photograph: **a)** fine-grained pyroxene diorite of unit 1 that occurs as a panel 5–10 m wide within unit 7; **b)** medium-grained grey tonalite gneiss of unit 2 with thin trondhjemitic segregations; **c)** medium-grained grey tonalite gneiss of unit 2 intruded by monzogranitic veining several millimetres to tens of centimetres in width; **d)** medium-grained 'leopard' gneiss of unit 3 with plagioclase phenocrysts; **e)** 'leopard' gneiss of unit 3 characterized by fine-grained enclaves of hornblende+biotite+epidote quartz diorite; **f)** mafic monzogranite of unit 4 containing abundant clinopyroxene- and orthopyroxene-bearing mafic enclaves and discontinuous layering. Abbreviation: qtz, quartz.
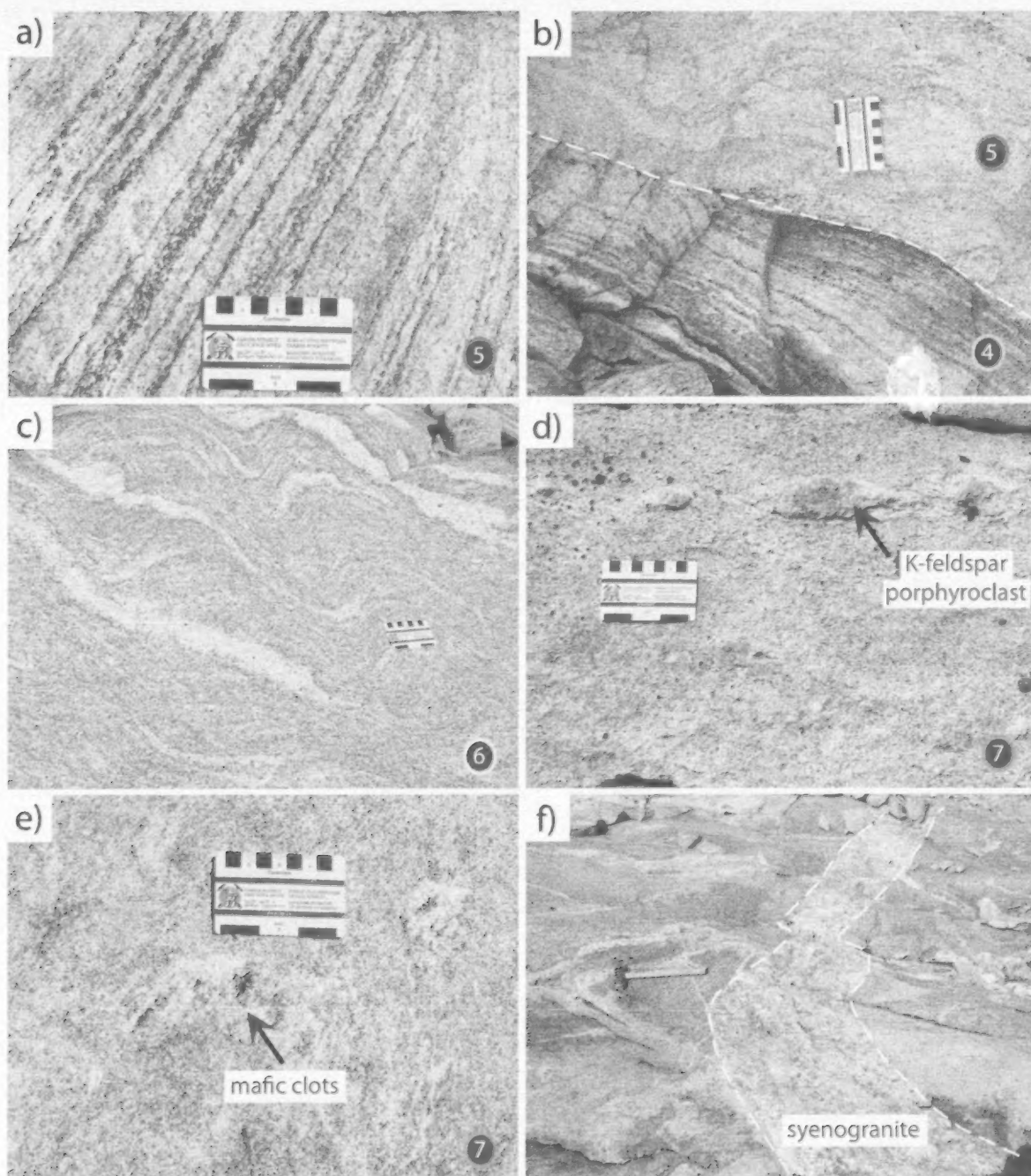
Figure 5: Field photographs from the study area, Hall Peninsula, Nunavut. Unit numbers and colour codes correspond to those of Figure 3 and are shown in the bottom right corner of each photograph: **a)** typical field aspects of the 'ribbon' granite gneiss from unit 5 with alternating bands of differential mineral composition giving a 'ribbon'-textured appearance; **b)** 'ribbon' granite gneiss of unit 5 crosscutting the foliation and layering in the mafic monzogranite gneiss of unit 4; **c)** magnetite-bearing monzogranite of unit 6 characterized by syntectonic melt segregations and depletion haloes enriched in mafic minerals; **d)** fine-grained porphyroclastic monzogranite of unit 7 characterized by K-feldspar porphyroclasts (disaggregated syenogranite veins); **e)** clots of biotite+hornblende±magnetite with light-coloured depletion haloes within the biotite+hornblende+epidote monzogranite of unit 7; **f)** weakly deformed syenogranite vein of unit 8 crosscutting foliation (parallel to the direction of the hammer) in grey tonalite gneiss of unit 2.

on the quartz. Rocks from unit 5 crosscut the gneissic layering of the mafic monzogranite gneiss in unit 4 (Figure 5b).

Magnetite-bearing monzogranite (unit 6)

Unit 6 consists of a greyish-white– and pinkish-weathering biotite- and magnetite-bearing monzogranite. Typically, the rocks of unit 6 are fine grained and characterized by melt segregations that have depletion haloes enriched in mafic minerals. The melt segregations also contain magnetite and are syndeformational as they locally crosscut the foliation but are in turn folded (Figure 5c).

Porphyroclastic monzogranite (unit 7)

Unit 7 rocks are typically greyish white on the weathered and fresh surfaces. The rocks are mainly fine grained and commonly contain biotite, hornblende and epidote. The unit is characterized by a K-feldspar porphyroclastic texture (Figure 5d), which is demonstrably derived from the disaggregation of syenogranitic veins. The rocks locally contain mineral clots consisting of relict orthopyroxene+clinopyroxene+hornblende and, elsewhere, abundant mineral clots of biotite±hornblende±magnetite. The clots of both compositions have light-coloured depletion haloes (Figure 5e). Locally, hornblende appears to be breaking down to biotite, which in turn is breaking down to epidote.

Syenogranite (unit 8)

The study area contains abundant occurrences of pegmatitic syenogranite, which forms dikes that crosscut all rock units in the area. These pegmatite dikes, too small to be shown on the map (Figure 3), are distinctively reddish pink on weathered and fresh surfaces. The rocks are coarse- to very coarse-grained and dominated by K-feldspar, with lesser amounts of quartz and biotite. The fact that these dikes crosscut the rocks from units 1 through 7 demonstrates that they are the youngest rock type in the study area. The pegmatite dikes have a varied structure; they are mainly undeformed, although locally some dikes are weakly folded (Figure 5f).

Structural and metamorphic character of the study area

The study area lies within the regionally extensive Archean orthogneiss complex that dominates eastern Hall Peninsula. The gneissic rocks in the study area broadly possess structural characteristics similar to those described by From et al. (2013). A summary of the structural context, with emphasis on observations made within the study area, is given here.

Field observations, including complex, superposed folding of gneissosity, demonstrate that multiple deformation events affected the gneissic rocks across Hall Peninsula during the Archean. In the study area, the deformational fabric, folding and metamorphism are labelled starting with the oldest recognizable deformation event. None of the

structures in the study area have been constrained by geochronology and their relative chronology is established based upon field observations. The pervasive gneissic fabric (S_1), developed in units 1 to 7, strikes east-southeast and dips moderately to steeply to the south-southwest. A mineral lineation (L_1), common in all units in the study area, plunges moderately to the west. This lineation is a common feature in Archean orthogneiss units of Hall Peninsula. Although F_1 folds, defined by folded S_1 gneissosity, were observed in rare, low-strain zones throughout the complex, they were not observed in the study area. Some rocks in the study area contain an S_2 fabric that strikes north-northwest to northwest and is defined as a local axial-planar foliation in F_2 folds of gneissosity. Parallel to the fold hinge, the F_2 folds display a shallowly plunging mineral-stretching lineation (L_2) defined by quartz+feldspar±hornblende±biotite. A quartz+feldspar rodding lineation (L_2) was also observed at the same orientation, plunging shallowly to the northwest.

The metamorphic assemblage seen most commonly throughout the study area is biotite+hornblende+epidote, indicating lower-amphibolite–facies metamorphism. However, the epidote is seen locally to be growing at the expense of biotite, which suggests that epidote is not a part of the peak metamorphic assemblage. The presence of clots that contain relict orthopyroxene+clinopyroxene+hornblende, where hornblende is observed to be breaking down to biotite and subsequently epidote, is indicative of a previous granulite-facies metamorphic grade. Other localities throughout the orthogneiss complex contain larger mafic enclaves or pods that also preserve a granulite-facies metamorphic assemblage of orthopyroxene+clinopyroxene+hornblende. It would seem from these observations that the orthogneiss complex was previously at granulite-facies metamorphic grade during the Archean. During subsequent episodes of metamorphism (Scott, 1999; Rayner, 2014), amphibolite-facies metamorphism overprinted the granulite facies, as shown by the retrogression of mineral assemblages.

Migmatitic textures are observed locally throughout the study area, appearing as layers of mineral segregation, leucosome development and irregular bodies of leucocratic material centimetres to several metres in size. It is possible that some of the monzogranitic to syenogranitic phases within these lithological units and within the orthogneiss complex are the result of partial melting and remobilization.

Conclusions

Previous regional-scale mapping within the Archean orthogneiss complex of Hall Peninsula labelled a vast area of gneissic rocks as tonalite and monzogranite gneiss. Contributing factors, including felsenmeer erosion, inaccessibility, snow cover and lichen-coated outcrops, left the tonalite and monzogranite units mainly undifferentiated at a

regional scale. However, the subtle yet distinct rock types mapped in the study area demonstrate the complexity of regional Archean rock units. The study area is dominated by porphyroclastic monzogranite (unit 7) that intrudes and entrains other older phases of plutonic rocks (units 1–6), including a small amount of truly grey tonalite gneiss from unit 2 (Figures 3, 4 and 5). Coarse-grained syenogranite (unit 8) crosscuts all other units and is itself relatively undeformed. Following the documentation of these eight distinct lithological units in the study area, further detailed analytical work will be required to establish the correlation of units across the Archean orthogneiss complex and to determine the plutonic history of the complex. Future work will further characterize the Archean Hall Peninsula block, revealing a fingerprint that can be used for comparison with adjacent Archean terrains, and will provide insight into paleoplate reconstructions for the Baffin Island and subarctic region as a whole.

Future work

Excellent exposures and well-defined crosscutting relationships between the plutonic phases within the study area makes this locality ideal for future detailed work to fully characterize the geological history of these rocks. A petrographic analysis of each phase will provide full mineral assemblage characterization. The SHRIMP will be used to carry out U-Pb geochronology on selected units to constrain the intrusive ages of these phases, as well as the timing of crosscutting relationships. Geochemistry will further characterize each unit according to major elements and rare-earth element concentrations. Lutetium-hafnium isotopic ratios in zircon grains having a known crystallization age from U-Pb geochronology will provide insight into the magmatic history of the plutonic rocks. The field and analytical work will then provide a baseline, from which to assess the spatial extent of plutonic units across the Archean orthogneiss complex. In addition, regional-scale east-west and north-south Sm-Nd transects across eastern Hall Peninsula will provide an assessment of any underlying crust not exposed at surface on Hall Peninsula and the comparison of àNd values to those of crustal blocks adjacent to Hall Peninsula.

Economic considerations

Each crustal block in the Baffin Island region has its own distinct metallotect and associated exploration parameters. The characterization of the Archean orthogneiss complex of Hall Peninsula and correlation with adjacent crustal blocks will allow already established exploration models to be applied to Hall Peninsula. This is especially interesting for future exploration opportunities given the presence of diamonds, base metals, gem-quality minerals, including spinel, apatite and garnet, and carving stone already estab-

lished on Hall Peninsula (Senkow, 2013), all of which are important for Nunavut's future economic development.

Acknowledgments

References

Blackadar, R.G. 1967: Geological reconnaissance, southern Baffin Island, District of Franklin; Geological Survey of Canada, Paper 66-47.

Connelly, J. N. 2001: Constraining the timing of metamorphism: U-Pb and Sm-Nd ages from a transect across the northern Torngat Orogen, Labrador, Canada; Canadian Journal of Geology, v. 109, p. 57–77.

Corrigan, D., Pehrsson, S., Wodicka, N. and De Kemp, E. 2009: The Palaeoproterozoic Trans-Hudson Orogen: a prototype of modern accretionary processes; Geological Society, London, Special Publications, v. 327, p. 457–479.

Creason C.G., Gosse, J.C. and Young, M.D. 2013: Rift flank uplift and landscape evolution of Hall Peninsula, Baffin Island, Nunavut: an exhumation model based on low-temperature thermochronology; in Summary of Activities 2012, Canada-Nunavut Geoscience Office, p. 75–84.

From, R.E., Camacho, A.L. and St-Onge, M.R. 2012. Preliminary observations on the nature and origin of the eastern orthogneiss complex of southern Hall Peninsula, Baffin Island, Nunavut; in Summary of Activities 2012, Canada-Nunavut Geoscience Office, p. 43–54.

Hoffman, P.F. 1988: United Plates of America, the birth of a craton: Early Proterozoic assembly and growth of Laurentia; Annual Review of Earth and Planetary Sciences, v. 16, p. 543–603.

Hollis, J. A., Frei, D., Van Gool, J. A. M., Garde A. A. and Persson, M. 2006: Using zircon geochronology to resolve the Archaean geology of southern West Greenland; Geological Survey of Denmark and Greenland, Bulletin 10, p. 49–52.

Knight, I. and Morgan, W.C. 1981: The Aphebian Ramah Group, northern Labrador; in Proterozoic Basins of Canada, F.H. A. Campbell (ed.), Geological Survey of Canada, Paper 81-10, p. 313–330.

Leblanc-Dumas, J., Allard, M. and Tremblay, T. 2013: Quaternary geology and permafrost characteristics in central Hall Peninsula, Baffin Island, Nunavut; in Summary of Activities 2012, Canada-Nunavut Geoscience Office, p. 101–106.

Machado, G., Bilodeau, C., Takpanie, R., St-Onge, M.R., Rayner, N.M., Skipton, D.R., From, R.E., MacKay, C.B., Creason

C.G. and Braden, Z.M. 2013: Hall Peninsula regional bedrock mapping, Baffin Island, Nunavut: summary of fieldwork; *in* Summary of Activities 2012, Canada-Nunavut Geoscience Office, p. 13–22.

MacKay, C.B., Ansdell, K.M., St-Onge, M.R., Machado, G. and Bilodeau, C. 2013: Geological relationships in the Qaqqanittuaq area, southern Hall Peninsula, Baffin Island, Nunavut; *in* Summary of Activities 2012, Canada-Nunavut Geoscience Office, p. 55–64.

Rayner, N.M. 2014: New U-Pb geochronological results from Hall Peninsula, Baffin Island, Nunavut; *in* Summary of Activities 2013, Canada-Nunavut Geoscience Office, p. 39–52.

Senkow, M.D. 2013: Characterization of ultramafic occurrences on southern Hall Peninsula, Baffin Island, Nunavut, and evaluation of their potential as a source of carving stone; *in* Summary of Activities 2012, Canada-Nunavut Geoscience Office, p. 163–168.

Scott, D.J. 1996: Geology of the Hall Peninsula east of Iqaluit, southern Baffin Island; *in* Current Research 1996-C, Geological Survey of Canada, p. 83–91.

Scott, D.J. 1999: U-Pb geochronology of the eastern Hall Peninsula, southern Baffin Island, Canada: a northern link between the Archean of West Greenland and the Paleoproterozoic Torngat Orogen of northern Labrador; Precambrian Research, v. 93, p. 5–26.

Scott, D.J. and Campbell, L.M. 1993. Evolution of the Paleoproterozoic Torngat orogen, Labrador Canada: recent advances using U-Pb geochronology and Nd isotopic systematics (abstract); Geological Society of America, Annual Meeting 1993, Boston, Massachusetts, Program with abstracts, v. 25, p. A23.

Scott, D.J. and Gauthier, G. 1996: Comparison of TIMS (U-Pb) and laser ablation microprobe ICP-MS (Pb) techniques for age determination of detrital zircons from Paleoproterozoic metasedimentary rocks from northeastern Laurentia, Canada, with tectonic implications; Chemical Geology, v. 131, p. 127–142.

Skipton, D.R., Schneider, D. A. and St-Onge, M.R. 2013: Preliminary observations on Archean and Paleoproterozoic metamorphism and deformation of the southern Hall Peninsula, Baffin Island, Nunavut; *in* Summary of Activities 2012, Canada-Nunavut Geoscience Office, p. 29–42.

Steenkamp, H.M. and St-Onge, M.R. 2014. Overview of the 2013 regional bedrock mapping program on northern Hall Peninsula, Baffin Island, Nunavut; *in* Summary of Activities 2013, Canada-Nunavut Geoscience Office, p. 27–38.

St-Onge, M.R., Van Gool, J.A.M., Garde, A. A. and Scott, D.J. 2009: Correlation of Archaean and Palaeoproterozoic units between northeastern Canada and western Greenland: constraining the pre-collisional upper plate accretionary history of the Trans-Hudson orogen; Geological Society of London, Special Publications, v. 318, p. 193–235, doi:10.1144/SP318.7.

Thrane, K. and Connelly J. N. 2006: Zircon geochronology from the Kangatsiaq-Qasigianguit region, the northern part of the 1.9–1.8 Ga Nagssugtoqidian orogen, West Greenland; Geological Survey of Denmark and Greenland Bulletin, no. 11, p. 87–99.

Van Gool, J.A.M., Garde, A.A. and Larsen, L. M. 2004: Correlation of Precambrian geology in Labrador and southern Greenland; Danmarks og Grønlands Geologiske Undersøgelse Rapport, 2004/29, 30 p.

Wardle, R.J., James D.T., Scott, D.J. and Hall, J. 2002: The southeastern Churchill Province: synthesis of a Palaeoproterozoic transpressional orogen; Canadian Journal of Earth Sciences, v. 39, p. 639–663, doi:10.1139/E02-004.

Whalen, J. B., Wodicka, N., Taylor, B. E. and Jackson, G. D. (2010). Cumberland batholith, Trans-Hudson Orogen, Canada: petrogenesis and implications for Paleoproterozoic crustal and orogenic processes; Lithos, v. 117, p. 99–118.

Paleoproterozoic deformation and metamorphism in metasedimentary rocks west of Okalik Bay: a field template for the evolution of eastern Hall Peninsula, Baffin Island, Nunavut

D.R. Skipton[1] and M.R. St-Onge[2]

[1]*Department of Earth Sciences, University of Ottawa, Ottawa, Ontario, dskip037@uottawa.ca*
[2]*Geological Survey of Canada, Natural Resources Canada, Ottawa, Ontario*

Abstract

Hall Peninsula on southeastern Baffin Island, Nunavut, occurs in the northeastern segment of the Paleoproterozoic collisional zone of the Trans-Hudson Orogen. Recent bedrock mapping at the scale of 1:250 000 by the Canada-Nunavut Geoscience Office has shown that western Hall Peninsula comprises high-grade Paleoproterozoic metasedimentary cover rocks that host orthopyroxene-bearing granitic intrusions and garnet-bearing leucogranite. Eastern Hall Peninsula is dominated by an Archean orthogneiss basement complex mostly composed of tonalite and monzogranite. Paleoproterozoic supracrustal cover rocks in the east occur as discrete packages overlying the orthogneiss, or as panels tectonically imbricated with the basement units by thick-skinned thrusting and folding. Targeted mapping during the 2013 field season has further elucidated the complex structural and metamorphic history recorded in the supracrustal rocks. Excellent exposure of supracrustal cover units in contact with tonalitic basement in the area about 40 km west of Okalik Bay enabled a detailed study of the tectonostratigraphic units, deformation fabrics and metamorphic mineral assemblages that characterize the eastern assemblage. The supracrustal rocks consist of interbedded psammite and pelite, with minor occurrences of amphibolite and quartzite. Based on detailed mapping, there are two dominant Paleoproterozoic deformation events recorded in this area: an early east-directed shortening (D_1), which formed a strong west-dipping foliation, and a subsequent south-directed shortening (D_3), which produced south-verging folds. These events were accompanied by amphibolite-facies metamorphism and minor partial melting. The nature and relative timing of deformation and metamorphism in this area is representative of those observed elsewhere on eastern Hall Peninsula, and will therefore help in developing a template for the tectonometamorphic evolution of this segment of the Trans-Hudson Orogen during the Paleoproterozoic.

Résumé

La péninsule Hall située dans la partie sud-est de l'île de Baffin, au Nunavut, fait partie du segment nord-est de la zone de collision de l'orogène trans-hudsonien. Des travaux de cartographie à l'échelle de 1/250 000 récemment entrepris par des chercheurs du Bureau géoscientifique Canada-Nunavut ont révélé la présence, dans la partie occidentale de la péninsule de Hall, de roches couverture métasédimentaires d'âge paléoprotérozoïque soumises à un métamorphisme intense; ces dernières renferment des intrusions granitiques à orthopyroxène et du leucogranite à grenat. La partie orientale de la péninsule Hall est en plus grande partie constituée d'un socle d'orthogneiss archéen composé principalement de tonalite et de monzogranite. Les roches de couverture supracrustales d'âge paléoprotérozoïque situées dans la partie orientale de la péninsule se manifestent sous forme d'ensembles discrets sus-jacents à l'orthogneiss ou sous forme de panneaux imbriqués

tectoniquement dans les unités du socle suite à l'action de chevauchements et de plissements des couches épaisses. Des travaux de cartographie sélective réalisés au cours de la saison de terrain 2013 ont permis d'éclaircir encore mieux l'histoire structurelle et métamorphique consignée dans les roches supracrustales. À partir d'excellents affleurements de roches supracrustales en contact avec le socle tonalitique dans une région située environ 40 km à l'ouest de la baie Okalik, on a pu étudier en détail les unités tectonostratigraphiques, la fabrique tectonique et les assemblages minéraux métamorphiques qui caractérisent l'assemblage oriental. Les roches supracrustales se composent de psammite et de pélite interstratifiées, accompagnées d'une petite quantité d'amphibolite et de quartzite. La cartographie détaillée a permis d'établir que la région a été sujette à deux événements de déformation prépondérants au cours du Paléoprotérozoïque : un premier raccourcissement de direction est (D1), qui est à l'origine d'une foliation à pendage prononcé vers l'ouest, suivi d'un raccourcissement de direction sud (D3), responsable de la formation de plis à vergence sud. Ces événements ont été accompagnés d'un épisode de métamorphisme au faciès des amphibolites et d'un faible taux de fusion partielle. La nature et le rythme relatif des épisodes de déformation et de métamorphisme dans cette région s'apparentent à ceux qui ont été notés ailleurs dans la partie orientale de la péninsule Hall. À l'aide de ces renseignements, il sera possible de mettre au point un modèle de l'évolution tectono-métamorphique de ce segment de l'orogène trans-hudsonien au cours du Paléoprotérozoïque.

Introduction

The Canada-Nunavut Geoscience Office (CNGO) conducted bedrock mapping at the scale of 1:250 000 on Hall Peninsula during the summers of 2012–2013. Based on regional mapping by the CNGO, and collaborative studies with several Canadian universities and the Geological Survey of Canada, Hall Peninsula is known to represent a lithologically diverse section of the middle crust in the northeastern Paleoproterozoic Trans-Hudson Orogen with a complex structural architecture and metamorphic history. This paper presents a detailed study of the deformation fabrics and metamorphic assemblages in Paleoproterozoic metasedimentary rocks and Archean tonalitic orthogneisses in a well-exposed area located 40 km west of Okalik Bay on eastern Hall Peninsula. The nature and relative timing of deformation and metamorphism in this area is representative of those observed elsewhere on eastern Hall Peninsula, and therefore contribute to a better understanding of the thermal and structural history of Hall Peninsula as a whole, and its role in the Trans-Hudson orogeny during crustal amalgamation.

Background geology

Hall Peninsula on southeastern Baffin Island, Nunavut, is part of the Paleoproterozoic collisional zone of the Trans-Hudson Orogen (Figure 1), a Paleoproterozoic collisional belt that extends in a broad arcuate shape from northeastern to south-central North America (Hoffman, 1988; Lewry and Collerson, 1990) and separates the lower-plate Superior craton from an upper-plate collage of Archean crustal blocks (Churchill Plate). The Churchill Plate includes the Wyoming craton, the Hearne Domain, the Slave craton, the Rae craton and, in Greenland and Labrador, the North Atlantic (Nain) craton. On Baffin Island, the well-exposed continental collisional zone records the southward migration of the Churchill Plate and its terminal collision with the Superior craton at 1.82–1.80 Ga (St-Onge et al., 2009). The up-

per Churchill Plate collage in the Quebec–Baffin segment of the Trans-Hudson Orogen consists of the Rae craton and several microcontinents, which were accreted to the southeastern Rae margin between ca. 1.88–1.84 Ga. One of these terranes, forming much of southern Baffin Island, is the Meta Incognita microcontinent, which accreted to the southeastern Rae margin between ca. 1.883 and 1.865 Ga (St-Onge et al., 2006). The Meta Incognita microcontinent comprises crystalline basement overlain by a Paleoproterozoic clastic carbonate-shelf succession (Lake Harbour Group) and ca. 1.865–1.848 Ga quartz-diorite to monzogranite plutons (Cumberland Batholith) that intrude both crystalline basement and the Lake Harbour Group (Scott and Wodicka, 1998; St-Onge et al., 2000, 2007; Corrigan et al., 2009).

The crystalline basement has been correlated with ca. 3.02–2.78 Ga orthogneisses in the lower-plate Superior margin in Northern Quebec (St-Onge et al., 2000). However, it remains unclear whether the basement of the Meta Incognita microcontinent rifted from the Superior or Rae craton, or whether it constitutes crust that is exotic to both cratons (St-Onge et al., 2009). Previous work on Hall Peninsula has shown that it consists of ca. 1.85–1.86 Ga granitic plutons that intruded ca. 1.93–1.89 Ga metasedimentary rocks, with eastern Hall Peninsula dominated by an Archean (ca. 2.92–2.80 Ga) orthogneiss basement complex (Blackadar, 1967; Scott, 1996, 1999). The plutonic rocks may be the eastern continuation of the Cumberland Batholith and the metasedimentary rocks have been correlated with the Lake Harbour Group of the Meta Incognita microcontinent. Possible parentage for the Archean orthogneiss complex includes the Superior craton, as suggested for the Meta Incognita microcontinent, the North Atlantic craton of southern Greenland, the Aasiaat domain in West Greenland, the Core Zone in northern Labrador, the upper-plate Rae craton or an Archean block of exotic affinity. Several purported suture zones, when extrapolated great distances onto the peninsula, ap-
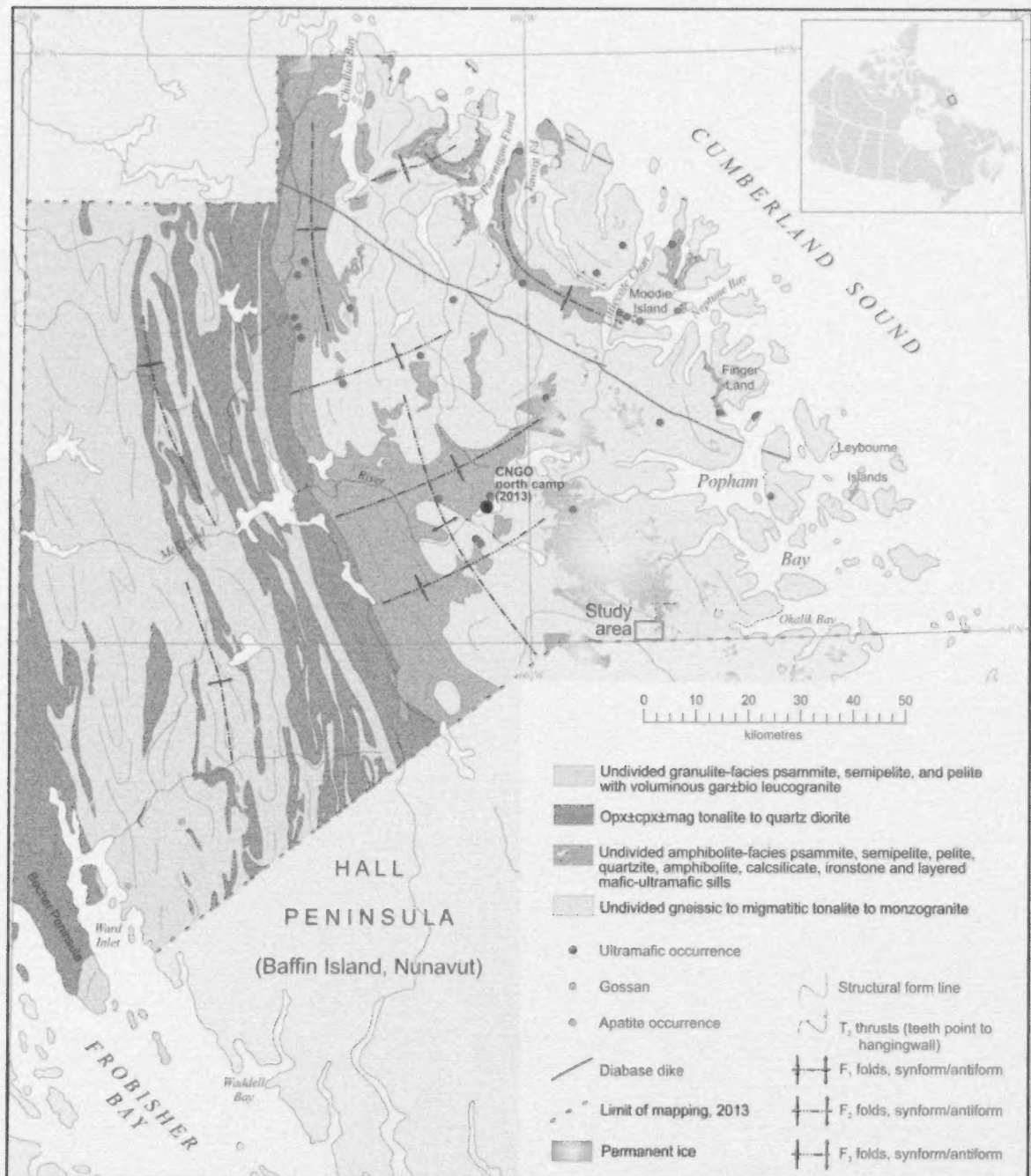
Figure 1: Geology of Hall Peninsula, Nunavut, based on mapping done by staff of the Canada-Nunavut Geoscience Office during the summers of 2012 and 2013 (Machado et al., 2013; Steenkamp and St-Onge, 2014). The inset map shows the location of Hall Peninsula in the Trans-Hudson Orogen. The study area, located approximately 40 km west of Okalik Bay, on Hall Peninsula, is indicated by the red box.

pear to converge on Hall Peninsula, including the approximately east-west striking Baffin suture, which forms the boundary between the Meta Incognita microcontinent and the Rae craton; the approximately east-west striking Disko Bugt and Nagssugtoqidian sutures, which separate the Aasiaat Domain (St-Onge et al., 2009) from the Rae craton to the north and the North Atlantic craton to the south in West Greenland; and the northwest-striking Abloviak Shear Zone and associated sutures in the Torngat Orogen, northern Labrador, which separate the North Atlantic craton from the Superior craton.

Consequently, the geology and tectonic history of Hall Peninsula may provide the needed constraints to resolve plate tectonic reconstructions of the Trans-Hudson Orogen in northern Canada and Greenland.

Metamorphic zircon and monazite from metasedimentary rocks and orthogneisses on Hall Peninsula dated regional amphibolite-facies metamorphism at ca. 1.86–1.83 Ga (Scott, 1999). Hints of a younger tectonothermal event are provided by ca. 1.76 Ga granitic veins (U-Pb zircon) and ca. 1.74–1.73 Ga titanite ages yielded by the Archean orthogneisses (Scott, 1999).

Updated geology of Hall Peninsula

Bedrock mapping at the scale of 1:200 000 undertaken during the summers of 2012–2013 (Figure 1) has shed light on the lithological complexity, deformation and metamorphism on Hall Peninsula (Machado et al. 2013; Steenkamp and St-Onge, 2014). Hall Peninsula records two principal lithological associations that differ in the eastern and western portions of the peninsula.

The western part of the peninsula is dominated by Paleoproterozoic metasedimentary rocks that host orthopyroxene-bearing granitic intrusions, garnet±biotite leucogranite sills and, locally, muscovite-sillimanite±garnet leucogranite dikes. The leucogranites generally exhibit transposed contacts with the host metasedimentary rocks and locally contain metasedimentary inclusions. The mineral assemblages and the presence of metasedimentary inclusions suggest that the leucogranite sills and dikes were produced by anatexis of the metasedimentary rock package (Dyck and St-Onge, 2014). Contacts between metasedimentary rocks and the orthopyroxene-bearing granitoid rocks are transposed and are interpreted as intrusive. Supracrustal rocks in the western portion of the peninsula include high-grade biotite-garnet-melt±sillimanite pelite and semipelite, biotite±garnet psammite, and minor biotite±garnet quartzite with localized occurrences of diopside-humite-phlogopite marble. The supracrustal rocks have been partially melted during metamorphism and are thus dominated by coarse-grained, garnet-rich diatexites that weather a rusty colour and transitional metatexites–diatexites with relict bedding.

The eastern portion of the peninsula is dominated by an Archean basement orthogneiss complex comprising mostly biotite±hornblende±magnetite tonalite and monzogranite that contain enclaves of diorite, mafic tonalite, amphibolite and pyroxenite, and are crosscut by undeformed monzogranite to syenogranite dikes (From et al., 2013, 2014). Paleoproterozoic supracrustal cover rocks in the eastern portion of Hall Peninsula form panels some 10 m to 10 km thick that occur structurally both above and below the Archean orthogneiss. The cover strata are separated from the basement by sharp contacts that are parallel to the dominant regional metamorphic foliation. In a number of localities, the contact between Paleoproterozoic cover units and the underlying Archean basement is relatively undeformed, suggesting it is stratigraphic in nature. The presence of basal quartzite beds resting directly on orthogneiss corroborates this interpretation.

The metasedimentary rocks of eastern Hall Peninsula include medium-grade biotite-garnet±sillimanite±muscovite pelite and semipelite, biotite psammite and minor occurrences of garnet-biotite quartzite, diopside-humite-phlogopite marble and tremolite±tourmaline calcsilicates. In contrast to the metasedimentary rocks to the west, those of the eastern assemblage almost always contain layers of amphibolite±ironstone and some supracrustal packages on northeastern Hall Peninsula are dominated by mafic rocks.

In several areas on Hall Peninsula, particularly along the northeastern coast in the Ptarmigan Fiord, Moodie Island and Finger Land regions (Figure 1), panels of supracrustal rock and basement orthogneiss that contain early synmetamorphic (D_1) structures are repeated by east-directed thick-skinned (D_2) thrusts, which occurred after the thermal peak. From outcrop-scale to map-scale basement and supracrustal rocks are also deformed by east-verging thick-skinned (D_2) folds and south-verging thick-skinned (D_3) crossfolds. A summary of structural elements and associated deformation fabrics on Hall Peninsula is provided in Steenkamp and St-Onge, (2014).

Study area

This paper focuses on a package of Paleoproterozoic supracrustal rocks in the east-central part of Hall Peninsula, located approximately 40 km west of Okalik Bay, adjacent to a glacier that is 6 km wide (Figures 1, 2). Due to the recent retreat of the glacier, there is continuous bedrock exposure in this area, which enabled detailed mapping through a succession of dominantly metasedimentary strata and across the underlying basement-cover contact. Most significantly, the excellent exposure of pelitic rocks provided an opportunity to examine the deformation fabrics and associated metamorphic mineral assemblages related to two Paleoproterozoic regional deformation events (D_1 and D_3), which

are representative of structures and assemblages observed elsewhere on eastern Hall Peninsula.

The D_2 event, comprising post-thermal peak thick-skinned thrusts and folds, as described above, is interpreted as representing a later phase of the east-directed shortening that produced the synmetamorphic structures of D_1. Thrust imbricates of basement and cover are not documented in the area west of Okalik Bay, leading to the conclusion that post-thermal peak thick-skinned thrusting did not occur in this area. However, thick-skinned folding (D_2) of basement and cover is indicated by the overturned nature of the western basement-cover contact (see below).

The supracrustal rocks consist dominantly of alternating beds 10–40 cm thick of biotite psammite and biotite–garnet–sillimanite–K-feldspar±muscovite pelite (Figure 3a), which exhibits a well-developed faserkiesel texture (Figure 3b). These rocks locally contain concordant layers of garnet-bearing amphibolite and ironstone. Near the overturned basement-cover contact on the western side of the basin (Figure 2), the metasedimentary rocks comprise dominantly psammite, with very few pelitic beds, and an interval of blue quartzite 24 m thick, which occurs at the basement-cover contact. Basement rocks consist of biotite tonalite intruded by monzogranite dikes and veins.

Deformation fabrics and metamorphic assemblages

East-directed shortening (D_1)

East-directed shortening during D_1 is responsible for the development of a west- to northwest-dipping S_{1a} fabric throughout the study area (Figures 2–5). The S_{1a} fabric in the metasedimentary rocks is defined by the orientation of the M_1 amphibolite-facies biotite–sillimanite–K-feldspar–melt±muscovite mineral assemblage (Figures 5a–d). The S_{1a} fabric generally dips slightly more steeply than bedding, suggesting that most of the supracrustal rocks in the study area lie on the upright limb of a large F_{1a} fold. East-verging F_{1a} folds of bedding occur at the outcrop scale, with the S_{1a} fabric clearly parallel to the F_{1a} axial plane (Figure 5b). A L_1 lineation is defined by aligned knots of sillimanite and garnet, and generally plunges northwest. Bedding and the S_{1a} fabric are reoriented by F_3 folds (Figures 4, 5c).

Upper-amphibolite–facies metamorphism (M_1)

The supracrustal rocks experienced upper-amphibolite–facies metamorphism early in their deformation history, as expressed by their metamorphic mineral assemblages. The M_1 assemblage in pelitic beds consists of biotite–garnet–sillimanite–K-feldspar–melt±muscovite. The pelite also locally contains muscovite with an oblique orientation to S_{1a}, suggesting that it represents in part a younger overprint (see below). Garnet forms ruby-red– to lilac-coloured euhedral crystals up to 1 cm wide, and is typically surrounded by sillimanite, which forms knots (faserkiesel) up to 2 cm wide (Figure 3b). Garnet and faserkiesel knots are hosted by a fine- to medium-grained matrix of biotite, quartz and feldspar. Biotite can also form coarse-grained crystals that surround the garnet, faserkiesel knots and the edges of leucosome. Partial melt forms discrete veins and lenses that comprise about 3–5%, and locally up to 10%, of total-rock volume (Figure 3c, d). The mineral assemblage and presence of partial melt indicate that these rocks achieved upper-amphibolite–facies temperatures exceeding the vapour-absent muscovite dehydration-melting reaction (mus+plag+qtz = als+kfs+melt; Spear et al., 1999; see Dyck and St-Onge, 2014).
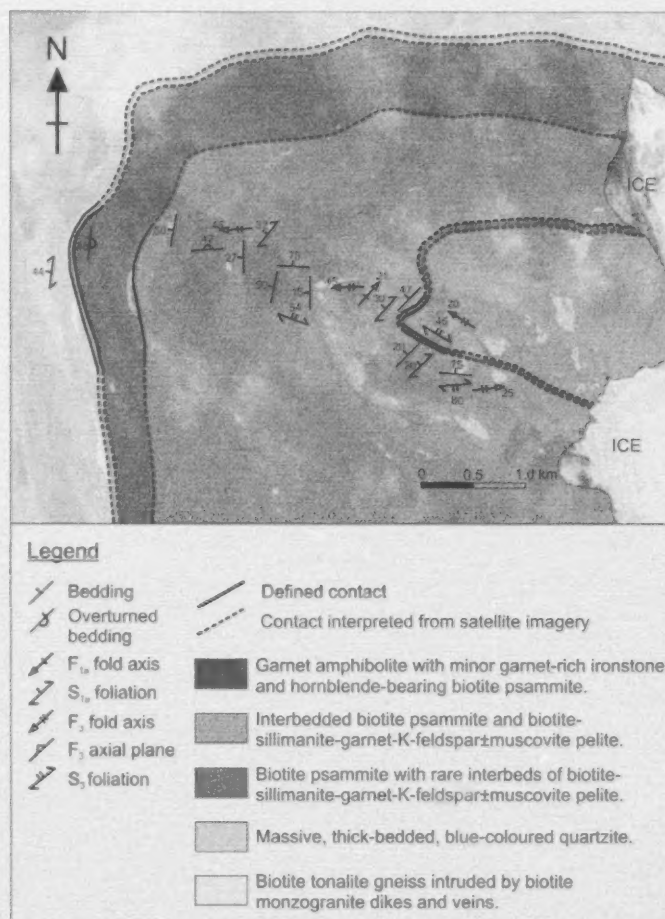
Figure 2: Geology of the study area, located approximately 40 km west of Okalik Bay on eastern Hall Peninsula, Baffin Island, Nunavut.

Legend

- ⟋ Bedding
- ⟋ Overturned bedding
- ⟋ F_{1a} fold axis
- ⟋ S_{1a} foliation
- ⟋ F_2 fold axis
- ⟋ F_3 axial plane
- ⟋ S_3 foliation

— Defined contact
--- Contact interpreted from satellite imagery

▨ Garnet amphibolite with minor garnet-rich ironstone and hornblende-bearing biotite psammite.

▨ Interbedded biotite psammite and biotite-sillimanite-garnet-K-feldspar±muscovite pelite.

▨ Biotite psammite with rare interbeds of biotite-sillimanite-garnet-K-feldspar±muscovite pelite.

▨ Massive, thick-bedded, blue-coloured quartzite.

▨ Biotite tonalite gneiss intruded by biotite monzogranite dikes and veins.

Figure 3: Field photographs of interbedded biotite psammite and biotite–garnet–sillimanite–K-feldspar±muscovite pelite on Hall Peninsula, Nunavut, showing, **a)** a typical outcrop of interbedded psammite and pelite with west-dipping bedding, and where S_{1a} is approximately parallel to bedding and S_3 crenulation cleavage dips to the northeast; **b)** ruby-red garnets surrounded by faserkiesel knots in pelite; **c)** a leucosome vein 1 cm thick in pelite, oriented parallel to S_{1a} and folded by F_3; **d)** a leucosome lens in pelite, oriented parallel to the S_3 crenulation cleavage.
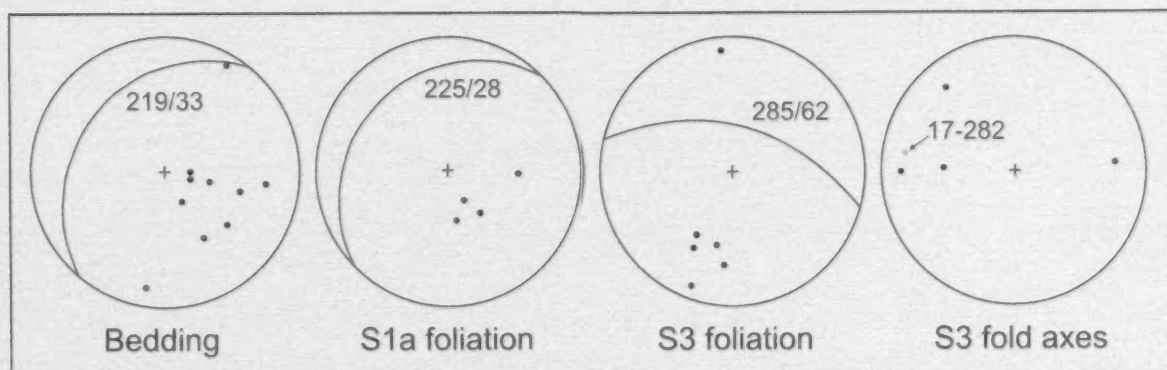
Figure 4: Representative structural measurements from the study area plotted on equal-area stereonets. Bedding and foliation are plotted as poles to planes, with mean orientations plotted as labelled great circles. The mean orientation of the fold axes is represented as a labelled grey dot.
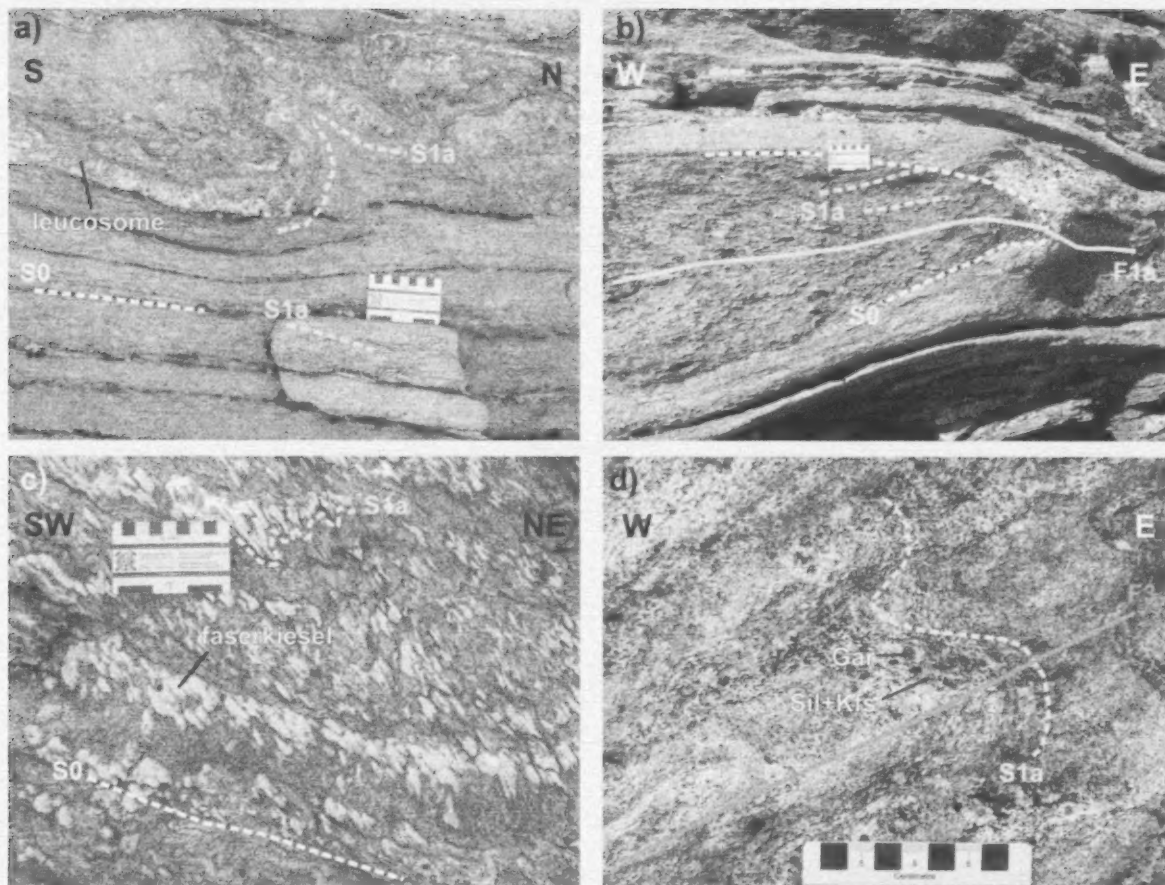
Canada-Nunavut Geoscience Office

Figure 5: Field photographs of interbedded biotite psammite and biotite–sillimanite–garnet–K-feldspar–melt (leucosome)±muscovite pelite on Hall Peninsula, Nunavut, showing **a)** S_{1a} and a leucosome folded by F_3 with faserkiesel knots, at the lower-centre of photo, slightly oblique to bedding, but not axial planar to F_3, and therefore interpreted as representing S_{1a}; **b)** isoclinal F_{1a} fold with axial-planar S_{1a} fabric; **c)** faserkiesel knots folded by F_3 and reoriented axial planar to F_3; **d)** M_1 metamorphic assemblage, including garnet (gar), K-feldspar (kfs) and sillimanite (sil), folded by F_3.

South-directed shortening (D₃)

The D_3 event is characterized by the widespread development of F_3 folds, which range in size from centimetre-scale, crenulation-style folds to much larger folds reaching 100 m in size, that result in the reorientation of bedding and D_1 fabrics. The D_3 event is interpreted as postdating M_1 and D_1 because the M_1 mineral assemblage (biotite–sillimanite–garnet–K-feldspar–melt±muscovite) and S_{1a} fabric are crenulated by F_3 folds (Figures 3, 5). The F_3 folds have west-plunging fold axes and north-dipping axial planes, and are generally asymmetric and verging to the south (Figure 5a). An S_3-crenulation cleavage is well-developed in pelitic beds (Figures 3a, d) and is locally accompanied by faserkiesel knots that are reoriented axial planar to the F_3 folds (Figure 5c). The S_3 fabric generally dips moderately to the north-northeast (Figure 4). The western segment of the study area, proximal to the basement-cover contact,

does not display D_3 structures as readily due to a relative paucity of pelitic beds.

Syn-D₃ amphibolite-facies metamorphism

There is limited field evidence for a distinct mineral assemblage associated with D_3. In D_3-crenulated muscovite-bearing pelite, muscovite, in addition to being strongly crenulated as part of the S_1a biotite–sillimanite–K-feldspar–melt assemblage, also occurs as neoblastic crystals oriented axial planar to the D_3 crenulations.

Granitic leucosome occurs as veins and lenses that are parallel to S_{1a} and crenulated by D_3 (Figures 3c, 5a), and also forms veins and lenses that are parallel to the S_3 crenulation cleavage (Figure 3d). Both sets of leucosome comprise roughly the same total-rock volume (3–5%), which suggests that a similar degree of partial melting occurred dur-

ing D_1 and D_3. The absence of new K-feldspar and the presence of apparently stable neoblastic muscovite and melt, both axial planar to the F_3 crenulations, suggest that P-T conditions during D_3 were slightly lower than the upper-amphibolite conditions associated with D_1 (see above). Therefore, the P-T conditions during D_3 are probably bracketed by the vapour-present muscovite breakdown reaction (mus+plag+qtz+v = als+melt) and the higher-temperature vapour-absent muscovite dehydration-melting reaction (mus+plag+qtz = als+Kfs+melt; Spear et al., 1999; see Dyck and St-Onge, 2014).

Discussion

Detailed field mapping in the area west of Okalik Bay provides clear evidence for two regional deformation events: an east-directed shortening during D_1 followed by a south-directed shortening during D_3. The D_1 event is responsible for the formation of a dominant west-northwest-dipping S_{1a} fabric, as well as east-verging folds of bedding. Based on bedding-foliation relationships and the overall map pattern, the study area is likely situated on a large F_{1a} fold several kilometres in size with dominantly west-dipping limbs. In the eastern part of the study area, the S_{1a} foliation is generally steeper than bedding in the metasedimentary rocks, suggesting that they lie on the upright limb of an F_{1a} fold. At the western end of the study area, the basement-cover contact is overturned and also west-dipping, with basement orthogneiss structurally folded over the supracrustal rocks. The presence of a thick quartzite sequence at the contact suggests that the contact is depositional in nature. As discussed above, there is no evidence of D_2 thrusting in this area; however, the presence of the overturned basement-cover contact is direct evidence of D_2 east-verging thick-skinned folding of basement and cover units.

Shortening during D_3 resulted in outcrop- to map-scale F_3 folds verging to the south, as well as a north-northeast-dipping S_3 crenulation cleavage. The roughly oval-shaped map pattern in the study area, the variable west-dipping bedding and S_{1a} fabric, and north-dipping S_3 fabric, are interpreted as resulting from fold interference between east-verging F_1 and F_2 folds and south-verging F_3 folds.

Evidence of east-directed shortening during D_1 and D_2 occurs throughout Hall Peninsula and includes the penetrative west-dipping metamorphic foliations that dominate the overall south-southeast-striking map pattern (Skipton et al., 2013). These deformation events are also characterized by the widespread occurrence of east-verging folds and associated northwest-plunging, hinge-parallel mineral lineation and, locally, west-southwest-dipping stretching lineation (Skipton et al., 2013). In the Ptarmigan Fiord area, thick-skinned thrusting during D_2 is evidenced by thrust repetition of basement orthogneiss and supracrustal rocks with west-over-east displacement (Steenkamp et al, 2014).

As the main regional fabric-forming event documented throughout Hall Peninsula, east-directed shortening during D_1 and D_2 (and associated M_1 metamorphism) represents the main Paleoproterozoic tectonometamorphic event in this segment of the Trans-Hudson Orogen. Preliminary U-Pb zircon and monazite geochronology suggests that regional amphibolite-facies metamorphism occurred during ca. 1.86–1.83 Ga (Scott, 1999). This period coincides, within errors, with other documented thermal events on southern Baffin Island, including granulite-facies metamorphism of the Lake Harbour Group at ca. 1.849–1.835 Ga and amphibolite-facies metamorphism at 1.820–1.813 Ga (Scott, 1999; St-Onge et al., 2007). Although it is presently uncertain whether the Hall Peninsula shares cratonic affinity with the Meta Incognita microcontinent, the Aasiaat domain in West Greenland, the Core Zone in northern Labrador or the North Atlantic craton, it is clear that the associated M_1 and D_1 event on Hall Peninsula represents ca. 1.86–1.83 Ga east-directed crustal shortening and, possibly continent-continent collision, involving Hall Peninsula and other cratonic blocks in the northeastern Trans-Hudson Orogen.

Several localities in the eastern portion of Hall Peninsula contain evidence of D_3, including south-verging, crenulation-style folds, as well as map-scale folds with axial planes striking east-west and fold hinges plunging west (Skipton et al., 2013). Also of note is the fact that evidence for D_3 is localized, whereas the dominant S_{1a} foliation is pervasive. This indicates that the intensity of deformation during D_1 was different from that of D_3: D_1 was widespread and penetrative, whereas D_3 was localized and occurred at lower metamorphic conditions and possibly higher crustal levels. Determining the nature and timing of D_1 metamorphism against that of D_3 on Hall Peninsula will require further investigation, including detailed pressure-temperature estimates of metamorphism coupled with geochronology.

Economic considerations

This paper provides a field template for the Paleoproterozoic tectonic evolution of eastern Hall Peninsula that may enable more effective mineral exploration. The Archean orthogneiss basement on Hall Peninsula hosts several diamond-bearing kimberlites, which were discovered by Peregrine Diamonds Ltd. in 2008. Understanding the Paleoproterozoic evolution of Hall Peninsula may shed light on the geometry and cratonic affinity of the Archean basement and the distribution of the kimberlites. The CNGO bedrock-mapping program (2012–2013) identified several additional targets for preliminary mineral exploration hosted by the supracrustal cover sequences, including layered mafic-ultramafic intrusions (potential for Ni-Cu-platinum group element mineralization), as well as iron formation and silicified gossans (Machado et al., 2013; Steenkamp et al., 2014). Since the distribution of these supracrustal pack-

ages was affected by east-directed shortening during D_1, east-directed, thick-skinned thrusting and folding during D_2, and south-verging thick-skinned folding during D_3, understanding the deformational history is a fundamental component of strategic exploration. Characterizing the metamorphic geology and discrete alteration patterns on Hall Peninsula will also help to evaluate zones of mineralization.

Conclusions

- The study area, west of Okalik Bay, Baffin Island, comprises a package of Paleoproterozoic metasedimentary rocks, with minor amphibolite and basal quartzite in stratigraphic contact with underlying Archean tonalitic orthogneiss.

- These rocks have been deformed by three Paleoproterozoic shortening events. East-directed shortening during D_1 produced a dominant west-northwest-dipping S_{1a} foliation that is axial planar to east-verging F_{1a} folds of bedding. East-verging thick-skinned folding during D_2 produced an overturned basement-cover contact. Subsequent south-directed shortening during D_3 produced south-verging F_3 folds, ranging in size from centimetre-scale crenulations to kilometre-scale folds, as well as a north-northeast-dipping crenulation cleavage. Interference between these structural events is responsible for the roughly oval-shaped map pattern displayed by the supracrustal package in this area.

- Early upper-amphibolite–facies metamorphism in the pelitic rocks west of Okalik Bay is characterized by the assemblage biotite–garnet–sillimanite–K-feldspar–melt±muscovite. Leucosome occurs as veins and lenses that form approximately 3–5% of the total-rock volume. The upper-amphibolite–facies assemblage is syn-D_1 and was folded during D_3. The occurrence of muscovite+melt (no K-feldspar) during D_3 suggests lower-temperature conditions than during D_1.

- The excellent bedrock exposure in the area west of Okalik Bay, and particularly the metamorphic assemblages and deformation fabrics in the pelitic rocks, allow for a detailed study of the nature and timing of tectonometamorphic events in this area. This field template for the Paleoproterozoic evolution of eastern Hall Peninsula provides a framework for pressure-temperature-time constraints and will help to elucidate the thermotectonic history of the northeastern Trans-Hudson Orogen.

Acknowledgments

References

Blackadar, R.G. 1967: Geological reconnaissance, southern Baffin Island, District of Franklin; Geological Survey of Canada, Paper 66–47.

Corrigan, D., Pehrsson, S., Wodicka, N. and de Kemp, E. 2009: The Palaeoproterozoic Trans-Hudson Orogen: a prototype of modern accretionary processes; Geological Society, London, Special Publication 327, p. 457–479.

Dyck, B.J. and St-Onge, M.R. 2014: Dehydration-melting reactions, leucogranite emplacement and the Paleoproterozoic structural evolution of Hall Peninsula, Baffin Island, Nunavut; in Summary of Activities 2013, Canada-Nunavut Geoscience Office, p. 73–84.

From, R., Camacho, A. and St-Onge, M.R. 2013: Preliminary observations on the nature and origin of the eastern orthogneiss complex of the southern Hall Peninsula, Baffin Island, Nunavut; in Summary of Activities 2012, Canada-Nunavut Geoscience Office, p. 43–54.

From, R.E., St-Onge, M.R. and Camacho, A.L. 2014: Preliminary characterization of the Archean orthogneiss complex of Hall Peninsula, Baffin Island, Nunavut; in Summary of Activities 2013, Canada-Nunavut Geoscience Office, p. 53–62.

Hoffman, P.F. 1988: United Plates of America, the birth of a craton: Early Proterozoic assembly and growth of Laurentia; Annual Review of Earth and Planetary Sciences, v. 16, p. 543–603.

Lewry, J.F. and Collerson, K.D. 1990: The Trans-Hudson Orogen: extent, subdivisions and problems; in The Early Proterozoic Trans-Hudson Orogen of North America, J.F. Lewry and M.R. Stauffer (ed.), Geological Association of Canada, Special Paper 37, p. 1–14.

Machado, G., Bilodeau, C., Takpanie, R., St-Onge, M.R, Rayner, N.M., Skipton, D.R., Young, M., From, R., MacKay, C., Creason, C.G. and Braden, Z.M. 2013: Hall Peninsula regional bedrock mapping, Baffin Island, Nunavut; in Summary of Activities 2012, Canada-Nunavut Geoscience Office, p. 13–22.

Scott, D.J. 1996: Geology of the Hall Peninsula east of Iqaluit, southern Baffin Island; in Current Research 1996-C, Geological Survey of Canada, p. 83–91.

Scott, D.J. 1999: U-Pb geochronology of the eastern Hall Peninsula, southern Baffin Island, Canada: a northern link between the Archean of West Greenland and the Paleoproterozoic Torngat Orogen of northern Labrador; Precambrian Research, v. 93, p. 5–26.

Scott, D.J. and Wodicka, N. 1998: A second report on the U-Pb geochronology of southern Baffin Island; Geological Survey of Canada, Paper 1998-F, p. 47–57.

Skipton, D., Schneider, D.A. and St-Onge, M.R. 2013: Preliminary observations on Archean and Paleoproterozoic metamorphism and deformation of the southern Hall Peninsula, Baffin Island, Nunavut; in Summary of Activities 2012, Canada-Nunavut Geoscience Office, p. 29–42.

Spear, F., Kohn, M., and Cheney, J. 1999, Pressure-temperature paths from anatectic pelites; Contributions to Mineralogy and Petrology, v. 134, p. 17–32.

St-Onge, M.R., Scott, D.J. and Lucas, S.B. 2000: Early partitioning of Quebec: microcontinent formation in the Paleoproterozoic; Geology, v. 28, p. 323–326.

St-Onge, M.R., Searle, M.P. and Wodicka, N. 2006: Trans-Hudson Orogen of North America and Himalaya–Karakorum–Tibetan Orogen of Asia: structural and thermal characteristics of the lower and upper plates; Tectonics, v. 25, p. 1–22, doi:10.1029/2005TC001907.

St-Onge, M.R., Wodicka, N. and Ijewliw, O. 2007: Polymetamorphic evolution of the Trans-Hudson Orogen, Baffin Island, Canada: integration of petrological, structural and geochronological data; Journal of Petrology, v. 48, p. 271–302.

St-Onge, M.R., Van Gool, J.A.M., Garde, A.A. and Scott, D.J. 2009: Correlation of Archaean and Palaeoproterozoic units between northeastern Canada and western Greenland: constraining the pre-collisional upper plate accretionary history of the Trans-Hudson orogen; Geological Society, London, Special Publication 318, p. 193–235.

Steenkamp, H.M., Bros, E.R. and St-Onge, M.R. 2014: Altered ultramafic and layered mafic-ultramafic intrusions: new economic and carving stone potential on northern Hall Peninsula, Baffin Island, Nunavut; in Summary of Activities 2013, Canada-Nunavut Geoscience Office, p. 11–20.

Dehydration-melting reactions, leucogranite emplacement and the Paleoproterozoic structural evolution of Hall Peninsula, Baffin Island, Nunavut

B.J. Dyck[1] and M.R. St-Onge[2]

[1]Department of Earth Sciences, University of Oxford, Oxford, United Kingdom, brendan.dyck@earth.ox.ac.uk

[2]Geological Survey of Canada, Natural Resources Canada, Ottawa, Ontario

Abstract

Hall Peninsula exposes an oblique cross-section through an eroded midcrustal segment of the Paleoproterozoic Trans-Hudson Orogen. The style of Paleoproterozoic deformation and structures progresses from a foreland fold-thrust belt on the eastern side of the peninsula to a region of ductile, east-verging, isoclinal folding in the west. The relative timing of deformation and fabric development records a transition from early thin-skinned folding and thrusting of supracrustal cover strata to later thick-skinned thrusting and folding of all tectonostratigraphic levels. The metamorphic grade increases structurally upward from amphibolite facies in the east to granulite facies in the west. Two suites of leucogranite dikes and sills, formed by the dehydration and breakdown of muscovite and biotite, preserve a record of partial melting of pelitic metasedimentary rocks and bracket the thick-skinned thrusting event. The earlier leucogranite suite forms sills within the supracrustal strata and acts as the rheologically competent unit during regional-scale isoclinal folding. Field observations suggest that the partial melting of metasedimentary rocks strengthened the crust by 1) creating a coarse-grained, megacrystic, garnet-rich restite, lacking abundant, rheologically weaker, biotite and muscovite and 2) crystallizing leucogranite that is more resistant to deformation than the host metasedimentary rocks. These findings suggest that partial melting, melt segregation and melt crystallization carry significant implications in addition to those generally evoked in the widely accepted melt-weakening and melt-flow models.

Résumé

Une coupe transversale oblique d'un segment érodé de la croûte intermédiaire de l'orogène trans-hudsonien du Paléoprotérozoïque se trouve exposée dans la péninsule Hall. Le style de la déformation et des structures paléoprotérozoïques fait preuve d'une progression, d'une ceinture de plissement et de chevauchement d'avant-pays dans la partie orientale de la péninsule à une zone de plissement isoclinal ductile à vergence est dans la partie occidentale. Le rythme relatif de la déformation et du développement de la fabrique géologique témoigne de la transition qui a eu lieu, d'une période de chevauchements et de plissements de couches minces des strates de roches supracrustales à une période postérieure de chevauchements et de plissements de couches épaisses de tous les niveaux tectonotratigraphiques. Structurellement, le degré de métamorphisme augmente et devient plus élevé, passant du faciès des amphibolites dans l'est à celui des granulites dans l'ouest. Deux suites de dykes et de filons-couches de leucogranite, formés par la déshydratation et la décomposition de la muscovite et de la biotite, conservent les traces de la fusion partielle de roches métasédimentaires pélitiques et encadrent l'épisode de chevauchements de couches épaisses. La suite plus ancienne de leucogranite forme des filons-couches au sein des strates de roches supracrustales et joue le rôle de couche compétente, en termes rhéologiques, au cours des épisodes de

formation de plis isoclinaux d'échelle régionale. Les observations sur le terrain semblent indiquer que la fusion partielle de roches métasédimentaires a contribué au renforcement de l'écorce en: 1) créant une restite macrocristalline à grains grossiers riche en grenats et dépourvue d'une abondance de biotite et de muscovite, éléments rhéologiquement plus faibles, et 2) cristallisant un leucogranite plus résistant aux effets de la déformation que les roches métasédimentaires encaissantes. Ces conclusions laissent supposer que la fusion partielle, la ségrégation des magmas et la cristallisation de ces derniers ont d'importantes conséquences qui viennent s'ajouter à celles habituellement soulevées dans les modèles largement acceptés d'affaiblissement et d'écoulement des magmas.

Introduction

The generation, emplacement and crystallization of anatectic melts have significant implications for the distribution of strain during the evolution of collisional mountain belts (Brown 2007). The localization of partial melts within the crust forms mechanically weak zones that will easily deform given a deviatoric/tectonic stress (Rosenberg and Handy, 2005). The effect of deformation on partially melted rocks is well documented in the literature (e.g., Rutter and Neumann, 1995; Vigneresse and Tikoff, 1999; Beaumont et al., 2001; Rosenberg and Handy, 2005), but the significance of melt segregation and emplacement on strain partitioning and deformation at the orogenic scale is poorly constrained.

Hall Peninsula, located on southern Baffin Island, Nunavut (Figure 1), exposes a superbly preserved cross-section through the eroded partially molten hinterland of the Paleoproterozoic Trans-Hudson Orogen. Building on previous reconnaissance mapping by Blackadar (1967) and Scott (1999), the Canada-Nunavut Geoscience Office (CNGO), Hall Peninsula Integrated Geoscience Program was established to improve knowledge of the tectonic history and economic potential of Hall Peninsula in the context of southern Baffin Island and the greater Trans-Hudson Orogen (northern Quebec and southern Baffin Island). In this paper, the authors present results from field mapping that outline the structural evolution, and relative timing of fabric and metamorphism for the northern portion of Hall Peninsula. Two suites of leucogranite sills and dikes are characterized in this paper, and the impact that leucogranite emplacement had on the Paleoproterozoic structural evolution of Hall Peninsula is outlined.

Geology of the northern portion of Hall Peninsula

The bedrock lithological units of Hall Peninsula can be grouped into three principal rock associations: Archean basement gneisses, overlying Paleoproterozoic cover/supracrustal strata, and Paleoproterozoic intrusive plutonic bodies. The basement gneisses, which are exposed on the eastern portion of the peninsula, comprise multiple plutonic phases of Archean mafic diorite, tonalite and granodiorite together with monzogranite and syenogranite (Scott 1999; From et al., 2014; Rayner, 2014). The Paleoprotero-

zoic cover rocks are found overlying the exposed basement gneisses and progressively become the dominant association in the western portion of the peninsula. Detrital zircon studies of the clastic sedimentary units (quartzite and psammite) yield maximum ages of deposition that range from 2126 ±16 Ma to 1906 ±9 Ma (Rayner, 2014). The cover strata include carbonate units, mafic sedimentary and volcanic rocks and their metamorphic equivalents. The supracrustal rocks are intruded by tonalitic- monzogranitic and leucogranite sills and dikes with crystallization ages between 1.89 and 1.87 Ga (Scott, 1999; Rayner, 2014).

There is a progressive change in the nature of the supracrustal units exposed on Hall Peninsula from east to west (Steenkamp and St-Onge, 2014). In the east, basal quartzite is typically overlain by psammite with calcsilicate, marble, altered pillow-basalt, magnetite-rich banded iron formation, mafic sedimentary rock and pelite. Sills of gabbro and retrogressed ultramafic rocks are parallel to compositional layering and are often boudinaged. A low- strain depositional contact separates the cover sequence from the underlying basement. Retrogressed ultramafic bodies with the same composition as the cover-sequence–hosted sills are found within the basement.

In the centre of the peninsula, the cover sequence contains marble and quartzite, but is overall more psammitic than in the east. Peridotite and pyroxenite, plus associated mafic gabbro, form sills hosted in the psammitic sedimentary units. Monzogranitic leucogranite sills crosscut all other units.

The western metasedimentary rocks are strongly migmatized and composed mostly of interbedded psammite and pelite with rare horizons of psammite-hosted calcsilicate. The supracrustal rocks are intruded by 5–500 m wide sills of granulite-facies mafic tonalite and granodiorite. Two generations of monzogranitic leucogranite cut across the metasedimentary units and sills in bodies 1–1000 m wide. The relative volume of leucogranite increases toward the west, becoming the dominant rock type at the western extent of the mapped area.

Late, crosscutting pegmatite of variable composition is most abundant in the east. The pegmatite dikes have S-type compositions, suggesting they were derived from a sedimentary source.
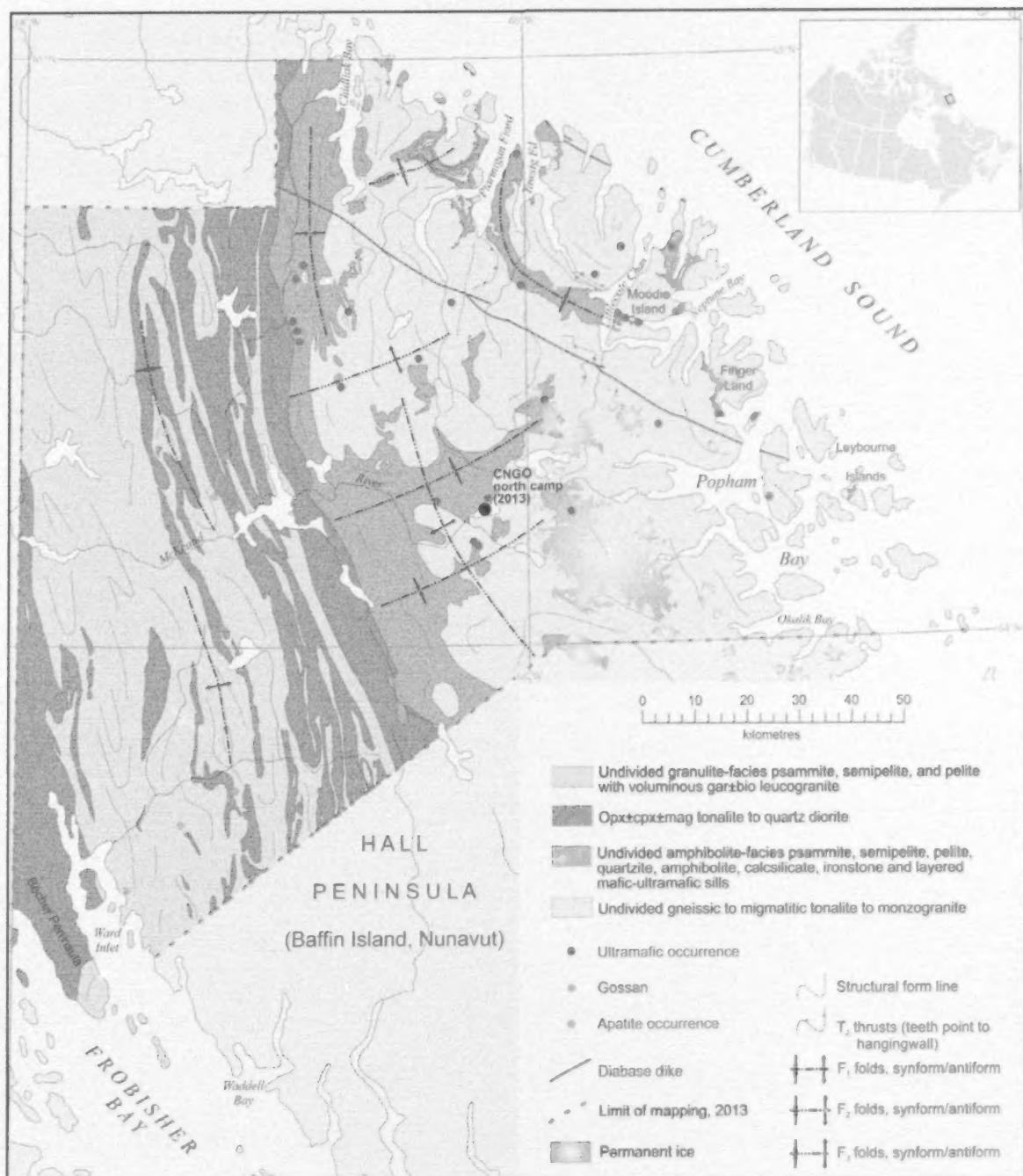
Figure 1: Map of southern Baffin Island, Nunavut, showing the location of Hall Peninsula.

Three coarse-grained gabbroic dikes that are 20–50 m in width crosscut all basement units in the northeastern part of Hall Peninsula. These are interpreted to belong to the 723–718 Ma Franklin swarm (Heaman et al., 1992), which formed during the breakup of the Rodinia supercontinent.

The latest magmatic event on Hall Peninsula is the emplacement of kimberlite pipes and dikes during the Jurassic 156–138 Ma (Heaman et al., 2012).

Structural elements, fabric development and relative timing of deformation/metamorphism

The mapping of Hall Peninsula has documented a progression in the style and character of the Paleoproterozoic deformation and related fabrics from east to west, and with time (Table 1).

The eastern portion of the peninsula preserves a record of ductile folding, thrust repetition and late cleavage development. The earliest Paleoproterozoic deformation observed (D_1) is largely restricted to the supracrustal rocks and interpreted as being thin-skinned in nature. The D_1 thrust repetition of supracrustal rocks is documented by 1) a repeating sequence of west-dipping 10–100 m thick mafic sedimentary rock, pelite and psammite layers and 2) the observation of high-strain sheared contacts between the psammite and mafic sedimentary rock. The D_1 isoclinal folding, termed (F_{1a}), is documented by ~100 m wide inclined isoclinal synformal and antiformal structures. The F_{1a} folds are east-verging with west-dipping axial planes (~180°/65°W) and shallow north- and south-plunging fold axes.

The earliest fabric observed within all mapped units, termed S_{1a}, is a strong, penetrative, metamorphic foliation.

Table 1: Structural table detailing the relative timing of deformation, fabric development and peak thermal metamorphism, Hall Peninsula, Nunavut.

S_0	Bedding
East-west shortening (pre-to syn-thermal peak): D_1	
F_{1a}	Isoclinal folds of bedding
S_{1a}	Metamorphic foliation axial planar to F_{1a}
F_{1b}	Isoclinal folds of S_{1a}
S_{1b}	Metamorphic foliation axial planar to F_{1b}
East-west shortening (post-thermal peak): D_2	
T_2	Thick-skinned thrusts
L_2	Mineral stretching and elongate growth
F_2	Thick-skinned folds
North-south shortening: D_3	
F_3	Thick-skinned folds
S_3	Axial planar crenulation cleavage

The S_{1a} fabric is axial planar to the F_{1a} isoclinal folds. In pelitic compositions S_{1a} is characteristically spaced (millimetre scale) and defined by aligned muscovite, biotite, sillimanite, platy quartz and elongation of feldspars. At higher metamorphic grades, it is defined by the alignment of thermal peak metamorphic minerals, as well as leucosome and melanosome, yielding a centimetre-spaced gneissosity in metasedimentary migmatites. The S_{1a} fabric is south-striking and predominantly west-dipping with an average orientation of ~190°/50°W, and an average dip steepening toward the west.

In the western portion of Hall Peninsula, F_{1b} outcrop-scale folds are defined by the folding of bedding, leucosome and/or the S_{1a} metamorphic foliation (Figure 2a, b). The folding is isoclinal and east-verging with northwest-trending (345°) fold axes, plunging ~15° and west-dipping axial planes orientated ~180°/55°W. The F_{1b} map-scale folding has the same orientation as the folds seen in outcrop, and is typically outlined by mapped lithological contacts between supracrustal strata, mafic tonalite and granodiorite sills, as well as one generation of monzogranitic leucogranite sills. Lobe-cuspate structures are recognized at map scale between leucogranite sills and host supracrustal rocks. The leucogranite forms the lobes of folds and the host rocks form the deformed cuspate structures (Figure 2c).

A second fabric, termed S_{1b}, is developed in the western portion of the peninsula and comprises a penetrative foliation axial planar to F_{1b} isoclinal folds. The S_{1b} fabric is defined by the alignment of platy quartz and biotite when present, and can only be observed at an angle to S_{1a} in F_{1b} fold hinges. The S_{1b} foliation strikes to the south and dips consistently west at ~55°. The S_{1b} fabric postdates crystallization of leucosome parallel to S_{1a}, and crystallization of map-scale leucogranite sills.

The D_2 structures involve both basement gneisses and cover strata and are documented in the well-exposed terrain between Ptarmigan Fiord and Chidliak Bay (Figure 2e). West-dipping panels of Archean basement gneiss and overlying supracrustal rocks are interpreted as a sequence of five thick-skinned (T_2) thrust imbricates based on 1) contacts between basement gneiss and overlying supracrustal rocks being typically low-strain and interpreted as primarily tectonostratigraphic, 2) the presence of high-strain shear zones separating the supracrustal rocks from structurally overlying basement gneiss and 3) shortening of the supracrustal sequence stratigraphy and the transposition of earlier basement structures. The primary tectonostratigraphic nature of the basement-overlain-by-cover contact is further evidenced by the presence of basement-hosted ultramafic 'pipes' structurally below cover sequences with ultramafic sills (Steenkamp et al., 2014). The shear zones separating the individual imbricates are shallowly west dipping, with an average orientation of ~185°/15°W. The
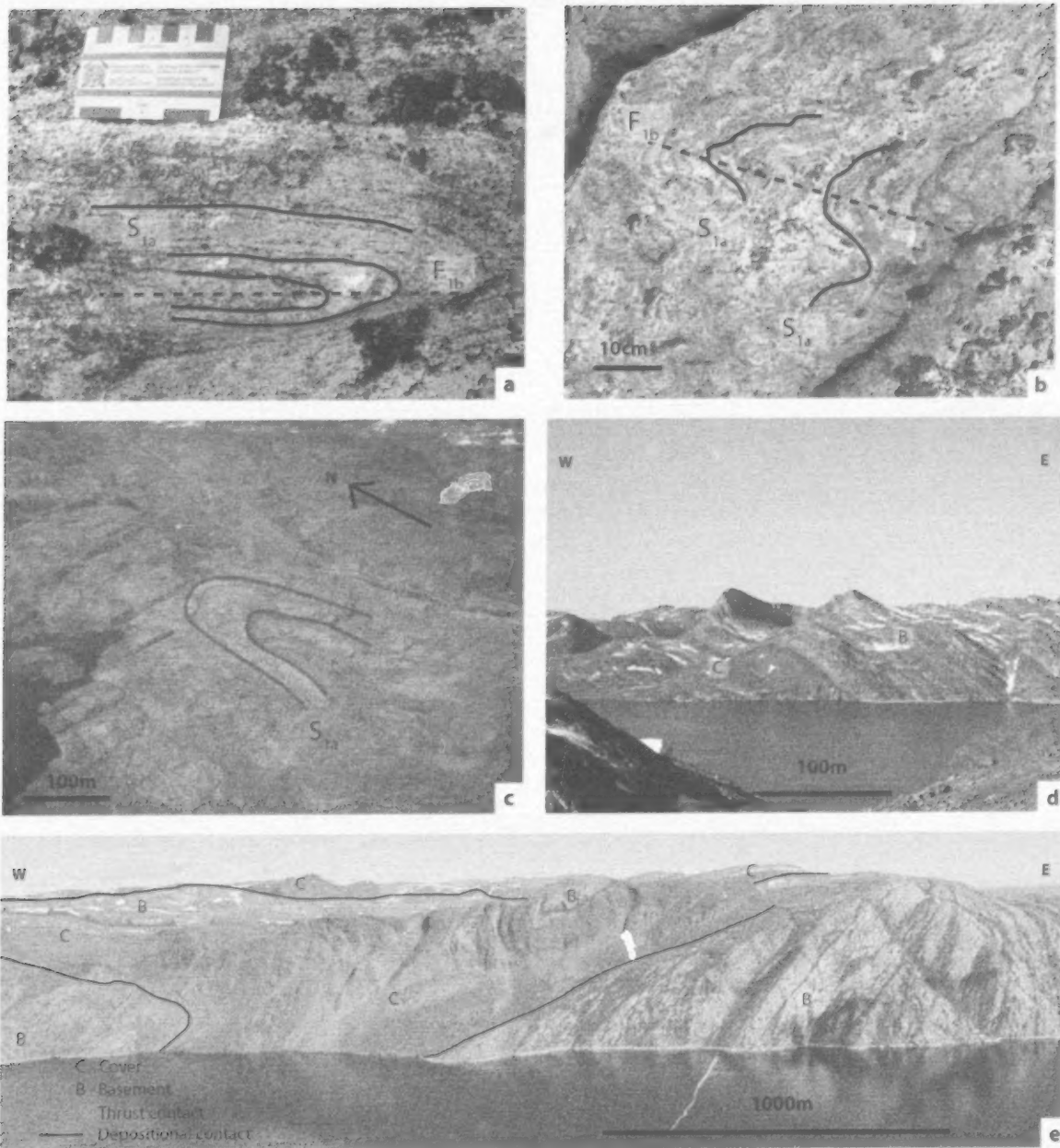
Figure 2: Structural elements, Hall Peninsula, Nunavut: **a)** isoclinal folding of a monzogranitic leucosome (S_{1a}) derived from the host granulite-facies granodiorite; **b)** outcrop-scale folding of the S_{1a} fabric in a partially melted metasedimentary rock; **c)** map-scale isoclinal fold outlined by a garnet-leucogranite sill hosted in metasedimentary rocks; **d)** overturned thrust fault with an apparent normal sense of shear placing Archean basement (B) on top of Paleoproterozoic cover (C); **e)** T_2 Thrust imbricates of Archean basement (B) and Paleoproterozoic cover (C) at Ptarmigan Fiord; basement and cover sequence of a second thrust imbricate are exposed in the background.

thickness of individual imbricates ranges from 100 to 750 m with varying thickness-ratios of basement and cover, and the horizontal length, measured east to west, ranges between 5 and 20 km. The D_2 west–over–east shear sense is documented in C-S fabrics and both σ-type and δ-type feldspar augens.

Structures and fabrics attributed to the D_2 event postdate the crystallization of leucosome and other melt structures. The L_2 fabric is a ductile, stretching and mineral-growth lineation developed on transposed S_{1b} foliation planes, and expressed as rodded quartz and amphibole, oriented sillimanite and aligned orthopyroxene. The L_2 fabric formed during the thick-skinned T_2 thrusting and is plunging west at ~25°. The west-over-east sense of thrust imbrication and displacement is consistent with D_2 east-verging folding found across Hall Peninsula. In the easternmost mapped area, gentle F_2 folding of T_2 shear planes resulted in east-dipping shear zones with apparent normal shear sense (Figure 2d). These folds occur at the kilometre scale and reoriented all earlier structures. The thick-skinned kilometre-scale F_2 open folding of the thrust imbricates is not associated with a recognizable fabric.

Late D_3 west-trending open folds involve all tectonostratigraphic levels in the eastern portion of Hall Peninsula. The folding is observed on a scale of 100 m to many kilometres. Open folding of the basement gneisses and overlying cover strata are recorded by a small deflection in foliation strike. In the mica-rich pelites, the late D_3 folding resulted in well-developed crenulation folds (F_3) with a north-dipping (S_3) axial planar crenulation cleavage (Skipton and St-Onge, 2014).

Metamorphic grade across Hall Peninsula

The peak metamorphic conditions associated with D_1 increase east to west from the foreland to hinterland (Steenkamp and St-Onge, 2014). Along the east coast of the peninsula, the rocks are amphibolite facies with a pelitic mineral assemblage comprising muscovite+biotite+garnet+sillimanite+quartz+plagioclase. Locally, the pelitic mineral assemblage biotite+garnet+sillimanite+K-feldspar+plagioclase+quartz+melt suggests an increase in tem-

perature to upper-amphibolite–facies conditions. Further toward the west, the metamorphic grade increases to granulite facies in the structurally highest T_2 thrust imbricates, where the pelitic mineral assemblage is garnet+ quartz+plagioclase+K-feldspar+melt± sillimanite±cordierite±biotite. Pelitic layers in the migmatitic western metasedimentary rocks contain up to 40 vol. % coarse-grained garnet and up to 15 vol. % K-feldspar megacrysts. The garnet+K-feldspar+melt mineral assemblage of the pelitic western metasedimentary rocks is interpreted to be a restitic granulite facies assemblage. The mafic tonalite and gabbroic sills contain granulite facies mineral assemblages with both orthopyroxene and clinopyroxene. The degree of melting also increases toward the west with the most voluminous partial melt fraction observed in the westernmost extent of the map area.

Leucogranites

Leucogranite is a product of anatexis, the partial melting of a source rock, typically developed during higher grade peak-metamorphic conditions. The prefix 'leuco', derived from the Greek leucos for white, when used to describe granite is generally reserved for leucocratic S-type monzogranites.

Characterization of Hall Peninsula leucogranites

Two suites of leucogranite sills and dikes occur in the western portion of the peninsula, and can be distinguished by their respective mineral assemblage and relative timing of emplacement (Table 2). Both suites are emplaced in high-grade metasedimentary rocks and cut across the mafic tonalite and granodiorite sills.

The older suite is a monzogranitic garnet-leucogranite characterized by the assemblage quartz+plagioclase+K-feldspar+garnet. Sillimanite is seldom found in equilibrium with the garnet-leucogranite mineral assemblage. Dark red, poikiloblastic garnet with quartz, plagioclase, biotite, and sillimanite inclusion-rich cores comprises up to 7 vol. % of the garnet-leucogranite. (Figure 3a). Subsolidus reaction rims of biotite+epidote form around garnet in retrogressed domains. The garnet-leucogranite is medium to coarse grained with heterogeneous grain size distribution between

Table 2: Comparison table, outlining the distinguishing characteristics for the garnet-leucogranite and muscovite-leucogranite from Hall Peninsula, Nunavut.

Characteristics	Garnet-leucogranite	Muscovite-leucogranite
Mineral assemblage	qz+pl+kfs+grt	qz+pl+kfs+sil+ms±grt
Garnet morphology	5–20 mm, poikioblastic, dark red	1–5 mm, inclusion-free, lilac
Grain size	4–20 mm	1–5 mm
Deformation	Strongly foliated, lineated, folded	Weakly foliated
Relative timing	Syn-S_{1a}, pre-F_{1b}, pre-L_2	Post-S_{1b}, post-L_2, post-T_2
Melt temperature	825–850°C	650–775°C

Abbreviations: grt, garnet; kfs, K-feldspar; ms, muscovite; pl, plagioclase; qz, quartz; sil, sillimanite
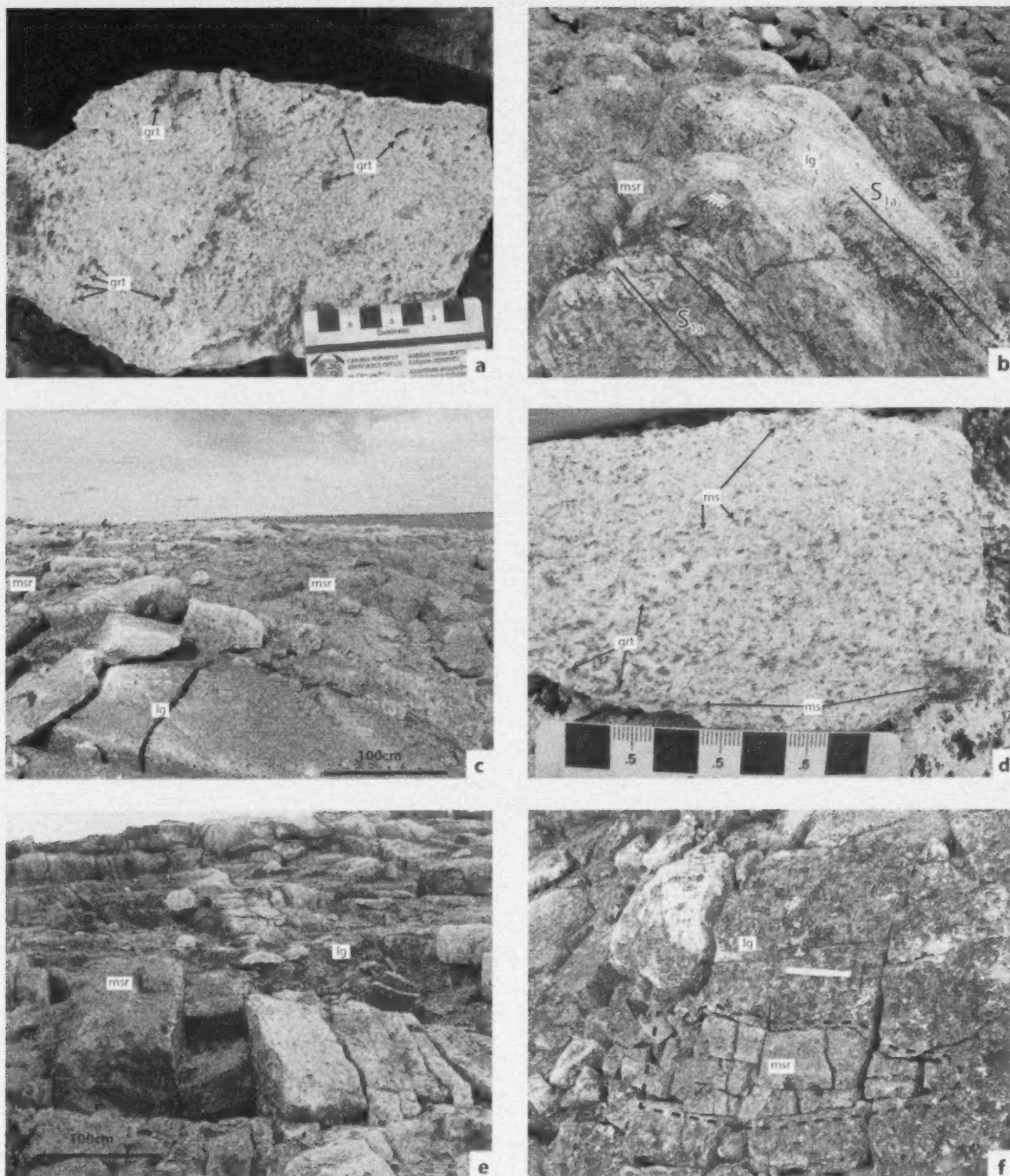
Figure 3: Leucogranite textures and contact relationships, Hall Peninsula, Nunavut: **a)** garnet-leucogranite texture (Note: mineral deformation and lineation of dark red coarse-grained garnet aggregates.); **b)** transposed contact between garnet-leucogranite sill and host metasedimentary rocks with a penetrative foliation (S_{1a}) developed in both units; **c)** 10 m long raft of host metasedimentary rock in garnet-leucogranite sill; **d)** muscovite-leucogranite texture. (Note: low-strain and millimetre-sized lilac-coloured garnets.); **e)** sharp vertical contact between muscovite-leucogranite dike and host granulite-facies metasedimentary rocks; **f)** 2 m long raft of host metasedimentary rock in muscovite-leucogranite dike. Abbreviations: grt, garnet; lg, leucogranite; ms, muscovite; msr, metasedimentary rock.

4 and 20 mm. Sills of the garnet-leucogranite are parallel to the peak-metamorphic fabric in the host metasedimentary rocks and are internally foliated by the penetrative S_{1a} foliation (Figure 3b). The sills share strongly transposed contacts with the host supracrustal package and the mafic tonalite and granodiorite sills, often containing metre-sized rafts of metasedimentary rock aligned parallel to foliation (Figure 3c). Elongate feldspars and aggregates of quartz as well as rodded/cylindrical garnet growth define the L_2 lineation in isolated domains. The garnet-leucogranite sills are folded by the F_{1b} isoclinal phase of folding, forming fold-defining hinge structures with distinct map-scale lobe-cuspate structures (Figure 2c). The garnet-leucogranite suite is a major component of the bedrock in the western portion of Hall Peninsula, with the sills typically continuously exposed as 10–1000 m wide panels that strike north-south for tens of kilometres. The composition and deformation textures detailed above suggest that the garnet-leucogranite formed and was emplaced during the thermal peak of metamorphism.

A second younger distinct suite of leucogranite is composed of monzogranitic muscovite-leucogranite that is characterized by a major mineral assemblage of quartz+plagioclase+K-feldspar+sillimanite+muscovite±garnet. Sillimanite accounts for greater than 5 vol. % of the rock and typically forms mineral-aligned clots. Muscovite occurs as randomly oriented sheets often associated with the sillimanite clots. Garnet accounts for less than 2 vol. % and is distinctively lilac coloured, a trait attributed to a peraluminous bulk composition. The garnet is often 'pinprick' in size (1–5 mm), and inclusion free. The muscovite-leucogranite is medium grained (1–5 mm) and contains K-feldspar megacrysts, up to 10 mm in diameter (Figure 3d). The muscovite-leucogranite suite forms dikes with moderately transposed margins (Figure 3e) and locally includes rafts of host metasedimentary rock (Figure 3f). Muscovite-leucogranite dikes are notably less deformed than the host rock types and are only weakly foliated. Textures and field relations suggest that the muscovite- leucogranite dikes were emplaced post S_{1b} and post L_2. The largest and best studied muscovite-leucogranite dike is south striking, vertical, 10 m wide and over 3 km long. Dikes of muscovite-leucogranite are less voluminous than the garnet-leucogranite sills, accounting for <5% surface area in the western portion of the peninsula.

Petrogenesis

Generating volumes of S-type leucogranite to the extent observed on Hall Peninsula requires a suitably fertile protolith and high temperatures (>750°C). The following observations strongly suggest that the source rocks for the leucogranite were pelitic in nature:

1) Leucogranite bodies are spatially associated with the pelitic and psammitic metasedimentary rocks, occur-

ring as sills within metasedimentary panels or at contacts between the metasedimentary rocks and the mafic tonalite and granodiorite sills.

2) The leucogranite mineral assemblages are S-type, indicating the source was a mica-rich metasedimentary rock (Chappell and White, 2001).

3) The relative volumes of leucogranite and pelitic restitic material are positively correlated, increasing toward the west.

4) The westward increase in leucogranite and metamorphic grade is consistent with generation of leucogranite from the prograde melting of a local metasedimentary source.

5) Garnet-monzogranite leucosome, within the pelitic layers in the metasedimentary rocks of the western portion of the peninsula, are compositionally and texturally similar to the sills of garnet-leucogranite.

The subsolidus mineral assemblage in the pelitic rocks is biotite+muscovite+garnet+quartz+plagioclase±sillimanite. In response to an increase in metamorphic grade toward the west and up structural section, pelitic rocks contain the product of two voluminous, melt- producing sets of reactions: the discontinuous muscovite breakdown/dehydration reactions and the semicontinuous biotite breakdown/dehydration reactions. An additional variable of considerable importance is the composition and abundance of an external fluid phase during melting. The presence of a water-rich vapour phase will lower the temperature required for melt production and increase the volumes of melt generated, but the key mineral reactants remain unchanged.

Muscovite breakdown/dehydration-melting reactions

Along a medium P/T trajectory (~6–8 kbar of pressure), which is a reasonable assumption for southern Baffin Island (St-Onge et al., 2007), the first melt-generating mineral reaction reached during prograde metamorphism of a pelite is the vapour present (K-feldspar absent) muscovite-breakdown reaction (Reaction 1).

muscovite + plagioclase + quartz + vapour
$= Al_2SiO_5$ (sillimanite) + melt (1)

muscovite + plagioclase + quartz
$= Al_2SiO_5$ (sillimanite) + K-feldspar + melt (2)
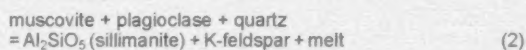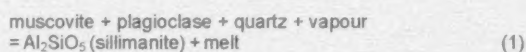
This reaction occurs at temperatures of 650–700°C until one reacting phase is fully exhausted (Figure 4; Spear, 1999; White, 2001). The assemblage produced by Reaction 1 is devoid of peritectic products, and is expected to result in a small amount of melt with no faserkiesel (sillimanite+quartz±K-feldspar) texture. Reaction 2, the muscovite dehydration-melting reaction, occurs between 650–775°C (depending on pressure) when muscovite breaks down in the absence of a free-vapour phase (Figure 4). Muscovite dehydration-melting is the first voluminous melting reac-
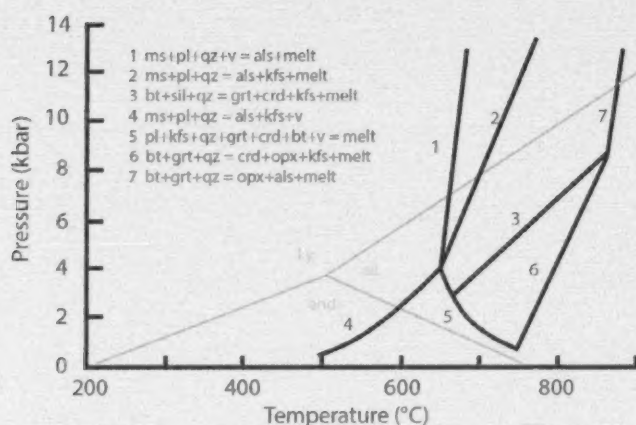
Figure 4: Pressure-temperature diagram showing the location of the important muscovite and biotite breakdown/dehydration reactions in the Na_2O-K_2O-FeO-MgO-Al_2O_3-SiO_2-H_2O chemical system (modified after Spear et al., 1999). The Al_2SiO_5 triple point is from Pattison (1992). Abbreviations: als, aluminosilicate; and, andalusite; bt, biotite; crd, cordierite; grt, garnet; kfs, K-feldspar; ky, kyanite; melt, silicate melt; ms, muscovite; opx, orthopyroxene; pl, plagioclase; qz, quartz; sil, sillimanite; v, vapour.

tion encountered and is capable of generating between ~7–15 vol. % melt depending on the volume of muscovite (White et al., 2001). The incongruent breakdown of muscovite forming peritectic sillimanite and K-feldspar is interpreted to result in the formation of the characteristic faserkiesel texture noted on Hall Peninsula.

Biotite dehydration-melting reaction

Following the exhaustion of muscovite, some melt is generated at the expense of quartz and plagioclase until temperatures reach ~825–850°C, at which point significant melt is generated by the vapour-absent biotite dehydration-melting Reaction 3 (Figure 4; LeBreton and Thompson, 1988; Spear et al., 1999).

biotite + plagioclase + quartz + sillimanite
= (garnet, cordierite) + K-feldspar + melt   (3)
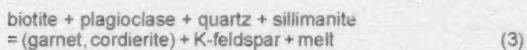
The peritectic product formed by biotite dehydration-melting is pressure dependent; garnet is produced when pressures are above ~5.5 kbar, whereas cordierite is produced at pressures below ~6 kbar, with a compositionally dependent overlapping stability field of both garnet and cordierite. Biotite dehydration-melting will generally produce ~20–30 vol. % melt depending on the volume of biotite. Thus with a pelitic source, a combination of both mica dehydration-melting reactions can generate 35–50 vol. % melt at ~850°C.

Tectonic implications of leucogranite generation, emplacement, crystallization

East-west shortening in the Paleoproterozoic Trans-Hudson Orogen culminated in the foreland fold-thrust belt exposed on eastern Hall Peninsula and the east-verging isocli-

nal folds of supracrustal strata that dominate the western portion of the peninsula. The progression in structural style documented on the eastern portion of the peninsula from thrusting and isoclinal folding of supracrustal strata to thrust imbrication and folding of basement and cover units preserves a record of the transition from thin-skinned foreland to thick-skinned hinterland structures.

The D_1 crustal shortening coincides with increasing metamorphic temperatures across the entire peninsula. Elevated temperatures at midcrustal levels in convergent orogenic belts result from thermal relaxation via crustal thickening (folding and faulting of cover units), and high internal heat production by the decay of radiogenic isotopes (England and Thompson, 1984). Intrusions of mantle-derived plutons and sills act to further thicken the supracrustal package. Advection of mantle heat through over-accretion of the plutonic bodies by magmatic additions at relatively shallow crustal levels can act as a thermal primer for later anatexis as well as bury the metasedimentary units, increasing metamorphic pressures (St-Onge et al., 2007). In the western portion of Hall Peninsula, deformation fabrics and associated metamorphic mineral assemblages document a regional east-west compression that led to the formation of the S_{1a} regional metamorphic foliation during an increase in midcrustal temperatures (i.e., through muscovite dehydration-melting conditions up to biotite dehydration-melting temperatures of ~850°C). At the highest metamorphic grades, evidence for products of the muscovite dehydration-melting Reaction 2 (sillimanite+K-feldspar+melt) are generally overprinted by the products of the higher temperature biotite melting Reaction 3 (garnet+K-feldspar+melt; Table 2), although the presence of sillimanite inclusions in garnet cores can be interpreted as a product of Reaction 2.

Field observations from Hall Peninsula have implications for the strength of the middle crust following anatectic melt generation and leucogranite emplacement that are not considered in the widely accepted melt-weakening and melt-flow models (Brown and Solar, 1998; Brown, 2007). The first implication is a strengthening of the crust with the resultant coarse-grained K-feldspar megacryst and garnet-rich restite that is depleted in quartz and plagioclase and devoid of easily deformed micas. The second and arguably most important implication is further strengthening of the middle crust by crystallization of porphyritic leucogranite that is more resistant to deformation than the host (or source protolith) unit. The emplacement of garnet-leucogranite sills, even if only partially crystallized, could provide a sufficient competency contrast to spur a change in mechanical behaviour during compression. Modelling of granitic folding mechanics shows that a partially crystallized leucosome with some interstitial melt will fold as a competent

layer in an incompetent host (i.e., high-grade metasedimentary rock; Hobbs et al., 2007, 2008). Field observations suggest the garnet-leucogranite has acted as the rheologically determinant unit, providing a competent backbone for the F_{1b} isoclinal folds (Figure 2c). The resulting kilometre-scale harmonic folding would have further thickened the crust, potentially leading to further melting at lower crustal levels.

The postmetamorphic peak (T_2) thick-skinned thrusts in the Ptarmigan Fiord area appear to have propagated structurally upsection emplacing progressively higher grade thrust imbricates on top of one another, 'telescoping' the supracrustal sequence stratigraphy. The thick-skinned thrusts (T_2) are interpreted to be out-of-sequence thrusts with a temporal progression toward the hinterland. The L_2 lineation is well developed within the ductile shear planes of the T_2 thrusts, and it constrains the relative timing of thick-skinned thrusting (see Table 1). The hangingwall of the structurally highest thrust imbricate juxtaposes granulite-facies supracrustal rocks (garnet+quartz+plagioclase+K-feldspar+melt±sillimanite±cordierite± biotite) on top of amphibolite-facies (biotite+garnet+sillimanite+K-feldspar+plagioclase+quartz+melt) supracrustal and basement rocks. Emplacement of the muscovite-leucogranite dikes demonstrably postdates the L_2 fabric and is interpreted as postdating the (T_2) thrusting.

The generation of muscovite-leucogranite dikes requires a lower temperature prograde melting reaction than the peak-metamorphic conditions recorded by the mineral assemblage in the host granulite-facies metasedimentary rocks. A possible scenario is that the overthrusting of high-temperature thrust imbricates led to a temperature increase in the footwall rocks, so that muscovite dehydration-melting (Reaction 2) took place at about 650°C, generating melts, which then migrated and crystallized upsection as muscovite-leucogranite.

Future studies and economic considerations

Samples have been collected to constrain the absolute timing of leucosome formation, leucogranite emplacement and associated fabric development and to provide a test of the model of thrust-induced footwall melting. A garnet-leucogranite crystallization age would provide a maximum age for F_{1b} folding and thick-skinned (T_2) thrusting as well as a date on thermal-peak metamorphism. An age on a muscovite-leucogranite would provide a minimum constraint on T_2 thrusting and date the metamorphism that resulted from thrust imbrication.

Continued studies on the generation and migration pathways of anatectic melts will help to constrain the metamorphic evolution of part of the eastern Trans-Hudson Orogen as well as continue developing the understanding of strain partitioning in orogenic belts. Constraining the Paleoproterozoic melting and deformation recorded on Hall Peninsula will further detail the structural and thermal evolution of the peninsula and provide a quantitative context for the consequent modification of any pre- to synthermal peak mineral occurrence it may contain. The link between crustal melting and deformation is inherently complex, but through careful study of melt reactions, deformation fabrics and field structures it is possible to decipher some of the fundamental tectonic processes that build mountain belts.

Acknowledgments

References

Beaumont, C., Jamieson, R.A., Nguyen, M.H. and Lee, B. 2001: Himalayan tectonics explained by extrusion of a low-viscosity crustal channel coupled to focused surface denudation; Nature, v. 414, p. 738–742.

Blackadar, R.G. 1967: Geological reconnaissance, southern Baffin Island, District of Franklin; Geological Survey of Canada.

Brown, M. 2007: Crustal melting and melt extraction, ascent and emplacement in orogens: mechanisms and consequences; Journal of Geological Society, London, v. 164, p. 709–730.

Brown, M. and Solar, G.S. 1998: Shear zone systems and melts: feedback relations and self organization in orogenic belts; Journal of Structural Geology, v. 20, p. 211–227.

Chappell, B.W. and White, A.J.R. 2001: Two contrasting granite types: 25 years later; Australian Journal of Earth Sciences, v. 48, p. 489–499.

England, P.C. and Thompson, A.B. 1984: Pressure-temperature-time paths of regional metamorphism I. Heat transfer during the evolution of regions of thickened continental crust; Journal of Petrology, v. 25, p. 894–928.

From, R.E., St-Onge, M.R. and Camacho A.L. 2014: Preliminary characterization of the Archean orthogneiss complex of Hall Peninsula, Baffin Island, Nunavut; in Summary of Activities 2013, Canada-Nunavut Geoscience Office, p. 47–56.

Heaman, L.M., Grütter, H.S., Pell, J., Holmes, P. and Grenon, H. 2012: U-Pb geochronology, Sr and Nd isotope compositions of groundmass perovskite from the Chidliak and Qilaq kimberlites, Baffin Island, Nunavut; 10th International Kimberlite Conference, Bangalore, India, Extended Abstract 10IKC-193, p. 4.

Heaman, L.M., LeCheminant, A.N. and Rainbird, R.H. 1992: Nature and timing of Franklin igneous events, Canada: implications for a Late Proterozoic mantle plume and the break-

up of Laurentia; Earth and Planetary Science Letters, v. 109, no. 1, p. 117–131.

Hobbs, B., Regenauer-Lieb, K. and Ord, A. 2007: Thermodynamics of folding in the middle to lower crust; Geology, v. 35, no. 2, p. 175–178.

Hobbs, B., Regenauer-Lieb, K. and Ord, A. 2008: Folding with thermal-mechanical feedback; Journal of Structural Geology, v. 30, no. 12, p. 1572–1592.

Le Breton, N. and Thompson, A.B. 1988: Fluid-absent (dehydration) melting of biotite in metapelites in the early stages of crustal anatexis; Contributions to Mineralogy and Petrology, v. 99, p. 226–237.

Rayner, N.M. 2014: New uranium-lead geochronological results from Hall Peninsula, Baffin Island, Nunavut; in Summary of Activities 2013, Canada-Nunavut Geoscience Office, p. 39–46.

Rosenberg, C.L. and Handy, M.R. 2005: Experimental deformation of partially melted granite revisited: implications for the continental crust; Journal of Metamorphic Geology, v. 23, no. 1, p. 19–28.

Rutter, E. and Neumann, D.H.K. 1995: Experimental deformation of partially molten Westerly granite under fluid absent conditions, with implications for the extraction of granitic magmas; Journal of Geophysical Research, v. 100, p. 15697–15715.

Scott, D.J. 1999: U-Pb geochronology of the eastern Hall Peninsula, southern Baffin Island, Canada: a northern link between the Archean of West Greenland and the Paleoproterozoic Torngat Orogen of northern Labrador; Precambrian Research, v. 93, p. 5–26.

Skipton, D.R. and St-Onge, M.R. 2014: Paleoproterozoic deformation and metamorphism in metasedimentary rocks west of Okalik Bay: a field template for the evolution of eastern Hall Peninsula, Baffin Island, Nunavut; in Summary of Activities 2013, Canada-Nunavut Geoscience Office, p. 57–66.

Spear, F., Kohn, M. and Cheney, J. 1999: Pressure-temperature paths from anatectic pelites; Contributions to Mineralogy and Petrology, v. 134, p. 17–32.

Steenkamp, H.M. and St-Onge, M.R. 2014: Overview of the 2013 regional bedrock mapping program on northern Hall Peninsula, Baffin Island, Nunavut; in Summary of Activities 2013, Canada-Nunavut Geoscience Office, p. 27–38.

Steenkamp, H.M., Bros, E.R. and St-Onge, M.R. 2014: Altered ultramafic and layered mafic-ultramafic intrusions: new economic and carving stone potential on northern Hall Peninsula, Baffin Island, Nunavut; in Summary of Activities 2013, Canada-Nunavut Geoscience Office, p. 11–20.

St-Onge, M.R., Wodicka, N. and Ijewliw, O. 2007: Polymetamorphic evolution of the Trans-Hudson Orogen, Baffin Island, Canada: integration of petrological, structural and geochronological data; Journal of Petrology, v. 48, no. 2, p. 271–302.

Pattison, D.R.M. 1992: Stability of andalusite and sillimanite and the Al_2SiO_5 triple point: constraints from the Ballachulish aureole, Scotland; Journal of Geology v. 100, p. 423–446.

Vigneresse, J.L. and Tikoff, B. 1999: Strain partitioning during partial melting and crystallizing felsic magmas; Tectonophysics, v. 312, p. 117–132.

White, R.W., Powell, R. and Holland, T.J.B. 2001: Calculation of partial melting equilibria in the system Na_2O–CaO–K_2O–FeO–MgO–Al_2O_3–SiO_2–H_2O (NCKFMASH); Journal of Metamorphic Geology, v. 19, no. 2, p. 139–153.

Geochemical study of mafic and ultramafic rocks from southern Hall Peninsula, Baffin Island, Nunavut

by C.B. MacKay[1] and K.M. Ansdell[1]

[1]Department of Geological Sciences, University of Saskatchewan, Saskatoon, Saskatchewan

Abstract

Whole-rock major- and trace-element geochemical analyses were carried out on 64 samples of mafic and ultramafic units collected from southern Hall Peninsula, Baffin Island, Nunavut. The mafic rocks have normal mid-ocean-ridge-basalt–normalized Th, Ce, Zr, Ti and Y concentrations typical of within-plate environments, and strongly negative Nb anomalies, suggesting that they were derived from partial melting of a subduction-modified mantle. The rarer ultramafic intrusions typically have high Ni and Cr (>1800 ppm) and may be either cumulates or high-degree partial melts. Geochemical modification of the mantle involved in partial melting to produce the mafic and ultramafic rocks of southern Hall Peninsula may have occurred during subduction around the margins of the Hall Peninsula block as the Manikewan Ocean closed during the accretionary phase of the middle Paleoproterozoic Trans-Hudson Orogen.

Résumé

On a procédé à l'analyse géochimique des éléments majeurs et des traces sur roche totale de 64 échantillons provenant d'unités cartographiques de nature mafique et ultramafique du sud de la péninsule Hall, dans l'île de Baffin, au Nunavut. La signature des roches mafiques se caractérise par des concentrations en Th, Ce, Zr, Ti et Y de basalte de dorsale médio-océanique normalisée représentatives de milieux intraplaque, et par de fortes anomalies négatives en Nb, ce qui semble indiquer qu'il s'agit de roches remaniées à partir de la fusion partielle du manteau modifié par l'action de la subduction. Les rares intrusions ultramafiques, qui présentent généralement de fortes concentrations en Ni et en Cr (>1800 ppm), peuvent être soit des cumulats, soit le produit d'un point de fusion partielle de premier ordre. La modification géochimique qui s'est produite au cours de la fusion partielle du manteau est à l'origine des roches mafiques et ultramafiques du sud de la péninsule Hall. Cet épisode de fusion a peut être eu lieu au cours de la subduction ayant touché la région marginale du bloc faillé de la péninsule Hall lors de la fermeture de l'océan Manikewan, événement qui s'est produit pendant la phase d'accrétion de l'orogène trans-hudsonien du moyen Paléoprotérozoïque.

Introduction

This paper summarizes preliminary results and interpretations that will contribute to the completion of an MSc thesis undertaken by the senior author as a thematic study within the context of the Canada-Nunavut Geoscience Office (CNGO) Hall Peninsula Integrated Geoscience Program (HPIGP). The study focuses on the geochemistry, petro-genesis, tectonic setting and mineral potential of the mafic and ultramafic rocks of Hall Peninsula. Further analysis of samples collected during the 2013 field season of the HPIGP will be carried out to characterize the mafic and ultramafic geochemistry of the entire Hall Peninsula. For a detailed description of the geology, deformation and metamorphism of Hall Peninsula, see Machado et al. (2013),

Skipton and St-Onge (2014) and Steenkamp and St-Onge (2014).

Mafic and ultramafic rocks are most commonly found as intrusions within metasedimentary packages in the east and central portions of southern Hall Peninsula; however, there are also mafic and ultramafic enclaves within the Archean tonalitic orthogneiss basement in the central and eastern regions and rare mafic and ultramafic units in western Hall Peninsula. All mafic and ultramafic rocks have undergone multiple phases of deformation and have been metamorphosed to at least amphibolite grade, thus only locally preserve primary igneous textures (Steenkamp et al., 2014). Age constraints provided by detrital zircons from quartzite within supracrustal panels in the central and eastern regions, and from crosscutting monzogranite dikes particularly in the area described by MacKay et al. (2013a), indicate that the mafic units within supracrustal packages are Paleoproterozoic (MacKay et al., 2013b; Rayner, 2014). It is not known whether all mafic and ultramafic bodies are the same age, or whether some of the enclaves in the tonalitic gneiss are possibly Archean in age.

Samples were taken from all mafic and ultramafic rock types and were chosen to maximize the geographic distribution of the sample dataset, both in the detailed study area and on southern Hall Peninsula as a whole (Figure 1).

Sample screening, analytical procedure and methodology

Care was taken to collect fresh, large, unaltered samples in the field. All weathered edges were removed with a rock saw. Geochemical preparation and analysis was carried out by Activation Laboratories Ltd. (Actlabs; Ancaster, Ontario) on 64 samples. Samples were pulverized using mild steel to reduce contamination, then mixed with a flux of lithium metaborate and lithium tetraborate and fused in an induction furnace. Major oxides were analyzed using a combination of simultaneous/sequential Thermo Jarrell-Ash ENVIRO II inductively coupled plasma (ICP). For trace-element analysis, the solutions prepared for major-element oxide analysis were spiked with Actlabs internal standard, diluted and run on a Perkin-Elmer SCIEX ELAN® inductively coupled plasma–mass spectrometer (ICP-MS). Sample introduction methods is proprietary to Activation Laboratories Ltd. Upon completion of geochemical analysis, 11 samples that had high (>1.5 wt. %) loss on ignition (LOI) values, suggesting they had been altered, were discarded. Spatial (latitude and longitude) and contextual (station notes) data were extracted from the CNGO database and appended to the geochemical dataset based on unique sampleIDs. This allowed the geochemical data to be analyzed and interpreted with spatial relationships and the broader geological context in mind. Based on the mafic and ultramafic rock classification schemes described herein, however, no geographic clustering of samples is observed.

Results

Element mobility

Samples were tested for evidence of major- and trace-element mobility that may have occurred during deformation and/or metamorphism. This was done by plotting major- and trace-element values against Zr, which is typically immobile in hydrothermal solutions due to its moderate ionic potential (Cann, 1970). Major-element oxides (Fe_2O_3, MgO, Na_2O and CaO) show a high degree of scatter when plotted versus Zr (Figure 2a–d), indicating that elements with low ionic potential were most likely mobilized during late thermotectonic events, limiting their potential usefulness in geochemical investigations. Conversely, the trace elements (Y, Ce, Ti and Nb), with the exception of a few notable outlier analyses, show a much higher degree of correlation (Figure 2e–h), allowing for elements with moderate ionic potential (high-field-strength elements, HFSE) to be used in primary geochemical discriminations.

Rock classification

When plotted on the Zr/Ti versus Nb/Y rock classification diagram (Pearce, 1996), which uses immobile trace elements, most of the mafic samples plot in the subalkaline basalt field, with three plotting in the alkali basalt field and three plotting in the basaltic andesite field (Figure 3a). Most mafic and ultramafic rocks exhibit characteristics typical of tholeiitic or transitional sequences based on the refined classification scheme (Figure 3b) of Ross and Bédard (2009).

Trace-element profiles

Trace-element profiles normalized to normal mid-ocean-ridge basalt (N-MORB) for the subalkaline basaltic composition rocks are shown in Figure 4. All samples show a pronounced negative Nb anomaly with respect to Th and Ce, which is typical of volcanic arcs and back-arcs. The negative anomaly arises during subduction, when Nb is fractionated from Th and Ce during the dehydration of subducted crust. Niobium is retained in amphibole and other minor minerals such as rutile and titanite, whereas Th and Ce preferentially enter the fluid phase (Pearce and Peate, 1995). In addition, all samples are enriched in the most incompatible elements relative to N-MORB typical of within-plate basalt (Pearce, 1996). Seven samples have high $(Ti/Y)_N$ ratios (2.5–5.0), suggesting the involvement of residual garnet during the melting process. Yttrium has a significantly higher bulk distribution coefficient than Ti for the melting of garnet lherzolite, thus is selectively retained within residual garnet, resulting in elevated $(Ti/Y)_N$ in the melt phase (Pearce and Parkinson, 1993). The three samples of alkali basalt composition and all ultramafic samples are excluded because they do not produce consistent trends.

Figure 1: Geology of southern Hall Peninsula, after Machado et al (2013). Green dots indicate the locations of mafic an̲ ̲mafic geochemical samples. Mineral abbreviations: Bi, biotite; Grt, garnet; Hbl, hornblende; Kfs, potassium feldspar; Mag. magn ̲ ̲, Ms, muscovite; Opx, orthopyroxene; Sil, sillimanite.
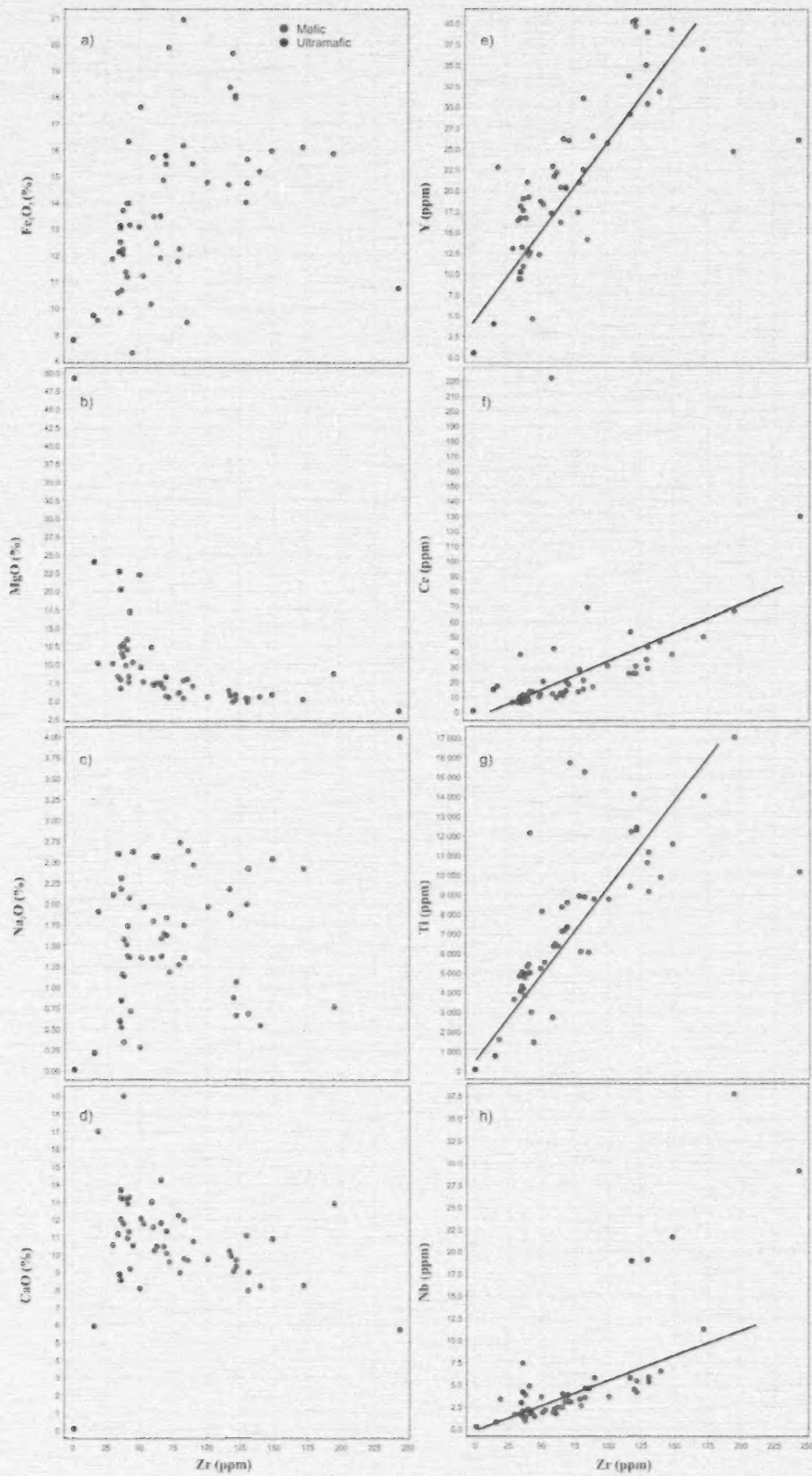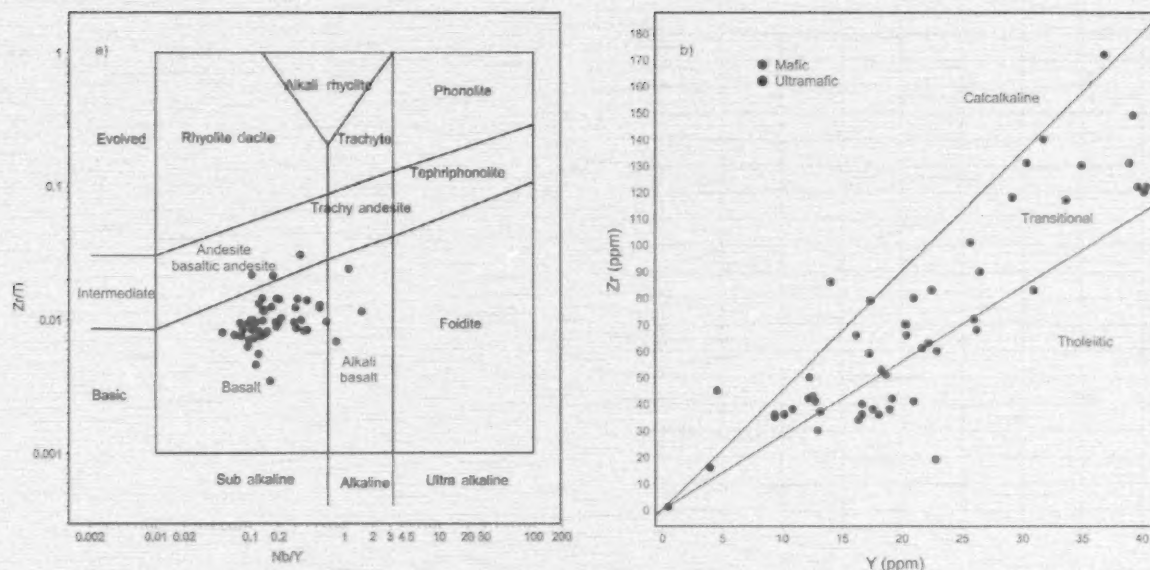
Figure 3: a) Volcanic rock type classification diagram (Zr/Ti versus Nb/Y; Pearce, 1996); **b)** subalkaline basalt classification diagram (Zr versus Y; Ross and Bédard, 2009).

Tectonic discrimination

Tectonic discrimination diagrams are derived from geochemical datasets of rocks whose tectonic setting is known with certainty. Most samples are taken from modern environments, and as such their accuracy and applicability—especially to rocks older than the Phanerozoic—is contentious (Pearce and Cann, 1973, 2008). That being said, tectonic discrimination diagrams can be used to identify chemical variations in similar rock types and form the basis for interpreting processes that give rise to identified differences. Samples plotted on the Th-Zr-Nb tectonic discrimination diagram (Wood, 1980) reveal a large scatter, but plot dominantly in the volcanic arc and within-plate transitional basalt fields (Figure 5).

Ultramafic rocks

Ultramafic rocks were identified in the field based on mineral composition: containing mafic minerals, with less than 10% plagioclase and no visible quartz. Geochemically, total silica is more than 45% in all cases, which is higher than expected, but silica concentration does not likely reflect a primary composition. Four of the five ultramafic intrusions analyzed have high (>1800 ppm) Ni and Cr. The bivariate plot (Figure 6) developed by Brand (1999) indicates that

four of the five samples are typical komatiitic melts and most of the Ni is likely bound in silicate phases, not in sulphides. Petrographic analysis will determine whether any of the samples may represent cumulates, although none of the intrusions from southern Hall Peninsula had any obvious igneous layering (in contrast to those reported by Steenkamp et al., 2014).

Discussion

Geochemically, all samples show characteristics that are intermediate between volcanic arc–related basalts and within-plate basalts. The consistency in geochemical signature may suggest that all subalkaline mafic rocks on southern Hall Peninsula resulted from one event. Alternatively, multiple events derived from the same mantle source may have occurred. The transitional geochemical character between volcanic arc basalts, exemplified by negative Nb anomalies, and within-plate basalts, which are enriched in incompatible elements relative to N-MORB, is best explained by subduction-related geochemical modification of the mantle below southern Hall Peninsula. The timing of enrichment is unknown but may have occurred during the Trans-Hudson Orogen as the Manikewan Ocean closed (Stauffer, 1984). The within-plate signature possibly resulted from the melting of the subduction-modified mantle during a mantle plume event, imparting a mixed geochemical signature to the resulting mafic rocks.

Figure 2: Binary plots of Zr versus **a)** Fe_2O_3, **b)** MgO, **c)** Na_2O, **d)** CaO, **e)** Y, **f)** Ce, **g)** Ti and **h)** Nb used to detect element mobility. Low-ionic-potential elements in a–d show a high degree of scatter, suggesting mobilization, whereas moderate-ionic-potential elements (HFSE) in e–h show a much stronger linear correlation, suggesting they reflect primary igneous compositions.

Economic considerations

Preliminary results indicate that the potential of finding mineral deposits commonly associated with mafic and ultramafic rocks including volcanogenic massive-sulphide (VMS) deposits, Ni–Cu–platinum group elements (PGEs) and Cr is low. All regions of Hall Peninsula have undergone at least middle-amphibolite metamorphism (Skipton and St-Onge, 2014; Steenkamp and St-Onge, 2014), which have not proven to be favourable for preserving these deposit types. Furthermore, the total volume of mafic and ultramafic rocks on the Hall Peninsula is low and those that are present are discontinuous. Finally, Ni values as high as 0.3 wt. % have been obtained from ultramafic rocks. Even though these values are high, they indicate that Ni will be bound dominantly within silicate phases, not in sulphides (Figure 6; Brand, 1999).

Low potential for mafic and ultramafic mineralized systems on Hall Peninsula—while disappointing—is not a total loss, as negative results can be useful. This knowledge can be used to inform members of industry so as to better direct their exploration programs and maximize their exploration dollars.

Figure 4: Trace-element diagrams normalized to normal mid-ocean-ridge basalt (N-MORB; Sun and McDonough, 1989) of **a)** tholeiitic basaltic composition, **b)** transitional basaltic composition, **c)** calcalkaline basaltic composition.
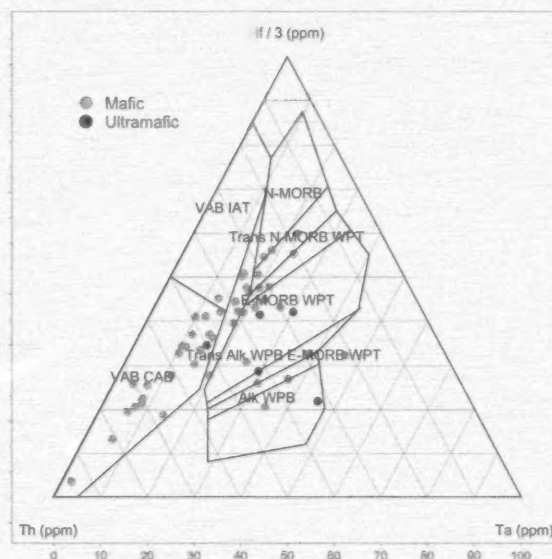
Figure 5: Tectonic discrimination ternary diagram (Wood, 1980). Abbreviations: Alk WPB, alkali within-plate basalt; E-MORB WPT, enriched mid-ocean-ridge basalt, within-plate transition; N-MORB, normal mid-ocean-ridge basalt; Trans Alk WPB E-MORB WPT, transitional alkali within-plate basalt, enriched mid-ocean-ridge basalt, within-plate transition; Trans N-MORB WPT, transitional normal mid-ocean-ridge basalt, within-plate transition; VAB CAB, volcanic arc basalt, calcalkaline basalt; VAB IAT, volcanic arc basalt, island arc transition.
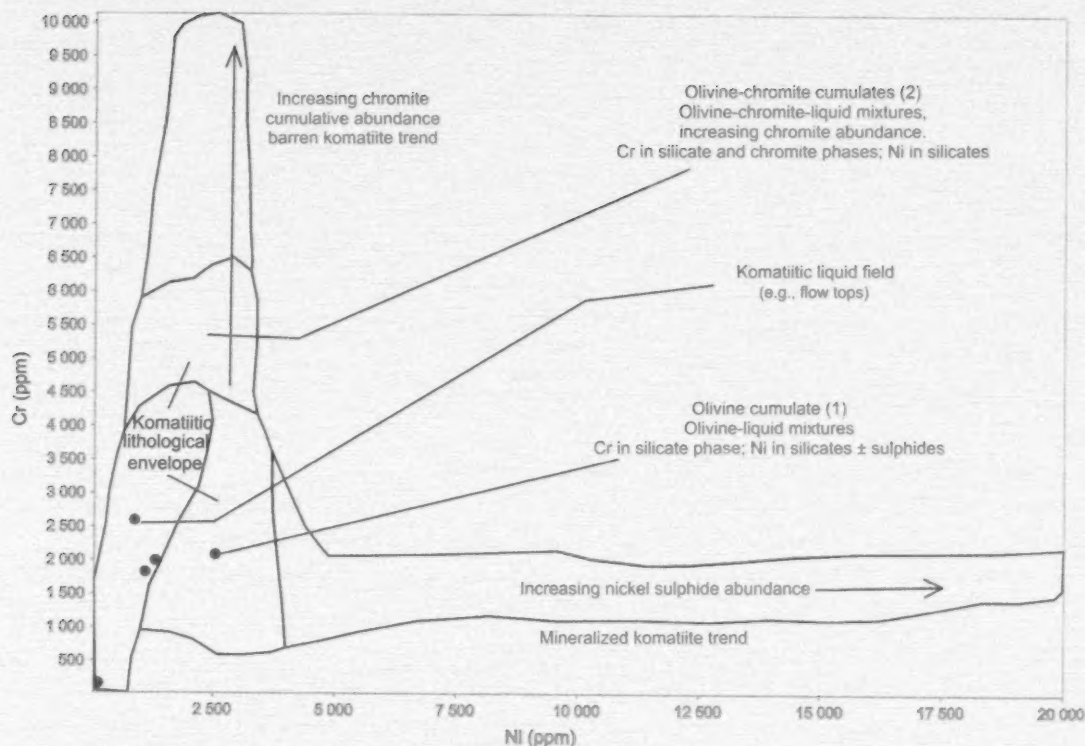
Figure 6: Binary plot of Ni versus Cr, indicating the type of and place within a komatiitic flow that samples of a given composition are found (Brand, 1999).

References

Brand, N.W. 1999: Element ratios in nickel sulphide exploration: vectoring towards ore environments; Journal of Geochemical Exploration, v. 67, p. 145–165.

Cann, J.R. 1970: Rb, Sr, Y, Zr, and Nb in some ocean floor basaltic rocks; Earth and Planetary Science Letters. v. 10, p. 7–11.

Machado, G., Bilodeau, C., Takpanie, R., St-Onge, M.R., Rayner, N.M., Skipton, D., From, R., MacKay, C.B., Creason, C.G. and Braden, Z.M. 2013: Hall Peninsula bedrock mapping, Baffin Island, Nunavut: summary of field work; *in* Summary of Activities 2012, Canada-Nunavut Geoscience Office, p. 13–21.

MacKay, C.B., Ansdell, K.M., St-Onge, M.R., Machado, G. and Bilodeau, C. 2013a: Geological relationships in the Qaqqanittuaq area, southern Hall Peninsula, Baffin Island, Nunavut; *in* Summary of Activities 2012, Canada-Nunavut Geoscience Office, p. 55–63.

MacKay C.B., Ansdell, K.M., St-Onge, M.R., Rayner N.M. and Mate, D. 2013b: Geological age and geochemical constraints on the evolution of the northeastern Paleoproterozoic Trans-Hudson Orogen from the southern Hall Peninsula, Baffin Island, Canada; Geological Society of America Abstracts with Programs, v. 45, no. 7, p. 309.

Pearce, J.A. 1996: A user's guide to basalt discrimination diagrams; *in* Trace Element Geochemistry of Volcanic Rocks: Applications for Massive Sulphide Exploration, D.A. Wyman (ed.), Short Course Notes, v. 12, Geological Association of Canada, p. 79–113.

Pearce, J.A. 2008: Geochemical fingerprinting of oceanic basalts with applications to ophiolite classification and the search for Archean oceanic crust; Lithos, v. 100, p. 14–48.

Pearce J.A. and Cann J.R. 1973: Tectonic setting of basic volcanic rocks determined using trace element analysis; Earth and Planetary Science Letters, v. 19, p. 290–300.

Pearce, J.A. and Parkinson, I.J. 1993: Trace element models for mantle melting: applications to volcanic petrogenesis; Geological Society, London, Special Publications, v. 76, p. 373–403.

Pearce, J.A. and Peate, D.W. 1995: Tectonic implications of the composition of volcanic arc magmas; Annual Review of Earth and Planetary Sciences, v. 23, p. 251–285.

Rayner, N.M. 2014: New uranium-lead geochronological results from Hall Peninsula, Baffin Island, Nunavut; *in* Summary of Activities 2013, Canada-Nunavut Geoscience Office, p. 39–46.

Ross, P.-S. and Bedard, J.H. 2009: Magmatic affinity of modern and ancient subalkaline volcanic rocks determined from trace-element discrimination diagrams; Canadian Journal of Earth Sciences, v. 46, p. 823–839.

Skipton, D. and St-Onge, M.R. 2014: Paleoproterozoic deformation and metamorphism in metasedimentary rocks west of Okalik Bay: a field template for the evolution of eastern Hall Peninsula, Baffin Island, Nunavut; *in* Summary of Activities 2013, Canada-Nunavut Geoscience Office, p. 57–66.

Stauffer, M.R. 1984: Manikewan: an early Proterozoic ocean in central Canada, its igneous history and orogenic closure; Precambrian Research, v. 25, p. 257–281.

Steenkamp, H.M. and St-Onge, M.R. 2014: Overview of the 2013 regional bedrock mapping program on northern Hall Peninsula, Baffin Island, Nunavut; *in* Summary of Activities 2013, Canada-Nunavut Geoscience Office, p. 27–38.

Steenkamp, H., Bros, E. and St-Onge, M.R. 2014: Economic potential of ultramafic rocks on Hall Peninsula, Nunavut; *in* Summary of Activities 2013, Canada-Nunavut Geoscience Office, p. 11–20.

Sun, S.-s. and McDonough, W.F. 1989: Chemical and isotopic systematics of oceanic basalts: implications for mantle composition and processes; Geological Society, London, Special Publications, v. 42, p. 313–345.

Wood, D.A. 1980: The application of the Th-Hf-Ta diagram to problems of tectonomagmatic classification and to establishing the nature of crustal contamination of basaltic lavas of the British Tertiary volcanic province; Earth and Planetary Science Letters, v. 50, p. 11–30.

Preliminary characterization of the Mesozoic–Cenozoic exhumation history of Hall Peninsula, Baffin Island, Nunavut, based on apatite and zircon (U-Th)/He thermochronology

C.G. Creason[1] and J.C. Gosse[2]

[1]Department of Earth Science, Dalhousie University, Halifax, Nova Scotia, creason@dal.ca
[2]Department of Earth Science, Dalhousie University, Halifax, Nova Scotia

Abstract

The thermochronometric data from the southeastern half of Hall Peninsula will provide a means of establishing the spatial and temporal patterns of rock cooling as the rocks were brought to the surface through tectonic and erosional processes. The ^{4}He concentrations in apatite (n = 130) and zircon (n = 35) grains from 26 samples reveal a strong sensitivity to radiation damage, which suggests a record of slow exhumation. After adjusting the He ages for the effects of radiation damage, two models will be used to interpret the cooling history. A widely used thermal modelling program used to simulate potential time-temperature (t-T) paths for various thermochronometers (HeFTy) will provide a means of establishing constraints for the cooling history of each sample. A three-dimensional thermokinematic finite-element modelling code (Pecube) will also be used to determine the t-T history of the rocks on Hall Peninsula, and test how regional tectonism and long-term climate changes were responsible for spatial and temporal variations in the cooling rates.

Résumé

Les données thermochronométriques recueillies dans la moitié sud-est de la péninsule Hall serviront à établir les profils spatiaux et temporels du refroidissement des roches, à mesure que ces dernières ont été entraînées vers la surface par les processus associés à la tectonique et à l'érosion. Les concentrations en ^{4}He dans les grains d'apatite (n = 130) et de zircon (n = 35) provenant de 26 échantillons accusent une forte sensibilité aux effets du rayonnement, phénomène qui semble indiquer que l'exhumation s'est faite sur une longue période de temps. Après avoir ajusté les âges du He pour compenser les effets du rayonnement, on aura recours à deux modèles afin d'interpréter le parcours des conditions de refroidissement des roches. Un logiciel de modélisation thermique à utilisation fort répandue (HeFTy), qui simule les trajets temps-température (t-T) possibles pour divers thermochronomètres, servira à préciser les contraintes propres aux conditions de refroidissement de chaque échantillon. En outre, un code de modélisation thermocinétique par éléments finis en trois dimensions (Pecube) servira à établir le parcours t-T des roches de la péninsule Hall et à vérifier à quel point les variations dans l'espace et le temps au niveau des vitesses de refroidissement sont imputables aux incidences du tectonisme à l'échelle régionale et aux changements climatiques à long terme.

Introduction

The cooling rate (temperature vs. time) of rocks during their ascent to the surface is a useful indication of the processes that have controlled regional topography and sediment flux to the nearby ocean. The cooling history can be obtained by using any of more than a dozen thermochronometers, depending on the rock depth (temperature) of interest, duration and rate of the process, and mineralogy available. Using multiple thermochronometers with different closure temperatures (temperatures at which the chronometer begins) in a single rock sample provides a means of establishing the change in the cooling rate with time (cooling history). Furthermore, by collecting multiple samples in space (i.e., bottoms of valleys, tops of mountains, across a fault zone), it is possible to link the cooling history

to process and thereby test hypotheses regarding the timing and extent of rock and surface uplift, incision and changes in the onshore sediment flux.

The low-temperature thermochronology samples for this study were collected during the 2012 Hall Peninsula field season (Figure 1). In total, 26 samples were selected for apatite (U-Th)/He (AHe) analysis; additionally, 7 of these samples were also analyzed for zircon (U-Th)/He (ZHe). Sample preparation was completed at the Dalhousie Geochronology Centre and the samples were analyzed at the (U-Th)/He Geo-and-Thermochronometry Lab, University of Texas, Austin (see Creason et al., 2013 for detailed descriptions of the sample lithology, sampling strategy and laboratory procedures for (U-Th)/He thermochronology). The (U-Th)/He thermochronology method is based on the
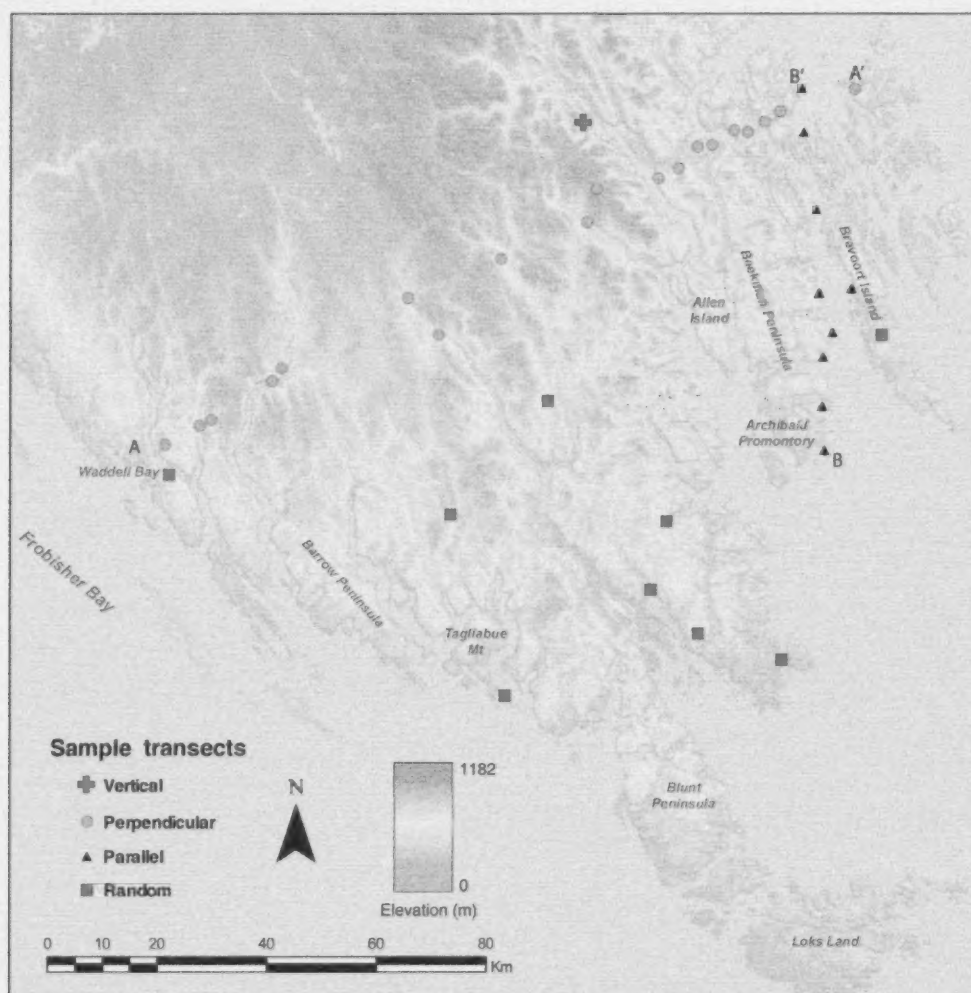
Figure 1: Locations of (U-Th)/He samples collected during the 2012 field season on Hall Peninsula, Baffin Island, Nunavut. Samples were collected from three transects: one vertical transect (capturing the maximum amount of relief) and two constant-elevation transects (one oriented perpendicular to the Cumberland Sound coastline, the other parallel). Additional samples were collected to serve as constraints for Pecube models. Figure from Creason et al. (2013).

diffusion of radiogenic ^{4}He (α-particles) from a grain until its temperature cools to a point at which ^{4}He diffusion is effectively halted (the grain is closed with respect to ^{4}He) and the abundance of ^{4}He within the grain increases proportionally with time since closure.

Preliminary results suggest that the rocks on Hall Peninsula have experienced a history of protracted slow cooling (Figure 2), exposing the samples to a high dose of radiation during their exhumation. Actinide radionuclide decay will cause damage to a crystal lattice. The radiation damage alters the diffusion of ^{4}He, necessitating a correction to the measured He ages, as they no longer conform to the standard He-diffusion kinetics (Shuster et al., 2006; Flowers et al., 2009). This paper focuses on the effect of radiation damage on He diffusion in the AHe thermochronometer and outlines the procedure for interpreting the AHe data. See Goldsmith et al. (2014) for a detailed discussion on the effects of radiation damage in ZHe thermochronometry and the means by which a radiation-damage correction will be applied to the ZHe thermochronology data from Hall Peninsula.

The paper summarizes progress on evaluating the applicability of corrections for existing radiation damage and devising a new correction for grains with high actinide concentrations. It briefly describes two different modelling programs, HeFTy and Pecube, that will be utilized to characterize the subsurface thermal history of Hall Peninsula using the radiation-damaged ^{4}He data. The program HeFTy

will be used to develop a time-temperature (t-T) path for each sample. Outputs from the HeFTy models will allow comparison of the corrected results with synthetic data from other low-temperature thermochronometers, such as apatite fission track, and justify the need for further analyses with different thermochronometers to validate the corrected He ages. The program Pecube will be used to derive an exhumation history of Hall Peninsula based on the thermochronometry data and results from HeFTy models, and test a hypothesis that north-south extension preceded the more recent east-west transtensional extension between Baffin and Greenland.

AHe thermochronometry and radiation damage

The (U-Th)/He thermochronology method is based on the thermally controlled retention of radiogenic α-particles (^{4}He) within a mineral (Farley, 2002). This method relies on the understanding that certain minerals only accumulate ^{4}He when they are cooled below a specific temperature, known as their closure temperature (T_c). At temperatures above T_c, secular equilibrium is achieved, whereby the α-particles diffuse through the grain at the same rate they are produced (Farley, 2002). Closure temperature varies with mineral type (e.g., zircon, apatite, magnetite), enabling investigation of many geological processes that affect geothermal fields spanning various depths in the Earth's crust. Selection of an appropriate thermochronometer depends on
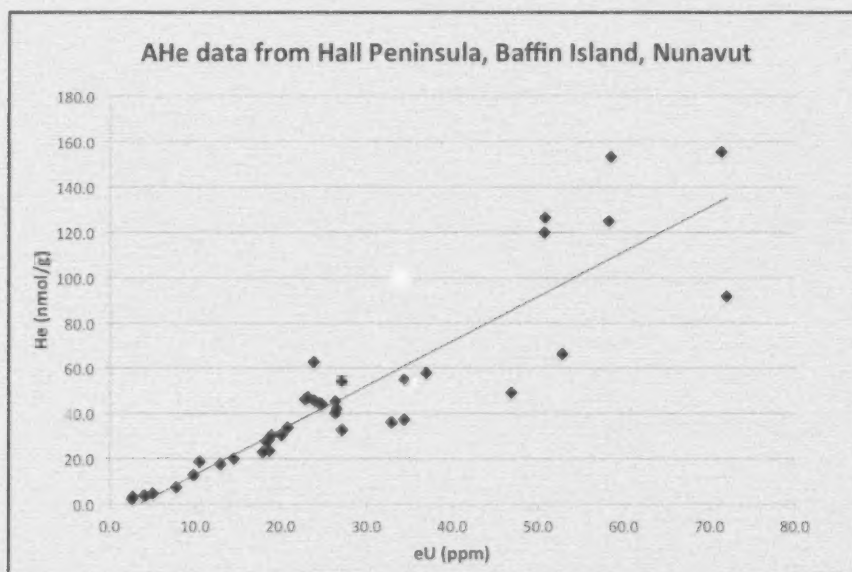
Figure 2: Preliminary AHe data from Hall Peninsula, Baffin Island, Nunavut, illustrating the linear relationship between ^{4}He concentration and the effective concentration of parent radionuclides (eU). This correlation suggests the influence of radiation damage on the diffusion kinetics of ^{4}He within the apatite grains. The plot comprises individual aliquots from several samples collected along a constant-elevation transect spanning southeastern Hall Peninsula and oriented perpendicular to the Cumberland Sound coastline (Creason et al., 2013).

the geological processes of interest to the study, and how those processes affect the subsurface thermal field. Previous studies investigating the landscape evolution of passive margins (e.g., Braun and van der Beek, 2004) demonstrated the appropriateness of apatite and zircon (U-Th)/He thermochronometers for determining the long-term landscape evolution and exhumation history of Hall Peninsula. Apatite-He has a very low T_c (40–75°C; Ehlers and Farley, 2003), making it sensitive to the tectonism- and climate-induced variations in exhumation of the upper crust of Hall Peninsula. In select samples, ZHe, with higher T_c (~180°C; Reiners, 2005), was also analyzed to serve as an added constraint in determining the earlier (higher temperature) thermal history with the thermokinematic models.

An underlying premise in (U-Th)/He thermochronometry is that the concentration of radiogenic ^{4}He in a grain is controlled primarily by the amount of time since it cooled below T_c (Wolf et al., 1996). However, several other factors control ^{4}He accumulation in a mineral, such as grain size, grain shape, and concentration and distribution of parent radioisotopes in the crystal lattice (Farley, 2002). These factors are considered in each cooling-age calculation. Additionally, the rate of cooling and residence time in the He partial-retention zone (HePRZ) can affect the amount of α-particles retained in the crystal; in cases of protracted slow cooling, these factors can alter the kinetics of ^{4}He diffusion within the grain (Shuster et al., 2006). Grains exposed to low temperatures for extended periods of time (i.e., tens to hundreds of millions of years) are susceptible to the effects of radiation damage caused by prolonged α-decay, which can alter the He-diffusion kinetics of the mineral (Flowers et al., 2009). The effect of α-induced lattice damage must be considered to account for any changes in ^{4}He diffusion, and it appears the effect varies with crystal type (apatite, zircon) and actinide concentration.

Radiation damage in the AHe system has been recognized for several decades (e.g., Hurley, 1954). Many studies have speculated on how radiation damage might alter the diffusivity characteristics of apatite (e.g., Wolf et al., 1996; Farley, 2000), but the effect has only recently been quantified (Shuster et al., 2006; Flowers et al., 2007; Flowers, 2009; Flowers et al., 2009; Gautheron et al., 2009). Radiation damage is the result of α-particle recoil damage during α-decay of ^{238}U, ^{235}U, ^{232}Th and ^{147}Sm, as well as the spontaneous fission of ^{238}U (Shuster et al., 2006). Damage begins to accumulate in the apatite crystal structure when the mineral is at or near ~120°C, the chemistry-sensitive temperature below which the crystal no longer anneals. In apatite, lattice damage acts to decrease the diffusivity of the mineral grains, causing an increased retention of ^{4}He. Furthermore, grains with a prolonged residence time in the HePRZ are much more sensitive to changes in ^{4}He diffusivity; in cases of extremely slow cooling (i.e., 1–0.1°C/

m.y.), radiation damage has been suggested as the primary control on ^{4}He diffusivity (Shuster et al., 2006; Flowers et al., 2009).

Shuster et al. (2006) proposed that radiation damage in apatite leads to the formation of ^{4}He 'traps', which increase the energy required for the ^{4}He to diffuse through the grain, thus effectively increasing T_c and yielding 'artificially older' AHe ages. This understanding led to development of the Helium Trapping Model (HeTM), a correction for radiation damage in apatite that accounts for altered ^{4}He diffusion (Shuster et al., 2006). The HeTM diffusion model by Shuster et al. (2006) uses ^{4}He concentration as a proxy for the amount of radiation damage present in the apatite crystal. However, this method is limited because ^{4}He abundance and damage within the crystal are not accumulated at the same rate. Flowers et al. (2009) built upon HeTM with the radiation-damage accumulation and annealing model (RDAAM). This model uses the effective spontaneous fission-track density (a byproduct of spontaneous ^{238}U fission, calculated in apatite fission-track thermochronology) to quantify the amount of radiation damage present in the apatite grain.

Previous studies on the effects of radiation damage in AHe thermochronometry have provided ways to recognize an altered ^{4}He diffusion profile (Flowers et al., 2007; Flowers, 2009; Flowers et al., 2009). For example, a key indicator of radiation-damage–induced ^{4}He diffusion in apatite is a strong positive linear correlation between the effective concentration of all ^{4}He-parent isotopes (eU) and concentration of ^{4}He within the grain, resulting in large amounts of scatter in several measured He ages of apatite grains from a single rock sample (Shuster et al., 2006; Flowers et al., 2007). The results from Hall Peninsula reveal a similar ^{4}He-eU relationship. Owing to very high eU in many of the apatite crystals (>50 ppm), the relationship can be studied over a large eU range. The results indicate that, at eU greater than 20 ppm, the relationship becomes much more scattered (Figure 2). The authors interpret an eU of 20 ppm to be the effective threshold for radiation damage in these apatite grains (i.e., for crystals below T_c for long durations, more radiation damage does not significantly or regularly increase the effect). A similar threshold was observed in the zircon data (Goldsmith et al., 2014). The observed ^{4}He-eU relationship provides a first-order interpretation of the exhumation and cooling history. The fact that the samples are so extensively altered by radiation damage indicates that the rocks on Hall Peninsula cooled very slowly. This alone provides a beneficial initial constraint for the thermal modelling in both HeFTy and Pecube.

HeFTy Model

The HeFTy modelling program calculates t-T histories for individual thermochronometers in a sample based on min-

eral type; grain geometry; measured U, Th, Sm and He concentrations; chemical zonation; and ^{4}He diffusion parameters (e.g., Farley (2000) Durango standard diffusion, Shuster et al. (2006) HeTM diffusion and Flowers et al. (2009) RDAAM diffusion). The program is capable of both forward and inverse modelling for many different thermochronometers (e.g., (U-Th)/He, fission track, vitrine reflectance and ^{40}Ar/^{39}Ar). The model computes potential thermal histories that fit the data in accordance with the input parameters and boundary conditions (Ketcham, 2005). The forward model provides an indication of appropriate ^{4}He diffusion profiles based on a prescribed t-T path.

The HeFTy program is not capable of determining the exact t-T path of a sample; it provides acceptable t-T histories based on the goodness-of-fit value calculated for the He-diffusion profile from all the aliquots in the sample (Ketcham, 2005). For the purposes of the Hall Peninsula thermochronology study, the t-T paths derived from HeFTy will serve two purposes: 1) testing the sensitivity of the RDAAM correction to the AHe data; and 2) establishing preliminary constraints for the three-dimensional (3-D) thermokinematic modelling by establishing the boundary thermal conditions and ^{4}He-diffusion characteristics necessary to yield corrected, geologically meaningful AHe ages. In many instances, inclusion of higher T_c thermochronometers can help constrain the early thermal history of the grain and improve the fit of the modelled histories. Using synthetic-apatite fission-track data, the authors observed that the HeFTy cooling histories in some samples were very sensitive to the early history. Therefore, apatite grains have

been strategically selected for fission-track analysis to help constrain the HeFTy models. The HeFTy output will not only provide guidance regarding the timing and therefore potential cause of changes in cooling (exhumation) rates, but it will help constrain the Pecube modelling of the 3-D diffusion throughout the region.

Pecube Model

A 3-D thermokinematic model (Pecube) will be used to predict the spatial distributions of thermochronological ages on Hall Peninsula, in order to test hypotheses regarding the possible rift-related controls on exhumation. Pecube is a finite-element code used to solve the heat-transport equation. It calculates the effect of time-varying finite-amplitude topography on the subsurface thermal field and links changes to the surface topography with the subsurface thermal history (Braun, 2003). After solving the heat-transport equation, Pecube interpolates the calculated 3-D subsurface temperature field onto particles as they travel to the sampled points at the surface, resulting in a time-temperature history controlled by the surface processes that altered the subsurface thermal field during exhumation (Braun, 2003; Braun et al., 2012). The end result is a time-temperature path for the rocks now at the surface, which yields a spatial distribution of He ages (Figure 3) and exhumation rates. Specific patterns in the distribution of He ages can be indicative of various exhumation styles typical of rifted continental margins (i.e., escarpment retreat versus pinned-divide exhumation; e.g., Gallagher and Brown, 1999; Braun and van der Beek, 2004) and if tilting of Hall Peninsula and
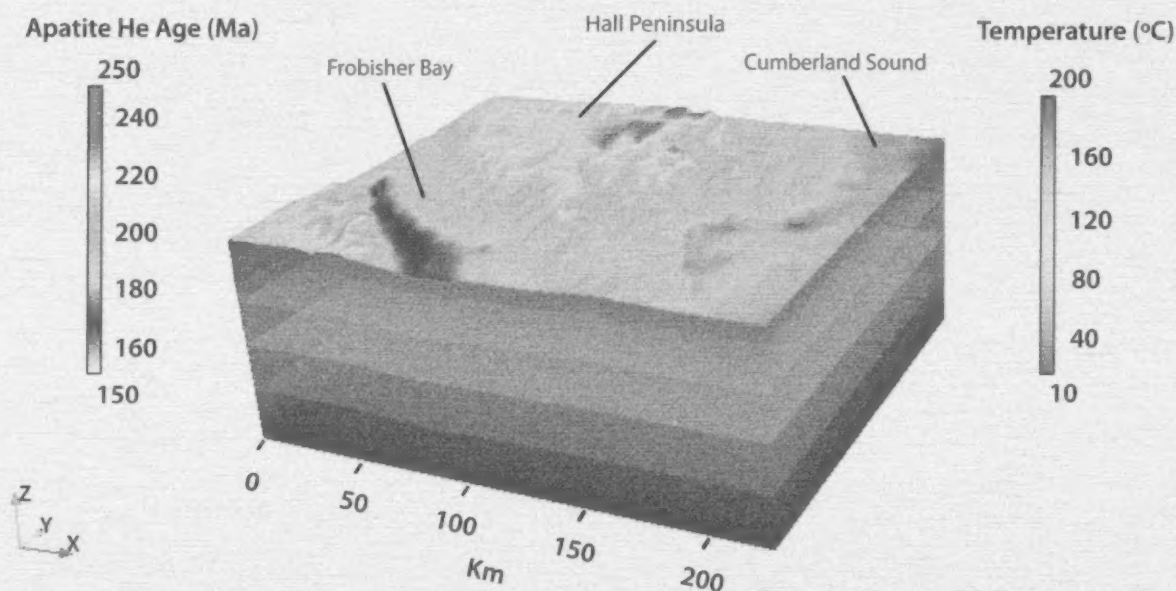
Figure 3: Semischematic Pecube model of Hall Peninsula, as viewed in the 3-D visualization program ParaView (Henderson, 2007). Colours at the surface reflect hypothetical AHe ages, as calculated by a simplified model with uniform uplift and steady-state topography. Subsurface layers represent planes of equal temperature. Vertical exaggeration (i.e., z-axis) is 5 times, to visibly enhance topography.

neighbouring peninsulas occurred during the initial rifting along reactivated Precambrian structures (sutures, faults).

The input requirements for Pecube are a digital-elevation model; spatial co-ordinates and measured cooling ages (He ages) of samples collected in strategically oriented transects; spatial co-ordinates and kinematics of any faults; and various geophysical parameters (e.g., uplift rate, crustal thickness, rock density, effective elastic thickness, thermal conductivity, basal crustal temperature and crustal heat production).

The Pecube program is capable of processing both forward and inverse t-T histories (Braun, 2003). In a forward model, the user defines the initial parameters and runs the scenario for a set time; the model is started at t = 0, simulating an evolution based on the initial model boundaries. Pecube first calculates a velocity field for all particles, then calculates the temperature field at specific user-defined time steps, providing a time window at each time step (Braun et al., 2012). The end result is a prediction of what the modern distribution of He ages at the surface should be, given the prescribed set of model parameters. A Pecube model provides a comparison of the simulated He ages to the measured data by calculating a misfit value for the difference, allowing the user to test various starting conditions and model parameters, and determine the ensuing distribution of surface He ages. The processing time for forward modelling is relatively short, allowing the user to test many different scenarios in a little as a few hours. Results from forward models are often used as boundary constraints for subsequent inverse models.

Inverse models in Pecube are implemented using the Neighbour Algorithm (NA) to create a best-fit scenario for the t-T history. In these models, the user defines a variable range for select parameters. The model is run multiple times (10 000+), modifying the variables within the predefined parameter space. After each model run, the NA analyzes the misfit values for these parameters and selects the next parameter set based on the minimized misfit values (Braun et al., 2012). For more details on the theory of the NA and its application in geophysical modelling, the reader is referred to Sambridge (1999a, b).

Inverse modelling is typically much more computationally intensive than forward modelling; depending on model size and resolution, processing times can range from days to weeks. The current expectation is that the forward models constructed in Pecube will be sufficient for characterizing the exhumation history and resultant long-term landscape evolution of Hall Peninsula.

Initial Pecube experiments involve a simple featureless crust (i.e., no topographic relief) to determine if there is a general spatial relationship between He ages and the location of large-scale structures and coastlines. Subsequent experiments will solve more complex scenarios, and may be scaled up to include data from other parts of Baffin Island.

Economic significance for Nunavut

Developing a quantitative model of the exhumation history of Hall Peninsula will give a detailed history of the Cenozoic sediment flux to Cumberland Sound and Frobisher Bay. However, because Hall Peninsula may be representative of eastern Baffin Island, the results of this study will provide the first land-based history of regional variations in sediment flux to Baffin Bay and Davis Strait, where stratigraphic characterization is of significance to the development of basin-sedimentation models for the petroleum industry. Although the sediment within Baffin Bay and Davis Strait may be, to some extent, far travelled, a detailed exhumation-history and landscape-evolution model of Hall Peninsula, derived from coupling of low-T thermochronology and 3-D thermokinematic modelling (Pecube), will help establish the portion of sediment flux that was derived from Hall Peninsula and, by proxy, eastern Baffin Island.

Acknowledgments

References

Braun, J. 2003: Pecube: a new finite-element code to solve the 3D heat transport equation including the effects of a time-varying, finite amplitude surface topography; Computers & Geosciences, v. 29, p. 787–794, doi:10.1016/S0098-3004(03)00052-9

Braun, J. and van der Beek, P. 2004: Evolution of passive margin escarpments: what can we learn from low-temperature thermochronology?; Journal of Geophysical Research, v. 109, F04009, doi:10.1029/2004JF000147

Braun, J., van der Beek, P., Valla, P., Robert, X., Herman, F., Glotzbach, C., Pedersen, V., Perry, C., Simon-Labric, T. and Prigent, C. 2012: Quantifying rates of landscape evolution and tectonic processes by thermochronology and numerical modeling of crustal heat transport using PECUBE; Tectonophysics, v. 524–525, p. 1–28.

Creason, C.G., Gosse, J.C. and Young, M.D. 2013: Rift flank uplift and landscape evolution of Hall Peninsula, Baffin Island, Nunavut: an exhumation model based on low-temperature thermochronology; *in* Summary of Activities 2012, Canada-Nunavut Geoscience Office, p. 75–84.

Ehlers, T.A. and Farley, K.A. 2003: Apatite (U-Th)/He thermochronometry: methods and applications to problems in tectonic and surface processes; Earth and Planetary Science Letters, v. 206, no. 1–2, p. 1–14, doi:10.1016/S0012-821X(02)01069-5

Farley, K.A. 2000: Helium diffusion from apatite: general behavior as illustrated by Durango fluorapatite; Journal of Geophysical Research, v. 105(B2), p. 2903–2914.

Farley, K.A. 2002: (U-Th)/He dating: techniques, calibrations, and applications; Reviews in Mineralogy and Geochemistry, v. 47, p. 819–844, doi:10.2138/rmg.2002.47.18

Flowers, R.M. 2009: Exploiting radiation damage control on apatite (U-Th)/He dates in cratonic regions; in Earth and Planetary Science Letters, v. 277, no. 1, p. 148–155.

Flowers, R.M., Ketcham, R.A., Shuster, D.L. and Farley, K.A. 2009: Apatite (U-Th)/He thermochronometry using a radiation damage accumulation and annealing model; Geochimica et Cosmochimica Acta, v. 73, no. 8, p. 2347–2365.

Flowers, R.M., Shuster, D.L., Wernicke, B.P. and Farley, K.A. 2007: Radiation damage control on apatite (U-Th)/He dates from the Grand Canyon region, Colorado Plateau; Geology, v. 35, no. 5, p. 447–450.

Gallagher, K. and Brown, R. 1999: Denudation and uplift at passive margins: the record on the Atlantic margin of southern Africa; Philosophical Transactions of the Royal Society of London, Series A, v. 357, p. 835–859.

Gautheron, C., Tassan-Got, L., Barbarand, J. and Pagel, M. 2009: Effect of alpha-damage annealing on apatite (U-Th)/He thermochronology; Chemical Geology, v. 266, no. 3, p. 157–170.

Goldsmith, A.S., Creason, C.G., Stockli, D.F. and Ketcham, R.A. 2014: Using zircons from Hall Peninsula, Baffin Island, Nunavut to understand the effects of radiation damage on helium diffusion; in Summary of Activities 2013, Canada-Nunavut Geoscience Office, p. 101–108.

Henderson, A. 2007: ParaView guide, a parallel visualization application; Kitware Inc., URL <www.paraview.org> [November 12, 2013].

Hurley, P.M. 1954: The helium age method and the distribution and migration of helium in rocks; in Nuclear Geology, H. Faul (ed.), J. Wiley & Sons, p. 301–329.

Ketcham, R.A. 2005: Forward and inverse modeling of low-temperature thermochronometry data; Reviews in Mineralogy and Geochemistry, v. 58, no. 1, p. 275–314.

Reiners, P.W. 2005: Zircon (U-Th)/He thermochronometry; Reviews in Mineralogy and Geochemistry, v. 58, no. 1, p. 151–179.

Sambridge, M. 1999a: Geophysical inversion with a neighbourhood algorithm—I. searching a parameter space; Geophysical Journal International, v. 138, no. 2, p. 479–494.

Sambridge, M. 1999b: Geophysical inversion with a neighbourhood algorithm—II. appraising the ensemble; Geophysical Journal International, v. 138, no. 3, p. 727–746.

Shuster, D.L., Flowers, R.M. and Farley, K.A. 2006: The influence of natural radiation damage on helium diffusion kinetics in apatite; Earth and Planetary Science Letters, v. 249, p. 148–161.

Wolf, R.A., Farley, K.A. and Silver, L.T. 1996: Helium diffusion and low-temperature thermochronometry of apatite; Geochimica et Cosmochimica Acta, v. 60, no. 21, p. 4231–4240.

Using zircons from Hall Peninsula, Baffin Island, Nunavut to understand the effects of radiation damage on helium diffusion

A.S. Goldsmith[1], C.G. Creason[2], D.F. Stockli[3] and R.A. Ketcham[3]

[1]Department of Geological Sciences, University of Texas at Austin, Austin, Texas, atom.goldsmith@utexas.edu
[2]Department of Earth Sciences, Dalhousie University, Halifax, Nova Scotia
[3]Department of Geological Sciences, University of Texas at Austin, Austin, Texas

Abstract

Zircon (U-Th)/He thermochronometry (ZHe) is a method of determining low-temperature thermal histories by measuring the concentrations of U, Th and He in zircon. Because the diffusion of He from the crystal is a function of temperature and time, the combined ratios of these elements contain valuable information about cooling of the host rock. Helium diffusion in zircon, however, is more complex than in previous models, in that it is now well known to be significantly and systematically affected by damage to the crystal lattice caused by the á-decay of U and Th, and the spontaneous fission of ^{238}U. Therefore, a thorough and quantitative understanding of the effects of radiation damage on He diffusion kinetics is critical to the accurate modelling of thermal histories. This is particularly useful for cases in which zircons have experienced significant radiation doses, or prolonged residence at temperatures above which radiation damage is annealed. This study uses (U-Th)/He thermochronology on zircon from Hall Peninsula, Baffin Island, which displays a negative correlation with radioactive element concentration, in combination with Raman spectroscopy and laser-ablation inductively coupled plasma–mass spectrometry, to quantify the effects of radiation dose on helium diffusivity. The ages produced from this study are anticipated to show the full range of variability in He diffusivity from radiation dose. These data and others will help in identifying the thresholds of radiation dose required for significant alteration of He diffusivity, and in developing a new and more accurate model for ZHe thermochronology.

Résumé

La thermochronométrie (U/Th)/He dans les zircons est une méthode qui permet d'établir les parcours thermiques de basse-température en mesurant les concentrations en U, Th et He dans les zircons. Puisque le comportement de l'He au sein des cristaux est fonction de la température et du temps, les rapports combinés de ces éléments renferment d'importants renseignements au niveau des vitesses de refroidissement des roches encaissantes. Le comportement de l'He qui s'échappe par diffusion des zircons est cependant un processus plus complexe que ne le décrivent les modèles antérieurs; en effet, il appert maintenant que ce processus est touché considérablement, et de façon systématique, par les dégâts causés au réseau cristallin par la réaction nucléaire de désintégration alpha de l'U et du Th, ainsi que la fission spontanée de l'^{238}U. La modélisation précise des parcours thermiques exige donc une connaissance approfondie et quantitative des effets des dégâts par rayonnement sur la cinétique de l'échappement par diffusion de l'hélium. De telles connaissances se révèlent surtout utiles dans les cas où les zircons ont été exposés à de fortes doses de rayonnement, ou sont restés en place pendant une période de temps prolongée à des températures au-dessus desquelles les dégâts par rayonnement se trouvent recuits. Pour

les besoins de la présente étude, on a eu recours aux résultats de la thermochronométrie (U-Th)/He dans les zircons de la péninsule Hall (île de Baffin), qui se caractérisent par une corrélation négative avec les concentrations en éléments radioactifs, combinés aux résultats provenant de la spectrométrie Raman et de l'ablation laser couplée à un spectromètre de masse à source à plasma inductif, afin de quantifier les effets de doses de rayonnement sur la diffusivité de l'hélium. Les résultats semblent indiquer que les âges obtenus et présentés dans ce rapport illustrent la gamme complète de la variabilité au niveau de la diffusion de l'He causée par les doses de rayonnement. Ces données, ajoutées à d'autres, aideront à déterminer les seuils de dose de rayonnement requis pour causer une importante altération au niveau de la diffusivité de l'He et à mettre au point de nouveaux modèles plus précis de thermochronométrie ZHe.

Introduction

The technique of (U-Th)/He thermochronology of zircon (ZrSiO$_4$) is an increasingly popular method of determining low-temperature thermal histories. This approach utilizes the high concentrations of U and Th (tens to thousands of ppm) in natural zircon. As U and Th undergo radioactive decay to Pb, they implant a series of á-particles into the crystal lattice. These á-particles, consisting of two protons and two neutrons, quickly become ^{4}He by electron capture. Each decay event also causes tens of thousands of localized atomic displacements, both from the energetic ejection of the daughter á-particle and recoil of the parent nuclide. The implanted He can be lost by thermally activated diffusion, the rate of which is in part a function of temperature but also a function of the properties of the mineral lattice, particularly the extent of radiation damage. Because of the thermal component of He retention, the 'ZHe' age, calculated from the concentrations of U, Th and He, contains significant information about the cooling history of the rock. For example, in the simplest scenario of a constant cooling rate of 10°C/m.y., zircon will 'close' to He diffusion and begin to retain significant concentrations of He at approximately 170–190°C (Reiners, 2005). These cooling ages, combined with geological and/or other thermochronometric constraints, are used to produce models of thermal histories by calculating ^{4}He production and diffusion over time. Such models are of great use in understanding the timing of geological processes, including upper-crustal structural deformation, basin formation and thermal evolution, and hydrothermal activity.

The overall accuracy of these models, however, is impeded by a lack of understanding of the full complexities of He diffusion kinetics, in particular with respect to damage to the crystal lattice caused both by the á-decay of U and Th, and by the spontaneous fission of ^{238}U. The systematic effects of this damage on He diffusion have long been recognized, particularly for rocks in which populations of zircon have accumulated significant radiation doses, and that have not experienced temperatures sufficient to allow the crystal lattice to reorder, or anneal (Nasdala et al., 2004; Reiners et al., 2004; Reiners, 2005; Guenthner and Reiners, 2009; Ketcham et al., 2013). For example, ZHe ages obtained from boreholes of assorted basement rock of the Egyptian Sinai Peninsula by Pujols (2011) yield a clear negative correlation with effective uranium concentration (eU), here used as a proxy for radiation damage (Figure 1). These data are significant for several reasons, the most important of which are 1) that the variation in ages is more than 500 m.y. and their negative correlation with eU is observed in several individual samples of rock from different locations; and 2) that these ages correlate with known regional tectonic events. These relationships suggest not only that accurate modelling of thermal histories recorded by zircon (U-Th)/He requires a quantitative knowledge of the effects of radiation dose on diffusivity, but that it is possible for a rock with zircons of sufficiently variable U and Th concentrations to record multiple thermal events.
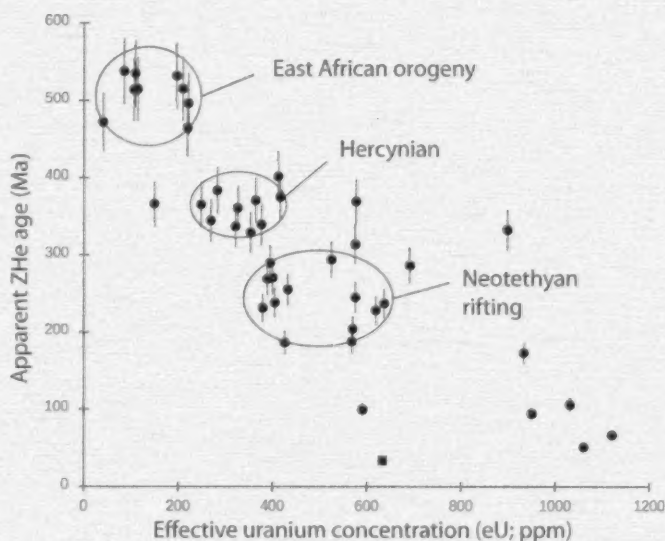
Figure 1: Compiled zircon (U-Th)/He (ZHe) ages from assorted basement rock of the Egyptian Sinai Peninsula obtained by Pujols (2011). These ZHe ages vary over 500 m.y. and show a negative correlation with effective uranium concentration (eU = [U] + 0.23[Th], which treats both elements as a single á-particle producer), here used as a proxy for radiation damage. This remarkable spread in ages is observed within individual samples of rock from various locations. Furthermore, these ages are interpreted as recording three successive tectonic events, as noted on the figure. These data provide strong evidence that zircon (U-Th)/He is a robust, dynamic thermochronometer capable of retaining significant information on complex thermal histories.

Similarly, ZHe ages from a transect of southern Hall Peninsula, collected by Creason et al. (2013) during the 2012 Hall Peninsula field season, show a strong and clear decrease in ZHe age of more than 700 m.y. with increasing eU (Creason, pers. comm., 2013). This study, and the future research described herein, utilizes further analysis of these zircons and others to understand these phenomena and develop a new model for ZHe thermochronology.

Background

Helium diffusion kinetics

Previous research

The diffusion of He from zircon is an Arrhenian process, meaning that diffusion coefficients are a function of temperature and time, for which quantitative information obtained over laboratory time scales may be extrapolated to geologically relevant settings. The He diffusion kinetics of zircon, described in detail by Reiners (2005), were primarily determined by step-heated, fractional-loss diffusion experiments on zircon from the Fish Canyon Tuff, Colorado and the rapidly exhumed Gold Butte block, Nevada (Reiners et al. 2002, 2004). One convenient method of visualizing the diffusive process is the closure temperature (T_c), generally given as the approximate temperature at which the system closes to bulk He diffusion given the simple thermal history of monotonic cooling at a rate of $10°C/m.y.$ (Dodson, 1973). Reiners et al. (2004) experimentally determined that zircon has a closure temperature of approximately $170–190°C$. For more information on the mathematics and design of these experiments, the reader is directed to Fechtig and Kalbitzer (1966), and Harrison and Zeitler (2005).

The effects of radiation doses exceeding $2–4 \times 10^{18}$ á-decays/g have been systematically observed to dramatically reduce the activation energy required for bulk He diffusion, leading to anomalously young ages (Nasdala et al., 2004; Reiners et al., 2004; Reiners, 2005; Guenthner and Reiners, 2009; Ketcham et al., 2013). This dosage threshold is thought to correspond to the overlapping of fission-track zones, which connect through and out of the crystal, creating low–activation energy diffusion pathways. This threshold is referred to as the fission-track percolation point, calculated by Ketcham et al. (2013) at approximately 1.9×10^{18} á-decays/g. Furthermore, Guenthner et al. (2013) documented an increase in diffusivity, corresponding to a decrease in T_c, of more than nine orders of magnitude at dosages exceeding this threshold, as well as a similar decrease in diffusivity of more than three orders of magnitude at lower levels of damage.

Producing a better model

The development of a newer, more accurate model for ZHe hinges not only on a quantitative understanding of the kinetics of He diffusion, but also on an understanding of the kinetics of radiation damage. The crystal lattice is affected by two distinct forms of damage: 'fission-track damage', caused by the spontaneous fission of ^{238}U; and 'á-damage', caused by the simultaneous ejection of the daughter á-particle and recoil of the parent nuclide. The accurate measurement of, and the ability to describe a model for, the accumulation and annealing of radiation damage over geological time and temperature and their evolving effects on diffusion are of critical importance to the accurate interpretation of ZHe thermochronometric data.

Although the similar radiation-damage accumulation and annealing model (RDAAM) for apatite, which describes a positive correlation between apatite closure temperature and radiation dose (Shuster et al., 2006; Flowers et al., 2009), and the new ZHe model proposed by Guenthner et al. (2013) provide an excellent framework for further research into the topic, both models are reliant on the assumption that fission-track (FT) density and/or ^{4}He concentration is an effective proxy for the α-dose present in a given grain; that is, á-recoil damage in the crystal lattice heals at approximately the same temperatures as He diffusion or fission-track annealing. While this might be an accurate proxy for apatite, the case for zircon is potentially more complex.

This study takes a different approach, focusing on datasets like those from Hall Peninsula on southern Baffin Island (Creason and Gosse, 2014, Figure 1). This study uses zircon from 16 samples collected during the Hall Peninsula field season of 2012. After standard (U-Th)/He mineral separation processes, including crushing and both magnetic and heavy liquid density separations, grains of zircon are hand selected for size and crystal quality, and analyzed using a combination of Raman spectroscopy, laser-ablation inductively coupled plasma–mass spectrometry (LA-ICP-MS), step-heated diffusion experiments and standard (U-Th)/He analysis. This combination of techniques will provide a dataset that will enable direct correlation between ZHe age and radiation dose, and quantitative statements about the effects of present radiation dose on diffusion constants.

Methodology

Raman spectroscopy

Raman spectroscopy is a technique that observes shifts in energy of a high-energy monochromatic laser resulting from low-frequency vibrations of molecular bonds due to inelastic collisions between photons and electron clouds. It has been well documented as an effective, nondestructive means of measuring radiation damage in zircon (Nasdala et al., 1995; Geisler et al., 2001; Geisler, 2002; Geisler and Pidgeon, 2002; Nasdala et al., 2003; Nasdala et al., 2004; Geisler et al., 2005; Marsellos and Garver, 2010). In this technique, the frequency and full width at half maximum

(FWHM) of the í3 [SiO₄] antisymmetric stretching peak are measured. The í3 stretching peak in highly crystalline zircon occurs at a frequency of approximately 1008 cm^{-1} and has an FWHM of approx. 1.2 cm^{-1} (Nasdala et al., 1995; Zhang et al., 2000a; Nicola and Rutt, 2001; Marsellos and Garver, 2010). With increasing radiation doses, the frequency decreases and the FWHM increases nearly linearly (Figure 2), reaching a limit at which the crystalline structure of the mineral is thought to be totally amorphous, or metamict, corresponding to a frequency of approximately 975–985 cm^{-1} and an FWHM of 25–38 cm^{-1} (Nasdala et al., 1995; Zhang et al., 2000b; Nasdala et al., 2001). For more information on this technique, the reader is directed to Nasdala et al. (1995) and Nasdala et al. (2004).

The majority of studies that use Raman spectroscopy to estimate zircon radiation doses do so on polished grain mounts, so that grains with a heterogeneous U and Th distribution can be identified prior to analysis by cathodoluminescence or back-scattered electron imaging. However, calculation of the á-ejection correction in (U-Th)/He, which estimates the amount of ^{4}He ejected outside the grain boundary by actinides near the grain boundary (Farley et al., 1996), is vastly simpler for whole grains; therefore, this study used whole grains rather than polished. This approach raises several potential issues, the most prominent of which is the commonly heterogeneous distribution of U and Th, which causes a similarly heterogeneous distribution of radiation dose. If a zircon's surface is enriched or depleted in U and/or Th with respect to the rest of the grain, Raman spectra taken on the surface will respectively over- or underestimate the radiation dose; likewise, due to an-

omalously high or low He ejection outside of the grain from near the grain boundary, the apparent ZHe age of the grain will be anomalously old or young, respectively. Another significant issue raised by the methodology of whole-grain Raman analyses is the effect of chemistry on the í3 peak, typically measured by electron microprobe, which has been documented by several researchers (Hurley and Fairbairn, 1953; Geisler et al., 2001; Kolesov et al., 2001; Nicola and Rutt, 2001; Geisler et al., 2005; Marsellos and Kidd, 2008; Marsellos and Garver, 2010). These issues are addressed by the use of LA-ICP-MS, described in the next section.

Measurements of Raman spectra were taken in the Mineral Physics Lab at the University of Texas at Austin with a 532 nm laser operating at 30–70 mW, and measured by an Andor Technology plc. spectrometer at 1800 grooves/mm. Calibrations were performed at the beginning of each experiment using a combination of a Si wafer and a polished mount of well-characterized Mud Tank zircon; the Mud Tank zircon was remeasured every 30 measurements to check for machine drift. Results from current Raman measurements and their respective radiation-dose estimates, calculated with equations from Nasdala et al. (2001), are given in Table 1.

Zircons were hand selected for size and quality to ensure that no features such as fractures or broken edges would affect the He measurements. For further information on selection of suitable grains for (U-Th)/He analysis, see Farley et al. (1996). Each grain was measured by Raman spectroscopy in at least three spatially separate, 25 μm spots on a crystalline surface; the spectra, such as those in Figure 2,
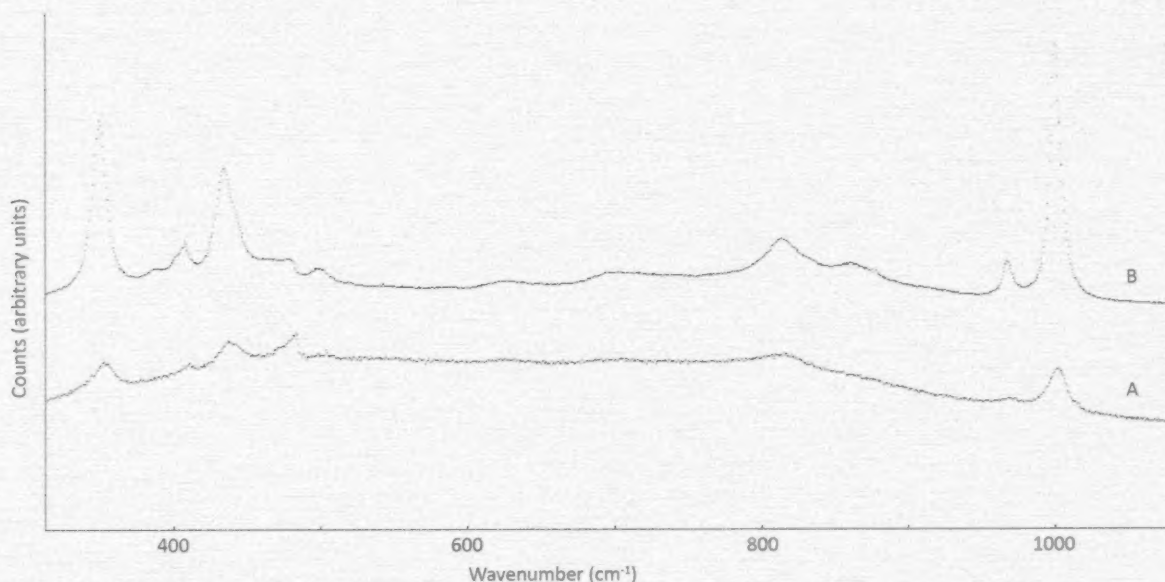
Figure 2: Raman spectra of two zircon grains from Hall Peninsula, southern Baffin Island, Nunavut. The í 3 peak, from which radiation damage is estimated, occurs at approximately 1000 cm^{-1}. Spectrum A is significantly more damaged than spectrum B, as indicated by the shorter, wider peak of A and the higher signal-to-noise ratio.

Table 1: Frequency and FWHM measurements of zircon from Hall Peninsula, southern Baffin Island, Nunavut, corrected for apparatus function, and the estimated radiation doses. Each value is the average of a minimum of three measurements taken at spatially separate points on a crystalline surface of the grain, together with the standard deviation. These data highlight the wide range of radiation doses experienced by the zircon. Abbreviations: FWHM, full width at half maximum; σ, standard deviation.

| Sample no. | Rock type | Frequency | | FWHM | | Estimated dose |
		(cm^{-1})	σ	(cm^{-1})	σ	$(10^{16} \, \alpha/mg)$
zR-C012-1	Biotite granite	1000.1	0.27	7.1	0.4	7.1
zR-C012-2	Biotite granite	1002.4	0.40	7.3	0.5	7.3
zR-C012-3	Biotite granite	1002.8	0.57	10.3	2.0	10.3
zR-C012-4	Biotite granite	1000.6	1.98	11.4	2.2	11.4
zR-C012-5	Biotite granite	992.8	4.77	7.1	0.3	7.1
zR-C013-1	Biotite granite	1003.8	0.40	6.5	0.1	6.5
zR-C013-2	Biotite granite	1003.8	0.32	7.8	0.5	7.8
zR-C013-3	Biotite granite	1003.1	0.75	12.7	0.9	12.7
zR-C013-4	Biotite granite	998.0	0.1	8.8	0.7	8.8
zR-C013-5	Biotite granite	1003.1	0.2	7.2	0.7	7.2
zR-C015-1	Biotite granite	1001.4	0.35	11.3	1.1	11.3
zR-C015-2	Biotite granite	1003.0	1.41	8.3	19	8.3
zR-C015-3	Biotite granite	1002.9	0.16	8.2	0.4	8.2
zR-C015-4	Biotite granite	1001.7	1.44	9.5	1.6	9.5
zR-C015-5	Biotite granite	997.5	0.89	12.5	0.5	12.4
zR-C016-1	Biotite granite	1002.3	1.68	6.9	1.9	6.9
zR-C016-2	Biotite granite	1001.3	2.04	9.0	2.1	9.0
zR-C016-3	Biotite granite	999.9	0.17	10.2	0.6	10.2
zR-C016-4	Biotite granite	1000.0	0.67	10.9	0.5	10.9
zR-C016-5	Biotite granite	1003.9	0.49	7.4	0.1	7.4
zR-Y080-1	Magnetite monzogranite	995.8	5.60	10.2	2.7	10.2
zR-Y080-2	Magnetite monzogranite	991.1	5.15	12.9	22	12.9
zR-Y080-3	Magnetite monzogranite	1001.7	1.65	9.1	1.6	9.1
zR-Y080-4	Magnetite monzogranite	998.0	2.46	12.3	2.6	12.3
zR-Y080-5	Magnetite monzogranite	998.8	1.76	9.5	1.5	9.5
zR-B099-1	Biotite tonalite	1002.3	1.13	9.1	06	9.1
zR-B099-2	Biotite tonalite	1001.2	1.08	90	2.3	9.0
zR-B099-3	Biotite tonalite	1000.5	0.61	11.1	0.2	11.1
zR-B099-4	Biotite tonalite	1001.1	1.16	9.6	0.9	9.6
zR-B099-5	Biotite tonalite	1001.3	0.52	11.1	0.8	11.1
zR-B102-1	Biotite diorite	1002.6	0.78	8.8	1.2	8.8
zR-B102-2	Biotite diorite	996.6	1.80	14.8	2.1	14.8
zR-B102-3	Biotite diorite	1002.2	0.56	11.6	25	11.6
zR-B102-4	Biotite diorite	999.2	1.76	11.3	1.3	11.3
zR-B102-5	Biotite diorite	996.0	0.78	13.7	1.8	13.7
zR-B106-1	Monzogranite	993.8	0.55	17.7	0.3	17.6
zR-B106-3	Monzogranite	999.9	1.62	13.6	0.4	13.6
zR-B106-4	Monzogranite	992.7	0.80	18.8	1.6	18.8
zR-B106-5	Monzogranite	997.2	1.24	13.9	1.0	13.9
zR-B106-7	Monzogranite	996.8	1.00	14.7	2.1	14.7

are averages collected over a minimum of five sequential, 10-second accumulation periods. Data were fitted and corrected for apparatus function using techniques described in Nasdala et al. (2001).

Laser-ablation inductively coupled plasma–mass spectrometry

Once characterized by Raman spectroscopy, zircon grains were placed on double-sided taped epoxy mounts and analyzed by laser-ablation inductively coupled plasma–mass spectrometry (LA-ICP-MS). This technique involves an excimer laser that ablates a pit 16–20 µm deep and 40 µm wide into the surface of the zircon, measuring concentrations of trace elements—most importantly U, Th and Hf—

and the results are calibrated against National Institute of Standards and Technology glass of known concentration. These data, which have been collected and are currently being evaluated, will

- ensure that Raman measurements made on the surface of the grain are estimating a relevant radiation dose. These measurements will allow comparison of the eU concentration used to calculate the grain's (U-Th)/He age with the eU value on the surface of the grain and help evaluate whether the Raman measurement is a reasonable estimation or an over/underestimate of the radiation dose.

- ensure that the He age is accurate. Natural zircon commonly has complex growth zoning or other chemical

heterogeneity. In the case of a grain that has a rim enriched or depleted in U or Th relative to the rest of the grain, a disproportionate amount of ^{4}He is either ejected from or not produced at the grain boundary, and the resulting age will be anomalously young or old, respectively. Therefore, LA-ICP-MS measurements of U and Th at the grain surface allow determination of whether the ZHe measured is over- or underestimated.

- facilitate corrections to shifts in the Raman spectrum caused by elements, such as Hf (which occurs in natural zircon up to 10 wt. %), U and Th, that have been noted by several researchers (Hurley and Fairbairn, 1953; Geisler et al., 2001, 2005; Kolesov et al., 2001; Nicola and Rutt, 2001; Marsellos and Kidd, 2008; Marsellos and Garver, 2010).

(U-Th)/He analysis and diffusion experiments

Following LA-ICP-MS analysis, whole-grain He, U and Th concentrations are measured at the (U-Th)/He Lab of the University of Texas at Austin. This is done via fractional-loss diffusion experiments, and by standard (U-Th)/He analysis. Although a limited number of these data have been collected, the bulk of these analyses are ongoing.

The first technique, step-heated fractional-loss diffusion experiments, are performed on zircons selected on the basis of chemical homogeneity, as measured by LA-ICP-MS, and radiation doses, as estimated by Raman spectroscopy. In these experiments, individual zircons are placed inside Pt foil capsules, wrapped in a Cu foil packet and placed in ultrahigh vacuum, wherein they are heated by a halogen bulb; heating takes place in a series of increasing and then decreasing temperatures for specified durations of time. The volume of ^{4}He released during each step is spiked with a known volume of ^{3}He, cryogenically purified and measured by quadrupole mass spectrometry (QMS). The Raman spectrum of each grain is remeasured after the experiment is complete to ensure that no significant annealing has occurred during exposure of the grain to high temperatures. Grains are then subjected to standard (U-Th)/He laser heating to ensure that >99% of the gas has been diffused from the grain.

Zircons not selected for diffusion experiments also undergo standard (U-Th)/He analysis. Single grains are placed in a Pt foil packet, placed in ultrahigh vacuum and laser heated until >99% of the total gas has been extracted. The resulting ^{4}He is spiked with a known quantity of ^{3}He, cryogenically purified and measured by QMS.

Following measurements of ^{4}He concentration, each grain is placed in a Teflon vial and spiked with a ^{235}U/^{230}Th tracer. Grains are dissolved in acid, in high-pressure digestion vessels over the course of one week, after which U and Th concentrations are measured by solution ICP-MS.

Preliminary results and future work

Although the dataset is thus far incomplete, it is expected that these data will clearly continue and elaborate on the trend observed in earlier Hall Peninsula ZHe results. Results from this study will both highlight the threshold at which radiation dose begins to affect He diffusion kinetics, and the threshold at which radiation dose is too high to permit systematic He retention by the grain (Creason, pers. comm., 2013). Once fully evaluated, LA-ICP-MS trace-element concentration data will allow identification of zonation and verify the relevance of the Raman measurement to the grain as a whole, as well as allow estimation of present radiation dose and back-calculation to the radiation dose at the time of the closure of He diffusion for that particular grain. Understanding radiation dose threshold at which He diffusivity begins to change is critical for obtaining accurate thermal histories from ZHe models.

These data will provide a critical piece of the puzzle. Ultimately, however, without an accurate model of the kinetics of radiation damage and accumulation and annealing as a function of temperature and time, it is impossible to truly accurately model how the evolving radiation dose changes He diffusivity over time. Perhaps even more critical is the lack of an independent measurement of the low-temperature thermal history of Hall Peninsula, without which it is impossible to develop a model that relates the thresholds provided by these data to temperature. Although step-heated fractional-loss diffusion experiments are helpful in relating diffusive constants to radiation dose, an independent measurement of thermal history is paramount to establish full confidence in these data. To the best of the authors' knowledge, no zircon fission-track (ZFT) or apatite fission-track (AFT) cooling ages are available for Hall Peninsula; however, it is possible that ZFT and AFT ages from these samples and others would provide the data necessary to derive a functional model.

Economic considerations

This study will yield better constraints on the effects of radiation dose on He diffusion kinetics and a better method of modelling thermal histories. Although Hall Peninsula perhaps represents a simple case of exceptionally slow cooling of crystalline rock (Stockli and Creason, pers. comm., 2013), the results of this study will provide a basis for addressing the more complex situation of the thermal history of sedimentary basins. The development of such a technique would be particularly useful in old basins in which zircons have experienced significant accumulation of damage, or basins that have complex thermal histories, consisting of multiple thermal events that could affect the presence, quality and maturation of hydrocarbon reserves. Therefore, the most significant economic contribution of this project is the improved ability to evaluate the prove-

nance and time-temperature evolution of economic sedimentary basins and associated structural deformation.

Conclusions

An understanding of the full complexity of He diffusion in zircon is critical to its use as a thermochronometer capable of recording a wide range of thermal events in a region. The development of a new model for ZHe that accounts for these complexities is particularly important for cases in which the zircons have accumulated significant amounts of radiation damage and have experienced slow cooling, such as on Hall Peninsula of Baffin Island, or complex cooling histories that involve multiple events at successively lower temperatures, as seen in the Egyptian Sinai Peninsula. The models for ZHe by Reiners (2005) and Guenthner et al. (2013) are an excellent beginning, but, as evidenced by the data presented herein, much work remains to be done.

Acknowledgments

References

Creason, C.G. and Gosse, J.C. 2014: Preliminary characterization of the Mesozoic–Cenozoic exhumation history of Hall Peninsula, Baffin Island, Nunavut, based on apatite and zircon (U-Th)/He thermochronology; *in* Summary of Activities 2013, Canada-Nunavut Geoscience Office, p. 93–100.

Creason, C.G., Gosse, J.C. and Young, M.D. 2013: Rift flank uplift and landscape evolution of Hall Peninsula, Baffin Island, Nunavut: an exhumation model based on low-temperature thermochronology; *in* Summary of Activities, 2012, Canada-Nunavut Geoscience Office, p. 75–84.

Dodson, M.H. 1973: Closure temperature in cooling geochronological and petrological systems; Contributions to Mineralogy and Petrology, v. 40, p. 259–274.

Farley, K., Wolf, R. and Silver, L. 1996: The effects of long alpha-stopping distances on (U · Th)/He ages; Geochimica et Cosmochimica Acta, v. 60, no. 21, p. 4223–4229.

Fechtig, H. and Kalbitzer, S. 1966: The diffusion of argon in potassium-bearing solids; *in* Potassium Argon Dating, O.A. Schaeffer and J. Zahringer (ed.), Springer-Verlag, p. 68–107.

Flowers, R.M., Ketcham, R.A., Shuster, D.L. and Farley, K.A. 2009: Apatite (U-Th)/He thermochronometry using a radiation damage accumulation and annealing model; Geochimica et Cosmochimica Acta, v. 73, no. 8, p. 2347–2365.

Geisler, T. 2002: Isothermal annealing of partially metamict zircon: evidence for a three-stage recovery process; Physics and Chemistry of Minerals, v. 29, no. 6, p. 420–429.

Geisler, T. and Pidgeon, R.T. 2002: Raman scattering from metamict zircon: comments on "Metamictisation of natural zircon: accumulation versus thermal annealing of radioactivity-induced damage" by L. Nasdala, M. Wenzel, G. Vavra, G. Irmer, T. Wenzel and B. Kober (Contributions to Mineralogy and Petrology, v. 141, p. 125–144); Contributions to Mineralogy and Petrology, v. 143, no. 6, p. 750–755.

Geisler, T., Burakov, B.E., Zirlin, V., Nikolaeva, L. and Philipp, P. 2005: A Raman spectroscopic study of high-uranium zircon from the Chernobyl 'lava'; European Journal of Mineralogy, v. 17, no. 6, p. 883–894.

Geisler, T., Pidgeon, R.T., van Bronswijk, W. and Pleysier, R. 2001: Kinetics of thermal recovery and recrystallization of partially metamict zircon: a Raman spectroscopic study; European Journal of Mineralogy, v. 13, no. 6, p. 1163–1176.

Guenthner, W. and Reiners, P. 2009: He diffusion in zircon: observations from (U-Th)/He age suites and ^{4}He diffusion experiments and implications for radiation damage and anisotropic effects; American Geophysical Union, Fall Meeting, 2009, abstract V52C-06.

Guenthner, W., Reiners, P., Ketcham, R.A., Nasdala, L. and Giester, G. 2013: Helium diffusion in natural zircon: radiation damage, anisotropy, and the interpretation of zircon (U-Th)/He thermochronology; American Journal of Science, v. 313, p. 145–198.

Harrison, T.M. and Zeitler, P.K. 2005: Fundamentals of noble gas thermochronometry; Reviews in Mineralogy and Geochemistry, v. 58, p. 123–149.

Hurley, P.M. and Fairbairn, H.W. 1953: Radiation damage in zircon: a possible age method; Geological Society of America Bulletin, v. 64, no. 6, p. 659–673.

Ketcham, R.A., Guenthner, W.R. and Reiners, P.W. 2013: Geometric analysis of radiation damage connectivity in zircon, and its implications for helium diffusion; American Mineralogist, v. 98, no. 2–3, p. 350–360.

Kolesov, B.A., Geiger, C.A. and Armbruster, T. 2001: The dynamic properties of zircon studied by single-crystal X-ray diffraction and Raman spectroscopy; European Journal of Mineralogy, v. 13, no. 5, p. 939–948.

Marsellos, A.E. and Garver, J.I. 2010: Radiation damage and uranium concentration in zircon as assessed by Raman spectroscopy and neutron irradiation; American Mineralogist, v. 95, no. 8–9, p. 1192–1201.

Marsellos, A. and Kidd, W. 2008: Extension and exhumation of the Hellenic forearc ridge in Kythera; Journal of Geology, v. 116, no. 6, p. 640–651.

Nasdala, L., Irmer, G. and Wolf, D. 1995: The degree of metamictization in zircon: a Raman spectroscopic study; European Journal of Mineralogy, v. 7, p. 471–478.

Nasdala, L., Reiners, P.W., Garver, J.I., Kennedy, A.K., Stern, R.A., Balan, E. and Wirth, R. 2004: Incomplete retention of radiation damage in zircon from Sri Lanka; American Mineralogist, v. 89, no. 1, p. 219–231.

Nasdala, L., Wenzel, M., Vavra, G., Irmer, G., Wenzel, T. and Kober, B. 2001: Metamictisation of natural zircon: accumulation versus thermal annealing of radioactivity-induced damage; Contributions to Mineralogy and Petrology, v. 141, no. 2, p. 125–144.

Nasdala, L., Zhang, M., Kempe, U., Panczer, G., Gaft, M., Andrut, M. and Plötze, M. 2003: Spectroscopic methods applied to zircon; Reviews in Mineralogy and Geochemistry, v. 53, no. 1, p. 427–467.

Nicola, J. and Rutt, H. 2001: A comparative study of zircon (ZrSiO4) and hafnon (HfSiO4) Raman spectra; Journal of Physics C: Solid State Physics, v. 7, no. 7, p. 1381.

Pujols, E.J. 2011: Temporal and thermal evolution of extensional faulting in the central Gulf of Suez and detrital zircon (U-Th)/He constraints on the thermo-tectonic Paleozoic and Mesozoic history of the Sinai, Egypt; M.Sc. thesis, The University of Kansas, Lawrence, Kansas, 246 p.

Reiners, P.W. 2005: Zircon (U-Th)/He thermochronometry; Reviews in Mineralogy and Geochemistry, v. 58, no. 1, p. 151-179.

Reiners, P.W., Farley, K.A. and Hickes, H.J. 2002: He diffusion and (U-Th)/He thermochronometry of zircon: initial results from Fish Canyon Tuff and Gold Butte; Tectonophysics, v. 349, no. 1, p. 297-308.

Reiners, P.W., Spell, T.L., Nicolescu, S. and Zanetti, K.A. 2004: Zircon (U-Th)/He thermochronometry: He diffusion and comparisons with $^{40}Ar/^{39}Ar$ dating; Geochimica et Cosmochimica Acta, v. 68, no. 8, p. 1857-1887.

Shuster, D.L., Flowers, R.M. and Farley, K.A. 2006: The influence of natural radiation damage on helium diffusion kinetics in apatite; Earth and Planetary Science Letters, v. 249, no. 3, p. 148-161.

Zhang, M., Salje, E.K.H., Capitani, G.C., Leroux, H., Clark, A.M., Schlüter, J. and Ewing, R.C. 2000a: Annealing of alpha-decay damage in zircon: a Raman spectroscopic study; Journal of Physics: Condensed Matter, v. 12, no. 13.

Zhang, M., Salje, E.K.H., Farnan, I., Graeme-Barber, A., Daniel, P., Ewing, R.C., Clark, A.M. and Leroux, H. 2000b: Metamictization of zircon: a Raman spectroscopic study; Journal of Physics: Condensed Matter, v. 12, no. 8.

Surficial geology of central Hall Peninsula, Baffin Island, Nunavut: summary of the 2013 field season

T. Tremblay[1], J. Leblanc-Dumas[2], M. Allard[2], M. Ross[3] and C. Johnson[3]

[1]Canada-Nunavut Geoscience Office, Iqaluit, Nunavut

[2]Département de Géographie et Centre d'études nordiques, Université Laval, Québec, Quebec

[3]Department of Earth and Environmental Sciences, University of Waterloo, Waterloo, Ontario

Abstract

This study is part of the Canada-Nunavut Geoscience Office's Hall Peninsula Integrated Geoscience Program, a multiyear bedrock and surficial geology mapping program. This paper presents the surficial geology component of the program conducted during the 2013 field season, completing a two-year program covering NTS map areas 25I, J, O, P, 26A and B at a scale of 1:100 000. A 1:50 000 scale segment of the surficial geology map for the peninsula, containing all key material types, is presented in this paper. Till and glaciofluvial sediment samples were collected to help understand regional mineral potential. Till geochemistry and heavy mineral results from summer 2012 are briefly presented, the full dataset is available in a separate publication. Glaciodynamic indicators were mapped to provide a regional understanding of ice-flow history on Hall Peninsula. Cold-based (limited glacial erosion, regolith material is present), intermediate cold-based (weak to moderate glacial erosion, a mix of till and regolith is dominant) and warm-based zones (moderate to strong glacial erosion, till and bedrock outcrops are abundant) are the principal glaciodynamic zones mapped. Along the coast, areas with linear selective erosion were also mapped, where fiords and U-shaped valleys are common features.

Résumé

La présente étude s'inscrit dans le cadre du Projet géoscientifique intégré de la péninsule Hall, un programme pluriannuel dirigé par le Bureau géoscientifique Canada-Nunavut mettant l'accent sur la cartographie du substratum rocheux et de la géologie de surface. Ce rapport fait état des aspects de ce projet liés à la géologie de surface réalisés au cours de la saison de terrain 2013, clôturant ainsi ce programme de deux ans dont l'objet était de porter sur les feuilles de carte 25I, J, O, P, 26A et B du SNRC la géologie de la région à l'échelle de 1/1 000 000. Suit la description d'une section de la carte de la géologie de surface de la péninsule dressée à l'échelle de 1/50 000, et des principaux types de matériaux qui s'y trouvent. Des échantillons de till et de sédiments fluvioglaciaires ont été recueillis en vue de fournir des renseignements susceptibles d'aider à mieux cerner le potentiel minéral de la région. Les résultats provenant de l'analyse géochimique du till et des minéraux lourds effectuée en 2012 font l'objet d'une brève description et l'ensemble de données complet fait partie d'une publication connexe. La carte de la répartition des indicateurs de l'activité glaciodynamique a été dressée afin de reconstituer l'histoire de l'écoulement glaciaire à l'échelle régionale dans la péninsule Hall. Les principales zones glaciodynamiques cartographiées sont les zones à base froide (peu d'érosion, présence de matériaux issus du régolithe), à base froide intermédiaires (degré d'érosion glaciaire faible à modéré, prédominance d'un mélange de till et de régolithe) et à base tempérée (degré d'érosion modéré à élevé, nombreux affleurements de till et de substratum rocheux). Le long des côtes, aux endroits où les fjords et les vallées en auge sont des formes de relief très répandues, les zones touchées par l'érosion sélective linéaire ont également été portées sur la carte.

Introduction

Reconnaissance fieldwork began in the summer of 2011 followed by two full field seasons undertaken in the summers of 2012 and 2013 (Figure 1; Tremblay et al., 2013; Leblanc-Dumas et al., 2013). The objective of this work is to produce framework surficial geology maps at a scale of 1:100 000 for Hall Peninsula (NTS 25I, J, O, P, 26A, B). Permafrost studies (LeBlanc et al., 2013; Leblanc-Dumas et al., 2013) are also part of the surficial research program. The surficial geology program encompasses a range of components that include surficial geology mapping; surficial materials characterization; ice-flow indicators; chronology and dynamics; traditional place names; and permafrost studies.

The project was conducted in a region where no surficial maps existed, except at a national scale (Fulton, 1995). Glacial geomorphology on southern Baffin Island has been the subject of much research (Andrews and Sim, 1964; Matthews, 1967; Miller, 1980; Dyke et al., 1982; Andrews et al., 1985; Stravers et al., 1992; Kaplan and Miller, 2003; Hodgson, 2005; Fréchette et al., 2006; Utting et al., 2007; Briner et al., 2009; Clements et al., 2009; Johnson et al., 2013). However, previous research did not completely address the diversity of polythermal glacial bed conditions and juxtaposition of alpine and ice-sheet glaciodynamics, which imparted the Quaternary geology observed on Hall Peninsula.

Surficial geology mapping

Surficial geology mapping at the scale of 1:100 000 was conducted across Hall Peninsula with helicopter support and foot traverses. Field observations, including landforms, surficial cover composition and ice-flow indicators, were compiled using the GanFeld application (Shimamura et al., 2008) developed by the Geological Survey of Canada (GSC). The office-based mapping procedure included an all-digital approach combining a mosaic of airphotos in an on-screen stereoscopic view, using Summit Evolution software (DAT/EM Systems International, 2012) and ArcGIS (Esri, 2012). Mapping was completed using the new GSC surficial geology integrated legend (Deblonde et al., 2012). Landsat, RapidEye, SPOT and WorldView-2 satellite imagery and a DEM (Gilbert, 2012) from CanVec 1:50 000 data (Natural Resources Canada, 2012; Figure 1) were also used in the mapping process. The area covered in 2013 was approximately 17 000 km^2, in addition to about 21 000 km^2 mapped in 2012. A preliminary and simplified version of the surficial geology from a portion of this area (covering 2100 km^2), which contains all of the key material types, is presented on Figure 2. Surficial material composition includes bedrock, mainly Precambrian granitic rocks and gneiss (Steenkamp and St-Onge, 2014), preglacial(?) weathered material (felsenmeer and regolith), till, glacio-

fluvial sediments, glaciolacustrine and marine sediments, colluvium, alluvium and coastal deposits.

In the central part of Hall Peninsula plateau, weathered bedrock material (regolith) is mapped as Wv (<1 m thick) or W (<3 m thick; Figure 3a). The material is a residual of in situ chemical alteration of the bedrock identified as a garnet granite and paragneiss, which probably occurred during the preglacial and interglacial periods. The occurrence of deeply weathered material is mapped with the stippled overlay pattern. The region of deeply weathered material is surrounded by a transition zone where the diamictic surficial material is composed of a mixture of regolith (often iron-stained an orange colour) and glacial sediment, mapped as Tb_Wv (>1 m thick) and Tv_Wv (<1 m thick). The consistent lithology of the material and the locally sharp lithological transitions of the sediment suggests that this material was not glacially transported, but the presence of rare erratics overlying the regolith indicates that the region was covered by glacial ice.

The glacial sediment (Tv, Tb) is a diamicton composed of sand, silt and pebbles of different lithologies. This material is associated with late glacial readvances of the Laurentide Ice Sheet. A moraine till (Tm), forming parallel, pronounced crests >100 m high, exists in the study area and is part of the Frobisher moraine complex (Miller, 1980). Hummocky till (Th) is associated with the ice-retreat moraine complex, such as the Hall and Frobisher moraines. Numerous kettles are found on the moraines, indicating the former presence of buried ice. Figure 1 illustrates the location of the known moraines in the area.

The moraine ridges and sediments are directly in contact with proglacial lacustrine and deltaic sediments (GLb, GLv and GLd; Figure 3b). Glaciolacustrine veneer (GLv) represents a thin and discontinuous deposit of fine, well-sorted glacial sediments, and the glaciolacustrine blanket (GLb) represents a thicker (1 m) continuous deposit. These sediments are composed of fine sand, silt and rare pebbles and were deposited during a period of postglacial flooding. Beach crests and terrace scarps are also found, forming small deposits, often too small to map individually. The glaciolacustrine deltas (GLd) are sometimes 25 m high, and are composed of stratified and sorted sand and silt with few pebbles. This unit was deposited by glacial meltwater in proglacial lakes during ice retreat. The dip direction of the foreset beds indicates that meltwater was draining toward the south and southeast. Accumulations of hummocky glaciofluvial sediments (GFh, Figure 3c, d), are generally composed of well-sorted to poorly sorted sand and gravel, which are found near the moraines and the glaciolacustrine sediments. Finally, recent accumulations of river alluvium (blankets as Ab and veneers as Av) are found within river valleys. The river alluvium is stratified and composed of sorted sand, silt and pebbles.
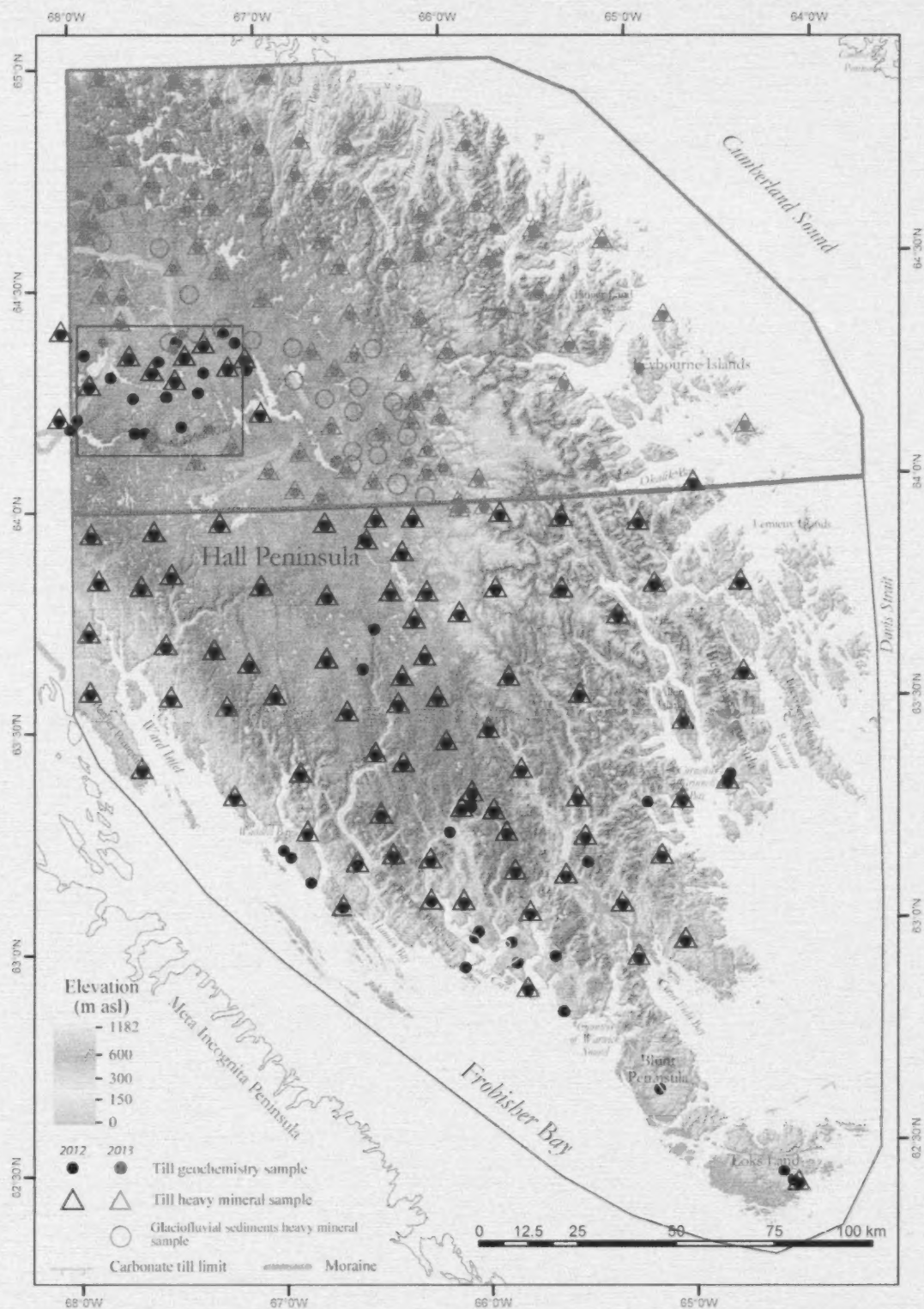
Figure 1: Location map displaying sample locations, principal moraines and carbonate till limit, Hall Peninsula, Baffin Island, Nunavut. Digital elevation model (Gilbert, 2012) derived from CanVec 1:50 000 data (Natural Resources Canada, 2012). The 2013 study area is outlined in blue, the 2012 study area is outlined in grey and the area of the 1:50 000 surficial map segment is outlined in black.
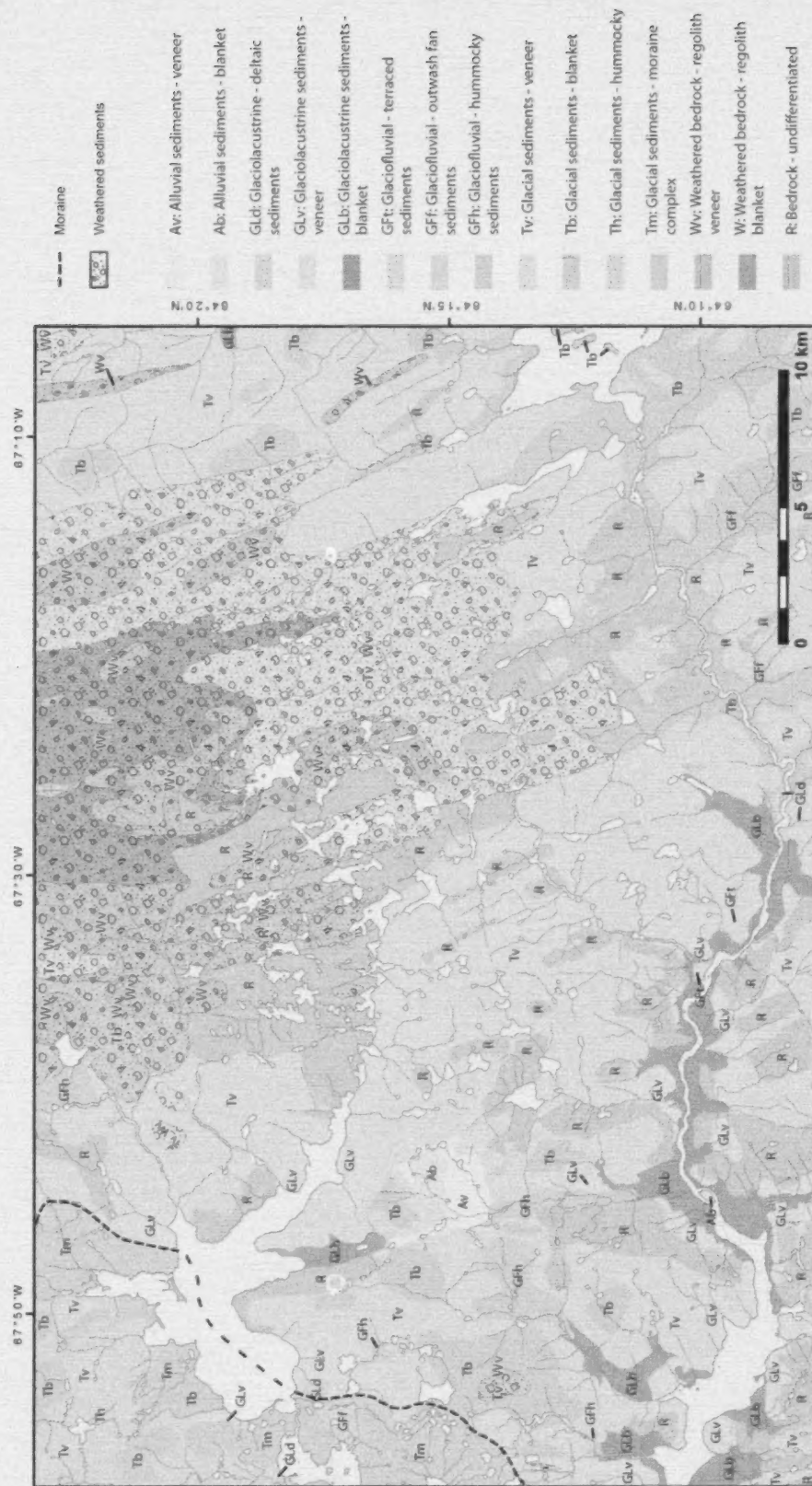
Figure 2: Preliminary map of the surficial geology and geomorphology of central Hall Peninsula, Nunavut.

Legend:

Moraine

Weathered sediments

Av: Alluvial sediments - veneer

Ab: Alluvial sediments - blanket

GLd: Glaciolacustrine - deltaic sediments

GLv: Glaciolacustrine sediments - veneer

GLb: Glaciolacustrine sediments - blanket

GFt: Glaciofluvial - terraced sediments

GFf: Glaciofluvial - outwash fan sediments

GFh: Glaciofluvial - hummocky sediments

Tv: Glacial sediments - veneer

Tb: Glacial sediments - blanket

Th: Glacial sediments - hummocky

Tm: Glacial sediments - moraine complex

Wv: Weathered bedrock - regolith veneer

W: Weathered bedrock - regolith blanket

R: Bedrock - undifferentiated

Figure 3: a) Regolith (W), with an orange (iron-stained), silty, coarse sand matrix and a pebble lag at the surface. **b)** Glaciolacustrine deltaic sediments (GLd), with silty layers (containing massive ice stringers) stratified with sandy layers. **c)** Poorly sorted, subangular to subrounded, gravelly, glaciofluvial sediments in a kame (forefront; GFh). The provenance of the sediments is proximal to the former ice margin. **d)** Well-sorted, gravelly sediments with subrounded to rounded clasts, overlain by stratified, well-sorted medium sand in a kame (GFh). The sediments are derived from a source distal to the former ice margin.

Surficial geochemistry

A till sampling program was also completed as part of surficial mapping on Hall Peninsula (Figure 1). In 2013, 109 till (or regolith) samples (2 kg each) were collected from the central part of Hall Peninsula with a spacing of 5–20 km between samples. A total of 115 heavy mineral samples (~10 kg bags) were collected to provide information on the potential for kimberlites, massive sulphides, gold, gemstones and other commodities. Ninety-three heavy mineral samples were collected from till and 22 heavy mineral samples were collected from glaciofluvial sediments. These sediments will be analyzed for geochemistry of the <63 μm fraction, heavy mineral content, grain size, carbonate content and mineralogy (X-ray diffraction). Seven mineralized boulders containing sulphides were also sampled. These datasets will be released in future reports.

From the 2012 survey, a total of 144 till matrix geochemistry samples (2 kg) were processed at the GSC Sedimentology Laboratory (Ottawa, Ontario; Tremblay and Leblanc-Dumas, 2014[4]). A portion of the matrix (<2 mm) of each sample was wet-sieved to 63 μm for geochemical analysis. Another <2 mm portion was sent for grain-size analysis and carbonate content analysis. Lastly, a portion was saved for archival purposes. A split of each 2 kg sample was dried and sieved at the GSC Sedimentology Laboratory and then submitted to Acme Analytical Laboratories Ltd. (Vancouver, British Columbia) for analysis of the <0.063 mm fraction (till matrix). A 30 g split was digested by aqua regia and analyzed by inductively coupled plasma–mass spectrometry (ICP-MS) for 72 elements, including gold, base metals, platinum and rare-earth elements. Another 2 g split was digested with lithium metaborate/lithium tetraborate fusion and then analyzed by inductively coupled plasma–emission spectrometry (ICP-ES) for 11 major elements. Analytical accuracy and precision was monitored by including GSC blind CANMET standards in the analytical analysis. Preparation laboratory duplicates of samples, Acme Analytical Laboratories Ltd. blanks, reference standards and analytical duplicates were also analyzed.

A total of 87 bulk samples (~10 kg) collected in 2012 were sent to Overburden Drilling Management Limited (Nepean, Ontario; Tremblay and Leblanc-Dumas, 2014) for heavy mineral analysis (cf. McClenaghan et al., 2012). The standard pre-analysis treatment was applied to all samples, which first included sieving of pebbles (>2 mm; the 4–8 mm fraction were separated for lithological counting) and preconcentration of heavy minerals by shaking table. Field sample duplicates and GSC blanks from granite grus and

---

[4]*CNGO Geoscience Data Series GDS2014-003, containing the data or other information sources used to compile this paper, is available online to download free of charge at http://cngo.ca/ summary-of-activities/2013/.*

till were inserted for quality control and quality assurance (Plouffe et al., in press). The gold grains from a panning concentrate were counted, described and replaced in the same fraction. The heavy mineral preconcentrate was then submitted for heavy liquid separation (methylene iodide, specific gravity=3.2) and ferromagnetic separation. The >0.25 mm fraction of nonferromagnetic heavy mineral concentrate (NFHMC) was examined by binocular microscope for the identification of various distinctive mineral species, namely, kimberlite-indicator minerals (KIMs) and metamorphic massive-sulphide–indicator minerals (MMSIMs), which notably include gahnite, red rutile, pyrite, chalcopyrite and arsenopyrite (Averill, 2001). The mineralogical picking was performed on three different size fractions (0.25–0.5 mm, 0.5–1 mm, 1–2 mm) of NFHMC. Following further preparation, binocular identifications of MMSIMs and KIMs were undertaken and supported in some cases by scanning electron micro- scope (SEM) analysis.

Preliminary results for gold (and gold grains) and platinum (and grains of sperrylite, a platinum-bearing mineral) are illustrated on Figure 4. Anomalies of up to 118 grains for gold (per 10 kg of table feed) and 41 ppb gold in the till <63 µm fraction occur in the 2012 study area. Platinum anomalies of up to 3.5 grains for sperrylite (per 10 kg of table feed) and 8 ppb platinum in the till <63 µm fraction also occur in the 2012 samples. In addition, two sapphire grains were found in the till heavy mineral fraction.

Ice-flow indicators and chronology

Preliminary ice-flow directions and chronology were established using striations, glacial landforms (macroforms, including ice-moulded bedrock forms and subglacial lineations observed on satellite images) and glacial sedimentology (Figure 5). Different phases of ice flow were recognized in the field by crosscutting relationships between striations and ice-retreat geochronology. Interpretation of this ice-flow history is in part based on previous work (Miller, 1980; Dyke and Prest, 1987; Stravers et al., 1992; Dyke et al., 2003; Johnson et al., 2013). The relative ice-flow chronology is based on the estimated time from the beginning of each phase and not the entire duration of the events, therefore chronological overlap is possible between phases.

Phase 1 ice flow

Last glacial maximum(?), main recorded ice-flow direction

This important ice-flow phase radiated from an ice divide located across the cold-based zone on the central plateau on Hall Peninsula (Figure 5). It is inferred that this phase occurred during the last glacial maximum (LGM). During that phase, Hall Peninsula was covered by ice, as were significant portions of the mountainous area of Baffin Island
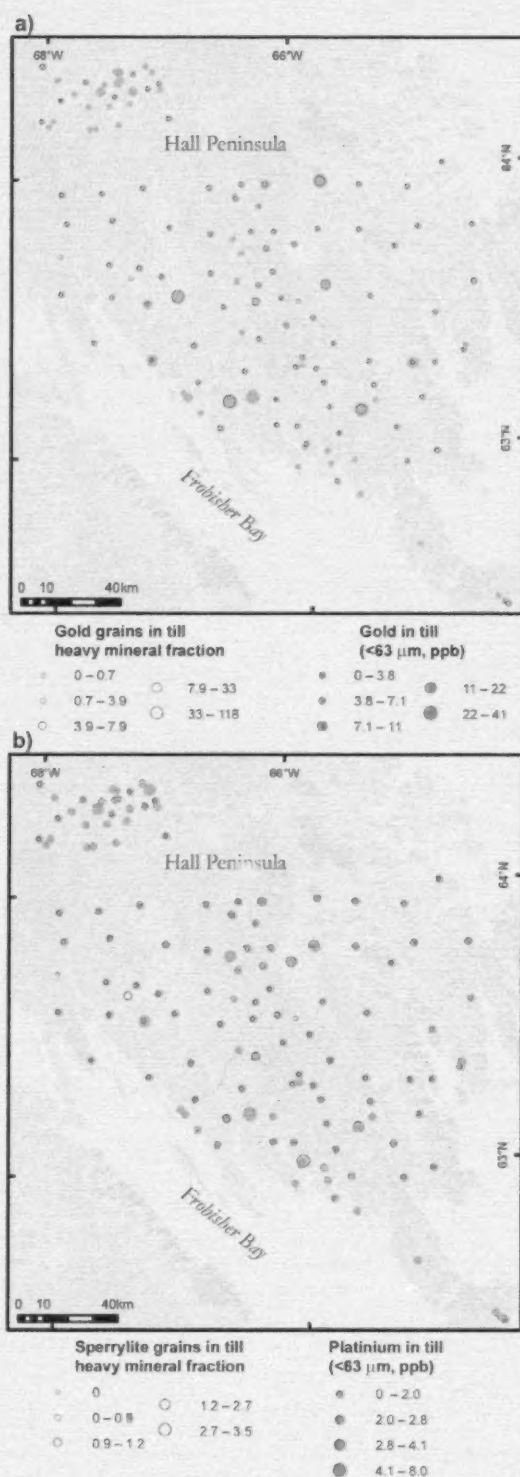
Figure 4: a) Distribution of gold (in ppb) and gold grains in till heavy mineral fraction (normalized to 10 kg table feed); **b)** Distribution of platinum (in ppb) and sperrylite (platinum-bearing mineral) grains in till heavy mineral fraction (normalized to 10 kg table feed). Till samples from central Hall Peninsula, Nunavut.
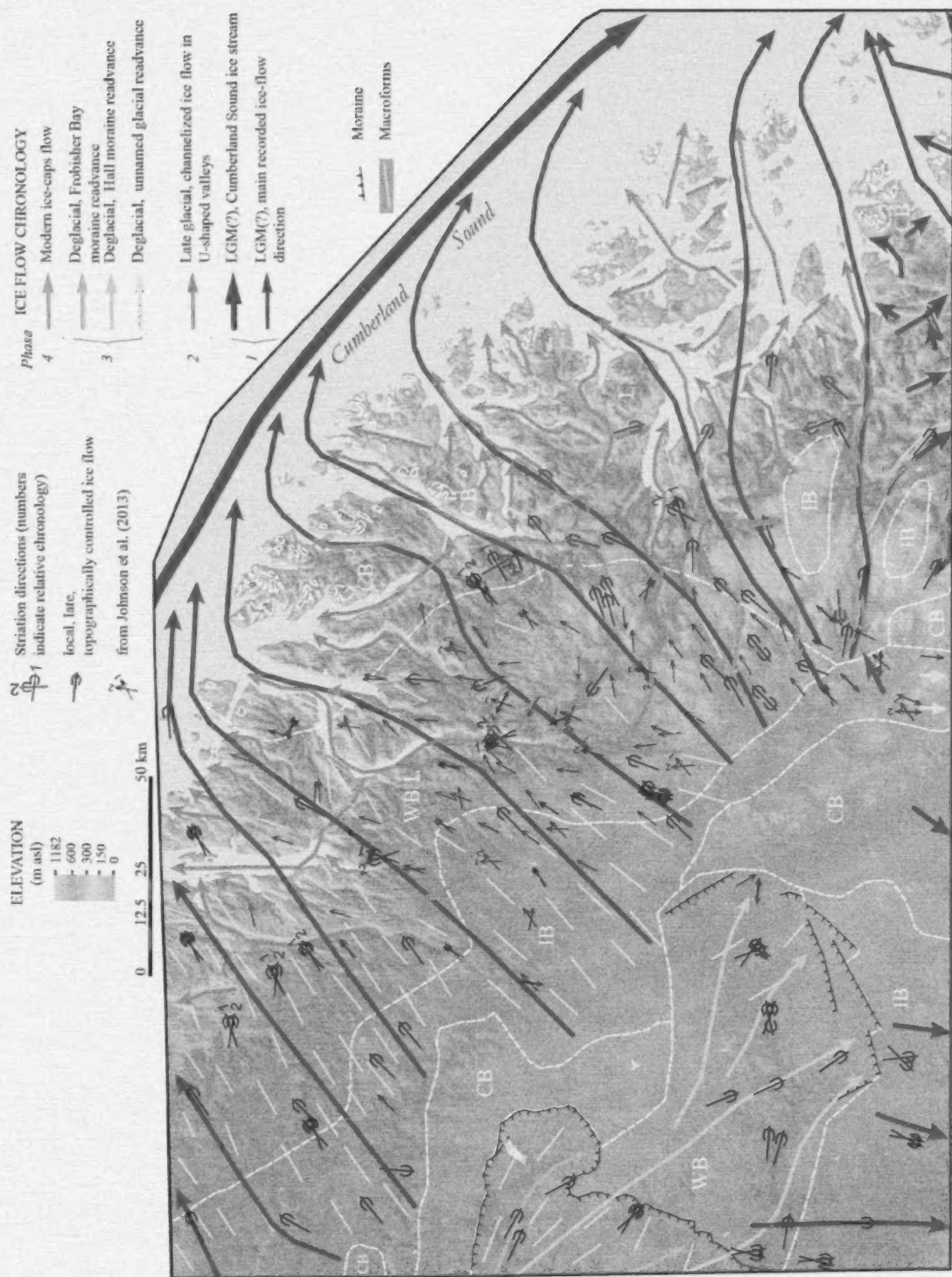
Figure 5: Preliminary ice flow and glaciodynamic setting in central Hall Peninsula, Nunavut. Digital elevation model (Gilbert, 2012) derived from CanVec 1:50 000 data (Natural Resources Canada, 2012). Abbreviations: CB, cold-based area; IB, intermediate cold-based area; WB/L, mix of warm-based and linear selective glacial erosion areas; L, linear selective glacial erosion area; WB, warm-based area; LGM, late glacial maximum.

(Marsella et al., 2000; Staiger et al., 2006). The ice was stagnant (cold-based) under the ice divide area, and became progressively more active toward Cumberland Sound. The ice flowed uniformly toward the northeast in the northern part of study area, whereas in the south, flow was more channelized in the valleys between highlands on the plateau and the outer rim of islands. Cold-based conditions protected the highlands as 'sticky spots' from glacial erosion, at least during the last glaciation. The northern portion of the highlands on the plateau bears striations, roches moutonnées and other marks of glacial erosion (Johnson et al., 2013), and this is not observed farther south on the highlands.

Last glacial maximum(?), ice stream in Cumberland Sound

High velocity zones of glacial flow, or ice streams, moved southeast along the main axis of Cumberland Sound (Dyke and Prest, 1987; De Angelis and Kleman, 2007; Johnson et al., 2013), to drain into Baffin Bay or into an ice shelf in Cumberland Sound (Jennings, 1993). The ice on the northeastern side of Hall Peninsula drained toward the Cumberland Sound ice stream, which likely caused considerable ice surface drawdown along the coast and toward the south.

Phase 2 ice flow

Late glacial, channelized ice flow in U-shaped valleys

It is inferred that this ice flow phase occurred from the late glacial period to the late Holocene and developed as a result of ice sheet thinning in the area, which made the subglacial topography increasingly important in controlling ice-flow direction. It is characterized by convergent patterns of ice flow into long U-shaped valleys located between highlands. As the ice thinned, presumably the conditions became cold-based adjacent to the U-shaped valleys, especially toward the coast into fiords (Johnson et al., 2013). Cirques commonly occurred adjacent to the major U-shaped valleys. Although it is possible that glacial advance and retreat occurred from the late glacial period to the present, the majority of ice flow was probably during the Holocene. Recently deglaciated, neoglacial tills and moraines are found at the margins of several modern glaciers.

On the plateau, phase 2 ice flow is marked by distinct inflexions of ice flows converging toward the main late-glacial valleys, especially toward Ptarmigan Fiord in the north (Johnson et al., 2013). Phase 2 ice flow is chronologically constrained by several later, crosscutting striae, relative to phase 1 ice flow.

Phase 3 ice flow

The three distinct events compiled under phase 3 ice flow share commonalities. They were all south- to southeast-trending flows, and left blankets of till on the plateau. These tills were often deposited over cold-based terrain, at least marginally, where a nonerosive thin lobate margin read-vanced partly over a landscape characterized by non-glacial features.

Deglacial, unnamed glacial readvance

This readvance represents localized southward ice flow related to a minor standstill of the ice-sheet margin or smaller alpine glaciers and is best characterized by nested recessional moraines. Ice was at least slightly sliding on its base. This warm-based ice transported sediment, deposited a blanket of till and constructed a subdued moraine made of hummocky, slightly thicker till. Evidence of glacial scouring and polish is found on outcrops throughout the landscape (e.g., lakes, bare outcrops and frequent fine striations on uppermost exposed bedrock surfaces).

Deglacial, Hall moraine readvance

The Hall moraine ice (Miller, 1980) was a local event that crosscut regolith and presumably former glacial and glaciolacustrine sediments, and deposited a blanket of till and scoured and exposed bedrock outcrops. This ice generally flowed toward the southeast. South of the large lake at the head of McKeand River some of this exceptionally fine, boulder-poor, thick and drumlinized till blanket may consist of re-entrained former glacial lake sediments. The Hall moraine itself consists of a 5 km wide swath of hummocky till, and occasionally hummocky ice-contact glaciofluvial sediments. Glacial lake sediments, littoral features (beaches and trim lines) and meltwater channels adjacent to the Hall moraine (Miller, 1985) provide evidence of a glacial stillstand. A few glacial lakes were dammed by the ice in some small valleys adjacent to this ice position (Miller, 1985).

Deglacial, Frobisher Bay moraine readvance

The Frobisher Bay moraine (dated to 9– 8 ka ^{14}C BP; Blake, 1966; Miller, 1980; Hodgson, 2005) is a major regional feature consisting of several tracts of large push moraines, smaller recessional moraines, hummocky till and glacio- fluvial ice-contact deposits, left by southeast-trending ice flow. It extends hundreds of kilometres to the south across Frobisher Bay onto Meta Incognita Peninsula, and to the north it seems to vanish a few tens of kilometres outside of the study area. On the Hall Peninsula plateau, this moraine contained several glacial lakes, marked by well-defined littoral features (beaches and trim lines), deltas and blankets of fine sediment (Figure 2). Behind the moraine, a thick blanket of till was deposited, sometimes streamlined or hummocky. Locally, the moraine crosscuts cold-based zones, and corresponds to a younger glacial re-advance episode.

Phase 4 ice flow

Modern ice cap flows

During the Holocene, the remaining ice cap located on the Hall Peninsula highlands flowed radially. It flowed west to-

ward the Hall Peninsula plateau, where it marked an ice flow reversal compared to phase 2 ice flow. On this western, land-based part of the local paleo-ice cap, the basal glaciodynamics were probably quite reduced due to cold-based conditions and relatively flat terrain. It is therefore rare to observe well-defined striae; but occasionally roches moutonnées, grooves, displaced boulders and erratics indicate ice flow reversal toward the west. Hummocky moraines consisting of bouldery till may also have been left by the west-flowing mountain glaciers. This late ice cap also flowed east toward Cumberland Sound, where it is parallel and therefore amalgamated to phase 2 ice flow.

Glaciodynamic zones

Building on work undertaken earlier on Hall Peninsula (Sugden, 1978; Hodder, 2012; Johnson et al., 2013; Tremblay et al., 2013), the mapping of glaciodynamic zones is based on an interpretation of the geomorphology, glacial erosion and glacial sediment in the area (Figure 5). It may help resolve enigmatic ice-flow histories at local scales, and provide first-order estimates of glacial sediment transport distances, which are useful to drift exploration as a means to discover buried mineral deposits.

The geomorphological indicators of glacial erosion are summarized as a broad classification of terrain types. The observations are primarily based on field observations and interpretation of digital elevation models, satellite imagery and airphotos. The presence of numerous small lakes, glacially eroded bare outcrops and streamlined hills are interpreted to represent erosive conditions (warm-based ice), whereas the persistence of a mix of thick nonglacial regolith, felsenmeer and till suggest cover by predominantly weakly erosive (cold-based) ice (Sugden, 1978; Miller, 1980; Dyke, 1993; Dredge, 2000; Tremblay et al., 2011; Hodder, 2012). The dynamic character of the former ice sheet (cold- versus warm-based) can thus be inferred from this classification, and can therefore help understand and outline the nature of glacial transport. The mapping includes theoretical and methodological elements from the central Canadian Arctic (Dyke, 1993), Melville Peninsula (Dredge, 2000; Tremblay et al., 2011; Tremblay and Paulen, 2012) and from Baffin Island (Miller, 1980; Andrews et al., 1985; Marsella et al., 2000; Staiger et al., 2006; Johnson et al., 2013). Hodder (2012) established criteria for a spatial assessment of subglacial dynamics on the Hall Peninsula plateau, and produced a map showing a glacial erosion index by using lake density, elevation and streamlined hill density with elongation ratios. The resulting maps illustrate important glacial erosion near the coast, and progressively less important glacial erosion toward the plateau. As a complement to Johnson et al.'s (2013) studies on northern Hall Peninsula, till geochemistry and cosmogenic isotopes on bedrock outcrops and tills will be used to assess the spatial distribution of glacial erosion during the late Quaternary on Hall Peninsula.

Cold-based area (CB)

Within this zone, the glacier was frozen on its base and little or no basal sliding occurred. On the Hall Peninsula plateau, this area coincides with the location of the main ice divide during the LGM (Figure 5). The landscape is not glacially scoured, as observed by the general absence of ice-scoured lakes and the rarity or absence of bedrock outcrops, and glacial sediments have been transported for short or negligible distances. Locally, a regolith is observed at surface, whereby the host rock was intensely chemically weathered to a thick, orange (iron-stained), clayey-sandy diamicton. Sharp lateral lithological boundaries are observed in the regolith content and correspond to underlying bedrock units, which eliminates a dominantly glacial origin for this material type (Leblanc-Dumas et al., 2013; Tremblay, 2013). Elsewhere in the cold-based zone, the ground cover is composed of in situ material that is reduced to fine material by the action of seasonal frost or chemical weathering (Figure 6a). Coverage by ice sheet during the Quaternary is indicated by abundant glaciofluvial channels and the presence of rare glacial erratics, some of those also intensively weathered (Miller, 1980).

Along the outer rim of islands on the Cumberland Sound coast, cold-based conditions occurred at least since the last interglacial, and allowed the preservation of flat surfaces covered with felsenmeer and displaying well-formed tors. The glacial erosion level was therefore much lower in elevation (200–400 m asl) than inland (600–700 m asl). The abrupt lowering of the paleoglacial profile toward the Cumberland Sound ice stream explains the preservation of these paleosurfaces on the outer rim of the islands.

Intermediate cold-based area (IB)

This glaciodynamic zone is transitional between cold- and warm-based terrains, and shares geomorphological and sedimentological characteristics of both. The cumulative effect of multiple glacial events (switching between cold- and warm-based conditions) has progressively affected the regolith terrains to expose more bedrock outcrops and deposit till (Figure 6b). The glacier was frozen at its base for long periods in this zone while warm-based erosion occasionally occurred with relatively restrained intensity. Scouring of the landscape gradually increases from the cold-based area toward warm-based zones and ice-scoured lakes and fresh bedrock outcrops are increasingly common. Within the intermediate cold-based area, field evidence shows that glacial sediments were transported for short to moderate distances (cf. Tremblay and Paulen, 2012). Some areas around the highest existing glaciers are considered to have been cold-based during the last glaciation, as no striae or glacial polish were found, and moderate chemical weathering occurs. However, outcrops are frequent indicating ear-
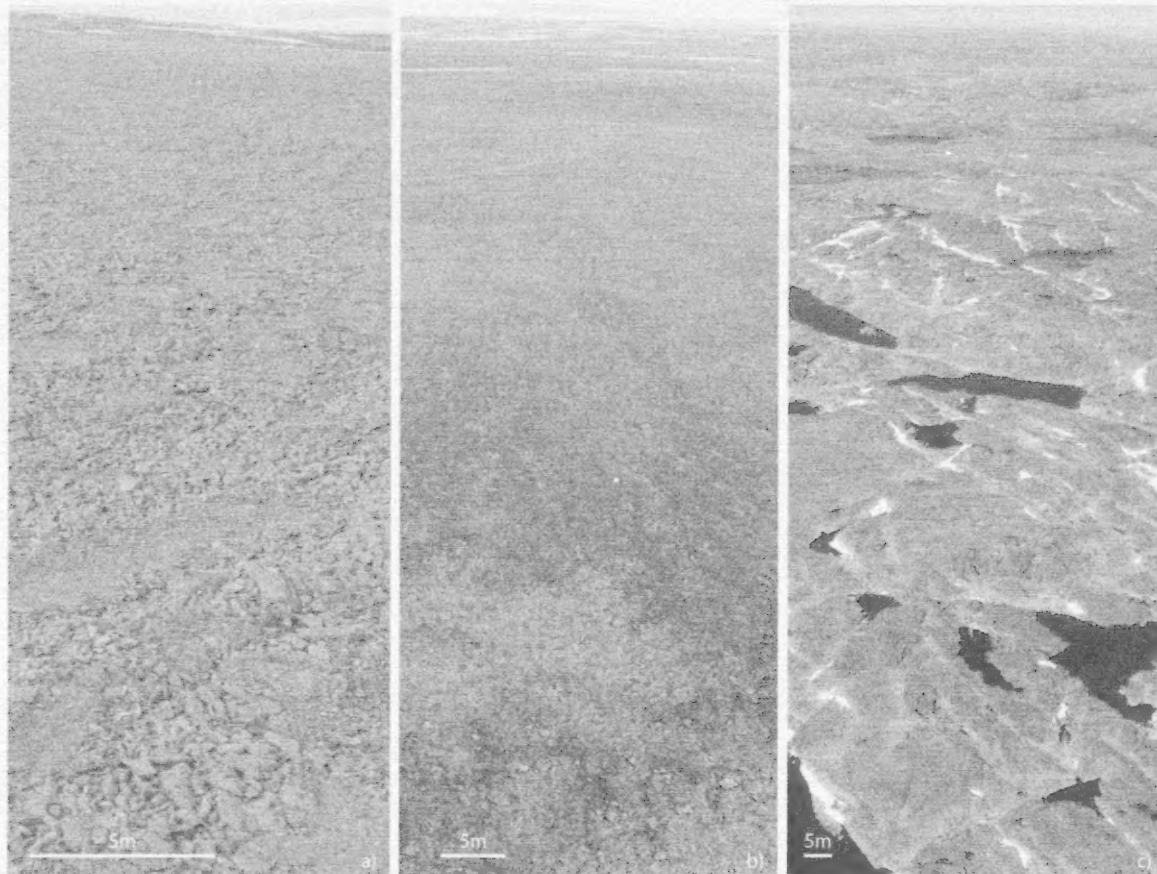
Figure 6: a) Cold-based terrain with slightly undulating topography. It is covered with a mixture of orange–matrix (iron-stained) regolith, formed from weathering of the underlying bedrock. b) Till blanket (mixed with regolith?) in intermediate cold-based zone. c) Till veneer and polished bedrock surfaces in glacially eroded, warm-based terrain.

lier glacial erosion, therefore they have been classified as intermediate cold-based zones.

Mix of warm-based and linear selective glacial erosion areas (WB/L)

In this zone, glacial thermal patterns were mixed, with extensive warm-based areas (and sparse intermediate cold-based areas) on plateaus, and linear glacial erosion in U-shaped valleys or fiords (Sugden, 1978; Johnson et al., 2013). Spatial and temporal variations in ice-flow velocity are implied by this complex glaciodynamic pattern, with ice flow in the U-shaped valleys being generally younger than the warm-based ice flow on the plateau.

Linear selective glacial erosion (L)

This is a landscape zone affected by patchy warm-based conditions in the numerous glacial valleys, juxtaposed with cold-based and intermediate cold-based zones on the plateaus and mountain tops (Sugden and Watts, 1977), where no evidence of strong regional glacial erosion is observed. The result was the generation of accentuated relief, caused by the deepening of glacial erosion and the preservation of

adjacent summit felsenmeer, where ice was kept relatively thin by dynamic and efficient drainage through the glacial valleys.

Warm-based area (WB)

This geomorphological landscape type reflects important glacial activity related to warm-based basal ice conditions, where ice melted at the base of the glacier, and sliding and deformation occurred at the bed. As observed in Figure 6c, glacial scouring is significant, as seen by the numerous lakes, polished or striated outcrops, and streamlined depositional or erosional landforms. Glacial transport distances are generally relatively long and glacial sediment thickness is variable.

Economic considerations

The surficial maps and geomorphological studies (glaciodynamic mapping, permafrost, satellite images and uplift history) will help to minimize risk associated with mineral exploration and optimize the design of infrastructure projects on Hall Peninsula. The surficial maps will also

help identify new sources of granular material, useful for road building and general construction. Zones of silty glaciolacustrine sediments have been mapped, which may contain ice lenses and represent challenges for infrastructure development. Till geochemical and mineralogical data will contribute to more efficient mineral exploration and assessment of environmental and geotechnical characteristics of soil. Gold and platinum mineral potential is present in the study area, and other elements might also be of interest for mineral exploration. Two sapphire grains were also found in the till heavy mineral fraction. Data from the 2012 field season can be downloaded online (Tremblay and Leblanc-Dumas, 2014), and all results will be analyzed and interpreted in future publications.

Acknowledgments

References

Andrews, J.T. and Sim, V.W. 1964: Examination of the carbonate content of drift in the area of Foxe Basin; Geographical Bulletin, v. 21, p. 44–53.

Andrews, J.T., Clark, P. and Stravers, J. 1985: The pattern of glacial erosion across the eastern Canadian Arctic; *in* Quaternary Environments: Eastern Canadian Arctic, Baffin Bay and West Greenland, J.T. Andrews (ed.), Allen and Unwin, Winchester, Massachusetts, p. 69–92.

Averill, S.A. 2001: The application of heavy indicator mineralogy in mineral exploration with emphasis on base metal indicators in glaciated metamorphic and plutonic terrains; Geological Society of London, Special Publication 185, p. 69–81.

Blake, W., Jr. 1966: End moraines and deglaciation chronology in northern Canada with special reference to southern Baffin Island; Geological Survey of Canada, Paper 66-26, 31 p.

Briner, J.P., Davis, P.T. and Miller, G.H. 2009: Latest Pleistocene and Holocene glaciation of Baffin Island, Arctic Canada: key patterns and chronologies; Quaternary Science Reviews, v. 28, p. 2075–2087.

Clements, B., Pell, J., Holmes, P. and Grenon, H. 2009: Following kimberlite indicator minerals to Chidliak, Baffin Island:

Canada's newest diamond district; *in* Workshop B: Indicator Mineral Methods in Mineral Exploration, 24th International Applied Geochemistry Symposium, Fredericton, New Brunswick, May 31, 2009, p. 83–88.

DAT/EM Systems International 2012: Summit Evolution software suite; software, DAT/EM Systems International, Anchorage, Alaska.

De Angelis, H. and Kleman, J. 2007: Palaeo-ice streams in the Foxe/Baffin sector of the Laurentide Ice Sheet; Quaternary Science Reviews, v. 26, p. 1313–1331.

Deblonde, C., Plouffe, A., Boisvert, É., Buller, G., Davenport, P., Everett, D., Huntley, D., Inglis, E., Kerr, D., Moore, A., Paradis, S.J., Parent, M., Smith, I.R., St. Onge, D. and Weatherston, A. 2012: Science language for an integrated Geological Survey of Canada data model for surficial geology maps, version 1.2; Geological Survey of Canada, Open File 7003, 238 p.

Dredge, L.A. 2000: Age and origin of upland block fields on Melville Peninsula, eastern Canadian Arctic; Geografiska Annaler, v. 82, no. 4, p. 443–454.

Dyke, A.S. 1993: Landscapes of cold-centred Late Wisconsinan ice caps, Arctic Canada; Progress in Physical Geography, v. 17, no. 2, p. 223–247.

Dyke, A.S. and Prest, V.K. 1987: Late Wisconsinan and Holocene history of the Laurentide Ice Sheet; Géographie physique et Quaternaire, v. 41, p. 237–263.

Dyke, A.S., Andrews, J.T. and Miller, G.H. 1982: Quaternary geology of Cumberland Peninsula, Baffin Island, District of Franklin; Geological Survey of Canada, Memoir 403, 32 p.

Dyke, A.S., Moore, A. and Robertson, L. 2003: Deglaciation of North America; Geological Survey of Canada, Open File 1574, 2 sheets, 1 CD-ROM.

Esri 2012: ArcGIS Desktop, release 10; software, Esri, Redlands, California.

Fréchette, B., Wolfe, A.P., Miller, G.H., Richard, P.J.H. and de Vernal, A. 2006: Vegetation and climate of the last interglacial on Baffin Island, Arctic Canada; Palaeogeography, Palaeoclimatology, Palaeoecology, v. 236, no. 1–2, p. 91–106.

Fulton, R.J. 1995: Surficial materials of Canada/Matériaux superficiels du Canada; Geological Survey of Canada, "A" Series Map 1880A, scale 1: 5 000 000, 1 sheet.

Gilbert, C. 2012: Hall Peninsula DEM derived from CanVec 1:50 000 topographical data; internal unpublished data, Canada-Nunavut Geoscience Office.

Hodder, T.J. 2012: A GIS analysis of subglacial erosion intensity of Hall Peninsula, Baffin Island, Nunavut; B.Sc. thesis, University of Waterloo, Waterloo, Ontario, 40 p.

Hodgson, D.A. 2005: Quaternary geology of western Meta Incognita Peninsula and Iqaluit area, Baffin Island, Nunavut; Geological Survey of Canada, Bulletin 582, 74 p., 1 CD-ROM.

Jennings, A.E. 1993: The Quaternary history of Cumberland Sound, southeastern Baffin Island: the marine evidence; Géographie physique et Quaternaire, v. 47, no. 1, p. 21–42.

Johnson, C., Ross, M. and Tremblay, T. 2013: Glacial geomorphology of north-central Hall Peninsula, southern Baffin Island; Geological Survey of Canada, Open File 7413, 57 p.

Kaplan, M. and Miller, G.H. 2003: Early Holocene delevelling and deglaciation of the Cumberland Sound region, Baffin Island, Arctic Canada; Geological Society of America Bulletin, v. 115, no. 4, p. 445–462.

LeBlanc, A.-M., Allard, M., Oldenborger, G.A., Short, N., Mathon-Dufour, V., L'Hérault, E. and Sladen, W.E. 2013: Permafrost characterization at the Iqaluit airport, Nunavut, in support of decision-making and planning; *in* Summary of Activities 2012, Canada-Nunavut Geoscience Office, p. 131–142.

Leblanc-Dumas, J., Allard, M. and Tremblay, T. 2013: Quaternary geology and permafrost characteristics in central Hall Peninsula, Baffin Island, Nunavut; *in* Summary of Activities 2012, Canada-Nunavut Geoscience Office, p. 101–106.

Marsella, K.A., Bierman, P.R., Thompson Davis, P. and Caffee, M.W. 2000: Cosmogenic ^{10}Be and ^{26}Al ages for the last glacial maximum, eastern Baffin Island, Arctic Canada; Geological Society of America Bulletin, v. 112, no. 8, p. 1296–1312.

Matthews, B. 1967: Late Quaternary marine fossils from Frobisher Bay (Baffin Island, N.W.T., Canada); Palaeogeography, Palaeoclimatology, Palaeoecology, v. 3, p. 243–263.

McClenaghan, M.B., Oviatt, N.M., Averill, S.A., Paulen, R.C., Gleeson, S.A., McNeil, R.J., McCurdy, M.W., Paradis, S. and Rice, J.M. 2012: Indicator mineral abundance data for bedrock, till and stream sediment samples from the Pine Point Mississippi Valley-type Zn-Pb deposits, Northwest Territories; Geological Survey of Canada, Open File 7267, 12 p.

Miller, G.H. 1980: Late Foxe glaciation of southern Baffin Island, N.W.T., Canada; Geological Society of America Bulletin, v. 91, no. 7, p. 399–405.

Miller, G.H. 1985: Moraines and proglacial lake shorelines, Hall Peninsula, Baffin Island; *in* Quaternary Environments, Eastern Canadian Arctic, Baffin Bay and Western Greenland, J.T. Andrews (ed.), Allen and Unwin, Boston, Massachusetts, p. 546–557.

Natural Resources Canada 2012: CanVec, topographic reference digital product; Natural Resources Canada, Topographic Information Centre, Sherbrooke, Quebec.

Plouffe, A., McClenaghan, M.B., Paulen, R.C., McMartin, I., Campbell, J.E. and Spirito, W.A. in press: Processing of glacial sediments for the recovery of indicator minerals protocols used at the Geological Survey of Canada; Geochemistry: Exploration, Environment, Analysis.

Shimamura, K., Williams, S.P. and Buller, G. 2008: GanFeld user guide: a map-based field data capture system for geologists; Geological Survey of Canada, Open File 5912, 90 p.

Staiger, J.W., Gosse, J.C., Little, E.C., Utting, D.J., Finkel, R., Johnson, J.V. and Fastook, J. 2006: Glacial erosion and sediment dispersion from detrital cosmogenic nuclide analyses of till; Quaternary Geochronology, v. 1, p. 29–42.

Steenkamp, H.M. and St-Onge, M.R. 2014: Overview of the 2013 regional bedrock mapping program on northern Hall Peninsula, Baffin Island, Nunavut; *in* Summary of Activities 2013, Canada-Nunavut Geoscience Office, p. 27–38.

Stravers, J.A., Miller, G.H. and Kaufman, D.S. 1992: Late glacial ice margins and deglacial chronology for southeastern Baffin Island and Hudson Strait, eastern Canadian Arctic; Canadian Journal of Earth Sciences, v. 29, p. 1000–1017.

Sugden, D. 1978: Glacial erosion by the Laurentide Ice Sheet; Journal of Glaciology, v. 20, no. 83, p. 367–391.

Sugden, D.E. and Watts, S.H. 1977: Tors, felsenmeer, and glaciation in northern Cumberland Peninsula, Baffin Island; Canadian Journal of Earth Sciences, v. 14, p. 2817–2823.

Tremblay, T. 2013: Surficial geology and geomorphology of southern Hall Peninsula, Baffin Island (abstract); Nunavut Mining Symposium 2013, Iqaluit, Nunavut, Program.

Tremblay, T. and Leblanc-Dumas, J., 2014: Geochemical and mineralogical data for southern Hall Peninsula, Nunavut; Canada-Nunavut Geoscience Office, Geoscience Data Series GDS2014-003, Microsoft® Excel® file.

Tremblay, T. and Paulen, R. 2012: Glacial geomorphology and till geochemistry of central Melville Peninsula, Nunavut; Geological Survey of Canada, Open File 7115, 47 p.

Tremblay, T., Lamothe, M. and Paulen, R.C. 2011: A spatial analysis of the geomorphology and geochemical alteration of cold-based zones transitional with warm-based zones, Melville Peninsula, Nunavut; Geological Association of Canada–Mineralogical Association of Canada, Joint Annual Meeting, Program with Abstracts, v. 34, p. 219.

Tremblay, T., Leblanc-Dumas, J., Allard, M., Gosse, J.C., Creason, C.G., Peyton, P., Budkewitsch, P. and LeBlanc, A.-M. 2013: Surficial geology of southern Hall Peninsula, Baffin Island, Nunavut: summary of the 2012 field season; *in* Summary of Activities 2012, Canada-Nunavut Geoscience Office, p. 93–100.

Utting, D.J., Gosse, J.C., Hodgson, D.A., Trommelen, M.S., Vickers, K.J., Kelley, S.E. and Ward, B. 2007: Report on ice-flow history, deglacial chronology, and surficial geology, Foxe Peninsula, southwest Baffin Island, Nunavut; Geological Survey of Canada, Current Research 2007-C2, 13 p.

Preliminary results from recent investigations of marine geological hazards in Baffin Bay, Nunavut and Greenland

D.C. Campbell[1] and J.R. Bennett[2]

[1]Geological Survey of Canada, Natural Resources Canada, Dartmouth, Nova Scotia, calvin.campbell@nrcan.gc.ca
[2]Geological Survey of Canada, Natural Resources Canada, Dartmouth, Nova Scotia

Abstract

Analysis of existing data reveals that several marine geological hazards in Baffin Bay pose a potential threat to coastal communities, the environment and infrastructure in the area. Since 2011, the Geological Survey of Canada (GSC) has actively undertaken research on this issue. In August and September 2013, the GSC conducted an expedition to the area to investigate marine geological hazards. Preliminary results of this research are provided. A range of geological and geophysical data was collected during the expedition in order to develop a geological framework for the area and to characterize geological hazards. Data collected during the expedition will be used to assess seafloor stability, sediment transport, the recurrence of large earthquakes, the recurrence of seabed failure and the characterization of natural hydrocarbon seeps. This information will be provided to northern communities, the Government of Nunavut and regulators in order to better manage these offshore areas.

Résumé

L'analyse des données existantes révèle que certains risques géologiques d'origine marine dans la baie de Baffin peuvent poser un danger pour les collectivités côtières, à l'environnement et aux infrastructures de la région. Depuis 2011, la Commission géologique du Canada (CGC) poursuit des études liées à ces questions. En août et septembre 2013, des chercheurs de la CGC ont mené une expédition dans la région en vue d'étudier ces risques géologiques d'origine marine. Le présent rapport fait état des résultats préliminaires provenant de cette étude. Une gamme de données géologiques et géophysiques ont été recueillies au cours de cette expédition en vue d'élaborer le cadre géologique de la région et de mieux cerner la nature des risques géologiques. Les données recueillies au cours de cette expédition serviront également à juger le degré de stabilité des fonds océaniques, les modes de transport des sédiments, la périodicité de tremblements de terre de grande envergure et de glissements des fonds marins, et la caractérisation des suintements d'hydrocarbures naturels. Cette information sera transmise aux collectivités du Nord, au gouvernement du Nunavut et aux organismes de réglementation afin de les aider à mieux gérer ces régions extracôtières.

Introduction

A geological hazard is an adverse geological condition capable of causing damage or loss of property and life. Since 2011, the Geological Survey of Canada (GSC) has conducted research on marine geological hazards in Baffin Bay. The Baffin Bay Geohazards Activity of the GSC's Public Safety Geoscience Program is aimed at improving the understanding of geological processes and hazards (geohazards) in Baffin Bay that could be a risk to coastal communities, the environment and infrastructure. Knowledge of geohazards is required in Baffin Bay to support community, Nunavut government and regulator decisions on the use of offshore areas and provide northern coastal communities with better knowledge for improving public safety.

Analysis of existing data suggest that geological hazards in Baffin Bay include hydrocarbon venting features, uneven seabed caused by glacial seafloor processes, submarine slope failures, ice scour and a high level of earthquake activity (Bennett et al., 2013). The magnitude (M) 7.3 earthquake of November 20, 1933 in Baffin Bay (Figure 1) is the largest passive-margin earthquake in North America and

the largest known earthquake north of the Arctic Circle (Bent, 2002). During community consultations in April 2013, several community members from Pond Inlet, Clyde River and Qikiqtarjuaq reported experiencing tremors and waves under the ice that may be evidence of possible past seismic activity, tsunamis and submarine landslides. The frequency of seismic events, combined with the region's high latitude, makes Baffin Bay unique compared to other glaciated margins. Despite the presence of these hazards, there are large portions of the seabed in Baffin Bay that have never been mapped or sampled, thus creating gaps in the understanding of geohazards in Baffin Bay.

During August–September 2013, the GSC conducted a scientific expedition to the Baffin Bay region (Figure 1) aboard Canadian Coast Guard Ship (CCGS) Hudson. The objectives of the expedition were to improve understanding of the surficial geology, seafloor properties and processes on the continental shelf and slope in the area, in order to better assess geological hazards. Specifically, the expedition

1) assessed the regional surficial geology framework in the area, including the shallow litho and acoustic stratigraphy, and physical properties;

2) collected data, including strategic coring in locations that may record an earthquake signature in the sediments, that should improve estimates of recurrence of large earthquakes in the area;

3) investigated natural hydrocarbon seeps on the seabed in the area; and

4) investigated slope instability features in the area.

This paper presents some preliminary results from the 2013 expedition.

Preliminary results

Slope off the Disko Trough

A portion of the Greenland shelf is located in Canada's Exclusive Economic Zone (Figure 1). The area is the seaward limit of the Disko Trough, which is incised into a large promontory extending into Baffin Bay. The seabed seaward of the trough is steep and historical data from this area are limited. The West Greenland Current sweeps the seabed along the slope in this area as it moves northward, and it is expected that the current strength is enhanced as it encounters the promontory. The area was traversed during a CCGS Hudson survey in 2008 while the ship was steaming north (Campbell and de Vernal, 2009). The 3.5 kHz sub-bottom data from that expedition showed irregular undulations on
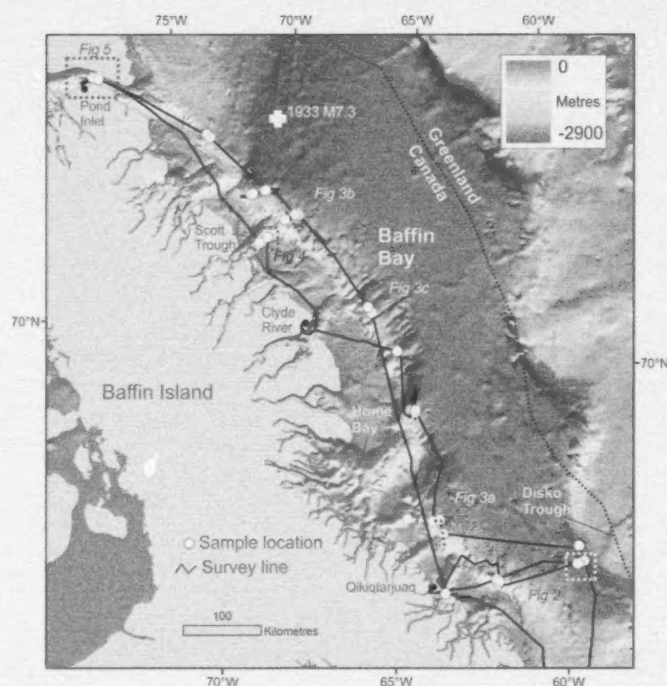
Figure 1: Digital elevation model of the Baffin Bay region, eastern Nunavut and western Greenland, showing the location of data collected during the 2013 expedition, as well as locations and features referred to in the text.

the seabed immediately south of the promontory. The undulations appeared to be gullies with depths of several tens of metres and relatively regular distance between crests. It was not clear from the 2008 data whether these undulations were due to down-slope sediment transport or seabed erosion by strong along-slope bottom currents.

During the 2013 expedition, multibeam bathymetry, sub-bottom profiler data and sediment sample data were collected on the slope off the Disko Trough in order to determine the origin of the gullies imaged in the 2008 data and to collect data for establishing the geological framework in this part of Baffin Bay (Figure 2). As the area lies within the Baffin Bay Narwhal Closure Area, a secondary objective was to collect seabed data to enable Fisheries and Oceans Canada to characterize the benthic biology.

The multibeam data reveal that the seabed morphology consists of both gullies that are oriented down slope and moats and smaller scours that are oriented along slope (Figure 2). The gullies are up to 60 m deep, while the scours are typically 20–30 m deep (Figure 2b). The floors of the gullies are draped by acoustically stratified sediments overlying an erosional unconformity. The drape thins substantially on the intervening ridges. The one moat that was crossed is not filled by the draped sediments, implying that it may still be active (Figure 2d), and shows upslope-migrating sediment waves on the adjacent contourite levée.
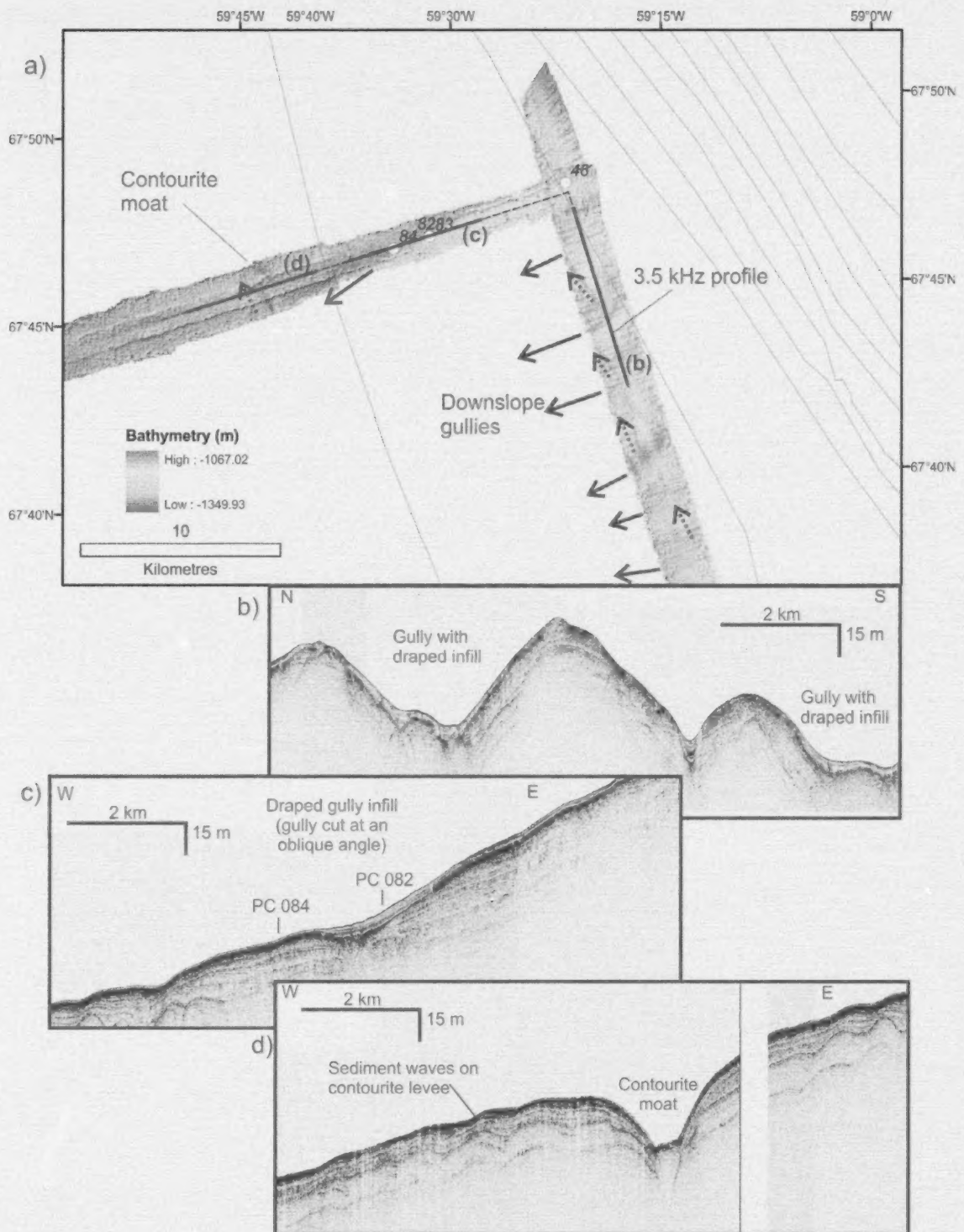
Figure 2: a) Bathymetry of the slope off the Disko Trough, western Greenland, showing the shaded-relief multibeam data and sample locations from the 2013 expedition; the seabed appears to show evidence of both down-slope and along-slope processes. **b)** 3.5 kHz sub-bottom strike profile across down-slope gullies; note the acoustically stratified sediments on the floor of the gullies that thin substantially on the ridge crests. **c)** 3.5 kHz sub-bottom dip profile that cuts a down-slope gully obliquely and shows the location of piston cores (PC) 084 and 082. **d)** 3.5 kHz sub-bottom dip profile that crosses a contourite moat; note the absence of acoustically stratified sediments in the floor of the moat and the upslope-migrating sediment waves on the contourite levée.

The observed thinning of draped sediments on the gully ridges is therefore interpreted to be due to the preferential winnowing by bottom currents of sediments on the ridge crests and their deposition in the gullies; the gullies are currently inactive except for occasional events. The piston cores collected in this area sampled the draped sediments and will help date the underlying erosional unconformity.

Slope seaward of Home Bay

The shallow acoustic stratigraphy of the slope seaward of Home Bay (Figure 1) is different than the slope north of Home Bay. The slope sediments seaward of Home Bay consist of relatively thick accumulations of acoustically stratified sediments, whereas the slope north of Home Bay is draped by relatively thin, acoustically transparent or stratified sediments over prolonged strong reflections.

High-resolution seismic-reflection data collected in 1978 show that the shallow seismic stratigraphy on the slope seaward of Home Bay is dominated by well-stratified sediments interrupted by mass-transport deposits (Figure 3a). The data show one such deposit that extends laterally for several kilometres. This deposit is overlain by several metres of sediment, making it likely Pleistocene in age. There is evidence in the data for rotational failure on the slope (Figure 3a), and there appears to be a recent mass-transport deposit on the seabed. Piston cores were collected in this area to date the shallowest mass-transport deposit and to establish the normal lithostratigraphy.

Slope north of Home Bay to Pond Inlet

The shallow acoustic stratigraphy of the eastern Baffin Bay slope extending from north of Home Bay to Pond Inlet is very consistent (Figures 1, 3). The typical stratigraphy consists of an acoustically transparent or stratified interval that overlies prolonged strong reflections (Figure 3b, c). The upper unit is interpreted to be mud-dominated glaciomarine sediments; it is variable in thickness but rarely exceeds a few metres. The upper unit is thickest on the mid-slope terrace that is located along the Baffin Bay slope seaward of Clyde River (Figure 3c). This stratigraphy is interrupted in a few locations by mass-transport deposits, interpreted to represent glaciogenic debris flows (Figure 3b). Holocene sedimentation rates on the floor of Baffin Bay are low (Simon et al., 2012). The interpretation of a glaciogenic debris flow at the seabed on the slope with little postglacial sediment overlying the deposit potentially indicates similarly low Holocene sedimentation rates on the slope. Piston cores were collected in this area to sample the typical shallow stratigraphy, as well as sample and date the mass-transport deposits.

Scott Trough

Data were collected in the Scott Trough during the 2013 expedition in order to date a mass-transport deposit identified from multibeam data collected by CCGS Amundsen (Figure 4a) and imaged on vintage seismic-reflection data. The deposits are located downslope from features interpreted to represent ice-margin gullies. A piston core (069, shown on Figure 4a) taken at the deposit had little recovery. It is interpreted that the mass-transport deposit was composed of till and coarse sediment that were deposited on the floor of the trough due to failure of the adjacent trough margin.

An additional objective in the Scott Trough was to investigate an area of a known seabed hydrocarbon seep in order to assess the geological characteristics of the seafloor in the vicinity of the seep (Figure 4). When the vessel arrived at the seep location, it was immediately noticed that the sea surface was scattered with several small slicks, ranging from less than 1 to several metres in diameter (Figure 4c, d). A camera transect and box core from the location did not show any obvious sign of active oil seepage at the seabed, but further detailed review of the data are required. Multibeam bathymetry data, collected upon departure from the area, showed extensive water-column anomalies in the pseudo–side-scan mode of the acquisition software (Figure 4b). Further analysis of the water-column data is necessary.

Pond Inlet

Earthquakes have been located along northeast-trending faults on Bylot Island immediately north of Pond Inlet (L. Currie, pers. comm., June 2013). Examination of multibeam data collected by CCGS Amundsen in Pond Inlet showed that these faults extend into the marine realm and trend toward the southwest (Figure 5).

During the 2013 expedition, sub-bottom profiler data and piston cores were collected in the vicinity of the faults in Pond Inlet to find evidence for slope failure associated with fault movement and potentially collect a long record of paleoseismicity in the inlet (Figure 5). It was difficult to image the base of the faults with the sub-bottom profiler because of the steepness of the escarpments (e.g., Figure 5b). However, slumping was observed at the base of a smaller escarpment, apparently related to a fault secondary to the main fault (Figure 5c). Several cores were taken in the area to ground truth and date these observations.

Economic considerations

The preliminary results of this study identified a number of features on the seabed in the area that are interpreted to represent geological hazards. Further analysis of the data collected in 2013 is planned for 2014. It is expected that this analysis will lead to more precise information on slope stability, the age and recurrence of submarine landslides, the recurrence of large earthquakes, and general understanding of the lithology and physical properties of the seabed in Baffin Bay. The outputs from this research will be used to
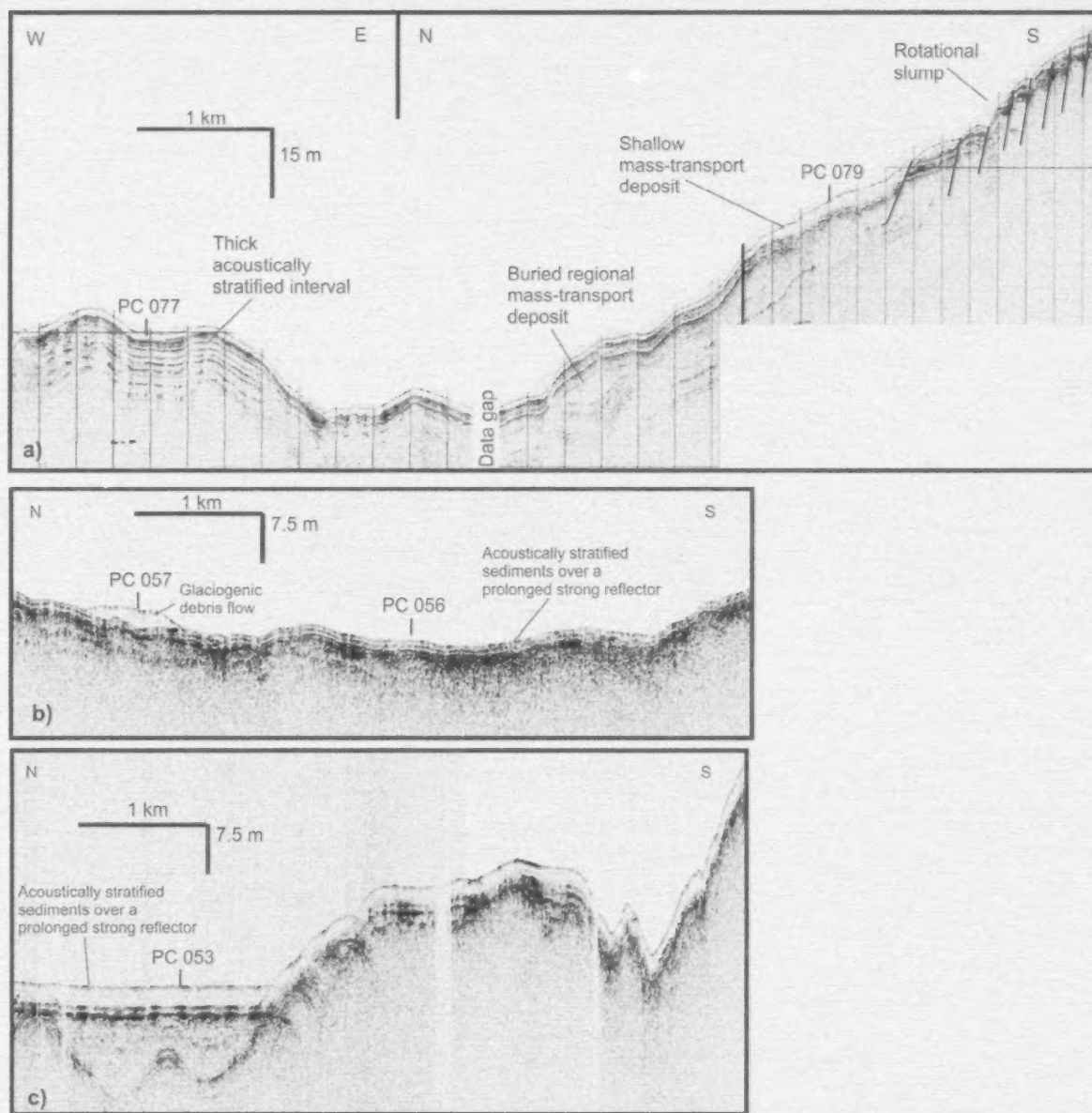
Figure 3: a) Huntec seismic-reflection profile collected in 1978, showing the shallow acoustic stratigraphy off Home Bay, east shore of Baffin Island, eastern Nunavut, and the locations of piston cores (PC) 077 and 079, collected during the 2013 expedition. **b)** 3.5 kHz profile from the slope near Scott Trough, east shore of Baffin Island, eastern Nunavut, showing an interpreted glaciogenic debris flow and stratified sediments overlying a prolonged strong reflection. **c)** 3.5 kHz profile, showing an example of a thick upper unit from the slope off Clyde River.
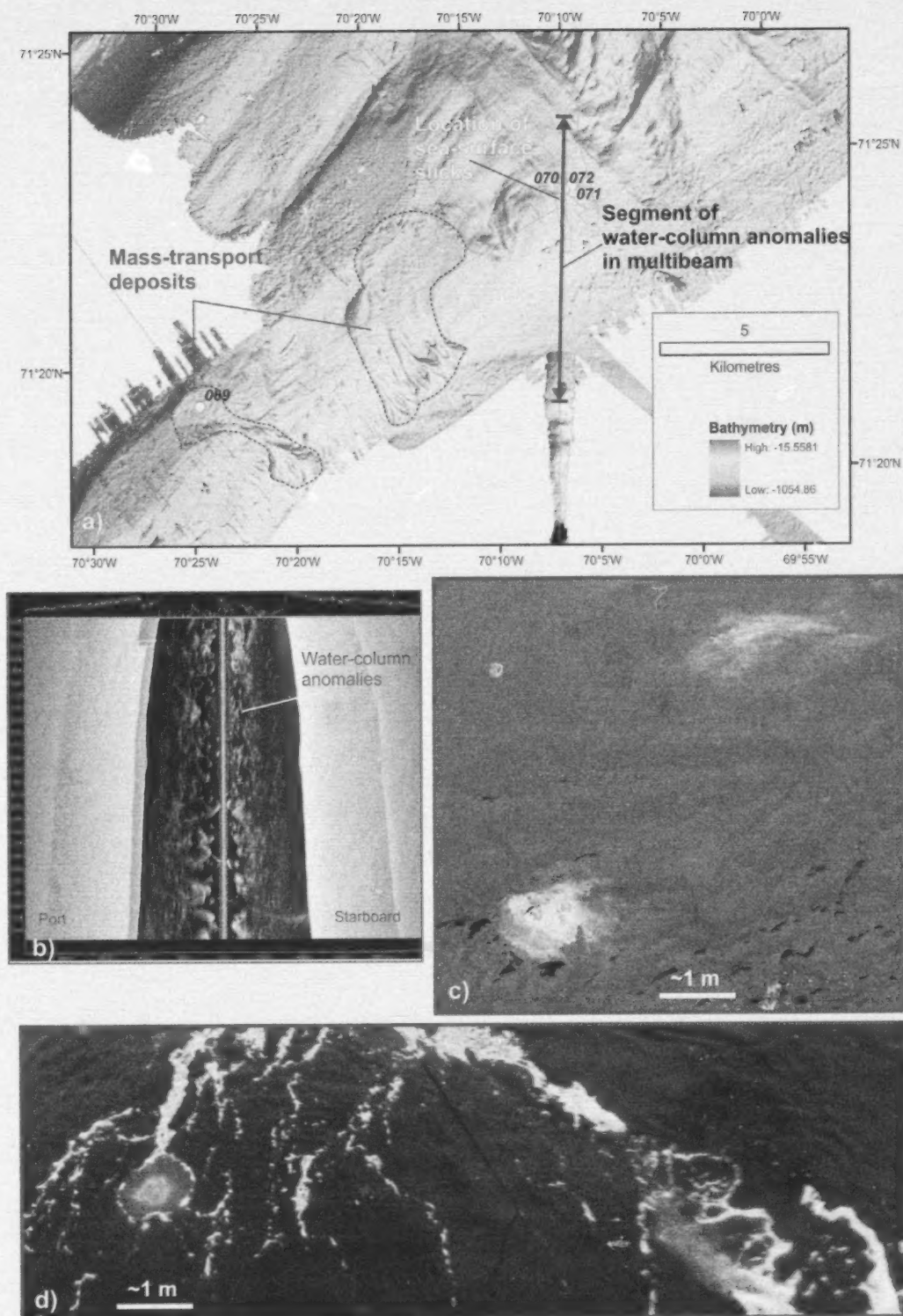
Figure 4: a) Bathymetry of the Scott Trough, east shore of Baffin Island, eastern Nunavut, showing the sampling locations during the 2013 expedition overlain on multibeam bathymetry data collected by CCGS Amundsen; shallow mass-transport deposits are indicated by dashed outlines. **b)** Screen grab of the multibeam bathymetry acquisition software, showing extensive water-column anomalies over the Scott seep. **c)** and **d)** Photographs of the sea-surface hydrocarbon slick observed at the location of the Scott seep; photos courtesy of L. Beazley, Fisheries and Oceans Canada.
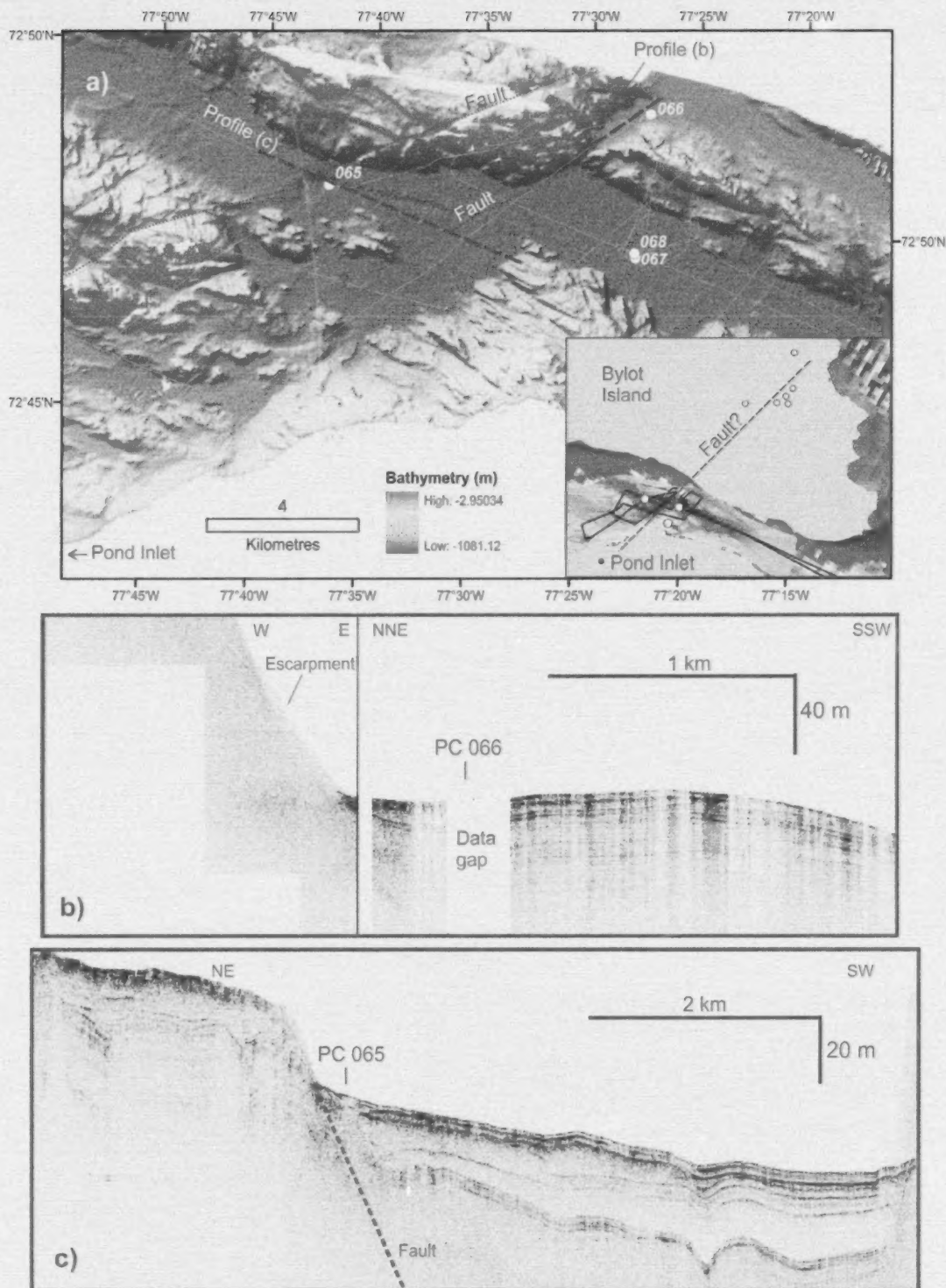
Figure 5: A) Data collected in Pond Inlet, east shore of Baffin Island, eastern Nunavut during the 2013 expedition, overlain on multibeam bathymetry data collected in the area by CCGS Amundsen; inset shows northern Baffin Island and Bylot Island with locations of recorded earthquakes (yellow circles), an interpreted fault and locations of data collected during the 2013 expedition. **B)** 3.5 kHz sub-bottom profile collected over the main fault escarpment, showing location of piston core (PC) 066. **C)** 3.5 kHz sub-bottom profile collected over a smaller fault, secondary to the main fault, that shows some slumping of sediments at the foot of the scarp; PC 065 was collected to determine the lithology of the sediment and when the slump occurred.

help formulate future regulations for infrastructure development, thus helping to ensure the safety of northerners.

Acknowledgments

References

Bennett, R., Campbell, C. and Furze, M., 2013: The shallow stratigraphy and geohazards of the northern Baffin Island shelf: studies to 2012; Geological Survey of Canada, Open File 7355, 41 p.

Bent, A. 2002: The 1933 Ms = 7.3 Baffin Bay earthquake: strike-slip faulting along the northeastern Canadian passive margin; Geophysical Journal International, v. 150, p. 724–736.

Campbell, D.C. and de Vernal, A. 2009: Marine geology and paleoceanography of Baffin Bay and adjacent areas, Nain, NL to Halifax, NS, August 28–September 23, 2008; Geological Survey of Canada, Open File 5989, 1 DVD.

Simon, Q., St-Onge, G. and Hillaire-Marcel, C. 2012: Late Quaternary chronostratigraphic framework of deep Baffin Bay glaciomarine sediments from high-resolution paleomagnetic data; Geochemistry Geophysics Geosystems, v. 13, Q0AO03, doi:10.1029/2012GC004272

Geophysical monitoring of permafrost conditions at Iqaluit International Airport, Baffin Island, Nunavut

by G.A. Oldenborger[1], A.-M. LeBlanc[2] and W.E. Sladen[2]

[1]Geological Survey of Canada, Natural Resources Canada, Ottawa, Ontario, greg.oldenborger@nrcan.gc.ca
[2]Geological Survey of Canada, Natural Resources Canada, Ottawa, Ontario

Abstract

Iqaluit International Airport presently suffers from instability and subsidence along its runway, taxiways and apron. Instability may be related to permafrost, permafrost degradation and associated drainage conditions. In particular, Taxiway Alpha is significantly impacted by permafrost degradation and thaw settlement. A suite of geophysical data was collected in 2012–2013 along a selected section of Taxiway Alpha to characterize permafrost conditions and investigate active permafrost processes, including seasonal changes in unfrozen water content. Even with cold permafrost temperatures, the data indicate material types with low electrical resistivity, suggesting fine-grained marine sediments and/or saline pore water with the potential for freezing-point depression and significant unfrozen water content. Observed seasonal changes in the data indicate that subsurface temperature fluctuations may result in significant ice formation near the thaw table and changes in unfrozen moisture content in the permafrost.

Résumé

L'instabilité et l'affaissement du sol risquent de causer des dommages à la piste de l'aéroport international d'Iqaluit, ainsi qu'à ses voies de circulation et son aire de trafic. Cette instabilité peut être le résultat de l'action du pergélisol, de la dégradation de ce dernier et des conditions de drainage qui lui sont associées. La voie de circulation Alpha est tout particulièrement touchée par les effets de la dégradation du pergélisol et du tassement dû au dégel. Une série de données géophysiques a été recueillie en 2012–2013 le long d'une section déterminée de la voie de circulation Alpha en vue d'établir les caractéristiques propres aux conditions du pergélisol et d'étudier les processus actifs liés au pergélisol, notamment les variations saisonnières au niveau de la teneur en eau non gelée. Même dans des conditions où les températures de surface du pergélisol sont froides, les données révèlent qu'il s'agit de types de matériel à faible résistivité électrique, ce qui semble indiquer la présence de soit des sédiments marins à grain fin, soit d'eau interstitielle saline, ou les deux, lesquels peuvent être aussi bien sujet à des affaissements lorsque le point de congélation est atteint que se caractériser par la présence d'une teneur élevée en eau non gelée. Des variations saisonnières dans les données semblent indiquer que les fluctuations de la température enregistrées en subsurface peuvent potentiellement entraîner la formation de quantités importantes de glace à proximité du plafond du pergélisol, ainsi que des changements au niveau de la teneur en eau non gelée au sein du pergélisol.

Introduction

Permafrost and associated ground ice can affect land-based infrastructure through their influence on ground stability and drainage patterns. Iqaluit International Airport, in the capital of Nunavut, experiences noticeable settlement and frost-cracking problems that affect engineered surfaces, such as the runway, taxiways, aprons and embankments. Deterioration requiring significant repair has been attributed to excessive permafrost degradation associated with the presence of water, possibly extending beneath engineered surfaces in places (Knapik and Hanna, 1998). Despite extensive studies and remediations, recurring settlement, deformation and noticeable damage have required several campaigns of resurfacing and reparation (Larochelle and Haché, 1991; Dietrich and Mitchell, 2011). Detailed and extensive characterization of permafrost and changing permafrost conditions is critical for understanding risks to airport infrastructure and to other land-based infrastructure

This publication is also available, free of charge, as colour digital files in Adobe Acrobat® PDF format from the Canada-Nunavut Geoscience Office website: http://cngo.ca/summary-of-activities/2013/.

across Canada's North. In addition, a better understanding of permafrost processes is required, particularly with respect to the role of groundwater and unfrozen water content, and the relationship to thaw susceptibility of materials.

To this end, the Geological Survey of Canada (GSC), in cooperation with the Canada-Nunavut Geoscience Office (CNGO), has established a geophysical test site on Taxiway Alpha of the Iqaluit International Airport to investigate the potential for electrical resistivity surveys to resolve important Earth features, such as sediment or terrain type, ice-bearing sediment, ice-rich regions, thaw zones and unfrozen water, in Canada's continuous permafrost region. The distinct electrical properties of frozen ground make electrical and electromagnetic geophysics a potential tool for spatially extensive and noninvasive characterization of permafrost terrain (e.g., Scott et al., 1990; Hauck et al., 2003; Ross et al., 2007; Fortier et al., 2008; Wolfe et al., 2013). An innovative experiment uses time-lapse data collection and integration of multiple data types to assess the ability to image subsurface changes in unfrozen water content, both spatially and temporally. Unfrozen water content is an important variable in calculating the thermal properties of sediment, which are used to predict the behaviour of the ground upon warming and thawing.

Study area

Iqaluit International Airport (YFB, CYFB) is located in Iqaluit, Nunavut, at the head of Frobisher Bay on Baffin Island (Figure 1a). It is built on flat terrain surrounded by hills and rocky plateaus of the Precambrian shield within the continuous permafrost zone (Heginbottom et al., 1995). The surficial geology was mapped by Allard et al. (2012). The present-day Runway 17/35 was originally constructed (in part) in 1942, followed by a runway extension in 1948. The 1942 portion of Runway 17/35 is built on glaciomarine delta deposits composed of sand, silt, boulders and gravel; the 1948 portion is built on glaciofluvial outwash, bedrock and fill. Alluvial channels and lacustrine deposits are present under the embankments of taxiways, aprons and access roads, and till and marine sediments are observed in the immediate area (Figure 1b). These smaller scale deposits (particularly former lake sediments and stream deposits that were covered by infilling during construction) may play a critical role in determining permafrost conditions due to their relationship with water channelling (alluvial sediments) or excess ice (fine-grained sediments); knowledge of their subsurface extent is therefore important.

This study focuses on Taxiway Alpha (Taxi A), which is a known area of distress that includes differential settlement, undulation and cracking, and displacement (LeBlanc et al., 2012; Short et al., 2012; Short et al., 2013). In response to this distress, the pavement was removed from a section of Taxi A in 2010, thus restoring it to a granular surface. The

stratigraphy underlying Taxi A comprises approximately 1–4 m of gravel embankment material (unlikely to be frost susceptible) overlying silty sand to sandy silt to depths of at least 7 m. The bedrock surface was encountered during cored drilling in the middle of Taxi A at approximately 7.4 m depth (M. Allard, pers. comm., 2013). Bedrock was also possibly encountered during air-track drilling (no recovery) along the shoulder of Taxi A at 16–17 m depth, demonstrating that the bedrock surface can be expected to have relatively strong topography in the area. Groundwater has been reported to flow in a northeast direction under Taxi A (Larochelle and Haché, 1991), presumably along the base of the active layer.

The mean annual ground temperature for southern Baffin Island is −5 to −10°C, with low to high occurrence of ground ice, including ice wedges and massive ice bodies (Heginbottom et al., 1995; Allard et al., 2012). As part of GSC-CNGO activities, thermistor cables were installed in 2010 and 2011 in the natural terrain and within the embankment infrastructures (LeBlanc et al., 2013). The permafrost temperature recorded in natural terrain is approximately −5°C at a depth of 10 m with an active-layer thickness of 1.5 m. Active-layer thickness is locally observed to be variable and can be in excess of 4 m under paved infrastructure (Larochelle and Haché, 1991; Dietrich and Mitchell, 2011).

Methods

Electrical resistivity

Electrical resistivity of Earth materials is a complicated function of many variables. However, in most near-surface sedimentary environments, it depends primarily on the amount and connectivity of the pore water and the mobility of charge-carrying ions in the pore water. Permafrost has a strong electrical signature because the freezing of water greatly reduces the availability and connectivity of pore water for electrolytic conduction, which results in a significant increase in electrical resistivity (King et al., 1988). Conversely, regions of unfrozen ground within permafrost terrain will have relatively low electrical resistivity. Although permafrost is generally electrically resistive, appreciable clay content or saline pore water can result in reduced electrical resistivity due to increased pore-water conductivity and freezing-point depression (e.g., Ross et al., 2007). Measurements of electrical resistivity in permafrost terrain can generally be used to interpret some combination of material type, temperature and the frozen or unfrozen state of pore water; measurements taken over time can be compared to infer changes in dynamic properties, such as temperature, moisture or ice content, while suppressing the effects of material heterogeneity or systematic errors (LaBrecque and Yang, 2001).

For time-lapse monitoring, a permanent array of 72 electrodes at 2 m spacing was buried along the shoulder of
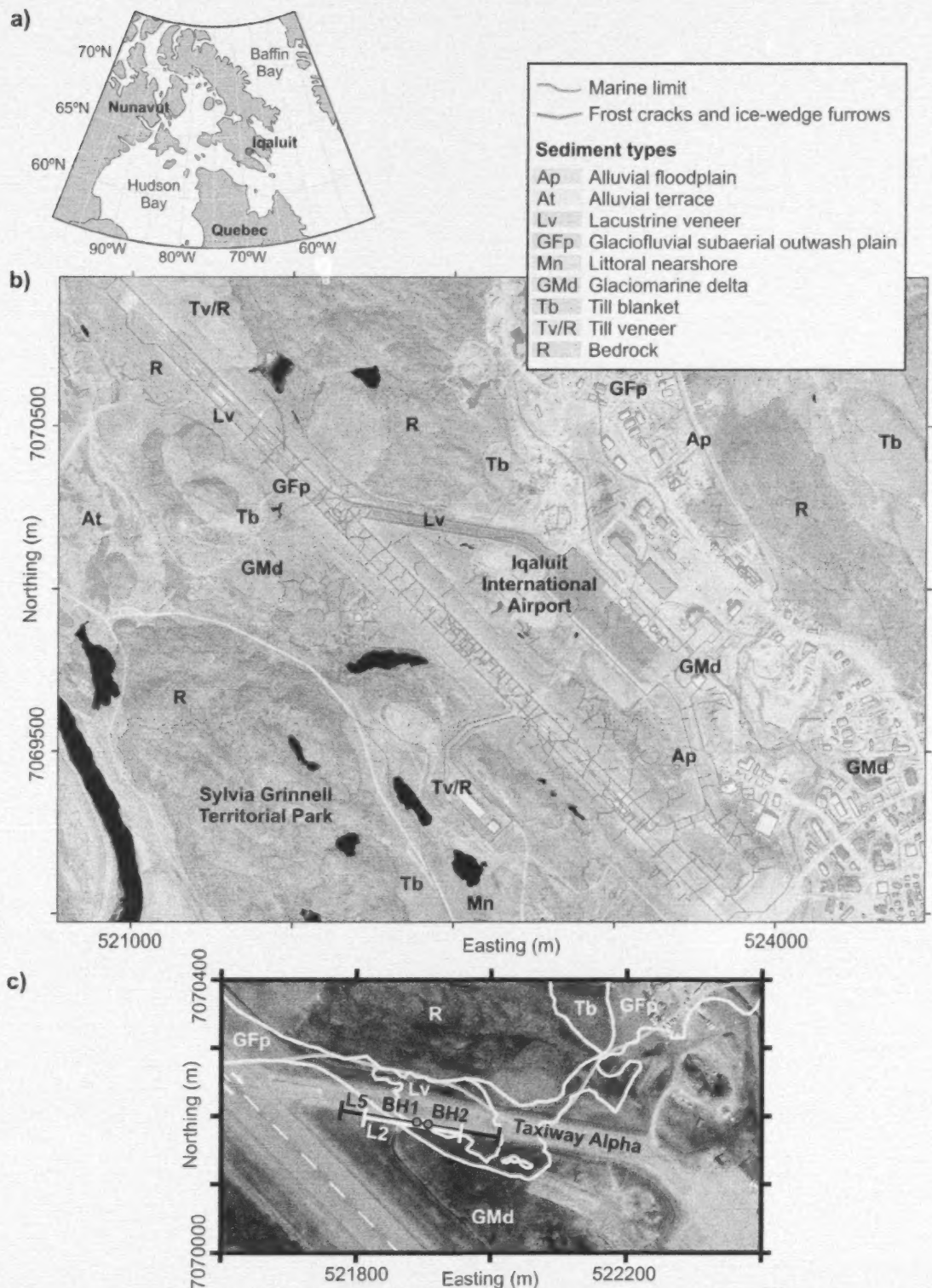
Figure 1: Iqaluit International Airport study area, showing **a)** location of Iqaluit at the head of Frobisher Bay, Baffin Island, Nunavut; **b)** mapped surficial geology of the airport and immediate area (Allard et al., 2012); **c)** Taxiway Alpha and locations of electrical resistivity survey lines L2 and L5 (white and black) and borehole installations BH1 and BH2 (red). QuickBird satellite image, July 25 2006, © DigitalGlobe Inc., all rights reserved.

Taxi A in July 2012 (L2 in Figure 1c). Installed electrodes help to reduce the contact resistance (which is high in permafrost terrain) and improve the stability of the data over time. Electrodes were constructed of 15 by 15 cm sheets of type 316 stainless-steel mesh wrapped over a small PVC ring to maximize surface area and buried at a depth of 0.3 m (Figure 2). Type 316 stainless-steel hose clamps physically connect each electrode to 18 AWG single-conductor direct-burial tracer wire with 600 V polyethylene insulation. Individual wires help to minimize errors associated with voltage leakage between electrodes in the active circuit. Wires were buried and routed to a central control box off the taxiway that could easily be accessed for data collection. Data collection is not automated. In addition to the installed electrode array, a one-time experiment using 48 removable electrodes at 5 m spacing was conducted in July 2012 to provide information at increased depth (L5 in Figure 1c; LeBlanc et al., 2013, Figure 5).

Borehole installations

The Taxi A monitoring installation was completed in 2013. In March, two air-track boreholes (10.2 cm diameter) were drilled by Canadrill Ltd. along Taxi A (Figures 1c, 3a). Borehole BH1 was instrumented with 31 electrodes at 0.5 m spacing from 0.5 to 15.5 m depth, installed on capped PVC casing (Figure 3b). The casing was filled with silicone oil in March and, in July, BH1 was completed with a string of 18 YSI 44033 thermistors from 0.5 to 14.75 m depth. Thermistor cables and electrode wires were buried and routed to near the L2 central control box for data collection (Figure 3c). No logger was installed for the thermistor cable and data collection is not automated for the electrodes. Borehole BH2 was instrumented with 24 electrodes at 0.5 m spacing from 0.5 to 12 m depth and 10 Decagon EC-5 dielectric moisture sensors from 0.3 to 11.8 m depth, installed on open PVC casing filled with sand (Figure 4a). In July, dielectric sensor cables and electrode wires were buried and routed to a control box off Taxi A for data collection

Figure 2: Installation of a permanent electrical resistivity monitoring system along Taxi A, Iqaluit International Airport study area, Baffin Island, Nunavut: a) single electrode; b) placement of electrodes at 30 cm depth; c) wiring of all electrodes in the array, looking toward Runway 17/35.
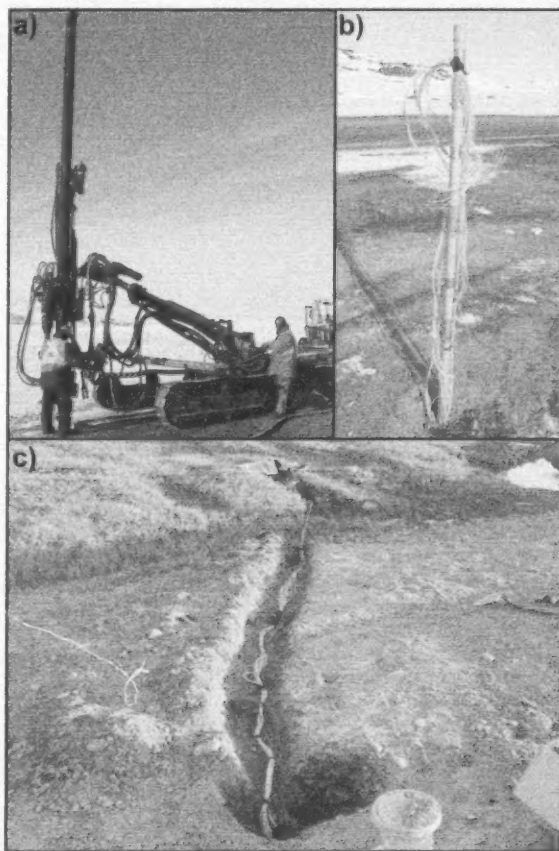
Figure 3: Installation of instrumentation in borehole BH1, Iqaluit International Airport study area, Baffin Island, Nunavut: a) air-track drilling of BH1 on Taxi A; b) installation of PVC casing and electrodes; c) completion of installation with electrode and thermistor cables routed to a common control area.

(Figure 4b). Decagon Em-50 data loggers were installed for the dielectric sensors and are currently recording data hourly. Data collection is not automated for the electrodes (Figure 4c).

Data collection

Electrical resistance data are collected during site visits. Data for the two-dimensional (2-D) resistivity array L2 were collected in the summer after installation (08/2012), the subsequent winter (11/2012) and the following summer (07/2013). After assessing noise levels, the resistance data are inverted using the smoothness-constrained least-squares algorithm of Loke et al. (2003). The resulting electrical resistivity image (ERI) is a 2-D model of subsurface electrical resistivity. Resistance data for the borehole electrodes were collected after installation this summer (07/2013). After assessment of noise, the data are presented as 1-D apparent resistivity.
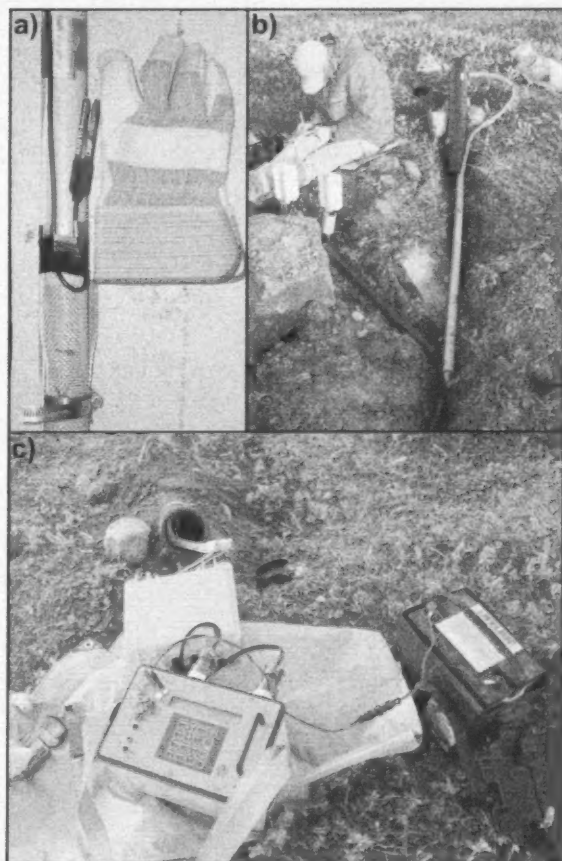
Figure 4: Installation of instrumentation in borehole BH2. Iqaluit International Airport study area, Baffin Island, Nunavut: **a)** Decagon EC-5 dielectric moisture sensor installed 20 cm above an electrode (on centres); **b)** Em-50 data loggers and electrode cables completed off Taxi A; **c)** collection of resistance data.

Temperature data from the thermistor cable were collected after installation this summer (07/2013) using a standard high-precision voltmeter, a full day after installation to allow for equilibration. Similarly, data from the dielectric sensors were collected manually after installation this summer (07/2013), although these data are currently logged continuously.

Preliminary results

The temperature data collected in the summer of 2013 for BH1 are shown in Figure 5a. The temperature trend is similar to that observed in past work, and shows a warming ac-
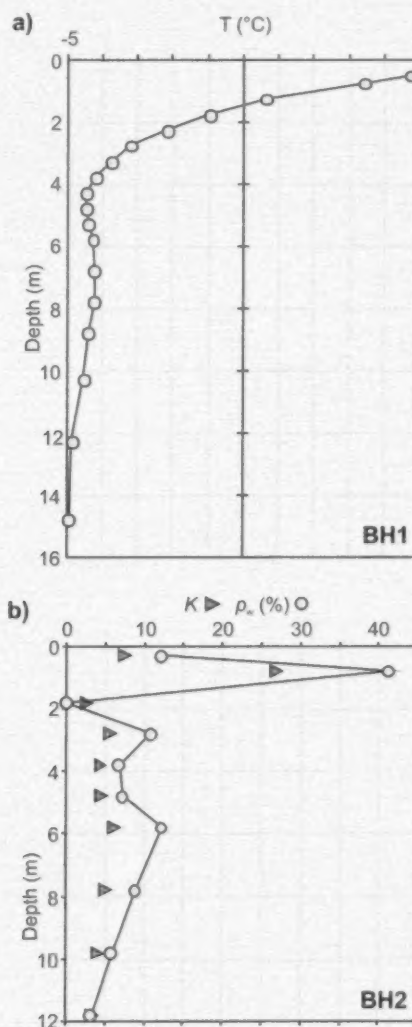
Figure 5: Preliminary monitoring results at the Iqaluit International Airport study area, Baffin Island, Nunavut: **a)** temperature as a function of depth in borehole BH1 on July 14, 2013; **b)** dielectric constant (K) and estimated volumetric percent unfrozen water content (p_w) as a function of depth in borehole BH2 on July 15, 2013.

tive layer with the 0°C point at approximately 1.5 m depth. Borehole BH2 is 16 m away from BH1 and variation of the dielectric constant with depth is shown in Figure 5b. The dielectric constant of Earth materials is a strong function of the unfrozen water content. The observed large increase in dielectric constant above 1.5 m depth is consistent with temperatures above freezing and water saturation during thawing of the active layer. Just below 1.5 m depth, the dielectric constant is at a minimum, which may be indicative of large amounts of ice formed at the onset of the previous winter with abundant water supply. It was noted that there is an apparent correlation between elevated temperature (BH1) and dielectric constant (BH2) at a depth of approximately 6 m.

Within the permafrost at depth, variations in dielectric constant may reflect variations in unfrozen water content, which can be estimated using a multiphase complex refractive-index model (CRIM; e.g., Knight and Endres, 2005). This study utilized dielectric constants of 5, 88, 3 and 1 for the matrix, water, ice and air, respectively, and it was assumed that total porosity was approximately 0.4 above the 0°C point and ice-filled porosity was 0.3 below the 0°C point. The CRIM model is most sensitive to the unknown of unfrozen water content, and realistic changes in the assumed parameters result in variations in estimated water content on the order of 1–2%. Larger errors likely result from void space near the borehole casing.

The resistance data collected in the summer of 2013 for boreholes BH1 and BH2 are shown in Figure 6. The data are presented as pseudo-logs of apparent resistivity for different dipole lengths that correspond to different regions of influence around the borehole. Data in BH1 are sparse due to poor data quality associated with high contact resistances that are inferred to result from excessive void space around the casing, the result of incomplete backfill of the hole after drilling. Nevertheless, a clear trend of decreasing resistivity with depth is evident in the top 6 m (Figure 6a). A similar trend in apparent resistivity is observed in BH2 (Figure 6b). Resistivity decreases significantly to approximately 5 m depth, at which point there is a moderate increase followed by a further decrease to 12 m depth. There are no measurements entirely above the 0°C point; the abrupt decrease in resistivity at 2 m depth is interpreted to be associated with the bottom of the engineered embankment and the top of natural ground (both below the 0°C point). Apparent resistivity decreases to less than 10 Ù·m at depth.

The borehole data can be compared to the 2-D ERI model recovered from the electrode-array data. The interpreted model from summer 2012 is shown in Figure 7, along with representations of the borehole results. At the surface, a resistive surface layer (1000–5000 Ù·m) approximately 2 m thick is interpreted to be the coarse-grained embankment material. This layer appears to thicken to the west. Low-re-

sistivity material (5–200 Ù·m) occurs below the resistive surface layer, the observed variability being interpreted to distinguish lacustrine sediments (Lv), glaciofluvial sediments (GFp) and glaciomarine sediments (GMd). The lowest resistivities are associated with GMd and are on par with those observed for the borehole data (Figure 6). The resis-
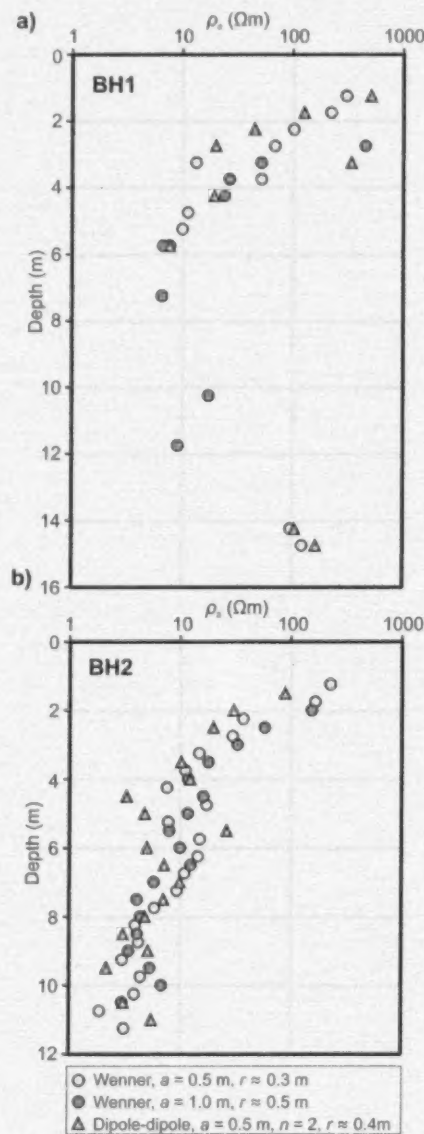
Figure 6: Resistance data collected in the summer of 2013 for boreholes BH1 and BH2 at the Iqaluit International Airport study area, Baffin Island, Nunavut: a) apparent resistivity (ñₐ) as a function of depth and dipole length in BH1 on July 14, 2013; b) apparent resistivity (ñₐ) as a function of depth and dipole length in BH2 on July 15, 2013; vertical resolution is approximately three times the dipole length (a); region of influence (r) around the borehole is a function of dipole length.
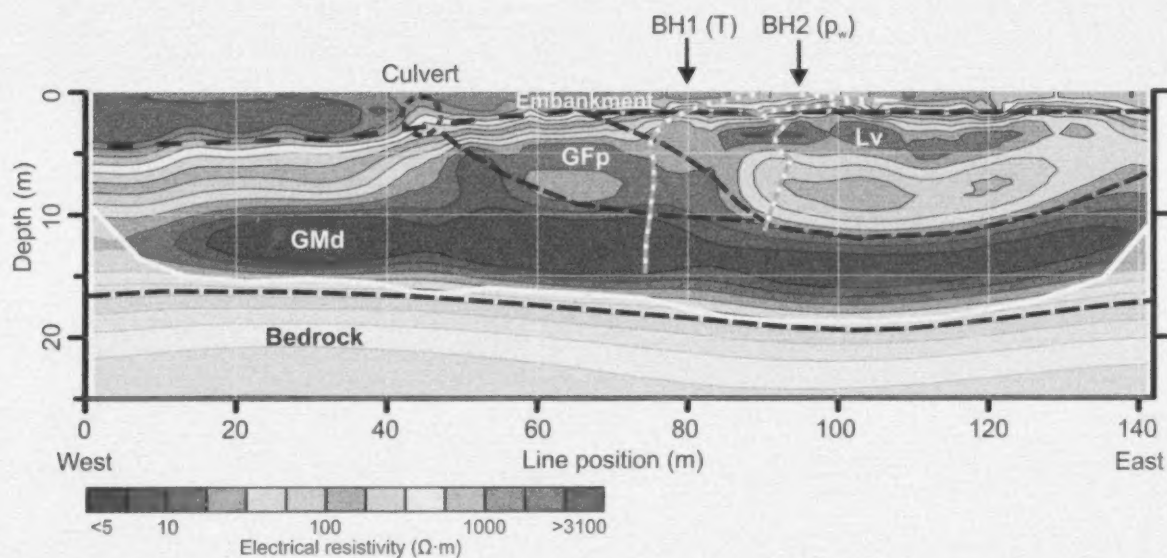
Figure 7: Interpreted electrical resistivity model for August 2, 2012, Iqaluit International Airport study area, Baffin Island, Nunavut. Locations of boreholes BH1 and BH2 are given, along with curves (dashed grey and white) for temperature (T) and estimated volumetric percent unfrozen water content (p_w). The bold white line shows the approximate limit of resolution for the given data and model. Vertical exaggeration is 1.5 times.

tivity structure of Lv is interpreted to be layered, with a transition at approximately 6 m depth to a more resistive signature, as observed in BH2 (Figure 6b). The bedrock surface is interpreted to be relatively flat along the section and is interpreted to be the cause of the elevated resistivity at the bottom of BH1 (Figure 6a). However, ERI resolution inevitably decreases with depth, and this is exacerbated by the highly conductive overburden such that the bedrock contact is poorly resolved and bedrock resistivity is uncertain.

Models recovered from time-lapse data can be compared to examine seasonal changes in the subsurface. Models from the summer of 2012 to the summer of 2013 are shown in Figure 8. Data quality in the winter suffers from poor electrical contact in the embankment material at the surface. The resulting dataset has a reduced number of reliable measurements, particularly at depth. The data scarcity results in a reduction in the interpretable depth of the winter model. Nevertheless, significant increases in winter resistivity can be observed for the ERI model of Taxi A, both at the surface and at intermediate depth. In some cases, this may indicate a thick active layer. In other cases, a reduction in the unfrozen water content is postulated within the permafrost in winter.

Discussion

The electrical resistivities observed in Figure 7 below the embankment material of Taxi A are considered low for permafrost terrain (e.g., Scott et al., 1990). However, there is good agreement between the borehole electrical data, the
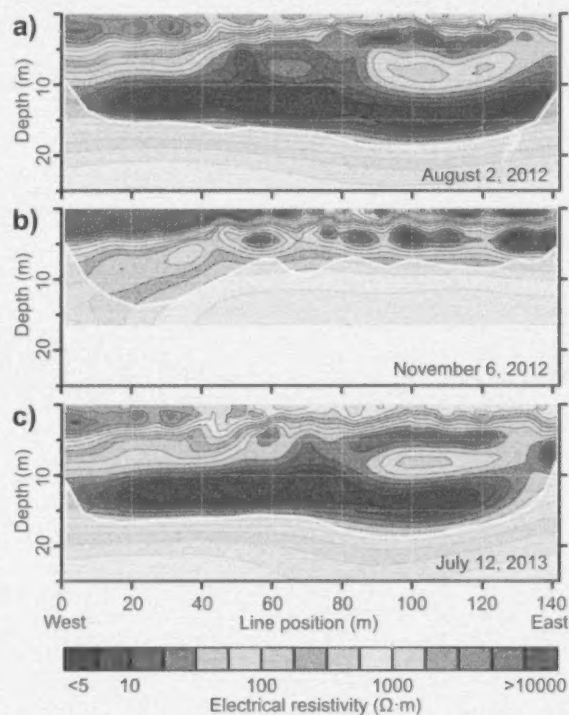
Figure 8: Time-lapse electrical resistivity models for the Iqaluit International Airport study area, Baffin Island, Nunavut: **a)** August 2, 2012; **b)** June 11, 2012; **c)** July 12, 2013. The bold white lines show the approximate limits of resolution for the given data and models. Vertical exaggeration is 2 times.

surface electrical data and data collected from nearby studies in the Iqaluit region using independent methods and equipment (LeBlanc et al., 2013; Oldenborger and LeBlanc, 2013). Observations while drilling suggest relatively homogeneous silt and sand below Taxi A, which alone would not typically account for the observed resistivity or the variations in resistivity. The observed variations in resistivity may result from changes in sediment that are too subtle to be detected in air-track cuttings. Alternatively, variations in resistivity may result from variations in unfrozen water content or variations in pore-water conductivity. The observed low resistivities would be consistent with elevated pore-water conductivity, which would also contribute to freezing point depression and increased unfrozen water content. Elevated pore-water conductivity could occur naturally in the region, given the glaciomarine nature of the sediments and the mapped marine limit (Figure 1). Limited water-conductivity measurements from disturbed borehole cutting samples on Taxi A indicate that salinity increases with depth up to 8 parts per thousand at 12 m; salinities approaching that of seawater have been reported in the vicinity at depths of 10 m (Knapik and Hanna, 1998).

Given the resistive surficial-embankment material, it is difficult to isolate the electrical signature of the summer active layer, which is typically a conductive anomaly in homogeneous ground. If the active layer is entirely within the embankment material, it will have the effect of reducing the summer bulk resistivity due to unfrozen water content. If the active layer extends below the resistive embankment material, it is likely indistinguishable from the conductive natural ground. However, a distinct and significant seasonal increase is observed in surface-layer resistivity, consistent with freezing of the active layer (Figure 8b). Based on this observation, the active layer appears to thicken substantially to approximately 5 m depth to the west where Taxi A joins Runway 17/35. This situation could lead to ponded water on the thaw table.

Within the active layer, there may be a temperature component to the electrical resistivity. Above the freezing point, the temperature of the pore water will affect the ionic mobility, resulting in an increase in the electrical conductivity of the pore water by approximately 2% per °C (Hayashi 2004). For the observed temperatures, this will correspond to a decrease in resistivity of less than 10% from the surface to the 0°C depth at 1.5 m, a variation that is neither significant nor resolvable with the given experiment. Below the freezing point, resistivity will be a function primarily of the freezing of pore water.

Economic considerations

Infrastructure forms an important foundation for Nunavut's economy in terms of community development and mineral exploration (Costello et al., 2011). Iqaluit International Airport is a critical component of Nunavut's infrastructure for activities in the Qikiqtaaluk Region and across Canada's North. Considerable action is planned by the Government of Nunavut to upgrade and repair Iqaluit International Airport, including runway resurfacing, apron expansion and new facility construction, at a cost of approximately $300 million. This expenditure emphasizes the importance of the airport, demonstrates the costs associated with infrastructure in permafrost terrain and stresses the value of a basic understanding of permafrost processes. This study provides baseline information on the current and evolving conditions of permafrost at Iqaluit International Airport and will contribute to a better understanding of permafrost processes that influence stability and degradation of land-based infrastructure.

Conclusions

A suite of geophysical data was collected in 2012–2013 along a selected section of Taxiway Alpha at the Iqaluit International Airport in order to characterize permafrost conditions and investigate active permafrost processes, including seasonal changes in unfrozen water content. The data indicate material types with low electrical resistivity despite the cold permafrost temperatures, suggesting fine-grained marine sediments and/or saline pore water with the potential for freezing-point depression and significant unfrozen water content. Observed seasonal changes in the data indicate that subsurface temperature fluctuation may result in significant ice formation near the frost table and changes in unfrozen water content in the permafrost. Changes in water content within the permafrost will affect the heat budget and will be accompanied by some degree of heave and subsidence associated with the phase change. The continued monitoring of the site will enable further understanding of the data and the active processes.

Acknowledgments

References

Allard, M., Doyon, J., Mathon-Dufour, V., LeBlanc, A.-M., L'Hérault, E., Mate, D., Oldenborger, G.A. and Sladen W.E. 2012: Surficial geology, Iqaluit, Nunavut; Geological Survey of Canada, Canadian Geoscience Map 64, scale 1:15 000.

Costello, K., Senkow, M., Bigio, A., Budkewitsch, P. and Ham, L. 2011: Nunavut mineral exploration, mining and geoscience overview 2011; Aboriginal Affairs and Northern Development Canada.

Dietrich, J.B. and Mitchell G. 2011: Geotechnical investigation, Taxiway A, Iqaluit Airport (CYFB), Iqaluit, Nunavut; unpublished report prepared by Peto MacCallum Ltd. for Genivar Inc., 11KF074.

Fortier, R., LeBlanc, A.-M., Allard, M., Buteau, S. and Calmels, F. 2008: Internal structure and conditions of permafrost mounds at Umiujaq in Nunavik, Canada, inferred from field investigation and electrical resistivity tomography; Canadian Journal of Earth Sciences, v. 45, p. 367–387.

Hauck, C., Vonder Muhll, D. and Maurer, H. 2003: Using DC resistivity tomography to detect and characterize mountain permafrost; Geophysical Prospecting, v. 51, p. 273–284.

Hayashi, M. 2004: Temperature-electrical conductivity relation of water for environmental monitoring and geophysical data inversion; Environmental Monitoring and Assessment, v. 96, p. 119–128.

Heginbottom, J.A., Dubreuil, M.H. and Harker, P.T. 1995: Canada, permafrost; in National Atlas of Canada, 5th edition, Plate 2.1, MCR 4177.

King, M.S., Zimmerman, R.W. and Corwin, R.F. 1988: Seismic and electrical properties of unconsolidated permafrost; Geophysical Prospecting, v. 36, p. 349–364.

Knapik, D.J. and Hanna A. J. 1998: Foundation soils investigation, settlement of Apron III extension, Iqaluit Airport, Iqaluit, NT; unpublished report prepared by AGRA Earth & Environmental Ltd. for the Government of the Northwest Territories, Department of Transportation.

Knight, R.J. and Endres, A.L. 2005: An introduction to rock physics principles for near-surface geophysics; in Near-Surface Geophysics, D.K. Butler (ed.), Society of Exploration Geophysicists, p. 31–70.

LaBrecque, D.J. and Yang, X. 2001: Difference inversion of ERT data: a fast inversion method for 3-D in-situ monitoring; Journal of Environmental and Engineering Geophysics, v. 6, p. 83–89.

Larochelle, Y.P. and Haché, J.G.A.R. 1991: Geotechnical study, Alpha Taxiway, Iqaluit Airport; unpublished report prepared by Jacques Whitford Ltd. for Public Works Canada.

LeBlanc, A.-M., Short, N., Oldenborger, G.A., Mathon-Dufour, V. and Allard, M. 2012: Geophysical investigation and InSAR mapping of permafrost and ground movement at the Iqaluit Airport; in Cold Regions Engineering 2012: Sustainable Infrastructure Development in a Changing Cold Environment, B. Morse and G. Doré (ed.), American Society of Civil Engineers, p. 644–654.

LeBlanc, A.-M., Mathon-Dufour, V., Allard, M., Oldenborger, G.A., Short, N., L'Hérault, E. and Sladen, W.E. 2013: Permafrost characterization at the Iqaluit International Airport, Nunavut, in support of decision-making and planning; in Summary of Activities 2012, Canada-Nunavut Geoscience Office, p. 131–142.

Loke, M.H., Acworth, I. and Dahlin, T. 2003: A comparison of smooth and blocky inversion methods in 2D electrical imaging surveys; Exploration Geophysics, v. 34, p. 182–187.

Oldenborger, G.A. and LeBlanc, A.-M. 2013: Capacitive resistivity inversion using effective dipole lengths for line antennas; Journal of Applied Geophysics, v. 98, p. 229–236.

Ross, N., Brabham, P.J., Harris, C. and Christiansen, H.H. 2007: Internal structure of open system pingos, Adventdalen, Svalbard: the use of resistivity tomography to assess ground-ice conditions; Journal of Environmental and Engineering Geophysics, v. 12, p. 113–126.

Scott, W.J., Sellmann, P.V. and Hunter, J.A. 1990: Geophysics in the study of permafrost; in Geotechnical and Environmental Geophysics, W.J. Ward (ed.), Society of Exploration Geophysicists, p. 355–384.

Short, N., LeBlanc, A.-M., Sladen, W.E., Allard, M. and Mathon-Dufour, V. 2012: Seasonal surface displacement derived from InSAR, Iqaluit, Nunavut; Geological Survey of Canada, Canadian Geoscience Map 66, scale 1:15 000.

Short, N., LeBlanc, A.-M., Sladen, W., Oldenborger, G. and Mathon-Dufour, V. and Briso, B. (2014): RADARSAT-2 D-InSAR for ground displacement in permafrost terrain, validation from Iqaluit Airport, Baffin Island, Canada; Remote Sensing of Environment, v 141, p. 40–51.

Wolfe, S., Stevens, C.W., Gaanderse, A.J. and Oldenborger, G.A. 2014: Lithalsa distribution, morphology and landscape associations in the Great Slave Lowland, Northwest Territories, Canada; Geomorphology, v. 204, p. 302–313, URL <http://dx.doi.org/10.1016/j.geomorph.2013.08.014> [November 13, 2013].

Coastal geoscience for sustainable development in Nunavut: 2013 activities

N.J. Couture[1,2], M.R. Craymer[3], D.L. Forbes[2,4], P.R. Fraser[2], J.A. Henton[5], T.S. James[6,7], K.A. Jenner[2], G.K. Manson[2], K.M. Simon[7], R.J. Silliker[3] and D.J.R. Whalen[2]

[1]Geological Survey of Canada, Natural Resources Canada, Ottawa, Ontario, ncouture@nrcan.gc.ca

[2]Geological Survey of Canada, Natural Resources Canada, Dartmouth, Nova Scotia

[3]Canadian Geodetic Survey, Natural Resources Canada, Ottawa, Ontario

[4]Department of Geography, Memorial University, St. John's, Newfoundland and Labrador

[5]Canadian Geodetic Survey, Natural Resources Canada, Sidney, British Columbia

[6]Geological Survey of Canada, Natural Resources Canada, Sidney, British Columbia

[7]School of Earth and Ocean Sciences, University of Victoria, Victoria, British Columbia

Abstract

Natural Resources Canada scientists and partners are assessing coastal conditions at various sites in Nunavut to help determine coastal stability and predict future changes. Mapping of coastal landforms and material composition has been carried out for over 2500 km of coastline in southern Coronation Gulf. Coastal stability was assessed at an existing mining port facility (Roberts bay[8]) and a planned one (Grays Bay). Results indicate that the shoreline at Roberts bay is relatively stable, although there is some sedimentation at the mouth of one river, and some erosion of ice-rich backshore cliffs. The coast around Grays Bay also shows little overall change due to the predominance of bedrock in the region. However, there are pockets where erosion is occurring and areas where progradation has occurred. A preliminary investigation shows that a method developed for the mapping of bottom-fast ice (BFI) in the Mackenzie Delta, using synthetic aperture radar imagery, can be successfully applied to identify BFI in the Coppermine River delta as well. Data indicative of past relative sea level were collected from 18 sites around the hamlet of Arviat and, together with previously published observations, were used to determine a regional Holocene sea-level curve. This information, together with results from a Global Positioning System (GPS) site near the hamlet, shows present-day crustal uplift of just under 10 mm/yr. Two new continuous GPS sites were installed at Ennadai Lake and Repulse Bay to measure vertical crustal motion. An improved model of vertical crustal motion is being developed that will assist with making projections of relative sea-level change in the territory.

Résumé

Les chercheurs de Ressources naturelles Canada et leurs partenaires procèdent à une évaluation des conditions côtières prévalant à divers sites au Nunavut dans le but d'analyser le niveau de stabilité des côtes et de prévoir les changements futurs. La cartographie des formes de relief côtières et de la composition des matériaux a été réalisée sur une distance couvrant 2500 km de trait de côte de la partie sud du golfe Coronation. Une évaluation de la stabilité des côtes a été complétée dans une installation portuaire minière (baie Roberts) et une autre est prévue (baie Grays). Les résultats révèlent que la ligne de rivage à la baie Roberts est relativement stable, bien que l'embouchure d'une des rivières fasse preuve d'un certain degré de sédimentation et que les falaises à forte teneur en glace de l'arrière-plage présentent des signes d'érosion. Le rivage autour de la baie Grays ne montre que peu de signes de modification globale en raison de la prédominance du substratum rocheux dans la région. On remarque cependant la présence de certains endroits où l'érosion se manifeste et d'autres qui, eux, sont touchés par la progradation. Une enquête préliminaire a établi qu'une méthode mise au point afin de cartographier les glaces de fond du delta du Mackenzie à l'aide d'images prises au moyen d'un radar à synthèse d'ouverture peut également servir à identifier les glaces de fond du delta de la rivière Coppermine. Des données témoignant de changements

---

[8]Place names with the generic in lower case are unofficial.

This publication is also available, free of charge, as colour digital files in Adobe Acrobat® PDF format from the Canada-Nunavut Geoscience Office website: http://cngo.ca/summary-of-activities/2013/.

relatifs du niveau marin antérieurs ont été recueillies à 18 sites entourant le hameau d'Arviat et, combinées aux renseignements préalablement publiés provenant d'observations sur le terrain, ont servi à établir une courbe régionale du niveau marin au cours de l'Holocène. En conjuguant cette information aux résultats obtenus d'un site de système mondial de localisation (GPS) situé à proximité du hameau, il a été possible de démontrer que le soulèvement actuel de la croûte terrestre ne dépasse pas 10 mm par année. Deux nouveaux sites GPS continus ont été installés au lac Ennadai et à la baie Repulse dans le but de mesurer le degré de mouvement vertical de la croûte terrestre. On procède actuellement à la mise au point d'un modèle amélioré des mouvements verticaux de la croûte terrestre qui devrait aider à l'établissement de prévisions quant aux changements relatifs du niveau marin dans le territoire.

Introduction

Scientists at Natural Resources Canada (NRCan), along with colleagues from the Canada-Nunavut Geoscience Office (CNGO) and academic partners, have been carrying out research to assess coastal conditions in Nunavut in order to support mining activities and other infrastructure development. A number of approaches are being used to determine the current stability of the coast as well as its vulnerability to future environmental changes. Some of the work is territorial or regional in nature and covers large areas, whereas other elements are tightly focused on local processes. The research encompasses a variety of timescales, ranging from interseasonal alterations in the morphology of delta channels, to multidecadal erosion rates, to long-term changes in relative sea level. The work summarized here focuses on analyses carried out in 2013, but these activities are part of larger multiyear research initiatives of NRCan's Climate Change Geoscience Program (CCGP), Environmental Geoscience Program (EGP), and the Canadian Geodetic Survey (CGS), as well as CNGO's 'Protecting Investments in Infrastructure' project.

Coastal information system (CIS) mapping for Coronation Gulf

With support from CNGO and EGP, scientists in the CCGP used seven hours of colour aerial video and WorldView-2 satellite imagery to map coastal landforms and material composition along 2653 km of the southern Coronation Gulf coast. The original aerial video coverage, with shore-zone commentary, was flown for Environment Canada from August 18 to 25, 1994 (Gillie, 1995), converted to DVD in 2012, and was determined to be of a suitable quality for detailed coastal mapping and interpretation. Aerial video coverage begins at Qikirrarnaq Bluff and continues southwestward to the hamlet of Kugluktuk (Figure 1). WorldView-2 imagery from July 11 and July 16, 2011 (DigitalGlobe Inc., 2011a, b) was used to map the hamlet of Kugluktuk, and eastward for 75 km, where aerial video coverage was unavailable. Aerial video coverage resumes just east of the WorldView-2 imagery and continues to Trap Point on Kiillinnguyaq (formerly Kent Peninsula).

Coastal form and material composition were mapped and interpreted using a coastal information system (CIS), which was developed at the Geological Survey of Canada (Atlantic) in 1994 for coastal information management purposes (Sherin and Edwardson, 1996). The interpreted physical features of the shoreline (Jenner et al., 2003; Sherin et al., 2003) were transferred into an existing ArcGIS-based database as individual layers for each of the backshore, foreshore and nearshore zones. These layers will also be used to populate NRCan's CanCoast geospatial database (Manson et al., 2012).

A sample query of the CIS database shows the variability within the backshore and foreshore zones of the southern Coronation Gulf coast (Figure 1; Table 1). A total of 1300 km (54.3%) of backshore forms are unconsolidated and, when broken down by form type, consist of slopes, wetlands, flats, unconsolidated cliffs, dunes and waterways. The remaining backshore (45.7%) is composed of solid forms, including cliffs and anthropogenic form types. By comparison, the foreshore consists predominantly of beaches (51.9%), with only 20.4% comprising solid outcrop (bedrock). These detailed form and material data are used to ground-truth rates of coastal change at Roberts bay and Grays Bay, which were determined from aerial photographs and satellite imagery (see next section). Furthermore, these coastal data provide specific attribute information for the hamlet of Kugluktuk and can also be used to quantify the variability of the remainder of the southern Coronation Gulf coastline in terms of understanding coastal stability at proposed port sites, coastal sensitivity to climate change, and coastal hazards.

Coastal stability assessments

Studies of historical coastal change at key sites provide baseline data for environmental assessment of these critical areas. Historical airphotos and more recent satellite imagery are used to assess coastal change for Roberts bay and Grays Bay within Coronation Gulf. Aerial oblique video is used to map the physical character of the coastline and to validate the coastal change results from historical photos. Results of this study are summarized here.

Roberts bay (Hope Bay)

Roberts bay extends 6 km into mainland Nunavut and is located 125 km southwest of Cambridge Bay. It has almost 30 km of coastline and provides open-water access for the
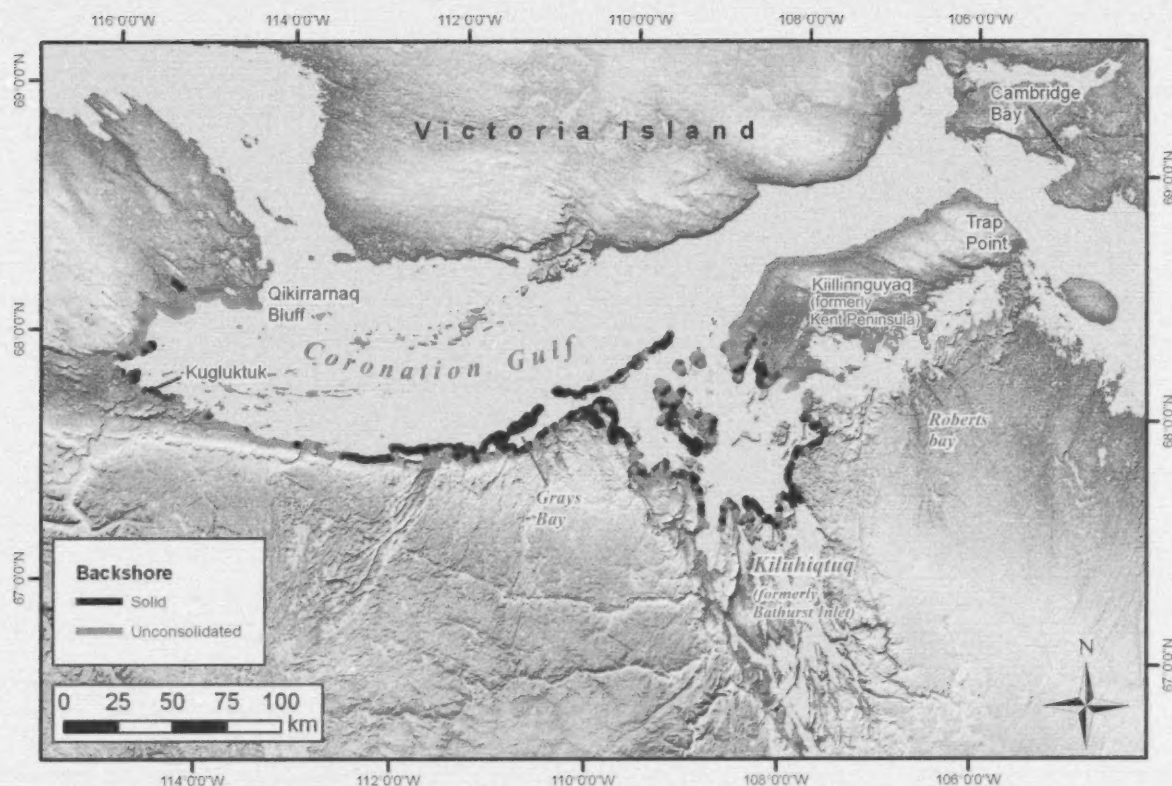
Figure 1: Location map showing the extent of the completed mapping for the southern Coronation Gulf coast, Nunavut. Most of the mapping was interpreted from aerial coastal video, with the exception of 75 km, beginning at the hamlet of Kugluktuk and continuing eastward, which was mapped from WorldView-2 imagery. These data show the distribution of solid versus unconsolidated forms along the backshore. Base image from GeoGratis (2013). Place names with the generic in lower case are unofficial.

Table 1: Summary showing the variability of backshore and foreshore coastal forms and the percentage of solid and unconsolidated backshore forms, Coronation Gulf coast, Nunavut.

Landform types		Length (km)	Percentage
Backshore form supertype			
Unconsolidated		1300	54.3
Solid		1092	45.7
	Total	**2392**	**100**
Backshore form type			
Unmapped		517	21.6
Unconsolidated cliff		36	1.5
Dune		10	0.4
Flat		40	1.7
Unconsolidated slope		1012	42.3
Wetland		55	2.3
Solid cliff		720	30.1
Solid anthropogenic		1	0.1
	Total	**2392**	**69.8**
Foreshore form type			
Unmapped		526	19.8
Beach		1377	51.9
Delta		36	1.4
Flat		170	6.4
Water body		2	0.1
Outcrop		542	20.4
	Total	**2653**	**100.0**

rich mineral deposits of the Hope Bay volcanic belt (AMEC, 2007). Comparison of historical airphotos (1956, 1984, 2000) at Roberts bay to more recent satellite imagery from August 4, 2011 has shown that this coastal region has remained relatively stable since 1956 (Figure 2). The calculated long-term mean shoreline change rate is 2 cm/yr. This slow erosion rate can be attributed to the abundance of bedrock cliffs and the reduced impact of ocean waves and mobile sea ice within the restricted fetch of Roberts bay. There is very little movement of the foreshore beach material, with the exception of the distributary mouth bar and outlet channels associated with one of the major rivers draining into Roberts bay located 0.6 km east of the port facility. Separated from the port site by a large rocky point, the sedimentation appears to be confined to the nearshore area at the river mouth and is unlikely to affect the bathymetry at the port facility (Figure 3). Bathymetric surveys acquired as part of the Roberts bay jetty fisheries authorization monitoring project show no major sedimentation changes for the area surrounding the jetty. In particular there is no evidence that may suggest any nearshore disruption of sediment transport patterns as a result of the jetty construction (Rescan, 2010). The backshore region is composed of bed-

Figure 2: Measurement of shoreline change calculated from comparison of historic airphotos and current satellite imagery at Roberts bay, Nunavut. Image (DigitalGlobe, Inc., 2011c) includes copyrighted material DigitalGlobe, Inc., all rights reserved. Place names with the generic in lower case are unofficial.

rock cliffs, ice-rich, glacially derived unconsolidated material, and raised marine beaches. The backshore cliffs show evidence of erosion and slumping of unconsolidated material, which can be attributed to thawing of ice-rich matter.

Grays Bay

Grays Bay is located east of Kugluktuk and west of Kiluhiqtuq (formerly Bathurst Inlet; see Figure 1). Grays Bay is a strong potential candidate site for a proposed port that would support numerous mining prospects to the south. A study of the coastline at the proposed port site shows very little change since the 1950s in areas dominated by bedrock, although there are pockets showing coastal changes on either side of the proposed port location (Figure 4). The foreshore region is made up primarily of unconsolidated beach material, whereas 33% of the shoreline consists of

low-lying (2–5 m high) bedrock granitoid cliffs. As expected, the coastal change along the cliffs is within the uncertainty of the shoreline measurement and is likely nil in most cases. The foreshore beach material is relatively stable, with the exception of a few localities along the coast that have experienced high levels of erosion (50 m since 1957); other areas have prograded by up to 42 m during the same time period. The backshore region of Grays Bay is characterized by mainly low-lying solid bedrock cliffs covering 61% of the region. The remainder of the backshore is characterized by gently sloping unconsolidated material consisting of glacial till, raised marine terraces and wetland areas. Although there is some sediment accumulation along the beach in front of the unconsolidated sediments, it is still unclear how much of the foreshore material is moving seaward on an annual basis and being deposited into the nearshore zone.

Figure 3: Although the shoreline itself has remained stable, there have been changes in the nearshore sediment extent for a river draining into Roberts bay (Nunavut). Comparison between 1956 and 2011 shows an increase seaward of the channel distributary mouth bar and a bifurcation of the channel. Image (DigitalGlobe, Inc., 2011c) includes copyrighted material DigitalGlobe, Inc., all rights reserved. Place names with the generic in lower case are unofficial.

Investigation of bottom-fast ice (BFI) off Kugluktuk

A series of RADARSAT-2, fine-mode, quad-pol synthetic aperture radar (SAR) images was acquired between November 2011 and June 2012, to observe the freezeup, winter growth, and breakup of nearshore ice in, and adjacent to, the Coppermine River delta at Kugluktuk. A major objective of this work was to test whether methods of SAR interpretation for mapping of bottom-fast ice (BFI) in the Mackenzie Delta could be applied in a smaller Arctic delta with lower freshwater discharge. Previous studies have successfully used SAR imagery for mapping BFI in Arctic lakes (Jefferies et al., 1996) and in Arctic nearshore areas where the water is sufficiently fresh that the SAR signal is able to penetrate through the ice (Eicken et al., 2005; Solomon et

al., 2008a). The imagery was acquired to explore the potential of SAR data for delineating the extent of BFI and for monitoring ice and flood conditions during spring breakup in the Coppermine delta. Understanding the BFI distribution is important as it provides information on shallow-seabed morphology and is also known to have effects on ground temperatures and permafrost aggradation (Solomon et al., 2008b). In addition, BFI restricts the flow of water and sediment during the spring freshet, which can lead to flooding over the nearshore ice and associated hazards, such as strudel scour (Solomon et al., 2008a, b; Dickins et al., 2011).

A preliminary examination of the imagery indicates that the SAR signal is able to penetrate the nearshore ice of the Coppermine delta and that there is potential BFI in channels be-
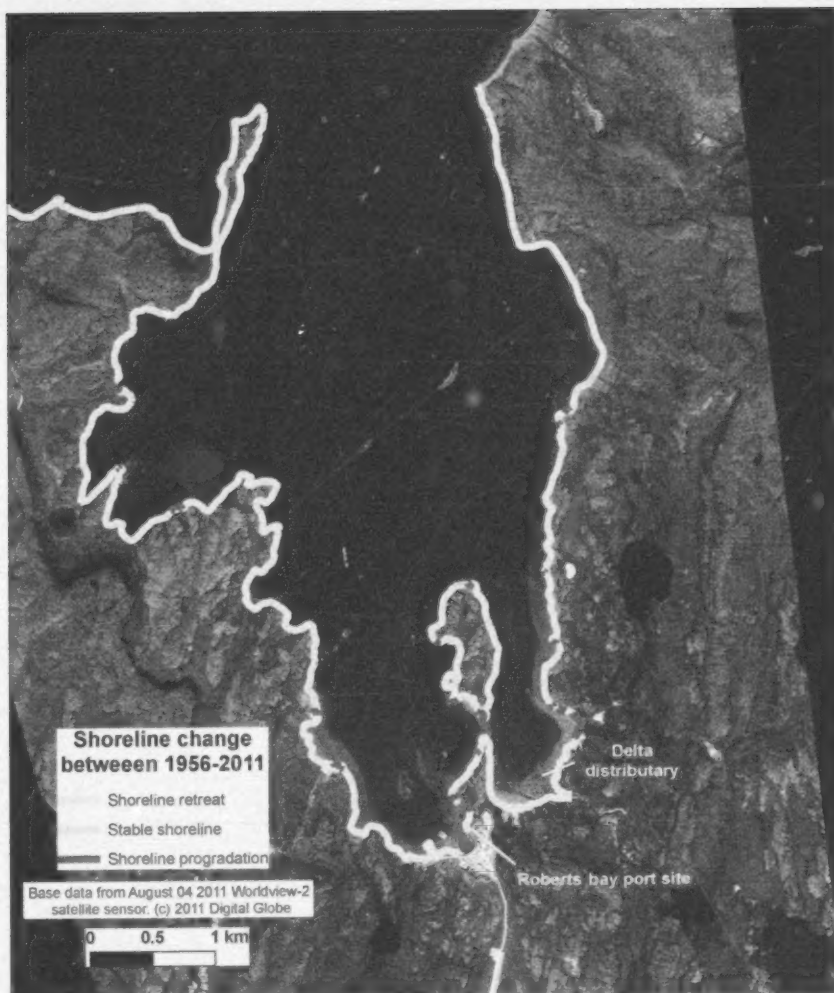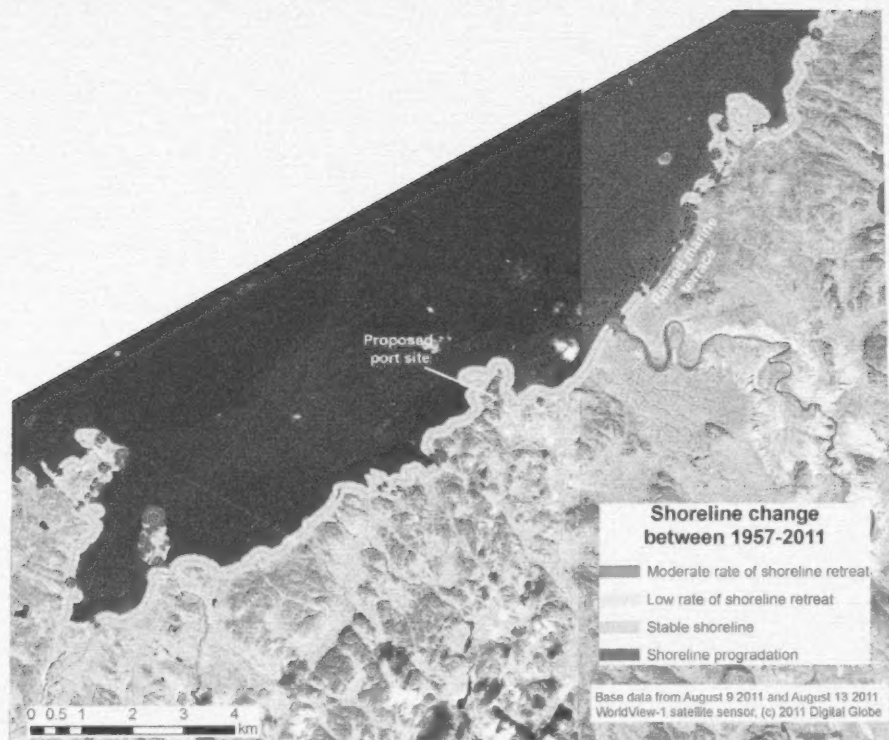
Figure 4: Measurement of coastline change calculated from comparison of historic airphotos and current satellite imagery at Grays Bay, Nunavut. Images (DigitalGlobe, Inc., 2011d, e) includes copyrighted material DigitalGlobe, Inc., all rights reserved.
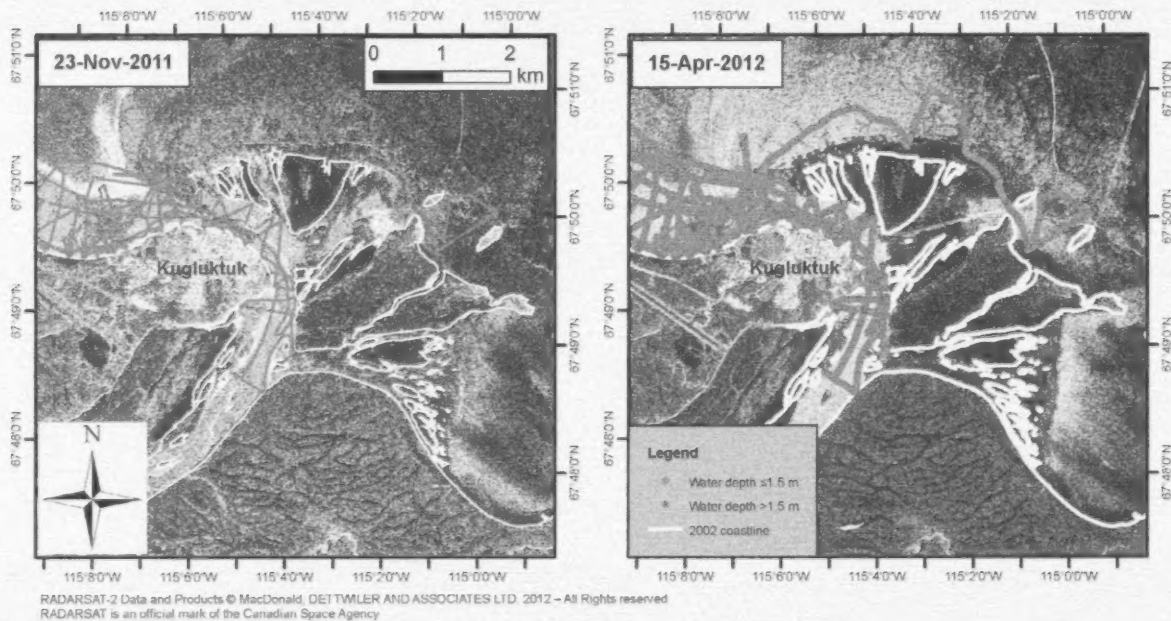
Figure 5: Colour composite (HH-HV-VV–RGB) RADARSAT-2 images of the Coppermine River delta, Nunavut, from November 23, 2011 and April 15, 2012. Green areas in the nearshore are interpreted as floating ice while the dark, low backscatter areas in the nearshore are interpreted as predominantly bottom-fast ice (BFI). The shoreline is shown in white. Red and blue points represent water depths measured using a single beam echo sounder in 2002, 2004 and 2009. Red points are depths ≤1.5 m where BFI development is likely. Blue points are depths >1.5 m. Images from MacDonald, Dettwiler and Associates Ltd. (2011, 2012).

tween islands in the delta, along the outer shore of the delta islands, and along the shore west of the hamlet of Kugluktuk. Figure 5 shows a comparison of RADARSAT-2 composite images from November 23, 2011 and April 15, 2012. Green-toned areas off the delta front are interpreted as floating ice, with the green tones brightening throughout the season as the ice thickens. Dark, low backscatter areas in the nearshore are interpreted as probable BFI and correspond well to water depths less than 1.5 m, as measured using a single-beam echo sounder during the summer months of 2002, 2004 and 2009 (Figure 5). Some channels between the delta islands are green (floating) in the November image but appear dark in the April image, suggesting the ice has thickened and become bottom-fast between the dates of the two images.

Further examination of the imagery is required along with the collection of validation data to gain a better understanding of the timing and extent of BFI and its effects on nearshore permafrost, sediment transport, and the initiation of over-ice flooding and associated hazards during the spring breakup period. Nevertheless, this initial investigation shows the potential for using RADARSAT-2 imagery to delineate BFI in the Coppermine delta.

Sea level change in Hudson Bay

In the summers of 2009 and 2010, fieldwork was carried out west of Hudson Bay, in the vicinity of the community of Arviat. The primary goal of the study was to develop an improved Holocene sea-level history for the region. The fieldwork focused on the collection of indicators of past relative sea level, such as marine shells and algae, driftwood and peat, at locations away from the present-day shoreline. The 25 sites (Figure 6), numbered from high to low elevation, include 18 new locations and 7 previously published locations. Radiocarbon ages of samples obtained from the new locations, when combined with previously published ages, determine a regional Holocene sea-level curve and tightly constrain late Holocene sea-level fall (Simon et al., work in progress).

In 2009, a campaign Global Positioning System (GPS) site, ARVI, was established on bedrock on the outskirts of Arviat (Figure 6b). The site was reoccupied in 2010 and 2012. The preliminary vertical uplift rate is slightly less than 10 mm/yr, similar in magnitude to the uplift rates measured with GPS at Churchill, Manitoba and Baker Lake, Nunavut. Additional occupations of the campaign site will refine the uplift rate and help to supplement sparse regional continuous GPS coverage. Both the improved sea-level curve and present-day uplift rate can be used to improve models of glacial isostatic adjustment. In particular, the observations place constraints on the thickness history of the Laurentide ice sheet west of Hudson Bay (Simon et al., work in progress).
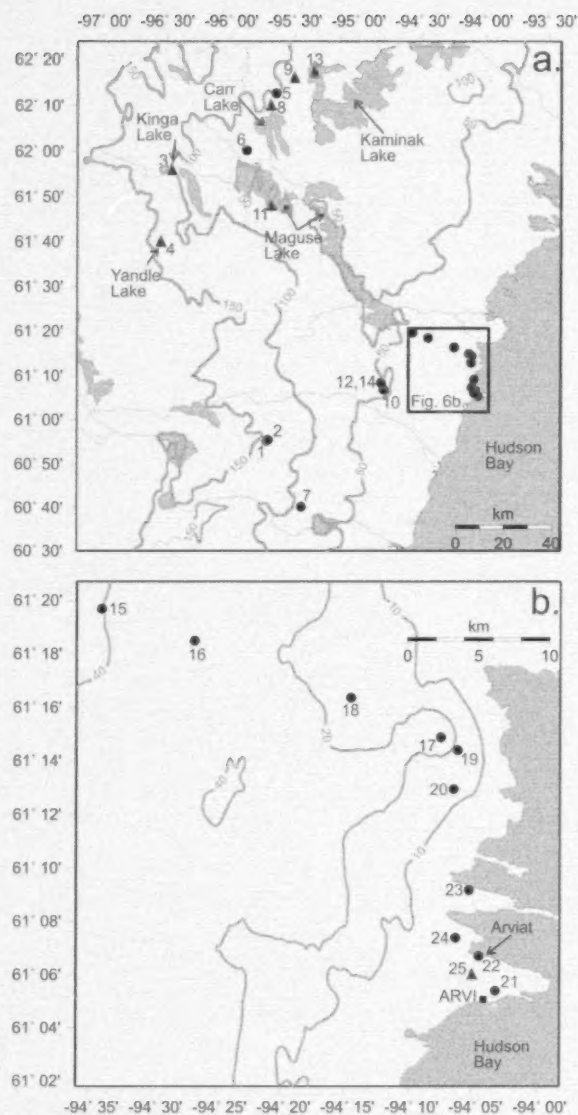
Figure 6: Site locations of previously published (triangle) and new (circle) relative sea-level observations near Arviat, Nunavut: **a)** Data from higher elevations are found up to 150 km away from the shoreline. **b)** Data from lower elevations are closer to the coastal community of Arviat. Site locations are numbered sequentially from high to low elevation; grey contours show regional elevations in metres. The location of the campaign GPS bedrock site, ARVI, is shown by the black square.

Territorial GPS coverage

In 2013, CGS, NRCan, installed two new continuous GPS sites in Nunavut, one at Ennadai Lake and the other at Repulse Bay (Figure 7). The two new sites augment the existing northern coverage of continuous sites operated by CGS, including eight sites in Nunavut.
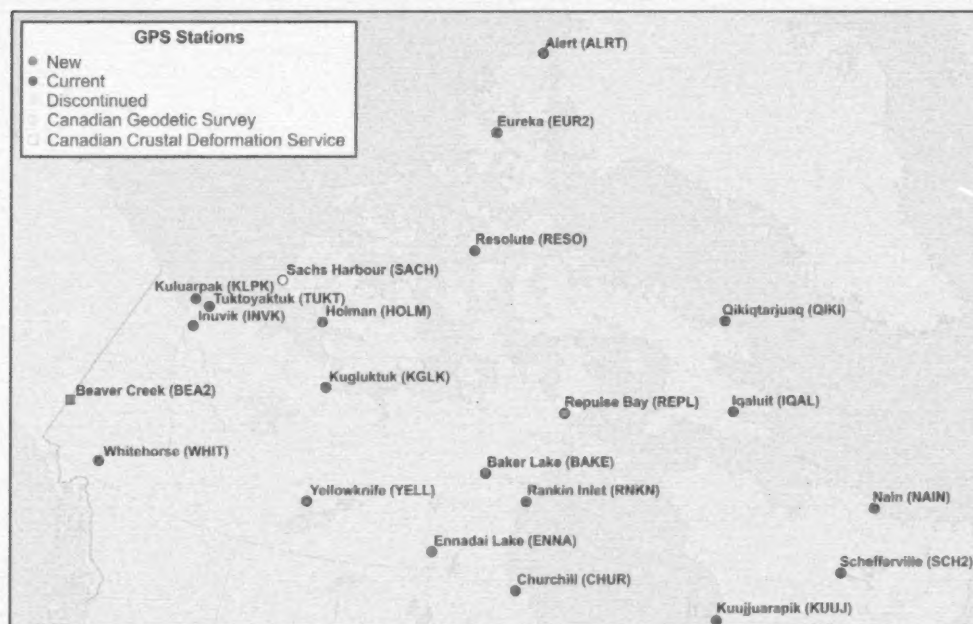
Figure 7: Location map of continuous GPS sites in northern Canada operated by Natural Resources Canada. The four-character station abbreviations are given in brackets.

The CGS maintains the vertical reference frame for Canada, including models of the vertical crustal motion. Across much of Canada, the land is rising and sinking due to glacial isostatic adjustment (GIA), which is the delayed response of the Earth to the surface loading and unloading caused by the continental ice sheets of the last ice age. The largest GIA uplift in Canada is thought to be located in mainland Nunavut and the adjacent Northwest Territories. The new site at Ennadai Lake was chosen to measure the expected large uplift rate. The second site, located at Repulse Bay, was chosen to fill a gap in northern coverage where crustal uplift rates are also expected to be large. The vertical motion observed from northern coastal GPS sites will be used for projections of relative sea-level change being generated by the CCGP of NRCan.

Links to other coastal research activities in Nunavut

The research described here furthers the investigations into coastal characterization and vulnerability of coastal infrastructure, carried out in 2012 with support from CNGO under NRCan's CCGP and EGP, as reported by James et al. (2013). Other studies provide additional information on specific coastal conditions in Nunavut. For instance, assessments of landscape hazards and climate change impacts for a number of Nunavut coastal communities can be found in the present volume, including reports on Arviat (Forbes et al., 2014), Cambridge Bay (Smith and Forbes, 2014), Kugluktuk (Smith, 2014) and Whale Cove (Allard et al., 2014). Similar studies which incorporated adaptation

planning have been conducted in the past for Iqaluit (Hatcher et al., 2011), Hall Beach (Forbes et al., 2008) and Clyde River (Forbes et al., 2007, 2008). Barrie et al. (1979) did reconnaissance for marine terminal planning in the high Arctic. Taylor et al. (2012) mapped the coastal geomorphology and physical characteristics of the islands known as the Findlay Group. The causes of current and former shoreline change have been examined at Kugluktuk (Manson et al., 2005), Lowther Island (St-Hilaire-Gravel et al., 2010), and along Barrow Strait and Lancaster Sound (Taylor and Frobel, 2006). Some studies have focused on specific coastal processes such as the effects of sea ice and shore ice (e.g., Taylor and McCann, 1976; Taylor, 1978; Forbes and Taylor, 1994), while insight into general geomorphology and processes for polar coasts is provided by Forbes and Hansom (2011), and for all of Canada's coasts by Shaw et al. (1998). Many of these studies are complementary and build on the results from earlier ones. Taken together, they help to deepen our understanding of coastal conditions in Nunavut, and provide stakeholders with the knowledge they need to make decisions about infrastructure planning and development.

Economic considerations

Coastal processes and shoreline dynamics are of paramount importance in Nunavut since almost all of its communities (26 of 27) and infrastructure are located on the coast. Only Baker Lake is located inland, but coastal issues are important there as well, given the importance of ship-based traffic to the community through Chesterfield Inlet. In addition,

numerous mining and energy projects are underway or in the planning stages throughout the territory, and many of these include development of ports and other infrastructure adjacent to the coast. Critical infrastructure for both communities and industry includes port facilities themselves, but also roads, buildings, power generation and transmission structures, water supplies, and railhead cargo handling facilities. This infrastructure may be vulnerable to direct damage by erosion and shoreline instability; the resulting transport of sediment in the nearshore zone can infill harbours and affect the navigability of channels. Even in areas where the coastline is stable, flooding can occur during high tides and storm surges. All of these processes may be exacerbated by changes in sea level (both rise and fall), increases in both air and water temperatures, and reductions in sea ice, which will lead to a longer open-water season and increased storminess and wave action. Knowledge of coastal materials, conditions and dominant processes is crucial in order to protect infrastructure, plan future development and generate strategies to adapt to changes in environmental conditions. The studies detailed here build on previous work by the authors to help provide information that will enable stakeholders to assess the sensitivity of existing and proposed coastal infrastructure and implement appropriate protection and adaptation measures. This will contribute to the viability of the mineral and energy industries in Nunavut and the well-being of its residents.

Acknowledgments

References

Allard M., Manson, G.K. and Mate, D.J. 2014: Reconnaissance assessment of landscape hazards and potential impacts of future climate change in Whale Cove, southern Nunavut; *in* Summary of Activities 2013, Canada-Nunavut Geoscience Office, p. 171–182.

AMEC 2007: Roberts Bay and Ida Bay abandoned mine sites geotechnical assessment in support of the site remediation program; prepared for Public Works and Government Service Canada by AMEC Earth and Environmental, Winnipeg, Manitoba, 61 p., URL <http://ftp.nirb.ca/01-SCREENINGS/COMPLETED%20SCREENINGS/2007/07CN007-INAC%20Roberts%20Bay%20 and%20Ida%20Bay/01-APPLICATION/Additional%20Information/Roberts-Ida%20Bay%20Geochemical%20Assessment.pdf> [November 26, 2013].

Barrie, W.B., Bornhold, B.D., Hodgson, D.A., Jubb, R.G., McLaren, P. and Taylor, R.B. 1979: Coastal reconnaissance for marine terminal planning in the high Arctic, District of Franklin; Geological Survey of Canada, Open File 633, 328 p., 55 maps, doi:10.4095/129575

Dickins, D., Hearon, G., Morris, K., Ambrosius, K. and Horowitz, W. 2011: Mapping sea ice overflood using remote sensing; Alaskan Beaufort Sea; Cold Regions Science and Technology, v. 65, p. 275–285.

Digital Globe, Inc. 2011a: WorldView-2 satellite image; DigitalGlobe, Inc., image, URL <https://browse.digitalglobe.com/imagefinder/showBrowseMetadata?catalogId=103001000C0FCC00> [November 13, 2013].

Digital Globe, Inc. 2011b: WorldView-2 satellite image; DigitalGlobe, Inc., image, URL <https://browse.digitalglobe.com/imagefinder/showBrowseMetadata?catalogId=103001000C575300> [November 13, 2013].

Digital Globe, Inc. 2011c: WorldView-2 satellite image; DigitalGlobe, Inc., image, URL <https://browse.digitalglobe.com/imagefinder/showBrowseMetadata?catalogId=103001000CBFE800> [November 13, 2013].

Digital Globe, Inc. 2011d: WorldView-1 satellite image; DigitalGlobe, Inc., image, URL <https://browse.digitalglobe.com/imagefinder/showBrowseMetadata?catalogId=102001001427DE00> [November 18, 2013].

Digital Globe, Inc. 2011e: WorldView-1 satellite image; DigitalGlobe, Inc., image, URL <https://browse.digitalglobe.com/imagefinder/showBrowseMetadata?catalogId=1020010015B04200> [November 18, 2013].

Eicken, H., Dmitrenko, K., Tyshko, K., Darovskikh, A., Dierking, W., Blahak, U., Groves, J. and Kassens, H. 2005: Zonation of the Laptev Sea landfast ice cover and its importance in a frozen estuary; Global and Planetary Change, v. 48, p. 55–83.

Forbes, D.L. and Hansom, J.D. 2011: Polar coasts; *in* Estuarine and Coastal Geology and Geomorphology, Treatise on Estuarine and Coastal Science, E. Wolanski and D.S. McLusky (ed.), Academic Press, Elsevier, Amsterdam, The Netherlands, v. 3, p. 245–283.

Forbes, D.L. and Taylor, R.B. 1994: Ice in the shore zone and the geomorphology of cold coasts; Progress in Physical Geography, v. 18, p. 59–89.

Forbes, D.L., Bell, T., James, T.S. and Simon, K.M. 2014: Reconnaissance assessment of landscape hazards and potential impacts of future climate change in Arviat, southern Nunavut; *in* Summary of Activities 2013, Canada-Nunavut Geoscience Office, p. 183–192.

Forbes, D.L., Manson, G.K., Mate, D. and Qammaniq, A. 2008: Cryospheric change and coastal stability: combining traditional knowledge and scientific data for climate change adaptation; Ice and Climate News, v. 11, p. 17–18.

Forbes, D.L., Mate, D., Bourgeois, J., Bell, T., Budkewitsch, P., Chen, W., Gearheard, S., Illauq, N., Irvine, M. and Smith, I.R. 2007: Integrated mapping and environmental change detection for adaptation planning in an Arctic coastal community, Clyde River, Nunavut; *in* Arctic Coastal Zones at Risk, G. Flöser, H. Kremer and V. Rachold, (ed.), Land-Ocean Interaction in the Coastal Zone *and* International Arctic Science Committee, Proceedings of Workshop,

Tromsø, Norway, October 2007, p. 42–47, URL <http://coast.gkss.de/events/arctic07/docs/proceedings.pdf> [November 6, 2013].

GeoGratis 2013: Canadian Digital Elevation Model; Natural Resources Canada, image, URL <http://geogratis.gc.ca/api/en/nrcan-rncan/ess-sst/C40ACFBA-C722-4BE1-862E-146B80BE738E.html> [November 13, 2013].

Gillie, R. 1995: Aerial video shoreline survey Coronation Gulf and Queen Maud Gulf, Northwest Territories, August 18–25; unpublished report prepared by AXYS Environmental Consulting Ltd. for Environment Canada, 32 p.

Hatcher, S.V., Forbes, D.L. and Manson, G.K. 2011: Coastal hazard assessment for adaptation planning in an expanding Arctic municipality; C-Change Secretariat (Canada), International Community-University Research Alliance Working Paper Series No. 23, 15 p., URL <http://www.coastalchange.ca/images/stories/Documents_Tab/workingpaper 23_hatcherforbes_manson_2011.pdf> [November 6, 2013].

James, T.S., Whalen, D.J.R., Jenner, K.A., Hatcher, S.V., Ulmi, M., Forbes, D.L., Manson, G.K., Henton, J.A. and Craymer, M.R. 2013: Coastal geoscience for sustainable development in Nunavut: 2012 activities; in Summary of Activities 2012, Canada-Nunavut Geoscience Office, p. 143–150.

Jefferies, M.O., Morris, K. and Liston, G. 1996: A method to determine lake depth and water availability on the North Slope of Alaska with spaceborne radar and numerical ice growth modelling; Arctic, v. 49, p. 367–374, URL <http://arctic.synergiesprairies.ca/arctic/index.php/arctic/article/view/1212> [November 5, 2013].

Jenner, K.A., Sherin, A.G. and Horsman, T. 2003: The use of dynamic segmentation in the Coastal Information System: adjacency relationships from southeastern Newfoundland, Canada; in Coastal and Marine Geo-Information Systems, D.R. Green and S.D. King (ed.), Kluwer Academic Publishers, The Netherlands, p. 371–384.

MacDonald, Dettwiler and Associates Ltd. 2011: RADARSAT-2 satellite image; MacDonald, Dettwiler and Associates Ltd., image, URL <http://gs.mdacorporation.com/SatelliteData/Radarsat2/Radarsat2.aspx> [November 29, 2013].

MacDonald, Dettwiler and Associates Ltd. 2012: RADARSAT-2 satellite image; MacDonald, Dettwiler and Associates Ltd., image, URL <http://gs.mdacorporation.com/SatelliteData/Radarsat2/Radarsat2.aspx> [November 29, 2013].

Manson, G.K., Couture, N.J., Forbes, D.L., Fraser, P.R., Frobel, D., James, T.S., Jenner, K.A., Lemmen, D.S., Lynds, T.L., Smith, C., Szlavko, B., Taylor, R.B., Wand, E. and Whalen, D.J.R. 2012: CanCoast: a national framework for characterising Canada's marine coasts; in Proceedings of the International Coastal Zone Canada Conference 2012, Coastal Zone Canada Association, June 9–14, 2012, Rimouski, Quebec.

Manson, G.K., Solomon, S.M., Forbes, D.L., Atkinson, D.E. and Craymer, M.R. 2005: Spatial variability of factors influencing coastal change in the western Canadian Arctic; Geo-Marine Letters, v. 25, p. 138–145.

Rescan 2010: Doris North Gold Mine Project: 2010 Roberts Bay Jetty Fisheries Authorization Monitoring Report; prepared by Rescan Environmental Services Ltd., Vancouver, British Columbia, for Hope Bay Mining Ltd., 121 p., URL <http://ftp.nirb.ca/03-MONITORING/05MN047-DORIS NORTH GOLD MINE/02-MONITORING AND MANAGEMENT PLANS/OTHER PLANS REQUIRED BY AA/Roberts Bay Fisheries Authorization Monitoring Report/110113- 2010 Roberts Bay Fisheries Authorization Monitoring Report.pdf> [November 13, 2013].

Sherin, A.G. and Edwardson, K.A. 1996: A coastal information system for the Atlantic provinces of Canada; Marine Technology Society Journal, v. 30, p. 20–27.

Sherin, A.G., Fraser, P.R., Solomon, S.M., Forbes, D.L., Jenner, K.A., Hynes, S., Lynds, T. and Gareau, P. 2003: A decade in the life of a coastal information system; International Geographical Union's Commission on Coastal Systems and International Cartographic Association's Commission on Marine Cartography, Proceedings, CoastGIS 2003, 5th International Symposium on GIS and Computer Cartography for Coastal Zone Management, October 16–18, 2003, Genoa, Italy, URL <http://www.gisig.it/coastgis/papers/sherin.htm> [November 6, 2013].

Shaw, J., Taylor, R.B., Forbes, D.L., Ruz, M.H. and Solomon, S.M. 1998: Sensitivity of the coasts of Canada to sea-level rise; Geological Survey of Canada, Bulletin 505, 1 CD-ROM, doi:10.4095/210075

Smith, I.R. 2014: Reconnaissance assessment of landscape hazards and potential impacts of future climate change in Kugluktuk, western Nunavut; in Summary of Activities 2013, Canada-Nunavut Geoscience Office, p. 149–158.

Smith, I.R. and Forbes, D.L. 2014: Reconnaissance assessment of landscape hazards and potential impacts of future climate change in Cambridge Bay, western Nunavut; in Summary of Activities 2013, Canada-Nunavut Geoscience Office, p. 159–170.

Solomon, S.M., Forbes, D.L., Fraser, P.R., Moorman, B., Stevens, C.W. and Whalen, D.J.R. 2008a: Nearshore geohazards in the southern Beaufort Sea, Canada; in Proceedings of the 7th International Pipeline Conference, Calgary, American Society of Mechanical Engineers, New York, v. 4, Paper IPC2008-64349, p. 281–289.

Solomon, S.M., Taylor, A.E. and Stevens, C.W. 2008b: Nearshore ground temperatures, seasonal ice bonding and permafrost formation within the bottomfast ice zone, Mackenzie Delta, NWT; in Ninth International Conference on Permafrost, Fairbanks, p. 1675–1680.

St-Hilaire-Gravel, D., Bell, T. and Forbes, D.L. 2010: Raised gravel beaches as proxy indicators of past sea-ice and wave conditions, Lowther Island, Canadian Arctic Archipelago; Arctic, v. 63, p. 213–226.

Taylor, R.B. 1978: The occurrence of grounded ice ridges and shore ice piling along the northern coast of Somerset Island, NWT; Arctic, v. 31, p. 133–149.

Taylor, R.B. and Frobel, D. 2006: Cruise report 2005-305: 2005 field survey of coastal changes along Barrow Strait, Bylot and northern Baffin islands, Nunavut; Geological Survey of Canada, Open File 5395, 89 p., 1 CD-ROM, doi:10.4095/223021

Taylor, R.B. and McCann, S.B. 1976: The effect of sea and nearshore ice on coastal processes in the Canadian Arctic Archipelago; La Revue de Géographie de Montréal, v. 30, p. 123–132.

Taylor, R.B., Frobel, D. and Forbes, D.L. 2012: Coastlines of the Findlay Island Group, Nunavut and Mackenzie King Island, Northwest Territories: aerial video surveys and ground observations; Geological Survey of Canada, Open File 6929, 17 p., doi:10.4095/289917

Reconnaissance assessment of landscape hazards and potential impacts of future climate change in Kugluktuk, western Nunavut

I.R. Smith[1]

[1]*Formerly of Geological Survey of Canada, Natural Resources Canada, Calgary, Alberta*

Smith, I.R. 2014: Reconnaissance assessment of landscape hazards and potential impacts of future climate change in Kugluktuk, western Nunavut; *in* Summary of Activities 2013, Canada-Nunavut Geoscience Office, p. 149–158.

Abstract

This paper examines environmental conditions and landscape hazards in the hamlet of Kugluktuk, Nunavut, based on observations made during a reconnaissance field survey in summer 2009, and an analysis of stereo airphotos. Conditions as they relate to permafrost, terrain and coastal stability and their potential impacts on infrastructure are assessed based on the present-day, and also how future climate change may positively or negatively increase perceived risk. This research is designed to assist future community planning activities by identifying the range of potential landscape hazards that currently exist, and indicating which conditions will require detailed analysis, monitoring and integration.

Résumé

Le présent rapport porte sur les conditions environnementales et les risques de nature géomorphologique auxquels fait face le hameau de Kugluktuk, au Nunavut, en fonction d'observations faites au cours d'un levé de reconnaissance sur le terrain effectué pendant l'été 2009, ainsi qu'à partir de l'analyse de stéréogrammes aériens. Les conditions associées au pergélisol, à la stabilité du terrain et des zones côtières, et leurs répercussions possibles sur l'infrastructure, ont fait l'objet d'une évaluation en fonction des circonstances qui prévalent, ainsi qu'en fonction de la façon dont les changements climatiques sont susceptibles d'accroître dans un sens soit positif, soit négatif, le risque perçu. Ces recherches peuvent contribuer à la mise au point d'outils susceptibles de venir en aide aux activités de planification communautaire futures en permettant d'identifier la gamme de risques de nature géomorphologique qui menacent la région à ce moment précis et de déterminer lesquelles de ces conditions exigent que l'on procède à leur analyse détaillée, à leur surveillance et à leur intégration dans le processus de planification.

Introduction

Arctic coastal communities are recognized as being particularly sensitive to projected climate change. Some of this sensitivity reflects the dynamic and direct linkage community members have with the land and surrounding seas, both in terms of their utilization of these for travel corridors, and as it pertains to traditional hunting and other country food harvesting. Changes in sea-ice regime, in terms of its seasonal extent, thickness and stability, will have the greatest immediate impact on arctic coastal communities. The focus of this reconnaissance assessment, however, is landscape stability as it pertains to potential impacts on existing infrastructure, and how such insights can be used to guide investigations supporting future adaptation strategies and hamlet planning guidelines.

Information presented here is based on a site visit to Kugluktuk on August 18–21, 2009. Information gathered during the community visit included field surveys and foot traverses throughout the townsite, tours provided of various infrastructure and development areas, and conversations with community members, local government officials and planning organizations. Additional information included in this assessment was derived from analysis of archival stereo airphotos.

Location and physiography

Kugluktuk (formerly known as Coppermine) is located on the north coast of mainland Canada, on the western edge of the Coppermine River where it empties into Coronation Gulf (67°49'N, 115°06'W; Figure 1). It lies north of the treeline in the southern Arctic tundra biome, a region commonly referred to as the Barren Grounds. Bedrock in the area is typically gabbro (Baragar and Donaldson, 1973) and the surface is often bare. Elsewhere, the landscape is covered by extensive shrub, herbaceous plant and moss cover. The terrain in the Kugluktuk area is characterized by coastal lowlands and a series of steplike terraces and deltas rising from ~10 m above sea level to 170 m above sea level at the marine-limit delta (which marks the highest position reached by the postglacial sea) situated 50 km up the Coppermine River at Muskox Rapids. These terraces and deltas formed during the retreat of the last ice age (more than 11 000 years ago) and throughout the period of Holocene isostatic uplift (Figure 2). Isostatic uplift is still ongoing and, in concert with eustatic (sea level) changes related to climate change, it is estimated it will account for a net rise of the land of up to 10 cm between 2010 and 2100 (James et al., 2011).

The surficial geology of the region surrounding Kugluktuk is depicted in maps by St. Onge (1988). Kerr et al. (1997) and Dredge (2001). A more detailed reconstruction based on airphoto interpretations is presented in Figure 3. Bedrock outcrops are prominent throughout the town. The majority of unconsolidated sediments within the town are related to submersion of the landscape during deglaciation, and its subsequent isostatic uplift. A prominent, flat delta terrace, upon which the airport runway was built, is situated approximately 30 m above sea level and is considered to have formed approximately 6000 years ago (Figures 2b, 3, unit Gd; Dredge, 2001). Around 5000 years ago, sea level was about 20 m higher than it is today, and the Coppermine River drained through both a west channel (west of present-day Kugluktuk [beyond the extent of Fig-

Figure 1: Location map of Kugluktuk (formerly Coppermine), situated at the mouth of the Coppermine River, in western Coronation Gulf, Nunavut. Black dots (with site number) represent ground thermal profile and lakewater monitoring stations from Wolfe's (2000) study; white circles (with site number) represent air and near-surface ground temperature stations (from Wolfe, 2000, p. 6).

Figure 2: Final stages of deglaciation and emergence of the land around Kugluktuk: **a)** land (white areas bounded by thick black lines) and sea (grey area) about 8000 years ago, and development of the terraces (stippled areas) at 70–80 m above present sea level along the Coppermine River; modern coastline indicated by thin grey line; **b)** development of the delta 6000 years ago and emergence of Saddleback hill; sea level was about 30 m above the present level; **c)** coastline about 5000 years ago, when the west channel of the Coppermine River was active and sea level was about 20 m above the present sea level; **d)** land and sea about 3500 years ago, when sea level was 10–15 m above present. Arrows on the figure represent proglacial drainage paths during deglaciation. Modified from Dredge (2001, p. 26).

Figure 3: Surficial geology, Kugluktuk, Nunavut. Background image (WorldView-1; DigitalGlobe, Inc., 2008) includes copyrighted material from DigitalGlobe, Inc., all rights reserved.

ANTHROPOGENIC DEPOSITS: **AN**, culturally made or modified materials, usually comprising infills and pad developments.

COLLUVIAL DEPOSITS: **C**, a thin and discontinuous cover of earth materials accumulated through gelifluction and other slope processes; **Ct**, talus debris accumulations below rock scarps.

ORGANIC DEPOSITS: **O**, peat and muck formed by accumulations of plant material in various stages of decomposition; generally occurs as flat, wet terrain overlying poorly drained substrates.

ALLUVIAL DEPOSITS: commonly stratified; **A**, sorted sand, silt, and minor gravel and organic detritus deposited by streams; **At**, sorted sand, silt and gravel deposited by the Coppermine River and tributaries at the time of a higher sea level; **Ap**, modern floodplain of the Coppermine River.

GLACIOFLUVIAL DELTAIC DEPOSITS: **Gd**, sorted sand, silt, and gravel delta terraces deposited by the deglacial Coppermine River.

MARINE DEPOSITS: **M**, a mixture of sand, silt and rocks, deposited during, or reworked by postglacial marine flooding; may include reworked diamict (till); postglacial thickness of material is generally thin (<2 m), but locally may infill deeper bedrock hollows.

HUMMOCKY MARINE DEPOSITS: **Mh**, a mixture of sand, silt and rocks deposited during postglacial marine flooding of the landscape, that were reworked into raised beach ridges; characterized by hummocky or irregular surface topography considered to reflect differential melt or content of underlying ground ice.

MARINE DEPOSITS - RAISED BEACH RIDGES: **Mb**, a mixture of sand, silt and rocks reworked into raised beach ridges; local ponding behind ridges is common; may contain significant quantities of buried ice.

MARINE DEPOSITS - THERMOKARST: **Mk**, a mixture of sand, silt and rocks, deposited during postglacial marine flooding of the landscape, that were reworked into raised beach ridges and, following isostatic uplift, have undergone extensive melting of buried ground ice leading to land subsidence and surface ponding.

BEDROCK: **R**, gabbro of the Proterozoic Coronation sills and associated dikes.

ure 3]) and along an east channel that followed a similar path to the modern river (Figure 2c). An extensive flat sand, silt and gravel terrace situated west of the community was formed during this period. By 3500 years ago, sea level was 10–15 m above present and drainage occurred along the modern Coppermine River channel only. Sand, silt and gravel terraces forming the northern shoreward margins of Kugluktuk and raised alluvial terraces east of the airport along the Coppermine River (Figure 3, unit At) were deposited at this time of a higher sea level (Figure 2d). Erosion of the raised alluvial terraces by the Coppermine River, over the past 3500 years of isostatic uplift, has produced the extensive alluvial plain (Ap) shown on Figure 3, much of which appears to experience seasonal or occasional flooding. Alluvial sediments are also found west of town along small streams (some of which may be ephemeral) that cut perpendicular downslope through areas of extensive beach ridges. In places west of town, these channels are over-deepened and -widened suggesting that they have incised into ice-rich terrain. The terrain underlying the central part of Kugluktuk comprises a marine-washed surface lag. Sediments are predominantly sandy, but may contain significant quantities of finer grained material (silt and clay) and clasts. Till was not identified in the field, but may underlie some areas. Thicknesses of unconsolidated sediments in the M terrain unit areas are generally thin (<2 m), but locally may infill deeper bedrock hollows. Ice content is unknown in this unit, but it may be significant in the areas of infill and small in the other areas based on an absence of thermokarst surface morphology. However, in the area of the sealift and port facility (west of the townsite; Figure 3), extensive pitting and surface ponding suggests that the predominantly marine sediments in this area have undergone thermokarst (Figure 3, unit Mk), that is, melting of ice-rich permafrost. Areas surrounding this exhibit a hummocky topography (Figure 3, unit Mh) also suggestive of differential ground ice melt. Most of the remaining terrain in the Kugluktuk area is characterized as beach ridges (Figure 3, unit Mb) where distinctive parallel ridges extend perpendicularly upslope, often with small ponds impounded behind ridge crests. Large ice wedges and extensive erosion by small streams in both the beach ridge (Mb) and glaciofluvial delta (Gd) deposits suggest that ice content may be significant, but highly variable in these deposits. Organic deposits are found in low-lying wet terrain, west and southwest of the airport. Thickness of organic matter in these areas is unknown.

Projecting through the terraced landscape is a series of parallel east-northeast–oriented, elongate bedrock hills characterized by cliffed southern faces and more gently sloping northern faces. Cliffed areas are frequently associated with talus accumulations. Prominent bedrock outcrops occur throughout the town and, based on their physiographic ex-

pression, bedrock is considered to shallowly underlie much of the central and southern extents of the townsite.

Climate

Kugluktuk's weather is influenced by arctic air masses year-round and is characterized by short, cool summers and long, cold winters. Based on the 1971–2000 Canadian climate normals (Environment Canada, 2013), Kugluktuk has a mean annual air temperature of –10.6°C, with monthly averages ranging from a low of –27.8°C in January to a high of 10.7°C in July. The coldest temperature was –47.2°C on February 20, 1998, and the warmest temperature was 34.9°C on July 15, 1989. Annual average precipitation is 249.3 mm, of which roughly half (133.4 mm) falls as rain, the rest (165.7 cm) as snow. Average maximum snow depth is ~0.5 m, and is typically present throughout February, March and April. Extreme daily rainfall was 53.7 mm on August 12, 1982, whereas extreme daily snowfall was 26.2 cm on January 1, 1988. This extreme rainfall event was eclipsed by the 55.7 mm of rain received July 20, 2007, immediately followed by the 115.0 mm received July 21, 2007 (Prno et al., 2011). Monthly average wind speed is fairly constant year-round, ranging from 19 km/h in January to 14 km/h in June. Wind direction does show seasonality, being predominantly from the southwest in winter and from the east in summer. Maximum monthly hourly wind speeds are almost always from the northwest, and maximum gusts range from 74 km/h in June to ~106 km/h in the December–March period. Over the period of 1978–2008, there appears to be a 1–1.5°C increase in mean annual air temperature (Figure 4; Environment Canada, 2013).

Permafrost

Kugluktuk lies within a region of continuous permafrost. Depth of seasonal thaw (active layer thickness) is unknown in Kugluktuk and is likely to be spatially variable depending on parent material, vegetation cover and seasonal snow
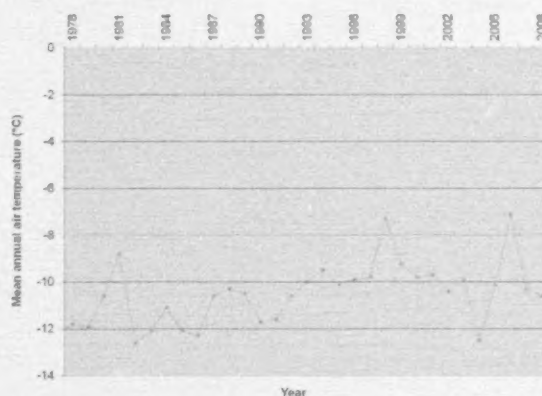

Figure 4: Graph of mean annual air temperature from 1978–2008, Kugluktuk, Nunavut (Environment Canada, 2013).
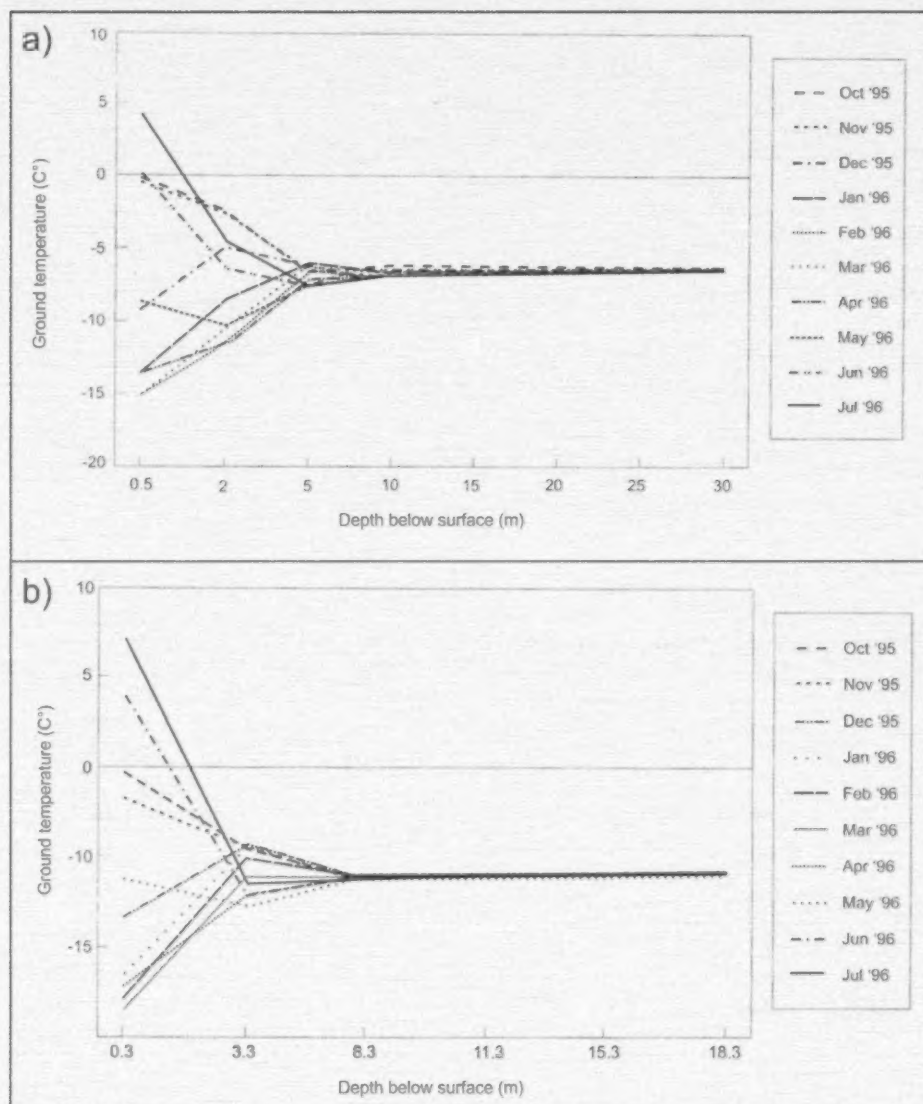
Figure 5: Ground temperature profiles for **a)** site GSC-001 (location shown on Figure 1; Wolfe, 2000, p. 39) and **b)** site GSC-002 (location shown on Figure 1; Wolfe, 2000, p. 40), near Kugluktuk, Nunavut.

cover. Short term (~1 yr) thermistor profiles collected for two near-coastal sites, ~20 km east of Kugluktuk (Figure 1, sites GSC 001, 002), show depth of thaw penetrating between 1.5 and >2 m (Figure 5; Wolfe, 2000).

Periglacial landforms are widespread in the Kugluktuk area, and garner consideration in any development proposal. While much of the marine sediments that blanket areas of Kugluktuk are predominantly sand, they do contain significant proportions of silt and clay. These sediments are conducive to water retention, which in a permafrost environment becomes ice. During initial permafrost aggradation into these sediments (following isostatic uplift), water would have migrated through the sediments to a freezing front, leading to the development of horizontal ice lenses. It

is suspected that such lenses (which can range from millimetres to decimetres thick) are present in the lower alluvial terrace sediments (Figure 3, unit At), upon which much of the northern part of Kugluktuk is built. An assessment of the ice content in these sediments is important for determining foundation stability of existing buildings and for future infrastructure design. Consideration should be given to the potentially increased thaw subsidence that may occur under climate warming. If ice lenses do occur in these alluvial terrace sediments, then their exposure to wave action along the shore, causing erosion and slumping of sediments (Figure 6), or their exposure to surface runoff, causing erosion and incision (Figure 7), could lead to increased and rapid coastal retreat, imperilling nearshore infrastructure.

Figure 6: Erosion of sandy alluvial terrace sediments along Kugluktuk's northern shore, Nunavut. Gabion baskets (foreground), which were installed to reduce erosion, are now being undercut and/or destabilized by wave-induced erosion. Wave-induced undercutting of vegetated slopes, seen in the background (marked by arrows), has resulted in slumping of sediments along the base of the active layer. Exposure of underlying frozen sediments along cracks will lead to further erosion.

Figure 7: Stream erosion atop alluvial terrace sediments beside the seashore, Kugluktuk, Nunavut. Channelling of meltwater and rainwater from the community through an unarmoured channel has resulted in physical erosion and incision. Incision of the channel has also likely led to melting of underlying permafrost, resulting in thermal erosion, and enhanced over-deepening of the channel. Slumping of sediments along channel margins points to ongoing instability and lateral propagation of the channel margins.

Saline permafrost (Biggar and Sego, 1993; Hivon and Sego, 1993) is also an issue throughout the Kugluktuk area. Because the whole region was inundated by the sea, and then subsequently isostatically uplifted, the marine sediments would naturally contain saline pore waters. During aggradation of permafrost into these sediments, brines would have formed, until they eventually became trapped within interstitial crystal lattices. The nature of saline permafrost is such that it weakens the bonds of the crystal structure, making the permafrost far more plastic and deformable than nonsaline permafrost. The presence of brines also depresses the freezing point, such that saline permafrost will melt at lower temperatures than regular permafrost, and thus is more susceptible to changes in ground temperature as may occur under projected climate warming.

Perceived sensitivities to climate change

Observations from this reconnaissance visit and subsequent research, presented above, are used to infer a range of landscape sensitivities in the Kugluktuk region to potential climate change. It is stressed, however, that these inferences require more field-based study and substantiation before they may be incorporated into a design/adaptation strategy. They are perhaps most useful in identifying knowledge needs/gaps that can be used to support the planning process.

1) In the specific context of climate warming, landscape and permafrost-related hazards in Kugluktuk appear to be of low risk. That is not to say that there could not be significant impacts on local infrastructure. It is just that as most of the town is situated on bedrock, or on a thin veneer of predominantly sandy sediments overlying bedrock, it can be regarded as occupying an enviably stable building platform.

2) Warming could have a potential influence on thaw subsidence in the alluvial terrace sediments (Figure 3, unit At) upon which the northern extents of the town are built. Sediment coring would have to be undertaken to determine and characterize this risk.

3) Based on the presence of thermokarst terrain along the beachfront regions in the port facility and west of there (Figure 3, unit Mk), it can be deduced that some of the areas covered by raised beaches contain significant quantities of buried ice. This is not unusual, as during the beach-forming process, ice push and subsequent burial of ice masses can occur. Urban development, such as roads and building pads in areas of beach ridges, would need to take into account the potential presence of buried ice. This includes any trenching activities that might expose ice-rich sediments.

4) Over-deepened and -widened alluvial channels, found adjoining the runway and elsewhere in regions of extensive raised beach cover, suggest that the stream channel morphology reflects melting of ice-rich sediments. Stream diversion efforts, such as has been undertaken along the western end of the airport runway, must take this into account. Simple excavation of ditches will not protect underlying pe   frost. Armouring of the bed with larger rock material will be required to ensure that easily eroded sandy sediments are not removed, as this could lead to further thermal erosion of underlying sediments and accentuated erosion.

5) The extensive network of ice wedge polygons and individual ice wedges in the glaciofluvial delta terrace (Figure 3, unit Gd) that underlies most of the airport merits significant attention. The large size (length and width) of ice wedges suggests significantly large ice masses underlie the active layer in this region. Climate warming could result in melting of the upper sections of these ice wedges leading to subsidence along the ice wedge depressions. These depressions then readily form drainage conduits, leading to increased thermal melting of the ice wedge, and continued subsidence. In extreme cases, channelling of meltwater along these ice wedge depressions can result in the rapid melting and incision of the entire ice wedge below, resulting in metres of incision and destabilization of the adjacent slope materials. The morphology of various tributary streams flowing east from this area down toward the Coppermine River suggests that they have formed in part by this process. Even though it can be argued that this area emerged from the sea over 5000 years ago and thus shows considerable stability, it must be recognized that the construction of infrastructure, and particularly the diversion of meltwater from pre-existing pathways, can have dramatic consequences upon a permafrost landscape. Changes in snow drifting can also be of potential significance here in terms of meltwater generation and thermal insulation of the ground. On the south side of the airport runway, a large area of surface sediments has been removed—presumably as part of the runway construction process. Removal of the surface layer will undoubtedly have exposed ice wedges or at least caused the active layer to now extend down below their top. It can be anticipated that ice wedges will exhibit pronounced melt and subsidence in this region until equilibrium conditions are re-attained. Attention would need to be paid to ensure that subsidence/erosion does not propagate headward into the runway pad.

6) In addition to the ice wedge polygons in the glaciofluvial delta terrace region, some areas east of the airport terminal pad show evidence of thermokarst, suggesting that the ice wedge polygons themselves may have significant ice contents below them. Under a climate-warming scenario, it could be anticipated that further subsidence may occur in this region. Any development considerations in this area would have to first assess subsurface ice content.

Climate warming is only one component of climate change, and thus a broader scope of environmental changes and potential impacts must be assessed with respect to determining risk in Kugluktuk.

7) Changes in sea ice are likely to produce the biggest impacts on day-to-day life for residents of Kugluktuk. Even though most of this research is beyond the scope of this assessment, impacts of reduced summer sea-ice cover, particularly as it pertains to reductions in the extent of shorefast ice and increases in wave fetch, need to be taken into account in regards to shore stability. This is likely to be less of an issue in the more gently inclined regions of the beach occupying the western part of the town. In the eastern part of the town, where there is a fairly steep shore profile (Figure 6), reductions in sea ice and increased wave action may accelerate shore erosion. Note, wave action also needs to take into account wakes from boats operating close to the shore. The present gabion baskets appear insufficient, and need to be reconstructed or bolstered in order to halt further erosion taking place. Several small shacks and two housing properties appear to be at direct risk to continued shore erosion and coastal slumping.

8) Even though Kugluktuk presently lies within a region that is continuing to experience positive isostatic uplift (projected to be up to 10 cm between 2010 and 2100 [James et al., 2011]), it is conceivable that under various climate-change scenarios, it may start to see net subsidence when eustatic (sea level) rise outpaces isostatic (land) uplift. James et al. (2011) project that sea level at Kugluktuk could rise up to 50 cm between 2010 and 2100. Significant changes could thus occur along various shore profiles, and indeed it is possible that storm surges could see flooding of low-lying thermokarst terrain around the port facility and west of there.

9) Protection of Kugluktuk's water supply must be examined in terms of its long-term sustainability. Currently, freshwater is drawn from the Coppermine River, by a large pipe system, into settling ponds and a holding tank. It was reported to the author that the town has experienced several saltwater incursion events that have temporarily contaminated their water supply. Reasons for this are potentially manifold, but it may be a consequence of increased storm surge brought about by higher winds and increased open-water fetch during periods of reduced summer sea-ice extent. Changes in channel geometry within the Coppermine River are also a likely contributor. Historical and ongoing surveys of beach and nearshore profiles by Natural Resources

Canada (D.L. Forbes and G.K. Manson, unpublished data, 2013) do not incorporate the region around the freshwater intake. It is suggested that a detailed bathymetric and hydrological survey be established near the freshwater intake in order to better understand the nature of the hydrological system, particularly as it applies to mechanisms leading to saltwater incursions. Such a survey could also be used as a bench mark upon which future changes can be assessed. It also needs to be recognized that changes in channel depth and sedimentation will naturally occur in this region of the Coppermine River as a consequence of continued isostatic uplift, eustatic rise and delta formation. Melting of ice-rich permafrost and increased formation of active-layer detachments along the banks of the Coppermine River (c.f. Dredge, 2001) may also result in increased sedimentation rates and shallowing of the Coppermine River, further exacerbating the problem.

10) Urban hydrology is universally identified as a problem in northern communities. Poorly maintained, often undersized drainage culverts and a lack of retrofitting of downstream drainage systems to handle new, upslope infrastructure development (which results in an increased and hurried routing of meltwater and precipita-

Figure 8: Erosion of Kugluktuk streets as a result of the extreme July 20–21, 2007, storm event (170.7 mm; Environment Canada, 2013). Photo by J.Prno, 2007.

tion) is a significant problem. In Kugluktuk, it has to be recognized that the sandy nature of the surface sediments and those used in road construction are particularly susceptible to stream erosion. The dramatic erosion of streets (Figure 8) during the July 20–21, 2007 extreme precipitation event (170.7 mm) points to the problem of insufficient urban drainage capacity. Routing of meltwater must be addressed from source, right down to output into the sea or Coppermine River. As demonstrated in Figure 8, free drainage across unprotected surface sediments can lead to rapid erosion and incision of drainage channels, which can then perpetuate thaw subsidence of underlying ice-rich permafrost leading to further erosion and channel incision. Drainage infrastructure built to handle existing meltwater and precipitation regimes may not be suitable to address what could occur under climate-change scenarios that foresee increased storm activity and seasonal rainfall.

11) Another component of urban hydrology that needs to be addressed is that of surface ponding of water. Construction of roads and building pads can lead to impoundment of meltwater and precipitation. In permafrost environments, ponding of surface water can lead to thermal erosion of underlying materials. When this occurs in ice-rich sediments bordering culverts, it can result in subsidence of land effectively stranding the culvert above the subsided surface—a positive feedback loop that leads to increased ponded water depth and greater thermal erosion and therefore further subsidence. Ponded water can also saturate coarse materials used in most building pad construction. Building pads purposefully use coarse materials in order to ensure free drainage of water away from them. If water is allowed to pond around a building pad, then it can be anticipated that ice will seasonally form within the pad, resulting in differential heave of the building above it and progressive disturbance and compromising of the pad's integrity.

12) Snow drifting is something that has to be considered in building design and community planning. In terms of climate change, there may be changes in both the amount of snow (increased) and perhaps more significantly, changes in wind direction and strength, particularly during storm events. This can result in significant changes in snowdrift patterns within the community. Snowdrifts must be considered in terms of their insulation properties and their eventual meltwater production and the routing of this meltwater. In permafrost terrain, it is often essential that materials be allowed to freeze deeply each winter in order to preserve the existing land stability. Snowdrifts act to insulate the ground materials and can significantly alter the seasonal thermal profile, allowing for a thickening of the active layer. Therefore, changes in snowdrift patterns or thicknesses, including consideration of where snow cleared from the airstrip or

community streets is dumped, needs to be taken into account during the planning process.

Economic considerations

This report illustrates existing environmental conditions and landscape and coastal hazards faced by infrastructure within and adjacent to the hamlet of Kugluktuk. It further considers how these factors may be compounded as a consequence of climate change. Understanding of these conditions and the risks they pose to infrastructure can be integrated with future community planning in order to enhance stability and sustainability, thereby reducing costs of infrastructure development and maintenance.

Acknowledgments

References

Baragar, W.R.A. and Donaldson, J.A. 1973: Geology, Coppermine, District of Mackenzie; Geological Survey of Canada, Map 1337A, scale 1:250 000.

Biggar, K.W. and Sego, D.C. 1993: The strength and deformation behaviour of model adfreeze and grouted piles in saline frozen soils; Canadian Geotechnical Journal, v. 30, p. 319–337.

Dredge, L.A. 2001: Where the river meets the sea: geology and landforms of the lower Coppermine River valley and Kugluktuk, Nunavut; Geological Survey of Canada, Miscellaneous Report 69, 76 p.

Environment Canada 2013: Canadian climate normals; Environment Canada, URL <http://climate.weather.gc.ca/climate_normals/index_e.html> [November 7, 2013].

Hivon, E.G. and Sego, D.C. 1993: Distribution of saline permafrost in the Northwest Territories, Canada; Canadian Geotechnical Journal, v. 30, p. 506–514.

James, T.S., Simon, K.M., Forbes, D.L., Dyke, A.S. and Mate, D.J. 2011: Sea-level projections for five pilot communities of the Canada-Nunavut Climate Change Partnership; Geological Survey of Canada, Open File 6715, 23 p.

Kerr, D.E., Dredge, L.A. and Ward, B.C. 1997: Surficial geology, Coppermine (east half), District of Mackenzie, Northwest Territories; Geological Survey of Canada, Map 1910A, scale 1:250 000.

Mate, D. and Reinhart, F., ed. 2011: Nunavut Climate Change Partnership workshop, February 15–16, 2011; Geological Survey of Canada, Open File 6867, 1 CD-ROM, doi:10.4095/288645

Prno, J. 2007: Living with change: community exposures and adaptations in Kugluktuk, Nunavut; University of Guelph, Department of Geography, unpublished report, 26 p.

Prno, J., Bradshaw, B., Wandel, J., Pearce, T., Smit, B. and Tozer, L. 2011: Community vulnerability to climate change in the context of other exposure-sensitivities in Kugluktuk, Nunavut; Polar Research, v. 30, p. 1–21, doi:10.3402/polar.v2010.7363

St. Onge, D.A. 1988: Surficial geology, Coppermine River, District of Mackenzie, Northwest Territories; Geological Survey of Canada, Map 1645A, scale 1:250 000.

Wolfe, S.A. 2000: Permafrost research and monitoring stations in west Kitikmeot, Slave geological province, Nunavut; Geological Survey of Canada, Open File 3848, 101 p.

Reconnaissance assessment of landscape hazards and potential impacts of future climate change in Cambridge Bay, western Nunavut

I.R. Smith[1] and D.L. Forbes[2,3]

[1]Formerly of Geological Survey of Canada, Natural Resources Canada, Calgary, Alberta
[2]Geological Survey of Canada, Natural Resources Canada, Dartmouth, Nova Scotia
[3]Department of Geography, Memorial University of Newfoundland, St. John's, Newfoundland and Labrador

Abstract

This paper presents observations of environmental conditions and landscape characteristics as they pertain to issues of infrastructure stability and sustainability that were recorded during a site visit in and around the hamlet of Cambridge Bay during the summer of 2009. Observational and model-based analysis of sea-level change was also investigated. This research is designed to assist the development of future community planning activities. It highlights issues of permafrost degradation, surface drainage, building pad construction and the potential for increased wave erosion in coastal areas, particularly beyond the hamlet's inner harbour where cabins may be located.

Résumé

Le présent rapport fait état des observations auxquelles les auteurs se sont livrés à l'étude des conditions environnementales et des caractéristiques géomorphologiques, dans la mesure où ces questions ont trait à la stabilité et à la durabilité des infrastructures, lors d'une visite des sites dans le hameau de Cambridge Bay et sa périphérie au cours de l'été 2009. Une analyse du changement du niveau marin a également été entreprise à partir de ces observations et à l'aide de modèles. L'objet de ces recherches est de fournir les outils nécessaires à la mise en œuvre d'activités de planification communautaire futures. Elles mettent en évidence les questions liées à la dégradation du pergélisol, au drainage en surface, à la construction de plates-formes de bâtiments et aux risques que pose l'augmentation de l'action érosive des vagues dans les régions côtières, surtout au-delà de l'arrière-port du hameau, où des cabines peuvent avoir été érigées.

Introduction

Arctic coastal communities are recognized as being particularly sensitive to projected climate change. Some of this sensitivity reflects the dynamic and direct linkage community members have with the land and surrounding seas, both in terms of their use as travel corridors and for traditional hunting and other country food harvesting. Changes in sea-ice regime, particularly in terms of the seasonal extent, thickness and stability of ice, are likely to have the greatest immediate impact on the residents of Arctic coastal communities. The focus of this reconnaissance assessment, however, is landscape stability and sea-level change as they pertain to potential impacts on existing infrastructure, and how such insights can be used to guide future adaptation strategies and land-use planning activities. This is a subject of growing interest and relevance given the rate of recent climate changes witnessed and the development pressures in many northern communities (cf. Furgal and Prowse, 2008; National Round Table on the Environment and the Economy, 2009; Forbes, 2011; Government of the Northwest Territories, 2011).

Information presented here is based on a site visit to Cambridge Bay from August 21 to 26, 2009, by the authors and Canadian Institute of Planners members C. Callihoo and

T. Romaine. Information gathered during the community visit included field surveys and foot traverses throughout the townsite and along the surrounding gravel roads, as well as conversations with community members and staff from various community and regional organizations.

Location and physiography

The hamlet of Cambridge Bay (population 1477 [Statistics Canada, 2006]; 69°07'02"N, 105°03'11"W) is located on southeastern Victoria Island in a protected setting near the head of an L-shaped harbour forming the inner part of Cambridge Bay (Figure 1). The bay lies on the north side of the narrows extending from Dease Strait in the west to Queen Maud Gulf in the east, between Victoria Island and the mainland (Kiillinnguyaq, formerly known as Kent Peninsula).

The inner bay forming the harbour is oriented northwest-southeast, protecting it from waves from the outer bay. At the inner end, a triangular embayment extends northeast to the mouth of Freshwater Creek. An inlet, Kangiqhuk (formerly known as West Arm), extends about 6 km west from the main body of the bay. The original settlement site was on the east side of the bay across Freshwater Creek from the

present hamlet. The present-day settlement lies at the head of the bay facing southeast toward the mouth of the harbour. An extensive gravel road network reaches about 15 km to the northeast, to Iqaluktuuttiaq (formerly known as Greiner Lake) and Uvayuq (formerly known as Mount Pelly), 15 km to the north, and 10 km to the west, with all-terrain vehicle trails continuing beyond. Community infrastructure extends 3 km inland (north) to the water-supply lake and almost 4 km to the west to the end of the airport runway, beyond which the gravel road extends another 6 km toward a large gravel pit and southwest-facing coastline where a number of houses and cabins have been built.

Bedrock in the area consists of mainly flat-lying, ancient (Precambrian or Cambrian) carbonate rocks (limestone or dolostone) with smaller proportions of sandstone, siltstone and shale (Okulitch, 1991). Bedrock is exposed along the eastern and western shores of the bay, at the mouth of Freshwater Creek, along the shores of Kangiqhuk, and in quarries on the west and north sides of the hamlet.

The Cambridge Bay townsite is situated on terrain mapped as till veneer, constituting a patchy, <1 m cover of clast-rich, sandy diamict deposited during the last glaciation (Sharpe, 1993; Figure 2). The area north of the town and
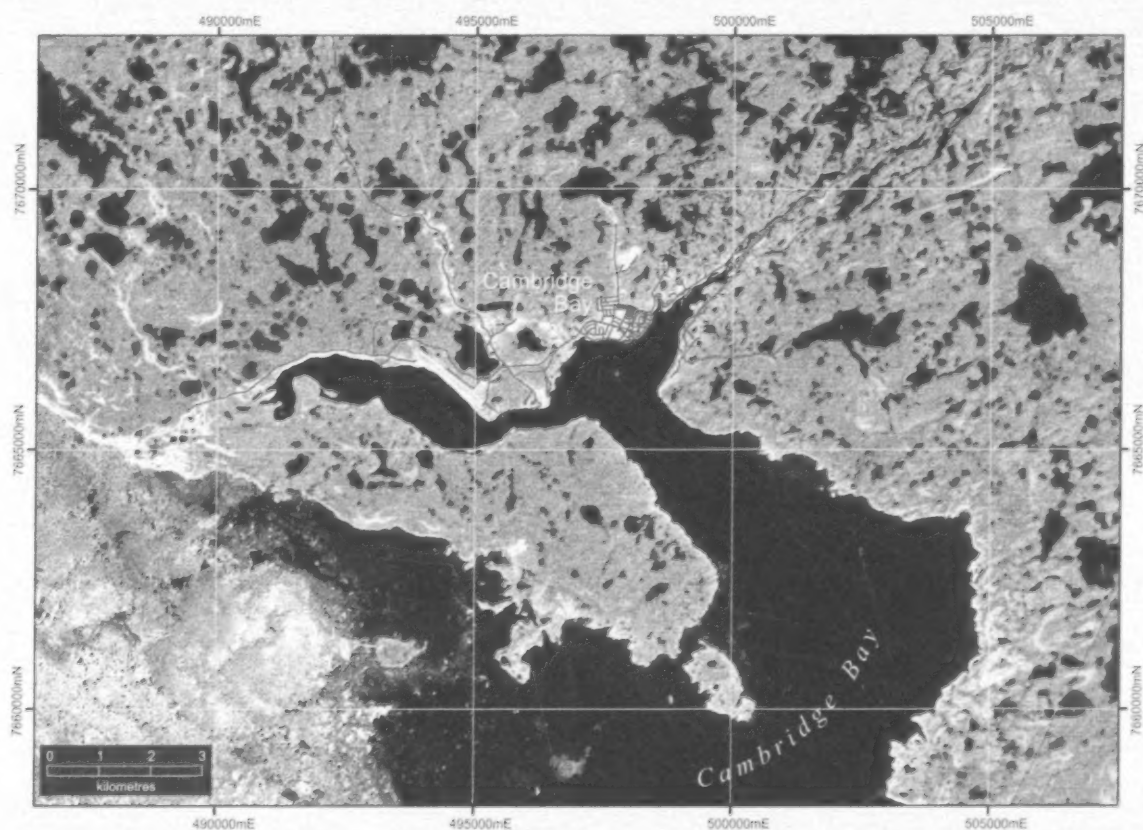
Figure 1: Cambridge Bay and vicinity on southeastern Victoria Island, Nunavut (UTM zone 13). Landsat 7 orthorectified panchromatic image (15 m resolution; GeoBase®, 1999–2003) with roads (magenta) from National Road Network (GeoBase®, 2009).

Canada-Nunavut Geoscience Office

Figure 2: Cambridge Bay area (Nunavut) of Sharpe's (1993) regional surficial geology map. Pale green terrain underlying Cambridge Bay townsite is till veneer, while thicker till accumulations (darker green) blanket much of the area north and east of the hamlet. Interpreted marine limit (which marks the highest position reached by the postglacial sea) is indicated by the red polygon atop the mountain, northeast of the hamlet. A prominent esker (chevron symbols) extends along the axis of Freshwater Creek, northeast of the hamlet. Place names on this figure reflect the official place names at the time of publication of the map.

west toward Kangiqhuk (including the airport and distant early warning [DEW] line station) is covered by a till blanket, with regional thicknesses indicated to be up to 5 m, locally interbedded with meltwater deposits of sand and gravel (Sharpe, 1993). Field observations as part of this reconnaissance survey suggest local till thicknesses are in the

Figure 3: Sandy esker ridge at mouth of Freshwater Creek, Nunavut. Esker trends northeast for ~10 km toward Uvayuq (formerly known as Mount Pelly) in the background. The community cemetery is situated along the flanks of the esker (foreground).

Figure 4: Beach shingle (washed till and weathered bedrock), up to 30 cm thick, exposed along Uvayuq road (formerly known as Mount Pelly road), Cambridge Bay, Nunavut.

Figure 5: Thermokarst pond adjacent to the airport road, northeast of the runway, Cambridge Bay, Nunavut. Construction of road blocked natural drainage allowing surface ponding of water that has then thawed ice-rich sediments below. Continued growth of the pond is seen by radially extending slump scars and collapse of 10–25 cm thick mats of peat into the pond. This exposes underlying sediments to thaw and further settlement.

order of 1–3 m. A prominent esker ridge (up to 6 m high) runs for ~10 km along the valley of Freshwater Creek (Figure 2). The community cemetery is situated atop the esker near the mouth of Freshwater Creek (Figure 3) and the Uvayuq road (formerly known as Mount Pelly road) follows the esker eastward. The esker is composed of fine to medium sand with little gravel content, making it unsuitable as a potential granular aggregate resource. Deglaciation occurred prior to 8.9 ka ^{14}C BP, after which the entire landscape, up to at least 180 m, was inundated by the sea (Sharpe, 1993). There is little evidence of marine sediments in the area; however, prominent flights of raised sandy beaches in the Tikiraaryuaq (formerly known as Long Point) area, and a washed surface lag (nearshore or beach shingle; Figure 4), which armours much of the terrain, records evidence of marine inundation.

Permafrost and periglacial environments

Cambridge Bay lies within the zone of continuous permafrost, with a thin (<1 m) active (seasonal thaw) layer, below which the ground materials and bedrock remain frozen year-round. Evidence of massive ground ice and excess ice (ice wedges and thermokarst depressions) are found in low-lying areas surrounding ponds. There is little evidence for the presence of excess ground ice in the present-day Cambridge Bay built-up area, but there are indications of excess ice in areas around the DEW line station and in isolated areas east of the airport runway (Figure 5). The absence of ground-ice features in much of the Cambridge Bay region likely reflects the generally thin cover of sediment overlying bedrock, the coarse nature of the sediment and the regional slope that has allowed this sediment to drain. Unconsolidated sediments in the region may well contain interstitial ice and potentially in sufficient quantities as to become a hazard to infrastructure development. Furthermore, because the area was submerged below sea level following deglaciation and has subsequently been uplifted, saline permafrost conditions likely exist in the Cambridge Bay area, and thus warrant study as part of any engineering assessment (cf. Biggar and Sego, 1993; Hivon and Sego, 1993).

Ice wedges are characteristic features of permafrost environments and form below the active layer due to the thermal contraction of the ground under extreme winter cold conditions. Spring meltwater seeps into the cracks and freezes at depth, leading to the formation of a vertical wedge of ice in the permafrost. Repeated cycles of winter cracking and infiltration of water lead to the progressive thickening and growth of ice wedges, which manifest as surface geomorphological features such as ice-wedge fissures, or where a number of these intersect, ice-wedge polygons. If the thermal equilibrium properties of an area change, either through increases in summer temperature or the removal of vegetation cover or sediments from the active layer, the top

of the ice wedges can begin to melt. Where thawing ice wedges intersect small ponds, they can serve as drainage conduits, resulting in the disappearance of small surface water bodies. An example of this was seen south of the Uvayuq road (Figure 6).

Where finer sediments and organic materials have accumulated, such as in regional depressions, and where slope wash may have carried them in, active periglacial landforms are found (Figure 7). These landforms are created by freezing and thawing of the active layer and frost-churning of finer sediments and clast material. They represent constraints on infrastructure development, requiring sediment and gravel pads to be placed atop them, in order to translocate the active layer upward into the pad materials, thus stabilizing the surface sediments within the permafrost zone prior to development.

Unconsolidated sediments on gentle to steep slopes in the area are subject to gelifluction, the slow downslope movement of earth materials on a frozen substrate. This is fairly inconsequential to the stability of infrastructure such as roads, as the rate of ground movement is so slight that the frequency of road regrading, as part of regular surface maintenance, would more than offset any ground move-

ment. Where infrastructure is fixed to the ground, or where it crosses areas undergoing differential rates of slope movement, problems can occur. This appears to be the case with the raised pipeline leading north from the community's fuel tank farm at the harbour (Figure 8). In a low-lying area, the pipeline is rigidly anchored to wooden crib foundations atop small gravel pads. Where the pipeline traverses a moderate slope, it is anchored to saucer disks designed to allow the pipe to flex and bend and at the same time 'float' above the underlying deforming sediments. A conspicuous angular kink in the pipe (Figure 8a) suggests that this system is not operating as it should, and that differential horizontal and vertical ground movement above and below the kink is bending the pipe, creating a potential for rupture. The displacement of the wooden cribbing also shows evidence of differential vertical movement, such that a second kink has formed (Figure 8b). This may relate to surface ponding of water around the structures and thawing of ice-rich sediments below, or to the formation of ice within underlying sediments. Gelifluction and slope sediment deformation may also be a long-term concern to the buried water pipeline servicing the hamlet, as there is potential for pressure buildup against the pipe in areas where it obliquely traverses slopes.

Sea-level change

The global mean sea level is rising. It rose about 1.8 ± 0.5 mm/yr from 1961 to 2003 (Meehl et al., 2007). During the decade 1993–2003, the rate was 3.1 ± 0.7 mm/yr, but it is not yet clear how much of that may have been due to decadal-scale variability rather than an acceleration in the trend. The effect of this sea-level rise at Cambridge Bay will depend on several factors. First, how the mean sea level in the Arctic Archipelago relates to the global mean sea level. Second, how fast the land is rising in the Cambridge Bay area. Third, the effects of ice melt from glaciers, ice caps and the Greenland and Antarctic ice sheets. The effects of
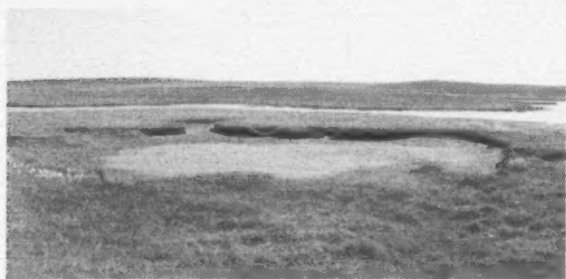
Figure 6: Small (8 m across) surface pond, south of the Uvayuq road (formerly known as Mount Pelly road), Nunavut, that has rapidly drained along thawing ice wedges, which intersected the pond.

Figure 7: a) Planners from the Canadian Institute of Planners and Government of Nunavut examining area of prominent periglacial activity (gelifluction and frost-churning) on lands proposed for development on the west side of the hamlet of Cambridge Bay, Nunavut. **b)** Well developed nonsorted circles up to 0.75 m wide in the same area.

Figure 8: a) Prominent kink in fuel pipeline outside Cambridge Bay, Nunavut, suggests that differential slope movement (gelifluction) is stressing and bending the pipeline. Several of the plastic saucers that the pipeline is affixed to are broken such that they appear to no longer 'float' atop the land surface, but instead, have become anchored to it. **b)** K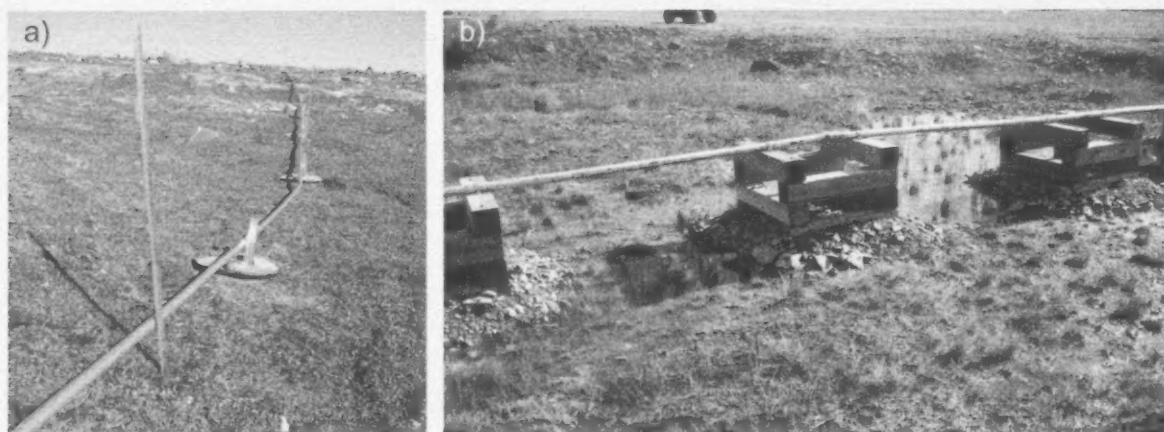ink in pipeline at right side of central wooden crib is likely the result of settling of the rightmost crib, to which the pipeline is rigidly adhered. Ponding of surface water in this area may have resulted in thawing of underlying ice-rich sediments leading to differential settling.

this melt will be variable around the globe. Counter-intuitively, the effect of Greenland ice melt will be to lower sea level in areas close to the ice sheet, including much of the Canadian Arctic. This is the so-called 'finger-printing' effect (Conrad and Hager, 1997; Mitrovica et al., 2001), which will serve to limit the rate of sea-level rise in most Canadian Arctic communities. These factors are explained and discussed at length in a Geological Survey of Canada report on projections of relative sea-level rise at the five pilot communities of the Nunavut Climate Change Partnership (James et al., 2011).

The present-day rate of postglacial uplift at Cambridge Bay, estimated by a self-consistent combination of geological evidence and from a geophysical model (see Allard et al., 2014), is 3.7 ±2 mm/yr (James et al., 2011). Thus, it is within the range of the reported rate of sea-level rise for 1993–2003 (Meehl et al., 2007). If local sea level rises more slowly than the rate of uplift, then sea level will appear to go down at Cambridge Bay (relative sea-level fall). However, if sea-level rise exceeds the rate of uplift, there will be a rise in relative sea level at a rate equal to the difference between the rate of sea level rise and the rate of uplift.

The effect of finger-printing will be to decrease the rates of sea-level rise in the Arctic. The various scenarios adopted by James et al. (2011) for projecting possible future relative sea-level rise at Cambridge Bay indicate a range for the next 90 years (2010–2100) from –25 cm (local sea-level fall) to +45 cm (local sea-level rise). They concluded that the most probable amount will be somewhere between –15 and +30 cm. Incorporating uncertainty in the estimate of land uplift, they estimated the range to be from –35 to +50 cm. The most recent report of the Intergovernmental Panel on Climate Change (2013) uses new emission scenarios and adjusts the estimates of the Meehl et al. (2007) re-

port, which was used for the local projections described above, but does not alter the conclusion that limited sea-level rise in Cambridge Bay is a possibility that needs to be considered in the planning process.

Short-term variability is also worth bearing in mind. Church and White (2006) showed that decadal average sea-level rise, on a global basis, ranged from –1 to +4 mm/yr between 1870 and 1995. This suggests that the recent acceleration documented from 1993 to 2003 is not anomalous, and there may be periods of several years when sea level rise is almost equal the rate of land uplift at Cambridge Bay and these may become more common with accelerated global sea-level rise.

The tidal range varies from neap to spring tides on a fortnightly pattern, and lesser variations occur at longer time scales. The tidal range at Cambridge Bay is small, 0.4 m at mean tides and 0.5 m at large (spring) tides, and the maximum recorded water level is 1.4 m (chart datum), 0.9 m higher than mean water level and 0.6 m above the level of higher high water at large tides (Canadian Hydrographic Service, 2002). During the late August 2009 field visit, there was a run of unusually high tides, with predicted high water at 1.0 m in the early afternoon from August 20 to 23 and 0.9 m in the mid-afternoon on August 24 and 25 (Figure 9a). This was apparent in observed flooding of *Puccinellia* sp. grass above the usual high-tide line along the shore below the airport road (Figure 9b). This grass typically occupies saline areas, above high tide, that are flooded intermittently by storm surges. On the afternoon of August 24, there was a brisk south wind forming small waves inside the harbour. These waves were able to rework beach gravel both southwest of the hamlet and along the shore southeast of the community and created a breach in the very thin fringing barrier beach a little farther west,

Figure 9: a) Local waves, generated inside bay by brisk southerly wind, mobilize gravel on small beach, southwest of the hamlet of Cambridge Bay, Nunavut. Water level near higher high tide, August 24, 2009. **b)** Water breaches a thin fringing barrier beach, southeast of the hamlet.

Figure 10: a) Rising tide, with onshore wind, flood *Puccinellia* sp. turf on gravel flats southwest of hamlet of Cambridge Bay, Nunavut, on August 24, 2009; approaching a 0.9 m (chart datum) high tide. **b)** Very small transgressive bayhead barrier beach in cove near fuel tanks, near the hamlet of Cambridge Bay, August 24, 2009.

flooding a saline meadow behind (Figures 9b, 10a). In a small cove nearby, a miniature bayhead barrier beach has formed (Figure 10b), suggesting that relative sea level is nearly stable.

Overall, coastal hazards at Cambridge Bay are thought to be minimal. The community is located on an excellent harbour with good protection from waves and mobile ice. The site also provides protection from storm surges and the gravel and rock shores in the harbour are reasonably resistant to erosion. Camps on the land along the coast to the west may be more exposed to waves from Coronation Gulf and more vulnerable to ice ride-up.

Urban hydrology

The ineffective and inefficient routing of meltwater and rainwater is universally identified as a problem in northern communities. Significant problems are created by poorly maintained (sometimes blocked) or undersized drainage culverts, insufficient grading of slopes and a lack of retro-

fitting of downstream drainage systems. The current systems cannot handle new upslope infrastructure development, which results in an increased and hurried routing of meltwater and precipitation. Examples of impeded drainage relating to these various factors were noted throughout the hamlet of Cambridge Bay (Figure 11).

Ponding of surface water was most prevalent in areas of western Cambridge Bay (Figures 11, 12). Surface water ponding is problematic for several reasons:

1) Water ponded on the surface absorbs solar energy more readily than surrounding earth materials. This heat is then transferred downward into the ground, potentially thawing underlying ice-bearing sediments.

2) The thawing of ice-bearing sediments leads to ground subsidence, which in turn leads to increased potential ponding of water. If water is allowed to pond in front of culverts, ground subsidence may eventually lead to stranding of the culverts above the lower water levels.
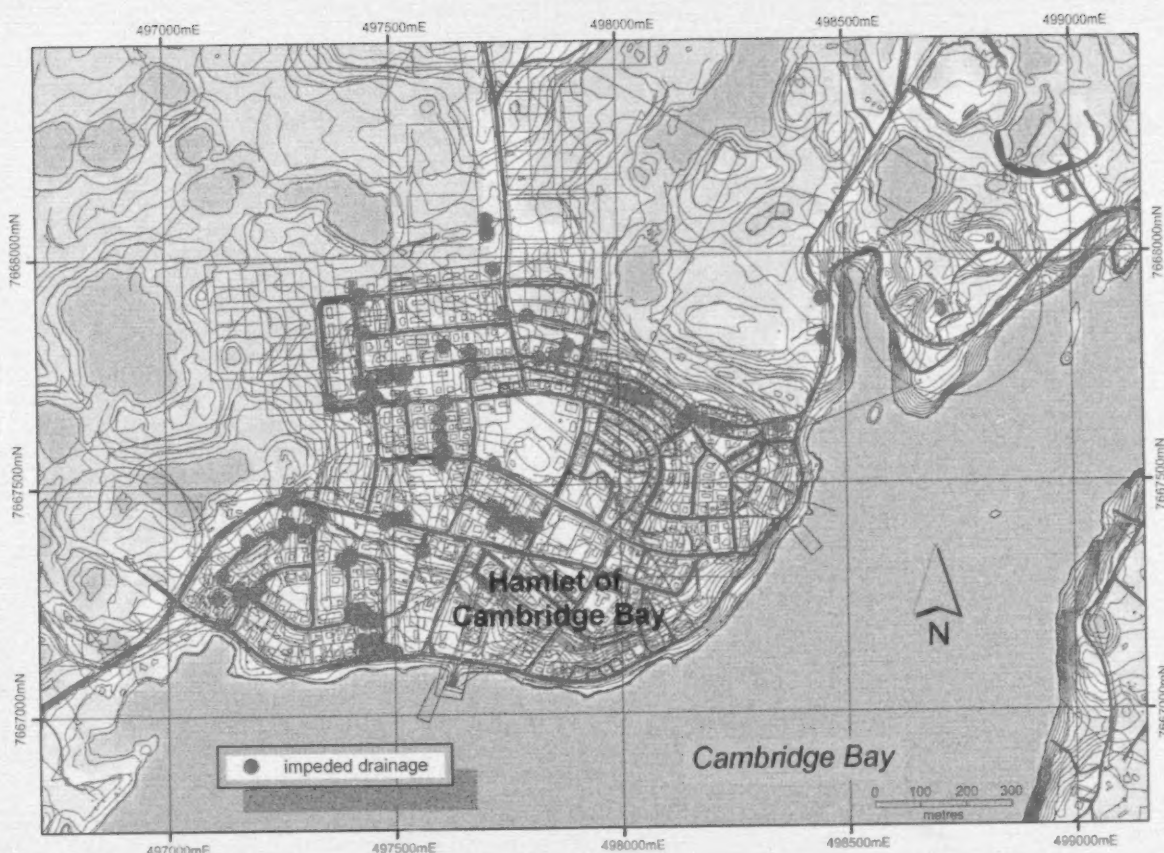
Figure 11: Sites noted in Cambridge Bay where surface water was impounded, or where culvert size, integrity or position appeared problematic, August 2009 (UTM zone 13N). Backdrop is orthorectified, 15 m resolution, panchromatic Landsat 7 imagery acquired in July 2001 (GeoBase®, 1999–2003); CAD vector mapping data (2009) courtesy of Government of Nunavut, Department of Community and Government Services, Kugluktuk; and National Road Network vector data from GeoBase® (2009).

Figure 12: Examples of ponded surface water in the hamlet of Cambridge Bay, Nunavut, owing to improper grading or positioning of drainage culverts.

Canada-Nunavut Geoscience Office

3) Ponding of surface water acts to saturate underlying active layer (seasonally thawed) sediments. During winter, these sediments will freeze and the volumetric expansion of ice accentuates ground heave, potentially causing damage to surrounding infrastructure.

4) Ponded, stagnant surface water will provide breeding habitat for mosquitoes, contributing to their nuisance factor. In addition, children playing in the stagnant water could be exposed to potentially harmful bacteria. Although the risk of this is lessened with the cool summer climate, future warming could lead to increased risk.

Surface water ponding was also identified along sections of the buried water pipeline servicing the community (Figure 13). Saturation of sediments surrounding the pipeline could lead to both differential heave and thaw settlement, affecting the pipeline's integrity over time. Improved grading/drainage may be required to address this issue if deemed a sufficient risk.

Snow drifting is also a significant component of urban hydrology planning, and is problematic in all Arctic communities. Several examples of former or derelict snow fences are found in the northwestern part of Cambridge Bay, clearly illustrating that it is a problem that the community has tried to mitigate in the past. In the planning of new infrastructure development, particularly in the peripheral and northwestern portions of Cambridge Bay, it would be wise to consider the potential for snow drifting when deciding on such things as building alignment and spacing and road design. The impacts of snow drifting go beyond issues of building access. Snow is a very effective insulator of the ground. Permafrost stability in the north is recognized in terms of both summer thaw potential and the intensity of winter freezing. If snow is allowed to accumulate in areas where it normally doesn't, then it will insulate the underlying permafrost preventing heat loss, which potentially

Figure 13: Surface water ponding adjacent to the buried water pipeline near the water-supply lake for the hamlet of Cambridge Bay, Nunavut. Surface water leads to saturation of underlying sediments and the seasonal formation of ice layers, resulting in increased ground heave.

leads to deeper summer thaw (downward expansion of the active layer) and thawing of ice-bearing sediments in summer. Snowdrifts also act to concentrate meltwater in spring and prolong the flow of water through the community.

Perceived sensitivities to climate change

Observations from this reconnaissance visit, and subsequent research presented above, are used to infer a range of landscape sensitivities to potential climate change in the Cambridge Bay region. It is stressed, however, that these inferences require more field-based study before they may be incorporated into a design/adaptation strategy. They are perhaps most useful in identifying knowledge needs/gaps that can be used to support the planning process.

1) In the specific context of climate warming, landscape hazards in Cambridge Bay appear to pose a low risk. This is not to say that there could not be significant impacts on local infrastructure. It is just that because most of the town is situated on a thin veneer of sand and clast-rich glacial sediments overlying stable bedrock, it can be regarded as occupying an enviable building platform. As the community expands into peripheral low-lying and sloped areas, where there is greater sediment thickness, ice content and periglacial activity, relative degrees of infrastructure risk may increase.

2) While increased open water and wave action brought on by reductions in summer sea ice create a significant threat to coastal stability in many Arctic communities, the protected setting of the Cambridge Bay harbour minimizes this risk. Houses, cabins and roads located near the seashore northwest of the airport and south of Tikiraaryuaq do potentially face increased threat of storm surge, wave action and ice ride-up or pile-up, as their exposure is much greater.

3) Thermokarst ponds, ice wedges and ground subsidence in areas of surface-water ponding demonstrate that varying quantities of excess ground ice occur within surficial deposits in the Cambridge Bay area. Assessment of ground ice content would be considered an integral part of any infrastructure expansion. While excess ground ice represents a potential hazard to infrastructure stability, in some cases it can be mitigated through effective engineering and design measures.

4) The coarse-grained, gravel-rich materials used to construct roads and building pads in the Cambridge Bay area are an asset to the region's infrastructure stability. Construction of roads and pads with more sand-rich material, as has been observed in other communities, makes them particularly vulnerable to washout from flooding during the spring snow melt and extreme summer rainfall events, as may be anticipated under various climate change scenarios. While the main community gravel pit north of the airport appears to be nearing its end, there are a number of sites near the townsite where

suitable bedrock is being quarried to produce granular aggregate. This is recognized as being costly, as well as having undesirable noise and dust issues associated with it, so undertaking a broader, regional, granular aggregate assessment may be beneficial to the community. Although the Freshwater Creek esker is too sandy to be of much use, other eskers in the region (Sharp, 1993) may have more promising sedimentological character, and could be accessed through winter-haul activities.

5) The use of gravel building pads and integrative space-frame foundations for new housing multiplexes appears well-adapted to environmental conditions in Cambridge Bay. In some cases, pad thicknesses were noted to vary between adjacent buildings, including sites where thicknesses appeared insufficient to ensure that foundations were raised above seasonal water ponding. The pads themselves appeared to be unable to fully thaw and drain each summer. Where expansion occurs to the northwest, attention will need to be paid to ensure sufficient pad thicknesses are used to mitigate periglacial activity in the area.

6) Urban hydrology will continue to be an area of focus and concern in reflection of present environmental conditions, as well as those that may occur as a result of future climate change. Attention to routing, integration and volume capacity of drainage networks will require reassessment with each stage of community expansion. Armouring of drainage ditches with coarser rock material may be required to prevent channel erosion, particularly in light of potentially extreme summer rainfall events or early season rain-on-snow events. As a general principle, surface ponding of water should be avoided wherever possible.

7) Snow drifting is a recognized development issue in Cambridge Bay. With a move to larger multiplex housing units, the importance of attention to drifting issues should increase, along with accordant concerns about access limitations, winter snow removal and spring melt. It is possible that large snow-fence structures, such as those employed upwind of the Road to Nowhere subdivision in Iqaluit, may be useful in mitigating some of the impacts of snow drifting in Cambridge Bay. Changes in snowfall amounts and storm trajectories projected to occur under various climate change scenarios may also require a reassessment of existing infrastructure adaptations.

Economic considerations

This paper seeks to illustrate existing environmental and landscape hazards in and around the hamlet of Cambridge Bay, and those that may be further compounded as a consequence of climate change. Understanding of these conditions and the risks they pose to infrastructure can be integrated with future community planning in order to enhance stability and sustainability, thereby reducing costs of infrastructure development and maintenance.

References

Allard, M., Manson, G.K. and Mate, D.J. 2014: Reconnaissance assessment of landscape hazards and potential impacts of future climate change in Whale Cove, southern Nunavut; *in* Summary of Activities 2013, Canada-Nunavut Geoscience Office, p. 171–182.

Biggar, K.W. and Sego, D.C. 1993: The strength and deformation behaviour of model adfreeze and grouted piles in saline frozen soils; Canadian Geotechnical Journal, v. 30, p. 319–337.

Canadian Hydrographic Service 2002: Canadian Tide and Current Tables, v. 4: Arctic and Hudson Bay; Fisheries and Oceans Canada, 88 p.

Church, J.A. and White, N.J. 2006: A 20th century acceleration in global sea-level rise; Geophysical Research Letters, v. 33, 4 p., L01602, doi:10.1029/2005GL024826

Conrad, C.P. and Hager, B.H. 1997: Spatial variations in the rate of sea level rise caused by the present-day melting of glaciers and ice sheets; Geophysical Research Letters, v. 24, p. 1503–1506.

Forbes, D.L., ed. 2011: State of the Arctic Coast 2010: Scientific Review and Outlook; International Arctic Science Committee, Land-Ocean Interactions in the Coastal Zone, Arctic Monitoring and Assessment Programme, International Permafrost Association, Helmholtz-Zentrum, Geesthacht, Germany, 178 p., URL <http://arcticcoasts.org> [October 5, 2013].

Furgal, C. and Prowse, T.D. 2008: Northern Canada; *in* From Impacts to Adaptation: Canada in a Changing Climate 2007, D.S. Lemmen, F.J. Warren, J. Lacroix and E. Bush (ed.), Government of Canada, Ottawa, Ontario, p. 57–118, URL <http://www.nrcan.gc.ca/earth-sciences/climate-change/community-adaptation/assessments/132> [October 5, 2013].

GeoBase® 1999–2003: GeoBase® Landsat 7 orthorectified imagery over Canada; Canadian Council on Geomatics, URL <http://www.geobase.ca/geobase/en/data/imagery/landsat/index.html> [November 7, 2013].

GeoBase® 2009: GeoBase® National Road Network, Nunavut, edition 4; Canadian Council on Geomatics, URL <http://www.geobase.ca/geobase/en/data/nrn/index.html> [September 16, 2009].

Government of the Northwest Territories 2011: Good building practice for northern facilities, 3rd edition; Government of the Northwest Territories, Department of Public Works and Services, 286 p., URL <http://www.pws.gov.nt.ca/pdf/GBP/GBP%202011.pdf> [October 5, 2013].

Hivon, E.G. and Sego, D.C. 1993: Distribution of saline permafrost in the Northwest Territories, Canada; Canadian Geotechnical Journal, v. 30, p. 506–514.

Intergovernmental Panel on Climate Change 2013: Summary for policymakers; *in* Climate Change 2013: The Physical Science Basis, Contribution of Working Group I to the Fifth Assessment Report of the Intergovernmental Panel on Climate Change, T.F. Stocker, D. Qin, G.-K. Plattner, M. Tignor, S.K. Allen, J. Boschung, A. Nauels, Y. Xia, V. Bex and P.M. Midgley (ed.), Cambridge University Press, Cambridge, United Kingdom and New York, New York, 27 p., URL <http://www.climate2013.org/images/uploads/WGI_AR5_SPM_brochure.pdf> [October 5, 2013].

James, T.S., Simon, K.M., Forbes, D.L., Dyke, A.S. and Mate, D.J. 2011: Sea-level projections for five pilot communities of the Canada-Nunavut Climate Change Partnership; Geological Survey of Canada, Open File 6715, 23 p.

Mate, D. and Reinhart, F., ed. 2011: Nunavut Climate Change Partnership workshop, February 15–16, 2011; Geological Survey of Canada, Open File 6867, 1 CD-ROM, doi:10.4095/288645

Meehl, G.A., Stocker, T.F., Collins, W.D., Friedlingstein, P., Gaye, A.T., Gregory, J.M., Kitoh, A., Knutti, R., Murphy, J.M., Noda, A., Raper, S.C.B., Watterson, I.G., Weaver, A.J. and Zhao, Z.-C. 2007: Global climate projections; *in* Climate Change 2007: The Physical Science Basis, Contribution of Working Group I to the Fourth Assessment Report of the Intergovernmental Panel on Climate Change, S. Solomon, D. Qin, M. Manning, Z. Chen, M. Marquis, K.B. Averyt, M. Tignor and H.L. Miller (ed.), Cambridge University Press, Cambridge, United Kingdom and New York, New York, p. 747–846.

Mitrovica, J.X., Tamisiea, M.E., Davis, J.L. and Milne, G.A. 2001: Recent mass balance of polar ice sheets inferred from patterns of global sea-level change; Nature, v. 409, p. 1026–1029.

National Round Table on the Environment and the Economy 2009: True north: adapting infrastructure to climate change in northern Canada; National Round Table on the Environment and the Economy, Ottawa, Ontario, 160 p., URL <http://nrt-trn.ca/climate/true-north> [October 5, 2013].

Okulitch, A.V. 1991: Geology of the Canadian Arctic Archipelago, Northwest Territories and North Greenland; Geological Survey of Canada, Map 1715A, scale 1:2 000 000.

Sharpe, D.R. 1993: Surficial geology, Cambridge Bay, District of Franklin, Northwest Territories; Geological Survey of Canada, Map 1825A, scale 1:250 000.

Statistics Canada 2006: 2006 community profiles; Statistics Canada, URL <http://www12.statcan.gc.ca/census-recensement/2006/dp-pd/prof/92-591/details/page.cfm?Lang=E&Geo1=CSD&Code1=6208073&Geo2=PR&Code2=62&Data=Count&SearchText=Cambridge Bay&SearchType=Begins&SearchPR=62&B1=All&Custom=> [November 7, 2013].

Reconnaissance assessment of landscape hazards and potential impacts of future climate change in Whale Cove, southern Nunavut

M. Allard[1], G.K. Manson[2] and D.J. Mate[3]

[1]Centre d'études Nordiques, Université Laval, Québec, Quebec, michel.allard@cen.ulaval.ca
[2]Geological Survey of Canada, Natural Resources Canada, Dartmouth, Nova Scotia
[3]Canada-Nunavut Geoscience Office, Iqaliut, Nunavut

Abstract

An assessment of terrain and coastal sensitivity to climate change in Whale Cove, Nunavut, on the west coast of Hudson Bay, was completed in 2009. Available climate data from 1986 to present show that significant warming is taking place and that inter-annual climate variability has increased. Community members reported on the impacts of these changes on living conditions and their traditional activities. The community was first established on low elevation beaches near the seashore and a small pond was filled to make room for early buildings. Currently, the community is expanding on relatively flat, glacially polished, bedrock surfaces, which make solid ground and are at little risk to be impacted by climate warming. Adapted foundations for buildings on unconsolidated surficial sediments will be necessary in the older part of the hamlet in preparation for warming permafrost and increased active layer depth. The shoreline in the townsite is primarily made of bedrock, but there are small pocket beaches, which host much of the coastal infrastructure. Sea-ice concentration is expected to decrease over the next few decades and it is anticipated that Whale Cove will experience higher and more frequent waves, which may cause localized erosion. With possible changes in storminess, storm surges may also become more frequent but will likely be no higher because storms are not expected to be significantly stronger. Relative sea level is falling in the area at a rate of approximately 6.4 mm/yr due to crustal uplift and sea-level change. This presents an issue for coastal infrastructure that will slowly be stranded above a lowering water line; wharfs may need to be lowered and extended. Accelerating global and regional sea-level rise may cause a slowing of the rate of emergence at Whale Cove in the future.

Résumé

Une évaluation de la sensibilité du terrain et des zones côtières aux changements climatiques a été réalisée en 2009 à Whale Cove, au Nunavut, sur la côte ouest de la baie d'Hudson. Les données climatiques recueillies depuis 1986 jusqu'à aujourd'hui révèlent que la région est sujette à un réchauffement important et que la variabilité interannuelle du climat a augmenté. Des membres de la communauté ont exprimé leur opinion au sujet de l'incidence de ces changements sur leurs conditions de vie et sur la poursuite de leurs activités traditionnelles. La collectivité a pris naissance sur les plages de faible élévation situées à proximité du rivage et un petit étang a dû être comblé afin de créer l'espace nécessaire à l'implantation des premiers immeubles. Actuellement, la collectivité continue de s'étendre sur des surfaces de substratum relativement plates, qui ont été polies par le passage des glaciers; il s'agit d'un sol ferme qui présente peu de risque de subir les répercussions du réchauffement du climat. Il faudra adapter les fondations des immeubles érigés sur des sédiments superficiels non consolidés dans la partie plus ancienne du hameau en prévision du réchauffement du pergélisol et de l'augmentation de la profondeur de la couche active. La ligne de rivage du lotissement urbain est constituée essentiellement de substratum rocheux, jalonnée de plages qui forment de petites enclaves sur lesquelles se dressent la plupart des infrastructures côtières. On s'attend à une diminution de la concentration en glace de mer au cours des prochaines décennies et il est alors possible que

Whale Cove subisse l'attaque de vagues plus fréquentes et plus hautes, susceptibles de causer de l'érosion à certains endroits. Les changements possibles au niveau de la sévérité des tempêtes laissent prévoir une fréquence accrue des ondes de tempête mais, puisque les tempêtes ne seront pas plus fortes, leur ampleur ne devrait pas changer. Le niveau relatif de la mer s'abaisse au rythme d'environ 6,4 mm/a en raison du soulèvement de la croûte et du changement du niveau de la mer. Cela pourrait causer des problèmes aux infrastructures côtières qui risquent de se trouver progressivement coincées au-dessus d'une ligne d'eau qui ne cesse de s'abaisser; il faudra possiblement procéder à l'abaissement et à l'extension des quais. À long terme, la vitesse croissante de l'augmentation du niveau de la mer à l'échelle mondiale et régionale pourrait entraîner un ralentissement du taux d'émergence à Whale Cove.

Introduction

Under a changing climate, Arctic communities, such as Whale Cove, Nunavut (Figure 1), are facing potential challenges related to the thawing of permafrost, expected sea-level changes, and evolving coastal erosion and storm-surge hazards. For example, the deepening of the active layer over time affects soil-bearing capacity, soil drainage and slope stability. Impacts are expected on building foundations and municipal infrastructure, as well as marine infrastructure at the shoreline. Adaptation planning is increasingly important to reduce the impacts of climate warming on terrain, coastal stability and community infrastructure.

Climate warming also generates impacts on the traditional way of life of Inuit, who harvest an important part of their food supply from the surrounding environment. This includes activities such as travelling, hunting, fishing and gathering on the land and at sea, notably in winter over the ice cover.

This short paper presents results of a brief assessment of terrain conditions collected during a field visit to Whale Cove on July 28–31, 2009. Some information relative to other impacts of climatic events and climate change was also obtained through discussions and meetings in the community.

Physiography and coastal geomorphology of Whale Cove

Whale Cove is located on the west coast of Hudson Bay (62°10'20"N, 92°34'47"W), between Arviat and Rankin In-
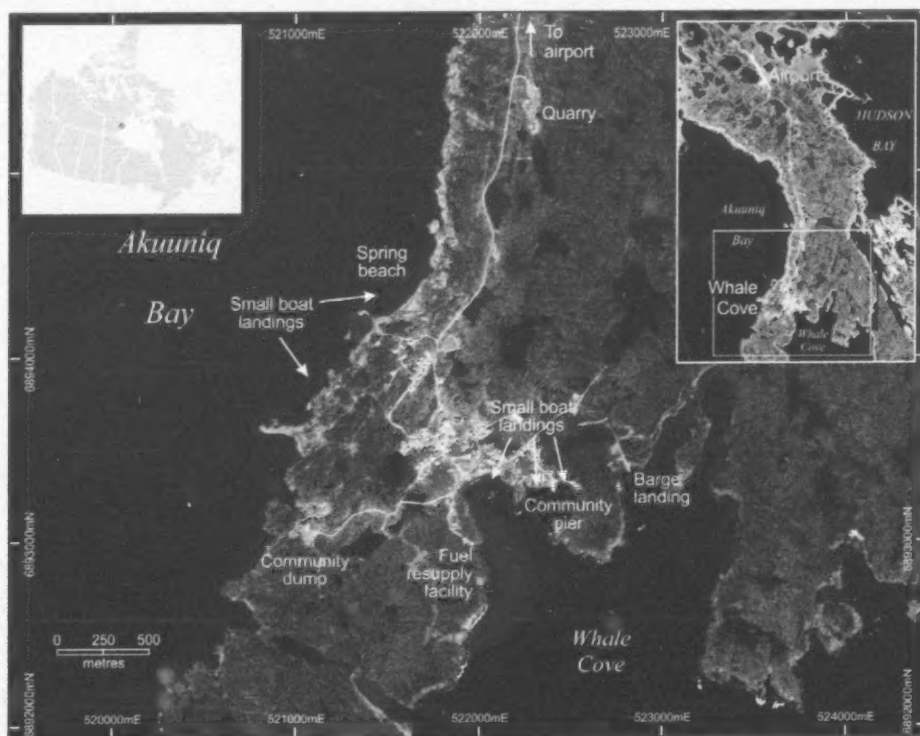

Figure 1: Satellite imagery of Whale Cove, Nunavut, showing coastal infrastructure. Background image (Quickbird; DigitalGlobe, Inc., 2006) includes copyrighted material DigitalGlobe, Inc., all rights reserved.

Canada-Nunavut Geoscience Office

let. The relief is generally low and the elevations in the hamlet gently rise from sea level to about 20 m above sea level (asl) on the rolling rock outcrops that make up most of the landscape. The airport, which is located 9 km inland, is built on a sandy plain at an elevation of only 8 m asl. Numerous lakes are located in rocky depressions.

The region is at the core of the Canadian Shield and the bedrock consists of various types of volcanic rocks, such as basalt, diorite and pillow lavas. Granite gneiss is also a widespread rock type. The outcrops are glacially profiled; roches moutonnées and striations are to be seen almost everywhere in the landscape.

Under the prevailing Arctic climate conditions, permafrost is present in the bedrock. This implies that water is frozen within structural features. The numerous bedrock heave features on outcrops across the region are the most widespread geomorphological evidence of the presence of permafrost in the bedrock (Figure 2). The region was deglaciated approximately 8000 years ago and was thereafter covered by the Tyrrell Sea. The peninsula emerged only recently.
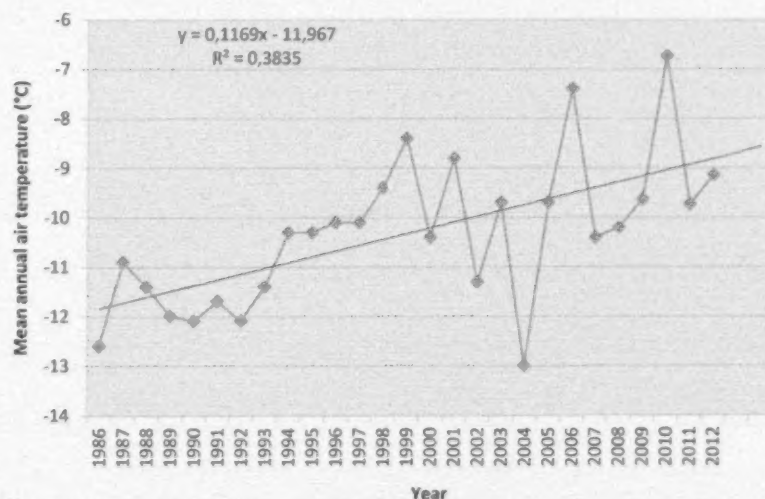
The townsite (Figure 1) is near the southern end of a rocky peninsula and flanked by a semi-enclosed bay to the west and Hudson Bay to the east. The shoreline is predominantly exposed bedrock covered in places by thin, raised, shelly, gravel beach deposits with thicker beach deposits accumulating in gullies between bedrock exposures. Beaches within the hamlet boundary are typically small pocket beaches confined between bedrock points, but farther north along the outer coast, fringing barrier beaches are common, as are multiple raised beach ridges on the emerged terrain behind.

The tidal range at Whale Cove is 2.2 m (large tides). Storms that bring high waves are typically easterly to southeasterly; waves can reach 3–4 m offshore in a 50 km/h wind but are lower once they impact the shoreline of the community (G. Enuapik, pers. comm., 2009). Based on 30-year medians (1981–2010) available from the Canadian Ice Service archives (Canadian Ice Service, 2013), freeze-up has typically occurred in early November and break-up of shorefast ice in early July.

Current climate and recent climatic trends

The nearest climate station with a good quality meteorological record is Rankin Inlet (airport). The normal (30-year average, 1971–2000) mean annual air temperature was –11°C (Environment Canada, 2013). Winter is very cold; from December to the end of March, the daily air temperature varies between –25 and –38°C. The midsummer months are typical of the shrub tundra ecoregion: mean temperatures are 10.6°C for July and 10.8°C for August. Mean long-term annual precipitation is about 300 mm. Total snowfall is about 120 cm and late-winter snow cover is on average 30 cm thick.

Mean annual air temperatures have significantly increased since 1986 (Environment Canada, 2013; Figure 3). The warming occurred in every month of the year (Environment Canada, 2013; Figure 4a, b). In the 1980s, mean annual air temperatures were around –12°C. However, temperatures have varied around –9.7°C since 1994. The average warming trend from 1982 to 2013 was 0.12°C/yr. The inter-annual variability is currently

Figure 2: Heaved bedrock disrupting a glacially polished rock surface, near Whale Cove, Nunavut.

$$y = 0,1169x - 11,967$$
$$R^2 = 0,3835$$

Figure 3: Mean annual air temperature in Rankin Inlet, Nunavut, 1986–2012 (Environment Canada, 2013).
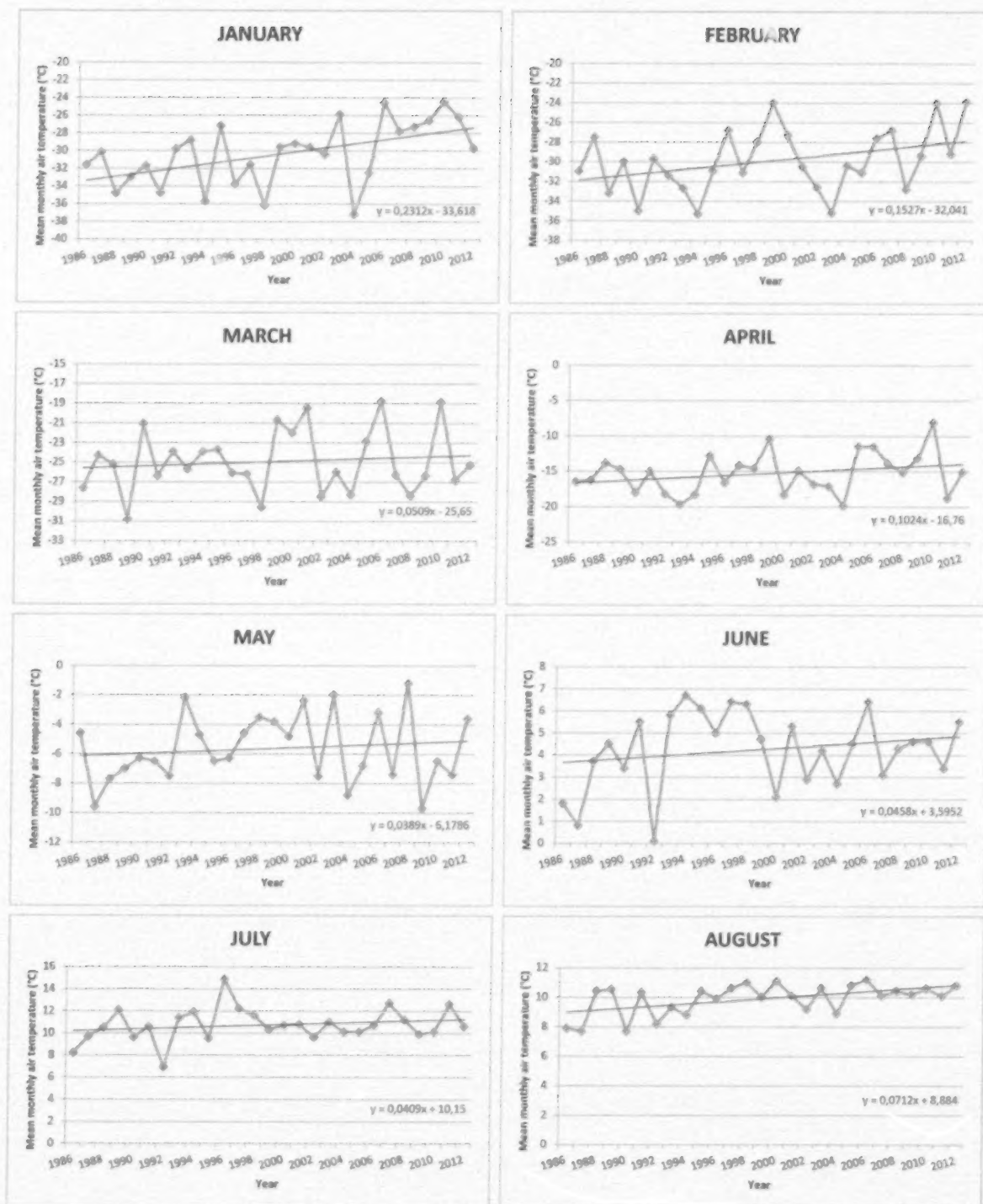
Figure 4a: Mean monthly air temperature changes in Rankin Inlet, Nunavut, January to August, 1986–2012 (Environment Canada, 2013).
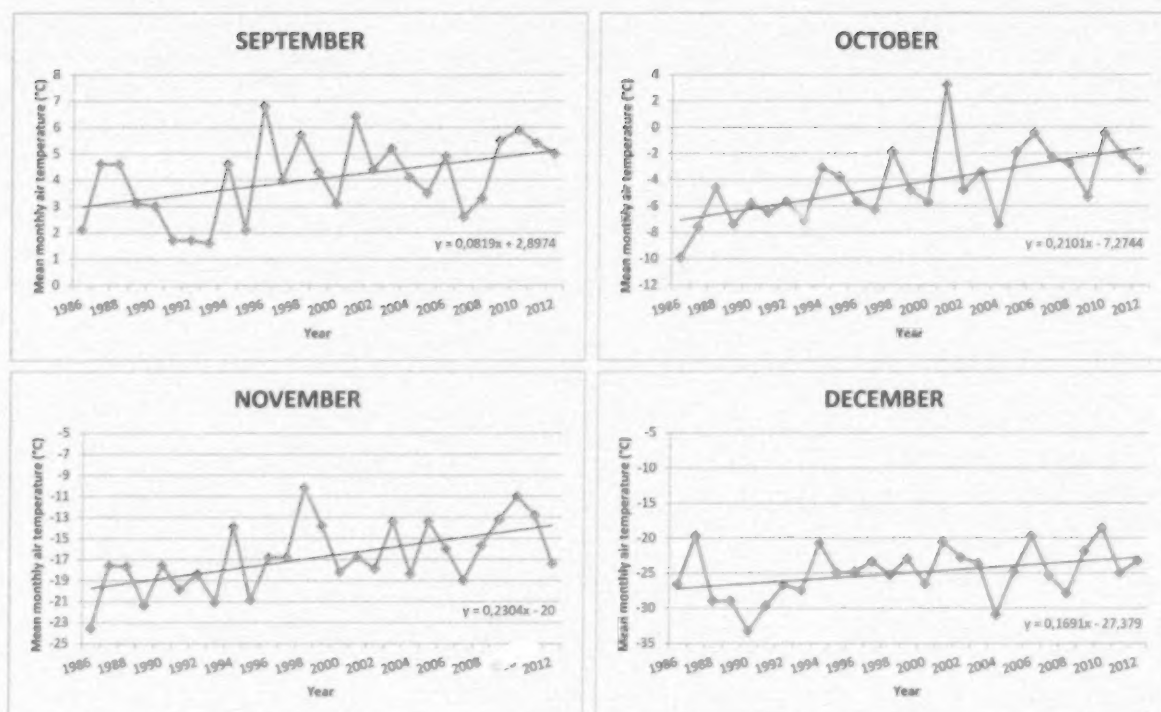
Figure 4b: Mean monthly air temperature changes in Rankin Inlet, Nunavut, September to December, 1986–2012 (Environment Canada, 2013).

greater than in the 1980s; for example, from 2004 to 2005 the mean annual air temperature jumped from –13 to –7.4°C. Such shifts imply important changes in daily and monthly temperatures and in seasonal effects, such as weather patterns, storm frequency and timing of ice formation on lakes and the sea. Analysis of Canadian Ice Service charts shows local sea-ice concentration at Whale Cove in November (freeze-up) has decreased significantly over the last few decades (Canadian Ice Service, 2013; Figure 5). This trend in sea-ice concentration and the increased variability in the weather make prediction of conditions more difficult, affecting traditional land-use practices.

Trend lines applied to mean monthly air temperatures indicate that the warming occurred principally over the fall and in early winter (Figure 4a, b). October, November, December and January temperatures increased at rates from 0.15 to 0.19°C/yr. In the spring, April also warmed at a rate of 0.10°C/yr. These values are in accordance with observations by community members of a delay in freeze-up of water bodies and sea-ice formation, as well as earlier and faster spring thaw accompanied by a fast freshet and sometimes flooding conditions along streams. Even though they remained cold, winters have definitely become shorter over the past 20 years.

Potential impacts on permafrost

The observed warming of air temperatures inevitably has an impact on permafrost. As ground temperatures increase, the summer thaw depth (the active layer) gets deeper. However, it cannot be said precisely how much the active layer has deepened in Whale Cove over recent years because there has been no monitoring of active layer depth and ground temperature. However, by general comparison with regions of comparable climate, it is estimated that the active layer may have increased by about 1 m in bedrock and by several centimetres, even decimetres, in sediments such as till (Smith et al., 2010). Permafrost thawing in the local bedrock has practically no impact on terrain stability because the rock is massive and contains very little ice. In areas of poorly drained surficial sediments, permafrost thawing makes the ground more sensitive to artificial disturbance. It may also destabilize some buildings and provoke some thaw settlement under roads and airport runways.

The landscape in Whale Cove is bedrock-dominated with a gently rolling topography, which makes it possible to continue development on stable ground (bedrock) while keeping away from the poorly drained sediment areas.

Map of ground conditions

As a support to decision making, a surficial geology map was prepared (Figure 6). The units of the legend represent broad
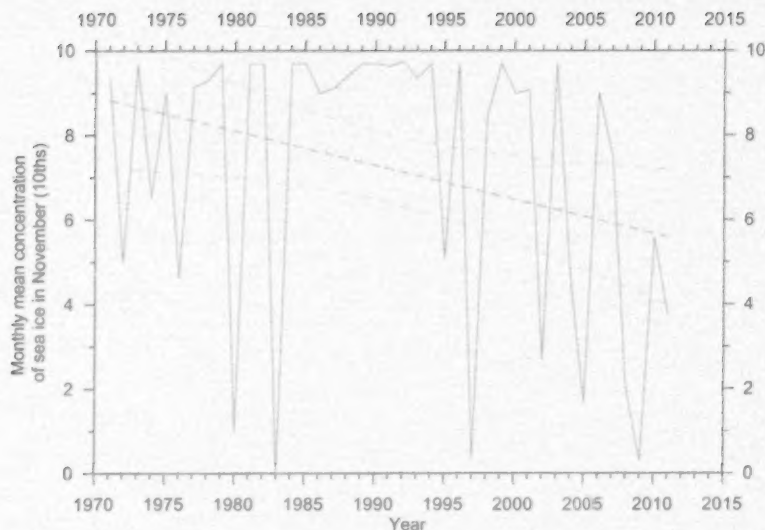
Figure 5: Trend in sea-ice concentration off Whale Cove, Nunavut, in November (1971–2011) showing a statistically significant decrease in sea-ice concentration at freezeup, implying a longer open-water season (Canadian Ice Service, 2013).

terrain categories that are representative of the site conditions that exist within the community and which so far have been taken into consideration by local managers and decision makers for urban planning.

The first map unit consists of poorly sorted sand and gravel, which is generally found at low elevations. A fraction of silt appears present in the sediments. This material is of marine origin. In many places within this map unit, drainage is poor in summer as the perched water table, overlying the permafrost, is close to the surface. This map unit includes an area of fill in the lower, older part of the community. This was the site of a small pond that was filled with marine sediments from nearby pits to allow building construction. The former pond area appears in the inset of Figure 6 as it was mapped from old airphotos. It must also be mentioned that the artificial soil at this former pond site was contaminated many years ago by a diesel fuel spill near the power station. One geotechnical study confirmed hydrocarbon contamination in this area (EBA Engineering Consultants Ltd., 1990). Dedicated geotechnical studies are recommended before establishing large buildings in this map unit. The new municipal garage in Whale Cove is a good example of an appropriate design as it was built on thermosyphons (Figure 7).

The second map unit consists of shallow (<6 m), shell-bearing, sandy-silty, poorly sorted sediments found in hollows between rock outcrops. In the deepest part of these deposits, some till appears to be present beneath these marine sediments. These marine sediments were reworked by waves and coastal ice during postglacial land emergence. They are the main source of fill and other aggregate material and are extracted from numerous local shallow pits.

Many of these pits have now been depleted and are mapped as bedrock in Figure 6.

The third map unit is bedrock that occurs over vast expanses of terrain. As the topography is rather flat and gently rolling over wide areas, this terrain type provides solid ground for construction. Some levelling is required and can be achieved by covering the bedrock surface with small quantities of fill material (Figure 8).

Airport site

The airport site was also inspected during the field visit. The gravel runway was in good condition. The surface is affected by numerous frost cracks that open in winter and sometimes sever buried cables, affecting runway lights that need to be fixed frequently. According to the person in charge of maintenance, the runway surface becomes soft during the spring thaw, which is normal for such infrastructure. Resurfacing is done every summer as part of normal maintenance. A concern was raised about its long distance from the community (>8 km), which makes efficient highway maintenance essential in order to maintain access to the airport but difficult after snowstorms as there is no garage for the machinery at the airport.

Coastal infrastructure

At Whale Cove, there are three main components of coastal infrastructure: the fuel resupply facility; the community pier; and the supply barge landing. There are several other areas where small boats are pulled ashore. These small boat landings range from skidways to landings on sand or gravel beaches cleared of boulders. The community dump is also close to the shoreline.

The fuel resupply facility (Figure 9) is located near the tank farm southwest of the community. Fuel barges moor offshore and connect temporarily to permanent onshore pipelines to refill tanks. No evidence of wave impact or flooding was observed on the infrastructure and the highest wrackline at time of observation was below the terminus of the pipeline.

The community pier (Figure 10) is a filled timber breakwater in a sheltered cove in the eastern part of the community. It was built circa 2004 and shows signs of ice damage at its southwestern corner. Its function is not clear as its deck is too high for use by the majority of boats in Whale Cove at the time of the field visit and its foot is too shallow for per-

Filled pond

········ Ditches
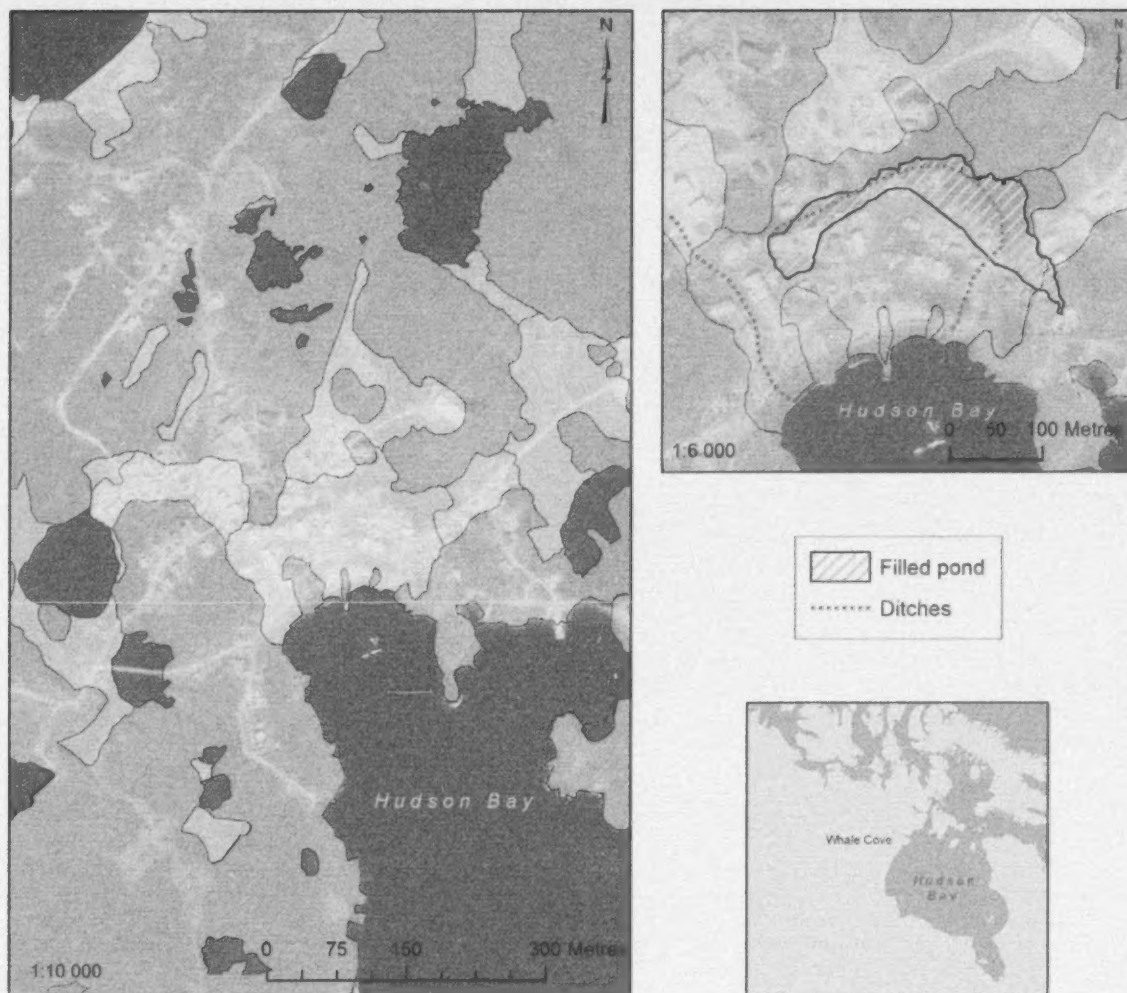
Surficial geology

Raised coastal, poorly sorted, silty sand and gravel. Includes fill material in former pond. Poorly drained.

Shallow cover (1-6 m) of surficial deposits. Shell-bearing, sandy-silty, poorly sorted sediments. Till sometimes found at depth between rock outcrops.

Bedrock (gneiss, basalt, pillow lavas). Includes areas where sediments have been extracted to bedrock.

Figure 6: Surficial geology of Whale Cove, Nunavut.

Figure 7: Garage built on thermosyphons, which keep the ground frozen under the concrete floor slab. Site is on fill material, which covers a former shallow pond, in Whale Cove, Nunavut. Note nearby poor terrain drainage.

Figure 8: Residential site built on bedrock in 2009, Whale Cove, Nunavut.
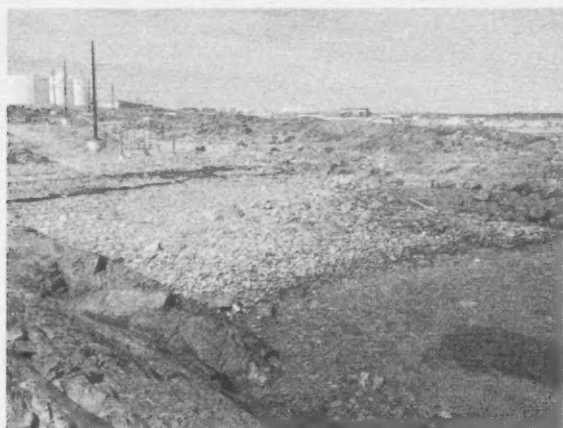
Figure 9: Fuel resupply facility with the tank farm and community in the background, Whale Cove, Nunavut.

Figure 10: The community pier showing ice damage and boats typical of the community, Whale Cove, Nunavut. Freighter canoes and Lund-style aluminum boats are also common.

manent mooring. There are two approximately 9 m vessels in the community that may use the pier for on- and off-loading at suitable tides.

The barge landing (Figure 11) receives supply barges. A floating dock is moored off the seaward end of the access road and connected to the road by a ramp. Gravel is pushed off the end to support the landward end of the ramp. Each September and October, the gravel at the end and sides of the causeway is lost. Some is recovered from the sides of the causeway the following year. There is a plan to stabilize the sides and front of the causeway with timbers, potentially solving the continued loss of gravel. Smaller landing barges, which unload sealift ships anchored offshore, will be able to dock at this modified facility.

The most significant of the small boat landings (Figure 12) is located in a narrow cleft just west of the community pier (middle arrow in Figure 1). The two largest boats in the community were pulled ashore at the time of the field visit. Other small boat landings are ad hoc on available beaches, sometimes with boulders removed to just below the low tide line.

The community dump (Figure 13) is located southwest of the community. It is partly located on raised beach deposits with intervening wetlands, and partly in blasted bedrock. The most seaward part of the facility impinges on recently active beach gravel. An earth retaining dam at this end of the dump is intended to prevent contaminated surface runoff entering the ocean.

Sea-level change

Whale Cove is currently experiencing falling relative sea level, which is a function of both vertical land motion and change in regional sea level. No tide-gauge records are available at Whale Cove, so the rate of relative sea-level fall

Figure 11: The causeway to the barge landing, Whale Cove, Nunavut. Piles of sand and gravel on the causeway have been recovered from the beach or newly excavated from inland sources.

Figure 12: The most significant small boat landing with skidway, Whale Cove, Nunavut. The two largest boats in the community were both pulled out though the green boat was relaunched the next day.

with respect to the land is unknown. James et al. (2011) use the rate of glacio-isostatic uplift given by ice model Ice-5G VM2 (Peltier, 2004; Figure 14) and a regional estimate of absolute sea-level rise under various scenarios of changing climate, including the effect of sea-level finger-printing, which depends on the global location of the source of meltwater flowing into the oceans. At Whale Cove, this analysis indicates glacio-isostatic uplift at approximately 8.2 mm/yr. Taking a globally averaged rate of absolute sea-level rise over the last four decades of 1.8 mm/yr (Intergovernmental Panel on Climate Change, 2007), this suggests a present-day rate of relative sea-level fall of approximately 6.4 mm/yr. Figure 15 shows how relative sea level can be falling while global (and regional) sea level is rising and also why coastal lagoons are shrinking—a phenomenon described by residents of Whale Cove.

Figure 13: The community dump adjacent to an active pocket beach showing surface runoff behind an earth containment dam, Whale Cove, Nunavut.

James et al. (2011) project future amounts of sea-level change at Whale Cove to the year 2100. Though the range in the different scenarios is 0.84 m, the results suggest that future rates of sea-level fall will probably be between 6.1 and 0 mm/yr. The range reflects that there is uncertainty and that regional and global sea-level rise is expected to increase over the projected time-frame. Whale Cove is not expected to switch to a regime of relative sea-level rise by 2100, but the relative rate of sea-level fall shall decrease over time.

Economic implications

Large expanses of bedrock-dominated terrain with a manageable topography are available for the future development of residential areas in Whale Cove. With proper but somewhat more expensive engineering designs, the other terrain types can also be used. Examples of well-constructed new buildings with adapted foundations, such as the hospital, the community centre and the garage, are found in the community.

The community has begun to adapt properly to permafrost thawing, thanks to rather favourable geological and topo-
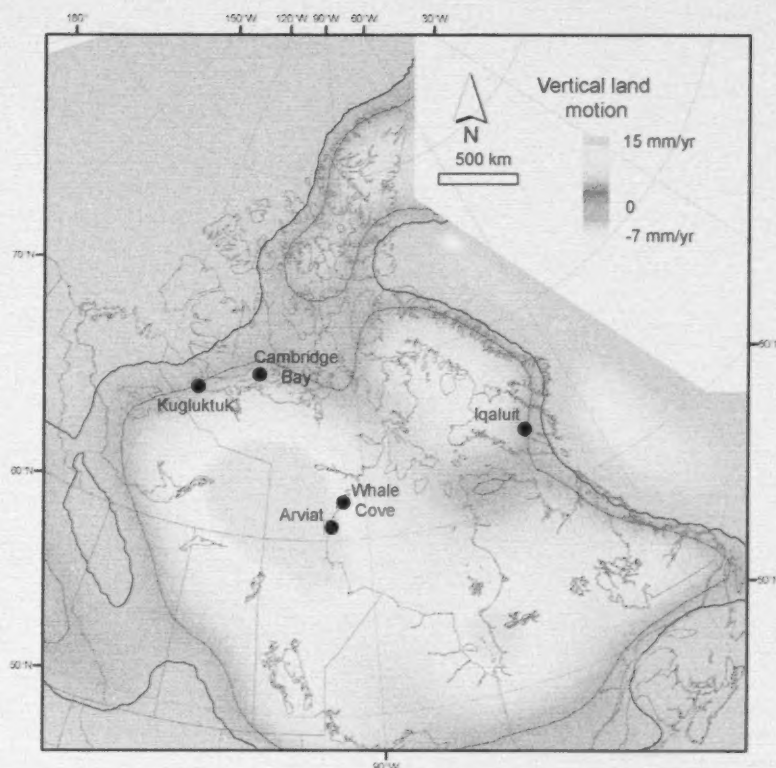
Figure 14: Rates of vertical land motion over the last 500 years from ice model Ice-5G Version 1.2/VM2, northern Canada (Peltier, 2004). Whale Cove and Arviat are located just east of a significant area of rapid uplift, Cambridge Bay is farther away from the area of uplift, and both Kugluktuk and Iqaluit are closer to zones of subsidence. The darker solid line between purple and brown represents the 0 mm/yr isobase (i.e., no vertical motion) and the lighter line shows the 2 mm/yr isobase where relative sea level may begin to rise over the next 100 years. Kugluktuk and Iqaluit lie very close to this line, but the other communities are less likely to experience sea-level rise.
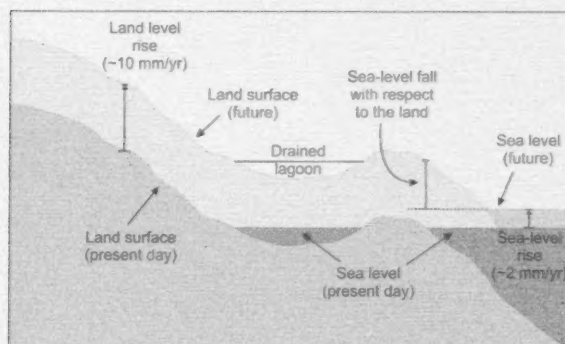

Figure 15: Schematic illustration of land uplift, sea-level rise and relative sea-level fall.

graphic conditions. Eventually, the airport could need more maintenance as the active layer deepens.

Under falling relative sea level, over time the elevation of storm-surge flooding decreases, assuming unchanging storminess and sea ice. Therefore, exposure and vulnerability to storm-surge flooding at Whale Cove is expected to decrease. Though there is little consensus on changing storminess under changing climate (e.g., Intergovernmental Panel on Climate Change, 2007), one scenario of changing storminess suggests increased frequency of the most severe storms (Lambert, 2004) with the potential for increased frequency of storm-surge flooding at Whale Cove. Under falling relative sea level, even with increased frequency of severe storms, over time the vulnerability of coastal infrastructure in Whale Cove is expected to decrease, resulting in reduced repair costs.

With falling relative sea level, storm-wave energy is focused lower on the shoreface and vulnerability of coastal infrastructure to erosion decreases. However, with anticipated reduction in sea ice, waves can grow higher and act on shorelines for a longer period of time in the year. As with storm surges, the more severe events may be expected to occur more often and Whale Cove may experience increased localized erosion of beaches due to more frequent and severe waves. Bedrock sections of the shoreline will not be significantly eroded. Given falling relative sea level and low exposure and sensitivity to storm-surge flooding and erosion, vulnerability is expected to remain low.

One implication of continued sea-level fall is that coastal infrastructure slowly becomes separated from the sea. Wharves become too high to be usable and the approaches become too shallow for the vessels for which the infrastructure was designed. Options include abandonment, or a planned strategy of lowering wharf levels and extending them offshore, with associated costs.

An area of concern is the earth dam at the community dump. Depending on the rate of increase in severity and frequency of storm waves relative to the rate of relative sea-level fall, the dam may be increasingly exposed and sensitive to erosion. Given the risk of contaminated surface water entering the marine ecosystem, should the earth dam be breached, and that the community is currently considering some improvements to the facility, there is an opportunity to redesign the surface water management strategy at the dump and reduce the potential for contaminated water to enter the marine ecosystem. Costs associated with redesigning the

community dump may be significant, but the present situation is unsustainable, even under falling relative sea level.

Conclusions

The geomorphology of Whale Cove is dominated by bedrock, which provides solid ground for new construction and limits the sensitivity to waves and erosion along the shore. However, the main coastal infrastructure is located on the several beaches in the community. These tend to be in protected bays and the risk of most infrastructure to coastal erosion is probably low. However, sea ice is expected to decrease (in concentration and seasonal duration), resulting in a longer open-water season and greater open-water fetch, allowing higher waves to build during storms. It is also possible that the frequency of severe storms may increase, which would cause more erosion and storm-surge events. The community dump site may be the infrastructure that is most vulnerable to erosion and storm-surge flooding, with potential for release of contaminated water into the marine environment.

These risks will be mitigated, over time, by relative sea-level fall. Climate change is not expected to cause a switch to relative sea-level rise in Whale Cove, but may reduce the rate of fall by a few millimetres per year. Storm surges will in the future reach lower shoreline elevations.

Sea-level fall does cause some impacts on the continued utility of coastal infrastructure. As the waterline recedes, the approaches to the community pier, the fuel resupply facility and the barge landing site will be more difficult with shallower water. It may be necessary in the future to extend or lower waterfront infrastructure, incurring added costs. Planning of future infrastructure should consider the implications of changing climate as presented here.

Climate warming and increasing variability in meteorological and sea-ice conditions will continue to affect the way of life of the people of Whale Cove.

Acknowledgments

References

Canadian Ice Service 2013: Canadian Ice Service archive; Environment Canada, Canadian Ice Service, URL <http://iceweb1.cis.ec.gc.ca/Archive20/?lang=en> [September 2, 2013].

DigitalGlobe, Inc. 2006: QuickBird-2 satellite image; Digital Globe, Inc., image, URL <https://browse.digitalglobe.com/imagefinder/showBrowseMetadata?catalogId=10100100051A2800> [October 8, 2013].

EBA Engineering Consultants Ltd. 1990: Final geotechnical evaluation report, proposed new arena, Whale Cove, NWT; Government of the Northwest Territories, Department of Public Works, Architecture Division, Report 071-10453, 27 p.

Environment Canada 2013: Canadian climate normals; Environment Canada, URL <http://climate.weather.gc.ca/climate_normals/index_e.html> [October 8, 2013].

Intergovernmental Panel on Climate Change 2007: Climate Change 2007: The Physical Science Basis, Contribution of Working Group 1 to the Fourth Assessment Report of the Intergovernmental Panel on Climate Change; Cambridge University Press, Cambridge, United Kingdom, 996 p.

James, T.S., Simon, K.M., Forbes, D.L., Dyke, A.S. and Mate, D.J. 2011: Sea-level projections for five pilot communities of the Nunavut Climate Change Partnership; Geological Survey of Canada, Open File 6715, 21 p.

Lambert, S.J. 2004: Changes in winter cyclone frequencies and strengths in transient enhanced greenhouse warming simulations using two coupled climate models; Atmosphere-Ocean, v. 42, p. 173–181.

Mate, D. and Reinhart, F., ed. 2011: Nunavut Climate Change Partnership workshop, February 15–16, 2011; Geological Survey of Canada, Open File 6867, 1 CD-ROM, doi:10.4095/288645

Peltier, W.R. 2004: Global glacial isostasy and the surface of the ice-age earth: the ICE-5G (VM2) model and GRACE; Annual Review of Earth and Planetary Science, v. 32, p. 111–149.

Smith, S.L., Romanovsky, V.E., Lewkowicz, A.G., Burn, C.R., Allard, M., Clow, G.D., Yoshikawa, K. and Throop, J. 2010: Thermal state of permafrost in North America: a contribution to the international polar year; Permafrost and Periglacial Processes, v. 21, p. 117–135.

Reconnaissance assessment of landscape hazards and potential impacts of future climate change in Arviat, southern Nunavut

D.L. Forbes[1,2], T. Bell[2], T.S. James[3,4] and K.M. Simon[4]

[1]*Geological Survey of Canada, Natural Resources Canada, Dartmouth, Nova Scotia, dforbes@nrcan.gc.ca*

[2]*Department of Geography, Memorial University of Newfoundland, St. John's, Newfoundland and Labrador*

[3]*Geological Survey of Canada, Natural Resources Canada, Sidney, British Columbia*

[4]*School of Earth and Ocean Sciences, University of Victoria, Victoria, British Columbia*

Abstract

This paper summarizes observations of surficial geology and landscape hazards relevant to infrastructure stability and community sustainability in Arviat, Nunavut. It is based on a site visit and rapid reconnaissance survey in July 2009 in support of climate-change adaptation planning. The scientific work focused on surficial deposits, permafrost and ground ice, slope stability, runoff and drainage, sea-level change, and coastal processes in relation to building foundation stability, building pad construction, safety and viability of coastal infrastructure, and land-use planning for community expansion. These issues were addressed by mapping surficial materials and landscape units based on a brief reconnaissance survey and interpretation of high-resolution optical imagery. Through a classification of relative risk to infrastructure for various surficial materials, a preliminary map of foundation stability risk was developed to support adaptation planning under the Nunavut Climate Change Partnership and to provide general guidance on the challenges facing future development in various parts of the community.

Résumé

Le présent rapport résume certaines observations faites au sujet de la géologie de surface et les risques géomorphologiques dans la région d'Arviat, au Nunavut, dans la mesure où ces questions ont trait à la stabilité des infrastructures et à la durabilité de la collectivité. Ces observations ont été faites au cours d'une visite sur place et d'un bref levé de reconnaissance réalisés en juillet 2009 dans le cadre d'activités de planification des mesures d'adaptation aux changements climatiques. Les travaux scientifiques ont surtout porté sur les dépôts de surface, le pergélisol et la glace dans le sol, la stabilité des pentes, le ruissellement et le drainage, le changement du niveau marin et les processus côtiers par rapport à leurs répercussions sur la stabilité des fondations d'immeubles, la construction de plates-formes de bâtiments, la sécurité et la viabilité des infrastructures littorales et la planification liée à l'aménagement des terres en vue d'une expansion communautaire future. Pour traiter ces questions, on a eu recours à la cartographie des matériaux de surface et des unités géomorphologiques à partir d'un levé de reconnaissance de brève durée et de l'interprétation d'images optiques à haute résolution. En se basant sur une classification du degré relatif de risque aux infrastructure en fonction de divers matériaux de surface, on a pu dresser une carte préliminaire du degré de risque à la stabilité des fondations. Non seulement cette carte peut-elle jouer un rôle au niveau du processus de planification des mesures d'adaptation dans le cadre du Partenariat sur les changements climatiques du Nunavut, mais encore peut-elle fournir des conseils d'ordre général au sujet des défis auxquels devront faire face toutes les activités futures de mise en valeur entreprises à différents endroits de cette collectivité.

Introduction

Arviat is located along the west coast of Hudson Bay at 61°09'N, 94°14'W, in the Kivalliq Region of Nunavut (Figure 1). The community (formerly Eskimo Point) is located 215 km south of Rankin Inlet and 260 km north of Churchill, Manitoba. It is the third largest urban centre in Nunavut with a population of 1810 in the 2011 census, a 1.4% growth since 2006 (Statistics Canada, 2013). There is a high demand for new housing, and the built-up area of Arviat has expanded rapidly in recent years. However, issues of foundation instability, specifically frost jacking, thaw settlement and possible instability related to saline permafrost, have emerged in both older and new construction. There is a need for information on foundation conditions, surface water drainage, slope stability and other issues relevant to infrastructure resilience. These other issues include coastal changes and hazards, such as land uplift and relative sea-level rise, the implications of falling local sea levels for navigation and sealift operations, potential hazards associated with storm surge and wind-driven waves in summer, changes in landfast sea ice and the duration of the open-water season. People in this region have vivid memories of starvation in the last century and are well aware of the need for adaptation, but today's dependence on built infrastructure places some limits on adaptive capacity and resilience. The purpose of this study was to gather an information base for adaptation planning.

This project was undertaken within the Nunavut Climate Change Partnership (NCCP; Mate and Reinhart, 2011) together with the Government of Nunavut (GN) and volunteer planners from the Canadian Institute of Planners (CIP). The Arviat work was mirrored in other NCCP pilot communities (Allard et al., 2014; Smith, 2014; Smith and Forbes, 2014), although specific methodology and products varied from site to site. The scientific team for the Arviat work carried out a number of other studies. These included an extensive sampling effort to improve knowledge of postglacial relative sea-level change, particularly within the past few thousand years, and also to quantify rates of uplift as a contribution to more robust projections of local sea-level change (James et al., 2011; Couture et al., 2014). In addition, a team from the Canada Centre for Remote Sensing (now the Canada Centre for Mapping and Earth Observation), Natural Resources Canada (NRCan), carried out work on freshwater resources and surveyed a number of lakes in the vicinity to identify potential backup sources of potable water (Budkewitsch et al., 2011).

Physical setting

Arviat lies within the Western Churchill Province of the Canadian Shield and specifically within the Hearne domain, which is composed of predominantly Archean early crust (Tella et al., 2007). The bedrock exposed in Arviat is Proterozoic dark grey paragneiss with lenses of quartz, forming low whalebacks carved by ice flow during and after the last glacial maximum (LGM). Following the LGM, the ice centre west of Hudson Bay shifted eastward to form the Keewatin Ice Divide, about 250 km west of the present-day coast. Outflow from this topographic high was approximately eastward in the Arviat region (Aylsworth and Shilts, 1989), creating elongated drumlins and large flutes over much of the landscape to the west of the community (Figure 1). A thin veneer of ice-contact deposits (glacial till) is present over much of the landscape as well as thicker till forming ribbed moraines in some areas. Evidence of ice flow and recession is also revealed by the many east-trending eskers (Aylsworth and Shilts, 1989).

The opening of Hudson Strait after 9 ka ^{14}C BP (10.2 ka cal. BP) triggered rapid recession of the ice-sheet margin on the west side of Hudson Bay, probably along a tidewater ice front, as esker deposits continued to be laid down and fine sediment (mud) settled out of suspension on the newly formed seafloor. The postglacial Tyrrell Sea was formed by the expansion of late-glacial Hudson Bay over the isostatically depressed land surface. It reached a maximum elevation of about 170 m above present sea level shortly after 8 ka cal. BP and extended as much as 150 km west of the current coast (Dyke, 2004). The subsequent isostatic rebound

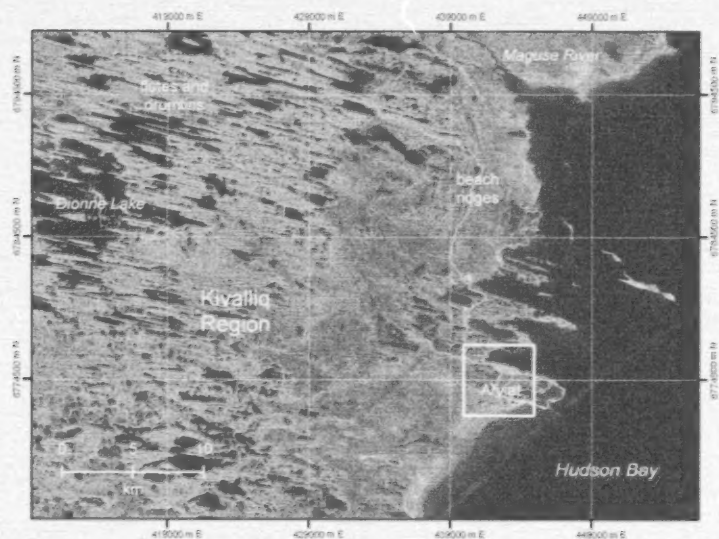**Figure 1:** Geographic setting of Arviat, Nunavut, on west coast of Hudson Bay, with partial road network (in orange) based on field surveys. The white box shows the area of the surficial geology and landscape hazards maps (Figures 3, 5). Backdrop is orthorectified, 15 m resolution, panchromatic Landsat 7 imagery acquired in July 2001 (GeoBase®, 1999–2003; UTM zone 15N).

Canada-Nunavut Geoscience Office

(uplift) and emergence resulted in reworking of the glacial and marine deposits into flights of raised beaches, visible in Figure 1 (north of Arviat).

Arviat is located on an esker ridge along the southern shore of the harbour (Figure 2a). This ridge forms the north side of a peninsula extending eastward into Hudson Bay (Figure 1). A second, parallel, esker ridge forms the southern edge of the peninsula. In previous work, Arsenault et al. (1981) mapped the two main esker ridges and an extensive cover of shallow-marine deposits, which includes raised beach ridges, thin sheets of sand representing emergent coastal reworking of marine mud and silty sand, and abandoned tidal flats with peat cover. The terrain is slightly rolling with a general increase in elevation westward away from the coast. Although the townsite on the esker ridge is about 10 m above mean sea level, the built-up area is fairly flat (Figure 2b). An extensive shallow wetland covers a large part of the subtle depression between the two esker ridges. Much of the wetland has been capped with gravel pads for construction of housing and infrastructure (Figure 2c).

The climate of Arviat is cold and dry, with mean daily temperatures from +11°C in July to –29°C in January and total annual precipitation of 286 mm, of which 112 mm (39%) falls as snow (Canadian climate normals, 1981–2010 [Environment Canada, 2013]). Arviat lies within the continuous permafrost zone (Brown et al., 2001). The thickness of the active layer (maximum depth of summer thaw) varies with the sediment properties, from <0.5 m in poorly drained organic-rich deposits to 1.5 m or more in well drained outwash sediments (Shilts et al., 1976). The tides are semidiurnal and the large (spring) tidal range is about 4 m (Canadian Hydrographic Service, 2002). Hudson Bay has extensive sea-ice cover in winter but the mean dates of freeze-up and break-up have been changing, resulting in a longer open-water season and a higher probability of fall storms occurring with open water (Forbes et al., 2008; Allard et al., 2014). Little information is available on storm characteristics, wave climate or storm surges in the Arviat region.

Methods and survey activities

Members of the science team were onsite for one week (July 6–13, 2009). On the first day, the team (including scientific staff, CIP planners, GN staff, a hamlet official and a local elder) toured the hamlet on foot and met in the council chamber for a discussion of issues. During this tour, it was apparent that surface drainage issues are a concern within the built-up area (Figure 2c, d). Water is retained at the surface because of the low surface slope, underlying ice-bonded and impermeable sediments or rock at shallow depth and poor drainage infrastructure. Differential movement of piles and damage due to local thaw subsidence was

apparent at a number of sites (Figure 2e), but most structures in the community were found to be supported on adjustable wooden blocks or, for more recent construction, on space frames (trihedral frame supports; Figure 2f). The morning discussion included a consideration of future development trends and siting options for construction of additional housing. The afternoon provided an opportunity for an initial survey of the area surrounding Arviat.

Landscape hazard mapping was carried out for a 25 km^2 area surrounding the built-up part of Arviat (Figure 1). Following the earlier work of Arsenault et al. (1981), the mapping reported here was carried out independently using high-resolution satellite imagery to discriminate built infrastructure, geomorphology, surficial geological units, shallow nearshore seabed and hydrological features (lakes and channels). The image interpretation was validated by ground observations of surface materials and examination of shallow sections in channel cuts and gravel pits. This information was used to create a surficial geology (surface materials and landscape units) map for the study area. Landscape hazards were identified in relation to sediments prone to slope failure (marine muds), ice-rich deposits susceptible to differential thaw settlement (shallow-marine sediments, organic cover including areas of high-centre polygons, and existing wetlands), coastal features open to nearshore ice pressure, storm-surge flooding, wave action and shoreline erosion, among others. A landscape hazards map was developed using a simple green-amber-red colour scheme pioneered in other pilot studies in Nunavut, notably Arctic Bay and Clyde River (Ford et al., 2006; Irvine et al., 2007).

A GPS survey monument (designated ARVI) was established on a rock knoll west of the south end of the runway. A geodetic-quality GPS antenna was set up over a steel pin cemented in bedrock, and the receiver was operated for five days. Subsequent GPS occupations in 2010 (three days) and 2012 (three days) and processing of data in International Terrestrial Reference Frame (ITRF) 2005, using the Canadian Spatial Reference System Precise Point Positioning (CSRS-PPP) tool of the Canadian Geodetic Survey (Natural Resources Canada, 2013), indicate an uplift rate of <10 mm/yr (Couture et al., 2014).

Elevations were determined for raised shoreline features and the sites of organic samples collected for radiocarbon age determination to improve knowledge of sea-level change. In 2009, a post-processed static differential GPS was used with a base station at Government of the Northwest Territories bench mark 6019210 on the c   of the former airstrip near the reservoir. The position   us monument was also determined by CSRS-PPP a   the geoidal correction was validated by surveys of water level.
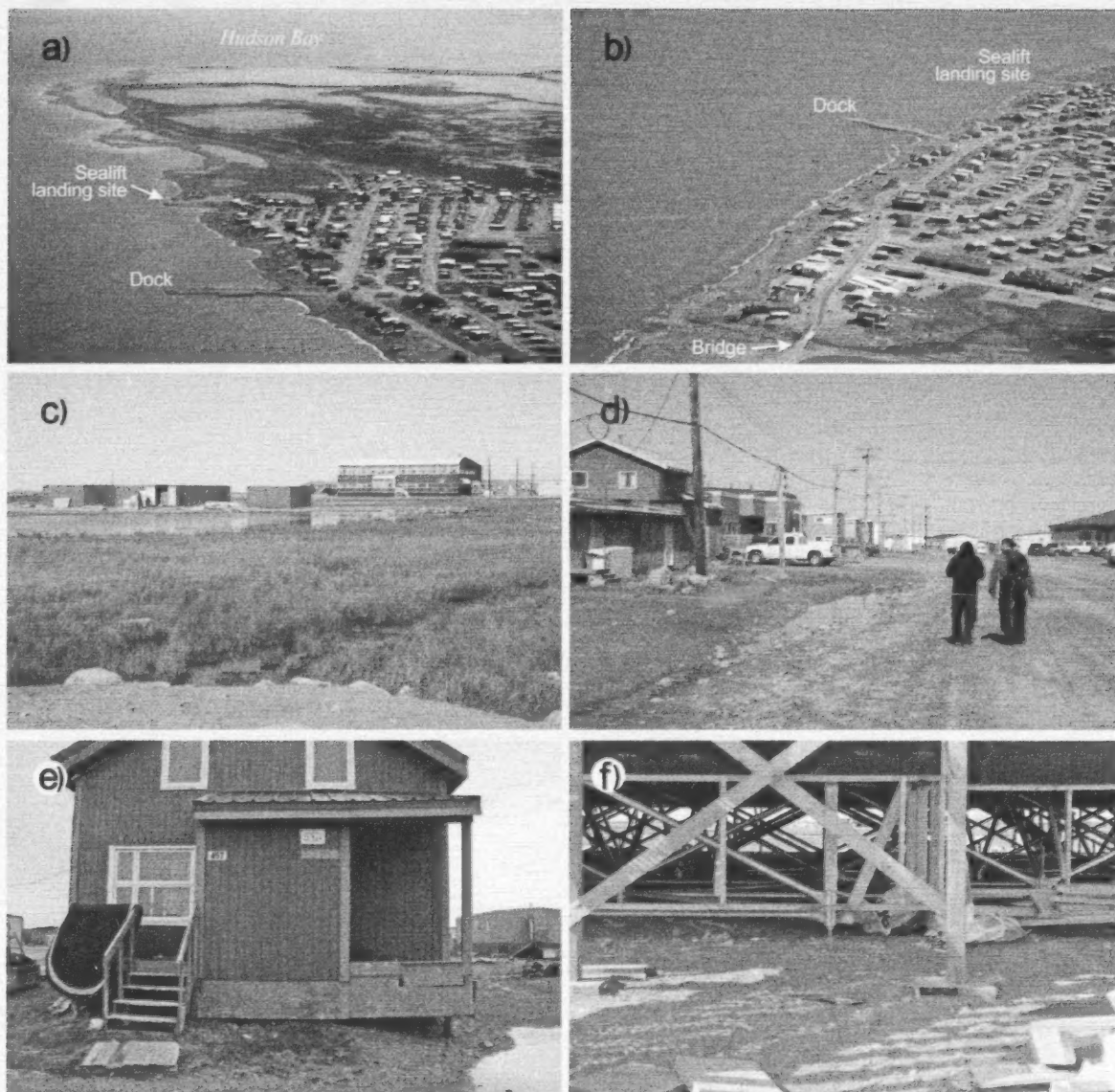
Figure 2: a) Oblique aerial view of Arviat, Nunavut, looking east with harbour at left and Hudson Bay in the background; note dock in foreground and sealift landing site in middle distance (July 13, 2009). **b)** Closer overview showing bridge over lake drainage channel (site of slope failure in Figure 4b) and development impinging on wetland in right foreground (July 13, 2009). **c)** Development expanding across wetland over thin layers of fill on south side of community (July 7, 2009). **d)** Ponded water in ditch along a major street in Arviat (July 7, 2009). **e)** House deformed by frost jacking of pile beside depression, which may have resulted from thaw subsidence under ponded water (July 11, 2009). **f)** Space-frame foundation of multiplex under construction on thin fill over wetland (July 7, 2009).

Results

Surficial geology

The surficial geology map (Figure 3) shows deposits exposed on the landscape around Arviat. The oldest unit is bedrock (*R*), occurring mostly in isolated, glacially sculpted, whaleback outcrops south of the airstrip, as well as off the map to the west and north. The rock is an ancient paragneiss (Tella et al., 2007) and is stable in outcrop near the coast. However, frost shattering and heaving of joint-defined blocks was observed to the west of the hamlet, beyond the limits of Figure 3.

The oldest exposed surficial unit (*Pgf*) is late-glacial outwash forming two prominent esker ridges extending east-southeast across the map area (Figures 2a, 4a–c). These deposits, primarily of sand and gravel with boulders, were laid down before and during the retreat of the ice front as the ice sheet contracted toward the west. Concurrent with
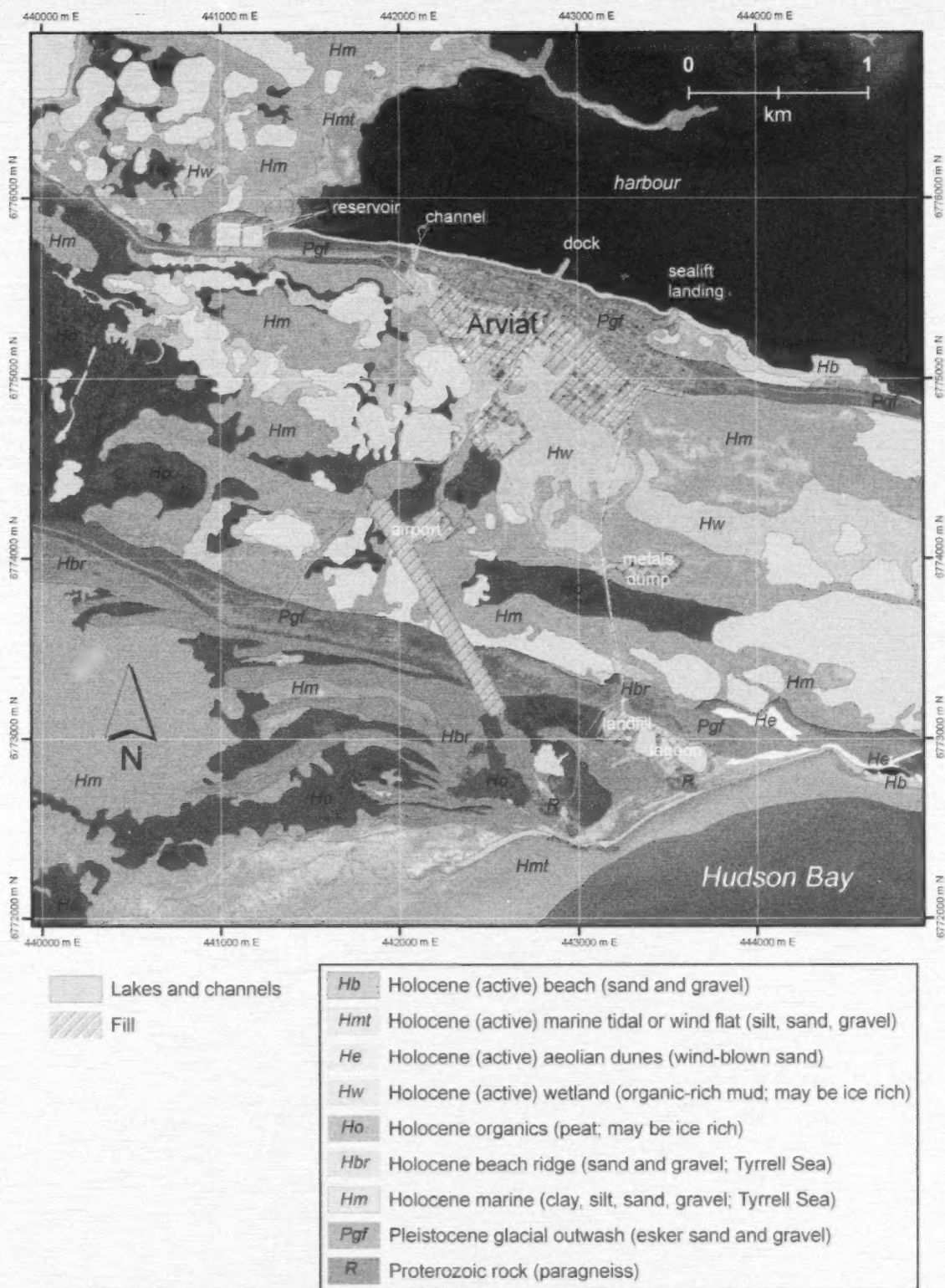
Figure 3: Surficial geology based on 2009 reconnaissance surveys and interpretation of 2006 satellite imagery (DigitalGlobe, Inc., 2006) for immediate vicinity of Arviat, Nunavut (area defined by white box in Figure 1; UTM zone 15N). See text for description of units. Contains copyrighted material DigitalGlobe, Inc., all rights reserved.

Legend:

| | Lakes and channels |
| | Fill |

Hb	Holocene (active) beach (sand and gravel)
Hmt	Holocene (active) marine tidal or wind flat (silt, sand, gravel)
He	Holocene (active) aeolian dunes (wind-blown sand)
Hw	Holocene (active) wetland (organic-rich mud; may be ice rich)
Ho	Holocene organics (peat; may be ice rich)
Hbr	Holocene beach ridge (sand and gravel; Tyrrell Sea)
Hm	Holocene marine (clay, silt, sand, gravel; Tyrrell Sea)
Pgf	Pleistocene glacial outwash (esker sand and gravel)
R	Proterozoic rock (paragneiss)

and following recession of the ice, after 10.2 ka cal. BP, marine deposits (*Hm*) of the Tyrrell Sea accumulated by settling of suspended sediment over the glacial units. As the land emerged from the sea, waves and nearshore ice reworked the eskers, other glacial sediments and deepwater deposits, leaving a large expanse of shallow-marine sediment cover, with wave-washed boulders scattered across the landscape, piles of boulders with little interstitial mate-

rial in places along esker flanks (Figure 4c), and mixtures of silt, sand and gravel forming a widespread veneer. Where sufficient sediment was exposed to wave action at the shoreline, beach ridges (*Hbr*) were formed and later stranded as the land continued to emerge. These ridges are composed of sand and gravel, have little vegetation cover and may be marked by orthogonal frost cracks. The esker ridges were also reworked, forming temporary beaches as
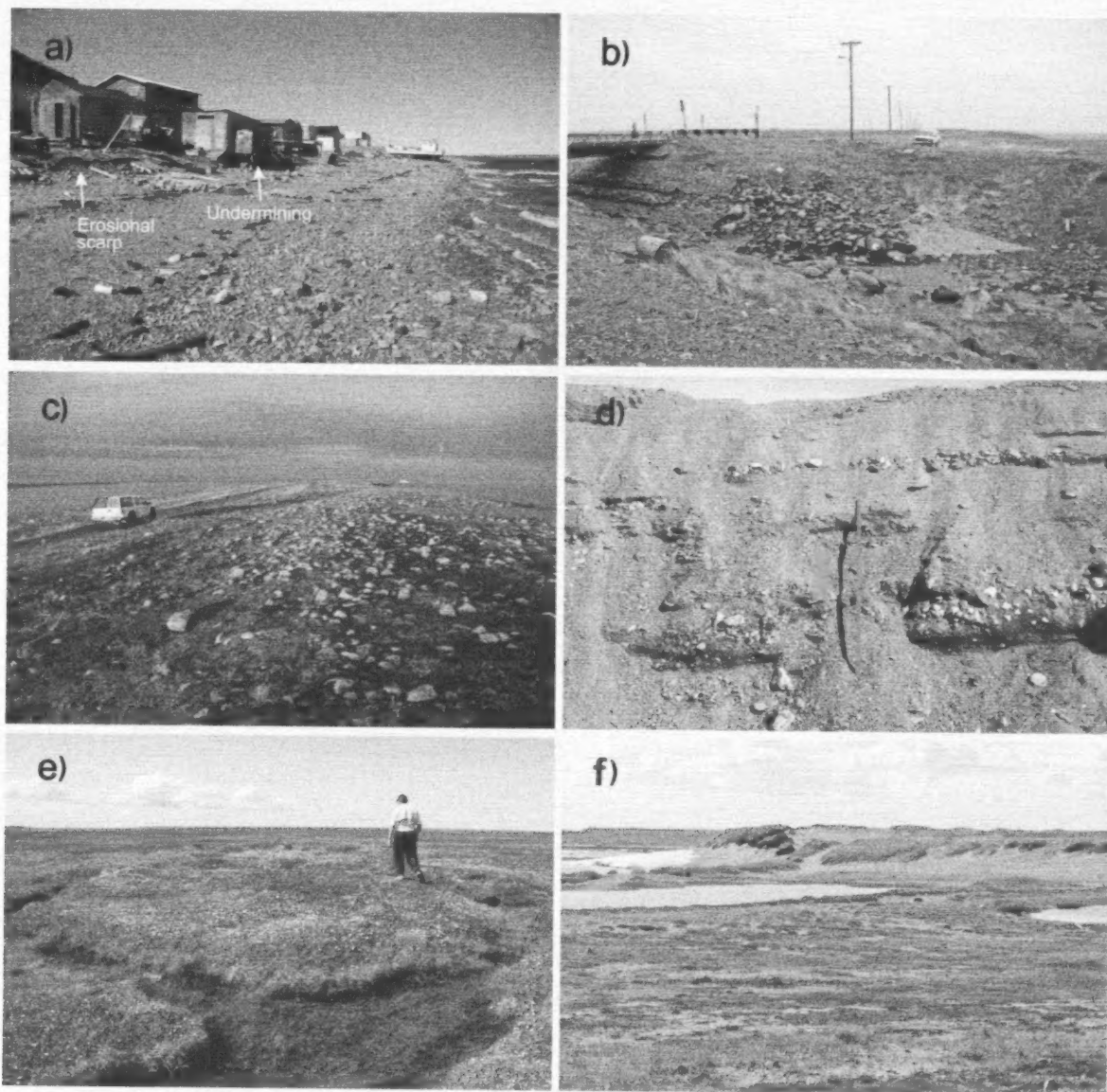
Figure 4: a) Harbour shore showing houses on the northern flank of the esker ridge (unit *Pgf* in Figure 3), with subsistence infrastructure above the high-tide line; note poorly sorted coarse gravel beach in foreground, low erosional scarp in turf at top of beach at left and partial undermining of shed in middle distance (July 13, 2009). **b)** Slope failure in marine muds (unit *Hm* in Figure 3) initiated by heavy rain on flank of esker at west end of community (July 10, 2009). **c)** Evening light on emerged boulder shoal along northern esker (July 12, 2009). **d)** Landward-dipping (to left) interbedded sand and gravel washover deposits (unit *Hbr* in Figure 3) on north side of southern esker north of landfill; attributed to storm waves from the southeast in Hudson Bay when water level was almost 10 m higher than this day (July 12, 2009); length of red scale is 1 m. **e)** High-centred polygons in area of thick Holocene organic cover (unit *Ho* in Figure 3; July 7, 2009). **f)** Dunes (unit *He* in Figure 3) along south-facing shore, in lower right corner of Figure 3 (July 7, 2009).

they emerged from the sea. Sediment washed over the ridges in places and formed landward-thinning wedges of washover deposits (sand and gravel) on the landward side (Figure 4d). A wide expanse of tidal flats (*Hmt*) with a higher proportion of fine sediments and a sparse gravel cover occurs in the wide bay south of the community (Figure 3). The modern beach (*Hb*) is typically coarse gravel (predominantly pebble and cobble) and the active storm ridge at the east end of the peninsula is relatively low for an exposed coast (orthometric crest elevation 3.3 m). Despite the coarse grain size and more restricted fetch, the beach along the waterfront facing the harbour is actively reworked by local waves (Figure 4a).

As the land surface rose above the influence of tides and waves, an organic cover of fibrous peat began to form over much of the area (*Ho*; Figure 3). The peat thickness is typically 0.4 m or more, but rarely >1 m (Arsenault et al., 1981). This organic cover continues to accumulate and its surface is marked by high-centred ice-wedge polygons (Figure 4e) and thaw ponds 2–3 m deep. Windblown dunes (*He*) occur along the esker ridge east of the landfill, extending intermittently to the east end of the peninsula (Figure 4f).

An extensive flat area between the two esker ridges is poorly drained and has been mapped as wetland (*Hw*). There are numerous lakes and smaller ponds in this area. The wetland has discontinuous organic cover and is underlain predominantly by shallow-marine deposits, reworked from underlying sediments. Thus, the wetland has characteristics both of shallow-marine and organic-cover units.

The other widespread unit in the map area is artificial fill. Aggregate resources are abundant in the Arviat area, particularly in the many accessible esker deposits close to the community, and lots for new development are being created on an ongoing basis by pushing fill out across the wetlands. The thickness of the fill is typically less than 1 m, but in some cases not much more than 0.5 m, which may provide insufficient insulation for stability.

All units are underlain by permafrost, with varying effects. Sediments without silt or clay generally have lower ice content and are not susceptible to heave or thaw settlement. Nevertheless, they may contain ice wedges. Deposits with finer sediments are more likely to contain excess ice, which may occur as lenses or more massive bodies of ice. It may have formed as permafrost progressed downward during and after land emergence. This excess ice can lead to settlement if seasonal thaw penetrates more deeply into the underlying permafrost with a warming climate. Relict shallow-marine sediments, emergent tidal flats, areas of organic cover and shallow wetlands may all have excess ice at shallow depth, posing a hazard to foundation stability. At present, there is little information on the thickness of permafrost, the mean ground surface temperature or the extent of excess ground ice in the Arviat area.

Another factor is saline permafrost. Because the entire area was covered by marine waters of the Tyrrell Sea, pore water in the sediments at the time of emergence and start of permafrost development would have been saline to some degree. Hivon and Sego (1993) reported porewater salinities in Arviat ranging from 0.8 to 38.3 parts per thousand (ppt). Because the freezing temperature is depressed in a saline solution, frozen soils with salinity >5 ppt have reduced strength and bearing capacity (Hivon and Sego, 1993).

Sea-level rise and coastal hazards

Coastal hazards are considered relatively minor in Arviat because of the continuing rapid uplift and emergence of the land. Local traditional knowledge points to many instances of shoaling, with channels becoming unnavigable, shoals appearing as islands and islands becoming peninsulas (Nasmith and Sullivan, 2010). Thus, the rapidly falling relative sea levels create issues for navigation, both for small boats and for larger sealift vessels, which may face more restricted access to the community landing facility (Figure 2a, b) in the future.

Development of a more energetic wave climate may be an outcome of declining concentrations and duration of sea ice in the region (Allard et al., 2014) as well as possible changes in storm climatology. Despite falling mean sea level, storm waves are still effective in reworking coarse gravel, reshaping the outer coastline and presumably reworking nearshore sediments. Small erosional scarps in the turf at the top of the beach along the community shorefront attest to erosional processes even within the harbour (Figure 4a, left side). Some small-scale subsistence infrastructure (storage sheds and platforms) appears to be at risk from storm waves or ice push (Figure 4a). No instances of ice ride-up or pile-up were mentioned in conversations with Arviat residents, but damaging ice pile-up is a recognized hazard (Forbes and Taylor, 1994; Forbes and Hansom, 2012).

James et al. (2011) have reviewed the state of knowledge on vertical land motion and sea-level rise as a basis for projecting future local sea-level rise at the NCCP communities. They provided an envelope of possible trends in relative sea level (the mean water level relative to the land surface) over 90 years from 2010 to 2100. Results for Arviat suggested that local sea level is unlikely to fall more than 0.70 m and unlikely to rise more than 0.25 m (these projections incorporate both land uplift and sea-level rise). This is obviously a wide range and it may be difficult to determine an appropriate response.

Should the rate of sea-level rise outpace the rate of uplift in the future, this would undoubtedly lead to shoreline dis-

equilibrium and readjustment. It would also open the door to more storm-surge flooding of low-lying land and likely to increasing erosion along the hamlet waterfront. These potential impacts are largely in the future, but form part of the framework for climate-change adaptation in this rapidly growing community.

Landscape hazards

A number of landscape-related issues were noted during the site visit in 2009. New construction on the southern and western fringes of the built-up area is founded on thin gravel pads pushed out over the wetland unit (*Hw*; Figures 2b, c, 3), which may contain excess ground ice at shallow depth. Drainage is poor throughout the community, with standing water common (Figure 2c, d), a condition that can induce thaw subsidence because water acts as a heat source. Many buildings in the hamlet show evidence of deformation related either to frost jacking of piles or to thaw subsidence and deformation (Figure 2e). Anecdotal evidence from the Arviat Housing Association pointed to many reports of cracked walls even in housing constructed on space-frame foundations over gravel pads (Figure 2f).

Although most of Arviat is flat, steep slopes occur along the flanks of the esker ridges and in a channel cut through the northern ridge at the west end of town. Heavy rain on July 10, 2009, triggered a slump in fine-grained marine sediments on the channel wall just below the bridge (Figure 4b). Further propagation of this slope failure could pose a threat to stability of the bridge abutment and approach road.

A preliminary landscape hazards map (Figure 5) was developed based on the properties, landscape characteristics, and exposure of the mapped units in Figure 3. Quantitative data on geotechnical properties, including permafrost and ground ice, are lacking for the most part in Arviat. For this reason, the map represents an interpretation of relative stability or instability, based on the surface expression of the units, some information on sediment grain size and knowledge of the properties of similar deposits elsewhere.

It is assumed that sites underlain by units containing fine-grained sediments (silt and clay) will be most susceptible to permafrost degradation, which may lead to thaw settlement. For this reason, wetland and organic cover units (including areas of high-centre polygons) have been classified as high risk and shallow-marine sediments as moderate risk, although it is apparent that some of the latter are fine-grained and entail a higher risk of thaw subsidence or slope failure (Figure 4b). More detailed surveys will be required to differentiate the risk within this unit. Also included in the high risk category are coastal units that may be susceptible to storm-surge flooding, wave run-up, shoreline erosion or ice ride-up. The remaining units (rock, esker deposits, raised beach deposits and modern windblown sediments) are classified as low risk for foundation instability or other hazards. These units represent a small proportion of the available land in the map area.

Perceived sensitivity to climate change

A number of climate-sensitive landscape hazard issues were identified during the reconnaissance survey. These include

- poor surface water drainage throughout the community, even in areas built on fill;
- slope failure (landslide) in marine sediments in the deep channel on the west side of the hamlet;
- differential pile movement and settlement of buildings;
- permafrost degradation indicated by high-centre polygons; and
- frost heaving of bedrock blocks evident on some outcrops.

The ongoing expansion of development on space-frame foundations over thin gravel pads across the wetland on the south side of the community may be problematic if pad thickness is inadequate and future warming leads to subsurface thaw settlement. More suitable building sites may exist on land west of the reservoir, but this would involve a commitment to extending services and would entail longer travel distance to community facilities.

Other climate-change impacts of concern include

- sea-level rise and whether it will exceed the rate of land uplift, changing the trend of relative sea level from falling to rising;
- implications of continuing emergence for future marine access to the current freight landing area;
- changes in sea ice, with implications both for the length of the open-water season and for safety of travel on landfast ice; and
- changes in wave climate related both to open-water fetch and to possible changes in storm characteristics.

All of the issues above are important considerations for land-use planning, development practices and policies to build a more resilient community.

Economic implications

This study addresses existing environmental and landscape hazards in and around Arviat and how these may be compounded by climate change now and in the future. Understanding of these conditions and the risks they pose to infrastructure can be integrated with future community planning in order to enhance stability and sustainability, thereby reducing costs of infrastructure development and maintenance.
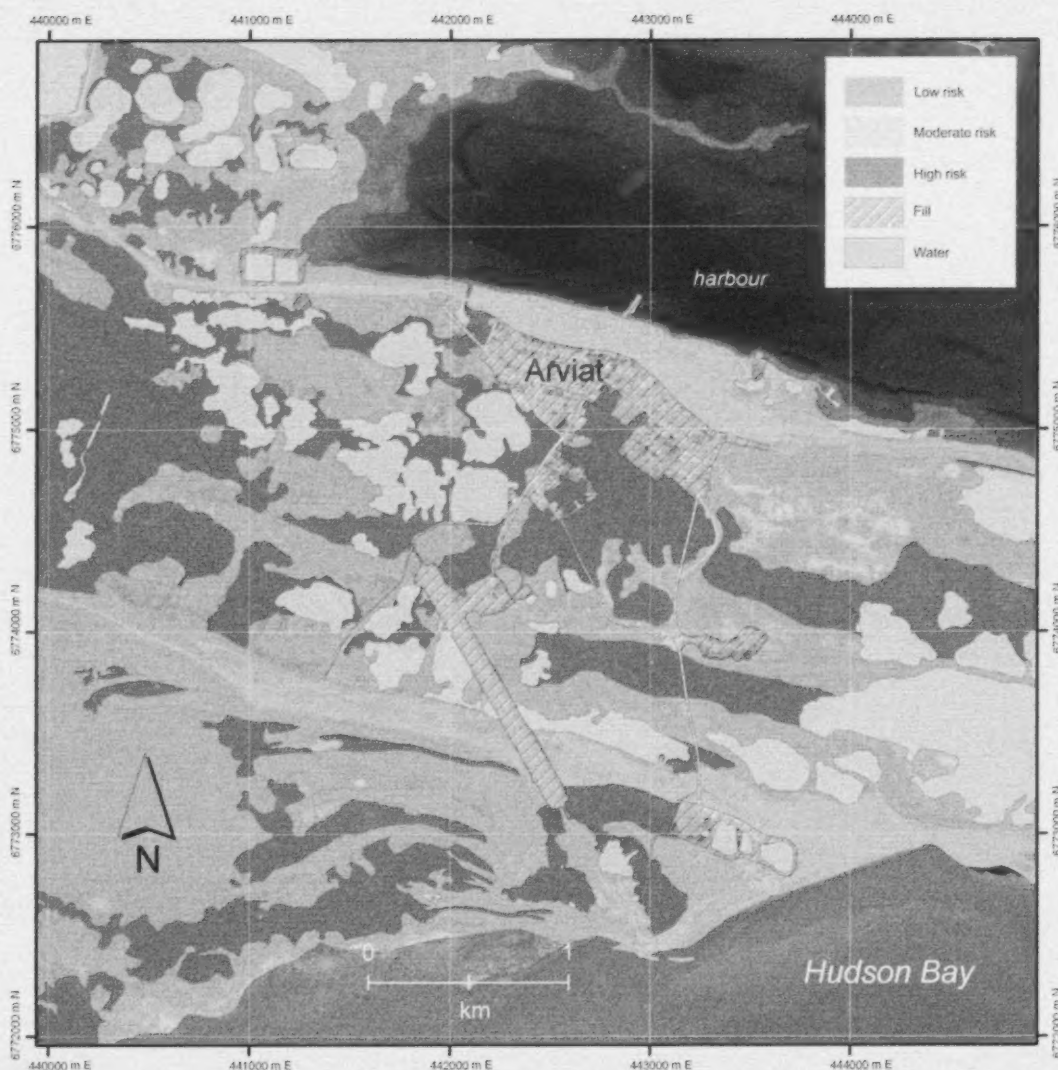
Figure 5: Preliminary landscape hazards map for Arviat, Nunavut, covering the same 25 km² area as Figure 3 (UTM zone 15N). Qualitative classification of risk to infrastructure stability derived directly from the map units in Figure 3. Contains copyrighted material (DigitalGlobe, Inc., 2006) DigitalGlobe, Inc., all rights reserved.

Acknowledgments

Natural Resources Canada, Earth Sciences Sector, contribution number 20130289.

References

Allard, M., Manson, G.K. and Mate, D.J. 2014: Reconnaissance assessment of landscape hazards and potential impacts of future climate change in Whale Cove, southern Nunavut; *in* Summary of Activities 2013, Canada-Nunavut Geoscience Office, p. 171–182.

Arsenault, L., Aylsworth, J.M., Cunningham, C.M., Kettles, I.M. and Shilts, W.W. 1981: Surficial geology, Eskimo Point, District of Keewatin; Geological Survey of Canada, Preliminary Map 8-1980, scale 1:125 000.

Aylsworth, J.M. and Shilts, W.W. 1989: Bedforms of the Keewatin Ice Sheet, Canada; Sedimentary Geology, v. 62, p. 407–428.

Brown, J., Ferrians, O.J., Jr., Heginbottom, J.A. and Melnikov, E.S. 2001: Circum-Arctic map of permafrost and ground ice conditions; National Snow and Ice Data Center, digital media, URL <http://nsidc.org/data/docs/fgdc/ggd318_map_circumarctic/> [November 10, 2013].

Budkewitsch, P., Prévost, C., Pavlic, G. and Pregitzer, M. 2011: New satellite images help to show the changing face of Arviat; *in* Changing Times: Impacts and Adaptation in Nunavut, Government of Nunavut, Government of Canada and Canadian Institute of Planners, Iqaluit, p. 6–7, URL <http://env.gov.nu.ca/sites/default/files/changing_times_-english_low_res.pdf> [November 4, 2013].

Canadian Hydrographic Service 2002: Canadian Tide and Current Tables, v. 4: Arctic and Hudson Bay; Fisheries and Oceans Canada, Ottawa, 88 p.

Couture, N.J., Craymer, M.R., Forbes, D.L., Fraser, P.R., Henton, J.A., James, T.S., Jenner, K.A., Manson, G.K., Simon, K.M., Silliker, R.J. and Whalen, D.J.R. 2014: Coastal geoscience for sustainable development in Nunavut: 2013 activities; *in* Summary of Activities 2013, Canada-Nunavut Geoscience Office, p. 139–148.

DigitalGlobe, Inc. 2006: QuickBird 2 satellite image; Digital-Globe, Inc., image, URL <https://browse.digitalglobe.com/imagefinder/showBrowseMetadata?catalogId=10100100050F4800> [November 28, 2013].

Dyke, A.S. 2004: An outline of North American deglaciation with emphasis on central and northern Canada; *in* Quaternary Glaciations - Extent and Chronology, part II, J. Ehlers and P.L. Gibbard (ed.), Developments in Quaternary Science 2, New York, p. 373–424.

Environment Canada 2013: Canadian climate normals; Environment Canada, URL <http://climate.weather.gc.ca/climate_normals/index_e.html> [October 7, 2013].

Forbes, D.L. and Hansom, J.D. 2012: Polar coasts; *in* Estuarine and Coastal Geology and Geomorphology, Treatise on Estuarine and Coastal Science, E. Wolanski and D.S. McLusky (ed.), Academic Press, Elsevier, Amsterdam, The Netherlands, v. 3, p. 245–283.

Forbes, D.L. and Taylor, R.B. 1994: Ice in the shore zone and the geomorphology of cold coasts; Progress in Physical Geography, v. 18, p. 59–89.

Forbes, D.L., Manson, G.K., Mate, D. and Qammaniq, A. 2008: Cryospheric change and coastal stability: combining traditional knowledge and scientific data for climate change adaptation; Ice and Climate News, v. 11, p. 17–18.

Ford, J., Bell, T., Parewick, K., St-Hilaire, D., Allurut, M. and Shappa, M. 2006: Climate change, infrastructure risks and vulnerability of Arctic coastal communities: a case study from Arctic Bay; ArcticNet Annual Science Meeting, Victoria, British Columbia, December 12–15, 2006 (poster presentation), URL <http://www.arcticnet.ulaval.ca/pdf/posters_2006/ford_et_al.pdf> [November 4, 2013].

GeoBase® 1999–2003: GeoBase® Landsat 7 orthorectified imagery over Canada; Canadian Council on Geomatics, URL <http://www.geobase.ca/geobase/en/data/imagery/landsat/index.html> [August 7, 2009].

Hivon, E.G. and Sego, D.C. 1993: Distribution of saline permafrost in the Northwest Territories, Canada; Canadian Geotechnical Journal, v. 30, p. 506–514.

Irvine, M., Smith, I.R. and Bell, T. 2007: Community-scale hazard mapping in the Canadian Arctic: a case study of Clyde River; ArcticNet Annual Science Meeting, Collingwood, December 11–14, 2007 (poster presentation), URL <http://www.arcticnet.ulaval.ca/pdf/posters_2007/irvine_et_al.pdf> [November 4, 2013].

James, T.S., Simon, K.M., Forbes, D.L., Dyke, A.S. and Mate, D.J. 2011: Sea-level projections for five pilot communities of the Canada-Nunavut Climate Change Partnership; Geological Survey of Canada, Open File 6715, 23 p.

Mate, D. and Reinhart, F., ed. 2011: Nunavut Climate Change Partnership workshop, February 15–16, 2011; Geological Survey of Canada, Open File 6867, 1 CD-ROM, doi:10.4095/288645

Nasmith, K. and Sullivan, M. 2010: Climate Change Adaptation Action Plan for Hamlet of Arviat; Canadian Institute of Planners, 27 p., URL <http://www.climatechange nunavut.ca/sites/default/files/arviat_community_adap plan_eng.pdf> [November 10, 2013].

Natural Resources Canada 2013: Tools and applications, Canadian Spatial Reference System-Precise Point Positioning; Natural Resources Canada, Canadian Geodetic Survey, URL <http://webapp.geod.nrcan.gc.ca/geod/tools-outils/index.php#ppp> [November 26, 2013].

Shilts, W.W., Kettles, I.M. and Arsenault, L. 1976: Surficial geology, southeast Keewatin; Geological Survey of Canada, Open File 356, 28 p.

Smith, I.R. 2014: Reconnaissance assessment of landscape hazards and potential impacts of future climate change in Kugluktuk, western Nunavut; *in* Summary of Activities 2013, Canada-Nunavut Geoscience Office, p. 149–158.

Smith, I.R. and Forbes, D.L. 2014: Reconnaissance assessment of landscape hazards and potential impacts of future climate change in Cambridge Bay, western Nunavut; *in* Summary of Activities 2013, Canada-Nunavut Geoscience Office, p. 159–171.

Statistics Canada 2013: Population and dwelling counts, for Canada, provinces and territories, and population centres, 2011 and 2006 censuses; Statistics Canada, URL <http://www12.statcan.gc.ca/census-recensement/2011/dp-pd/hlt-fst/pd-pl/Table-Tableau.cfm?LANG=Eng&T=802&PR=62&S=51&O=A&RPP=999> [October 7, 2013].

Tella, S., Paul, D., Berman, R.G., Davis, W.J., Peterson, T.D., Pehrsson, S.J. and Kerswill, J.A. 2007: Bedrock geology compilation and regional synthesis of parts of the Hearne and Rae domains, Western Churchill Province, Nunavut-Manitoba; Geological Survey of Canada, Open File 5441, scale 1:550 000.

Geology, history and site-management planning of the Kangiqsukutaaq carving stone quarry, southern Baffin Island, Nunavut

H.M. Steenkamp[1], M. Pizzo-Lyall[2], C.J. Wallace[3], M.A. Beauregard[4] and B.J. Dyck[5]

[1]*Canada-Nunavut Geoscience Office, Iqaluit, Nunavut, holly.steenkamp@nrcan.gc.ca*

[2]*Department of Land and Resources, Qikiqtani Inuit Association, Iqaluit, Nunavut*

[3]*De Beers Canada Exploration Inc., Toronto, Ontario*

[4]*Minerals and Petroleum Resources, Department of Economic Development and Transportation, Government of Nunavut, Arviat, Nunavut*

[5]*Department of Earth Sciences, University of Oxford, Oxford, United Kingdom*

Abstract

The Kangiqsukutaaq quarry, located approximately 160 km east of Cape Dorset, Nunavut, has been providing excellent-quality serpentinite carving stone to Inuit carvers within the southern Baffin Island region for over 50 years. Geological mapping by the Canada-Nunavut Geoscience Office, and a high-resolution ground magnetic survey by De Beers Canada Exploration Inc., were recently carried out at the quarry to identify the extent of at-surface and surface-accessible carving stone. The Qikiqtani Inuit Association requires this information to develop a site-management plan that reduces risks associated with quarrying, and to better understand the resource potential remaining at the site. Geological field observations indicate that there is very little at-surface and surface-accessible serpentinite remaining at Kangiqsukutaaq, which has traditionally been quarried by hand. However, magnetic survey data suggest that subsurface serpentinite underlies the wasterock and overburden between the two established quarry pits. Considerations and recommendations for future development and site management at the Kangiqsukutaaq quarry are provided, as well as techniques for future exploration of new potential carving stone deposits.

Résumé

La carrière Kangiqsukutaaq, située environ 160 km à l'est de Cape Dorset, au Nunavut, fournit depuis plus de 50 ans de la serpentinite d'excellente qualité aux sculpteurs inuits de la région méridionale de l'Île de Baffin. Des travaux de cartographie géologique, entrepris par des chercheurs du Bureau géoscientifique Canada-Nunavut, et un levé magnétique au sol à haute résolution, réalisé par la société De Beers Canada Exploration Inc., ont récemment eu lieu à l'endroit de la carrière en vue de déterminer l'étendue de roche à sculpter se trouvant en surface ou accessible à partir de la surface. L'Association des Inuits de Qikiqtani a besoin de ces données afin de mettre au point un plan de gestion du site conçu en vue de réduire les risques associés à l'exploitation des carrières, et afin de pouvoir mieux estimer l'importance des ressources potentielles encore disponibles à ce site. À partir des observations géologiques faites sur place, il appert qu'il ne reste que peu de serpentinite, que ce soit en surface ou accessible à partir de la surface, dans la carrière Kangiqsukutaaq, carrière qui a toujours été exploitée manuellement. Cependant, les données obtenues lors du levé magnétique semblent indiquer la présence à faible profondeur de serpentinite sous-jacente aux roches stériles et aux morts-terrains qui occupent l'espace entre les deux mines établies. Les points à examiner et les recommandations soulevés dans le présent rapport portent sur la mise en valeur future et la gestion de la carrière Kangiqsukutaaq, ainsi que sur des techniques pouvant servir à déceler de nouveaux gisements de pierre à sculpter lors de travaux d'exploration futurs.

Introduction

Kangiqsukutaaq (also known as Korok Inlet; lat. 64°23'44"N, long. 73°19'24"W) hosts a serpentinite carving stone deposit located approximately 160 km east of Cape Dorset and approximately 240 km northwest of Kimmirut. Since the 1960s, the site has been one of the preferred carving stone quarries accessed by people from across southern Baffin Island. Quarrying is done manually, using jackhammers, shovels, pry bars and wheelbarrows. The Kangiqsukutaaq quarry site belongs to the Inuit of Cape Dorset under Inuit Owned Lands parcel #CD39, and the land is managed by the Qikiqtani Inuit Association (QIA) Department of Lands and Resources.

The demand for excellent-quality carving stone in the territory is rising, as the art form is becoming more popular and reaching global markets. Therefore, the few known excellent-quality surface-available deposits are being rapidly consumed to meet the demand. Since 2010, the Government of Nunavut Department of Economic Development and Transportation (EDT) has been evaluating the resource potential and quantifying deposit volumes at existing quarry sites across the territory through the Nunavut Carving Stone Deposit Evaluation Program (NCSDEP; Beauregard et al., 2013). This initiative found that carvers usually compare the quality of other carving stone to that produced from the Kangiqsukutaaq quarry. This stone is highly regarded for its overall consistency, toughness, holding of fine detail and smooth finished polish. Kangiqsukutaaq carving stone can be quarried in large blocks and has a Mohs hardness of 2.0–2.5.

The QIA has been working with the Community Lands and Resources Committees of Kimmirut, Cape Dorset and Iqaluit, as well as users of the Kangiqsukutaaq quarry, to determine future site-management actions. Safety is a primary concern at the site after many years of unmanaged quarrying. Accumulation of wasterock and overburden in both the upper and lower pits, garbage around the site, and lack of equipment to manage overhanging rock and soil are all problems requiring attention. Thus, after several meetings, the QIA and quarry stakeholders have concluded that there is a definite need to create a collective plan to further manage the site.

In August 2013, the QIA, the Canada-Nunavut Geoscience Office (CNGO), De Beers Canada Exploration Inc. and EDT conducted geological mapping (Figure 1a), a high-resolution walking magnetic survey (Figure 1b) and a preliminary land survey of the Kangiqsukutaaq quarry. Logistics support and transportation from Cape Dorset were provided by a local outfitter, who also established a camp on site and monitored wildlife. Representative rock samples were collected for geochronological and geochemical analyses in support of an M.Sc. thesis by R. Pikor (supervised

by A. Camacho) at the University of Manitoba on the geological development of select carving stone deposits on southern Baffin Island. The extent of the carving stone deposit, and the quality and quantity of remaining surface-accessible carving stone in the two quarry pits and around the site were investigated. The geological observations and interpretations from the quarries presented in this paper will assist the QIA and quarry stakeholders to develop management strategies for future work and increased site safety at Kangiqsukutaaq.

Geological observations

The northern end of Kangiqsukutaaq is underlain by Paleoproterozoic metasedimentary units of the Lake Harbour Group and relatively younger Paleoproterozoic intrusive biotite-granite gneiss (Jackson and Taylor, 1972; Scott et al., 2002; St-Onge et al., 2007; Sanborn-Barrie et al., 2008). The mapped carving stone comprises serpentinite derived from metasomatized ultramafic rock found within the Lake Harbour Group (Figure 1a). All rock units experienced regional granulite-facies metamorphism, pervasive amphibolite-facies overprinting and deformation associated with the 2.0–1.8 Ga terminal collision of the Trans-Hudson Orogen (Sanborn-Barrie et al., 2008; St-Onge et al., 2009).

Rock types

Lake Harbour Group metasedimentary units

The metasedimentary rocks in the vicinity of the quarry comprise white to grey impure marble structurally overlain by psammitic and pelitic strata that contain a large amount of monzogranitic partial melt. The coarse-grained marble is about 35 m thick near tidewater and up to about 50 m thick approximately 300 m inland. The marble displays a regionally consistent, steeply eastward-dipping compositional foliation defined by layers of medium-grained serpentine pseudomorphs after olivine, and lesser magnetite, apatite, phlogopite and diopside (Figure 2a). Several calcsilicate layers were observed near the upper quarry continuing to the north within the marble unit (Figure 2b). These layers range from 0.3 to 2 m wide, are generally oriented parallel to the regional north-south foliation, and contain tremolite, actinolite, phlogopite, calcite and minor diopside.

The Lake Harbour Group psammite and pelite units also display the pervasive north-south regional foliation recorded in the marble. The foliation is defined by compositional layering of monzogranitic partial-melt seams and garnet+biotite±orthopyroxene restite. The abundance of melt and presence of orthopyroxene confirm that this area has experienced granulite-facies metamorphism. Retrogression from granulite-facies conditions is inferred from the presence of porphyroblastic garnet, up to 4 cm wide, that displays symplectite textures with quartz (Figure 2c).

Figure 1: Kangiqsukutaaq quarry and surrounding area, southern Baffin Island, Nunavut: **a)** geology and structures; map area detailed in Figure 4 is outlined in black; **b)** high-resolution ground magnetic survey overlain with geological contacts and faults for geographic reference; a strong magnetic dipole signature coincides with the serpentinite-bearing marble unit.

Figure 2: Photographs of the Kangiqsukutaaq quarry, southern Baffin Island, Nunavut: **a)** Paleoproterozoic marble with layers of serpentine+magnetite+diopside are cut and offset by minor faults, looking south-southwest from just west of the upper quarry; **b)** deformed calcsilicate layer hosted in marble, looking north-northeast; **c)** garnet+quartz symplectite in psammite east of the lower quarry; **d)** west wall of the lower quarry exposing the highest quality carving stone (type 1 serpentinite), typically found within the core of the deposit; quarry walls are marked with several orientations of slickenlines, dominantly indicating sinistral motion' **e)** banded serpentine and calcite (type 3 serpentinite) common to the outer rim of the serpentinite body; eraser pen for scale is 1 cm in diameter; **f)** two generations of leucosome were documented in the biotite-granite gneiss; the earlier leucosome and associated restite boundaries are folded (yellow dashed line) and cut by the later, more voluminous leucosome; both leucosome generations are subsequently deformed; hammer for scale is 40 cm long. Abbreviations: bio, biotite; cal, calcite; di, diopside; gar, garnet; ksp, K-feldspar; mag, magnetite; qtz, quartz; srp, serpentine.

Serpentinite

The carving stone extracted from the Kangiqsukutaaq quarry comes from a 7–10 m wide serpentinized ultramafic sill hosted in the Lake Harbour Group marble. The serpentinite outcrop is restricted to the two quarry pits (upper and lower), which are mostly covered with wasterock by quarry users to minimize oxidation and weathering of the fresh surfaces.

The serpentinite can be divided compositionally into three types. Type 1 is the most abundant and is dominated by cryptocrystalline antigorite (Fe-rich serpentine end-member) with minor fine-grained magnetite. Brittle fracture planes 1–2 mm wide criss-cross through the massive host and are filled with prismatic chrysotile (Mg-rich serpentine end-member) oriented perpendicular to the fracture planes and minor calcite. Type 1 is found at the centre of the serpentinite body and ranges in colour from medium to dark green, black or dark brown (Figure 2d).

Type 2 is found within the outer 0.5–2 m of the serpentinite body. Cryptocrystalline antigorite is the dominant component of the Type 2 serpentinite, and chrysotile is also present as 2–4 mm long grains. Minor magnetite, brucite and calcite were observed in varying proportions throughout the Type 2 serpentinite. Weathered rock faces are black with a white polka-dot texture, and fresh faces are generally dark green.

Type 3 is less abundant than type 2 and occurs as a 10–50 cm wide rim around the serpentinite body at the metamorphosed contact with the Lake Harbour Group marble. Other than antigorite and chrysotile, type 3 serpentinite also contains a major calcite component that was found to increase with proximity to the marble. Fine-grained serpentine dominantly pseudomorphs medium-grained euhedral olivine, and phlogopite occurs as 0.5–1.5 cm thick books concentrated in 2–5 cm thick discontinuous lenses. This rock type has a banded or layered texture that appears black and white on weathered faces (Figure 2e), but fresh or polished surfaces show the green colour of the serpentine against the white calcite.

Biotite-granite gneiss

Intrusive biotite-granite gneiss lies to the northwest of the Lake Harbour Group units at the northern end of Kangiqsukutaaq (St-Onge et al., 2007). The gneiss is characterized by a compositional foliation that is defined by fine-grained leucosome with thin restite boundaries (Figure 2f). The fabric is tightly folded axial planar to the north-south regional foliation and crosscut by a second generation of coarse-grained leucosome. Isolated, boudinaged mafic pods within the biotite-granite gneiss are wrapped by the earlier leucosome and crosscut by the later, more voluminous, coarse-grained leucosome.

Randomly oriented syenogranite dikes crosscut all metamorphic features in the biotite-granite gneiss. These dikes are generally medium grained and locally contain magnetite, amphibole and epidote where the dikes are in contact with mafic components in the gneiss.

Monzogranitic leucogranite

The contact between the biotite-granite gneiss and the Lake Harbour Group marble is marked by a 10–15 m wide, steeply east-dipping, pegmatitic monzogranitic leucogranite dike. The leucogranite lower (western) contact with the gneiss is straight and clearly defined. Rare enclaves of the host biotite-granite gneiss are incorporated in the leucogranite 30–50 cm from the contact. The leucogranite upper (eastern) contact with the marble is also clear and well defined, and is associated with a calcsilicate layer that pinches and swells from 0.2 to 2 m wide along strike (Figure 3a). The leucogranite contains individual and clustered orthopyroxene crystals up to 1 cm long within 2 m of the marble contact, and displays a weak foliation defined by elongated aggregates of quartz.

The Lake Harbour Group marble-psammite contact is marked by a similar 5 m wide leucogranite dike that forms the competent overhanging eastern wall of the lower quarry (Figure 3b). North of the upper quarry, 1.5–4 m wide leucogranite dikes were also observed cutting through the marble unit parallel to the regional north-south foliation.

Late structures

The serpentinite at Kangiqsukutaaq is variably sheared due to sinistral movement along a 6–8 m wide northeast-southwest fault that runs through the host marble parallel to the eastern contact with the leucogranite dike and structurally overlying psammite unit. A later, major, northwest-southeast sinistral fault system (Figures 1a, 3b) that runs through the end of the bay cuts the regional north-south foliation and truncates the southern end of the serpentinite deposit in the lower quarry. Observable at low tide, a 2 m by 2 m serpentinite body in contact with marble is juxtaposed with psammite, indicating about 27 m of left-lateral displacement along a parallel, relatively minor fault (Figure 3c). Several minor northwest-southeast faults with centimetres to metres of sinistral displacement were observed within the marble unit near the upper quarry. The major fault system cutting through the bay is responsible for delimiting and offsetting segments of the serpentinite body; however, serpentinite was not identified during field investigations of the marble southeast of the bay fault.

Serpentinization of the ultramafic unit at Kangiqsukutaaq is restricted to zones affected by late faulting (Figure 2a). Serpentinite is interpreted to have formed during brittle deformation when faulting opened pathways for metamorphic fluids to interact with the ultramafic unit and hostrocks. In the ultramafic unit, the primary and/or previ-
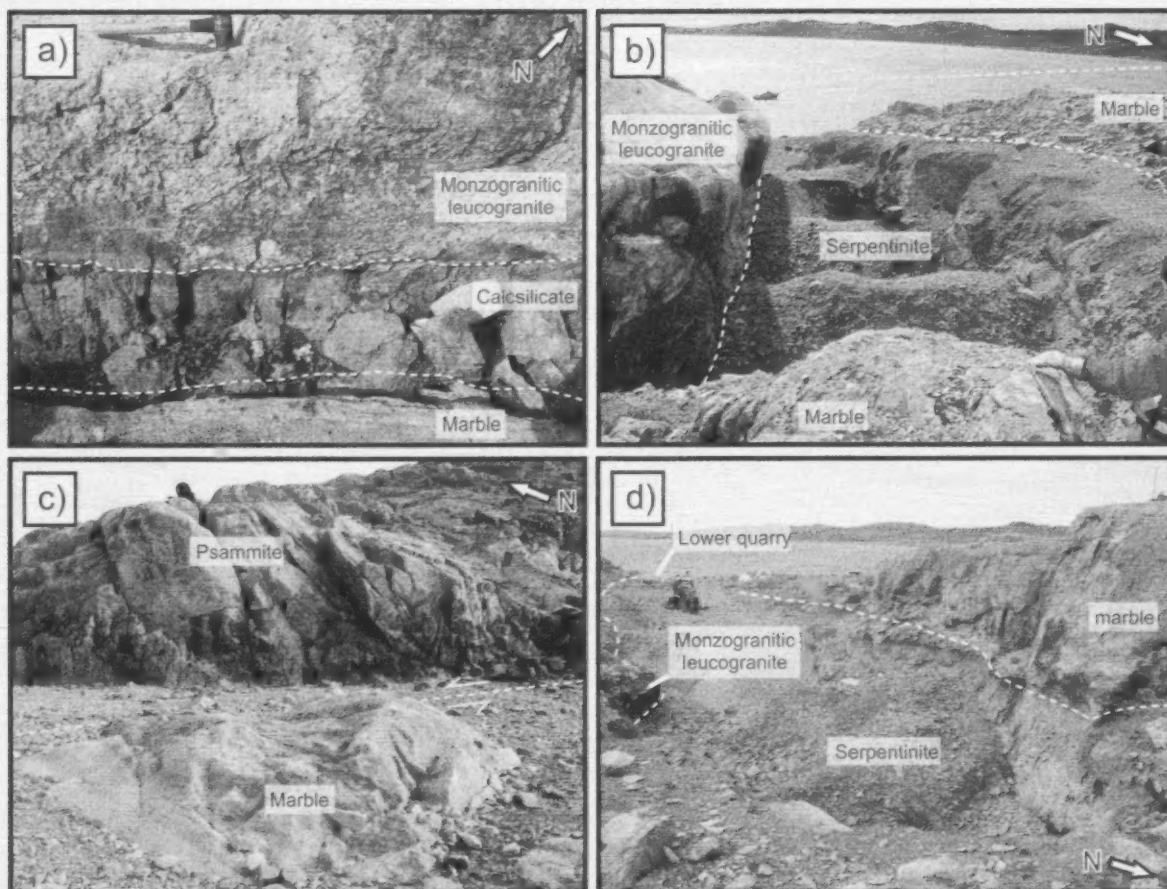
Figure 3: Photographs of the Kangiqsukutaaq quarry, southern Baffin Island, Nunavut: **a)** the western contact of the marble unit with the monzogranitic leucogranite is marked by a calcsilicate layer containing an amphibolite-facies mineral assemblage; hammer for scale is 40 cm long; **b)** view of the lower quarry from above the north wall, looking southwest; a major northwest-southeast sinistral fault (yellow dashed line) truncates the southern end of the serpentinite body; boat in the bay is approximately 9 m long; **c)** juxtaposed marble and psammite indicate 27 m of sinistral displacement along a local minor fault parallel to the major fault in Figure 3b; geologist is 1 m tall; **d)** view of the upper quarry from above the north wall, looking southwest downhill to the lower quarry; excavator for scale is approximately 4 m tall and is situated on the upper quarry ramp, a location with potential for subsurface serpentinite.

ously stable metamorphic mineral assemblages have been completely overprinted by the low-grade, serpentine-bearing mineral assemblages, suggesting that fluid interaction occurred within lower greenschist-facies conditions. The differences in major mineral assemblages and proportions documented in the three types of carving stone suggest a change in chemical composition across the deposit, which is interpreted to result from fluid interaction within the marble, at the contact between the marble and the ultramafic unit, and within the ultramafic unit.

The boudinaged character of the ultramafic unit is interpreted to be tectonic in nature, likely occurring at granulite-facies conditions during the Trans-Hudson orogeny. The important implication of this interpretation is that the ultramafic unit is potentially discontinuous, occurring as isolated bodies along a deformed horizon.

High-resolution ground magnetic survey

High-resolution ground magnetic surveys are commonly conducted in the exploration industry to identify subsurface magnetic anomalies often associated with Fe-bearing geological features. De Beers Canada Exploration Inc. completed a 0.5 km^2 walking magnetic survey at the Kangiqsukutaaq site to help constrain the subsurface extent and geometry of the serpentinite bodies. Using a GEM Systems GSM19W GPS-integrated magnetometer, the team collected 17.9 km of magnetic data along 40 lines averaging 450 m in length. The lines were run perpendicular to the northeast-southwest strike of the ultramafic body at 25 m spacing. The survey area is centred over the two quarry pits, and extends from the shoreline to the low-lying marsh north of the upper quarry (Figure 1b).

The survey results show a 500 m long high-magnetic dipole signature, ranging in amplitude from 1000 to 4000 nT, that corresponds to the observed serpentinite-bearing marble unit at Kangiqsukutaaq. The dipole signature is most intense along the shoreline boundary of the lower quarry. Preliminary geometric modelling of the signature suggests that the serpentinite body is subvertical and could continue down to a depth of about 100 m. The survey results also show a high-magnetic dipole signature between the two established quarries, suggesting a subsurface continuation of serpentinite at this location (Figure 3d). In the northern half of the survey area, the dipole signature fades to background signal levels, indicating a possible termination of the serpentinite unit approximately 500 m north of the shoreline. No other magnetically similar dipole signatures were observed in the surveyed area.

Deposit evaluation and recommendations

Carving stone deposits in Nunavut are typically quarried by hand, and therefore must be exposed at the ground surface or be reasonably surface accessible. The limited surface-accessible serpentinite remaining at Kangiqsukutaaq after five decades of quarrying is confined to the north walls and quarry floors of both upper and lower pits. Based on the current dimensions of the two quarry pits, an estimated 50 000 tonnes (110,000,000 lbs.) of rock has been extracted in that time and, considering the amount of wasterock on site, approximately 30% of that material has been transported to communities for artisan use.

A volumetric evaluation of the remaining carving stone deposit at Kangiqsukutaaq requires that the serpentinite unit be accurately geometrically constrained. Considering the results from the walking magnetic survey and geological mapping, there is a high probability that the serpentinite exposed in the upper quarry could extend southward below the pit ramp and overburden (Figures 3d, 4), and possibly connect with the northern wall of the lower quarry (Figure 3b). To confirm this prediction, it is recommended that the wasterock in the upper quarry and overburden to the south be removed to expose the bedrock surface and establish the lateral extent of serpentinite. Additionally, systematic drilling into the bedrock would be useful to define the geometry of the serpentinite at depth.

Given the subvertical nature of the carving stone deposit at Kangiqsukutaaq, further downward quarrying could lead to instability of the highly fractured pit walls and therefore increased safety risks for quarry workers. To minimize risks, it may be necessary to transition away from the traditional hand-mining methods and consider suitable mechanized excavation techniques.

With the information from this study, the QIA, with input from quarry stakeholders, can begin to develop a site-management plan for the Kangiqsukutaaq quarry. It is impor-

tant to remember, however, that natural resource deposits such as carving stone are finite. Therefore, new sources of easily accessible high-quality carving stone need to be identified in the territory. This study has shown that the discrete high-amplitude magnetic signature associated with the Kangiqsukutaaq serpentinite could be a useful tool when assessing the subsurface extent of carving stone at other known localities with similar geological settings. Exploration for new serpentinite locations is highly recommended, and could initially be done using high-quality airborne magnetic survey data coupled with detailed geological mapping along coastal areas and near communities. Prospective targets should be followed up with a site visit by
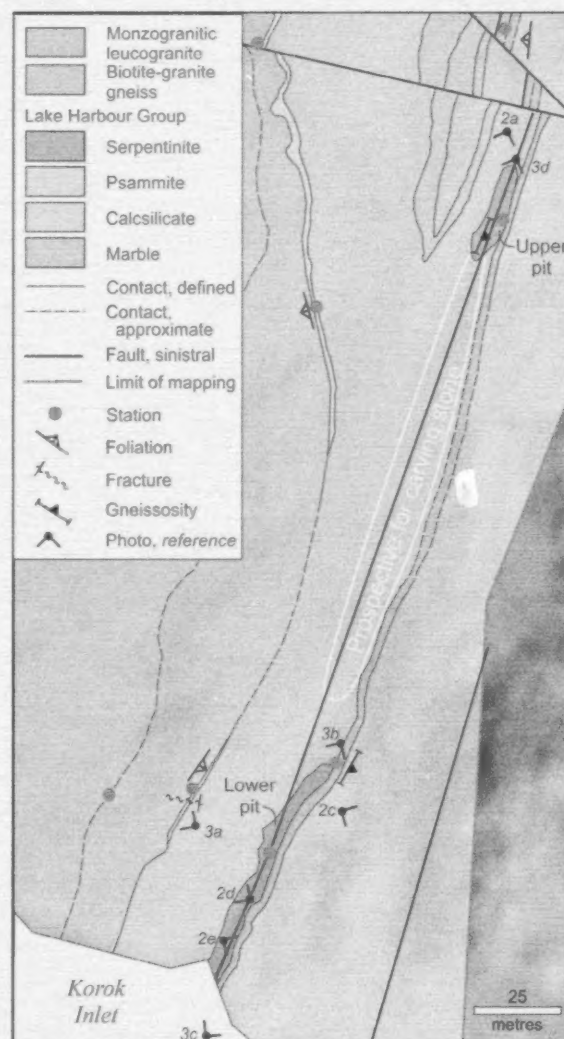

Figure 4: Detailed geology of the immediate Kangiqsukutaaq quarry area, southern Baffin Island, Nunavut, showing the upper and lower pit locations, the recommended location to begin initial subsurface exploration for more carving stone resources, and the locations where several photographs referenced in Figures 2 and 3 were taken.

geologists and local carvers to sample and test the quality of any potential carving stone finds (e.g., Beauregard et al., 2013; Senkow, 2013).

Acknowledgments

The authors thank the Alariaq family for their generous hospitality in Cape Dorset, and professional logistics support and guidance in the field. M. Akavak is gratefully recognized for sharing his knowledge of the history of carving stone quarrying at Kangiqsukutaaq and providing field assistance. The authors also thank A. Camacho, M. St-Onge, and D. Mate for providing thoughtful comments to improve this paper.

Natural Resources Canada, Earth Science Sector contribution 20130296.

References

Beauregard, M.A., Ell, J., Pikor, R.K. and Ham, L.J. 2013: Nunavut Carving Stone Deposit Evaluation Program (2010–2013): third year results; in Summary of Activities 2012, Canada-Nunavut Geoscience Office, p. 151–162.

Jackson, G.D. and Taylor, F.C. 1972: Correlation of major Aphebian rock units in the northeastern Canadian Shield; Canadian Journal of Earth Sciences, v. 9, p. 1650–1669.

Sanborn-Barrie, M., St-Onge, M.R., Young, M.D. and James, D.T. 2008: Bedrock geology of southwestern Baffin Island, Nunavut: expanding the tectonostratigraphic framework with relevance to mineral resources; Geological Survey of Canada, Current Research 2008-6, 16 p.

Scott, D.J., Stern, R.A., St-Onge, M.R. and McMullen, S.M. 2002: U-Pb geochronology of detrital zircons in metasedimentary rocks from southern Baffin Island: implications for the Paleoproterozoic tectonic evolution of northeastern Laurentia; Canadian Journal of Earth Sciences, v. 39, p. 611–623.

Senkow, M.D. 2013: Characterization of ultramafic occurrences on southern Hall Peninsula, Baffin Island, Nunavut, and evaluation of their potential as a source of carving stone; in Summary of Activities 2012, Canada-Nunavut Geoscience Office, p. 163–168.

St-Onge, M.R., Sanborn-Barrie, M. and Young, M.D. 2007: Geology, Mingo Lake, Baffin Island, Nunavut; Geological Survey of Canada, Open File 5433, scale 1:200 000.

St-Onge, M.R., Van Gool, J.A.M., Garde, A.A. and Scott, D.J. 2009: Correlation of Archaean and Palaeoproterozoic units between northeastern Canada and western Greenland: constraining the pre-collisional upper plate accretionary history of the Trans-Hudson orogen; in Earth Accretionary Systems in Space and Time, P.A. Cadwood and A. Kröner (ed.), Geological Society, London, Special Publications, 318, p. 193–235.

Resource potential for industrial limestone on Southampton Island, Nunavut: summary of fieldwork and geochemical data

S. Zhang[1], E.C. Prosh[2] and D.J. Mate[3]

[1] *Canada-Nunavut Geoscience Office, Iqaluit, Nunavut, Shunxin.Zhang@NRCan-RNCan.gc.ca*

[2] *Mineral and Petroleum Resources, Department of Economic Development and Transportation, Government of Nunavut, Iqaluit, Nunavut*

[3] *Canada-Nunavut Geoscience Office, Iqaluit, Nunavut*

Abstract

In 2009, an assessment of the resource potential for industrial limestone in the Upper Ordovician strata near the community of Coral Harbour on Southampton Island was completed. These strata contained only medium- to low-purity limestone. In 2013, new fieldwork focused on the resource potential of the Lower Silurian Ekwan River and Attawapiskat formations on western Southampton Island. Three major areas underlain by these formations were explored, and 49 samples, each weighing >3 kg, were collected for whole-rock major- and minor-element analysis. In order to quantitatively grade the resource potential of the Ekwan River and Attawapiskat limestone formations, all samples were analyzed by X-ray fluorescence (XRF). The preliminary data suggest that high-calcium limestone occurs in the Ekwan River Formation on western Southampton Island.

Résumé

On a complété, en 2009, une évaluation dont l'objet était de déterminer la présence de ressources potentielles de calcaire industriel dans les strates de l'Ordovicien supérieur situées à proximité de la collectivité de Coral Harbour dans l'île Southampton. Ces strates ne renfermaient que du calcaire dont la pureté variait de faible à moyenne. De nouveaux travaux sur le terrain, entrepris en 2013 dans l'ouest de l'île Southampton, ont porté sur la présence de ressources potentielles dans les formations d'Ekwan River et d'Attawapiskat du Silurien inférieur. Trois zones importantes reposant sur ces formations ont fait l'objet d'explorations et 49 échantillons d'un poids de plus de 3 kg chacun ont été recueillis aux fins d'analyse géochimique sur roche totale pour les éléments majeurs et mineurs. Tous les échantillons ont été analysés par fluorescence X en vue d'établir de façon quantitative le potentiel économique des formations calcaires d'Ekwan River et d'Attawapiskat. Les données préliminaires obtenues semblent indiquer que la formation d'Ekwan River dans l'ouest de l'île Southampton renferme du calcaire à haute teneur en calcium.

Introduction

Quicklime (CaO) is a chemical reagent that has many uses in the mining industry. In particular, it is used in the recovery of gold and silver in cyanide-leaching processes to curtail the loss of cyanide, and for pH control in tailings processes. With the projected growth of the mining industry in the Kivalliq Region of Nunavut alone, 4 000 000, 4 700 000 and 4 000 000–10 000 000 kg of quicklime would be required annually at the Meadowbank mine (gold) and the proposed Kiggavik (uranium) and Meliadine (gold) mines, respectively.

Quicklime (CaO) is a product of thermal decomposition of limestone, consisting principally of calcite ($CaCO_3$). Limestone containing >97% calcite is ideal for producing such a product. Finding limestone resources suitable for quicklime on Southampton Island could potentially meet mining-industry needs, reduce transportation costs for mine operators and provide significant opportunities for economic development and local employment in the Kivalliq Region of Nunavut. The Canada-Nunavut Geoscience Office (CNGO) conducted a research project to evaluate the industrial-mineral potential of the Upper Ordovician limestone near the

community Coral Harbour in 2009 (Figure 1). Unfortunately, according to Zhang et al. (2011), most limestones in the Upper Ordovician Bad Cache Rapids and Churchill River groups are of only medium (93.5–97% $CaCO_3$; 52.4–54.3% CaO) to low purity (85–93.5% $CaCO_3$; 47.6–52.4% CaO).

The Silurian Ekwan River and Attawapiskat formations in northern Ontario (Moose River Basin) yield high-purity limestone resources (Kelly, 1996). Since these formations developed similar facies in both the Moose River and Hudson Bay basins during the Early Silurian (Figure 1), a new study was initiated by CNGO and the Department of Economic Development and Transportation (EDT), Government of Nunavut (GN) to see if high-purity limestone exists in the Silurian Ekwan River and Attawapiskat formations on Southampton Island, located on the northern margin of the Hudson Bay Basin. The primary objectives of this study are to:
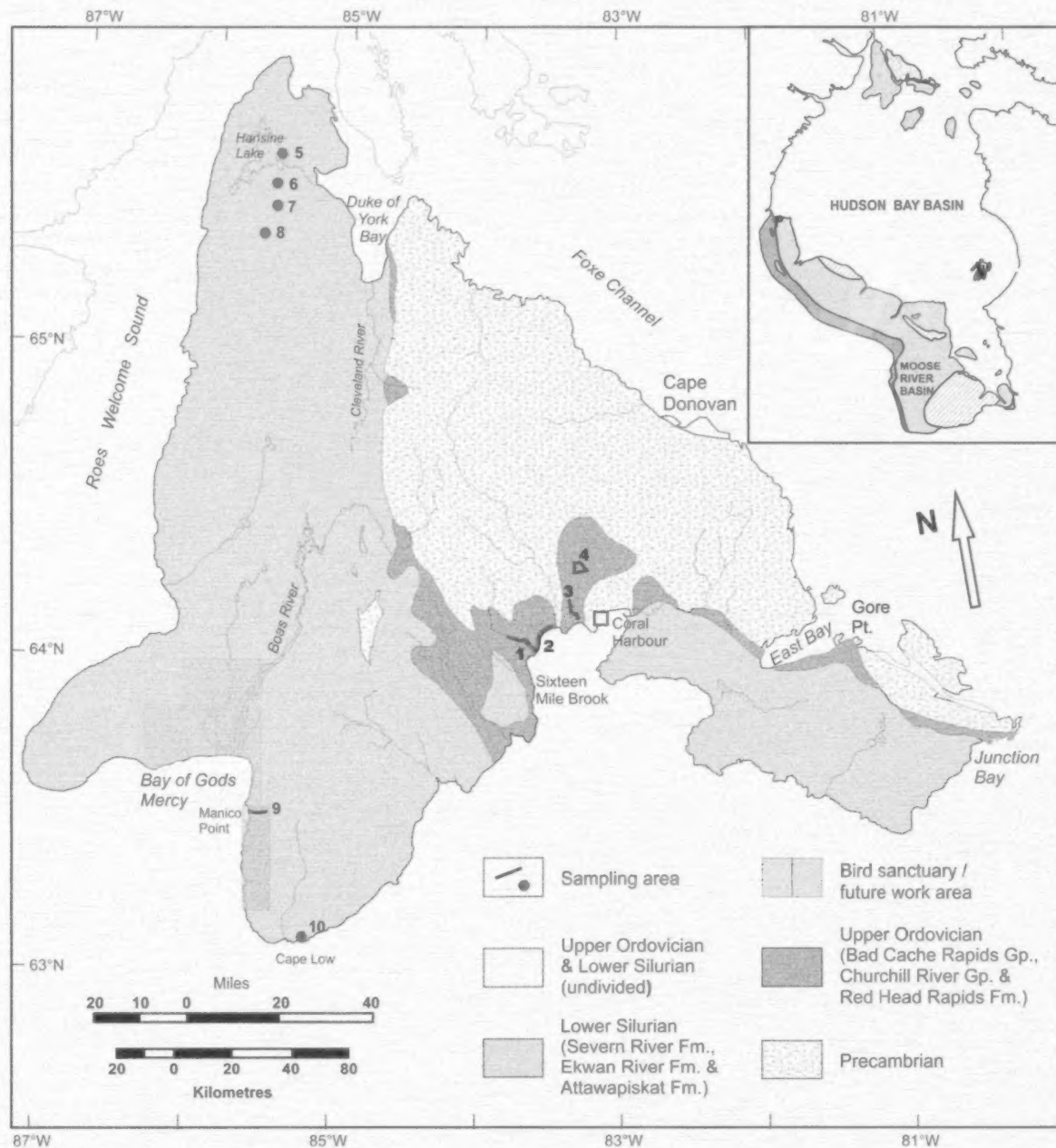

Figure 1: Simplified geology of Southampton Island, south-central Nunavut, modified from Heywood and Sanford (1976) and Zhang (2008), with sample locations. Areas 1–4 were sampled in 2009 (see Zhang et al., 2011); areas 5–10 were sampled during this study.

- better understand the stratigraphic and geographic distribution of relatively pure Silurian limestone intervals on Southampton Island;
- provide an assessment of limestone purity based on detailed geochemical data; and
- identify potential quarry locations, based on limestone thickness and lateral continuity, that may be of interest to industry.

This paper summarizes fieldwork that took place during the 2013 field season, and geochemical data from the samples that were collected during that fieldwork.

Lower Paleozoic stratigraphy on Southampton Island

The lower Paleozoic strata on Southampton Island (Figure 1) include 1) the Upper Ordovician Bad Cache Rapids and Churchill River groups and Red Head Rapids Formation, and 2) the Lower Silurian Severn River, Ekwan River and Attawapiskat formations (Heywood and Sanford, 1976), which are composed entirely of carbonate with minor shale and distributed throughout the southern and western parts of Southampton Island (Figure 1). Over broad areas, these carbonate rocks are almost horizontally distributed, undeformed and unmetamorphosed; therefore, they are exposed as subcropping rubble, although layered outcrops are commonly found along rivers and creeks.

Bad Cache Rapids Group

The Bad Cache Rapids Group unconformably overlies the Precambrian crystalline basement. It is dark grey or brown-grey fossiliferous limestone with a thin layer (about 1–2 m) of basal sandstone. It is characterized by yellowish-orange irregular zones of mottling on almost all bedding. The group has a maximum thickness of approximately 65 m. This unit was systematically sampled for geochemical analysis (Zhang et al., 2011), which indicates its medium purity and low purity based on the content of both calcite ($CaCO_3$) and calcium oxide (CaO).

Churchill River Group

The Churchill River Group conformably overlies the Bad Cache Rapids Group (Zhang, 2011). It consists of greenish-grey or grey-brown, argillaceous dolomitic limestone. No complete section of the formation was found; therefore, the maximum thickness of the group is unknown on Southampton Island. The lower part of the group was sampled for geochemical analysis (Zhang et al., 2011), which indicates mainly medium purity and low purity based on the content of both calcite ($CaCO_3$) and calcium oxide (CaO).

Red Head Rapids Formation

The Red Head Rapids Formation conformably overlies the Churchill River Group; the contact between these two units

is transitional. The Red Head Rapids Formation has a distinctive orange-tan colour, and is composed mostly of dolostone; therefore, no samples were collected for testing limestone purity during the previous and recent field seasons. The Red Head Rapids Formation is divided (Zhang, 2008) into laminated beds (unit 1), breccia beds (unit 2), biostromal beds (unit 3) and biohermal beds (unit 4). The maximum thickness of the formation is greater than 61 m on Southampton Island (Zhang, 2011).

Severn River Formation

The Severn River Formation disconformably overlies the Red Head Rapids Formation. It consists primarily of brown microcrystalline limestone and dolostone; at a number of localities, Severn River strata have been intensely dolomitized (Heywood and Sanford, 1976, p. 15–29); therefore, no samples were collected for analysis of limestone purity during the previous and recent field seasons. The thickness of the formation on Southampton Island is unknown.

Ekwan River and Attawapiskat formations

The Ekwan River Formation, which conformably overlies the Severn River Formation, consists of well-bedded, skeletal and peloidal limestone and fine-grained dolostone. The upper part of the formation passes laterally into the Attawapiskat Formation, consisting of a reef-bearing carbonate unit with algal and stromatoporoid bioherms. The Ekwan River Formation is nowhere exposed in a complete section; the formation probably has a composite thickness of about 91 m, according to Sanford (Heywood and Sanford, 1976, p. 15–29). These two formations occur on western Southampton Island and are the focus of the present study.

Samples, sample-site selection and areas

According to Kelly (1996), analyses from samples collected from the Ekwan River and Attawapiskat formations in the Moose River Basin (northern Ontario) indicate the potential for high-calcium limestone, with $CaCO_3$ concentrations of 96.86–97.40% (54.3–54.57% CaO) in the Ekwan River Formation and 98.03–100% (54.8–56.03% CaO) in the Attawapiskat Formation. These formations developed similar facies in both the Moose River and Hudson Bay basins during the Early Silurian. Since Southampton Island was located on the northern margin of the Hudson Bay Basin during the Paleozoic, it was targeted by this study. Therefore, from north to south, the following areas were selected (Figure 1; Zhang et al., 2014, sheet 1[3]):

- Hansine Lake: area 5 and north of area 5

- south of Hansine Lake: areas 6, 7 and 8
- Manico Point: area 9
- Cape Low: area 10

Sampling stratigraphically targeted the Lower Silurian Ekwan River and Attawapiskat formations.

Hansine Lake (area 5; stations 7–19)

Hansine Lake is located near the northern tip of Southampton Island (Figures 1, 2a), about 200 km northwest of Coral Harbour. Based on information from K. Dewing (pers. comm., 2012), the Silurian 'reef' is exposed on the east shore of Hansine Lake (Figure 2a, b, e). Actually, at this locality, three flat 'reef' patches are lined up in a northerly direction and occupy an area measuring about 1200 by 400 m (light grey colour in Figure 2b, e). Due to the strong glacial erosion and frost shattering, the rocks here do not outcrop. The three flat 'reef' patches are actually formed by the in situ limestone rubble (light grey colour in Figure 2b, e), and the surrounding rocks are heavily covered by vegetation (brown colour in Figures 2b, e). Many macrofossils, mainly corals, stromatoporoids and brachiopods, are scattered among the rubble. Based on the topography at this locality, it is difficult to determine the three-dimensional distribution of the fossiliferous rocks (i.e., whether they are bioherms or biostromes, or just simply layered limestone rich in fossils).

The Hansine Lake locality was originally mapped as Upper Ordovician Red Head Rapids Formation (Heywood and Sanford, 1976, p. 15–29); however, one of the fossils, *Pentamerus* sp. (or *Pentameroides* sp.), indicates that its age is Silurian.

Thirty rubble samples, each weighing >3 kg, were collected for geochemical analysis from the three flat 'reef' patches (Zhang et al., 2014, sheet 1); each sample covers an area measuring about 76 by 76 m.

In order to determine the relative age of the three flat 'reef' patches of fossiliferous limestone, six rubble samples were collected for microfossil conodont processing (Zhang et al., 2014, sheet 1). Another six samples (Zhang et al., 2014, sheet 1) were collected from the dolomitic limestone outcrop in the area north-northeast of area 5 (station 4) for conodont processing; this outcrop is stratigraphically higher than the three flat patches of fossiliferous limestone in area 5 and geographically about 500–1000 m north of area 5.

South of Hansine Lake

Area 6 (station 20)

The second flat patch of fossiliferous limestone (area 6, station 20) was found about 13 km south of area 5, and measures about 700 by 500 m (Figure 2a, c, f). Similar to the patches in area 5, this patch is composed of limestone rubble (dark brown colour in the foreground of Figure 2f), which is rich in fossil corals, stromatoporoids and brachiopods. Unlike the patches in area 5, it is apparently surrounded by dolomitic limestone and dolostone rubble (yellowish colour in the background of Figure 2f). Topographically, the patch of fossiliferous limestone is ~1 m higher than the surrounding dolomitic limestone and dolostone at some spots, and almost at the same level in others. This may indicate that the patch of fossiliferous limestone at this location is stratigraphically higher than the surrounding dolomitic limestone and dolostone, and is therefore just an erosional remnant.

Three rubble samples, each weighing >3 kg, were collected for geochemical analysis from the central, northern and southern ends of the patch (Zhang et al., 2014, sheet 1); each of them covers an area measuring about 76 by 76 m.

For determining the relative age of the patch of fossiliferous limestone, four rubble samples were collected for conodont processing from the surrounding dolomitic limestone and dolostone that is probably stratigraphically beneath the patch of fossiliferous limestone.

Area 7 (station 21)

The third flat patch of fossiliferous limestone was found about 7 km south of area 6, and measures about 1200 by 1000 m (Figure 2a, 2d, g). Similar to the patch in area 6, dark grey limestone rubble (dark grey colour in the middle of Figure 2g) is rich in fossil corals, stromatoporoids and brachiopods, and the patch is surrounded by dolomitic limestone and dolostone rubble (yellowish colour in the foreground of Figure 2g). Both topographically and stratigraphically, this patch of fossiliferous limestone is apparently higher than the surrounding dolomitic limestone and dolostone rubble; it may therefore be an erosional remnant.

Only one sample, weighing >3 kg, was collected from this area for geochemical analysis (Zhang et al., 2014, sheet 1).

Area 8 (station 22)

This area is covered by thinly layered dolomitic limestone and dolostone rubble; no fossils were found among the rubble. Only one sample, weighing >3 kg, was collected from this area for geochemical analysis (Zhang et al., 2014, sheet 1).

Manico Point (area 9; stations 23 and 24)

Manico Point is about 135 km southwest of Coral Harbour. The brown-coloured limestone is well exposed along a creek that flows into the Bay of Gods Mercy about 6–7 km south-southeast of Manico Point (Figure 3a). The rocks here were mapped as Ekwan River Formation by Sanford (Heywood and Sanford, 1976, p. 15–29). They are nearly
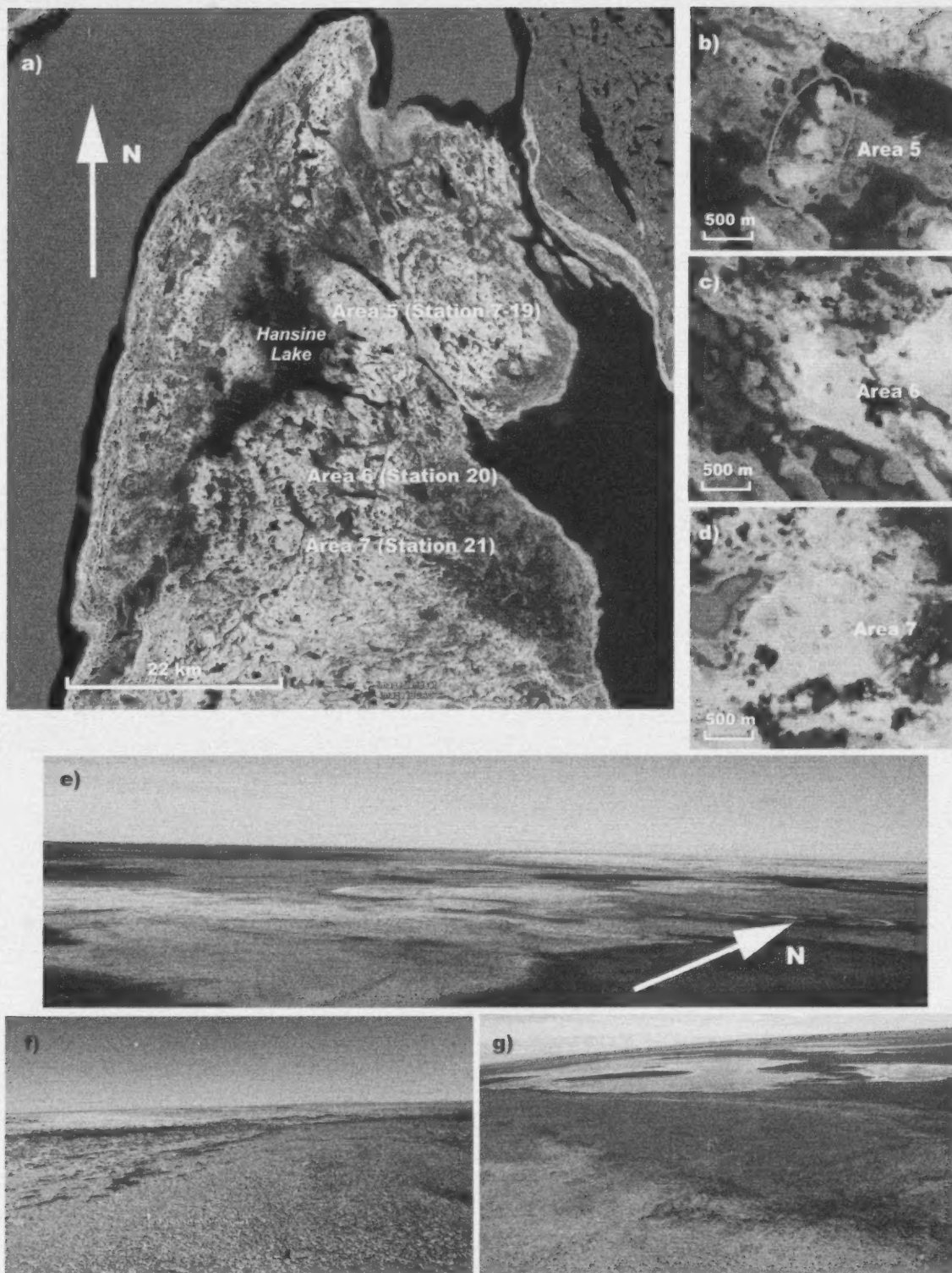
Figure 2: a) Locations of Silurian fossiliferous limestone around Hansine Lake, northern Southampton Island, south-central Nunavut, on a Google Maps base (Imagery ©2013 Terrametrics, Map data ©2013 Google, data downloaded Sep. 15, 2013). **b), c), d)** close-ups of areas 5 (stations 7–19), 6 (station 20) and 7 (station 21), respectively. **e), f), g)** Field photos from areas 5 (stations 7–19), 6 (station 20) and 7 (station 21), respectively.

horizontally distributed; based on the contour lines in Figure 3a), the limestone is about 90 m in thickness; it is distributed along this creek and exposed off and on for approximately 3.5 km between stations 23 and 24. It is uncertain whether all the 90 m thick strata in this area belong to the Ekwan River Formation or include parts of the Attawapiskat Formation at station 23 or the Severn River Formation at station 24.

At station 23, the upper reach of the creek (Figure 3a), the rubble on the top of the two sides of the creek is similar to that in the vicinity of Hansine Lake and south of Hansine Lake. A fossiliferous limestone with a thickness of about 6–7 m is well exposed along the two sides of the creek (Figure 3b–e). Several layers are full of fossil brachiopods and corals, which are apparently a biostrome. Figure 3d and e show a 15–20 cm thick layer full of brachiopod shells and a large colony of corals, respectively. However, at the bottom of the outcrop, there is a nonlayered bioherm-like structure (Figure 3c), but no macrofossils were found within it.

At station 24, the mouth of the creek (Figure 3f), the rocks are deeply cut by a waterfall and a thickness of about 12–15 m of strata is exposed. The rocks here appear to be stratigraphically lower than those at station 23, and some intervals above the waterfall are dolomitic. The fossils in these rocks are not as abundant as at station 23, but are more diverse. Besides corals and stromatoporoids, gastropods and trilobites are also found.

Four and eight samples, weighing >3 kg, were collected for geochemical analysis from outcrops at stations 23 and 24, respectively (Zhang et al., 2014, sheet 1). All sample intervals are =1.5 m; within each 1.5 m interval, uniform-sized chips were taken at nearly equal spacings. Weathered surfaces were avoided where possible, and the weathered rind on the chips was discarded. Unfortunately, the strata between these two stations, representing a thickness of about 60–70 m, were not sampled. In 2007, four samples were collected by the senior author from station 23, and another six samples were collected from three additional localities between stations 23 and 24 along the creek for microfossil conodonts; these samples have been processed, but the conodonts have not yet been examined.

Cape Low (area 10; stations 1 and 2)

Cape Low is located on the south coast of western Southampton Island, about 135 km southwest of Coral Harbour (Figure 1). The rocks here were mapped as Attawapiskat Formation by Sanford (Heywood and Sanford, 1976, p. 15–29). The formation is composed of inter-reef dolomitic limestone and dolostone, and small algal bioherms. At this locality, the small bioherms (<1 m high and less than 10 m long) are seen both on the surface (Figure 4a, b) and as a 'lens' interbedded with the inter-reef dolomitic limestone and dolostone (Figure 4c). The majority of rocks at this lo-

cality are thick to massive dolomitic limestone and dolostone (Figure 4d, e). Chert and limestone nodules were found on the surface of the thick dolomitic limestone and dolostone (Figure 4e), which is an indication that some of the rocks at this locality were possibly deposited in the fore-reef transition zone. No macrofossils were found within the bioherms, but brachiopods, corals and crinoids were found among the inter-reef dolomitic limestone and dolostone.

Because of the dolomitization, only two samples were collected from the 'limestone' nodules and the small bioherm 'lens' within the inter-reef dolomitic limestone and dolostone (Zhang et al., 2014, sheet 1).

Results of whole-rock major- and trace-element analysis by X-ray fluorescence (XRF)

Forty-nine samples were sent to Acme Analytical Laboratories Ltd. (Vancouver, British Columbia) for whole-rock major- and trace-element geochemical analysis. Each sample weighed >3 kg. The entire sample was crushed to 80% passing 10 mesh, then a 1000 g portion was pulverized to 85% passing 200 mesh. The samples were analyzed by X-ray fluorescence (XRF; Acme method 4X01), with total S and C determined by LECO carbon-sulphur analyzer. The results for major oxides are summarized in Table 1, and complete geochemical data are presented in Zhang et al. (2014, sheet 2). Application of the British Geological Survey scheme for the classification of limestone by purity (percentage of CaO) (Harrison et al., 1998; Table 2) was employed by this study to evaluate the limestones sampled in the various areas.

Hansine Lake (area 5)

Of the 30 rubble samples collected from Hansine Lake (area 5; Figures 1, 2a, b, e), only one is of high purity (55% CaO), whereas four and twenty-five samples are of medium (54.3–52.4% CaO) and low (<52.4% CaO) purity, respectively (Figure 5a; Tables 1, 2; Zhang et al., 2014, sheet 2). Therefore, 83% of the collected samples are classified as low-calcium and impure limestone.

South of Hansine Lake (areas 6, 7 and 8)

Three and one rubble samples, respectively, were collected in areas 6 and 7, south of Hansine Lake (Figures 1, 2c, d, f, g). Two of the four samples contain >55.2% CaO, indicating very high purity, and the other two contain 54.3–55.2% CaO, indicating high purity (Figure 5b; Tables 1, 2; Zhang et al., 2014, sheet 2).

Only one rubble sample (SZ13-08-01) was collected from south of Hansine Lake in area 8 (Figure 1). It contains only 47.69% CaO (Zhang et al., 2014, sheet 2), and can therefore be classified as low-calcium limestone (Table 2).
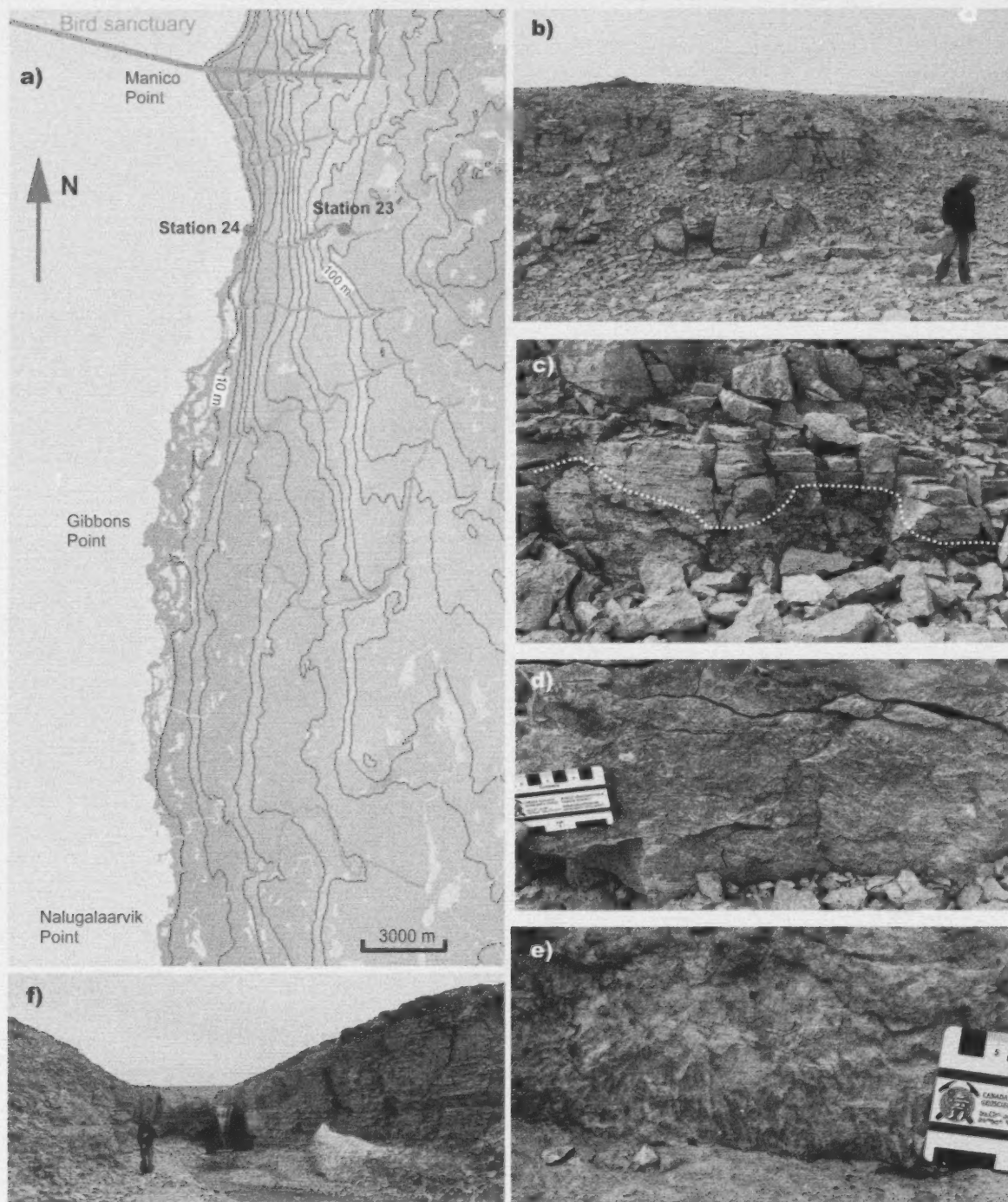
Figure 3: a) Topography of the coastline south of Manico Point, southwestern Southampton Island, south-central Nunavut, showing a creek (highlighted by orange line) and two localities (red dots) where the samples were collected for this study, and other creeks (highlighted by light blue lines) from north of Manico Point to Nalugalaarvik Point where future studies are being considered. **b)** Part of the outcrop at station 23. **c)** Contact (dotted white line) between the layered fossiliferous limestone and nonlayered bioherm at station 23. **d)** Fossiliferous limestone full of brachiopod shells and corals at station 23. **e)** Corals in the outcrop at station 23. **f)** Outcrop at station 24.
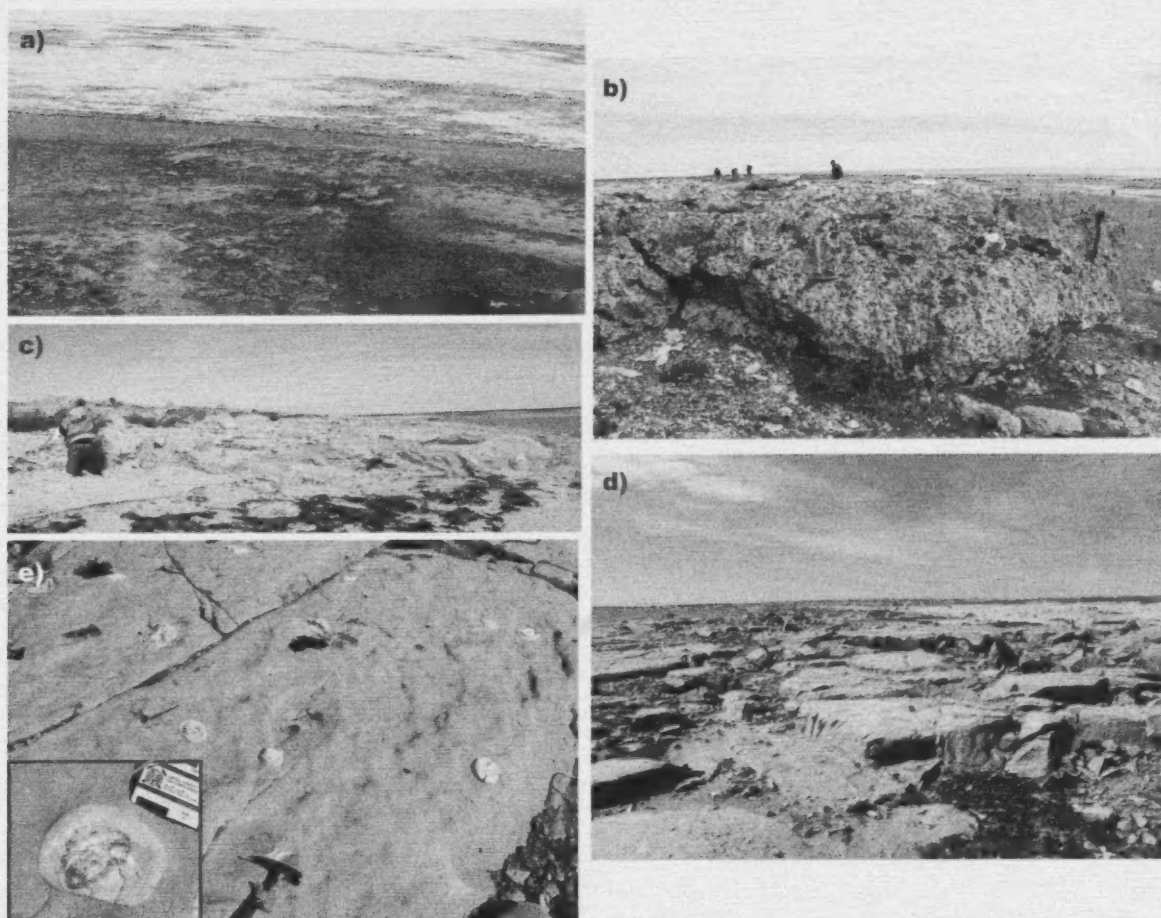
Figure 4 Outcrops and fossils of the Attawapiskat Formation at Cape Low, southwestern Southampton Island, south-central Nunavut:
a) bird's-eye view of a small algal bioherm exposed on the coast; **b)** close-up of the algal bioherm in (a); **c)** small bioherm interbedded within thick dolostone; **d)** inter-reef dolostone; **e)** chert nodules on the surface of dolostone.

Manico Point (area 9)

Twelve samples were collected from outcrops along a creek in the Manico Point area (area 9; Figure 3), of which ten are of very high (>55.2% CaO) or high (55.2–54.3% CaO) purity (Figure 5c; Tables 1, 2; Zhang et al., 2014, sheet 2). Therefore, 83% of the collected samples can be classified as very high or high-calcium limestone.

Cape Low (area 10)

Only two samples were collected from Cape Low (Figures 1, 4). One (SZ13-01-01) is from a limestone nodule and the other (SZ13-02-01) from a small 'bioherm'. The first sample contains 54.89% CaO and is classified as high-calcium limestone. The second contains 34.11% CaO (Zhang et al., 2014, sheet 2) and can therefore be considered impure limestone.

Economic considerations

The purpose of the project was to identify high-purity limestone within the Silurian Ekwan River and Attawapiskat formations on western Southampton Island. Samples were collected (Figure 1) near Hansine Lake (area 5), south of Hansine Lake (areas 6, 7, 8), and near Manico Point (area 9) and Cape Low (area 10).

Because the rubble samples collected from Hansine Lake and south of Hansine Lake are weathered, all CaO concentrations presented in Table 1 and sheet 2 of Zhang et al. (2014) are likely to be lower than if they had been unweathered. Although a few rubble samples can be classified as high- and medium-calcium limestone (Table 1; Figure 5a, b; Zhang et al., 2014, sheet 2) in these areas, lack of outcrop makes it difficult to determine their thickness in the stratigraphic sequence. Drilling would be required to collect nonweathered samples for more reliable geochemical

analysis and to get information on the thickness and three-dimensional distribution of the higher concentrations.

Samples from Manico Point have the highest CaO concentrations, with 83% of the samples from the sampled stations 23 and 24 containing 54.76%–55.99% CaO, which is suitable for many industrial purposes. More importantly, this limestone is well exposed along a creek, and the total thickness of the sampled units is clear. Therefore, it is recommended that further investigation is focused in the Manico Point area, to confirm if a locally mineable high-calcium limestone deposit exists. If so, this could become an extremely valuable resource for Nunavut and the community Coral Harbour.

Future studies at Canada-Nunavut Geoscience Office (CNGO)

Future studies by the CNGO will focus on examining conodont microfossils to determine the relative age of these sampled rock units, and continuing to evaluate materials collected during the summers of 2007 and 2013. New field work may also be initiated for

- more detailed sampling along the creek (highlighted by orange line in Figure 3a) in the Manico Point area (area 9) to understand the change in CaO content and to identify the mineable intervals with very high and high-calcium limestone; and

- expanding the prospective area near Manico Point by sampling along other creeks in the region between Manico Point and Nalugalaarvik Point (highlighted by light blue lines in Figure 3a; area north of Manico Point is within a bird sanctuary). Paleozoic strata are nearly horizontally distributed on Southampton Island, so exposures between Manico Point and Nalugalaarvik Point should be from the same stratigraphic units.

Acknowledgments

Table 1: Results for major oxides in carbonate samples collected from areas 5–10, western Southampton Island, south-central Nunavut.

Sample	Oxide (%)				
	SiO$_2$	Al$_2$O$_3$	Fe$_2$O$_3$	CaO	MgO
SZ13-01-01	0.03	<0.01	0.02	54.89	1.46
SZ13-02-01	0.24	0.06	0.08	34.11	18.86
SZ13-05-01	0.11	0.01	0.02	52.11	3.68
SZ13-05-01A	0.47	0.02	0.02	47.97	6.66
SZ13-05-02	0.45	0.02	0.02	47.52	6.6
SZ13-05-02A	0.52	0.03	0.04	44.11	10.34
SZ13-05-03	0.04	<0.01	0.01	53.24	2.91
SZ13-05-03A	0.04	<0.01	0.01	53.29	2.78
SZ13-05-04	0.23	0.02	0.03	50.87	5.14
SZ13-05-04A	0.2	0.02	0.02	43.13	11.21
SZ13-05-05	0.17	0.01	0.03	49.82	5.7
SZ13-05-05A	0.35	0.02	0.03	45.55	9.1
SZ13-05-06	0.07	<0.01	<0.01	53.23	1.47
SZ13-05-06A	0.22	0.02	0.02	45.85	8.92
SZ13-05-06B	0.3	0.02	0.03	48.17	6.69
SZ13-05-07	0.08	<0.01	0.01	53.92	1.88
SZ13-05-07A	0.18	0.02	0.04	44.07	10.62
SZ13-05-07B	0.32	<0.01	0.03	50.52	4.98
SZ13-05-08	0.04	<0.01	<0.01	55	1.51
SZ13-05-08A	0.15	<0.01	0.02	48.59	6.77
SZ13-05-09	0.58	0.05	0.04	48.57	6.59
SZ13-05-09A	0.25	0.05	0.04	41.34	12.78
SZ13-05-10	0.16	0.02	0.02	51.26	4.65
SZ13-05-10A	0.27	0.02	0.04	44.26	10.41
SZ13-05-11	0.47	0.03	0.03	43.72	10.46
SZ13-05-11A	0.08	<0.01	0.02	48.74	6.76
SZ13-05-11B	1.03	0.03	0.04	38.08	15.21
SZ13-05-12	0.12	0.01	0.04	48.83	6.46
SZ13-05-12A	0.28	0.03	0.04	36.5	16.48
SZ13-05-12B	0.08	<0.01	0.02	50.03	5.63
SZ13-05-13A	0.08	<0.01	0.02	45.95	9.05
SZ13-05-13B	0.15	0.02	0.03	49.13	6.2
SZ13-06-01	0.29	0.02	0.03	55.34	0.91
SZ13-06-02	0.07	<0.01	0.02	55.74	0.87
SZ13-06-03	0.14	<0.01	0.02	54.56	1.5
SZ13-07-01	0.6	0.01	0.02	55.05	0.67
SZ13-08-01	0.27	0.05	0.05	47.69	7.47
SZ13-09-01	0.12	0.02	0.03	54.96	1.24
SZ13-09-02	0.13	0.02	0.03	55.56	0.49
SZ13-09-03	0.08	<0.01	0.02	55.78	0.39
SZ13-09-04	0.08	<0.01	0.02	55.79	0.39
SZ13-09-05	0.4	<0.01	0.02	55.54	0.39
SZ13-09-06	0.07	<0.01	0.02	55.99	0.38
SZ13-09-07	0.18	<0.01	0.01	55.69	0.4
SZ13-09-08	0.84	0.02	0.02	54.76	1.16
SZ13-09-09	3.8	0.06	0.05	53.69	0.52
SZ13-09-10	1.18	0.04	0.03	55.03	0.8
SZ13-09-11	3.44	0.02	0.07	53.89	0.42
SZ13-09-12	0.93	0.02	0.04	55.21	0.74

References

Harrison, D.J., Inglethorpe, S.D.J., Mitchell, C.J., Kemp, S.J., Chaodumrong, P. and Charusribandhu, M. 1998: Procedures for the rapid assessment of limestone resources; British Geological Survey, Technical Report WC/98/1, 120 p.

Heywood, W.W. and Sanford, B.V. 1976: Geology of Southampton, Coats and Mansel Islands, District of Keewatin, Northwest Territories; Geological Survey of Canada, Memoir 382, 35 p.

Table 2: Classification of limestone by purity (after Harrison et al., 1998) and grade of limestone on Southampton Island, south-central Nunavut, based on data (CaO) determined by X-ray fluorescence.

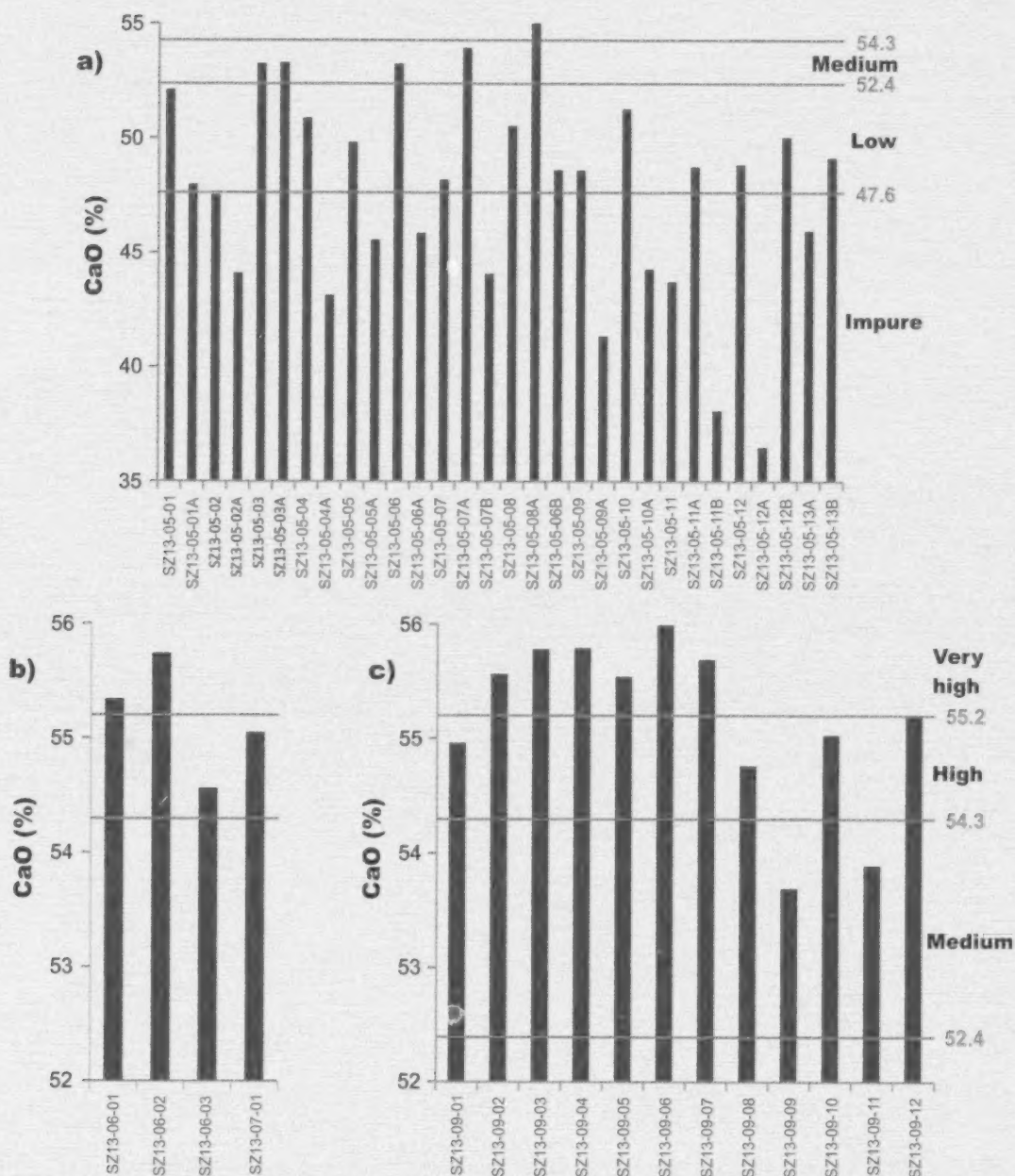| Sample no.	Percentage of		Category	Limestone on Southmpton Island		
	CaO	Equivalent CaCO₃		Area 5	Areas 6 & 7	Area 9
1	55.2–56.03	98.5–100	Very high purity	0% (0/30)	50% (2/4)	50% (6/12)
2	55.2–54.3	98.5–97.0	High purity	3% (1/30)	50% (2/4)	33% (4/12)
3	54.3–52.4	97.0–93.5	Medium purity	13% (4/30)	0% (0/4)	17% (2/12)
4	52.4–47.6	93.5–85.0	Low purity	43% (13/30)	0% (0/4)	0% (0/12)
5	< 47.6	< 85.0	Impure	40% (12/30)	0% (0/4)	0% (0/12)

Figure 5: Percentage of CaO in the samples collected on western Southampton Island, south-central Nunavut, from **a)** area 5, Hansine Lake; **b)** areas 6 and 7, south of Hansine Lake; and **c)** area 9, Manico Point. Classification of limestone by purity after Harrison et al. (1998).

Kelly, R.I. 1996: High-purity calcite and dolomite resources of Ontario; Ontario Geological Survey, Open File Report 5954, 39 p.

Zhang, S. 2008: New insight into Ordovician oil shales in Hudson Bay: their number, stratigraphic position, and petroleum potential; Bulletin of Canadian Petroleum Geology, v. 56, p. 300–324.

Zhang, S. 2011: Late Ordovician conodont biostratigraphy and redefinition of the age of oil shale intervals on Southampton Island; Canadian Journal of Earth Sciences, v. 48, p. 619–643.

Zhang, S., Prosh, E.C. and James, D.T. 2011: An assessment of a potential source of industrial limestone on Southampton Island, Nunavut; Geological Survey of Canada, Open File 6827, 30 p.

Zhang, S., Prosh, E.C. and Mate, D.J. 2014: Field localities and whole rock analysis of limestone samples from the 2013 field season on Southampton Island, Nunavut; Canada-Nunavut Geoscience Office, Geoscience Data Series GDS2014-002, Microsoft® Excel® file.

Geoscience field training for Nunavut students: a collaboration between the Canada-Nunavut Geoscience Office and Dalhousie University

M.D. Young[1], D.J. Mate[2], P.J. Peyton[2], C. Sudlovenick[2], and H.M. Steenkamp[2]

[1]*Department of Earth Sciences, Dalhousie University, Halifax, Nova Scotia, Mike.Young@Dal.Ca*
[2]*Canada-Nunavut Geoscience Office, Iqaluit, Nunavut*

Abstract

In 2013, the Canada-Nunavut Geoscience Office (CNGO) and Dalhousie University piloted a collaborative geoscience training program for Nunavut students. The main objective of this program is to engage students from Nunavut in the geosciences by providing intensive hands-on geoscience training that could lead to exciting careers in the public and private sectors. Two candidates from the Nunavut Arctic College's Environmental Technology Program were chosen to participate in the four-component program: 1) introductory geoscience lessons delivered by CNGO staff (early spring), 2) participation in Dalhousie University's advanced field school in California (May), 3) working as a geological field assistant with CNGO (summer), and 4) assisting with this paper for the CNGO's *Summary of Activities 2013* volume.

Résumé

En 2013, le Bureau géoscientifique Canada-Nunavut, en collaboration avec l'Université Dalhousie, a mené pour la première fois un programme de formation en géoscience à l'intention d'étudiants du Nunavut. Le programme avait comme objectif principal d'encourager les étudiants à s'engager dans les sciences de la Terre en leur offrant une formation pratique en géoscience susceptible de mettre à leur portée des carrières passionnantes dans les domaines public ou privé. Deux candidats provenant du programme de techniques environnementales du Collège de l'Arctique du Nunavut ont été sélectionnés pour participer à ce programme à quatre composantes, à savoir 1) des leçons d'introduction au domaine géoscientifique présentées par le personnel du Bureau au début du printemps, 2) la participation au programme de séances avancées sur le terrain offert par l'Université Dalhousie et se déroulant en Californie en mai, 3) une expérience de travail à titre d'aide-géologue sur le terrain avec des chercheurs du Bureau à l'été et, 4) l'occasion de contribuer à la rédaction de la présente édition du *Sommaire des activités* du Bureau géoscientifique Canada-Nunavut.

Introduction

Geoscience training for postsecondary students in Nunavut is one of the priorities of the Canada-Nunavut Geoscience Office (CNGO). Numerous activities and initiatives have been conducted by the CNGO in the past, including community presentations, summer jobs and geoscience-awareness campaigns in schools that promote geoscience as a relevant field of study that can lead to various employment opportunities. The training activities described in this paper are designed to expand upon these ongoing initiatives, as well as to deliver a longer duration and fully immersed geoscience-training experience for students in Nunavut. In the summer of 2013, two students from the Nunavut Arctic College's (NAC) Environmental Technology Program (ETP) were identified by CNGO staff to participate in this training. The first student was Patricia Peyton from Pangnirtung, Nunavut, who is a recent graduate of the ETP and is currently enrolled in the NAC's Inuktitut Interpreter/Translator Program. The second student was Candice Sudlovenick from Iqaluit, Nunavut, who is currently enrolled in her second year of the ETP.

Geoscience training program

The geoscience training program was developed with the goal of providing students from Nunavut with meaningful training opportunities that would open doors to careers in

the public and private sectors and/or higher education. It was designed to take a student through a structured process that involved understanding key geological concepts and processes, observing and collecting geological data in the field, and using the learned knowledge to interpret the geological meaning of the data. The training began in March 2013, was delivered over the course of six months, and consisted of four components (Table 1). The first component, a series of classroom lectures and hands-on learning activities, was followed by field training, a work placement and then map making and report writing. A brief description of each component is provided in the following sections.

Classroom teaching

The first component of the training program comprised eight evening and weekend seminars, during which content from a typical first-year university geology course was taught. Although both Patricia and Candice had taken introductory geoscience courses in the ETP, these lectures provided an invaluable review of fundamental geological concepts. The classes were taught by Holly Steenkamp at the CNGO and included such topics as the geological cycle, plate tectonics, mountain building, earthquakes and volcanos, and folds and faults. Lectures were complemented by in-class exercises that focused on rock and mineral identification, answering short questions, and calculations based on lecture topics. The students learned specific skills required for geological fieldwork, including how to take a strike and dip measurement with a compass, and how to record field observations and data in an organized and effec-

tive way. The knowledge and skills that Patricia and Candice learned in the classroom were specifically designed to prepare them for the next two program components: field school and summer fieldwork.

Field school

In the second component of the training program, the students took the observational and practical skills learned in the classroom and applied them in a realistic outdoor environment. Patricia and Candice participated in Dalhousie University's advanced field school in the White-Inyo Mountains of eastern California (Figure 1a) from May 19 to 29, 2013. Alongside 21 senior Dalhousie University students, they participated in group field trips, fieldwork exercises for the entire group, customized exercises designed to develop field skills, and camp life. Patricia and Candice learned the basic principles of geological mapping, including how to recognize and record folds and faults, while they continued to improve upon their rock and mineral identification skills (Figure 1b).

To introduce the concepts of field relationships between different rock types, Patricia and Candice participated in a customized field trip in an area where sedimentary rocks had been metamorphosed by a granitic pluton. This provided the opportunity to observe igneous, sedimentary and metamorphic rocks, and discuss the associated regional- to hand sample–scale processes involved in such an event. Patricia and Candice made their first paper map, detailing the observed field relationships, and continued with basic mineral and rock identification of hand samples.

Table 1: Sequence of activities completed during the geoscience training program for the Nunavut students.

Dates	Location	Activities	Learning Objectives
March/April, 2013	Iqaluit	Evening and weekend lecture and seminar series.	To review basic principles of Earth systems and the rock cycle To develop a better understanding of the various rock types and structures To prepare the students for rigorous field work including mapping
Late May, 2013	White/Inyo Mountains, California	Field trips, rock and mineral identification, geological mapping.	To introduce the students to field relationships and field work To introduce the students to 4th year university students To develop a basic understanding of geological mapping and cross sections
Late June to late August, 2013	Hall Peninsula, Baffin Island	Summer job as geological field assistants.	To gain an appreciation for the rigors of a long field work season (8 weeks) To learn how professionals map in northern terrain To semi-independently map a small area and produce a cross section
August to October, 2013	Various	Produce final versions of map and cross-section from field work and assist with this report.	To gain an appreciation for the various steps involved after field work is completed To develop some writing proficiency

Figure 1: a) Candice (left) and Patricia (right) in the White-Inyo Mountains, eastern California. **b)** Candice (left) and Patricia (right) learn to identify minerals in the field at the Obsidian Dome group field trip in California. **c)** Patricia (left) and Candice (right) sketching the folded and faulted strata in the cliff section prior to mapping the Poleta Folds area, California. **d)** Candice collects field observations while on traverse on Hall Peninsula, Nunavut (CNGO-HPIGP photo no. Y002P05)[3]. **e)** Patricia examines a hand sample while on traverse on Hall Peninsula, Nunavut (CNGO-HPIGP photo no. Y011P01). **f)** Candice (left) and Patricia (right) collect samples from their study area on Hall Peninsula.

---

[3]*Unless otherwise indicated, all numbered photos are from the Canada-Nunavut Geoscience Office Hall Peninsula Integrated Geoscience Program database.*

During the last four days of the field school, Patricia and Candice systematically mapped a small area with guidance from instructors and teaching assistants. They produced a geological map of folded and faulted early Cambrian sedimentary rocks in the Poleta Folds area in the White Mountains of eastern California (Figure 1c). They also constructed a topographic profile across their map area and, using their structural measurements, created a geological cross-section. Through this process, they learned the importance of recording detailed and accurate observations in the field, and how to compile field data to produce a three-dimensional picture. Additionally, they were shown how their observations could be used to interpret a geological story through time. Patricia and Candice wrote photo essays on their own experiences during this field school, which are posted on the CNGO website (Peyton, 2013; Sudlovenick, 2013).

Summer fieldwork with the CNGO

Following the field school, both students returned to Nunavut and transitioned seamlessly into summer jobs with the CNGO as geological field assistants. These jobs were part of the Hall Peninsula Integrated Geoscience Program (Steenkamp and St-Onge, 2014). Prior to beginning fieldwork, Patricia and Candice, along with the rest of the field crew, completed compulsory health and safety training that included helicopter safety and firearms shooting practice. In the field, their primary duties were to accompany more experienced geologists on helicopter-supported field traverses to collect geological samples and field observations. In this capacity they were able to put their new skills to work and received further 'on-the-job' training from senior geologists. At the same time, the Hall Peninsula mapping team benefitted from having two trained assistants who could contribute meaningfully to the mapping work. By the end of the 6-week mapping campaign, Patricia and Candice could effortlessly collect field data (Figure 1d), such as structural measurements and mineral and rock names (Figure 1e), and ask relevant and thoughtful questions about what they were observing in the field. They actively participated in and contributed to the daily 'geo-wrap' sessions, where each traverse team summarized their observations from that day to the broader group.

During their summer work, Patricia and Candice were tasked with conducting a semi-independent field project focused on producing a small map and cross-section of a previously unmapped region of the study area. The chosen site (Figure 2) has excellent bedrock exposure and low relief, is located in the centre of the study area, and contains features relevant to answering some of the broader mapping-project questions.

The selected map area contains a doubly plunging syncline overturned to the west. The structurally lowest and presumably oldest mapped unit is tonalitic gneiss, which surrounds the map area. Internal to the donut-shaped structure, the rocks comprise regionally metamorphosed sedimentary strata with mafic and felsic intrusive components. The stratigraphic sequence, including monzogranite, quartzite, diorite gneiss, iron formation, semipelite and tonalite, was documented in detail by Patricia and Candice and found to be comparative with other stratigraphic sections in the study area (Steenkamp and St-Onge, 2014).

To conduct this work, Patricia and Candice spent a day creating base maps and doing a lineament analysis and predictive mapping using airphotos and satellite imagery. Under the supervision of senior geologists, they spent three days mapping in the area and another three days drafting their maps and cross-sections (Figure 3). While mapping, they were expected to identify the various rock types, pay close attention to any lithological changes while walking across strike, take structural measurements and representative samples (Figure 1f), plot their locations on a base map and take detailed notes of their observations.

Map making and report writing

The final component of the geoscience training program required the compilation and critical analysis of recorded field data to understand the three-dimensional geometry of the observed features and the geological history of the mapped area, including the relative timing of events and associated processes. Patricia and Candice compiled their map data from Hall Peninsula during evenings and on weather days in order to produce their own maps, cross-sections and a written summary of the geological history of their map areas. In doing so, they gained an appreciation for attention to detail and how careful observations lead to a robust interpretation. Also, they developed an understanding of the geological history of the area, which led to an appreciation of the collective goals of the mapping team.

Economic considerations

Mineral exploration, mining, natural-resource management and land-use planning jobs are going to be in demand in Nunavut for the foreseeable future. Recently, the Conference Board of Canada noted that nearly 17 000 additional northerners will be required to meet the growth in mining (metallic and nonmetallic) between 2011 and 2020 (Conference Board of Canada, 2013). Although Nunavut communities are located near mining and exploration activities and their demographics are skewed heavily toward youth (51% under the age of 25 based on the 2011 Statistics Canada census), they are struggling to provide skilled workers. Part of the reason for this is that residents lack experience, education and training, and often cannot afford the associated costs (Mining Industry Human Resources Guide for Aboriginal Communities; Howard et al., 2012). Clearly, innovative and comprehensive training programs that expose students and residents from Nunavut to classroom teach-
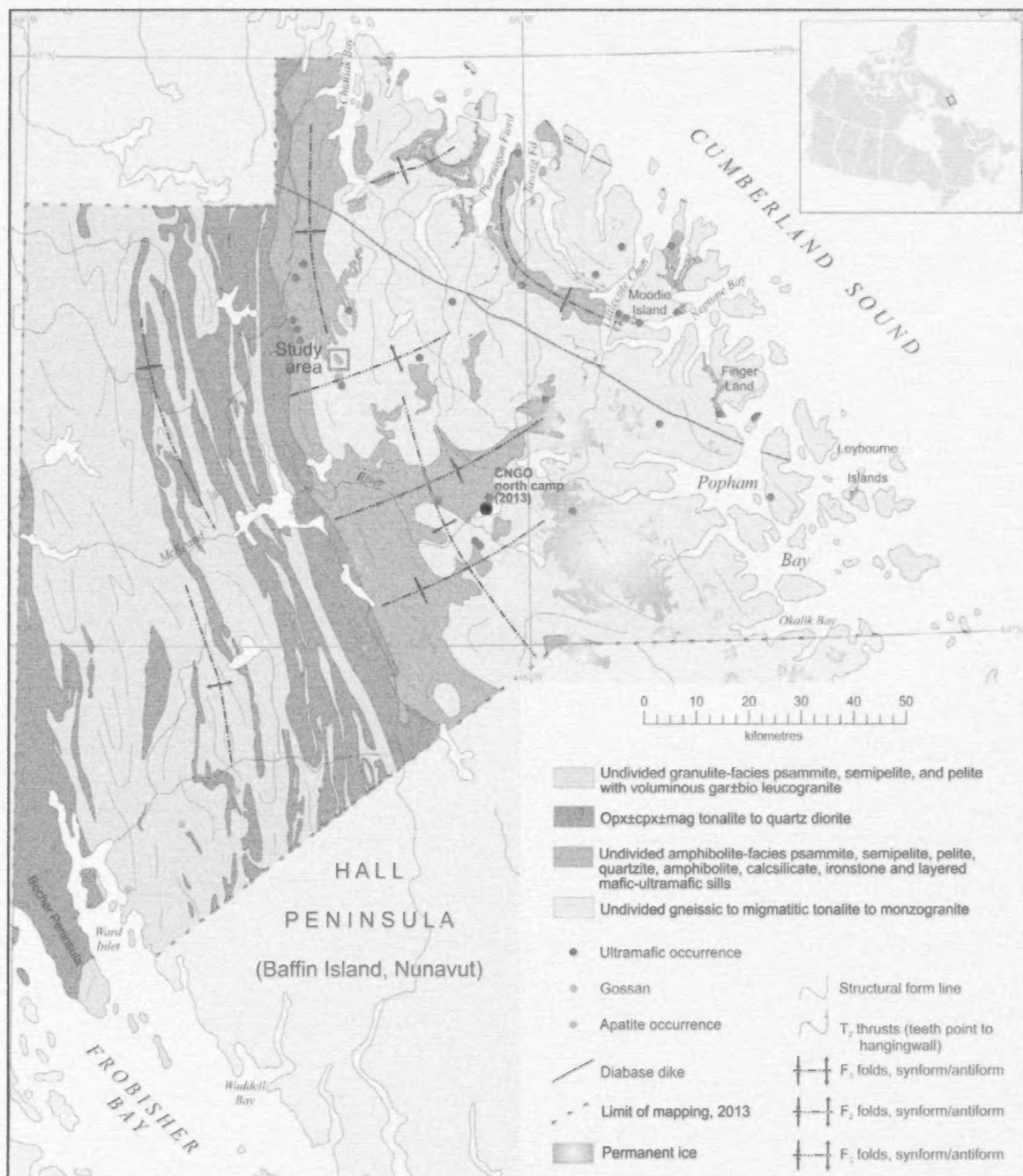
Figure 2: Location of the study area on Hall Peninsula, southeastern Baffin Island, Nunavut for detailed map and cross-section work by Patricia and Candice. Map after Steenkamp and St-Onge (2014).
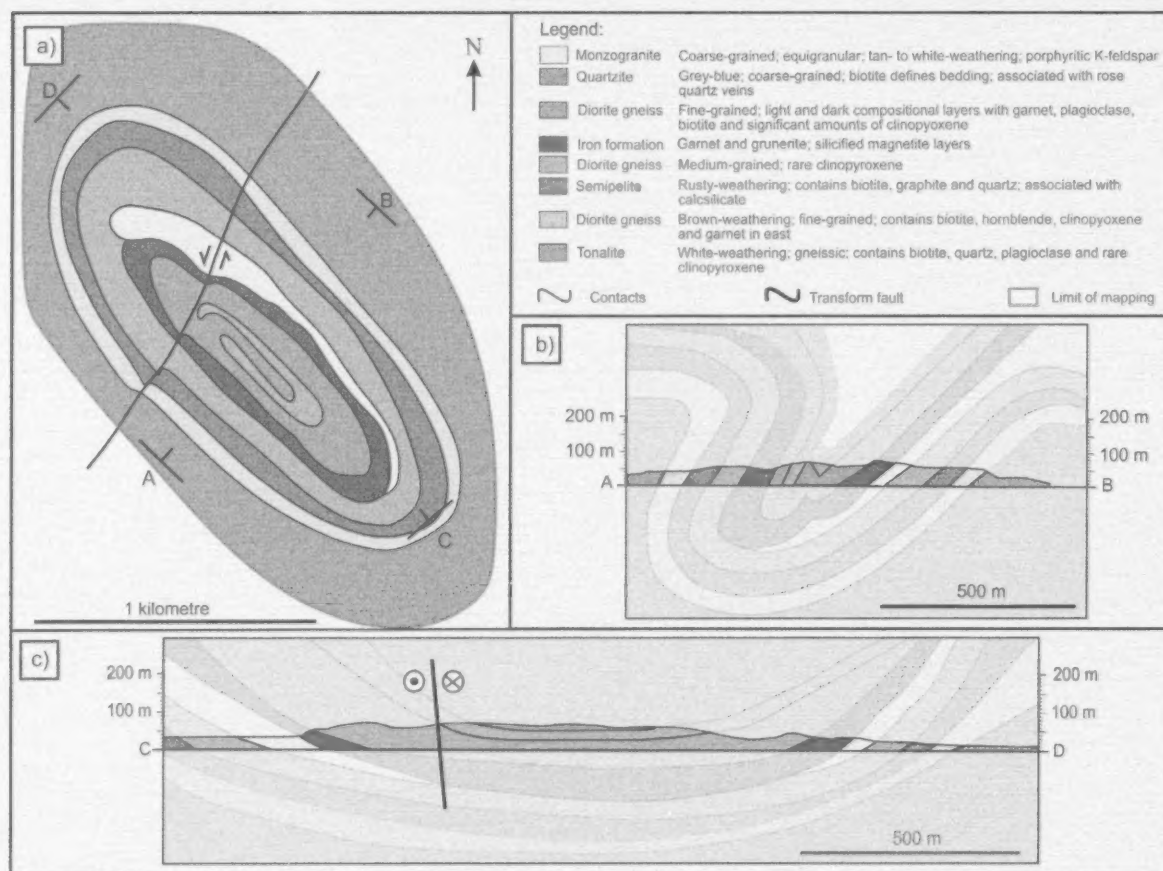
Figure 3: a) Geological map produced by Patricia and Candice from the detailed map area shown in Figure 2. **b)** A–B cross-section produced by Patricia and Candice from the detailed map area shown in Figure 2. **c)** C–D cross-section produced by Patricia and Candice from the detailed map area shown in Figure 2.

ing, hands-on learning and on-the-job experience are essential.

This was the aim of the CNGO–Dalhousie University geoscience training program. It is an attempt to provide students in Nunavut with meaningful geoscience experience and support for training that could open the door to exciting career possibilities. The structured sequence of classroom lessons, field school training, on-the-job experience and report writing appears to be an effective way to teach the essential fundamentals and field mapping skills required for a broad range of career opportunities in both the public and private sectors. The diverse exposure that this program offered provides skills and experience relevant to careers in the natural-resources sector that include, but are not limited to, mining and exploration. For example, Patricia is currently enrolled in the NAC Interpreter-Translator Program. Her experience working with the CNGO and participating in this training program will enable her to better interpret and translate geoscience concepts, terminology and expressions. Because of the importance of community consultations, stakeholder meetings and communication regarding natural-resource development, interpreting and translating are becoming skills in high demand in Nunavut.

Summary

The overall goal of the geoscience training initiative was to provide a thorough educational experience for students in Nunavut and expose them to geological fieldwork and semi-independent mapping. This training enabled Patricia and Candice to efficiently and confidently produce a detailed geological map of a small area on Hall Peninsula and be contributing members to a large mapping team. An unforeseen benefit from this training was that it exposed Patricia and Candice to senior university students, providing them the opportunity to learn about what it takes to get to that level of education. Patricia and Candice made many friends with the Dalhousie students in California and quickly realized that they, too, are capable of attaining a higher education.

Although this training program was successful, an appreciation for the complicated nature of such an ambitious endeavour was gained. Communication between trainees, facilitators and support staff is key. Additionally, managing expectations of how much can be achieved by a student in a program like this is crucial. Enthusiasm at the beginning of the training led to unrealistic expectations for what could be achieved. A dedicated person should be in place to manage the training program to ensure that all goals are met, there is effective communication and the northern students are integrated into all aspects of the field school and summer fieldwork.

The authors are planning to build on the successes of this training program and hope to continue similar training in the future. Some combination of classroom teaching, field school and summer fieldwork will be incorporated. Financial constraints and personnel schedules are major factors in planning and delivering this training program. An arrangement between the CNGO and Dalhousie provided support to the university, which co-ordinated the logistics for the Nunavut students participating in the field school. The delivery of this training program was rewarding for all involved.

Acknowledgments

References

Conference Board of Canada 2013: The future of mining in Canada's North; Conference Board of Canada, Centre for the North, Publication 13-201.

Howard, A., Edge, J. and Watt, D. 2012: Understanding the value, challenges, and opportunities of engaging Métis, Inuit and First Nations workers; Conference Board of Canada, 46 p., URL <http://www.conferenceboard.ca/e-library/abstract.aspx?did=4886> [November 15, 2013].

Mining Industry Human Resources Council 2013: Canadian mining industry employment, hiring requirements and available talent 10-year outlook; Mining Industry Human Resources Council, URL <http://www.mihr.ca/en/resources/MiHR_10_Year_Outlook_2013.pdf> [November 15, 2013].

Peyton, P. (2013): Patricia Peyton's experience with the CNGO-Dalhousie Collaborative Geoscience Training Initiative for Northerners; Canada-Nunavut Geoscience Office photo essay, June 27, 2013, URL<http://cngo.ca/2013/06/27/patricia-peytons-experience-with-the-cngo-dalhousie-collaborative-geoscience-training-initiative-for-northerners/> [November 15, 2013].

Steenkamp, H.M. and St-Onge, M.R. 2014: Overview of the 2013 regional bedrock mapping program on northern Hall Peninsula, Baffin Island, Nunavut; in Summary of Activities 2013, Canada-Nunavut Geoscience Office, p.27–38.

Sudlovenick, C. (2013): Candice Sudlovenick's experience with the CNGO-Dalhousie Collaborative Geoscience Training Initiative for Northerners; Canada-Nunavut Geoscience Office, photo essay, June 27, 2013, URL <http://cngo.ca/2013/06/27/candice-sudlovenicks-experience-with-the-cngo-dalhousie-collaborative-geoscience-training-initiative-for-northerners/> [November 15, 2013].

The **Canada-Nunavut Geoscience Ofice** conducts new geoscience mapping and research, supports geoscience-capacity building, disseminates geoscience information and develops collaborative geoscience partnerships for Nunavut.

www.cngo.ca